Two-Phase Flows with Phase Transitions

Modelling - Analysis - Numerics

Habilitation
zur Erlangung des akademischen Grades

doctor rerum naturalium habilitatus
(Dr. rer. nat. habil.)

von Dr. rer. nat. Maren Hantke
geb. am 03.12.1977 in Magdeburg

genehmigt durch die Fakultät für Mathematik
der Otto-von-Guericke-Universität Magdeburg

Gutachter:
Prof. Dr. Gerald Warnecke
Prof. Dr. Dietmar Kröner
Prof. Dr. Eleuterio F. Toro

eingereicht am 23.06.2017
verteidigt am 01.02.2018

Contents

Introduction 7

1 Deutsche Zusammenfassung 9
1.1 Klassifizierung von Zweiphasenströmungen . . . 9
1.2 Modellierung und Simulation - eine große Herausforderung . . . 10
1.3 Ausblick . . . 10

2 Compendium 19
2.1 Classification of Two-Phase Flows . . . 19
2.2 Modeling and simulation - a great challenge . . . 20
2.3 Outline . . . 20

Bibliography 27

I Sharp interface models 29

3 Euler equations with phase transition 31
(Joint work with Wolfgang Dreyer and Gerald Warnecke)
3.1 Introduction . . . 31
3.2 Isothermal Euler equations . . . 33
3.3 Equations of state . . . 33
3.4 Riemann problem . . . 34
3.5 Generic solution . . . 34
3.6 Explicit solutions . . . 43
3.7 3-Phase flow . . . 49
3.8 Numerical results . . . 53
References . . . 59

4 A general existence result 61
(Joint work with Ferdinand Thein)
4.1 Introduction . . . 61
4.2 Isothermal Euler Equations . . . 62
4.3 Solution at the Interface . . . 67
4.4 Solution of the Two Phase Riemann Problem . . . 74
4.5 Phase Creation in Single Phase Flows . . . 84
4.6 Conclusion . . . 88
References . . . 93

5 Singular and selfsimilar solutions for Euler equations 95
(Joint work with Ferdinand Thein)
5.1 Introduction . . . 95
5.2 Balance laws and entropy inequality . . . 96
5.3 Selfsimilar solutions . . . 97
5.4 Singular solutions . . . 98
References . . . 101

6 A non-existence result **103**
(Joint work with Ferdinand Thein)
6.1 Introduction . . . 103
6.2 The Euler model . . . 104
6.3 Equation of state . . . 105
6.4 Condensation by compression . . . 106
6.5 Extension to the real equation of state for water . . . 109
6.6 Cavitation by expansion . . . 112
6.7 Conclusions . . . 114
References . . . 117

II Diffusive Interface models **119**

7 Modeling Phase Transition for Two Phase Flows **121**
(Joint work with Ali Zein and Gerald Warnecke)
7.1 Introduction . . . 121
7.2 Mathematical model . . . 124
7.3 Numerical method . . . 126
7.4 Thermal relaxation, modeling of heat and mass transfer . . . 130
7.5 Modeling phase transition for the six-equation model . . . 139
7.6 Numerical results . . . 144
7.7 Conclusion . . . 154
7.A Appendix: Mathematical properties of the seven-equation model . . . 155
7.B Appendix: Derivation of the six-equation model . . . 156
7.C Appendix: Determination of $T_{sat}(p_{equi})$ . . . 161
References . . . 163

8 A Laser-Induced Cavitation Bubble **167**
(Joint work with Ali Zein and Gerald Warnecke)
8.1 Introduction . . . 167
8.2 Mathematical Model . . . 170
8.3 Equations of state (EOS) . . . 173
8.4 Numerical method . . . 178
8.5 Numerical Results . . . 181
8.6 Conclusion . . . 196
8.A Appendix: Mathematical properties of the three-phase model . . . 196
References . . . 199

9 Closure conditions for multi-component models **203**
(Joint work with Siegfried Müller and Pascal Richter)
9.1 Introduction . . . 203
9.2 Mathematical model . . . 204
9.3 Primitive variables . . . 207
9.4 Mathematical properties: hyperbolicity and sub-characteristic condition . . . 209
9.5 Frame invariance, objectivity and Galilean transformation . . . 215
9.6 Thermodynamical properties: 2nd law of thermodynamics . . . 217
9.7 Relaxation model . . . 224
9.8 Conclusion . . . 232
References . . . 233

10 Efficient and robust relaxation procedures **237**
(Joint work with Ee Han and Siegfried Müller)
10.1 Introduction . . . 237
10.2 Mathematical formulation of the model . . . 239
10.3 Relaxation procedures . . . 243
10.4 Discretization . . . 251

10.5 Numerical results . . . 253
10.6 Conclusion . . . 260
References . . . 263

III Particle flows **267**

11 Bubble evolution models **269**
(Joint work with Wolfgang Dreyer, Frank Duderstadt, and Gerald Warnecke)
11.1 Introduction . . . 269
11.2 Variables, equations of balance and local entropy principle . . . 272
11.3 The Göttingen laser induced bubble experiment . . . 278
11.4 Special cases . . . 279
11.5 Detailed derivations . . . 282
11.6 Numerical results . . . 286
11.7 Conclusions . . . 290
References . . . 291

12 Mixture theories for dispersed particles **293**
(Joint work with Wolfgang Dreyer and Gerald Warnecke)
12.1 Introduction . . . 293
12.2 Local spatial averaging techniques . . . 294
12.3 Mixture balance laws . . . 300
12.4 Closure relations . . . 303
12.5 Mathematical properties of the radial symmetric system . . . 306
12.6 Production terms . . . 307
12.7 Numerical results . . . 309
12.A Appendix: Newton's second law with non-constant mass . . . 312
12.B Appendix: Distributional derivatives . . . 313
12.C Appendix: Exterior potential flow . . . 314
12.D Appendix: Surface integrals . . . 318
References . . . 319

Eigene Veröffentlichungen **321**

Part

Introduction

Chapter 1

Deutsche Zusammenfassung

Zwei- und Mehrphasenströmungen spielen in zahllosen Anwendungen eine wesentliche Rolle, beispielsweise in der Luft- und Raumfahrt, in der Verkehrs- und Schiffstechnik, in der Geo- und der Astrophysik oder auch in der Elektrochemie oder Meteorologie. Sie treten auf in Siede-, Kühlungs- oder Verbrennungsprozessen. Dabei finden i.a. Phasenübergänge und chemische Reaktionen statt. Die Modellierung und Simulation solcher Prozesse ist eine Herausforderung und Gegenstand der aktuellen Forschung.

Figure 1.1: Die Abbildung[1] zeigt ein System zur Kühlung, Befeuchtung und Reinigung von Luft. Dabei wird mittels Druck Wasser in Form von Nebel der Luft zugeführt. Der Kühleffekt entsteht durch die sofortige Verdunstung des Wassers.

1.1 Klassifizierung von Zweiphasenströmungen

In den Materialwissenschaften, der Thermodynamik und der physikalischen Chemie bezeichnet eine Phase einen räumlichen Bereich, in welchem die chemische Zusammensetzung und wesentliche physikalische Eigenschaften wie z.B. die Dichte homogen sind. Das bedeutet, bestimmende Parameter sind innerhalb gewisser Größenordnungen etwa konstant. Die wichtigsten Phasen sind die Aggregatzustände gasförmig, flüssig und fest, die sich wesentlich z.B. in ihren Dichten unterscheiden. Auch innerhalb eines Aggregatzustandes einer chemischen Substanz können verschiedene Phasen auftreten, man denke an Graphit und Diamant. Eine Phase kann sich aus mehreren Komponenten zusammensetzen, Luft z.B. besteht hauptsächlich aus den Komponenten Stickstoff und Sauerstoff. Mitunter ist das Abgrenzen von Phasen und Komponenten schwierig und kann von der Genauigkeit der Betrachtung, also der verwendeten Längenskala, abhängen. In der Literatur ist die Bezeichungsweise teilweise ungenau. Nicht selten werden die Begriffe nicht unterschieden.

Liegen mindestens zwei Phasen vor, so bildet sich zwischen den Phasen eine Phasengrenze, an der sich die Materialeigenschaften sprunghaft ändern. Eine Phasengrenze ist im mathematischen Sinne eine Gren-

[1] https://www.lubing.de/top-klima-system.de

zfläche, an der physikalische Größen unstetig sein können. An dieser finden i.a. Phasenübergangsprozesse statt, z.B. Kondensation oder Verdampfung, aber auch chemische Reaktionen.

Eine Klassifizierung von Zweiphasenströmungen kann mit Hilfe der Charakterisierung der Phasengrenze erfolgen. Hierbei werden sog. disperse, separierte und Übergangsströmungen unterschieden.

Zu den separierten Strömungen gehören u.a. Jet- und Filmströmungen. Hierbei sind die Phasen klar voneinander getrennt. Liegt eine disperse Strömung vor, überwiegt der Volumenanteil der umgebenden (Träger)-Phase den Volumenanteil der strömenden Partikel bei weitem. Dagegen ist der Volumenanteil beider Phasen in sog. Übergangströmungen von etwa gleicher Größenordnung.

1.2 Modellierung und Simulation - eine große Herausforderung

Sowohl die korrekte mathematische Beschreibung als auch die numerische Behandlung der Phasen und insbesondere der Phasengrenzen sind zentrale Fragestellungen in der Theorie von Mehrphasenströmungen. Besondere Schwierigkeiten bereitet die physikalisch korrekte Modellierung der Prozesse an der Phasengrenze wie Energie- und Massentransfer durch Phasenübergänge. In der Literatur finden sich verschiedene Modellklassen zur Beschreibung von Zwei- und Mehrphasenströmungen, die sich nach ihrer Behandlung der Phasengrenzen einteilen lassen.

Sind die Phasen wohl separiert und wird die Phasengrenze als freier Rand explizit verfolgt, spricht man von sog. *sharp-interface*-Modellen. Die Beschreibung der Prozesse an der Phasengrenze ist dabei vergleichsweise einfach und erfolgt durch *Sprungbedingungen* und *kinetische Relationen*. Sprungbedingungen sind Erhaltungseigenschaften über die Phasengrenze hinweg und ergeben sich unmittelbar aus den Erhaltungssätzen für Masse, Impuls und Energie in Abhängigkeit von den zu berücksichtigenden physikalischen Effekten. Kinetische Relationen quantifizieren die Phasenübergänge und sind thermodynamisch konsistent zu bestimmen.

Sharp-interface-Methoden erfordern besonderen Aufwand für die Behandlung der Phasengrenze. Euler-Methoden wie die *level-set*-Methode oder die *volume-of-fluid*-Methode arbeiten auf fixen Gittern. Hierbei ist die Phasengrenze aufwendig zu rekonstruieren. Dagegen arbeiten Lagrange-Methoden auf sich mit dem Interface mitbewegenden Gittern. Ihre Implementierung ist aufwendig. Ebenfalls aufwendig ist die Implementierung kombinierter Euler-Lagrange-Methoden, sog. *front-tracking*-Verfahren.

Die zweite wichtige Modellklasse sind die sog. *diffusive-interface*-Modelle. Die Phasengrenze ist hierbei eine diffusive Zone, d.h. eine Mischung der Phasen. Die numerische Behandlung dieser Modelle ist teilweise etwas einfacher, da die Lösung auf festen Gittern mit einheitlichen Methoden erfolgen kann.

Der wohl prominenteste Vertreter dieser Klasse ist das *Baer-Nunziato*-Modell, das ursprünglich als Zwei-Phasen-Modell formuliert wurde. Obwohl dieses Modell bereits von vielen Autoren diskutiert wurde, ist es nach wie vor Gegenstand der aktuellen Forschung. Aus analytischer und numerischer Sicht bereitet das Auftreten sog. nicht-konservatier Produkte Schwierigkeiten. Schwache Lösungen können nicht formuliert werden und die Diskretisierung erfordert besondere Sorgfalt. Weitere Herausforderungen sind die Modellierung der Austauschterme und thermodynamisch konsitenter Grenzflächengrößen.

Schließlich seien an dieser Stelle noch Partikelströmungen erwähnt. Die Berechnung kann mit Hilfe *direkter numerischer Simulation* erfolgen, wobei Phasengrenzflächen explizit aufgelöst werden. Diese Berechungen sind aufwendig und werden für Strömungen mit bis zu etwa 100 Partikeln durchgeführt. Alternativ kann die Simulation mit Zweifluidmodellen erfolgen, wobei zusätzlich Partikelgrößenverteilungen zu berechnen sind. Zusätzlicher Modellierungsaufwand ist für die Bestimmung von Austauschtermen erforderlich.

1.3 Ausblick

Die vorliegende Arbeit gliedert sich in drei Hauptteile und befasst sich mit Aspekten der Modellierung, analytischen Fragestellungen und der Numerik von Zweiphasenströmungen:

I Modelle mit Grenzflächen

II Diffusive Modelle

III Partikelströmungen

Die drei Teile dieser Arbeit setzen sich zusammen aus veröffentlichten Artikeln und einer zur Veröffentlichung eingereichten Arbeit. Es wurden keinerlei inhaltliche Änderungen oder Änderungen der Notation vorgenommen.

1.3.1 Modelle mit Grenzflächen

Der erste Teil der vorliegenden Arbeit enthält vor allem analytische Resultate und untersucht Riemann-Probleme für Zweiphasenströmungen, die mit Hilfe der (isothermen) Eulergleichungen beschrieben werden. Dieses System partieller Differentialgleichungen besteht im allgemeinen Fall aus den Bilanzen für Masse (1.3.1), Impuls (1.3.2) und Energie (1.3.3)

$$\partial_t \rho + \partial_x(\rho v) = 0 \tag{1.3.1}$$

$$\partial_t(\rho v) + \partial_x(\rho v^2 + p) = 0 \tag{1.3.2}$$

$$\partial_t(\rho e + \rho\frac{v^2}{2}) + \partial_x(\rho(e + \frac{v^2}{2})v + pv) = 0 \tag{1.3.3}$$

und im Falle konstanter Temperatur aus den Gleichungen (1.3.1) und (1.3.2). Geschlossen wird dieses System durch Zustandsgleichungen

$$p = p(\rho, e) \qquad \text{bzw.} \qquad p = p(\rho) \tag{1.3.4}$$

für die betrachteten Phasen. Das System wird ergänzt durch eine zusätzliche Gleichung, die kinetische Relation, die Phasenübergänge über etwaige Phasengrenzen beschreibt.

Riemann-Probleme sind Anfangswertprobleme mit sog. Riemann-Anfangsdaten; dies sind stückweise konstante Daten mit genau einer Unstetigkeit. Riemann-Probleme treten in natürlicher Weise bei der Diskretisierung partieller Differentialgleichungen auf. Die Kenntnis und Charakterisierung ihrer exakten Lösung ist von besonderer Bedeutung für die Konstruktion effizienter Lösungsverfahren, sog. Riemann-Löser.

Ausgangspunkt von Teil I - **Kapitel 3** - ist eine gemeinsame Veröffentlichung mit Wolfgang Dreyer und Gerald Warnecke, [H8]. Diese Publikation ist gleichzeitig Grundlage des DFG-Projektes HA 6471/2-1, aus welchem unter anderem die in den Kapiteln 4, 5 und 6 vorgestellten Ergebnisse hervorgegangen sind.

In Kapitel 3 werden isotherme Phasenübergänge zwischen flüssigem Wasser und Wasserdampf untersucht. Der Zusammenhang zwischen Dichte und Druck wird dabei in beiden Phasen als linear angenommen. Die gewählten Materialparametern sind den Dampftafeln [13] entnommen. Isotherm bedeutet konstante Temperatur bzw. unendlich schneller Wärmetransport. Entsprechend werden Phasenübergänge von den Differenzen der jeweiligen Gibbs-Energien angetrieben. Dies ergibt sich unmittelbar aus dem zweiten Hauptsatz der Thermodynamik. Die Differenz der Gibbs-Energien geht linear in die kinetische Relation ein. Der gewählte Koeffizient, die sog. Mobilität, stammt aus der klassischen Hertz-Knudsen-Theorie und basiert auf der Annahme, dass jedes Dampfmolekül, das auf die Phasengrenze trifft, kondensiert, siehe [1].

Für die Konstruktion exakter Riemann-Lösungen folgen wir der Vorgehensweise in Toro [11]. Die sich in den einzelnen Phasen ausbreitenden Wellen sind klassisch. Die durchlässige Phasengrenze ist eine zusätzliche Welle, ein sog. nicht-klassischer Stoß. Mathematisch bedeutet das, dass die Bilanzgleichungen über die Phasengrenze hinweg nicht genügen, die Welle eindeutig zu charakterisieren. Entsprechend ist eine zusätzliche Bedingung erforderlich, die kinetische Relation, welche den Massentransfer quantifiziert.

In einem ersten Schritt wird die Phasengrenze charakterisiert bzw. die Lösung eines nichtlinearen Gleichungssystems untersucht. Dazu wird mit Hilfe des Satzes über implizite Funktionen gezeigt, dass zu gegebenem Dampfzustand auf einer Seite der Grenzfläche der Zustand der flüssigen Phase auf der anderen Seite eindeutig bestimmt ist und umgekehrt. Geometrisch entspricht dies der eineindeutigen Abbildung von Zuständen des einen Phasenraumes in den jeweils anderen. In einem weiteren Schritt wird die Lösung des Riemann-Problems in ein Nullstellenproblem überführt, für welches wiederum die Eindeutigkeit der Lösung nachzuweisen ist. Dies entspricht der Bestimmung des (eindeutigen) Schnittpunktes sog. Wellenkurven bzw. ihrer Projektionen.

Neben dem Nachweis der Eindeutigkeit der Lösung des Riemann-Problemes gelingt es, Existenzaussagen anzugeben und Vorhersagen für das Vorliegen von Verdampfungs- bzw. Kondensationsprozessen anhand der Anfangsdaten zu formulieren.

Wird Wasserdampf isotherm komprimiert, so kann Kondensation erzwungen werden (Nukleation). Umgekehrt kann durch isotherme Expansion von flüssigem Wasser Wasserdampf erzeugt werden (Kavitation). Für die geschilderten Sachverhalte werden Nukleations- und Kavitationskriterien formuliert, exakte Lösungen zu Riemann-Anfangsdaten konstruiert und Existenz- und Eindeutigkeitsaussagen bewiesen.

Im anschließenden **Kapitel 4** gelingen weitreichende Verallgemeinerungen der Resultate aus [H8]. Die Resultate entstanden in Zusammenarbeit mit dem Doktoranden Ferdiand Thein, der aus oben genanntem DFG-Projekt finanziert wurde. Die Ergebnisse aus Kapitel 4 sind zur Veröffentlichung eingereicht und befinden sich derzeit in Begutachtung, siehe [H17].

Für die Beweise der Ergebnisse in [H8] waren umfangreiche Abschätzungen erforderlich. Diese benutzen die speziell getroffenen Annahmen, d.h., die Linearität der Zustandsgleichungen, die Parameterbereiche von Wasser und die Annahme über die Mobilität, d.h., die Wahl der kinetischen Relation. Auf diese Annahmen wird im folgenden verzichtet. Stattdessen werden hinreichende und notwendige Bedingungen für die Existenz und Eindeutigkeit des verallgemeinerten Riemann-Problems mit Phasenübergang formuliert und nachgewiesen. Ebenfalls gelingt die Konstruktion exakter Lösungen für den Nukleations- und den Kavitationsfall und der Beweis analoger Eindeutigkeitsresultate.

Es erfolgt eine kritische Diskussion der formulierten Bedingungen. Tatsächlich stellt sich heraus, dass sich diese im wesentlichen auf (wenig restriktive) Schranken für die dimensionslosen isothermen Schallgeschwindigkeiten beschränken. Die übrigen Bedingungen ergeben sich aus den Hauptsätzen der Thermodynamik bzw. sind auch für den einphasigen Fall zu erfüllen, d.h., sind keine zusätzlichen problemspezifischen Einschränkungen.

Abschließend werden die formulierten Bedingungen anhand verschiedener Zustandsgleichungen diskutiert. Die bewiesenen Resultate sind - nach unserem Kenntnisstand - die allgemeinsten Resultate für diesen Problemtyp.

Eine weitere Verallgemeinerung betrifft die Ausdehnung der Fragestellung auf den nicht-isothermen Fall, d.h., die entsprechende Fragestellung für das System (1.3.1-1.3.3). Erste Ergebnisse dazu werden in **Kapitel 5** bzw. in [H14], einer gemeinsamen Veröffentlichung mit Ferdinand Thein, diskutiert.

Dazu ist zunächst eine geeignete thermodynamisch konsistene kinetische Relation zu bestimmen. Ausgangspunkt dafür sind die Bilanzgleichungen über die Phasengrenze sowie die Entropieungleichung in ihrer allgemeinsten Form. Werden selbstähnliche Riemann-Lösungen für das Euler-System gesucht, so lässt sich zeigen, dass Phasenübergänge von den Differenzen der Entropien der Phasen getrieben werden. Dies hat weitreichende Konsequenzen. Da die Entropie der Dampfphase (in einem physikalisch sinnvollen Temperatur- und Druckbereich) stets größer ist als die der flüssigen Phase, besitzt die Entropiedifferenz ein festes Vorzeichen. Folglich existieren keine Gleichgewichtszustände und ausschließlich Verdampfungsprozesse können abgebildet werden. Eine mögliche Folgerung ist, dass das adiabate Modell in dieser Formulierung ungeeignet ist, Phasenübergänge zu beschreiben.

Ein Ausweg ist die Verallgemeinerung der zugrunde liegenden Annahmen, d.h., die Berücksichtigung von Wärmeleitung oder eine allgemeinere Beschreibung der Phasengrenze. Im zweiten Fall wird angenommen, dass das Interface eine zeitlich veränderliche Energie besitzt, die von der Oberflächenspannung der Phasengrenze abhängt. Als Konsequenz kann die Grenzfläche Energie speichern, eine Singularität bildet sich heraus und die Selbstähnlichkeit der Lösung geht verloren.

Das letzte Kapitel des ersten Teils - **Kapitel 6** - enthält ein Nicht-Existenzresultat, welches in [H12] erschienen ist. Wird Wasserdampf komprimiert, so steigt die Dichte der Dampfphase. Man könnte erwarten, dass durch hinreichend starkes Komprimieren ein Phasenübergang erzwungen werden kann. Überraschenderweise stellt sich heraus, dass es unmöglich ist, Kondensation von Wasserdampf durch adiabate Kompression zu erzielen. Dieses Verhalten kann in Experimenten beobachtet werden und ist bereits im Buch von Landau und Lifshitz [6] erwähnt worden. Ein mathematischer Nachweis lag bislang

nicht vor und wird in [H12] geliefert.

Dazu wird in einem ersten Schritt die Dampfphase mit Hilfe der *stiffened-gas*-Zustandsgleichung beschrieben. Zu beliebigen Anfangszuständen werden die Wellenkurven konstruiert. Anschließend wird nachgewiesen, dass diese keinen Schnittpunkt mit der Sättigungskurve besitzen, d.h., dass kein Kondensationsprozess stattfinden kann.

Natürlich ist die spezielle Wahl der Zustandsgleichung sehr einschränkend und es ist nicht möglich, mit einem einzigen beliebigen Parametersatz Wasser im gesamten Temperatur-Druck-Bereich realistisch zu beschreiben. Deshalb wird in einem weiteren Schritt die offizielle Standardformulierung IAPWS-IF97 für Wasser untersucht. Dies ist der seit 1997 geltende Industriestandard zur Beschreibung von flüssigem Wasser und Wasserdampf, siehe [13] or [12]. Diese Formulierung besteht aus einem Satz komplizierter Gleichungen für die verschiedenen Zustands- und Geltungsbreiche. Obwohl es nahezu unmöglich ist, die IAPWS-IF97 analytisch zu diskutieren, lässt sich zeigen, dass sie sich lokal in einer Umgebung der Sättigungslinie einschließlich ihrer Ableitungen beliebig genau durch geeignete Paramterwahl mit Hilfe der stiffened-gas-Gleichung approximieren lässt. Damit gelingt der Nachweis obiger Nicht-Existenzaussage sowohl für die IAPWS-IF97 als auch für beliebige Zustandsgleichungen, die Wasser hinreichend gut beschreiben.

Im Anschluss wird der umgekehrte Fall - Kavitation durch Expansion - betrachtet. Hierbei werden die Fälle *schwache Kavitation* (Erzeugung von sog. Nassdampf) und *starke Kavitation* (Erzeugung einer reinen Dampfphase) unterschieden. Mit einer analogen Strategie wird bewiesen, dass durch adiabate Expansion keine starke Kavitation zu erzwingen ist. Immerhin der Fall schwacher Kavitation ist realisierbar, also die Erzeugung von Nassdampf, einer Mischung aus flüssigem Wasser und Wasserdampf. Dabei ist der Volumenanteil des Dampfes beschränkt, eine entsprechende Schranke wird angegeben.

Die gewonnenen theoretischen Resultate sind ebenfalls gültig für Zweiphasenmodelle, die auf den Eulergleichungen basieren, wie z.B. das Baer-Nunziato-Modell. Sie sind in Übereinstimmung mit numerischen Resultaten in der Literatur, siehe dazu z.B. [H3] oder [3].

1.3.2 Diffusive Modelle

Teil II der vorliegenden Arbeit enthält überwiegend numerische Resultate. Hierbei werden Zwei-Phasenströmungen mit Phasenübergängen mit Hilfe des Baer-Nunziato-Modelles simuliert. Dieses ist für den Zwei-Komponentenfall gegeben durch

$$\frac{\partial \alpha_1}{\partial t} + V_I \frac{\partial \alpha_1}{\partial x} = S_\alpha \tag{1.3.5}$$

$$\frac{\partial (\alpha_1 \rho_1)}{\partial t} + \frac{\partial (\alpha_1 \rho_1 v_1)}{\partial x} = S_\rho \tag{1.3.6}$$

$$\frac{\partial (\alpha_1 \rho_1 v_1)}{\partial t} + \frac{\partial (\alpha_1 \rho_1 v_1^2 + \alpha_1 p_1)}{\partial x} = P_I \frac{\partial \alpha_1}{\partial x} + S_{\rho v} \tag{1.3.7}$$

$$\frac{\partial (\alpha_1 \rho_1 E_1)}{\partial t} + \frac{\partial (\alpha_1 (\rho_1 E_1 + p_1) v_1)}{\partial x} = P_I V_I \frac{\partial \alpha_1}{\partial x} + S_{\rho E} \tag{1.3.8}$$

$$\frac{\partial (\alpha_2 \rho_2)}{\partial t} + \frac{\partial (\alpha_2 \rho_2 v_2)}{\partial x} = -S_\rho \tag{1.3.9}$$

$$\frac{\partial (\alpha_2 \rho_2 v_2)}{\partial t} + \frac{\partial (\alpha_2 \rho_2 v_2^2 + \alpha_2 p_2)}{\partial x} = -P_I \frac{\partial \alpha_1}{\partial x} - S_{\rho v} \tag{1.3.10}$$

$$\frac{\partial (\alpha_2 \rho_2 E_2)}{\partial t} + \frac{\partial (\alpha_2 (\rho_2 E_2 + p_2) v_2)}{\partial x} = -P_I V_I \frac{\partial \alpha_1}{\partial x} - S_{\rho E} \tag{1.3.11}$$

Die Größen P_I und V_I beschreiben den Druck an der Phasengrenze bzw. deren Geschwindigkeit und sind thermodynamisch konsistent zu modellieren. Mit Hilfe der Terme S_α, S_ρ, $S_{\rho v}$ und $S_{\rho E}$ können Massen-, Impuls- und Energietransfer zwischen den Phasen bzw. Komponenten beschrieben werden. Auch diese Terme sind geeignet zu modellieren.

Abschnitt II beginnt mit **Kapitel 7**, dessen Inhalt in [H3] publiziert ist. In dieser Arbeit wird das Baer-Nunziato-Modell in der oben genannten Form erstmals unter Berücksichtigung aller Quellterme S_α, S_ρ, $S_{\rho v}$ und $S_{\rho E}$ für Flüssigkeit-Dampf-Gemische diskutiert. Frühere Arbeiten in der Literatur behan-

deln entweder das Baer-Nunziato-Modell ohne Berücksichtigung von Phasenübergängen oder reduzierte Varianten, siehe z.B. [10].

Der Fokus der Arbeit beruht dabei auf den Austauschtermen. Massen-, Impuls- und Energietransfer werden mit Hilfe von Relaxationen für die Geschwindigkeiten, die Drücke, die Temperaturen und die Gibbs-Energien der Phasen realisiert. Der Modellierung liegt die Annahme zugrunde, dass alle Relaxationszeiten extrem kurz sind, wobei angenommen wird, dass die Geschwindigkeiten und Drücke schneller ins Gleichgewicht relaxieren als die Temperaturen und Gibbs-Energien. In entsprechender Reihenfolge werden die Quellterme behandelt.

Besonderes Augenmerk gilt den Relaxationen für die Temperaturen und die Gibbs-Energien. Es ist bekannt, dass sich zwei Phasen im thermodynamischen Gleichgewicht befinden, wenn ihre Gibbs-Energien übereinstimmen. Ist dies nicht der Fall, finden Phasenübergänge statt. Entsprechend wird der Massentransfer durch Relaxation der Gibbs-Energien modelliert, während der damit einhergehende Wärmetransport durch die Relaxation der Temperaturen realisiert wird. Motiviert durch eine Arbeit von [10] werden in [H3] metastabile Flüssigkeiten und damit einhergehend Verdampfungsprozesse untersucht.

Zur Modellierung der Austauschterme für Temperatur- und Gibbs-Relaxation werden insgesamt drei Relaxationsparameter eingeführt und für diese explizite Ausdrücke in Abhängigkeit von den Variablen des Systems hergeleitet. Die numerische Lösung der sich aus den Relaxationen ergebenden Systeme gewöhnlicher Differentialgleichungen ist aufwendig und erfordert verschachtelte Iterationen. Zudem sind diese Systeme extrem steif und erfordern kleine Zeitschrittweiten. Dies zieht erhebliche Rechenzeiten für die Lösung des Systems (1.3.5-1.3.11) nach sich. Entsprechend werden Temperatur- und Gibbs-Relaxation nur im Bereich der Phasengrenze ausgeführt. Dieser wird anhand der Volumenfraktionen der Phasen identifiziert.

Die Arbeit [H3] enthält umfangreiche numerische Resultate und Vergleiche mit der Literatur. Weiterhin wird ein reduziertes Zwei-Phasen-Modell untersucht und verglichen.

Das anschließende **Kapitel 8** baut auf den in Kapitel 7 präsentierten Ergebnissen auf und enthält weitreichende Verallgemeinerungen bzw. Erweiterungen. Motiviert durch die deutsch-französische DFG-CNRS-Forschergruppe *Micro-Macro Modelling and Simulation of Liquid-Vapour Flows* und in diesem Zusammenhang an der Universität Göttingen durchgeführte Experimente sollen nun Kavitationsblasen simuliert werden.

In den durchgeführten Experimenten, siehe [9], wird mit Hilfe eines Lasers eine Kavitationsblase in einem Behältnis mit Wasser erzeugt. Es lässt sich beobachten, dass die Blase zunächst aufschwingt und dann auf einen minimalen Radius zusammenfällt. Es folgen weitere Blasenschwingungen. Eine reine Wasserdampfblase kann unter den Bedingungen des Experiments ein solches Verhalten nicht aufweisen, siehe z.B. [7], [8] oder [H5]. Folglich enthält die erzeugte Blase mindestens eine weitere inerte Komponente, z.B. Sauerstoff, einem Bestandteil von Luft, der zunächst im Wasser gelöst war.

Für eine erfolgreiche Simulation des genannten Experimentes wurde in [H10] das Zweikomponentenmodell (1.3.5-1.3.11) auf drei Komponenten erweitert und die entsprechenden Relaxationsterme verallgemeinert. Der Massentransfer wird wiederum mit Hilfe der Gibbs-Relaxation realisiert. Die durchgeführten Simulationen zeigen ein dem Experiment qualitativ ähnliches Verhalten der Blase. Insbesondere die erste Blasenschwingung ist in sehr guter Übereinstimmung mit dem Experiment.

Für praxisrelevante Anwendungen ist die Verwendung eines Zweikomponentenmodelles oftmals nicht ausreichend. Dies wurde bereits im Kapitel 8 deutlich: Ein Zweikomponentenmodell, das Phasenübergänge berücksichtigt, kann das Experiment nicht beschreiben - in Übereinstimmung mit den Gesetzen der Thermodynamik. Abseits von Laborbedingungen kann das Vorliegen absolut reiner Komponenten i.a. nicht erwartet werden. Die Gegenwart weiterer Bestandteile bzw. etwaige Verunreinigungen können jedoch wesentlichen Einfluss auf den Ablauf einer chemischen Reaktion oder eines physikalischen Prozesses nehmen und sind bei entsprechenden Simulationen zu berücksichtigen.

Die Erweiterung des o.g. Zweikomponentenmodells auf n Komponenten mit Phasenübergang ist nicht trivial. Diese Verallgemeinerung hat wesentlichen Einfluss auf die mathematischen und physikalischen Eigenschaften des Systems. Besondere Sorgfalt ist erforderlich, um zu garantieren, dass der zweite Hauptsatz der Thermodynamik nicht verletzt wird. Dieser Fragestellung widmet sich **Kapitel 9** der vorliegenden Arbeit, veröffentlicht in [H13].

Neben der Diskussion zahlreicher mathematischer Eigenschaften des n-Komponentenmodells wie Hyperbolizität oder Galilei-Invarianz widmet sich Kapitel 9 den Interfacegrößen V_I und P_I sowie der Modellierung der Quellterme. Ausgehend vom zweiten Hauptsatz der Thermodynamik werden Bedingungen für die Modellierung der Interfacegrößen hergeleitet, die thermodynamische Konsistenz garantieren. Insbesondere werden spezielle Wahlen für diese Größen vorgeschlagen. In einem weiteren Schritt werden die Relaxationsterme für die Geschwindigkeiten, Drücke, Temperaturen und Gibbs-Energien bzw. chemische Potentiale einzeln untersucht und die Gewährleistung der Gesetze der Thermodynamik nachgewiesen.

Das letzte Kapitel des zweiten Teils dieser Arbeit - **Kapitel 10** - stellt effiziente Verfahren zur Behandlung der Relaxationsterme für den n-Komponentenfall vor. Die in [H3] und [H10] verwendeten Lösungsverfahren sind äußerst aufwendig und ziehen lange Rechenzeiten nach sich, verursacht durch eine große Steifheit der Relaxationsterme einerseits und verschachtelte Iterationen andererseits. Daher wurden als Kompromiss vereinfachende Annahmen getroffen:

- Temperatur- und Gibbs-Relaxation wurden nur im Bereich der Phasengrenze angewendet. Zur Identifikation des entsprechenden Bereiches wurden die Volumenanteile der Komponenten betrachtet. Die Wahl der zugehörigen Schranken ist relativ willkürlich.
- Die Berücksichtigung von Phasenübergängen wurde auf metastabile Flüssigkeiten bzw. auf Verdampfung beschränkt.
- Bei der Bestimmung der Gleichgewichtszustände im 3-Komponentenfall wurden vereinfachend Gibbs-Energien relaxiert, d.h. Mischungsentropien vernachlässigt.

In der Literatur vorgestellte Relaxationsverfahren berücksichtigen entweder nur zwei Komponenten, siehe z.B. oder treffen ähnliche vereinfachende Annahmen, siehe [4] oder [5]. Die Existenz von physikalisch sinnvollen Lösungen wird nicht diskutiert.

Im vorliegenden Kapitel 10 gelingen zahlreiche wesentliche Verbesserungen, mit denen u.a. auch eine Implementierung zweidimensionaler Probleme ohne weiteres möglich ist.

Zunächst wird festgestellt, dass die Steifheit des Systems von der Druckrelaxation verursacht wird. Die Bestimmung des Druckgleichgewichts kann zu Instabilitäten führen und die Verwendung extrem kleiner Zeitschritte bzw. extrem kleiner CFL-Zahlen, CFL$\ll$1 erfordern. Weiter kann gezeigt werden, dass der Gleichgewichtszustand unabhängig von der Relaxationsreihenfolge ist. Daher wird eine simultane Druck-Temperatur-Relaxation eingeführt. Eine explizite Formel für das Temperatur-Druck-Gleichgewicht wird bestimmt. Dadurch werden zum einen aufwendige Iterationen zur Bestimmung des Druckgleichgewichtes vermieden. Andererseits führt dies zu einer erheblichen Stabilisierung. Infolgedessen ist die Verwendung von CFL=0.9 ohne weiteres möglich.

Eine weitere Verbesserung besteht darin, dass die Temperatur-Relaxation im gesamten Rechengebiet ausgeführt wird. Dies ist physikalisch sinnvoll, da auch ohne Massentransfer ein Wärmeaustausch zwischen den Komponenten erwartet werden kann.

Anstelle der Gibbs-Energien werden chemische Potentiale relaxiert, d.h. Mischungsentropien werden berücksichtigt. Damit wird auch im Mehrkomponentenfall das physikalisch korrekte Gleichgewicht bestimmt.

Sowohl die Temperaturrelaxation als auch die Relaxation der Gibbs-Energien bzw. chemischen Potentiale wird signifikant verbessert. Die neuen Verfahren vermeiden die Berechnung von Relaxationsparametern. Insbesondere werden verschachtelte Iterationen vermieden.

Weiterhin entfällt die Beschränkung auf metastabile Zustände, so dass auch Kondensationsprozesse behandelt werden können.

Schließlich gelingt der Beweis der Existenz und Eindeutigkeit von Gleichgewichtszuständen. Insbesondere kann gezeigt werden, dass die Gleichgewichtszustände physikalisch sinnvoll sind und die numerischen Verfahren gegen diese konvergieren.

Die Veröffentlichung wird abgerundet durch zahlreiche numerische Beispiele.

1.3.3 Partikelströmungen

Der dritte und letzte Teil der vorliegenden Arbeit widmet sich Partikelströmungen und enthält Resultate aus dem Bereich der Modellierung.

In **Kapitel 11** werden verschiedene Evolutionsgesetze für Dampfblasen hergeleitet, die in [H5] veröffentlicht sind. Motiviert wurde diese Arbeit durch die bereits erwähnte deutsch-französische DFG-CNRS-Forschergruppe und das bereits im vorhegehenden Abschnitt vorgestellte Experiment für Kavitationsblasen.

Die in diesem Experiment erzeugte Blase schwingt mehrfach im Beobachtungszeitraum. Dabei erreicht die Blase beim ersten Aufschwingen den mit Abstand größten Radius. Bereits beim zweiten Aufschwingen erfährt der Blasenradius eine erhebliche Dämpfung und wird auch in den folgenden Schwingungen kontinuierlich kleiner.

Die im Experiment gewonnenen Daten beschränken sich im wesentlichen auf den Radius der Blase, gemessen in kürzesten Zeitabständen. Dagegen gibt das Experiment keine Auskunft über die genaue Zusammensetzung der Blase, Geschwindigkeitsfelder, den Druck in der Blase oder herrschende Temperaturen. Dies macht die Modellierung bzw. Simulation des Experiments äußerst schwierig.

Wird eine einfache Blasenschwingung in einem inkompressiblen Medium unter Vernachlässigung von Gravitation, Phasenübergang und Wärmeleitung beschrieben, so handelt es sich dabei um eine ungedäpfte Schwingung. Tatsächlich kommt es natürlich auch in nahezu inkompressiblen Flüssigkeiten wie Wasser zu Dichteunterschieden und auch die übrigen genannten Effekte üben Einfluss auf die Schwingung aus.

Ziel von [H5] ist es, diese Effekte mit einfachen Mitteln zu untersuchen und insbesondere die im Experiment beobachtete starke Dämfung zu erklären. Zu diesem Zweck werden verschiedene einfache Blasenevolutionsgesetze hergeleitet. Selbstverständlich sind solche reduzierten Modelle nicht in der Lage, eine Kavitationsblase zufriedenstellend zu beschreiben. Dennoch erlauben sie Rückschlüsse auf die einzelnen Mechanismen. Insbesondere geben sie Auskunft darüber, welche Effekte in komplexeren Simulationen unbedingt zu berücksichtigen oder aber vernachlässigbar sind.

Es wurde bereits diskutiert, dass die Blase neben Wasserdampf mindestens eine inerte Komponente enthalten muss. Zudem wurde angenommen, dass die Blase sphärisch ist und Größen wie Dichte und Temperatur innerhalb der Blase homogen sind. Phasenübergänge werden mit Hilfe einer kinetischen Relation beschrieben, die sich unmittelbar in der Massenevolution niederschlägt.

Um den Einfluss der Kompressibilität der umgebenden Flüssigkeit zu untersuchen, werden diese zunächst als inkompressibel angenommen. Unter dieser Annahme gelingt es, ein System gewöhnlicher Differentialgleichungen zur Beschreibung der Blasenevolution herzuleiten. Wird dagegen die umgebende Flüssigkeit als schwach kompressibel angenommen, so erhält man ein System von Delaygleichungen.

Zur Untersuchung des Einflusses von Phasenübergängen werden Modelle mit und ohne Massentransfer betrachtet. Insbesondere kann der Massenanteil der inerten Phase variiert werden.

Für die Untersuchung des Dämpfungseffektes durch Wärmeleitung werden die Evolutionsgleichungen mit der Wärmeleitungsgleichung in der umgebenden Flüssigkeit gekoppelt.

Die resultierenden Systeme werden mit Hilfe von Standardverfahren numerisch gelöst. Es stellt sich heraus, dass Phasenübergänge den Dämpfungseffekt nicht erklären können. Andererseits haben sie wesentlichen Einfluss auf die herrschenden Temperaturen. Ebenfalls führt Wärmeleitung zu keinen nennenswerten Dämpfungseffekten. Vielmehr stellt sich heraus, dass die Kompressibilität der umgebenden Flüssigkeit weitestgehend für die Dämpfung verantwortlich ist. Es kann geschlussfolgert werden, dass inkompressible Modelle zur Beschreibung solcher und ähnlicher Prozesse ungeeignet sind.

Überraschenderweise kann mit dem reduzierten kompressiblen Modell eine relativ gute Übereinstimmung des Radiusses mit den Daten des Experiments erzielt werden, auch wenn dieses Modell natürlich keine detailierten Rückschlüsse auf weitere physikalische Größen zulässt. Dennoch können mit den hergeleiteten Modellen qualitative Aussagen für moderate Blasenschwingungen getroffen werden. Insbesondere sind die reduzierten Modelle geeignet zur Verwendung als Quellterme in Gemischmodellen zur Beschreibung disperser Strömungen.

Ein solches Gemischmodell wird in [H11] bzw. in **Kapitel 12** der vorliegenden Arbeit hergeleitet. Sollen Strömungen mit vielen Partikeln, z.B. Tropfen- oder Blasenströmungen, simuliert werden, ist das explizite Verfolgen sämtlicher Phasengrenzen sehr aufwendig. Mitunter ist die detailierte Betrachtung jedes einzelnen Partikels nicht notwendig, stattdessen genügt eine qualitative Beschreibung. In diesem Fall bieten sich zur Simulation Gemischmodelle, ähnlich dem Baer-Nunziato-Modell, an, die zusätzlich

Partikelgrößenverteilungen bestimmen.

Die Herleitung des Modells benutzt Volumenmittelungstechniken gemäß [2]. Zugrunde liegt die Annahme einer Mischung aus kleinen sphärischen, wohl separierten Partikeln und eines umgebenden Fluids. Obwohl in der Veröffentlichung [H11] ausdrücklich von Wasserdampfblasen in flüssigem Wasser die Rede ist, ist die Herleitung sowohl für beliebige andere Fluide als auch den umgekehrten Fall von Tropfen in ihrem Dampf gültig.

Während für die Bestimmung gemittelter Größen für die Trägerphase eine kontinuierliche Volumenmittelung benutzt wird, wird für die Bestimmung entsprechender disperser Größen ein vereinfachter Ansatz verwendet. Dieser wird durch Homogenitätsannahmen gerechtfertigt.

Zunächst wird ein Transportsatz für die disperse Phase bewiesen. Damit lassen sich Bilanzgleichungen für die Partikel herleiten, insbesondere lässt sich eine Bilanz für die Anzahldichte und damit eine Bilanz für die mittlere Partikelgröße bestimmen. Diese Bilanzen weisen eine Besonderheit auf: Da die Partikel als wohl separiert angenommen werden, besteht keine Wechselwirkung untereinander. Entsprechend enthalten die Bilanzgleichungen keinen Druckterm. In einem weiteren Schritt werden mit Hilfe des Reynoldschen Transportsatzes Bilanzen für die Trägerphase ermittelt.

Es stellt sich heraus, dass sowohl die Bilanzen für die disperse als auch für die Trägerphase unmittelbar von der Evolution der Partikel abhängen. Konkret ergeben sich Quellterme in Abhängigkeit von der Evolution der Masse, des Radiusses und der Temperatur der Partikel.

Um das Modell zu schließen, werden also entsprechende Evolutionsgesetze benötigt. Für den Fall von Dampfblasen stehen mit [H5] geeignete Modelle zur Verfügung. Natürlich sind auch andere Wahlen für die Quellterme denkbar.

Eine Besonderheit des Modelles ist das Fehlen von nichtkonservativen Termen wie etwa im Baer-Nunziato-Modell. Somit lassen sich für dieses Modell schwache Lösungen formulieren. Für den homogenen Anteil des isothermen Untermodelles lassen sich Riemann-Lösungen explizit konstruieren und Eindeutigkeitsaussagen beweisen. Insbesondere können sich δ-Stoß-Lösungen herausbilden. Eine Publikation dazu befindet sich in Vorbereitung.

Chapter 2

Compendium

Two- and multi-phase flows occur in many applications, for instance in aerospace, traffic engeneering, geo- or astrophysics, electrochemistry or meteorology. They play an important role in boiling, cooling or combustion processes. Within such flows usually phase transitions and chemical reactions take place. The modelling as well as the simulation of the considered processes is a challenge and in the focus of the ongoing research.

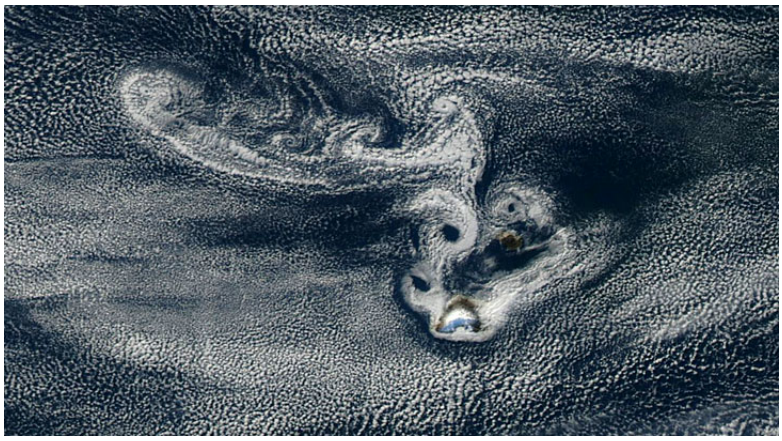

Figure 2.1: The picture[2] shows the structure of clouds. It is taken by the NASA.

2.1 Classification of Two-Phase Flows

In materials science, thermodynamics or physical chemistry a phase denotes a spatial domain where the chemical composition and essential physical properties like density are homogeneous. This means that constitutive parameters are nearly constant within appropriate bounds. The most important phases are the aggregate states gaseous, liquid and solid, which differ amongst other things in the densities. Also within a certain aggregate state a specific substance may exhibit different phases, see for instance diamonds and graphite. It is possible that a phase consists of several components, for instance air mainly consists of nitrogen and oxygen. Occasional it is difficult to distinguish phases and components. This depends on the required accuracy of the observation and accordingly on the considered length scale. In the literature sometimes the notation is imprecise. Often these terms are mixed.

In the case of at least two phases an interface is formed. Across the interface material properties may change significantly. This means that in mathematical sense a phase boundary is a discontinuity. Across the interface usually mass transfer processes take place, i.e. condensation, evaporation or chemical reactions.

[2] www.top-wetter.de/themen/wolken/htm

Two-phase flows may be classified by the characterization of phase interfaces. Dispersed, separated and transitional flows were considered.

Examples for separated flows are jet or film flows. In dispersed flows the volume fraction of the surrounding carrier phase is much larger than the volume fraction of the particles. In contrast to that the volume fraction of the phases is of the same order in transitional flows.

2.2 Modeling and simulation - a great challenge

The accurate mathematical description as well as the numerical treatment of phases, in particular the treatment of phase interfaces is in the focus of recent research concerning multi-phase flows. The precise physical modelling of interface processes, especially the transfer of mass and energy, are a challenge. In the literature several types of multi-phase models may be found. They can be classified by the methods to treat phase interfaces.

A first class are the so-called *sharp-interface-modells*. Here the interface is treated as a free boundary. Interface processes can be characterized by *jump conditions* and *kinetic relations*. Jump conditions are conservation properties that are satisfied across phase boundaries and arise from conservation laws for mass, momentum and energy, depending on the physical effects accounted for. Kinetic relations quantify the mass transfer and have to be determined in a thermodynamically consistent manner.

Sharp-interface-methods require special effort concerning the treatment of interfaces. Euler-methods like the *level-set-method* or the *volume-of-fluid-method* work on fixed grids. The necessary interface reconstruction is complex and costly. In contrast to that, Lagrangian methods work on moving meshes coupled to the phase boundaries. They require an extensive implementation. The same is true for combined Euler-Lagrangian methods, so-called *front-tracking-methods*.

A further important class is given by the *diffusive-interface-models*. Here the interface is a diffusive zone, given by a mixture of the phases. In some parts the numerical treatment is less complex, since numerical methods may work on fixed grids.

Probably the most famous model in this class is the *Baer-Nunziato-model*. Originally this model was introduced as a two-phase model. Even though this model was discussed by numerous authors it is still in the focus of recent research. From an analytical and a numerical point of view the presence of non-conservative products causes difficulties. Weak solutions canot be formulated. The discretization of these terms requires extraordinary diligence. Further challenges are the modelling of source terms and thermodynamically consistent interphase quantities.

Finally we refer to particle flows. Computations may be performed by *direct numerical simulations*. Here phase interfaces are treated explicitly. Such computations are time consuming and are performed for flows up to about 100 dispersed particles. Alternatively two-fluid modells can be used where in addition particle size distributions have to be determined. Additional effort is required for the determination of exchange terms.

2.3 Outline

The thesis consists of three main parts and considers aspects of modelling, analysis and numerics of two-phase flows:

I Sharp interface modells

II Diffusive interface modells

III Particle flows

These three parts consist of published articles and in addition one submitted article. No changes in their content and no changes of the notations were made.

2.3.1 Sharp interface models

The first part of this theses mainly presents analytical results. Riemann problems for two phase flows were considered. We use the system of (isothermal) Euler equations to describe the flows. In the general

case this system consists of the balance equations for mass (2.3.1), momentum (2.3.2) and energy (2.3.3)

$$\partial_t \rho + \partial_x(\rho v) = 0 \tag{2.3.1}$$
$$\partial_t(\rho v) + \partial_x(\rho v^2 + p) = 0 \tag{2.3.2}$$
$$\partial_t(\rho e + \rho\frac{v^2}{2}) + \partial_x(\rho(e + \frac{v^2}{2})v + pv) = 0\,. \tag{2.3.3}$$

In the isothermal case the system reduces to equations (2.3.1) and (2.3.2). The system is closed by equations of state

$$p = p(\rho, e) \qquad \text{resp.} \qquad p = p(\rho) \tag{2.3.4}$$

for the phases under consideration. In addition a kinetic relation is considered. This equation quantifies the mass transfer across phase interfaces.

Riemann problems are initial value problems using Riemann initial data. These data are the simplest, non-trivial initial conditions. The data are piecewise constant with a single discontinuity. Riemann problems inherently occur in certain discretization of these partial differential equations. The knowledge of the exact solutions and their structure is a key ingredient for the construction of efficient numerical Riemann solvers.

Chapter 3, the beginning of the first part of this thesis is formed by a publication together with Gerald Warnecke und Wolfgang Dreyer, [H8]. This article is the basis of the DFG-project HA 6471/2-1. Within this project the results presented in the chapters 4, 5 and 6 are developed.

In Chapter 3 we consider isothermal phase transitions between liquid water and water vapor. Here a linear dependency of densities and pressures is assumed in both phases. The chosen material parameters are taken from steam tables [13]. In an isothermal process the temperature is assumed to be constant. This correlates with infinitely fast heat conduction. Due to this assumption phase transitions are driven by the differences of the Gibbs free energies of the phases, which is a consequence of the second law of thermodynamics. The kinetic relation is modeled by a linear relation of this difference. The mobility coefficient is obtained from the classical Hertz-Knudsen theory. It is based on the assumption that vapor particles hitting the interface will condensate, cf. [1].

For the construction of exact Riemann solutions we follow the strategy presented in the book of Toro [11]. Waves propagating through the bulk phases are classic. The phase boundary is an additional wave that possesses the properties of a non-classical shock. From a mathematical point of view this means that the balances across the phase boundary are not sufficient for a unique characterization of this wave. Accordingly an additional equation is required, the kinetic relation, quantifying the mass transfer.

In a first step we investigate the phase boundary. This corresponds to the solution of a non-linear system of equations. Using the implicit function theorem we prove that a given vapor state located at the interface uniquely defines the corresponding liquid state and vice versa. In other words a bijective map between the phase spaces is defined. In a further step the solution of the Riemann problem is converted to the problem of finding roots of non-linear systems. Geometrically we are looking for intersection points of wave curves resp. their projections.

Beside proofs uniqueness of the Riemann problem, we succeed in formulating existence results and we are able to forecast evaporation or condensation processes on the basis of the initial data.

Assume, water vapor is isothermally compressed. In that case it is possible to enforce condensation (nucleation). Contrarily, by isothermal expansion of liquid water water vapor may be created (cavitation). For these two circumstances nucleation and cavitation criteria are formulated, exact solutions for Riemann initial data are constructed and existence as well as uniqueness results are proven.

In **Chapter 4** we obtain significant generalizations of the results discussed in Chapter 3 resp. in [H8]. These new results were derived together with Ferdinand Thein within the DFG-project mentioned above. The outcome of Chapter 4 is submitted for publication.

For the proofs of the results in [H8] many extensive estimations were required. These estimations use special assumptions like the linearity of the equation of state, the range of parameters for water or assumptions on the mobility, this means the choice of the kinetic relation. In the following we give up all

these assumptions. Instead we give sufficient and necessary conditions for existence and uniqueness of Riemann solutions for the generalized phase transition problem. Moreover, exact solutions for nucleation and cavitation problems are constructed. Uniqueness results are proven.

Subsequently we critically discuss the formulated conditions. It turns out that basically only restrictions for the dimensionless isothermal sound speed are needed. Further conditions result from the laws of thermodynamic. These conditions must also be fulfilled for single phase flows, this means that these conditions are no additional problem-specific requirements.

Finally, these conditions are discussed on the basis of examples. The results proven in Chapter 4 are - to our knowledge - the most general results in this context.

Further generalizations concern the extension of the problem to non-isothermal flows, this means the extension to the system (2.3.1-2.3.3). First results are discussed in **Chapter 5** resp. [H14].

In a first step an appropriate thermodynamic consistent kinetic relation has to be determined, using the balance equations across the phase boundary as well as the entropy inequality in their general form. Looking for selfsimilar Riemann solutions to the Euler system one can prove that mass transfer is driven by the difference of the specific entropies of the phases. This has extensive consequences. Because the entropy of the vapor phase (in a meaningful pressure-temperature regime) is always larger than the liquid entropy the entropy difference has a fixed sign. Accordingly no equilibrium states exists and exclusively evaporation processes can be described.

To overcome this problem further generalizations have to be made, i.e. taking into account heat conduction or a more general description of the interface. In the second case one assumes that the interface exhibits a time-depending energy depending on surfacial tension. Hence the phase boundary is able to accumulate energy, a singularity is forming and the selfsimilarity of solutions is lost.

The last chapter of the first part - **Chapter 6** - presents a non-existence result, which is published in [H12]. If water vapor is compressed its density will increase. One may assume that for sufficiently strong compression a phase transition will be enforced. Surprisingly it turns out that it is impossible to achieve condensation of water vapor by an adiabatic compression. This behavior can be observed in experiments and was already mentioned in the book of Landau and Lifshitz [6]. Nevertheless, a mathematical proof was missing until now and is given in [H12].

To prove this statement, in a first step we characterize the vapor phase by the *stiffend-gas equation of state*. We construct wave curves for arbitrary initial data. After that we show that there are no intersection points of the saturation line and any wave curve. This implies that condensation processes due to compressions are impossible.

Of course, the specific choice of the equation of state is a strong restriction. Moreover, it is not possible to give a realistic characterization of water vapor in the whole pressure-temperature regime using a single set of parameters. Therefore in the next step we use the IAPWS-IF97 for water. IAPWS-IF97 is the industrial formulation for the properties of liquid water and steam, see [13] or [12]. This formulation consists of a set of complicated equations for the certain ranges of validity. Although it is nearly impossible to discuss the IAPWS-IF97 analytically, it can be shown that locally in a neighborhood of the saturation line this curve can be approximated to arbitrary precision using the stiffened gas law and a proper set of parameters. The same is true for the corresponding derivatives. This fact is crucial to the proof of the non-existence statement for the IAPWS-IF97 as well as arbitrary equations of state.

Further, we discuss the opposite case - cavitation by expansion. We distinguish the cases (i) *weak cavitation* (the creation of wet steam) and (ii) *strong cavitation* (the creation of pure vapor). Using an analogous strategy we prove the non-existence of adiabatic strong cavitation. Anyway, weak cavitation can be realized, this means the creation of wet steam. This is a mixture of water vapor and liquid water. It is clear that in this case the volume fraction for water vapor is bounded. A bound is given in [H12].

The results obtained are also valid for two-phase models that are based on the Euler equations, for instance the Baer-Nuntiato model. They are in agreement with numerical results that can be found in the literature, see [H3] or [3].

2.3.2 Diffusive interface models

Part II of the present thesis mainly includes numerical results. We consider two-phase flows with phase transition using the Baer-Nunziato model. For two components this model is given by

$$\frac{\partial \alpha_1}{\partial t} + V_I \frac{\partial \alpha_1}{\partial x} = S_\alpha \tag{2.3.5}$$

$$\frac{\partial (\alpha_1 \rho_1)}{\partial t} + \frac{\partial (\alpha_1 \rho_1 v_1)}{\partial x} = S_\rho \tag{2.3.6}$$

$$\frac{\partial (\alpha_1 \rho_1 v_1)}{\partial t} + \frac{\partial (\alpha_1 \rho_1 v_1^2 + \alpha_1 p_1)}{\partial x} = P_I \frac{\partial \alpha_1}{\partial x} + S_{\rho v} \tag{2.3.7}$$

$$\frac{\partial (\alpha_1 \rho_1 E_1)}{\partial t} + \frac{\partial (\alpha_1 (\rho_1 E_1 + p_1) v_1)}{\partial x} = P_I V_I \frac{\partial \alpha_1}{\partial x} + S_{\rho E} \tag{2.3.8}$$

$$\frac{\partial (\alpha_2 \rho_2)}{\partial t} + \frac{\partial (\alpha_2 \rho_2 v_2)}{\partial x} = -S_\rho \tag{2.3.9}$$

$$\frac{\partial (\alpha_2 \rho_2 v_2)}{\partial t} + \frac{\partial (\alpha_2 \rho_2 v_2^2 + \alpha_2 p_2)}{\partial x} = -P_I \frac{\partial \alpha_1}{\partial x} - S_{\rho v} \tag{2.3.10}$$

$$\frac{\partial (\alpha_2 \rho_2 E_2)}{\partial t} + \frac{\partial (\alpha_2 (\rho_2 E_2 + p_2) v_2)}{\partial x} = -P_I V_I \frac{\partial \alpha_1}{\partial x} - S_{\rho E} \tag{2.3.11}$$

Here P_I and V_I denote the interfacial pressure resp. the interface velocity. These quantities have to be modeled thermodynamically consistent. The terms S_α, S_ρ, S_{rhov} and $S_{\rho E}$ describe the transfer of mass, momentum and energy between phases resp. components. Also these terms have to be modeled.

The content of **Chapter 7**, the first chapter in Part II, is published in [H3]. In this article the Baer-Nunziato model is discussed the very first time in the above presented form taking account the source terms S_α, S_ρ, S_{rhov} and $S_{\rho E}$ for liquid-vapor mixtures. Previous papers discuss either the Baer-Nunziato model without phase transitions or reduced models, i.e. [10].

Our main focus is on the transfer terms. We realise the transfer of mass, momentum and energy by relaxation terms for the velocities, the pressures, the temperatures and the Gibbs free energies of the phases. The modelling bases on the assumption that all relaxation times are extremely short. Further, we assume that velocities and pressures relax much faster than temperatures and Gibbs energies. This assumption determines the order of the relaxations.

Special attention is given to the relaxation terms for the temperature and the Gibbs free energies. It is known that two phases are in thermodynamic equilibrium if their Gibbs free energies coincide. If this is not the case, phase transitions will take place. Accordingly mass transfer is modelled by Gibbs free energy relaxation. Heat exchange is achieved by temperature relaxation. Motivated by [10] in [H3] we investigate metastable liquids and evaporation processes.

For the modelling of the temperature and Gibbs free energy relaxation three relaxation parameters have to be introduced. For these parameters explicit expressions are derived depending on the variables of the considered system. The computation of numerical solutions for the system of ordinary differential equations resulting from the relaxations is very expensive and requires nested iterations. Moreover, the relaxation terms introduce strong stiffness to the system. Accordingly very small time steps have to be used and numerical computations for the system considered are very time consuming. Therefore the relaxation procedures for temperature and Gibbs free energy are only used in an interfacial region. This region is identified by the volume fractions of the phases.

In [3] one can find numerous numerical results and comparisons to the existing literature. Moreover, a reduced modell is discussed.

In the subsequent **Chapter 8** that continues the previous work significant generalizations and extensions are made. Motivated by the German-French DFG-CNRS research group *Micro macro Modelling and Simulation of Liquid-Vapour Flows* and experiments provided at the Göttingen university we now investigate cavitation bubbles.

In the experiments, cf. [9], a cavitation bubble is created in a water filled cuvette, using a laser pulse. One can observe that the bubble is created and grows up to a certain radius. After that it shrinks to

a minimal radius. Several damped oscillations follow. A pure vapor bubble is not able to show such a behavior, cf. [7], [8] or [H5]. The conclusion is that the bubble contains at least one inert component, maybe components of air that were dissolved in the water.

Fur successful simulations of the experiment in [H10] we extend the two-component model (2.3.5 - 2.3.11) to three components. Furthermore, we generalize the relaxation terms. As before the mass transfer is modelled using the Gibbs free energy relaxation. The performed simulations show a qualitatively similar behavior of the bubble. In particular, the first rebound of the bubble is in very good agreement with the experiment.

For many applications two-components models are not sufficient to give a fairly good description of the processes. This was already discussed in Chapter 8: A two-component model that takes phase transitions into account cannot reproduce the experiment - this is in agreement with thermodynamics. Apart from laboratory conditions the presence of absolutely pure components cannot be expected. However, the presence of further constituents or contaminations may strongly impact physical or chemical processes. Therefore they have to be taken into account in the simulations.

The extension of the two-component model to n components is not trivial. The generalizations modify the mathematical and physical properties of the system. Reasonable care is required to guarantee that the second law of thermodynamics is not violated. This problem is in the focus of **Chapter 9**, published in [H10].

Beside the discussion of mathematical properties of the n-component model, like hyperbolicity or Galilean invariance, Chapter 9 discusses the consistent modelling of the interface velocity V_I and the interface pressure P_I as well as the modelling of the source terms. Using the second law of thermodynamics conditions for a correct modelling of the interfacial quantities are derived that guarantee thermodynamic consistency. In particular, a special choice for these quantities is proposed. In further steps the relaxation procedures for the velocities, the pressures, the temperatures and the Gibbs free energies resp. the chemical potential are proven.

Chapter 10 of this thesis introduces efficient and robust procedures to handle the relaxation terms of the n-component model. The methods used in [H3] and [H10] are very expensive and lead to very long computational times due to the stiffness of the relaxation terms and nested iterations. Therefore in [H3] and [H10] some simplifications were made:

- Temperature and Gibbs free energy relaxation were only used in the interfacial region. To identify this region the volume fractions of the components were considered. The choice of proper bounds is an arbitrary assumption.
- The consideration of phase transition was restricted to metastable liquids, i.e. evaporation processes.
- To evaluate equilibrium states in the three-component case, Gibbs free energies were relaxed, i.e. the mixture entropy was neglected.

Relaxation procedures proposed in the literature either take into account only two components or use similar simplifying assumptions, see [4] or [5]. Moreover, the existence of physically meaningful solutions is not discussed.

In Chapter 10 of this thesis many improvements are achieved that enable also two-dimensional computations within short computational times.

First we point out that the stiffness of the system is introduced by the pressure relaxation. The evaluation of pressure equilibria may cause instabilities and requires very small time steps resp. very small CFL numbers, CFL$\ll$1. One can show that that the final equilibrium state does not depend on the order of relaxation. Therefore we propose a simultaneous pressure-temperature relaxation. Thereby, we avoid expensive iterations. Moreover, this simultaneous procedure stabilizes the simulations and one may use CFL=0.9.

In addition, we use the temperature relaxation in the whole computational domain. This is physically reasonable. Apart from phase transitions, energy transfer between components can be expected.

We do not relax the Gibbs free energies but the chemical potentials, i.e. we take into account the mixture entropy. Accordingly also in the multi-component case the physically correct equilibrium state will be determined.

We significantly improve the temperature relaxation procedure as well as the relaxation of Gibbs free energies resp. chemical potentials. On the one hand we avoid the calculation of relaxation parameters. On the other hand we are able to avoid nested iterations.

Moreover, we do not restrict ourselves to metastable liquids and are able to handle condensation processes. We prove existence as well as uniqueness of physically meaningful equilibrium states and prove convergence of the methods. Finally we present numerous numerical examples.

2.3.3 Particle flows

The last part of this thesis considers particle flows and gives results in the field of modelling.

In **Chapter 11** we derive several evolution laws for vapor bubbles, published in [H5]. This work was motivated by the German-French DFG-CNRS research group mentioned above and the experiment on cavitation bubbles, introduced in the last subsection.

The bubble created in the experiment shows repeated oscillations in the observation period. The maximum radius is reached initially. After that the radius is significantly damped and shrinks during the following oscillations.

More or less, the only experimental data that can be determined during the observation are the bubble radii measured in very short time intervals. The experiment does not provide any information about the composition of the bubble, the velocity fields, the pressure inside the bubble or the temperature. Accordingly, the modelling resp. the simulation of the experiment is extremely difficult.

The oscillation of a bubble surrounded by an incompressible fluid, neglecting gravitation, phase transitions and heat conduction, gives an undamped oscillation. Actually, also in nearly incompressible fluids like water density differences can be observed that affect the process.

The aim of [H5] is to investigate the effects mentioned and in particular to explain the damping mechanism observed in the experiment. Therefore, we derive several evolution laws. Of course, these reduced models are not able to simulate a cavitation bubble. Nevertheless, they allow conclusions concerning the particular effects. Especially, we can conclude which terms can be neglected and which necessarily have to be taken into account.

It was already discussed in the previous subsection that at least one inert component must be present inside the bubble. We assume the bubble to be spherical and homogeneous. Phase transitions are described by a kinetic relation resulting in a mass evolution equation.

To investigate the influence of the compressibility of the surrounding fluid in a first step, we assume the liquid to be incompressible. Under the listed assumptions one can derive a system of ordinary differential equations describing the bubble evolution. If the liquid is modeled weakly compressible, we obtain a system of delay equations.

For investigations concerning the influence of phase transitions we derive models with and without mass transfer. In particular, one can vary the mass fraction of the inert components. Effects due to heat conduction are investigated by coupling the heat equation for the liquid to the system.

The resulting systems are solved numerically using standard techniques. It turns out that phase transitions cannot cause the observed damping. On the other hand they significantly influence the temperature. Also heat conduction is not responsible for the damping. Instead we determine that the compressibility generates the damping. We conclude that incompressible models are inappropriate to describe such and similar processes.

Surprisingly the reduced compressible model gives results for the radius evolution that are in good agreement with the experiment, although the model does not allow further conclusions for other quantities. Nevertheless, the reduced models give qualitative statements for moderate bubble oscillations. In particular, the reduced models are suitable as source terms in mixture models for dispersed flows.

Such a mixture model is derived in **Chapter 12** of this thesis. If flows with many dispersed particles, i.e. droplets or bubbles, have to simulated, than the explicit treatment of the interfaces is very expensive.

Often a detailed description of each particle is not required. Instead a qualitative description is sufficient. In that case one can use mixture models, similar to the Baer-Nunziato model, that in addition determine particle size distributions.

The derivation of the model uses volume averaging techniques according to [2]. It is based on the assumption of a mixture of many dispersed spherical well separated particles and a surrounding fluid. Although in [H11] water vapor bubbles are discussed explicitly, the derivation is also valid for other fluids or the opposite case of droplets in gas.

We use a continuous type of averaging to derive averaged quantities for the carrier phase but a simplified method for the dispersed phase. This simplification of the averaging is reasonable due to the homogeneity assumption inside the particles.

We prove a transport theorem for the dispersed phase. This theorem is used to obtain balance equations for the particles, especially a balance for the number density resp. the particle size. These balances feature a special property: Because the particles are well separated, there is no particle interaction. As a consequence there are no pressure terms in the dispersed balances. In a further step, balances for the carrier fluid are derived using the Reynolds transport theorem.

It turns out that all balance equations depend on the evolution for the dispersed phase. In detail the source terms depend on the evolution of mass, radius and temperature of the particles.

To close the model, appropriate evolution laws are required. If vapor bubbles are considered, the models derived in [H5] are suitable. Of course, other choices are possible.

A special feature of the model is the absence of non-conservative terms. Accordingly weak solutions can be formulated. For the homogeneous part of the isothermal submodel exact Riemann solutions can be constructed and uniqueness results can be proven. In particular δ-shock solutions can develop. A further publication on this topic is in preparation.

Bibliography

[1] M. Bond and H. Struchtrup. Mean evaporation and condensation coefficients based on energy dependent condensation probability, *Phys. Rev. E.*, **70** (2004) 061605.

[2] D.A. Drew and S.L. Passman. T*heory of multicomponent fluids*, Springer-Verlag, New York (1999)

[3] M. Dumbser, U. Iben, and C.-D. Munz. Efficient implementation of high order unstructured WENO schemes for cavitating flows, *Computers & Fluids*, **86** (2013), pp. 141 - 168.

[4] M.H. Lallemand, A. Chinnayya, and O.L. Metayer. Pressure relaxation procedures for multiphase compressible flows. *Int. J. Numer. Meth. Fluids*, 49(1):1-56, 2005.

[5] M.H. Lallemand and R. Saurel. Pressure relaxation procedures for multiphase compressible flows, *Technical Report* 4038, INRIA, 2000.

[6] L.D. Landau and E.M. Lifshiz. *Lehrbuch der theoretischen Physik*, Bd.V Statistische Physik, Akad.-Verl., 1987.

[7] I. Müller and W. Müller. *Fundamentals of Thermodynamics and Applications*, Springer-Verlag, Berlin 2009.

[8] I. Müller. *Thermodynamics*, Pitman, London 1985.

[9] S. Müller, M. Bachmann, D. Kröninger, T. Kurz, and P. Helluy. Comparison and Validation of Compressible Flow Simulations of Laser-Induced Cavitation Bubbles, *Computers and Fluids*, DOI: 10.1016/j.compfluid.2009.04.004, (2009).

[10] R. Saurel, F. Petitpas, and R. Abgrall. Modelling phase transition in metastable liquids: application to cavitating and flashing flows., *J. Fluid. Mech.*, 607:313-350, 2008.

[11] E. F. Toro, *Riemann Solvers and Numerical Methods for Fluid Dynamics*, Springer-Verlag, Berlin - Heidelberg, 1999.

[12] W. Wagner and H.-J. Kretzschmar. *International Steam Tables*, Springer-Verlag, Berlin - Heidelberg, 2008.

[13] W. Wagner and A. Kruse. *Properties of Water and Steam - The Industrial Standard IAPWS-IF97 / Zustandsgrößen von Wasser und Wasserdampf - Der Industriestandard IAPWS-IF97*, Springer-Verlag, Berlin, 1998.

For further literature we refer to the references in the chapters.

Part I

Sharp interface models

Chapter 3

Euler equations with phase transition

Bibliographic note: The content of this chapter is published in [H8]: M. Hantke, W. Dreyer, and G. Warnecke. Exact solutions to the Riemann problem for compressible isothermal Euler equations for two phase flows with and without phase transition, *Quarterly of Applied Mathematics*, vol. LXXI 3 (2013), pp. 509-540.

Abstract: We consider the isothermal Euler equations with phase transition between a liquid and a vapor phase. The mass transfer is modeled by a kinetic relation. We prove existence and uniqueness results. Further, we construct the exact solution for Riemann problems. We derive analogous results for the cases of initially one phase with resulting condensation by compression or evaporation by expansion. Further we present numerical results for these cases. We compare the results to similar problems without phase transition.

3.1 Introduction

We study compressible multi phase flows without and with phase transitions relying on the isothermal Euler equations with a non-monotone pressure-density function. Our main objective is a detailed discussion of a thermodynamically based kinetic relation that controls the mass transfer across a sharp interface between two coexisting phases. The derivation of the kinetic relation is based on thermodynamics, especially on classical Hertz-Knudsen theory, see Bond and Struchtrup [4]. To this end we study Riemann problems and show for various classes of initial data the existence and uniqueness of solutions. We consider single phase initial data describing condensation by compression or evaporation by expansion, as well as initial data describing two differing adjacent phases. The case of multi phase flows without phase transition mainly serves as illustration and as comparison with other treatments of the same subject in the literature.

Phase transitions can be treated either by sharp interface models or by models that describe the interface between two adjacent phases by a smooth transition within the setting of phase field models. Sharp interface models are physically better founded while phase field models may have numerical advantages. The available sharp interface models are surveyed in Zein [23].

The phase field model of Euler-Korteweg type by Dreyer et al. [9] establishes a sharp interface limit that produces our kinetic relation, whereupon the mass flux across the interface is proportional to the jump of the Gibbs free energy. A similar study of the same model by Benzoni-Gavage et al. [3] ends up with a kinetic relation describing local equilibrium at the interface, i.e. the Gibbs free energy is continuous.

The seminal paper by Abeyaratne and Knowles [1] considers a solid-solid phase transition and describes the Riemann problem of the corresponding Euler system in Lagrangian coordinates. For this reason the nonlinearities appearing there are different from the current study. The kinetic relation in [1] relies on the same driving force as we use here. However, Abeyaratne and Knowles relate the mass flux to the jump of the Gibbs free energy in a nonlinear manner.

A very interesting review on the Riemann problem for a large class of thermodynamic consistent constitutive models in the setting of Euler equation models by Menikoff and Plohr [14] is restricted to a simple kinetic relation that results from the assumption of local equilibrium at the interface. For isothermal processes local interfacial equilibrium is guaranteed by the continuity of the Gibbs free energy.

Merkle [15] also considered the Riemann problem for the isothermal Euler system. Differences to the current work are: He used the van der Waals equation to model the non-monotone pressure-density dependence. We observed that it is better to model the pressure-density function by pieces of by three linear functions. This leads to a closer agreement with measured data, e.g. for a substance like water. The kinetic relation introduced by Merkle does arise from thermodynamic motivations. But there are initial data for which it must be supplemented by further assumptions in order to pick up a unique solution. Furthermore the structure of the solutions is essentially different from those that we obtain here. Our solutions consist exclusively of three types of elementary waves, namely classical shocks, rarefaction waves and phase transitions, that separate a certain number of constant states. Merkle needs composite waves to construct the solution.

The isothermal Euler system was also studied by Müller and Voss [18], [21]. They modeled the fluid by a van der Waals equation, however, instead of a kinetic relation they exclusively applied the Liu entropy condition in order to establish uniqueness. Consequently Müller and Voss also need composite waves.

There are also studies of the same subject that use the Euler equations in a different manner than they are used here. Despite the fact that in those studies the nonisothermal case is considered, the main difference to our study concerns the application of a full Euler system to each phase everywhere in space.Thus the number of balance equations is doubled. Additionally there is an equation determining the local phase fraction. The basic paper is that of Baer and Nunziatio [2]. However, it is restricted to 2-phase flows without phase transition. The main aim of those models is to study phase mixtures such as e.g. bubbly flows or sprays. Zein et al. [24] started from this approach and added the continuity of the Gibbs free energy across the interface in order to allow for a phase transition.

For basics on conservation laws see the books of Toro [20], Lax [12], LeVeque [13], Smoller [19], Kröner [11], Dafermos [5] and others. For thermodynamics see for instance Müller and Müller [16] as well as Müller [17].

Next we describe the main results of the current study. Our kinetic relation can be obtained in two different ways. It follows in the sharp interface limit that starts with the isothermal Navier-Stokes-Korteweg model and ends up with the corresponding isothermal Euler equations, see Dreyer et al. [9]. In this case the kinetic relation gives the mass flux across the interface as a linear function of the jump of the Gibbs free energy and it is proportional to the Navier-Stokes viscosities. A more physical derivation of the kinetic relation can be given in the setting of the Hertz-Knudsen theory, its non-isothermal version is described in Bond and Struchtrup [4]. Here the only difference between the two derivations is the factor of proportionality that is related to the sound velocity at the gas side of the interface.

As a main consequence of this kinetic equation is the absence of composite waves in the solution to Riemann problems. If we consider a Riemann problem where the left and right state correspond to two different phases, our kinetic relation implies a solution that exclusively consists of two classical waves and a phase transition in between. This construction is unique and generates classes of initial data, for which existence of solutions is guaranteed.

If we consider a Riemann problem where the left a right state correspond to the same phase, two cases may occur. Either the two states can be connected by only classical waves or if this is not possible, nucleation of a the other phase is enforced by the kinetic relation. Also here we prove existence and uniqueness.

The paper is organized as follows. In Section 3.2 we introduce the system of balances in the bulk and across the interface. Details of the equations of state are given in Section 3.3, whereas the entropy inequality is discussed in the following section. In Section 3.5 we obtain mathematical properties of the system considered. Moreover we discuss rarefactions and shocks for the isothermal case. The main part of this section is Subsection 3.5.3. Here we introduce the kinetic relation and prove a uniqueness result for the pressures at the phase interface. Moreover, we derive monotonicity results for interface quantities. Based on these results we construct the exact solution for the isothermal Euler euqations with phase transition, presented in Subsection 3.6.2. We prove uniqueness results within the class of Riemann problems as well as sufficient conditions for solvability. In Section 3.7 we discuss the cases of condensation by compression as well as evaporation by expansion. As before we prove several existence

and uniqueness results. Also we present the exact solution for the Riemann problems considered. Finally we give numerical examples for all cases considered. These are presented in Section 3.8.

3.2 Isothermal Euler equations

In our study we consider inviscid fluids under the isothermality assumption. This means, that the temperature T_0 is fixed. The phases are indicated by the value of mass density ρ and we have the velocity v as a variable. The physical fields are assumed to depend on time $t \in \mathbb{R}_{\geq 0}$ and space $x \in \mathbb{R}$. In regular points of the bulk phases we have the local mass conservation law (3.2.1) and the balance law for momentum (3.2.2). These are

$$\frac{\partial \rho}{\partial t} + \frac{\partial (\rho v)}{\partial x} = 0 \tag{3.2.1}$$

$$\frac{\partial (\rho v)}{\partial t} + \frac{\partial (\rho v^2 + p)}{\partial x} = 0\,. \tag{3.2.2}$$

In the momentum balance equation (3.2.2) there is a further quantity, pressure p. It is not among the basic variables and is therefore called a constitutive quantity. This quantity is related to the variable ρ in a material dependent manner by an equation of state. This will be given in Section 3.3. The system (3.2.1-3.2.2) is called system of isothermal Euler equations.

Across any discontinuity we have the jump conditions

$$[\![\rho(v - W)]\!] = 0 \tag{3.2.3}$$

$$\rho(v - W)[\![v]\!] + [\![p]\!] = 0\,. \tag{3.2.4}$$

Here we use the jump brackets $[\![\Psi]\!] = \Psi'' - \Psi'$ for any physical quantity Ψ, where $'$ and $''$ denote the one sided limits to the left left and right of the discontinuity, respectively, on the horizontal x-axis. Further, W denotes the propagation speed of the discontinuity. The mass flux Z across the discontinuity is given by

$$Z = -\rho(v - W) \tag{3.2.5}$$

with

$$Z = \begin{cases} Q & \text{shock wave} \\ z & \text{phase boundary} \end{cases} \quad \text{and} \quad W = \begin{cases} S & \text{shock wave} \\ w & \text{phase boundary} \end{cases}. \tag{3.2.6}$$

For more details on interface relations see Dreyer [7, Sections 5-14] and Müller [17, Section 2.2.2, Chapter 3].

3.3 Equations of state

The pressure is related to the density by the equation of state

$$p = p(\rho) \quad \text{with} \quad p'(\rho) = a^2 = \text{const}\,, \tag{3.3.1}$$

where a denotes the speed of sound.

In particular, for the vapor phase V we use the ideal gas law

$$p_V = \rho_V \frac{kT_0}{m} \tag{3.3.2}$$

for given temperature T_0. Here k denotes the Boltzmann constant and m is the mass of a single water molecule. The liquid phase L is modeled as a compressible fluid whose pressure is related to the liquid density by

$$p_L = p_0 + K_0 \left(\frac{\rho_L}{\rho_0} - 1 \right), \tag{3.3.3}$$

where the pressure p_0 and the density ρ_0 denote arbitrary reference values. The constant K_0 is the modulus of compression, which is temperature dependent. For convenience we choose p_0, ρ_0, K_0 at the saturation state, tabled in [22]. The data can also be found in [10].

In order to characterize the two phases we introduce two constant parameters, that will be properly defined later on. Within a range $0 \leq \rho_V \leq \tilde{\rho}$ the fluid is assumed to be in the vapor state. For $\rho_L \geq \rho_m$ the liquid phase is present. Between the pure phases there are intermediate states, whose pressure is defined by a linear function of negative slope, cf. Figure 3.1. For more details see Section 3.5.3.

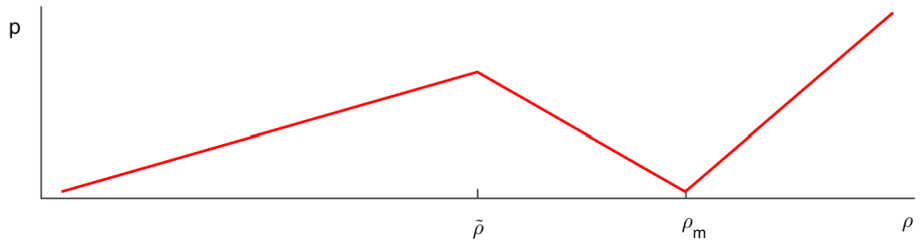

Figure 3.1: Equation of state: $p(\rho)$

According to the second law of thermodynamics the pressure is the derivative of the Helmholtz free energy with respect to $1/\rho$

$$p = -\frac{\partial \psi}{\partial 1/\rho}\,.$$

The Gibbs free energy is defined by

$$g = \psi + \frac{p}{\rho}\,.$$

This quantity occurs in the entropy inequality for isothermal processes

$$Z[\![g + \frac{1}{2}(v - W)^2]\!] \leq 0\,. \tag{3.3.4}$$

For details see Dafermos [5], Merkle [15], Müller and Voss [18].

3.4 Riemann problem

In our study we consider the Riemann problem for the isothermal Euler equations. This is given by the balances (3.2.1-3.2.2), the equation of state (3.3.1) and the corresponding Riemann initial data

$$\rho(x,0) = \begin{cases} \rho_- & \text{for} \quad x < 0 \\ \rho_+ & \text{for} \quad x > 0 \end{cases} \qquad \text{and} \qquad v(x,0) = \begin{cases} v_- & \text{for} \quad x < 0 \\ v_+ & \text{for} \quad x > 0\,. \end{cases} \tag{3.4.1}$$

We denote the solution to the Riemann problem by $\mathbf{W}$. The solution consists of constant states $\mathbf{W} = const$, that are separated by waves or phase boundaries. We will denote neighboring states by $'$ and $''$, as done in Section 3.2. The Riemann problem is solved by self-similar solutions of type $\mathbf{W}(t,x) = \hat{\mathbf{W}}(x/t)$.

3.5 Generic solution

In order to give the mathematical properties of the Euler system (3.2.1-3.2.2), we rewrite the system in quasilinear form in terms of ρ and v

$$\begin{pmatrix} \rho \\ v \end{pmatrix}_t + \begin{pmatrix} v & \rho \\ \frac{a^2}{\rho} & v \end{pmatrix} \begin{pmatrix} \rho \\ v \end{pmatrix}_x = \begin{pmatrix} 0 \\ 0 \end{pmatrix}\,.$$

The Jacobian matrix is

$$\mathbf{A} = \begin{pmatrix} v & \rho \\ \frac{a^2}{\rho} & v \end{pmatrix}$$

with the eigenvalues

$$\lambda_1 = v - a \qquad \text{and} \qquad \lambda_2 = v + a$$

as well as the corresponding right eigenvectors

$$\mathbf{r}_1 = \begin{pmatrix} \rho \\ -a \end{pmatrix} \qquad \text{and} \qquad \mathbf{r}_2 = \begin{pmatrix} \rho \\ a \end{pmatrix} .$$

The system is strictly hyperbolic. Finally we give the Riemann invariants

$$I_1 = v + a \ln \rho = const \qquad \text{and} \qquad I_2 = v - a \ln \rho = const \tag{3.5.1}$$

across the left and right wave, respectively.

3.5.1 Rarefaction wave fans

Assume, the wave corresponding to λ_1 is a (left) 1-rarefaction, then we use the Riemann invariant given in $(3.5.1)_1$ to obtain

$$v' + a \ln \rho' = v'' + a \ln \rho'' . \tag{3.5.2}$$

For a left rarefaction the head speed is given by $v' - a$ whereas the tail speed is given by $v'' - a$. The slope inside the rarefaction fan is given by

$$\frac{dx}{dt} = \frac{x}{t} = v - a .$$

Using (3.5.2) we obtain, that the solution $\mathbf{W}$ inside the fan is given by

$$\mathbf{W}_{1fan} = \begin{cases} v = a + \frac{x}{t} \\ \rho = \exp\left(\frac{v'-v}{a} + \ln \rho' \right) \end{cases} \tag{3.5.3}$$

On the other hand, using $(3.5.1)_2$ for a (right) 2-rarefaction we get

$$v' - a \ln \rho' = v'' - a \ln \rho'' . \tag{3.5.4}$$

Analogously to the above calculations for a 2-rarefaction wave we have the head speed $v'' + a$ and the tail speed $v' + a$. The solution inside the fan is then given by

$$\mathbf{W}_{2fan} = \begin{cases} v = -a + \frac{x}{t} \\ \rho = \exp\left(\frac{v-v''}{a} + \ln \rho'' \right) \end{cases} . \tag{3.5.5}$$

3.5.2 Shocks

3.5.2.1 Entropy inequality across a shock wave

In this section we want to prove, that the Lax condition is equivalent to the entropy condition for the systemconsidered. We take the case, where the states

$$\begin{pmatrix} \rho' \\ v' \end{pmatrix} \qquad \text{and} \qquad \begin{pmatrix} \rho'' \\ v'' \end{pmatrix}$$

are separated by a shock wave, that propagates with speed S. W.l.o.g. we assume, that $v' = 0$. This assumption is used to simplify the following calculations and is only used in Section 3.5.2.1. Due to $v' = 0$ we have $v'' < 0$. Then from the Rankine-Hugeniot conditions we obtain for S

$$S = -\frac{\rho'' v''}{\rho' - \rho''} \tag{3.5.6}$$

$$\text{and} \qquad S = \frac{-\rho'' v''^2 + a^2(\rho' - \rho'')}{-\rho'' v''} .$$

This gives

$$v''^2 = a^2 \frac{(\rho' - \rho'')^2}{\rho' \rho''} . \tag{3.5.7}$$

Further, the entropy inequality is given by

$$\rho' S \left(a^2 \ln \frac{\rho'}{\rho''} + \frac{1}{2} S^2 - \frac{1}{2} (v'' - S)^2 \right) \leq 0 \,.$$

For the second factor we obtain using (3.5.1) twice, then (3.5.6) and (3.5.7)

$$\begin{aligned}
a^2 \ln \frac{\rho'}{\rho''} + \frac{1}{2} S^2 - \frac{1}{2} (v'' - S)^2 &= a^2 \ln \frac{\rho'}{\rho''} + \frac{Q^2}{2} \left(\frac{1}{\rho'^2} - \frac{1}{\rho''^2} \right) \\
&= a^2 \ln \frac{\rho'}{\rho''} + \frac{\rho'^2 S^2}{2} \left(\frac{1}{\rho'^2} - \frac{1}{\rho''^2} \right) \\
&= a^2 \ln \frac{\rho'}{\rho''} + \frac{\rho'^2 \rho''^2 v''^2}{2(\rho' - \rho'')^2} \left(\frac{1}{\rho'^2} - \frac{1}{\rho''^2} \right) \\
&= a^2 \ln \frac{\rho'}{\rho''} + a^2 \frac{\rho' \rho''}{2} \left(\frac{1}{\rho'^2} - \frac{1}{\rho''^2} \right) \\
&= a^2 \left(\ln \frac{\rho'}{\rho''} + \frac{\rho' \rho''}{2} \left(\frac{1}{\rho'^2} - \frac{1}{\rho''^2} \right) \right) \begin{array}{l} = 0 \ , \rho' = \rho'' \\ > 0 \ , \rho' < \rho'' \\ < 0 \ , \rho' > \rho'' \end{array}
\end{aligned}$$

For the case $\rho' < \rho''$ we have from (3.5.7) $S < 0$, whereas for the second case $\rho' > \rho''$ this leads to $S > 0$. In the first case we thus have from (3.5.6) and (3.5.7) that

$$S = \frac{\rho''}{\rho'' - \rho'} v'' > v'' \qquad \text{and} \qquad S = -a \frac{\rho''}{\sqrt{\rho' \rho''}} < -a \,.$$

This implies the Lax condition $a > -a > S > v'' - a$, which in general notation is given by

$$v' + a > v' - a > S > v'' - a \,,$$

see Lax [12]. Obviously in that case we have a left or 1-shock. Similarly in the second case we have a right or 2-shock and we obtain the corresponding Lax condition

$$v' + a > S > v'' + a > v'' - a \,.$$

In summary, for the isothermal Euler equations the entropy condition and the Lax condition are equivalent. For this special system this is a more general result than that given in Dafermos [5]. Based on the explicit constitutive functions used here this statement is true for arbitrarily strong shocks.

3.5.2.2 Shock relations

Let us assume that the left wave is a shock wave, propagating with speed S_1. As done in Toro [20] we define relative velocities

$$\hat{v}' = v' - S_1 \qquad \text{and} \qquad \hat{v}'' = v'' - S_1 \,. \tag{3.5.8}$$

We obtain the corresponding Rankine-Hugeniot conditions

$$\rho' \hat{v}' = \rho'' \hat{v}'' \tag{3.5.9}$$

$$\rho' \hat{v}'^2 + p' = \rho'' \hat{v}''^2 + p'' \,. \tag{3.5.10}$$

For the mass flux Q_1 we have

$$-Q_1 = \rho'(v' - S_1) = \rho''(v'' - S_1) = \rho' \hat{v}' = \rho'' \hat{v}'' \,. \tag{3.5.11}$$

We substitute Q_1 into (3.5.10) to obtain

$$-Q_1 \hat{v}' + a^2 \rho' = -Q_1 \hat{v}'' + a^2 \rho'' \,.$$

Solving for $-Q_1$ and using the entropy condition discussed above this leads to

$$-Q_1 = -\frac{a^2(\rho'' - \rho')}{\hat{v}'' - \hat{v}'} = -\frac{a^2(\rho'' - \rho')}{v'' - v'} > 0 \,, \tag{3.5.12}$$

which gives us

$$v'' = v' + \frac{a^2(\rho'' - \rho')}{Q_1}\,. \tag{3.5.13}$$

On the other hand using (3.5.11) to substitute $\hat{v}'$ and $\hat{v}''$ in (3.5.12) we derive the relation

$$-Q_1 = -\frac{a^2(\rho'' - \rho')}{-\frac{Q_1}{\rho''} + \frac{Q_1}{\rho'}} \tag{3.5.14}$$

and get

$$Q_1^2 = a^2\rho'\rho''\,. \tag{3.5.15}$$

In combination with (3.5.13) and $Q_1 < 0$ this gives us across a left shock

$$v'' = v' - \frac{a^2(\rho'' - \rho')}{\sqrt{a^2\rho'\rho''}}\,.$$

Finally, from (3.5.11) and (3.5.15) we obtain the speed of a left shock

$$S_1 = v' + \frac{Q_1}{\rho'} = v' - \frac{\sqrt{a^2\rho'\rho''}}{\rho'}\,.$$

For a right shock the calculations are very similar. We obtain $Q_2 > 0$ and

$$v'' = v' + \frac{a^2(\rho'' - \rho')}{\sqrt{a^2\rho'\rho''}}\,.$$

as well as

$$S_2 = v' + \frac{Q_2}{\rho'} = v' + \frac{\sqrt{a^2\rho'\rho''}}{\rho'}\,.$$

In general terms the result is given by

$$v'' = v' - \frac{a^2|\rho'' - \rho'|}{\sqrt{a^2\rho'\rho''}} \qquad \text{and} \qquad S = v' + \frac{Q}{\rho'}\,. \tag{3.5.16}$$

Remark 3.5.1. *Note that our notation is similar to, but slightly different from the notation in the book of Toro [20].*

3.5.3 Phase transition

3.5.3.1 Definition of the phases

In case, that the discontinuity represents a boundary between two phases we always have

$$\rho_V < \rho_L\,. \tag{3.5.17}$$

Furthermore, from the mass and momentum balances (3.2.3-3.2.4) across the phase boundary together with (3.2.5) and (3.2.6) we obtain

$$z^2 = -\frac{p' - p''}{\frac{1}{\rho'} - \frac{1}{\rho''}}\,.$$

With the above relation for the densities (3.5.17) we conclude

$$p_L \geq p_V \qquad \text{and with} \qquad p_V \geq 0 \qquad \text{we have} \qquad p_L \geq 0\,. \tag{3.5.18}$$

The second statement is due to the fact that we ignore surface tension. We define, see (3.3.3),

$$\rho_m = \frac{\rho_0}{K_0}(K_0 - p_0)\,, \tag{3.5.19}$$

which gives $p_L(\rho_m) = 0$. Corresponding to ρ_m we have to find $\tilde{\rho}$. This value is uniquely defined by the equation of state (3.3.1), equation (3.5.19) and the Maxwell condition

$$\int_{\frac{1}{\rho_0}}^{\frac{1}{\rho_V(p_0)}} p(\rho)\, d\frac{1}{\rho} = \left(\frac{1}{\rho_V(p_0)} - \frac{1}{\rho_0}\right) \cdot p_0\,.$$

After some calculations we obtain

$$\frac{K_0}{\rho_0} \ln \frac{\rho_0}{\rho_m} + \frac{kT_0}{m} \ln \frac{\rho_m}{\rho_V(p_0)} - \frac{\rho_m}{\rho_m - \tilde{\rho}} \frac{kT_0}{m} \ln \frac{\rho_m}{\tilde{\rho}} = 0\,. \tag{3.5.20}$$

This relation defines $\tilde{\rho}$ uniquely for sufficiently low temperatures $T \leq 633.15K$. For higher temperatures the definition of ρ_m gives a negative value. The critical temperature T_c for water is given by $T_c = 647.096K$. For $T_0 = 573.15K$ we obtain $\tilde{\rho} = 36.515kg/m^3$, see Figure 3.2.

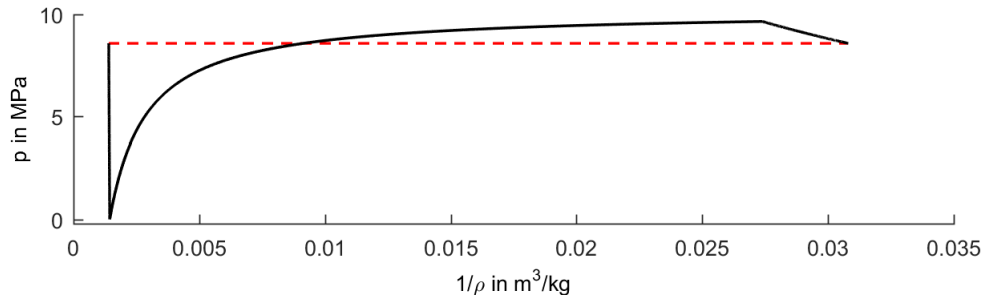

Figure 3.2: Equation of state: $p(1/\rho)$ for $T_0 = 573.15K$, dashed red: Maxwell line

The corresponding reference values are given by $p_0 = 18.6664MPa$, $\rho_0 = 1/0.00189451kg/m^3$ and $K_0 = 1/36.627 \cdot 10^9 Pa$.

Furthermore we give the curves $\rho_m(T)$ and $\tilde{\rho}(T)$, see Figure 3.3*a* and the quotient $\tilde{\rho}(T)/\rho_m(T)$, see Figure 3.3*b*. Obviously one has

$$\tilde{\rho}(T)/\rho_m(T) < 1/4 \tag{3.5.21}$$

for all temperatures $273.15K \leq T_0 \leq 623.15K$.

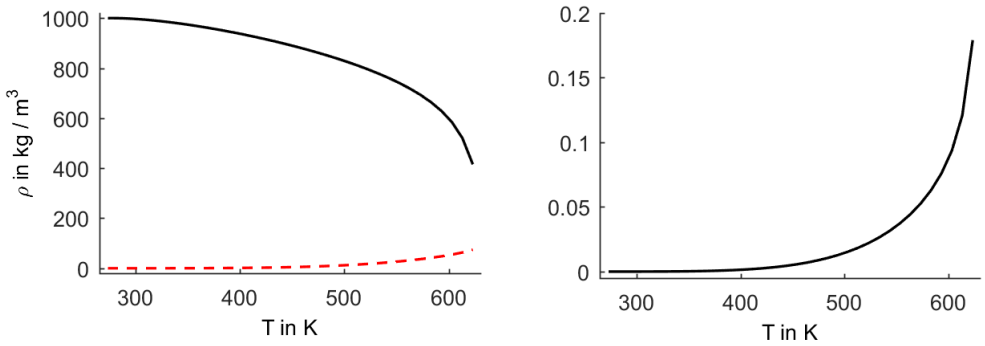

Figure 3.3: *a*) dashed red: $\tilde{\rho}(T)$, solid black: $\rho_m(T)$ *b*) $\tilde{\rho}(T)/\rho_m(T)$

Remark 3.5.2. *In our notation all temperature dependent constants have index 0. If we choose T_0 we have to use corresponding reference values ρ_0, p_0, K_0.*

Remark 3.5.3. *Most estimations in this paper are based on the data tabled in [22]. Accordingly for all temperatures usually means the finite number of discrete temperature values tabled in [22]. For the not tabled intermediate temperatures we have: If for monotonic temperature changes the temperature dependent constants change monotonically, the estimations are also valid for the intermediate temperatures.*

3.5.3.2 A simple kinetic relation to describe phase transitions

Besides the balances for mass (3.2.3) and momentum (3.2.4) at the phase boundary we need a further equation, that is called kinetic relation. This equation describes the rate of change of mass across the interface. We choose

$$z = \frac{p_V}{\sqrt{2\pi}} \left(\frac{m}{kT_0}\right)^{(3/2)} [\![g + e_{kin}]\!] , \tag{3.5.22}$$

where V denotes the vapor phase. For details of the derivation see Dreyer et a. [8]. If the vapor phase is to the left of the liquid phase, this results in

$$z = \frac{p_V}{\sqrt{2\pi}} \left(\frac{m}{kT_0}\right)^{\frac{3}{2}} \left[\frac{K_0}{\rho_0} \ln \frac{\rho_L}{\rho_0} - \frac{kT_0}{m} \ln \frac{p_V}{p_0} + \frac{1}{2}(v_L - w)^2 - \frac{1}{2}(v_V - w)^2 \right] . \tag{3.5.23}$$

Here V and L denote the vapor and the liquid phase, respectievely. Equation (3.5.24) gives the kinetic relation for the case, that the vapor phase is to the right

$$-z = \frac{p_V}{\sqrt{2\pi}} \left(\frac{m}{kT_0}\right)^{\frac{3}{2}} \left[\frac{K_0}{\rho_0} \ln \frac{\rho_L}{\rho_0} - \frac{kT_0}{m} \ln \frac{p_V}{p_0} + \frac{1}{2}(v_L - w)^2 - \frac{1}{2}(v_V - w)^2 \right] . \tag{3.5.24}$$

For the moment we restrict ourselves to the case, that the vapor phase is on the left side. Therefore in this section we identify $'$ (left state) with the vapor and $''$ (right state) with the liquid phase.

If condensation and evaporation are excluded, we replace (3.5.22) by the new kinetic relation

$$z = 0 . \tag{3.5.25}$$

This implies that $v_V = v_L$ at the phase boundary, see (3.2.5) and (3.2.6).

3.5.3.3 Uniqueness of p_L for given p_V

If p_V is given, we have to determine 4 unknowns, namely p_L, v_L, v_V and z. At the interface we have 4 conditions: two mass flux conditions (3.2.5), the interface momentum balance (3.2.4) and furthermore the kinetic relation (3.5.23). Our goal is to determine an equation for p_L. The interface momentum balance can be written as

$$[\![p]\!] = -z^2 [\![\frac{1}{\rho}]\!] . \tag{3.5.26}$$

Because $\rho_L > \rho_V$ we have

$$p_L = p_V \quad \Leftrightarrow \quad z = 0 .$$

This is the equilibrium case $p_L = p_V = p_0$. Otherwise we have $p_V < p_L$.

In the following lemma we will make the assumption

$$-a_V \rho_V \leq z \leq a_L \rho_L . \tag{3.5.27}$$

It simplifies the calculations and later it turns out to be automatically satisfied due to physical considerations, see Remark 3.5.6.

Lemma 3.5.1. *Consider the isothermal case with $273.15K \leq T_0 \leq 623.15K$. Then for given interface pressure p_V of the vapor phase with $0 \leq p_V \leq \tilde{p}$, the conditions (3.5.27) and the corresponding equations of state (3.3.2), (3.3.3) define the liquid interface pressure p_L, uniquely. Furthermore by these relations the mass flux z is uniquely defined.*

Proof. We replace z in (3.5.26) by the kinetic relation (3.5.23) and get

$$[\![p]\!] + \left(\frac{m}{kT_0}\right)^3 \frac{p_V^2}{2\pi} \left[\frac{K_0}{\rho_0} \ln \frac{\rho_L}{\rho_0} - \frac{kT_0}{m} \ln \frac{p_V}{p_0} - \frac{1}{2}[\![p]\!] \left(\frac{1}{\rho_L} + \frac{1}{\rho_V} \right) \right]^2 [\![\frac{1}{\rho}]\!] = 0 . \tag{3.5.28}$$

Next we define the functions

$$h(p_V, p_L) = \left(\frac{m}{kT_0}\right)^{3/2} \frac{1}{\sqrt{2\pi}} \left[\frac{K_0}{\rho_0} \ln \frac{\rho_L}{\rho_0} - \frac{kT_0}{m} \ln \frac{p_V}{p_0} - \frac{1}{2}[\![p]\!] \left(\frac{1}{\rho_L} + \frac{1}{\rho_V} \right) \right] \tag{3.5.29}$$

and

$$f(p_V, p_L) = [\![p]\!] + h^2(p_V, p_L) p_V^2 [\![\frac{1}{\rho}]\!]$$

for $p_V \geq 0$ and $p_L \geq p_V$. The roots of the latter function are the solutions of (3.5.28).

1. Let us consider, $p_V = p_0$, i.e. the saturation pressure. Then for $p_L = p_0$ we have $f(p_0, p_L) = 0$. So (p_0, p_0) is a solution of (3.5.28). It obviously satisfies (3.5.27) with $z = 0$.

2. We note, that
$$\frac{\partial f}{\partial p_V}(p_0, p_0) = -1 \qquad \text{and} \qquad \frac{\partial f}{\partial p_L}(p_0, p_0) = 1\,.$$
Accordingly in a neighborhood of $p_V = p_0$ relation (3.5.28) implicitely defines a function $p_L(p_V)$ with $p_L'(p_V) > 0$. This means, in a neighborhood of $p_V = p_0$ relation (3.5.28) has a solution, that satisfies the inequalities (3.5.27).

3. By our assumption we consider a temperature regime, where in (3.3.3) we have
$$p_L = p_0 + K_0 \frac{\rho_L}{\rho_0} - K_0 < p_0 + K_0 \frac{\rho_L}{\rho_0} - (p_0 - p_V)\,.$$
Therefore
$$1 - \frac{p_L - p_V}{K_0} \frac{\rho_0}{\rho_L} > 0$$
and we conclude that
$$\frac{\partial h}{\partial p_L}(p_V, p_L) = \left(\frac{m}{kT_0}\right)^{3/2} \frac{1}{\sqrt{2\pi}} \left[\frac{1}{2}\left(\frac{1}{\rho_L} - \frac{1}{\rho_V}\right) + \frac{1}{2}\frac{p_L - p_V}{K_0}\frac{\rho_0}{\rho_L}\frac{1}{\rho_L}\right] < 0\,.$$
For any fixed p_V the function $h(p_V, p_L)$ is strictly decreasing in p_L. Due to $p_L \geq p_V$ it attains its maximum at $p_L = p_V$.

4. Next we calculate
$$\frac{\partial f}{\partial p_L}(p_V, p_L) = 1 - p_V^2 \cdot h^2(p_V, p_L)\frac{1}{\rho_L^2}\frac{\rho_0}{K_0} + p_V^2 h(p_V, p_L)\frac{\partial h}{\partial p_L}(p_V, p_L)[\![\frac{1}{\rho}]\!]\,,.$$
Let us consider any p_V^*, p_L^* such that $f(p_V^*, p_L^*) = 0$ and (3.5.27) is satisfied. Let us further consider that $z > 0$. Then we obtain
$$\frac{\partial f}{\partial p_L}(p_V^*, p_L^*) > 1 - \frac{K_0}{\rho_0}\frac{\rho_0}{K_0} = 0\,.$$
On the other hand, if $z < 0$ then
$$\frac{\partial f}{\partial p_L}(p_V^*, p_L^*) > 1 - \frac{\rho_V^{*2}}{\rho_L^{*2}}\frac{a_V^2}{a_L^2} - \left(\frac{m}{kT_0}\right)^{3/2} \frac{p_V^*}{\sqrt{2\pi}} \rho_V a_V \frac{1}{\rho_V^{*2}} > 0\,.$$
So p_L^* is a simple root of $f(p_V^*, \cdot)$ with $\frac{\partial f}{\partial p_L}(p_V^*, p_L^*) > 0$.

5. Because of $f(p_V^*, \cdot) \to -\infty$ for $p_L \to \infty$ it is clear, that f has a further root $p_L^{**} > p_L^*$ with $\frac{\partial f}{\partial p_L}(p_V^*, p_L^{**}) \leq 0$. Accordingly (p_V^*, p_L^{**}) does not satisfy the inequality (3.5.27), see step 4. Moreover, by monotonicity of h there is no further root $p_L > p_L^*$, that satisfies (3.5.27), see step 3.

   By the same arguments as before there is no further root $p_L < p_L^*$.

6. We have seen that in a neighborhood of $p_V = p_0$ for every fixed p_V^* there exists a unique p_L^* such that $f(p_V^*, p_L^*) = 0$ and (3.5.27) are satisfied. Next we want to show that this is true for every $0 \leq p_V < p_0$.

   Assume, there exists a $p_V < p_0$ such that there is no solution p_L with $f(p_V, p_L) = 0$. Then by the previous results we conclude that there exist p_V^*, p_L^* with $p_V < p_V^* < p_0$ such that $f(p_V^*, p_L^*) = 0$

and $\frac{\partial f}{\partial p_L}(p_V^*, p_L^*) = 0$. Accordingly the solution (p_V^*, p_L^*) does not satisfy the right hand side of inequalities (3.5.27). For (p_V^*, p_L^*) we estimate

$$z(p_V^*, p_L^*) < p_V^* h(p_V^*, p_V^*) < -\left(\frac{m}{kT_0}\right)^{(3/2)} \frac{p_V^*}{\sqrt{2\pi}} \frac{kT_0}{m} \ln \frac{p_V^*}{p_0} = -\frac{a_V}{\sqrt{2\pi}} \rho_V^* \ln \frac{p_V^*}{p_0} .$$

The expression $-\frac{a_V}{\sqrt{2\pi}} \rho_V^* \ln \frac{p_V^*}{p_0}$ attains its maximum at $\hat{p}_V = p_0 \exp(-1)$. Accordingly we get

$$-\frac{a_V}{\sqrt{2\pi}} \rho_V^* \ln \frac{p_V^*}{p_0} \leq \frac{a_V}{\sqrt{2\pi}} \hat{\rho}_V < a_L \rho_L .$$

This contradicts the above statement that (p_V^*, p_L^*) does not satisfy the right hand side of inequalities (3.5.27). We conclude, that for every fixed $0 < p_V^* < p_0$ there exists a unique p_L^*, such that $f(p_V^*, p_L^*) = 0$ and (3.5.27) are satisfied.

7. Taking $p_V^* = \tilde{p}$ one can easily check, that the root $(\tilde{p}, p_L(\tilde{p}))$ satisfies (3.5.27). Accordingly by an argumentation analogously to step 6 this is true for every p_V^* with $p_0 \leq p_V^* < \tilde{p}$. Now the first statement of Lemma 3.5.1 is proven for all $0 \leq p_V^* < \tilde{p}$.

Applying this solution to the kinetic relation (3.5.23) we obtain the mass flux z across the interface. □

Remark 3.5.4. *For shorter and more clear notation we will often use instead of ρ_L the quantity $\left(\frac{p_L - p_0}{K_0} + 1\right)\rho_0$ given by the equation of state (3.3.3). This fact one should keep in mind when calculating partial derivatives $\partial/\partial p_L$.*

Proposition 3.5.1. *For every temperature $273.15K \leq T_0 \leq 623.15K$ and given p_V^* the first root of $f(p_V^*, \cdot)$ satisfies (3.5.27).*

Proof. It is obvious, that for $p_V = p_L > p_0$ the function h is negative whereas for $p_V = p_L < p_0$ the function h is positive. Accordingly in the latter case we have

$$p_V \cdot h(p_V, p_L) < -\left(\frac{m}{kT_0}\right)^{3/2} \frac{p_V}{\sqrt{2\pi}} \frac{kT_0}{m} \ln \frac{p_V}{p_0} \leq \frac{p_0 \exp(-1)}{a_V \sqrt{2\pi}} < a_L \rho_L . \tag{3.5.30}$$

This proves the statement, that the right hand side of (3.5.27) is always satisfied.

For the left hand side of (3.5.27) this statement is clear by step 7 of the proof of Lemma 3.5.1. □

3.5.3.4 Monotonicity of $p_L^*(p_V^*)$

Lemma 3.5.2. *By (3.5.28) the implicitely defined function $p_L^*(p_V^*)$ is strictly increasing. Here p_L^* denotes the uniquely defined root of (3.5.28) for given p_V^*.*

Proof. By the implicit function theorem we know that

$$p_L^{*\prime}(p_V^*) = -\frac{\partial f}{\partial p_V}(p_V^*, p_L^*) \Big/ \frac{\partial f}{\partial p_L}(p_V^*, p_L^*) .$$

From the last subsection we know that $\frac{\partial f}{\partial p_L}(p_V^*, p_L^*) > 0$. So we only have to show, that

$$\frac{\partial f}{\partial p_V}(p_V^*, p_L^*) < 0 .$$

We calculate

$$\frac{\partial f}{\partial p_V}(p_V^*, p_L^*) = -1 + p_V^* \cdot h^2(p_V^*, p_L^*) \left(\frac{2}{\rho_L^*} - \frac{1}{\rho_V^*}\right) + p_V^2 \cdot h(p_V^*, p_L^*) \frac{\partial h}{\partial p_V}(p_V^*, p_L^*) [\![\frac{1}{\rho^*}]\!] .$$

Let us assume that $z < 0$. Then

$$\begin{aligned} \frac{\partial h}{\partial p_V}(p_V^*, p_L^*) &= \left(\frac{m}{kT_0}\right)^{3/2} \frac{1}{\sqrt{8\pi}} \left([\![\frac{1}{\rho^*}]\!] + \frac{[\![p^*]\!]}{\rho_V^* p_V^*}\right) \\ &= \left(\frac{m}{kT_0}\right)^{3/2} \frac{1}{\sqrt{8\pi}} \left(1 - \frac{z^2}{p_V^* \rho_V^*}\right) [\![\frac{1}{\rho^*}]\!] < 0 \end{aligned}$$

and consequently $\frac{\partial f}{\partial p_V}(p_V^*, p_L^*) < 0$. If $z > 0$ and $z \leq \rho_V^* a_V$ then

$$\frac{\partial f}{\partial p_V}(p_V^*, p_L^*) < -1 + \left(\frac{m}{kT_0}\right)^{3/2} \frac{p_V^*}{\sqrt{2\pi}} \rho_V^* \left(\frac{kT_0}{m}\right)^{1/2} \frac{1}{\rho_V^{*2}} < 0\,.$$

Finally, for $z > 0$ and $z > \rho_V^* a_V$ the above statement is obvious. □

Proposition 3.5.2. *During a condensation process both pressures are larger than the saturation pressure*

$$p_0 < p_V < p_L$$

whereas during an evaporation process we have

$$p_V < p_L < p_0\,.$$

This is a direct consequence of the last lemma and the fact $p_L(p_0) = p_0$.

3.5.3.5 Monotonicity of $z[\![\frac{1}{\rho^*}]\!]$

Due to Lemma 3.5.1, for given p_V^* the mass flux z is uniquely defined, because $f(p_V^*, p_L) = 0$ has only a single admissible solution. Next we prove a further monotonicity relation.

Lemma 3.5.3. *For given temperature $273.15K \leq T_0 \leq 623.15K$ the expression $z[\![\frac{1}{\rho^*}]\!]$ is strictly increasing in p_V^*, where z depends on the function $p_L^*(p_V^*)$ implicitely defined by (3.5.28).*

Proof. We have

$$\frac{dz[\![\frac{1}{\rho}]\!]}{dp_V}(p_V^*, p_L^*) = \left(\frac{\partial z[\![\frac{1}{\rho}]\!]}{\partial p_V} + \frac{\partial z[\![\frac{1}{\rho}]\!]}{\partial p_L} p_L^{*\prime}\right)(p_V^*, p_L^*) = \left(\frac{\partial z[\![\frac{1}{\rho}]\!]}{\partial p_V} - \frac{\partial z[\![\frac{1}{\rho}]\!]}{\partial p_L} \frac{\frac{\partial f}{\partial p_V}}{\frac{\partial f}{\partial p_L}}\right)(p_V^*, p_L^*)$$

Using previous results we will show that

$$\left(\frac{\partial z[\![\frac{1}{\rho}]\!]}{\partial p_V}\frac{\partial f}{\partial p_L} - \frac{\partial z[\![\frac{1}{\rho}]\!]}{\partial p_L}\frac{\partial f}{\partial p_V}\right)(p_V^*, p_L^*) > 0\,. \tag{3.5.31}$$

Calculating all the derivatives we obtain

$$\begin{aligned}\left(\frac{\partial z[\![\frac{1}{\rho}]\!]}{\partial p_V}\frac{\partial f}{\partial p_L} - \frac{\partial z[\![\frac{1}{\rho}]\!]}{\partial p_L}\frac{\partial f}{\partial p_V}\right)(p_V^*, p_L^*) = \left(\frac{m}{kT_0}\right)^{3/2} \frac{1}{\rho_V^*\sqrt{2\pi}} \Bigg\{ [\![\frac{1}{\rho^*}]\!]^2 \left(\rho_V^* p_V^* - z^4 \frac{1}{\rho_L^{*2}} \frac{\rho_0}{K_0}\right) \\ + \left[\frac{K_0}{\rho_0} \ln\frac{\rho_L^*}{\rho_0} - \frac{kT_0}{m} \ln\frac{p_V^*}{p_0} - \frac{1}{2}[\![p^*]\!]\left(\frac{1}{\rho_L^*} + \frac{1}{\rho_V^*}\right)\right] \frac{\rho_V^*}{\rho_L^*}\left(1 - \frac{\rho_0}{K_0}\frac{p_L^*}{\rho_L^*}\right)\Bigg\}\,.\end{aligned}$$

Let us first consider, that $z > 0$. Then for $z^2 \leq \rho_V^* \rho_L^* a_V a_L$ the above statement is obvious.

Assume, z is positive with $z^2 > \rho_V^* \rho_L^* a_V a_L$. Then because $z > 0$ we conclude

$$\begin{aligned} & -\frac{kT_0}{m} \ln\frac{p_V^*}{p_0} - \frac{1}{2}[\![p^*]\!]\left(\frac{1}{\rho_L^*} + \frac{1}{\rho_V^*}\right) > 0 \\ \Longrightarrow \quad & -\frac{kT_0}{m} \ln\frac{p_V^*}{p_0} + \frac{1}{2}[\![\frac{1}{\rho^*}]\!]\left(\frac{1}{\rho_L^*} + \frac{1}{\rho_V^*}\right)\rho_V^*\rho_L^* a_V a_L > 0 \\ \Longrightarrow \quad & -\frac{kT_0}{m} \ln\frac{p_V^*}{p_0} - \frac{\rho_L^*}{2\rho_V^*} a_V^2 > 0 \\ \Longleftrightarrow \quad & \rho_L^* + 2\rho_V^* \ln\frac{p_V^*}{p_0} < 0\,. \end{aligned} \tag{3.5.32}$$

By some simple calculations we find, that for fixed ρ_L^* the expression $\rho_L^* + 2\rho_V^* \ln\frac{p_V^*}{p_0}$ attains its minimum for $\hat{p}_V = p_0 \cdot \exp(-1)$. Accordingly we have

$$\rho_L^* + 2\rho_V^* \ln\frac{p_V^*}{p_0} \geq \rho_L^* - 2\hat{\rho}_V > 0\,.$$

This is a contradiction to (3.5.32) and we conclude $z^2 \leq \rho_V^* \rho_L^* a_V a_L$. This implies the above statement for positive z.

Now let us consider $z < 0$. We obtain

$$\begin{aligned}
&[\![\frac{1}{\rho^*}]\!]^2 \left(\rho_V^* p_V^* - z^4 \frac{1}{\rho_L^{*2}} \frac{\rho_0}{K_0}\right) \\
&+ \left[\frac{K_0}{\rho_0} \ln \frac{\rho_L^*}{\rho_0} - \frac{kT_0}{m} \ln \frac{p_V^*}{p_0} - \frac{1}{2}[\![p^*]\!] \left(\frac{1}{\rho_L^*} + \frac{1}{\rho_V^*}\right)\right] \frac{\rho_V^*}{\rho_L^*} \left(1 - \frac{\rho_0}{K_0} \frac{p_L^*}{\rho_L^*}\right) \\
&> [\![\frac{1}{\rho^*}]\!]^2 \left(\rho_V^{*2} a_V^2 - \frac{\rho_V^{*4} a_V^4}{\rho_L^{*2} a_L^2}\right) + \left[\frac{K_0}{\rho_0} \ln \frac{\rho_L^*}{\rho_0} - \frac{kT_0}{m} \ln \frac{p_V^*}{p_0} - \frac{1}{2}[\![p^*]\!] \left(\frac{1}{\rho_L^*} + \frac{1}{\rho_V^*}\right)\right] \frac{\rho_V^*}{\rho_L^*} \\
&\geq a_V^2 \left([\![\frac{1}{\rho^*}]\!]^2 \rho_V^{*2} \left(1 - \frac{\rho_V^{*2} a_V^2}{\rho_L^{*2} a_L^2}\right) - \sqrt{2\pi} \frac{\rho_V^*}{\rho_L^*}\right).
\end{aligned}$$

This expression is obviously positive, because $\rho_V/\rho_L < 1/4$, cf. (3.5.21). Accordingly the proof of Lemma 3.5.3 is complete. □

Remark 3.5.5. *If we exclude phase transition, this means that we use the trivial kinetic relation $z = 0$, Lemma 3.5.1 and Lemma 3.5.2 remain valid. It is quite evident, that we have $p_L^* = p_V^*$. The expression $z[\![\frac{1}{\rho}]\!]$ of Lemma 3.5.3 becomes zero and is clearly non-strictly increasing in p_V^*.*

Remark 3.5.6. *During the proof of Lemma 3.5.3 we observe that the smallest $p_L \geq 0$ with $f(p_V^*, p_L) = 0$ identically satisfies the inequalities*

$$-a_V \rho_V \leq z \leq \sqrt{a_V a_L} \sqrt{\rho_V \rho_L} < a_L \rho_L\,, \tag{3.5.33}$$

which is a sharper result than the inequality (3.5.27).

3.6 Explicit solutions of the Riemann problem for isothermal Euler equations for two phases with different equations of state

Now let us consider two phase flows, where from now on for all examples the left phase (initially $x < 0$) is assumed to be water vapor, whereas the right phase (initially $x > 0$) is assumed to be liquid water. The different phases are characterized by different equations of state, given in (3.3.2) and (3.3.3). We consider the Riemann problem

$$\rho(x,0) = \begin{cases} \rho_- = \rho_V & \text{for} \quad x < 0 \\ \rho_+ = \rho_L & \text{for} \quad x > 0 \end{cases} \qquad \text{and} \qquad v(x,0) = \begin{cases} v_- = v_V & \text{for} \quad x < 0 \\ v_+ = v_L & \text{for} \quad x > 0\,. \end{cases} \tag{3.6.1}$$

The solution consists of 4 constant states, that are separated by 2 classical waves and the phase boundary. Accordingly we have three possible wave patterns, see Figure 3.4.

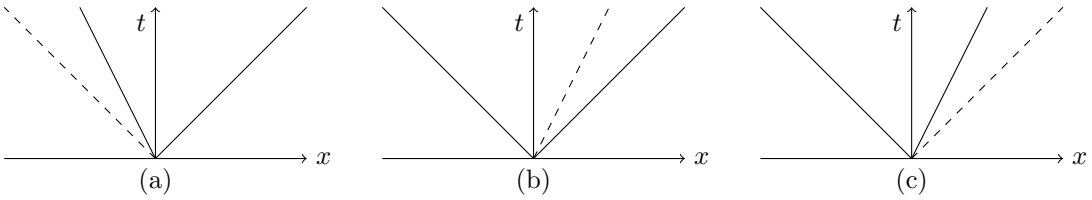

Figure 3.4: Wave patterns. Solid line: classical waves. Dashed line: Vapor-liquid interface

3.6.1 Case 1: Two-phase flow without phase transition

Let us first consider the case, where the phase transition is excluded, i.e. $z = 0$. In this case we have

Lemma 3.6.1. *There exists no solution of wave pattern types a) and c), which include the cases of the coincidence of the classical waves with the phase boundary.*

The lemma will be proven at the end of this section.

Now we consider Case *b*). For solutions of that type we use the following notations for the 4 constant states

$$\mathbf{W}_V = \begin{bmatrix} \rho_V \\ v_V \end{bmatrix} \quad \mathbf{W}_V^* = \begin{bmatrix} \rho_V^* \\ v_V^* \end{bmatrix} \quad \mathbf{W}_L^* = \begin{bmatrix} \rho_L^* \\ v_L^* \end{bmatrix} \quad \mathbf{W}_L = \begin{bmatrix} \rho_L \\ v_L \end{bmatrix} . \tag{3.6.2}$$

To find the exact solution we extend the procedure that is described for single gas flows by Toro in [20]. We aim to derive a function

$$f(p, \mathbf{W}_V, \mathbf{W}_L) = f_V(p, \mathbf{W}_V) + f_L(p, \mathbf{W}_L) + (v_L - v_V) , \tag{3.6.3}$$

such that the only root $p = p^*$ is the solution for the pressure p_V^* of the Riemann problem (3.2.1-3.2.2), (3.6.1). The functions f_V and f_L are the increments that relate the initial velocities v_V, v_L to v_V^* and v_L^* resp., only in terms of the initial data and the unknown solution p^*. This means that

$$v_V^* = v_V - f_V(p_*, \mathbf{W}_V) \qquad \text{and} \qquad v_L^* = v_L + f_L(p_*, \mathbf{W}_L) . \tag{3.6.4}$$

This procedure makes use of the constancy of pressure and velocity across the phase boundary, $v_V^* = v_L^*$ and $p_V^* = p_L^*$, which is due to $z = 0$.

Because p is constant in the star region, we choose p^* to be the unknown and eliminate ρ_V^*, ρ_L^*. However, for shorter notation we keep the initial data ρ_V, ρ_L.

We use the results in (3.5.2), (3.5.4) and (3.5.16). For a left wave we replace $'$ and $''$ by $_V$ and $^*_V$, resp. On the other hand, for a right wave $'$ and $''$ are replaced by $^*_L$ and $_L$. We end up with the following

Theorem 3.6.1 (**Solution of isothermal two-phase Euler equations without phase transition**). *Let $f(p, \mathbf{W}_V, \mathbf{W}_L)$ be given as*

$$f(p, \mathbf{W}_V, \mathbf{W}_L) = f_V(p, \mathbf{W}_V) + f_L(p, \mathbf{W}_L) + \Delta v \ , \ \Delta v = v_L - v_V$$

where the functions f_V and f_L are given by

$$f_V(p, \mathbf{W}_V) = \begin{cases} \frac{p - p_V}{\sqrt{\rho_V p}} & \text{if } p > p_V \ \textit{(shock)} \\ -a_V \ln p_V + a_V \ln p & \text{if } p \le p_V \ \textit{(rarefaction)} \end{cases}$$

$$f_L(p, \mathbf{W}_L) = \begin{cases} \frac{p - p_L}{\sqrt{K_0 \rho_L \left(\frac{p - p_0}{K_0} + 1\right)}} & \text{if } p > p_L \ \textit{(shock)} \\ -a_L \ln \frac{\rho_L}{\rho_0} + a_L \ln \left(\frac{p - p_0}{K_0} + 1\right) & \text{if } p \le p_L \ \textit{(rarefaction)} \end{cases} .$$

If the function $f(p, \mathbf{W}_V, \mathbf{W}_L)$ has a root p^* with $0 < p^* \le \tilde{p}$ and with $\tilde{p}$ as in Section 3.3, this root is unique and is the unique solution for pressure p_V^* of the Riemann problem (3.2.1-3.2.2), (3.6.1). The velocity v_V^* can be calculated as follows

$$v_V^* = \frac{1}{2}(v_V + v_L) + \frac{1}{2}\left(f_L(p_*, \mathbf{W}_L) - f_V(p_*, \mathbf{W}_V)\right) .$$

Proof. The function f is strictly monotone increasing in p with $f(p, \mathbf{W}_V, \mathbf{W}_L) \to -\infty$ for $p \to 0$. Therefore f has at most one unique root, which is by construction the solution for the pressure p_V^* of the Riemann problem considered. The second part of the theorem is an immediate consequence of (3.6.4). □

For given initial data one can define the sets of states that can be connected to the initial states by a single shock or rarefaction wave. These sets define curves in the p-v-phase plane, where the intersection point (p^*, v^*) is the solution due to Theorem 3.6.1, see Figure 3.5. In Figure 3.5 the black curve C_V belongs to the vapor phase, whereas the red curve C_L belongs to the liquid phase. The solid lines denote those states, that can be connected to the initial states, indicated by a star, by a rarefaction wave. Along the dash-dotted lines we have states, that may be connected to the initial states by a shock wave. The wave curves in Figure 3.5 belong to the data of the second example in Section 3.8.

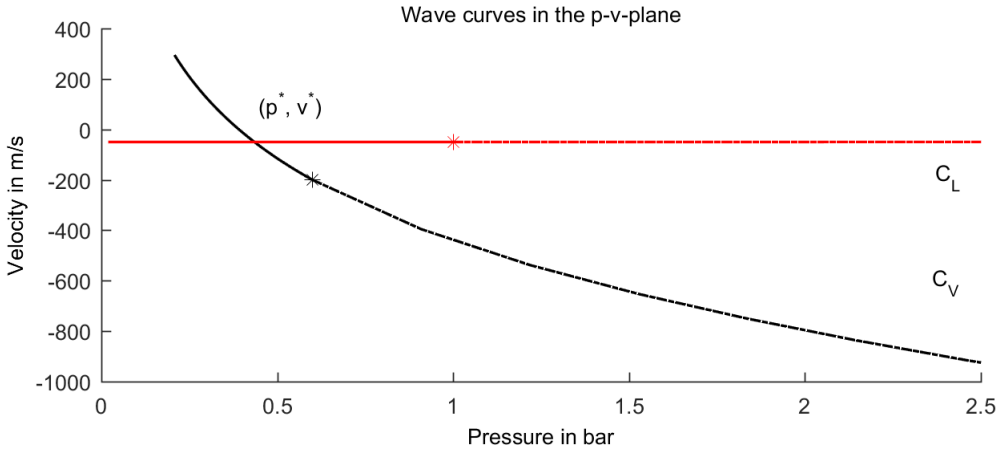

Figure 3.5: Wave curves in the p-v-phase plane

Theorem 3.6.2 (Sufficient condition for solvability). *Let us consider the Riemann problem (3.2.1-3.2.2), (3.6.1). We have two cases.*

- *For $p_L < p_V(\tilde{\rho}) = \tilde{p}$ the above Riemann problem is solvable if and only if*

$$f(\tilde{p}, \mathbf{W}_V, \mathbf{W}_L) = \frac{\tilde{p} - p_V}{\sqrt{\rho_V \tilde{p}}} + \frac{\tilde{p} - p_L}{\sqrt{\rho_L}(\tilde{p} - p_0 + K_0)} + \Delta v \geq 0\,.$$

- *For $p_L \geq \tilde{p}$ the above Riemann problem is solvable if and only if*

$$f(\tilde{p}, \mathbf{W}_V, \mathbf{W}_L) = \frac{\tilde{p} - p_V}{\sqrt{\rho_V \tilde{p}}} + a_L \ln\left(\frac{p_L - p_0 + K_0}{\tilde{p} - p_0 + K_0}\right) + \Delta v \geq 0\,.$$

Proof. As seen before f is strictly monotone increasing in p with $f(p, \mathbf{W}_V, \mathbf{W}_L) \to -\infty$ for $p \to 0$. Accordingly f has a unique root if and only if $f(p, \mathbf{W}_V, \mathbf{W}_L) \geq 0$ for $p \to \tilde{p}$. □

Remark 3.6.1 (Complete solution). *Theorems 3.6.1 and 3.6.2 allow us to calculate the pressure and the velocity in the star region as well as the interface velocity. From the equations of state (3.3.2) and (3.3.3) we find the densities ρ_V^*, ρ_L^* of the star region respectively. In the case of shock waves the relation (3.5.16) gives the shock speeds.*

For a left (right) rarefaction wave the head and tail speeds can be obtained from (3.5.2) or (3.5.4) respectively. The solution inside the fans is given by (3.5.3) respectively (3.5.5).

Finally we give the proof of Lemma 3.6.1.

Proof. We denote the states between the classical waves with two stars. The states between the right wave and the phase boundary have one star, also see Figure 3.6.

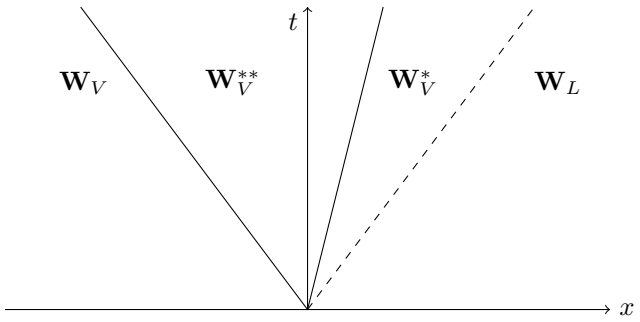

Figure 3.6: Wave pattern of type (c) with notation

Assume that the solution is of wave pattern type c). Then the interface is moving with speed $w = v_L = v_{V*}$. Let us further assume that the right wave is a shock wave moving with speed S_2. Obviously the condition $w \geq S_2$ must hold. To find S_2 we use $(3.5.16)_1$ and $(3.5.16)_2$. We replace $'$ and $''$ by $_{V**}$ and $_{V*}$ resp. We obtain

$$S_2 = w + \frac{a_V \rho_{V*}}{\sqrt{\rho_{V*}\rho_{V**}}},$$

which contradicts the condition $w \geq S_2$.

On the other hand if the right wave is a rarefaction wave, then the head speed is given by $a_V + v_{V*}$, see Subsection 3.5.1. This is likewise a contradiction to the condition $w = v_L = v_{V*} \geq a_V + v_{V*}$. If the phaseboundary lies within the rarefaction wave or at its tail we obtain the analogous contradiction in the wave speeds.

Accordingly there is no solution of type c). In an analogous manner we may discuss the case of wave pattern type a). □

3.6.2 Case 2: Two-phase flow with phase transition

The lemma corresponding to Lemma 3.6.1 is much more complicated in this case. For this reason we must discuss all three cases from Figure 3.4 and we start with Case b).

3.6.2.1 Solutions of type b)

To find the solution for the Riemann problem (3.2.1-3.2.2), (3.6.1) with phase transition we use the same strategy as before. Due to phase transition we have $v_L^* \neq v_V^*$ at the interface, which gives us a further term in the resulting algebraic equation. Moreover, a further challenge results from the inequality of the pressures $p_L^* \neq p_V^*$. Nevertheless we are able to construct a function

$$f_z(p, \mathbf{W}_V, \mathbf{W}_L) = f_V(p, \mathbf{W}_V) + f_L(p_L^*(p), \mathbf{W}_L) + z[\![\frac{1}{\rho}]\!] + (v_L - v_V) \tag{3.6.5}$$

such that the only root $p = p^*$ is the solution for the pressure p_V^* of the Riemann problem (3.2.1-3.2.2), (3.6.1) with phase transition. The functions f_V and f_L relate the initial velocities v_V, v_L to v_V^* and v_L^* respectively, only in terms of the initial data and the unknown solution p^* as well as the implicitely defined function $p_L^*(p^*)$.

As before we use the results in (3.5.2), (3.5.4) and (3.5.16). For a left wave we repalce $'$ and $''$ by $_V$ and $^*_V$, respectively. On the other hand, for a right wave $'$ and $''$ are replaced by $^*_L$ and $_L$. We end up with the following

Theorem 3.6.3 (Solution of isothermal two-phase Euler equations with phase transition). *Let $f_z(p, \mathbf{W}_V, \mathbf{W}_L)$ be given as*

$$f_z(p, \mathbf{W}_V, \mathbf{W}_L) = f_V(p, \mathbf{W}_V) + f_L(p_L^*(p), \mathbf{W}_L) + z[\![\frac{1}{\rho}]\!] + \Delta v\ ,\ \Delta v = v_L - v_V \tag{3.6.6}$$

where the functions f_V and f_L are given by

$$f_V(p, \mathbf{W}_V) = \begin{cases} \frac{p - p_V}{\sqrt{\rho_V p}} & \text{if } p > p_V \text{ (shock)} \\ -a_V \ln p_V + a_V \ln p & \text{if } p \leq p_V \text{ (rarefaction)} \end{cases}$$

$$f_L(p, \mathbf{W}_L) = \begin{cases} \frac{p_L^*(p) - p_L}{\sqrt{K_0 \rho_L \left(\frac{p_L^*(p) - p_0}{K_0} + 1\right)}} & \text{if } p_L^*(p) > p_L \text{ (shock)} \\ -a_L \ln \frac{\rho_L}{\rho_0} + a_L \ln\left(\frac{p_L^*(p) - p_0}{K_0} + 1\right) & \text{if } p_L^*(p) \leq p_L \text{ (rarefaction)}. \end{cases}$$

The function $p_L^*(p)$ is implicitely defined by (3.5.28) and z is given by (3.5.23).
If the function $f_z(p, \mathbf{W}_V, \mathbf{W}_L)$ has a root p^* with $0 < p^* \leq \tilde{p}$, see Section 3.3, this root is unique.

If further

$$p^* > p_V \qquad \text{we must have} \qquad z > -a_V \sqrt{\rho_V \rho_V^*}\,. \tag{3.6.7}$$

In this case the root p^* is the unique solution for the pressure p_V^* for a b)-type solution of the Riemann problem (3.2.1-3.2.2), (3.6.1) with phase transition and the complete solution is uniquely determined.

If there is no root or condition (3.6.7) is not satisfied the Riemann problem has no solution.

Proof. The function f_z is strictly increasing in p. This follows from Lemma 3.5.2 and Lemma 3.5.3. Further we have $f_z \to -\infty$ for $p \to 0$. Therefore f_z has at most one unique root, which is by construction the solution for p_V^* of the considered Riemann problem.

Then by Lemma 3.5.1 the pressure $p_L^*(p)$ and the mass flux z are uniquely defined. The corresponding densities can be obtained from the equations of state (3.3.2), (3.3.3). To find the velocities in the star regions one can use (3.5.2), (3.5.4) for rarefactions or (3.5.16) for shocks. The interface velocity can be obtained from (3.2.5).

The further calculations are the same as in the case of isothermal Euler equations without phase transition, see the proof for Theorem 3.6.1 and the remarks following. □

Remark 3.6.2. *The additional condition (3.6.7) in Theorem 3.6.3 is necessary to guarantee, that $S_1 \leq w$ in the case of a 1-shock propagating through the gas. If this condition is not satisfied, the root p^* of (3.6.6) is meaningless.*

As in the case of no phase transition in the previous section, one can construct the solution in the $p-v-$phase plane. We define the same sets of states as before. Moreover, for every state, that can be connected to (p_V, v_V) by a single wave, there exists a uniquely defined state (p_L^*, v_L^*), that can be connected to (p_V, v_V) by a phase boundary due to the kinetic relation (3.5.23). These states define a further wave curve $C_{L'}$, see Figure 3.7. The red and black curves C_L and C_V are identical to the case

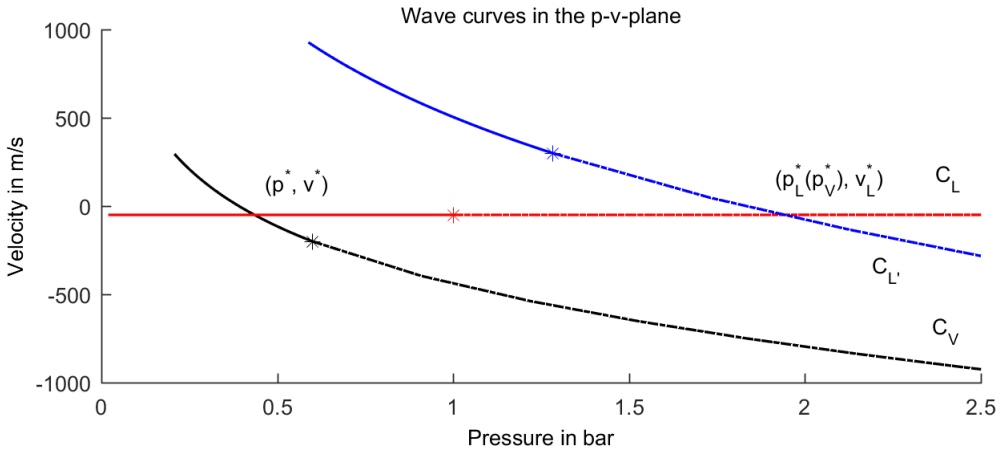

Figure 3.7: Wave curves in the $p-v-$phase plane

before. The blue curve $C_{L'}$ is newly defined, where the blue solid (dash-dotted) part of $C_{L'}$ corresponds to the black solid (dash-dotted) part of C_V. The intersection point of the blue and red curves $C_{L'}$ and C_L is the solution for $(p_L^*(p_V^*), v_L^*)$ due to Theorem 3.6.3. As before the wave curves in Figure 3.7 belong to the data of the second example in Section 3.8.

Theorem 3.6.4 (Sufficient condition for solvability I). *Let us consider the Riemann problem (3.2.1-3.2.2), (3.6.1). If the Riemann problem considered for Case 1 is solvable, then the same Riemann problem is also solvable taking into account phase transition due to the kinetic relation (3.5.23).*

The proof is obvious by the monotonicity properties of f_z. For details see the following corollary and its proof.

Proposition 3.6.1. *Let p^* be the solution of the pressure in the star region of the Riemann problem (3.2.1-3.2.2), (3.6.1) for Case 1. Then for the solutions p_V^* and $p_L^*(p_V^*)$ of the same Riemann problem for Case 2 we have*

1. $p^* = p_0$ *implies that* $p_V^* = p_L^*(p_V^*) = p_0$.
2. $p^* < p_0$ *implies that* $p^* < p_L^*(p_V^*) < p_0$.
3. $p^* > p_0$ *implies that* $p_0 < p_V^* < p^*$.

Proof. The first statement is obvious. Now let us consider $p^* < p_0$. Consider that $p_L^*(p_V^*) = p_0$. Then we have an equilibrium and therefore $p_V^* = p_0$ and further $f_z(p_0, \mathbf{W}_V, \mathbf{W}_L) = f(p_0, \mathbf{W}_V, \mathbf{W}_L) > 0$. Now $f_z(p_0, \mathbf{W}_V, \mathbf{W}_L) > 0$ and we obtain due to the monotonicity of f_z that $p_L^*(p_V^*) < p_0$. On the other hand, if $p_L^*(p_V^*) = p_*$ then $f_z(p_V^*, \mathbf{W}_V, \mathbf{W}_L) < f(p^*, \mathbf{W}_V, \mathbf{W}_L) = 0$ and we conclude the other inequality $p^* < p_L^*(p_V^*)$. The argumentation for the third statement is analogous. □

Theorem 3.6.5 (Sufficient condition for solvability II). *Let us consider the Riemann problem (3.2.1-3.2.2), (3.6.1) with phase transition. This Riemann problem is solvable by a b)-type solution if and only if*

$$f_z(\tilde{p}, \mathbf{W}_V, \mathbf{W}_L) \geq 0$$

and (3.6.7) is satisfied.

Proof. The statement is obvious, because the above requirement guarantees, that the function f_z has a root. □

3.6.2.2 Further solutions

As in Section 3.6.1 we want to discuss the existence of further solutions for the Riemann problem (3.2.1-3.2.2), (3.6.1) with phase transition. We obtain

Lemma 3.6.2. *There is no solution of type a).*

Proof. Assume, there is a solution of type a). Then analogously to solutions of type c) in Section 3.6.1 we denote the constant states by (ρ_V, v_v), (ρ_{L*}, v_{L*}), (ρ_{L**}, v_{L**}), (ρ_L, v_L), see Figure 3.6. Obviously in that case we have a condensation process and therefore $z < 0$. Assume the left wave is a rarefaction wave, then the head speed is given by $v_{L*} - a_L$ and

$$w = \frac{z}{\rho_{L*}} + v_{L*} \leq v_{L*} - a_L \tag{3.6.8}$$

must hold. We obtain $z \leq -a_L \rho_{L*}$. This contradicts (3.5.27) and therefore there is no solution of type a) with a left rarefaction.

Similarly, for a left shock wave

$$w = \frac{z}{\rho_{L*}} + v_{L*} < v_{L*} - a_L \sqrt{\frac{\rho_{L**}}{\rho_{L*}}}$$

must hold. This is a stronger inequality than (3.6.8) and therefore it cannot be satisfied. This proves the above statement. □

Lemma 3.6.3. *Consider the Riemann problem (3.2.1-3.2.2), (3.6.1) with phase transition. If $p_L \geq p_0$ there is no solution of type c).*

Proof. A solution of type c) implies an evaporation process. This requires that $p_L < p_0$. □

Lemma 3.6.4. *Consider the Riemann problem (3.2.1-3.2.2), (3.6.1) with phase transition. For sufficiently large p_L with $p_L \leq p_0$ there is no solution of type c).*

Proof. Assume, there is a solution of type c). Then analogously to the previous case of an a)-type solution for a right rarefaction

$$w = \frac{z}{\rho_{V*}} + v_{V*} \geq v_{V*} + a_V$$

must hold. On the other hand for a right shock wave we have

$$w = \frac{z}{\rho_{V*}} + v_{V*} > v_{V*} + a_V \sqrt{\frac{\rho_{V**}}{\rho_{V*}}}.$$

Accordingly

$$\frac{z}{\rho_{V*}} + v_{V*} < v_{V*} + a_V \qquad \Longleftrightarrow \qquad \frac{z}{\rho_{V*} a_V} < 1$$

is sufficient to guarantee, that there is no solution of type c). Due to $z > 0$ we obtain from (3.5.23) by a simple estimate

$$\frac{z}{\rho_{V*} a_V} < -\frac{1}{\sqrt{2\pi}} \ln \frac{p_{V*}}{p_0} .$$

Therefore, if

$$-\frac{1}{\sqrt{2\pi}} \ln \frac{p_{V*}}{p_0} \leq 1 \qquad \Longleftrightarrow \qquad p_{V*} \geq p_0 \exp(-\sqrt{2\pi})$$

there is no solution of type c). By the strict monotonicity of $p_L(p_{V*})$ the proof is complete, see Lemma 3.5.2. □

Remark 3.6.3. *Note that the inequality $p_L \geq p_L(p_0 \exp(-\sqrt{2\pi}))$ is sufficient, but not necessary for the statement of the above lemma.*

3.7 3-Phase flow

3.7.1 Condensation by compression

Now let us consider the Riemann problem for the isothermal Euler equations with the following initial data for $\rho_{V\pm} \in [0, \tilde{p}]$

$$\rho(x,0) = \begin{cases} \rho_- = \rho_{V-} & \text{for} \quad x < 0 \\ \rho_+ = \rho_{V+} & \text{for} \quad x > 0 \end{cases} \qquad \text{and} \qquad v(x,0) = \begin{cases} v_- = v_{V-} & \text{for} \quad x < 0 \\ v_+ = v_{V+} & \text{for} \quad x > 0 \,. \end{cases} \tag{3.7.1}$$

This means, we have a Riemann problem for a vapor phase only. Using the results of Section 3.5 we easily obtain

Theorem 3.7.1 (Solution of classical isothermal Euler equations). *Let the function f_{VV} be given as*

$$f_{VV}(p, \mathbf{W}_{V-}, \mathbf{W}_{V+}) = f_{V-}(p, \mathbf{W}_{V-}) + f_{V+}(p, \mathbf{W}_{V+}) + \Delta v \ , \ \Delta v = v_{V+} - v_{V-}$$

where the functions f_{V-} and f_{V+} are given by

$$f_{V-}(p, \mathbf{W}_{V-}) = \begin{cases} \frac{p - p_{V-}}{\sqrt{\rho_{V-} p}} & \text{if } p > p_{V-} \ \textit{(shock)} \\ -a_V \ln p_{V-} + a_V \ln p & \text{if } p \leq p_{V-} \ \textit{(rarefaction)} \end{cases}$$

$$f_{V+}(p, \mathbf{W}_{V+}) = \begin{cases} \frac{p - p_{V+}}{\sqrt{\rho_{V+} p}} & \text{if } p > p_{V+} \ \textit{(shock)} \\ -a_V \ln p_{V+} + a_V \ln p & \text{if } p \leq p_{V+} \ \textit{(rarefaction)} \end{cases} .$$

If the function $f_{VV}(p, \mathbf{W}_{V-}, \mathbf{W}_{V+})$ has a root p^* with $0 < p^* \leq \tilde{p}$, this root is unique and is the unique solution for pressure p_V^* of the Riemann problem (3.2.1-3.2.2), (3.7.1). The velocity v_V^* is given by

$$v_V^* = \frac{1}{2}(v_{V-} + v_{V+}) + \frac{1}{2}\left(f_{V+}(p_*, \mathbf{W}_{V+}) - f_{V-}(p_*, \mathbf{W}_{V-})\right) .$$

In principle this result is known with some small modifications, see for instance the book of Toro [20]. In the literature one usually looks for a pressure p^*, that is a root of the above algebraic equation. Due to $f_{VV} \to -\infty$ for $p \to 0$ and $f_{VV} \to +\infty$ for $p \to +\infty$ there is always a solution. The latter case is physically not meaningful because a sufficiently high pressure in a gas will lead to a phase transition to a liquid or solid phase. In contrast we only consider solutions, that satisfy the inequality $0 < p^* \leq \tilde{p}$, where $\tilde{p}$ denotes the maximally possible gas pressure. As a consequence one can find Riemann initial data without solution. If this happens we follow the following strategy.

Definition 3.7.1 (Nucleation criterion). *If there is no solution to the Riemann problem (3.2.1-3.2.2), (3.7.1) according to Theorem 3.7.1, then nucleation occurs.*

If this criterion is fulfilled, we look for a solution with two transition fronts (phase boundaries) and two classical waves. Next we discuss the possible wave patterns for condensation.

Lemma 3.7.1. *If there is a solution of the Riemann problem (3.2.1-3.2.2), (3.7.1) consisting of two classical waves and two phase boundaries, then no wave is propagating through the liquid. Waves may only occur in the gas.*

Proof. Assume, there is a solution with a classical wave propagating through the liquid phase. W.l.o.g. this wave is a left going wave. We denote the states to the left and right of this wave by $_{L*}$ and $_{L**}$, respectively. Furthermore, on the left hand side of this wave there is a phase boundary propagating with speed w_1. The state left to the phase boundary is denoted by $_{V*}$.

Obviously we have a condensation process. Accordingly $p_* > p_0$ and $p_{L*} > p_0$. This configuration is impossible due to Lemma 3.6.2. Analogously we discuss the case of a right going wave. □

We conclude, both waves propagate through the vapor phase. The possible wave patterns are given in Figure 3.8.

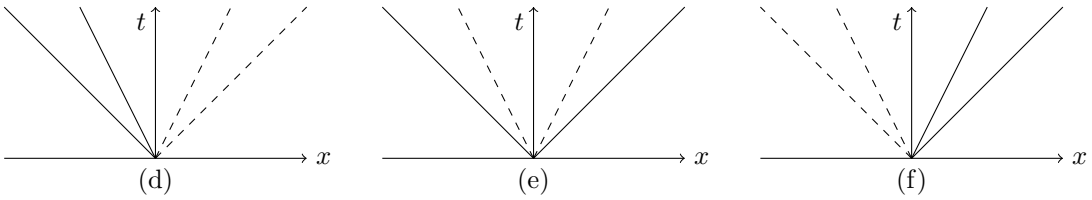

Figure 3.8: Wave patterns. Solid line: classical wave. Dashed line: phase boundary

Lemma 3.7.2. *There are no solutions of wave pattern types d) and f).*

Proof. Let us assume, that the solution is of wave pattern type *d)*. This corresponds to solutions of wave pattern type *c)* in Section 3.6.2.2, see Figure 3.4. We have seen, that such solutions only can occur for very low pressures, that imply evaporation, see Lemma 3.6.3 and Lemma 3.6.4. Here we have a condensation process, so wave pattern type *d)* is impossible. Analogously we can exclude solutions of wave pattern type *f)*. □

Accordingly the only possible wave configuration is of type *e)*. We use the notation as given in Figure 3.9 and obtain

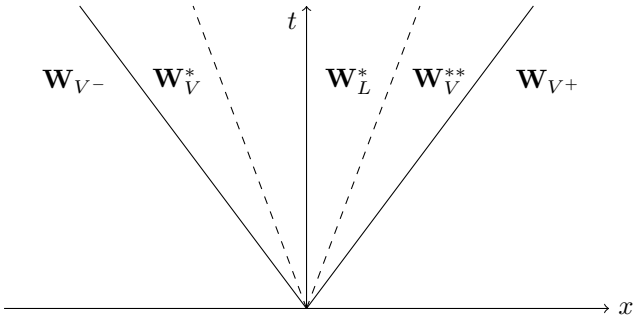

Figure 3.9: Notations, wave pattern type e).

Lemma 3.7.3. *Assume, there is a solution of wave pattern type e). Then* $p_{V*} = p_{V**}$.

Proof. For given p_{V*} the pressure p_{L*} is uniquely defined, cf. Lemma 3.5.1. The function $p_{L*}(p_{V*})$ is strictly monotone, see Lemma 3.5.2. For the second phase boundary we have to use the modified kinetic relation (3.5.24). We obtain the same pressure function $p_{L*}(p_{V**}) = p_{L*}(p_{V*})$ with the same monotonicity properties as in Section 3.5.3.4. □

Using the results of the previous sections and taking into account, that there are two phase boundaries we can formulate the following

Theorem 3.7.2 (Solution of isothermal Euler equations for two gases with phase transition). *Consider the Riemann problem (3.2.1-3.2.2), (3.7.1) and assume the nucleation criterion is satisfied. Let $f_{VVz}(p, \mathbf{W}_{V-}, \mathbf{W}_{V+})$ be given as*

$$f_{VVz}(p, \mathbf{W}_{V-}, \mathbf{W}_{V+}) = f_{V-}(p, \mathbf{W}_{V-}) + f_{V+}(p, \mathbf{W}_{V+}) + 2z[\![\frac{1}{\rho}]\!] + v_{V-} - v_{V+} = 0\,,$$

where the functions f_{V-} and f_{V+} are given by

$$f_{V-}(p, \mathbf{W}_{V-}) = \begin{cases} \frac{p-p_{V-}}{\sqrt{\rho_{V-}\,p}} & \text{if } p > p_{V-} \text{ (shock)} \\ -a_V \ln p_{V-} + a_V \ln p & \text{if } p \le p_{V-} \text{ (rarefaction)} \end{cases}$$
$$f_{V+}(p, \mathbf{W}_{V+}) = \begin{cases} \frac{p-p_{V+}}{\sqrt{\rho_{V+}\,p}} & \text{if } p > p_{V+} \text{ (shock)} \\ -a_V \ln p_{V+} + a_V \ln p & \text{if } p \le p_{V+} \text{ (rarefaction)} \end{cases}.$$

Here z is given by (3.5.23) and $[\![\frac{1}{\rho}]\!] = \frac{1}{\rho_{L*}} - \frac{1}{\rho_{V*}}$. The function $p_L^*(p)$ is implicitely defined by (3.5.28).

If the function f_{VVz} has a root with $p_0 < p \le \tilde{p}$, then this root is the only one. Furthermore, this root is the unique solution for pressure $p_{V*} = p_{V**}$ of the Riemann problem (3.2.1-3.2.2), (3.7.1) for the vapor pressure in the star regions. The liquid velocity v_{L*} can be calculated by

$$v_{L*} = \frac{1}{2}(v_{V-} + v_{V+}) + \frac{1}{2}\left(f_{V+}(p_*) - f_{V-}(p_*)\right)\,.$$

By previous results it is obvious, that the function f_{VVz} has at most one root. By construction this root is the solution for the pressure of the vapor phase in the two star regions in Figure 3.9.

The further calculations to find the complete solution are analogous to previous calculations.

Remark 3.7.1. *Note, that $v_{V*} \neq v_{V**}$ with $v_{V*} + v_{V**} = 2v_{L*}$.*

Theorem 3.7.3 (Sufficient condition for solvability I). *Consider the Riemann problem (3.2.1-3.2.2), (3.7.1). This problem is solvable without phase transition if and only if*

$$f_{VV}(\tilde{p}, \mathbf{W}_{V-}, \mathbf{W}_{V+}) \ge 0\,.$$

Proof. This statement is obvious by the monotonicity of f_{VV}. □

Theorem 3.7.4 (Sufficient condition for solvability II). *Consider the Riemann problem (3.2.1-3.2.2), (3.7.1) and assume that the nucleation criterion due to Definition 3.7.1 is satisfied. Taking into account phase transition this problem is solvable if and only if*

$$f_{VVz}(\tilde{p}, \mathbf{W}_{V-}, \mathbf{W}_{V+}) \ge 0\,.$$

Proof. This statement is obvious due to the monotonicity of f_{VVz}. □

3.7.2 Evaporation by expansion

In the following we consider the Riemann problem for the isothermal Euler equations with initial data $\rho_{L\pm} \ge \rho_{\min}$

$$\rho(x,0) = \begin{cases} \rho_- = \rho_{L-} & \text{for} \quad x < 0 \\ \rho_+ = \rho_{L+} & \text{for} \quad x > 0 \end{cases} \qquad \text{and} \qquad v(x,0) = \begin{cases} v_- = v_{L-} & \text{for} \quad x < 0 \\ v_+ = v_{L+} & \text{for} \quad x > 0\,, \end{cases} \tag{3.7.2}$$

i.e. the initial data only contain two states in a liquid phase.

We have seen, that at a planar phase boundary the liquid pressure is always positive. It is known from applications, that negative liquid pressures are possible. They give rise to cavitation in the liquid, see Doering [6]. Recall that in the liquid-vapor case a negative liquid pressure is forbidden, see (3.5.18). Now, in the liquid-liquid case we may meet negative pressures. The smallest pressure in the liquid is $p_{\min}$.

Using that definition we obtain

Theorem 3.7.5 (Solution of isothermal Euler equations for two states of a liquid without phase transition). *Let $f_{LL}(p, \mathbf{W}_{L-}, \mathbf{W}_{L+})$ be given as*

$$f_{LL}(p, \mathbf{W}_{L-}, \mathbf{W}_{L+}) = f_{L-}(p, \mathbf{W}_{L-}) + f_{L+}(p, \mathbf{W}_{L+}) + \Delta v \ , \ \Delta v = v_{L+} - v_{L-}$$

where the functions f_{L-} and f_{L+} are given by

$$f_{L-}(p, \mathbf{W}_{L-}) = \begin{cases} \frac{p-p_{L-}}{\sqrt{\rho_{L-}\, p}} & \text{if } p > p_{L-} \ \text{(shock)} \\ -a_L \ln \frac{\rho_{L-}}{\rho_0} + a_L \ln\left(\frac{p-p_0}{K_0} + 1\right) & \text{if } p \le p_{L-} \ \text{(rarefaction)} \end{cases}$$

$$f_{L+}(p, \mathbf{W}_{L+}) = \begin{cases} \frac{p-p_{L+}}{\sqrt{\rho_{L+}\, p}} & \text{if } p > p_{L+} \ \text{(shock)} \\ -a_L \ln \frac{\rho_{L+}}{\rho_0} + a_L \ln\left(\frac{p-p_0}{K_0} + 1\right) & \text{if } p \le p_{L+} \ \text{(rarefaction)} \end{cases} .$$

If the function $f_{LL}(p, \mathbf{W}_{L-}, \mathbf{W}_{L+})$ has a root p^* with $p_{\min} \le p^*$, this root is unique and is the unique solution for pressure p_L^* of the Riemann problem (3.2.1-3.2.2), (3.7.2). The velocity v_L^* is calculated from

$$v_L^* = \frac{1}{2}(v_{L-} + v_{L+}) + \frac{1}{2}\left(f_{L+}(p_*) - f_{L-}(p_*)\right) .$$

Remark 3.7.2. *For simplicity in our calculations we choose $p_{\min} = 0$, but also lower values are possible. Our theoretical results are general and do not depend on the special value of $p_{\min}$.*

Analogous to the above nucleation criterion we give the

Definition 3.7.2 (Cavitation criterion). *If there is no solution of the Riemann problem (3.2.1-3.2.2), (3.7.2) according to Theorem 3.7.5, then we may encounter cavitation.*

If this criterion is fulfilled, we look for a solution involving a vapor phase with two transition fronts (phase boundaries) and two classical waves. As before we discuss the possible wave patterns.

Lemma 3.7.4. *Assume there is a solution of the Riemann problem (3.2.1-3.2.2), (3.7.2) consisting of two classical waves and two phase boundaries. If further p_{L-}, p_{L+} are sufficiently large then no wave is propagating through the vapor.*

The proof is analogous to the proof of Lemma 3.6.4. A sufficient lower bound for p_{L-}, p_{L+} is given in Remark 3.6.3.

Lemma 3.7.5. *There is no solution of type d) and f), see Figure 3.8.*

The proof is analogous to the proof of Lemma 3.6.2.
Accordingly we construct solutions of type e), the notations are analogous to the notations in Figure 3.9. We obtain

Lemma 3.7.6. *Assume, there is a solution of wave pattern type e). Then $p_{L*} = p_{L**}$.*

The proof is analogous to the proof of Lemma 3.7.3.
The next theorem addresses wave pattern type e).

Theorem 3.7.6 (Solution for isothermal Euler equations for two liquids with phase transition). *Consider the Riemann problem (3.2.1-3.2.2), (3.7.2) and assume the cavitation criterion is satisfied. Let $f_{LLz}(p, \mathbf{W}_{L-}, \mathbf{W}_{L+})$ be given as*

$$f_{LLz}(p, \mathbf{W}_{L-}, \mathbf{W}_{L+}) = f_{L-}(p_L(p), \mathbf{W}_{L-}) + f_{L+}(p_L(p), \mathbf{W}_{L+}) + 2z[\![\frac{1}{\rho}]\!] + v_{L-} - v_{L+} = 0 \ ,$$

with f_{L-} and f_{L+} according to

$$f_{L-}(p_L^*(p), \mathbf{W}_{L-}) = \begin{cases} \frac{p_L^*(p)-p_{L-}}{\sqrt{\rho_{L-}\, p_L^*(p)}} & \text{if } p_L^*(p) > p_{L-} \ \text{(sh.)} \\ -a_L \ln \frac{\rho_{L-}}{\rho_0} + a_L \ln\left(\frac{p_L^*(p)-p_0}{K_0} + 1\right) & \text{if } p_L^*(p) \le p_{L-} \ \text{(rf.)} \end{cases}$$

$$f_{L+}(p_L^*(p), \mathbf{W}_{L+}) = \begin{cases} \frac{p_L^*(p)-p_{L+}}{\sqrt{\rho_{L+}\, p_L^*(p)}} & \text{if } p_L^*(p) > p_{L+} \ \text{(sh.)} \\ -a_L \ln \frac{\rho_{L+}}{\rho_0} + a_L \ln\left(\frac{p_L^*(p)-p_0}{K_0} + 1\right) & \text{if } p_L^*(p) \le p_{L+} \ \text{(rf.)} . \end{cases}$$

Here z is calculated from (3.5.23) and $[\![\frac{1}{\rho}]\!] = \frac{1}{\rho_{L*}} - \frac{1}{\rho_{V**}}$. The function $p_L^*(p)$ is implicitely defined by (3.5.28).

If the function f_{LLz} has a root with $p_{\min} \leq p$, then this root is unique. Further, this root uniquely determines the pressure p_V^* of the Riemann problem (3.2.1-3.2.2), (3.7.2) for the vapor pressure in the star region. Further, the vapor velocity v_{V*} is given by

$$v_{V*} = \frac{1}{2}(v_{L-} + v_{L+}) + \frac{1}{2}\left(f_{L+}(p_L^*(p_*)) - f_{L-}(p_L^*(p_*))\right) .$$

Proof. Due to our previous results it is obvious, that the function f_{LLz} has at most one root. By construction this root is the solution for the pressure of the vapor phase in the star region.

The further calculations leading to the complete solution are analogous to previous calculations. □

Theorem 3.7.7 (Sufficient condition for solvability I). *Consider the Riemann problem (3.2.1-3.2.2), (3.7.2). This problem is solvable without phase transition if and only if*

$$f_{LL}(p_{\min}, \mathbf{W}_{V-}, \mathbf{W}_{V+}) \leq 0 .$$

Proof. This statement is obvious due to monotonicity of f_{LL}. □

Theorem 3.7.8 (Sufficient condition for solvability II). *Consider the Riemann problem (3.2.1-3.2.2), (3.7.2) and assume the cavitation criterion is satisfied. If we admit phase transition, this problem is always solvable.*

Proof. This statement is obvious due to the fact that $z[\![\frac{1}{\rho}]\!] \to -\infty$ for $p_V^* \to 0$. □

3.8 Numerical results

In the following section we discuss some numerical examples. The calculations need the Boltzmann constant k and the mass of a single water molecule m_W

$$k = 1.380658 \cdot 10^{-23} J/K \qquad \text{and} \qquad m_W = \frac{2 \cdot 1.0079 + 15.9994}{6.02205 \cdot 10^{26}} kg .$$

The reference values used are tabled in [22].

3.8.1 Example 1: 2 phase flow, wave structure independent of phase transition

We consider an example in which the wave structure does not depend on whether a phase transition is modeled or not. The initial data and reference values for the first example are given by

$v_V = -100m/s$	$v_L = 100m/s$	$T_0 = 293.15K$	$K_0 = 10^9/0.45836Pa$
$p_V = 2300Pa$	$p_L = 1000Pa$	$\rho_0 = 1000/1.00184kg/m^3$	$p_0 = 2339Pa.$

Figure 3.10 shows for $z = 0$ the solution for velocity, pressure and density as well as the wave pattern. The phase boundary is indicated by the dotted red line. Figure 3.11 gives the solution for the same problem with $z \neq 0$, i.e. with phase transition. Both solutions have similar wave pattern.

Note that in the plots for density and velocity the jump across the shock wave is so small that it is not visible in the chosen scale. This is generally true for classical waves inside the liquid phase. The difference is only visible in a local zoom.

The solutions to Example 1 for the intermediate states $v_{V*}, p_{V*}, v_{L*}, p_{L*}$ for both cases are summarized in the following table

$v_{V*} = 100.0002m/s$	$v_{L*} = 100.0002m/s$	$v_{V*} = 42.5m/s$	$v_{L*} = 100.0004m/s$
$p_{V*} = 1335.3Pa$	$p_{L*} = 1335.3Pa$	$p_{V*} = 1561Pa$	$p_{L*} = 1699.5Pa .$

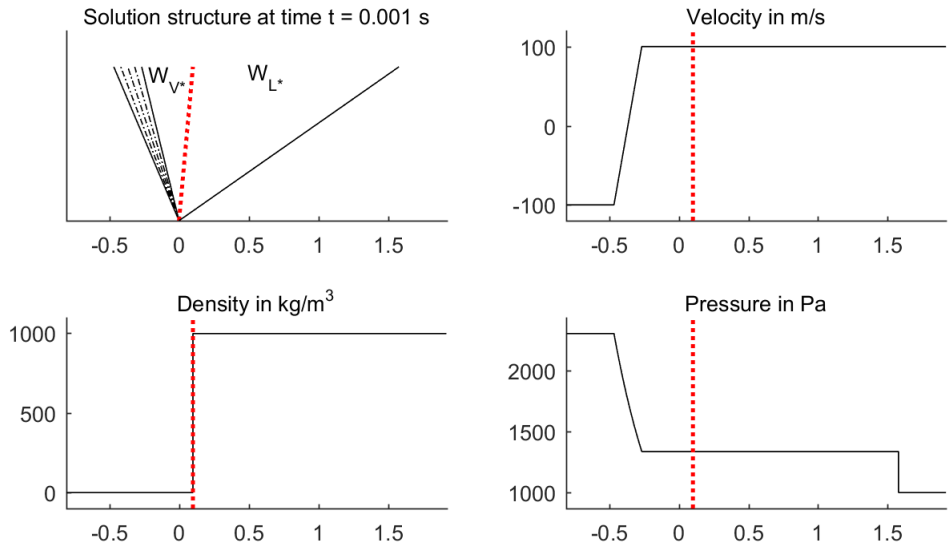

Figure 3.10: Example 1, without phase transition

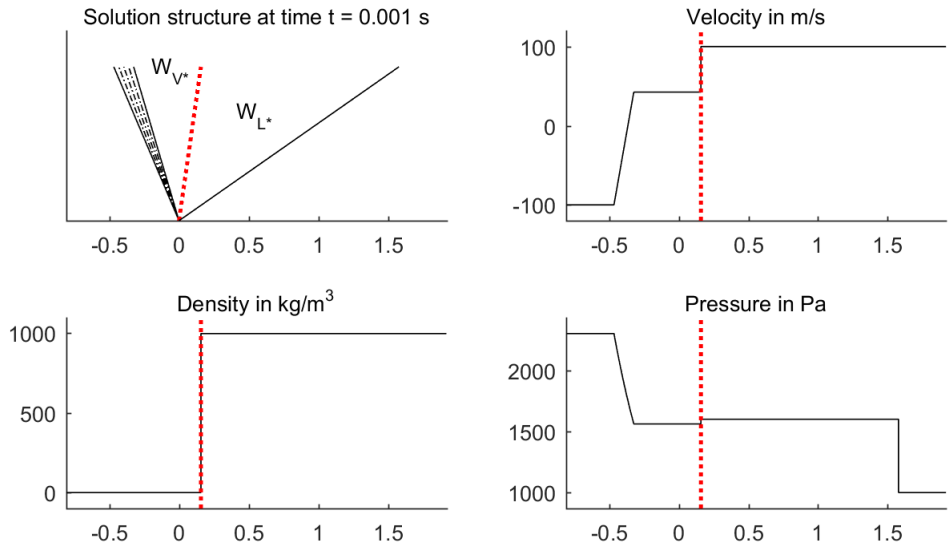

Figure 3.11: Example 1, with phase transition

3.8.2 Example 2: 2 phase flow, wave structure depending on phase transition

We now consider an example in which the wave type changes when a phase transition is introduced. The second example relies on

$v_V = -200m/s$	$v_L = -50m/s$	$T_0 = 473.15K$	$K_0 = 10^9/0.88383Pa$
$p_V = 60000Pa$	$p_L = 100000Pa$	$\rho_0 = 1000/1.15651kg/m^3$	$p_0 = 1554670Pa\,.$

In the case without phase transition the solution is composed of two rarefaction waves, see Figure 3.12, whereas the solution with phase transition possesses two shock waves, see Figure 3.13. The corresponding wave curves are given in Figure 3.5 of Subsection 3.6.1 and Figure 3.7 of Subsection 3.6.2. The solutions to Example 2 for the intermediate states $v_{V*}, p_{V*}, v_{L*}, p_{L*}$ for both cases are summarized in the following table

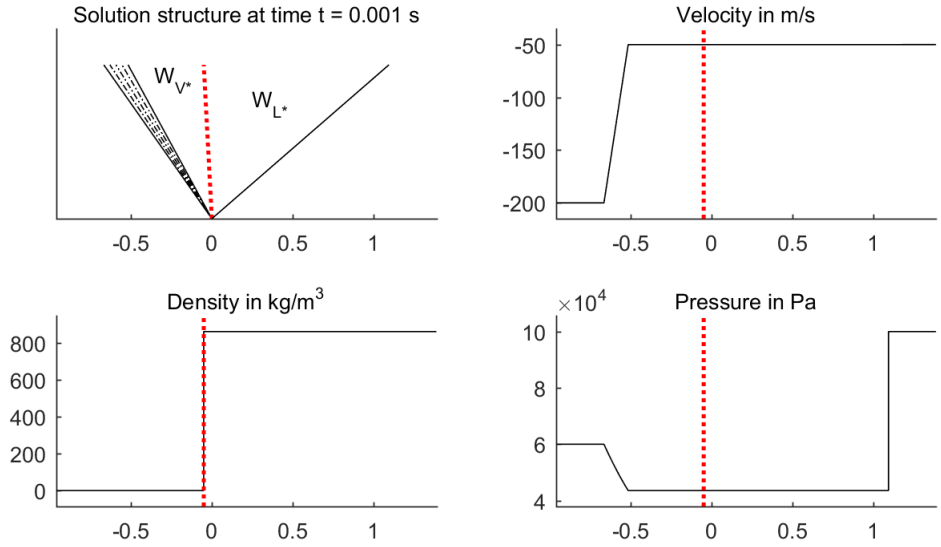

Figure 3.12: Example 2, without phase transition

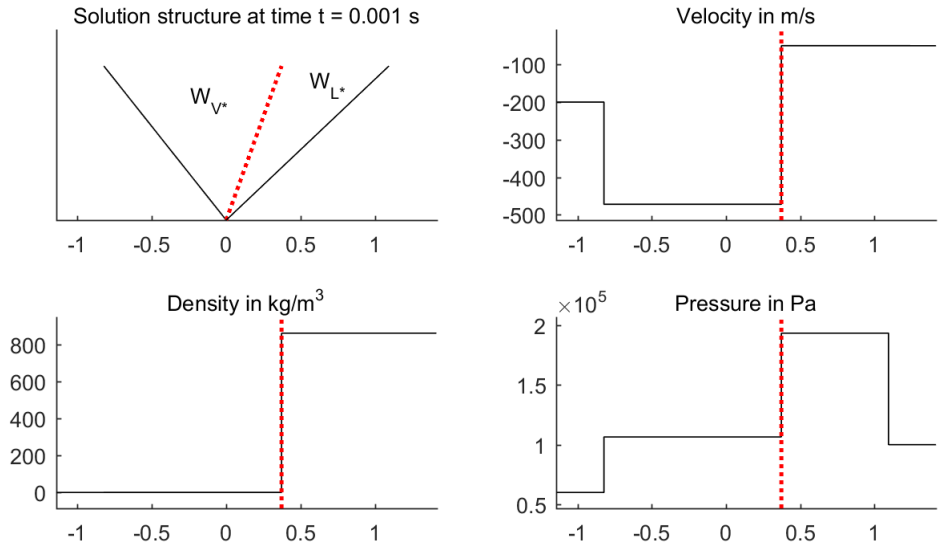

Figure 3.13: Example 2, with phase transition

$v_{V*} = -50.057m/s$	$v_{L*} = -50.057m/s$	$v_{V*} = -472m/s$	$v_{L*} = -49.905m/s$
$p_{V*} = 43531Pa$	$p_{L*} = 43531Pa$	$p_{V*} = 10652Pa$	$p_{L*} = 19346Pa\,.$

3.8.3 Example 3: Condensation by compression

In the third example the data are

$v_{V-} = 2.7m/s$	$v_{V+} = -2.7m/s$	$T_0 = 363.15K$	$K_0 = 10^9/0.47316Pa$
$p_{V-} = 70000Pa$	$p_{V+} = 70000Pa$	$\rho_0 = 1000/1.03594kg/m^3$	$p_0 = 70182.4Pa.$

The solution at time $t = 0.001s$ is illustrated in Figure 3.14, including a zoom plot to show the details. Further, the solutions to Example 3 for the intermediate states $v_{V*}, p_{V*}, v_{L*}, p_{L*}, v_{V**}, p_{V**}$ are summarized in the following table

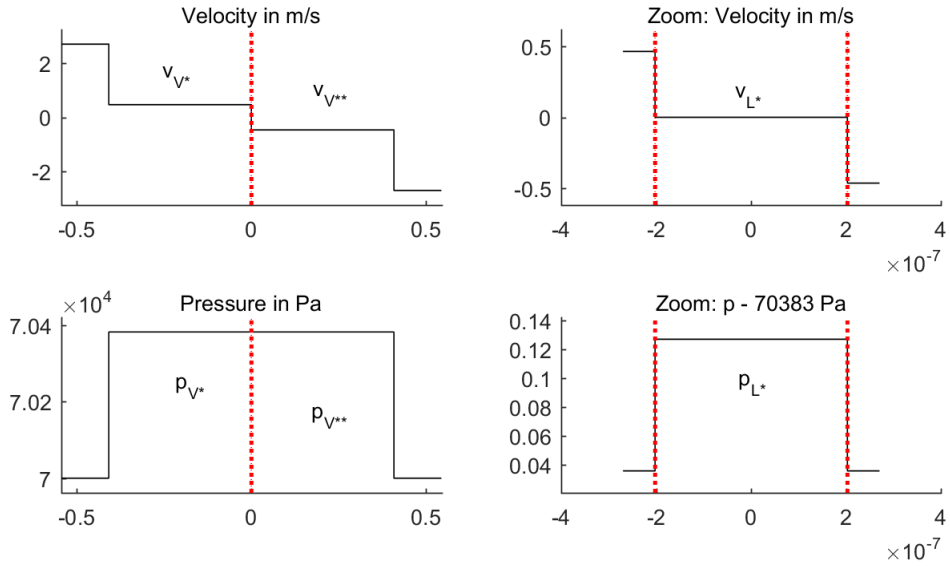

Figure 3.14: Example 3, condensation by compression

$v_{V*} = 0.465m/s$	$v_{L*} = 0$	$v_{V**} = -0.465m/s$
$p_{V*} = 70383.04Pa$	$p_{L*} = 70383.13Pa$	$p_{V**} = 70383.04Pa\,.$

3.8.4 Example 4 and 5: Evaporation by expansion

At first we start from the data

$v_{L-} = -40m/s$	$v_{L+} = 40m/s$	$T_0 = 363.15K$	$K_0 = 10^9/0.47316Pa$
$p_{L-} = 60000Pa$	$p_{L+} = 60000Pa$	$\rho_0 = 1000/1.03594kg/m^3$	$p_0 = 70182.4Pa$

and show the result at time $t = 0.001s$ in Figure 3.15. The same phenomenon is produced now by different data, namely

$v_{L-} = -20m/s$	$v_{L+} = 30m/s$	$T_0 = 363.15K$	$K_0 = 10^9/0.47316Pa$
$p_{L-} = 30000Pa$	$p_{L+} = 40000Pa$	$\rho_0 = 1000/1.03594kg/m^3$	$p_0 = 70182.4Pa.$

The Example 4 consists of two rarefaction waves and two phase transitions, whereas Example 5 exhibits two shock waves and two phase transitions, see Figure 3.16. The data for the intermediate states $v_{L*}, p_{L*}, v_{V*}, p_{V*}, v_{L**}, p_{**}$ for both examples are given in

$v_{L*} = -39.996m/s$	$v_{V*} = 0$	$v_{L**} = 39.996m/s$
$p_{L*} = 55188Pa$	$p_{V*} = 54665Pa$	$p_{L**} = 55188Pa$

and

$v_{L*} = -23.9m/s$	$v_{V*} = 4.3m/s$	$v_{L**} = 32.5m/s$
$p_{L*} = 59185Pa$	$p_{V*} = 58905Pa$	$p_{L**} = 59185Pa\,.$

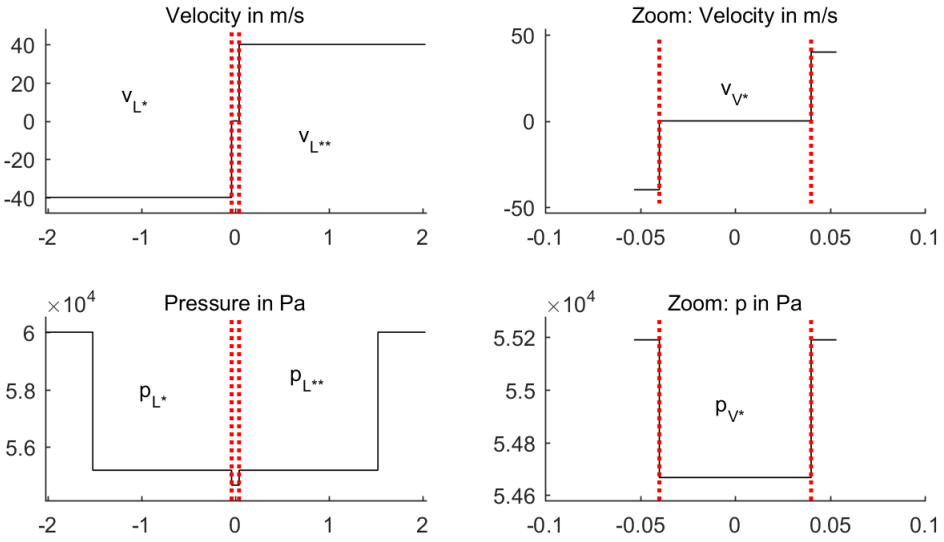

Figure 3.15: Example 4, evaporation by expansion

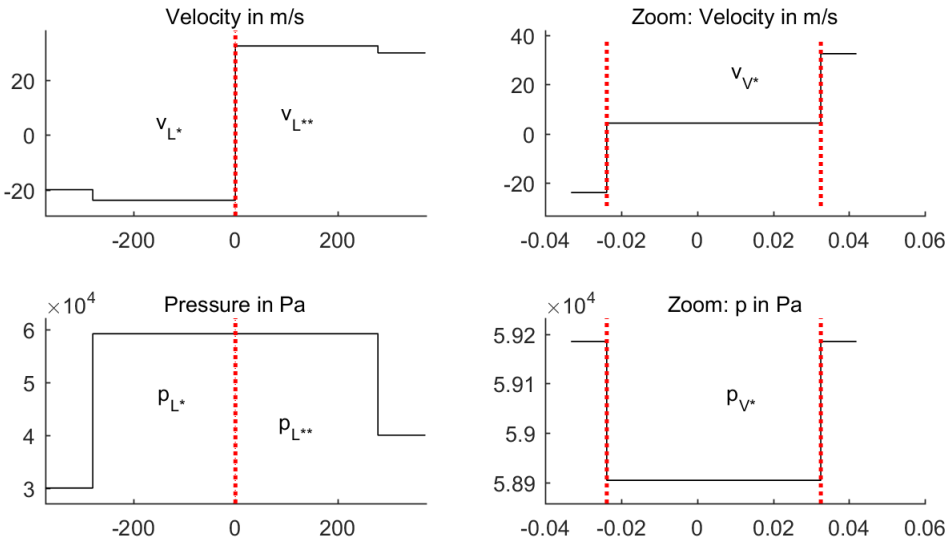

Figure 3.16: Example 5, evaporation by expansion

References

[1] R. Abeyaratne and J. K. Knowles. Kinetic relations and the propagation of phase boundaries in solids, *Arch. Rational Mech. Anal.*, **114** (1991), pp. 119-154.

[2] M. Baer and J. Nunziato. A two-phase mixture theory for the deflagration-to-detonation transition (DDT) in reactice granular materials, *Int. J. Multiphase Flows*, **12** (1986), pp. 861-889.

[3] S. Benzoni-Gavage, R. Danchin, S. Descombes, and D. Jamet. Stability issues in the Euler-Korteweg model, *Contemp. Math.*, **246** (2007), pp. 103-127.

[4] M. Bond and H. Struchtrup. Mean evaporation and condensation coefficients based on energy dependent condensation probability, *Phys. Rev. E.*, **70** (2004) 061605.

[5] C. M. Dafermos. *Hyperbolic Conservation Laws in Continuum Physics,* Springer-Verlag, Berlin - Heidelberg, 2010.

[6] W. Döring. Die Überhitzungsgrenze und Zerreißfestigkeit von Flüssigkeiten, *Z. physikal. Chem.*, Abt. B, Bd. **86** (1937), Heft 5/6.

[7] W. Dreyer. On jump conditions at phase boundaries for ordered and disordered phases, *WIAS Preprint*, **869** (2003).

[http://www.wias-berlin.de/main/publications/wias-publ/]

[8] W. Dreyer, F. Duderstadt, M. Hantke, and G. Warnecke. On phase change of a vapor bubble in liquid water, *WIAS Preprint*, **1424** (2009).

[http://www.wias-berlin.de/main/publications/wias-publ/]

[9] W. Dreyer, J. Giesselmann, C. Kraus, and C. Rohde. Asymptotic Analysis for Korteweg models, *WIAS Preprint*, **1545** (2010).

[http://www.wias-berlin.de/main/publications/wias-publ/]

[10] U. Grigull, S. Straub, and P. Schiebener. *Steam Tables in SI-Units, Wasserdampftafeln*, Springer-Verlag, Berlin, 1990.

[11] D. Kröner. *Numerical schemes for conservation laws*, John Wiley and Sons, Chichester, 1997.

[12] P. Lax. *Hyperbolic Systems of Conservation Laws and the Mathematical Theory of Shock Waves*, Society for Industrial and Applied Mathematics, Philadelphia, 1990.

[13] R. LeVeque. Numerical Methods for Conservation Laws, *Lectures in Mathematics ETH Zürich*, Birkhäuser Verlag, Basel - Boston - Berlin, 1990.

[14] R. Menikoff and B. J. Plohr. The Riemann problem for fluid flow of real materials, *Rev. of mod. Phys.*, **61** (1989), pp. 75-104.

[15] C. Merkle. *Dynamical Phase Transitions in Compressible Media*, Doctoral Thesis, Univ. Freiburg, 2006.

[16] I. Müller and W. Müller. *Fundamentals of Thermodynamics and Applications*, Springer-Verlag, Berlin, 2009.

[17] I. Müller. *Thermodynamics*, Pitman, London, 1985.

[18] S. Müller and A. Voss. The Riemann Problem for the Euler equations with nonconvex and nonsmooth equation of state: Construction of wave curves, *SIAM J. Sci. Comput.*, **28** (2006), pp. 651-681.

[19] J. Smoller. *Shock Waves and Reaction-Diffusion Equations*, Springer-Verlag, New York, 1994.

[20] E. F. Toro. *Riemann Solvers and Numerical Methods for Fluid Dynamics*, Springer-Verlag, Berlin - Heidelberg, 1999.

[21] A. Voss. *Exact Riemann Solution for the Euler Equations with Nonconvex and Nonsmooth Equation of state*, Doctoral Thesis, RWTH Aachen 2005.

[22] W. Wagner and H.-J. Kretzschmar. *International Steam Tables*, Springer-Verlag, Berlin - Heidelberg, 2008.

[23] A. Zein. *Numerical methods for multiphase mixture conservation laws with phase transition*, Doctoral Thesis, Univ. Magdeburg, 2010.

[24] A. Zein, M. Hantke, and G. Warnecke. Modeling phase transitions for compressible two-phase flows applied to metastable liquids, *J. Comput. Phys.*, **229** (2010), pp. 2964-2998.

Chapter 4

A general existence result

Bibliographic note: The content of this chapter contains the recently submitted work. F. Thein, M. Hantke. A general existence result for isothermal two-phase flows with phase transition. *Preprint:* https://arxiv.org/abs/1703.09431.

Abstract: Liquid-vapor flows with phase transitions have a wide range of applications. Isothermal two-phase flows described by a single set of isothermal Euler equations, where the mass transfer is modeled by a kinetic relation, have been investigated analytically in (Quarterly of applied Mathematics, vol. LXXI 3 (2013), pp. 509-540.). This work was restricted to liquid water and its vapor modeled by linear equations of state. The focus of the present work lies on the generalization of the primary results to arbitrary substances, arbitrary equations of state and thus a more general kinetic relation. We prove existence and uniqueness results for Riemann problems. In particular, nucleation and cavitation are discussed.

4.1 Introduction

Compressible liquid-vapor flows have a wide range of applications. Two-phase flow models are used to describe such processes, e.g. the formation of clouds, cavitation near moving objects in liquids such as ship propellers or certain phenomena in biology. Main difficulties in the modeling result from the phase interactions, especially from mass and energy transfer due to condensation or evaporation processes. Several two-phase flow models are available in the literature. They are mainly distinguished in sharp and diffusive interface models. For a detailed discussion of these models we refer to Zein [35] and concerning sharp interface models we exemplary refer to Bedeaux et al. [3]. In our work we study compressible two-phase flows with phase transitions across a sharp interface. Phase transitions are modeled using a kinetic relation. This concept was introduced by Abeyaratne and Knowles [1] for solid-solid phase transitions. This kinetic relation controls the mass transfer across the interface between the two adjacent phases. For a more general context of kinetic relations see LeFloch [19]. A detailed and very interesting survey on the Riemann problem for a large class of thermodynamic consistent constitutive models in the setting of Euler equations models can be found in Menikoff and Plohr [21]. Here the considerations are restricted to a simple kinetic relation that results from the assumption of local equilibrium at the interface.
In a recent work by Hantke et al. [12] Riemann problems relying on the isothermal Euler equations with a non-monotone pressure-density function are considered. This function is composed of three parts: the equations of state for the two single phases and an arbitrary relation for the intermediate state. The two phases are distinguished using the Maxwell construction, also known as the Equal-Area-Rule. The mass transfer is modeled via a kinetic relation, derived in [8], based on classical Hertz-Knudsen theory, see [4]. The authors discussed Riemann problems for various different cases of initial data and showed existence and uniqueness. Furthermore Hantke et al. also covered the cases of cavitation and nucleation. The constructed Riemann solutions are selfsimilar. They consist of constant states, separated by classical rarefaction and shock waves or phase boundaries. Nevertheless, the basic assumptions are very restrictive. Existence and uniqueness results are proven for liquid water and its vapor, modeled by linear equations of state.
Also Müller and Voss [26], [32] considered the isothermal Euler system. In contrast to the above men-

tioned work they modeled the fluid using the van der Waals equation of state. Instead of a kinetic relation the Liu entropy condition is used to achieve uniqueness. As a consequence Müller and Voss need non-classical composite waves to construct solutions. Further literature in this context is given by Merkle [22], Merkle and Rohde [23]. The focus of our present work is on the distinguished generalization of the results of Hantke et al. [12] resp. Menikoff and Plohr [21]. We consider two-phase flows for any regular fluid. Both phases can be modeled by any thermodynamic relevant equation of state. Further we construct exact Riemann solutions and prove existence and uniqueness results that advance achievements in the actual literature.
The paper is organized as follows. In Section 4.2 we present the balance equations in the bulk phases and the corresponding jump conditions across discontinuities. Further we give the thermodynamic framework needed throughout this work and discuss the Riemann problem in the isothermal case including the entropy inequality. In Section 4.3 we prove existence and uniqueness of a solution at the interface under certain appropriate assumptions. The following Section 4.4 contains a monotonicity argument needed to solve the two-phase Riemann problem, which is done subsequently. In Section 4.5 we present solutions to initial one-phase Riemann data leading to nucleation or cavitation, i.e. the creation of a new phase. We conclude this work with Section 4.6 where we give a detailed discussion of the assumptions made to state the previous results followed by some examples and the conclusion.

4.2 Isothermal Euler Equations

In this work we study inviscid, compressible and isothermal two phase flows.The two phases are either the liquid or the vapor phase of one substance. The phases are distinguished by the *mass density* ρ and further described by the *velocity* u. Sometimes it is convenient to use the *specific volume* $v = 1/\rho$ instead of the mass density. We will make the reader aware of such situations. The physical quantities depend on time $t \in \mathbb{R}_{\geq 0}$ and space $x \in \mathbb{R}$. In regular points of the bulk phases we have the conservation law for mass and the balance law for momentum, i.e.

$$\partial_t \rho + \partial_x(\rho u) = 0, \tag{4.2.1}$$
$$\partial_t(\rho u) + \partial_x(\rho u^2 + p) = 0. \tag{4.2.2}$$

The system of equations (4.2.1) and (4.2.2) is referred to as the *isothermal Euler equations*. The additional quantity p denotes the *pressure* and is related to the mass density via the *equation of state (EOS)* $p = p(\rho)$. Sometimes one also refers to the EOS as *pressure law*. Such an EOS crucially depends on the considered substance and how this substance is modeled. Across any discontinuity we have the following jump conditions

$$[\![\rho(u - W)]\!] = 0, \tag{4.2.3}$$
$$\rho(u - W)[\![u]\!] + [\![p]\!] = 0. \tag{4.2.4}$$

Here we write $[\![\Psi]\!] = \Psi^+ - \Psi^-$, where Ψ^+ is the right and Ψ^- the left sided limit of the physical quantity Ψ. Furthermore every discontinuity satisfies the following *entropy inequality*

$$\rho(u - W)[\![g + e^{kin}]\!] \leq 0. \tag{4.2.5}$$

Further, W denotes the speed of the discontinuity and $Z = -\rho(u - W)$ the *mass flux* where we will distinguish between a classical shock wave and the phase boundary (non-classical shock)

$$Z = \begin{cases} Q, & \text{shock wave} \\ z, & \text{phase boundary} \end{cases} \quad \text{and} \quad W = \begin{cases} S, & \text{shock wave} \\ w, & \text{phase boundary} \end{cases}.$$

4.2.1 Definition and Requirements for the *EOS*

Usually one only works with the pressure law when dealing with the Euler equations. Nevertheless the pressure law does not contain all the information about a fluid or more general a thermodynamic system. From a thermodynamic point of view a system in (local) equilibrium can be described relating the extensive quantities *energy* E, *volume* V and *entropy* S, i.e. $E(V, S)$. In the following we will use the

corresponding (intensive) densities and thus we use small letters (e.g.: e, v, s). Given this relation every other quantity can be derived using the first and second law of thermodynamics and the so called Maxwell relations. A condensed overview, including the difference between a complete and an incomplete EOS, can be found in [21]. For detailed information about EOS we refer to standard literature, cf. [2,18,24,25,28]. A discussion using the ideal gas EOS and the Tait EOS can also be found in [8]. From this point on we assume that we have an EOS for each phase with consistent thermodynamic properties. There are different possible thermodynamic potentials which can be used to describe a system and they are all connected to each other using the Legendre transform. Thus one can start from any potential and will get similar results. For the discussion of the equations at the interface we need the Gibbs energy and hence shortly summarize the most important features, i.e. those we need for our purpose. More details can be found in the above mentioned literature and references therein.

Definition 4.2.1 (Gibbs Energy and Sound Speed)**.** *The Gibbs energy is a function of the pressure p and the temperature T. The (complete) differential is given by*

$$\mathrm{d}g = -s\mathrm{d}T + v\mathrm{d}p.$$

Further we define the isothermal sound speed as

$$a = \sqrt{-v^2 \left(\frac{\partial p}{\partial v}\right)_T}.$$

From Definition 4.2.1 we obtain

$$\left(\frac{\partial g}{\partial p}\right)_T = v > 0, \quad \left(\frac{\partial^2 g}{\partial p^2}\right)_T = \left(\frac{\partial v}{\partial p}\right)_T = -\left(\frac{v}{a}\right)^2 < 0. \tag{4.2.6}$$

Since thermodynamic quantities may be expressed using different choices of independent variables the brackets with the subscript simply denote which quantity is held constant when calculating the derivative. In the isothermal case the Gibbs potential just depends on the pressure and hence we omit writing the brackets with subscript T. Here the volume v and the speed of sound a are strictly positive functions of the pressure p. Furthermore the inequality for the second derivative is due to the requirement of thermodynamic stability for an isothermal system. In short this can be seen by considering the requirements for the full case. There, thermodynamic stability requires the energy to be a convex function, both in the entropy and the volume. This implies that the Hessian of the energy is non negative. If we now assume the temperature to be constant, what remains is

$$0 \leq \frac{\mathrm{d}^2 e}{\mathrm{d}v^2} = -\frac{\mathrm{d}p}{\mathrm{d}v}. \tag{4.2.7}$$

In the following we use the subscripts $\{V, L\}$ when it is necessary to distinguish the vapor and the liquid phase. Since we are concerned with two phases we write g_L for the Gibbs energy of the liquid phase and g_V for the vapor phase, respectively. Further we require

$$\frac{\partial g_i}{\partial p_j} = 0, \ i \neq j, \ i, j \in \{V, L\}.$$

Since we only consider one substance the condition for two phases to be in equilibrium is

$$g_L(p_L) = g_V(p_V). \tag{4.2.8}$$

Due to the monotonicity of $g_K, \ K \in \{V, L\}$ we have

$$g_L(p_L) = g_V(p_V) \quad \Leftrightarrow \quad p_L = p_V$$

and we write in this case

$$p_L = p_V =: p_0 \quad \text{and} \quad g_L(p_0) = g_V(p_0).$$

A crucial point when dealing with different phases is how to discriminate them and how to connect them thermodynamically consistent. Equations of state describing two phases (e.g. *van der Waals* EOS) have

a so called spinodal region which is avoided by the Maxwell construction (or equal area rule). We want to discriminate the phases using the specific volumes. Therefore we need an upper bound for the liquid volume v_m and a lower bound for the vapor volume $\tilde{v}$. This should still be consistent with the Maxwell construction. Therefore we may proceed as follows. We use the EOS for each phase and prescribe the minimum liquid pressure p_{min} (e.g. $p_{min} = 0$) and from this we obtain v_m. Further we know the saturation pressure p_0 for a given temperature T_0 from a calculation or from tables which are available for many substances, such as for water [34]. Now we connect our two EOS monotonically and then obtain the maximum vapor pressure $\tilde{p}$ using the Maxwell construction, see [25].

Definition 4.2.2 (Maximum Vapor Pressure)**.** *Given a fixed temperature T_0 the corresponding saturation pressure p_0 is given by (4.2.8). Furthermore p_{min} is defined to be the minimum liquid pressure. Let $\bar{v}(p)$ be a function such that*

$$v_L(p_{min}) = \bar{v}(p_{min}), \quad v_V(\tilde{p}) = \bar{v}(\tilde{p}) \quad \text{and} \quad \bar{v}'(p) > 0.$$

Then the maximum vapor pressure $\tilde{p}$ is found as the solution of the following equation

$$0 = p_0(v_V(p_0) - v_L(p_0)) - \int_{v_L(p_0)}^{v_V(p_0)} p(v)\,\mathrm{d}v.$$

The function $p(v)$ given by

$$p(v) = \begin{cases} p_L(v),\ v \in \big(0, v_L(p_{min})\big] \\ \bar{p}(v),\ v \in \big(v_L(p_{min}), v_V(\tilde{p})\big), \\ p_V(v),\ v \in \big[v_V(\tilde{p}), \infty\big) \end{cases} .$$

Finally, analogous to [21] we introduce dimensionless quantities which we will use later on.

Definition 4.2.3 (Dimensionless Quantities)**.** *We define the (isothermal) dimensionless speed of sound as*

$$\gamma := -\frac{v}{p}\frac{\mathrm{d}p}{\mathrm{d}v}.$$

and the (isothermal) fundamental derivative

$$\mathcal{G} := -\frac{1}{2} v \frac{\dfrac{\mathrm{d}^2 p}{\mathrm{d}v^2}}{\dfrac{\mathrm{d}p}{\mathrm{d}v}}.$$

It is straight forward to verify and no surprise that these quantities are completely analogue to those defined in [21]. In fact, by using the relations given in [21] and assuming the temperature to be fixed, one also obtains the results given above. However we want to emphasize that γ and $\mathcal{G}$ defined here are *not equal* to those defined in [21]. This is because we assume the temperature to be constant, whereas in [21] the derivatives are taken at constant entropy. To clarify this, let us for the moment write γ_S for the isentropic quantity defined in [21]. Then we have (cf. [21])

$$\frac{\gamma}{\gamma_S} = \frac{c_V}{c_p}$$

and hence $\gamma \leq \gamma_S$ for thermodynamic stable systems. Further we have for γ, using Definition 4.2.1

$$\gamma = \frac{a^2}{pv}. \tag{4.2.9}$$

For the fundamental derivative one may also write

$$\mathcal{G} = \frac{1}{2}\frac{v^2}{p\gamma}\frac{\mathrm{d}^2 p}{\mathrm{d}v^2} = -\frac{v}{a}\frac{\mathrm{d}a}{\mathrm{d}v} + 1 \tag{4.2.10}$$

or when expressed in terms of the pressure

$$\mathcal{G} = \frac{a}{v}\frac{\mathrm{d}a}{\mathrm{d}p} + 1. \tag{4.2.11}$$

The *isotherms* in the $p - v$ plane are convex if $\mathcal{G} > 0$, which we will assume from now on.

4.2.2 Riemann Problem

In the following we briefly discuss the solution of the Riemann problem for the isothermal Euler equations (4.2.1)-(4.2.2) for a single phase. In order to do so we will discuss the elementary wave types that can occur, which are shock or rarefaction waves. The Riemann problem is given by equations (4.2.1)-(4.2.2), the EOS and the Riemann initial data

$$\rho(x,0) = \begin{cases} \rho_-,\, x<0 \\ \rho_+,\, x>0 \end{cases} \quad \text{and} \quad u(x,0) = \begin{cases} u_-,\, x<0 \\ u_+,\, x>0 \end{cases}. \tag{4.2.12}$$

We rewrite the system (4.2.1) - (4.2.2) in quasilinear form in terms of the primitive variables, i.e. the density ρ and the velocity u

$$\begin{pmatrix} \rho \\ u \end{pmatrix}_t + \begin{pmatrix} u & \rho \\ \frac{a^2}{\rho} & u \end{pmatrix} \begin{pmatrix} \rho \\ u \end{pmatrix}_x = 0. \tag{4.2.13}$$

The Jacobian matrix

$$\mathbf{A} = \begin{pmatrix} u & \rho \\ \frac{a^2}{\rho} & u \end{pmatrix} \tag{4.2.14}$$

has the following eigenvalues and corresponding eigenvectors

$$\lambda_1 = u - a, \quad \mathbf{r}_1 = \begin{pmatrix} \rho \\ -a \end{pmatrix}, \quad \lambda_2 = u + a, \quad \mathbf{r}_2 = \begin{pmatrix} \rho \\ a \end{pmatrix}. \tag{4.2.15}$$

Due to the requirement of thermodynamic stability (4.2.7) this system is hyperbolic. We have strict hyperbolicity for

$$\gamma > 0. \tag{4.2.16}$$

Furthermore one can immediately verify that the waves corresponding to the eigenvalues and eigenvectors are genuine nonlinear if and only if the fundamental derivative

$$\mathcal{G} = \frac{\rho}{a}\frac{\mathrm{d}a}{\mathrm{d}\rho} + 1.$$

does not vanish, i.e.

$$\nabla\lambda_{1/2} \cdot \mathbf{r}_{1/2} = \mp\frac{a}{\rho}\mathcal{G} \neq 0. \tag{4.2.17}$$

Here this is in fact the case, since we assumed $\mathcal{G} > 0$. For systems with genuine nonlinear waves the Lax condition is enough to pick the right solution, cf. [19] and also [21] for the full system. The Riemann invariants for this system are

$$I_1 = u + \int \frac{a}{\rho}\,\mathrm{d}\rho \quad \text{and} \quad I_2 = u - \int \frac{a}{\rho}\,\mathrm{d}\rho. \tag{4.2.18}$$

4.2.2.1 Entropy Inequality across a Shock Wave

Hantke et al. proved, that the Lax condition is equivalent to the entropy condition for an isothermal system. This holds true for the general entropy inequality given by (4.2.5)

$$Q[\![g + e^{kin}]\!] = -\rho(u - S)[\![g + e^{kin}]\!] \geq 0.$$

Consider two states

$$\begin{pmatrix} \rho_1 \\ u_1 \end{pmatrix} \quad \text{and} \quad \begin{pmatrix} \rho_2 \\ u_2 \end{pmatrix}$$

separated by a shock wave moving with speed S. Using the specific volume $v = 1/\rho$ one obtains

$$\frac{a(p_1)^2}{v(p_1)^2} < Q^2 < \frac{a(p_2)^2}{v(p_2)^2}. \tag{4.2.19}$$

which gives the Lax condition for a left Shock ($Q > 0$) and a right shock ($Q < 0$).

4.2.2.2 Rarefaction Wave

For a rarefaction wave we use the Riemann invariants (4.2.18) and hence obtain for a left rarefaction wave (corresponding to λ_1)

$$u_2 - u_1 = -\int_{\rho_1}^{\rho_2} \frac{a}{\rho}\,\mathrm{d}\rho. \tag{4.2.20}$$

Furthermore the slope inside the rarefaction is given by

$$\frac{\mathrm{d}x}{\mathrm{d}t} = \frac{x}{t} = \lambda_1 = u - a \tag{4.2.21}$$

and hence we obtain for the solution inside the rarefaction fan

$$u = \frac{x}{t} - a \quad \text{and} \quad F(\rho) = u - u_1 + \int_{\rho_1}^{\rho} \frac{a}{\sigma}\,\mathrm{d}\sigma = 0. \tag{4.2.22}$$

Here ρ is obtained as the root of $F(\rho)$. Similar we obtain the results for a right rarefaction

$$\begin{aligned} u_2 - u_1 = \int_{\rho_1}^{\rho_2} \frac{a}{\rho}\,\mathrm{d}\rho, \quad \frac{\mathrm{d}x}{\mathrm{d}t} = \frac{x}{t} = \lambda_2 = u + a, \\ u = \frac{x}{t} + a \quad \text{and} \quad F(\rho) = u - u_1 - \int_{\rho_1}^{\rho} \frac{a}{\sigma}\,\mathrm{d}\sigma = 0. \end{aligned} \tag{4.2.23}$$

4.2.2.3 Shock Wave

The relation across a shock wave is given by

$$[\![u]\!]^2 = -[\![p]\!][\![v]\!] = \frac{[\![p]\!][\![\rho]\!]}{\rho_1\rho_2} \quad \Leftrightarrow \quad [\![u]\!] = -\sqrt{-[\![p]\!][\![v]\!]} = -\sqrt{\frac{[\![p]\!][\![\rho]\!]}{\rho_1\rho_2}}. \tag{4.2.24}$$

4.2.2.4 Solution of the Riemann Problem

If we now want to solve the Riemann problem for the isothermal Euler equations we just have to connect the three constant states separated by the waves using the equations obtained above. Therefore we assume the left and right state to be given and use that the velocity between the waves is constant. The solution is obtained as the root of the following function

$$f(\rho, W_L, W_R) = f_R(\rho, W_R) + f_L(\rho, W_L) + u_R - u_L = 0, \tag{4.2.25}$$

$$f_K(\rho, W_K) = \begin{cases} \sqrt{\dfrac{[\![p]\!][\![\rho]\!]}{\rho\rho_K}}, \ \rho > \rho_K \ \text{(Shock)} \\ \displaystyle\int_{\rho_K}^{\rho} \frac{a(\sigma)}{\sigma}\,\mathrm{d}\sigma, \ \rho \le \rho_K \ \text{(Rarefaction)} \end{cases}, \quad K \in \{L, R\}.$$

Due to $p'(\rho) > 0$ we could also state this problems in terms of the unknown pressure p, i.e.

$$f(p, W_L, W_R) = f_R(p, W_R) + f_L(p, W_L) + u_R - u_L = 0, \tag{4.2.26}$$

$$f_K(p, W_K) = \begin{cases} \sqrt{-[\![p]\!][\![v]\!]}, \ p > p_K \ \text{(Shock)} \\ \displaystyle\int_{p_K}^{p} \frac{v(\zeta)}{a(\zeta)}\,\mathrm{d}\zeta, \ p \le p_K \ \text{(Rarefaction)} \end{cases}, \quad K \in \{L, R\}.$$

In order to investigate $f(p, W_L, W_R)$ we need information about the asymptotic behavior

$$v(p) \overset{p\to\infty}{\to} 0, \quad v(p) \overset{p\to 0}{\to} \infty \quad \text{and further} \quad \frac{\mathrm{d}v(p)}{\mathrm{d}p} \overset{(4.2.6)_2}{=} -\frac{v(p)^2}{a(p)^2} < 0.$$

We obtain for $f_K(p, W_K)$ in the case of a shock wave

$$\begin{aligned}\frac{\mathrm{d}}{\mathrm{d}p} f_K(p, W_K) &= \frac{-[\![v]\!] + [\![p]\!]\frac{v^2}{a^2}}{2\sqrt{-[\![p]\!][\![v]\!]}} > 0, \\ \frac{\mathrm{d}^2}{\mathrm{d}p^2} f_K(p, W_K) &= -\frac{1}{4(-[\![p]\!][\![v]\!])^{3/2}} \left(-4[\![p]\!]^2[\![v]\!]\frac{v^3}{a^4}\mathcal{G} + \left([\![p]\!]\frac{v^2}{a^2} - [\![v]\!] \right)^2 \right) < 0\end{aligned} \tag{4.2.27}$$

For a rarefaction wave we yield

$$\begin{aligned}\frac{\mathrm{d}}{\mathrm{d}p} f_K(p, W_K) &= \frac{v(p)}{a(p)} > 0, \\ \frac{\mathrm{d}^2}{\mathrm{d}p^2} f_K(p, W_K) &= -\frac{v(p)^2}{a(p)^3}\mathcal{G} < 0\end{aligned} \tag{4.2.28}$$

Combining (4.2.27) with (4.2.28) gives

$$\frac{\mathrm{d}}{\mathrm{d}p} f(p, W_L, W_R) > 0 \quad \text{and} \quad \frac{d^2}{dp^2} f(p, W_L, W_R) < 0. \tag{4.2.29}$$

Using the asymptotic behavior of $v(p)$ gives

$$f(p, W_L, W_R) \overset{p\to 0}{\to} -\infty \quad \text{and} \quad f(p, W_L, W_R) \overset{p\to\infty}{\to} +\infty \tag{4.2.30}$$

and hence we have a unique root which determines the solution of our system.

4.3 Solution at the Interface

The phase boundary separating the liquid and the vapor phase is a non-classical or under compressive shock, see [5] or [19] and references therein. Hence the Lax criterion alone will not give us a unique solution and we need a further relation at the interface. This equation is called *kinetic relation*. We use the kinetic relation derived by Dreyer et al. [8]. The kinetic relation is chosen such that the mass flux z is proportional to the jump term in the entropy inequality (4.2.5)

$$z[\![g + e^{kin}]\!] \geq 0.$$

If we assume the vapor left to the liquid phase the kinetic relation reads

$$z = \tau p_V [\![g + e^{kin}]\!] = \tau p_V [g_L - g_V + e_L^{kin} - e_V^{kin}]. \tag{4.3.1}$$

Otherwise we can use

$$z = -\tau p_V [g_L - g_V + e_L^{kin} - e_V^{kin}]. \tag{4.3.2}$$

In the following we will assume the first case. In this section we will prove that there exists a unique solution of the equations at the interface provided certain conditions hold. By this we mean that there exists a unique liquid (vapor) state for a prescribed vapor (liquid) state such that the following equations hold

$$\begin{aligned}[\![z]\!] &= 0, \\ -z[\![u]\!] + [\![p]\!] &= 0, \\ z &= \tau p_V [\![g + e^{kin}]\!].\end{aligned}$$

Here e^{kin} denotes the *kinetic energy*. Furthermore we have for the so called *mobility* $0 < \tau \in \mathbb{R}$. Usually one uses

$$\tau = \frac{1}{\sqrt{2\pi}} \left(\frac{m}{kT_0} \right)^{\frac{3}{2}} \tag{4.3.3}$$

where m denotes the mass of a single molecule, k the Boltzmann constant and T_0 the fixed temperature, see [4, 8]. Using the jump conditions (4.2.3)-(4.2.4) we can rewrite (4.3.1) and obtain

$$z = \tau p_V [\![g - \frac{1}{2} p(v_L + v_V)]\!]. \tag{4.3.4}$$

Furthermore we can combine the jump conditions and obtain

$$[\![p]\!] + z^2 [\![v]\!] = 0. \tag{4.3.5}$$

Together with the EOS and (4.3.4) equation (4.3.5) is a single equation for one unknown given one state at the phase boundary. For example we will prescribe the vapor pressure and then obtain the liquid pressure as the solution of equation (4.3.5). In the following we will assume as before that $\gamma_V \geq 0$ and $\mathcal{G}_K > 0$, $K \in \{V, L\}$. From the mathematical point of view we need further assumptions to solve the problem. A discussion will be given later on and it will turn out that these assumptions are rather liberal from a physical point of view, see Subsection 4.6.1. In the following we need the quotient of the specific volumes to be uniformly bounded as well as the corresponding sound speeds

$$\begin{aligned} &0 < \frac{v_L}{v_V} \leq \alpha < 1, \quad 0 < \frac{v_L}{v_V}\frac{a_V}{a_L} \leq \alpha\beta < 1, \quad \tau(1-\alpha)^2 a_V^3 < \gamma_V \quad \text{and} \\ &0 < p_V \leq \sigma_{max} p_0 \quad \text{with} \quad \sigma_{max} = \frac{1 + \sqrt{11 - 6\alpha}}{2}. \end{aligned} \tag{4.3.6}$$

Remark 4.3.1. *The specific volume and the speed of sound depend on the pressure but for convenience we often will not write out this dependence explicitly.*

Now we can state one of the main results of this work.

Theorem 4.3.1 (Existence and Uniqueness of a Solution at the Interface)**.** *For two phases each described by a thermodynamic consistent equation of state meeting the requirements (4.3.6) and*

$$-a_V/v_V \leq z \leq a_L/v_L$$

exists a unique solution of equation (4.3.5). Furthermore the mass flux z is uniquely defined. The liquid pressure can be written as a function of the vapor pressure and has the following properties

$$p_L^* = \varphi(p_V^*) \geq p_V^*, \ \varphi(p_0) = p_0, \ \frac{\mathrm{d}\varphi(p_V^*)}{\mathrm{d}p_V^*} > 0$$

In the remaining part of this section we will give the proof of this theorem.

4.3.1 Proof

The proof of Theorem 4.3.1 is based on the *implicit function theorem*. The main steps are the following

(i) We define a function $f(p_V, p_L)$, see (4.3.7), which we will analyze and where the roots correspond to the solution of (4.3.5).

(ii) The local existence of an admissible root, see Definition 4.3.1, for the equilibrium case (p_0, p_0) is given in Remark 4.3.2.

(iii) Lemma 4.3.2 and Lemma 4.3.3 state that the first order derivatives of $f(p_V, p_L)$ each have a sign for an admissible solution.

(iv) Uniqueness is shown in Lemma 4.3.4 and global existence is stated and proven in Lemma 4.3.5.

Replacing z in (4.3.5) using (4.3.4) we obtain

$$[\![p]\!] + \left(\tau p_V [\![g - \frac{1}{2} p(v_L + v_V)]\!] \right)^2 [\![v]\!] = 0.$$

According to this equation we define the following functions

$$\begin{aligned} h(p_V, p_L) &:= \tau[\![g - \frac{1}{2}p(v_L + v_V)]\!] \\ &= \tau\left[g_L(p_L) - g_V(p_V) - \frac{1}{2}(p_L - p_V)(v_L(p_L) + v_V(p_V))\right], \\ f(p_V, p_L) &:= [\![p]\!] + (p_V h(p_V, p_L))^2 [\![v]\!]. \end{aligned} \tag{4.3.7}$$

Obviously every root of (4.3.7) is a solution of (4.3.5) and we easily see

$$0 = f(p_V^*, p_L^*) \overset{[\![v]\!]\leq 0}{\Rightarrow} [\![p]\!] \geq 0. \tag{4.3.8}$$

Let us furthermore define the following

Definition 4.3.1 (Admissible Solution)**.** *Let (p_V^*, p_L^*) be a solution of $f(p_V^*, p_L^*) = 0$. We say this solution is admissible if further the following inequalities hold*

$$-\frac{a_V(p_V^*)}{v_V(p_V^*)} \leq p_V^* h(p_V^*, p_L^*) \leq \frac{a_L(p_L^*)}{v_L(p_L^*)}.$$

The quantities a_K and v_K with $K \in \{L, V\}$ are functions of the pressure as already mentioned in Remark 4.3.1. Thus the bounds are evaluated at the pressures (p_V^*, p_L^*) which solve $f(p_V^*, p_L^*) = 0$.

Remark 4.3.2. *It is immediately verified that a solution $f(p_V^*, p_L^*) = 0$ with $p_V^* = p_L^* =: p_0$ implies equilibrium $g_L(p_L^*) = g_V(p_V^*)$ and vice versa. Thus we further obtain*

$$f(p_0, p_0) = 0,\ \partial_{p_V} f(p_0, p_0) = -1,\ \partial_{p_L} f(p_0, p_0) = 1 \quad \textit{with} \quad p_0 h(p_0, p_0) = 0. \tag{4.3.9}$$

Hence there exists a neighborhood of $p_V = p_0$ such that (4.3.5) implicitly defines a function $p_L = \varphi(p_V)$ with $\varphi'(p_V) > 0$. Additionally (p_0, p_0) is an admissible solution with $z = 0$.

Lemma 4.3.1. *The function $h(p_V, p_L)$ is strictly monotonically decreasing in p_L under the given assumptions, i.e.*

$$\partial_{p_L} h(p_V, p_L) < 0.$$

Proof. We obtain for the partial derivative of $h(p_V, p_L)$ using $(4.2.6)_2$

$$\partial_{p_L} h(p_V, p_L) = \frac{\tau}{2}\left\{[\![v]\!] + [\![p]\!]\frac{v_L^2}{a_L^2}\right\}.$$

Let us consider $[\![p]\!] \geq 0$ since it is the only relevant case and the statement is obvious for $[\![p]\!] \leq$ anyway. Since $\mathcal{G}_L > 0$ we yield for the second partial derivative with respect to p_L using $(4.2.6)_2$ and (4.2.11)

$$\partial_{p_L}^2 h(p_V, p_L) = -\tau[\![p]\!]\frac{v_L^3}{a_L^4}\mathcal{G}_L < 0.$$

For $p_L = p_V$ we know that the Lemma is true and if we increase p_L the function is decreasing. Keep in mind that we have $[\![p]\!] > 0$. Hence we conclude $\partial_{p_L} h(p_V, p_L) < 0$. □

Corollary 4.3.1. *Every root of (4.3.7) with $z > 0$ is admissible.*

Proof. Using Lemma 4.3.1 one obtaines for $f(p_V^*, p_L^*) = 0$ with $z = p_V^* h(p_V^*, p_L^*)$

$$z^2 = (p_V^* h(p_V^*, p_L^*))^2 \overset{(4.3.7)}{=} -\frac{[\![p^*]\!]}{[\![v(p^*)]\!]} \overset{\text{Lemma}4.3.1}{<} \frac{a_L^2}{v_L^2}.$$

□

Lemma 4.3.2. *Let (p_V^*, p_L^*) be an admissible solution of $f(p_V^*, p_L^*) = 0$. Then the following inequality holds*

$$\partial_{p_L} f(p_V^*, p_L^*) > 0.$$

Proof. For the equilibrium solution (4.3.9) the stated relation is obvious. Let us consider $p_V^* h(p_V^*, p_L^*) > 0$. Using Lemma 4.3.1 and $[\![v]\!] < 0$ we have

$$\partial_{p_L} f(p_V^*, p_L^*) = 1 + 2\underbrace{(p_V^* h(p_V^*, p_L^*))}_{>0}\underbrace{(p_V^* \partial_{p_L} h(p_V^*, p_L^*))[\![v]\!]}_{>0} - \underbrace{(p_V^* h(p_V^*, p_L^*))^2 \frac{v_L^2}{a_L^2}}_{<1} > 0.$$

It remains to prove the Lemma for the case $p_V^* h(p_V^*, p_L^*) < 0$. We can write

$$\begin{aligned}
\partial_{p_L} f(p_V^*, p_L^*) &= 1 + 2(p_V^* h(p_V^*, p_L^*))(p_V^* \partial_{p_L} h(p_V^*, p_L^*))[\![v]\!] - (p_V^* h(p_V^*, p_L^*))^2 \frac{v_L^2}{a_L^2} \\
&= 1 + \tau p_V^* (p_V^* h(p_V^*, p_L^*))[\![v]\!]^2 \left(1 - (p_V^* h(p_V^*, p_L^*))^2 \frac{v_L^2}{a_L^2}\right) - (p_V^* h(p_V^*, p_L^*))^2 \frac{v_L^2}{a_L^2} \\
&= \left(1 - (p_V^* h(p_V^*, p_L^*))^2 \frac{v_L^2}{a_L^2}\right)\left(1 + \tau p_V^* (p_V^* h(p_V^*, p_L^*))[\![v]\!]^2\right).
\end{aligned}$$

The first term is positive, because of $-a_V/v_V \le p_V^* h(p_V^*, p_L^*) < 0$ and $a_V^2/v_V^2 < a_L^2/v_L^2$. For the second term we have

$$0 < 1 + \tau p_V^* (p_V^* h(p_V^*, p_L^*))[\![v]\!]^2 \quad \overset{p_V^* h(p_V^*, p_L^*) < 0}{\Leftrightarrow} \quad \tau < -\frac{1}{p_V^* (p_V^* h(p_V^*, p_L^*))[\![v]\!]^2}.$$

Indeed we obtain

$$-\frac{1}{p_V^* (p_V^* h(p_V^*, p_L^*))[\![v]\!]^2} > \frac{v_V}{p_V^* a_V [\![v]\!]^2} = \frac{1}{p_V^* v_V a_V \left(\frac{v_L}{v_V} - 1\right)^2} \overset{(4.3.6)_1}{\ge} \frac{\gamma_V}{(1-\alpha)^2 a_V^3} \overset{(4.3.6)_3}{>} \tau.$$

This proves the Lemma. □

Lemma 4.3.3. *Let (p_V^*, p_L^*) be an admissible solution of $f(p_V^*, p_L^*) = 0$. Then the following inequality holds*

$$\partial_{p_V} f(p_V^*, p_L^*) < 0. \tag{4.3.10}$$

Proof. Since we have $f(p_V^*, p_L^*) = 0$ we can write for $\partial_{p_V} h(p_V^*, p_L^*)$

$$\partial_{p_V} h(p_V^*, p_L^*) = \frac{\tau}{2}\left\{[\![v]\!] + [\![p]\!]\frac{v_V^2}{a_V^2}\right\} \overset{(4.3.7)}{=} \frac{\tau}{2}[\![v]\!]\left(1 - (p_V^* h(p_V^*, p_L^*))^2 \frac{v_V^2}{a_V^2}\right) \tag{4.3.11}$$

and hence we conclude

$$\partial_{p_V} h(p_V^*, p_L^*) \begin{cases} < 0, & (p_V^* h(p_V^*, p_L^*))^2 < \dfrac{a_V^2}{v_V^2}, \\ \ge 0, & (p_V^* h(p_V^*, p_L^*))^2 \ge \dfrac{a_V^2}{v_V^2}. \end{cases}$$

In the following we will discuss three cases depending on $p_V^* h(p_V^*, p_L^*)$.

First Case: We discuss the case where $-a_V/v_V \le p_V^* h(p_V^*, p_L^*) \le 0$. It is obvious to see

$$\partial_{p_V} f(p_V^*, p_L^*) = \left\{\begin{matrix} -1 & , & p_V^* h(p_V^*, p_L^*) = 0, \\ 2\dfrac{a_V^2}{p_V^* v_V^2}[\![v]\!] & , & p_V^* h(p_V^*, p_L^*) = -\dfrac{a_V}{v_V} \end{matrix}\right\} < 0.$$

In between we have $-a_V/v_V < p_V^* h(p_V^*, p_L^*) < 0$ and so all together

$$\begin{aligned}
&\partial_{p_V} f(p_V^*, p_L^*) = \dots \\
&= -1 + 2\underbrace{(p_V^* h(p_V^*, p_L^*))}_{<0}\underbrace{(h(p_V^*, p_L^*) + p_V^* \partial_{p_V} h(p_V^*, p_L^*))}_{<0}[\![v]\!] + \underbrace{(p_V^* h(p_V^*, p_L^*))^2 \frac{v_V^2}{a_v^2}}_{<1} < 0.
\end{aligned}$$

For $0 < p_V^* h(p_V^*, p_L^*) < a_L/v_L$ we split the proof into two parts. First we discuss the interval up to a_V/v_V and then the remaining part smaller than a_L/v_L.

Second Case: Using $0 < p_V^* h(p_V^*, p_L^*) \leq a_V/v_V$ we obtain

$$\begin{aligned}
&\partial_{p_V} f(p_V^*, p_L^*) = \dots \\
&= -1 + 2(p_V^* h(p_V^*, p_L^*))(h(p_V^*, p_L^*) + p_V^* \partial_{p_V} h(p_V^*, p_L^*))[\![v]\!] + (p_V^* h(p_V^*, p_L^*))^2 \frac{v_V^2}{a_V^2} \\
&\overset{(4.3.11)}{=} \underbrace{\left(1 - (p_V^* h(p_V^*, p_L^*))^2 \frac{v_V^2}{a_V^2}\right)}_{\geq 0} \left(\tau {p_V^*}^2 h(p_V^*, p_L^*)[\![v]\!]^2 - 1\right) + \underbrace{2p_V^* (h(p_V^*, p_L^*))^2 [\![v]\!]}_{<0}.
\end{aligned}$$

For the second term we obtain (as before in the proof of Lemma 4.3.2)

$$0 > \tau p_V^* (p_V^* h(p_V^*, p_L^*))[\![v]\!]^2 - 1 \quad \overset{p_V^* h(p_V^*, p_L^*) > 0}{\Leftrightarrow} \quad \tau < \frac{1}{p_V^* (p_V^* h(p_V^*, p_L^*))[\![v]\!]^2}.$$

and again we have

$$\frac{1}{p_V^* (p_V^* h(p_V^*, p_L^*))[\![v]\!]^2} \geq \frac{v_V}{p_V^* a_V [\![v]\!]^2} = \frac{1}{p_V^* v_V a_V \left(\frac{v_L}{v_V} - 1\right)^2} \overset{(4.3.6)_1}{\geq} \frac{\gamma_V}{(1-\alpha)^2 a_V^3} \overset{(4.3.6)_3}{>} \tau.$$

This proves the Lemma for $0 < p_V^* h(p_V^*, p_L^*) \leq a_V/v_V$.

Third Case: We discuss $a_V/v_V < p_V^* h(p_V^*, p_L^*) < a_L/v_L$ and rewrite $\partial_{p_V} f(p_V^*, p_L^*)$ to obtain with an analogue argument as used before

$$\begin{aligned}
&\partial_{p_V} f(p_V^*, p_L^*) = \dots \\
&= -1 + 2(p_V^* h(p_V^*, p_L^*))(h(p_V^*, p_L^*) + p_V^* \partial_{p_V} h(p_V^*, p_L^*))[\![v]\!] + (p_V^* h(p_V^*, p_L^*))^2 \frac{v_V^2}{a_V^2} \\
&= -\left(1 - (p_V^* h(p_V^*, p_L^*))^2 \frac{v_V^2}{a_V^2}\right) + 2(p_V^* h(p_V^*, p_L^*))(p_V^* \partial_{p_V^*} h(p_V^*, p_L^*))[\![v]\!] + 2p_V^* h(p_V^*, p_l^*)^2 [\![v]\!] \\
&\overset{(4.3.11)}{=} -\frac{2}{\tau [\![v]\!]} \partial_{p_V} h(p_V^*, p_L^*) + p_V^* h(p_V^*, p_L^*))(p_V^* \partial_{p_V^*} h(p_V^*, p_L^*))[\![v]\!] + 2p_V^* h(p_V^*, p_l^*)^2 [\![v]\!] \\
&= \underbrace{-\frac{2}{\tau [\![v]\!]} \partial_{p_V} h(p_V^*, p_L^*)}_{>0} \underbrace{\left(1 - \tau p_V^* [\![v]\!]^2 p_V^* h(p_V^*, p_L^*)\right)}_{\substack{(4.3.6) \\ <0}} + \underbrace{2p_V^* h(p_V^*, p_l^*)^2 [\![v]\!]}_{<0} < 0.
\end{aligned}$$

This ends the proof. □

Corollary 4.3.2 (Monotonicity of the Implicit Function)**.** *Let (p_V^*, p_L^*) be an admissible solution $f(p_V^*, p_L^*) = 0$. Then there exists a function φ with $p_L^* = \varphi(p_V^*)$ which is strictly monotonically increasing, i.e. $\varphi'(p_V^*) > 0$.*

Proof. This follows using the implicit function theorem together with Lemma 4.3.2 and 4.3.3. □

Corollary 4.3.3. *During a condensation process both pressures are larger than the saturation pressure*

$$p_0 < p_V < p_L$$

whereas during evaporation both pressures are smaller than the saturation pressure

$$p_V < p_L < p_0.$$

Proof. This follows from Corollary 4.3.2 and $p_L(p_0) = p_0$. □

Lemma 4.3.4 (Uniqueness)**.** *Let (p_V^*, p_L^*) be an admissible solution of $f(p_V^*, p_L^*) = 0$. Then this root is unique in the sense that for a given p_V^* the solution p_L^* is unique.*

Proof. First we assume that there exists a $p_L^{**} > p_L^*$ such that $f(p_V^*, p_L^{**}) = 0$. From Lemma 4.3.2 we know that $\partial_{p_L} f(p_V^*, p_L^*) > 0$. Hence we have (monotonicity argument) $\partial_{p_L} f(p_V^*, p_L^{**}) \leq 0$. Therefore we have

$$\underbrace{p_V^* h(p_V^*, p_L^{**}) < -\frac{a_V}{v_V}}_{\mathbf{I}} \quad \dot{\vee} \quad \underbrace{p_V^* h(p_V^*, p_L^{**}) > \frac{a_L}{v_L}}_{\mathbf{II}} \tag{4.3.12}$$

otherwise we would meet the requirements of Lemma 4.3.2. Since $p_V^* h(p_V^*, p_L^*) \leq a_L/v_L$ and Lemma 4.3.1 we can exclude **II**. Assuming **I** is true we have that the root (p_V^*, p_L^{**}) itself is not admissible and every possible further root with $p_L > p_L^{**}$ would also fulfill relation **I** due to Lemma 4.3.1 and thus is not admissible.
Now we assume that there exists a $p_L^{**} < p_L^*$ such that $f(p_V^*, p_L^{**}) = 0$. As in the first case we have the two possibilities (4.3.12). The arguments are now quite analogue to the first case. We can exclude **I** since

$$-\frac{a_V}{v_V} \leq p_V^* h(p_V^*, p_L^*) < p_V^* h(p_V^*, p_L^{**}).$$

Therefore relation **II** must hold and p_L^{**} is no admissible root. Due to Lemma 4.3.1 every further solution $p_L < p_L^{**}$ also fulfills **II**. This proves uniqueness. □

Lemma 4.3.5 (Global Existence)**.** *For every $p_V^* \in [0, \sigma_{max} p_0]$ exists a $p_L^* \in [p_V^*, \infty)$ such that (p_V^*, p_L^*) is an admissible root of $f(p_V^*, p_L^*) = 0$.*

Proof. We already have local existence in a neighborhood of (p_0, p_0) due to the implicit function theorem. In the following we discriminate the cases depending on whether p_V is smaller or larger than the saturation pressure p_0.

First Case ($\mathbf{0 \leq p_V < p_0}$): Assume that there exists a $p_V < p_0$ such that there exists *no* p_L with $f(p_V, p_L) = 0$. Using the above results we know that there exists an admissible root (p_V^*, p_L^*) in the neighborhood of (p_0, p_0) and due to monotonicity/continuity a further root $p_V < \bar{p}_V < p_V^*$ and $\bar{p}_L$ such that

$$f(\bar{p}_V, \bar{p}_L) = 0 \ \wedge \ \partial_{p_L} f(\bar{p}_V, \bar{p}_L) = 0.$$

Hence this root is *not* admissible due to Lemma 4.3.2. On the other hand we have, due to the behavior of the function $h(p_V, p_L)$ in (p_0, p_0) and the fact that

$$f(p_V, p_L) = 0 \ \wedge \ h(p_V, p_L) = 0 \quad \Leftrightarrow \quad [\![p]\!] = 0,$$

that $h(\bar{p}_V, \bar{p}_L) > 0$ for $\bar{p}_V < p_0$. Together with Corollary 4.3.1 this gives

$$0 < \bar{p}_V h(\bar{p}_V, \bar{p}_L) \leq \frac{a_L}{v_L}.$$

This contradicts the above statement that the root $\bar{p}_V$ is not admissible. Therefore the nonexistence assumption is wrong and we have global existence for $0 \leq p_V < p_0$.

Second Case ($\mathbf{p_0 < p_V \leq \sigma_{max} p_0}$): The idea is again to show, that there exists no $p_0 < p_V^* \leq \sigma_{max} p_0$ such that

$$f(p_V^*, p_L^*) = 0 \ \wedge \ \partial_{p_L} f(p_V^*, p_L^*) = 0. \tag{4.3.13}$$

Let us assume we have (p_V^*, p_L^*) such that the above relation holds. From that we can conclude

$$\begin{aligned} &\partial_{p_L} f(p_V^*, p_L^*) = 0 \quad \Leftrightarrow \\ &(p_V^* h(p_V^*, p_L^*))^2 = (1 + 2(p_V^* h(p_V^*, p_L^*))(p_V^* \partial_{p_L} h(p_V^*, p_L^*))[\![v]\!]) \frac{a_L^2}{v_L^2}. \end{aligned}$$

Inserting this expression in $0 = f(p_V^*, p_L^*)$ gives

$$\begin{aligned}
0 = f(p_V^*, p_L^*) &= [\![p]\!] + (p_V^* h(p_V^*, p_L^*))^2 [\![v]\!] \\
&= [\![p]\!] + (1 + 2(p_V^* h(p_V^*, p_L^*))(p_V^* \partial_{p_L} h(p_V^*, p_L^*))[\![v]\!]) \frac{a_L^2}{v_L^2} [\![v]\!] \\
&= [\![p]\!] + [\![v]\!] \frac{a_L^2}{v_L^2} + 2(p_V^* h(p_V^*, p_L^*))(p_V^* \partial_{p_L} h(p_V^*, p_L^*))[\![v]\!]^2 \\
&= \frac{2}{\tau} \frac{a_L^2}{v_L^2} \partial_{p_L} h(p_V^*, p_L^*) + 2(p_V^* h(p_V^*, p_L^*))(p_V^* \partial_{p_L} h(p_V^*, p_L^*))[\![v]\!]^2 \\
&= \frac{2}{\tau} \partial_{p_L} h(p_V^*, p_L^*) \frac{a_L^2}{v_L^2} \left(1 + \tau \, {p_V^*}^2 h(p_V^*, p_L^*)[\![v]\!]^2\right)
\end{aligned}$$

We define the function

$$H(p_V, p_L) = 1 + \tau p_V^2 h(p_V, p_L)[\![v]\!]^2.$$

Due to Lemma 4.3.1 we have $H(p_V^*, p_L^*) = 0$ and hence

$$p_V^* h(p_V^*, p_L^*) = -\frac{1}{\tau p_V^* [\![v]\!]^2}. \tag{4.3.14}$$

Further we can rewrite $\partial_{p_L} f(p_V, p_L)$ in terms of $H(p_V, p_L)$, i.e.

$$\partial_{p_L} f(p_V, p_L) = -\frac{v_L^2}{(\tau p_V a_L [\![v]\!]^2)^2} (H(p_V, p_L) - 1)^2 + \left(1 + \frac{[\![p]\!]}{[\![v]\!]} \frac{v_L^2}{a_L^2}\right) (H(p_V, p_L) - 1) + 1.$$

From this we immediately get

$$\begin{aligned}
H(p_V, p_L) = \partial_{p_L} f(p_V, p_L) \quad &\Leftrightarrow \\
0 = (H(p_V, p_L) - 1) &\left(-\frac{v_L^2}{(\tau p_V a_L [\![v]\!]^2)^2} (H(p_V, p_L) - 1) + \frac{[\![p]\!]}{[\![v]\!]} \frac{v_L^2}{a_L^2}\right).
\end{aligned}$$

For the considered root (p_V^*, p_L^*) we can exclude the first case since $H(p_V^*, p_L^*) = 1$ if and only if $p_V^* h(p_V^*, p_L^*) = 0$. Hence we further look at the second term which must vanish for (p_V^*, p_L^*) and obtain

$$H(p_V^*, p_L^*) = \left(\tau p_V^* [\![v]\!]^2\right)^2 \frac{[\![p]\!]}{[\![v]\!]} + 1 \quad \Leftrightarrow \quad p_V^* h(p_V^*, p_L^*) = \tau p_V^* [\![p]\!][\![v]\!]. \tag{4.3.15}$$

Summing up we can state that there are two conditions (4.3.14) and (4.3.15) which need to be true for (p_V^*, p_L^*) when (4.3.13) holds. For equation (4.3.14) we easily verify

$$p_V^* h(p_V^*, p_L^*) = -\frac{1}{\tau p_V^* [\![v]\!]^2} \overset{(4.3.6)_1}{\leq} -\frac{1}{\tau p_V^* v_V^2 (1 - \alpha)^2} \overset{(4.3.6)_3}{<} -\frac{a_V}{v_V}. \tag{4.3.16}$$

Now we investigate (4.3.15) and prove that this implies $p_V^* h(p_V^*, p_L^*) > -a_V / v_V$. This would contradict (4.3.16) and hence finish the proof.
First we introduce the following functions for fixed p_V^*

$$\begin{aligned}
F(p_L) &:= p_V^* h(p_V^*, p_L), & F'(p_L) &= p_V^* \partial_{p_L} h(p_V^*, p_L), \\
G(p_L) &:= \tau p_V^* [\![p]\!][\![v]\!], & G'(p_L) &= \tau p_V^* \left\{ [\![v]\!] - [\![p]\!] \frac{v_L^2}{a_L^2} \right\}.
\end{aligned}$$

We immediately verify for all $p_L \geq p_V^*$

$$G'(p_L) < F'(p_L) < 0.$$

Furthermore we have

$$G(p_V^*) = 0 \overset{p_V^* > p_0}{>} F(p_V^*) = p_V^* h(p_V^*, p_V^*) = \tau p_V^* [\![g(p_V^*)]\!].$$

Surely there is a $\bar{p}_L > p_V^*$ such that

$$G(\bar{p}_L) = -\frac{a_V}{v_V} \quad \text{with} \quad \bar{p}_L = p_V^* - \frac{a_V}{\tau p_V^* v_V [\![v]\!]} \leq p_V^* + \frac{a_V}{\tau p_V^* v_V^2 (1-\alpha)}. \tag{4.3.17}$$

Now we investigate $F(\bar{p}_L)$ and obtain

$$F(\bar{p}_L) = p_V^* h(p_V^*, \bar{p}_L) = \tau p_V^* \left\{ [\![g]\!] - \frac{1}{2} [\![p]\!] (v_L + v_V) \right\} \overset{(4.3.17)}{=} \tau p_V^* ([\![g]\!] - v_V [\![p]\!]) + \frac{1}{2} \frac{a_V}{v_V}.$$

We have for $p_V^* = \sigma p_0$ with $\sigma \in [1, \sigma_{max}]$

$$\begin{aligned}
&\tau p_V^* \left([\![g]\!] - v_V [\![p]\!] \right) \overset{g_L(\bar{p}_L) > g_L(p_V^*)}{>} \tau p_V^* \left([\![g(p_V^*)]\!] - v_V [\![p]\!] \right) \\
&\overset{(4.3.17)}{\geq} \tau p_V^* \left\{ [\![g(p_V^*)]\!] - \frac{a_V}{\tau p_V^* v_V (1-\alpha)} \right\} = \tau p_V^* [\![g(p_V^*)]\!] - \frac{a_V}{v_V (1-\alpha)} \\
&\overset{\text{Taylor}}{\geq} \tau p_V^* [\![v(p_0)]\!] (p_V^* - p_0) - \frac{a_V}{v_V (1-\alpha)} > \frac{v_V(p_0)}{a_V(p_0) [\![v(p_0)]\!]} \sigma(\sigma - 1) p_0 - \frac{a_V}{v_V (1-\alpha)} \\
&\geq -\frac{a_V(p_0)}{v_V(p_0)} \frac{\sigma(\sigma-1)}{1-\alpha} - \frac{a_V}{v_V(1-\alpha)} \\
&\overset{\frac{\mathrm{d}}{\mathrm{d}p} \frac{a(p)}{v(p)} > 0}{>} -\frac{a_V(p_V^*)}{v_V(p_V^*)} \frac{\sigma(\sigma-1) - 1}{1-\alpha} \\
&\overset{\sigma \leq \sigma_{max}}{\geq} -\frac{3}{2} \frac{a_V}{v_V}.
\end{aligned}$$

This gives us $F(\bar{p}_L) > G(\bar{p}_L)$ and so there exists a $p_L^{**} \in (p_V^*, \bar{p}_L)$ such that

$$F(p_L^{**}) = G(p_L^{**}) > -\frac{a_V}{v_V}. \tag{4.3.18}$$

Thus condition (4.3.15) contradicts the first condition (4.3.14). Hence there exists *no* (p_V^*, p_L^*) such that

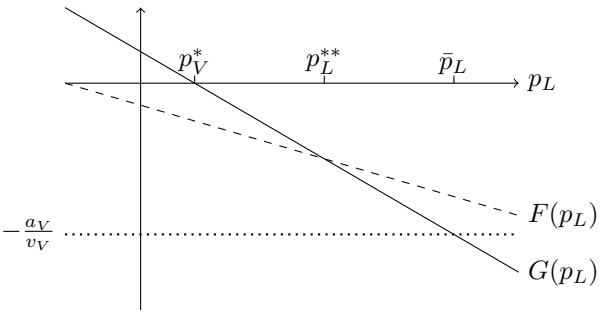

Figure 4.1: Idea for the contradiction argument

relation (4.3.13) holds. This implies global existence for all $p_0 < p_V \leq \sigma_{max} p_0$ and finishes the proof. □

4.4 Solution of the Two Phase Riemann Problem

In this section we want to solve the Riemann problem. Therefore we follow the strategy of constructing *wave curves* and obtain the solution as the intersection of the wave curves, as for example done in [21,31]. Due to the phase boundary we have an additional term, but we still want to show uniqueness of a solution

to the Riemann problem. Hence we need a further monotonicity argument which we will prove in the following.
To this end we additionally need bounds for the dimensionless speed of sound γ_V and γ_L. We distinguish two relevant cases, each with an appropriate condition needed to prove monotonicity. This is necessary especially for EOS (or equivalently fluids) near the critical point, e.g. *van der Waals* EOS. Further these conditions show that the dimensionless quantities are not independent of each other. We consider the following relevant cases

$$(\mathbf{I}) \begin{cases} \gamma_V & \leq 1 \quad \text{and} \quad 1 \leq \gamma_L \quad \text{with,} \\ \dfrac{1}{\gamma_L} & \geq 1 + \dfrac{\varepsilon(\gamma_V)}{\alpha}. \end{cases} \tag{4.4.1}$$

$$(\mathbf{II}) \begin{cases} \gamma_V & < 1 \quad \text{and} \quad \gamma_L < 1 \quad \text{with,} \\ \alpha & \leq \dfrac{1 - \frac{1}{\gamma_V}}{1 - \frac{1}{\gamma_L}} \quad \text{and} \quad \varepsilon(\gamma_V) \leq 0. \end{cases}$$

The quantity $\varepsilon(\gamma_V)$ is defined as follows, using all quantities as introduced before,

$$\varepsilon(\gamma_V) := \frac{1}{\gamma_V} - 1 - \frac{\tau a_V^3}{\gamma_V^2}(1-\alpha)^2\left(1 - (\alpha\beta)^2\right). \tag{4.4.2}$$

So far we proved in Section 4.3 that there exists a unique solution of the jump conditions at the interface. Furthermore we can express the pressure in the liquid phase as a strictly monotone increasing function of the vapor pressure

$$p_L^* = \varphi(p_V^*) \quad \text{with} \quad \varphi'(p_V^*) > 0.$$

Lemma 4.4.1. *Given the requirements (4.3.6) and (4.4.1). For an admissible solution $f(p_V^*, p_L^*) = 0$ the following monotonicity holds*

$$\frac{\mathrm{d}}{\mathrm{d}p_V}\left(p_V^* h(p_V^*, p_L^*)[\![v]\!]\right) \geq 0.$$

Proof. We have

$$\begin{aligned} \frac{\mathrm{d}}{\mathrm{d}p_V}\left(p_V^* h(p_V^*, p_L^*)[\![v]\!]\right) &= \partial_{p_V}\left(p_V^* h(p_V^*, p_L^*)[\![v]\!]\right) + \partial_{p_L}\left(p_V^* h(p_V^*, p_L^*)[\![v]\!]\right)\varphi'(p_V^*) \\ &= \left(h(p_V^*, p_L^*) + p_V^* \partial_{p_V} h(p_V^*, p_L^*)\right)[\![v]\!] + p_V^* h(p_V^*, p_L^*)\frac{v_V^2}{a_V^2} \\ &\quad + \left\{ p_V^* \partial_{p_L} h(p_V^*, p_L^*)[\![v]\!] - p_V^* h(p_V^*, p_L^*)\frac{v_L^2}{a_L^2} \right\}\varphi'(p_V^*). \end{aligned}$$

For (p_0, p_0) the statement is obvious and hence we assume $p_V^* h(p_V^*, p_L^*) \neq 0$ from now on. Now we can write

$$\begin{aligned} \frac{\mathrm{d}}{\mathrm{d}p_V}\left(p_V^* h(p_V^*, p_L^*)[\![v]\!]\right) &= \frac{1}{2p_V^* h(p_V^*, p_L^*)}\left(\partial_{p_V} f(p_V^*, p_L^*) + 1\right) + \frac{1}{2} p_V^* h(p_V^*, p_L^*)\frac{v_V^2}{a_V^2} \\ &\quad + \left\{ \frac{1}{2p_V^* h(p_V^*, p_L^*)}\left(\partial_{p_L} f(p_V^*, p_L^*) - 1\right) - \frac{1}{2} p_V^* h(p_V^*, p_L^*)\frac{v_L^2}{a_L^2} \right\}\varphi'(p_V^*). \end{aligned}$$

We multiply with $\partial_{p_L} f(p_V^*, p_L^*) > 0$ and use

$$\varphi'(p_V^*) = -\frac{\partial_{p_V} f(p_V^*, p_L^*)}{\partial_{p_L} f(p_V^*, p_L^*)}.$$

Thus we obtain

$$
\begin{aligned}
&\partial_{p_L} f(p_V^*, p_L^*) \frac{\mathrm{d}}{\mathrm{d}p_V} \left(p_V^* h(p_V^*, p_L^*)[\![v]\!]\right) = \dots \\
&= \left\{ \frac{1}{2p_V^* h(p_V^*, p_L^*)} (\partial_{p_V} f(p_V^*, p_L^*) + 1) + \frac{1}{2} p_V^* h(p_V^*, p_L^*) \frac{v_V^2}{a_V^2} \right\} \partial_{p_L} f(p_V^*, p_L^*) \\
&- \left\{ \frac{1}{2p_V^* h(p_V^*, p_L^*)} (\partial_{p_L} f(p_V^*, p_L^*) - 1) - \frac{1}{2} p_V^* h(p_V^*, p_L^*) \frac{v_L^2}{a_L^2} \right\} \partial_{p_V} f(p_V^*, p_L^*) \\
&= \frac{1}{2p_V^* h(p_V^*, p_L^*)} (\partial_{p_V} f(p_V^*, p_L^*) + \partial_{p_L} f(p_V^*, p_L^*)) \\
&+ \frac{1}{2} p_V^* h(p_V^*, p_L^*) \left(\partial_{p_V} f(p_V^*, p_L^*) \frac{v_L^2}{a_L^2} + \partial_{p_L} f(p_V^*, p_L^*) \frac{v_V^2}{a_V^2} \right) \\
&= (h(p_V^*, p_L^*) + p_V \partial_{p_V} h(p_V^*, p_L^*)) \left(1 + (p_V^* h(p_V^*, p_L^*))^2 \frac{v_L^2}{a_L^2} \right) [\![v]\!] \\
&+ p_V \partial_{p_L} h(p_V^*, p_L^*) \left(1 + (p_V^* h(p_V^*, p_L^*))^2 \frac{v_V^2}{a_V^2} \right) [\![v]\!] + p_V^* h(p_V^*, p_L^*) \left(\frac{v_V^2}{a_V^2} - \frac{v_L^2}{a_L^2} \right) \\
&= h(p_V^*, p_L^*) [\![v]\!] \left(1 + (p_V^* h(p_V^*, p_L^*))^2 \frac{v_L^2}{a_L^2} \right) - p_V^* h(p_V^*, p_L^*) [\![\frac{v^2}{a^2}]\!] \\
&+ \tau p_V [\![v]\!]^2 \left(1 - (p_V^* h(p_V^*, p_L^*))^4 \frac{v_V^2}{a_V^2} \frac{v_L^2}{a_L^2} \right) \\
&= h(p_V^*, p_L^*) \left([\![v]\!] + [\![v]\!] (p_V^* h(p_V^*, p_L^*))^2 \frac{v_L^2}{a_L^2} - p_V^* [\![\frac{v^2}{a^2}]\!] \right) \\
&+ \tau p_V [\![v]\!]^2 \left(1 - (p_V^* h(p_V^*, p_L^*))^4 \frac{v_V^2}{a_V^2} \frac{v_L^2}{a_L^2} \right) \\
&= h(p_V^*, p_L^*) \left(v_L \left(1 - \frac{p_L^* v_L}{a_L^2} \right) - v_V \left(1 - \frac{p_V^* v_V}{a_V^2} \right) \right) \\
&+ \tau p_V [\![v]\!]^2 \left(1 - (p_V^* h(p_V^*, p_L^*))^4 \frac{v_V^2}{a_V^2} \frac{v_L^2}{a_L^2} \right)
\end{aligned}
$$

Due to the bounds for the *EOS* we can show

$$
\left(v_L \left(1 - \frac{p_L^* v_L}{a_L^2} \right) - v_V \left(1 - \frac{p_V^* v_V}{a_V^2} \right) \right) \geq 0.
$$

and hence we can immediately verify the Lemma for

$$
0 < p_V^* h(p_V^*, p_L^*) \leq \sqrt{\frac{a_V}{v_V} \frac{a_L}{v_L}}. \tag{4.4.3}
$$

Now we want to prove the result for $0 > p_V^* h(p_V^*, p_L^*) \geq -a_V/v_V$. We have

$$
\begin{aligned}
& h(p_V^*, p_L^*) \left(v_L \left(1 - \frac{p_L^* v_L}{a_L^2} \right) - v_V \left(1 - \frac{p_V^* v_V}{a_V^2} \right) \right) + \tau p_V^* [\![v]\!]^2 \left(1 - (p_V^* h(p_V^*, p_L^*))^4 \frac{v_V^2}{a_V^2} \frac{v_L^2}{a_L^2} \right) \\
& \geq -\frac{a_V}{p_V^* v_V} \left(v_L \left(1 - \frac{1}{\gamma_L} \right) - v_V \left(1 - \frac{1}{\gamma_V} \right) \right) + \tau p_V^* [\![v]\!]^2 \left(1 - \frac{a_V^2}{v_V^2} \frac{v_L^2}{a_L^2} \right) \\
& \geq -\frac{\gamma_V}{a_V} \left(v_L \left(1 - \frac{1}{\gamma_L} \right) - v_V \left(1 - \frac{1}{\gamma_V} \right) \right) + \tau v_V^2 p_V^* (1-\alpha)^2 \left(1 - (\alpha\beta)^2 \right) \\
& = -\frac{v_V}{a_V} \left(\frac{\gamma_V}{\gamma_L} \frac{v_L}{v_V} (\gamma_L - 1) + (1 - \gamma_V) \right) + \tau v_V^2 p_V^* (1-\alpha)^2 \left(1 - (\alpha\beta)^2 \right) \\
& = -\frac{v_V}{a_V} \left(\frac{\gamma_V}{\gamma_L} \frac{v_L}{v_V} (\gamma_L - 1) + (1 - \gamma_V) - \frac{\tau a_V^3}{\gamma_V} (1-\alpha)^2 \left(1 - (\alpha\beta)^2 \right) \right) \qquad (+) \\
& \overset{\gamma_L \geq 1}{\geq} -\frac{v_V}{a_V} \left(\alpha \frac{\gamma_V}{\gamma_L} (\gamma_L - 1) + (1 - \gamma_V) - \frac{\tau a_V^3}{\gamma_V} (1-\alpha)^2 \left(1 - (\alpha\beta)^2 \right) \right) \\
& \geq \alpha \gamma_V \frac{v_V}{a_V} \left(\frac{1}{\gamma_L} - \left(1 + \frac{\varepsilon(\gamma_V)}{\alpha} \right) \right) \\
& \overset{(4.4.1)(\mathbf{I})}{\geq} 0.
\end{aligned}
$$

Starting from (+) we obtain for the case $1 > \gamma$ for both phases

$$
\begin{aligned}
& -\frac{v_V}{a_V} \left(\frac{\gamma_V}{\gamma_L} \frac{v_L}{v_V} (\gamma_L - 1) + (1 - \gamma_V) - \frac{\tau a_V^3}{\gamma_V} (1-\alpha)^2 \left(1 - (\alpha\beta)^2 \right) \right) \\
& \geq -\frac{v_V}{a_V} \left(1 - \gamma_V - \frac{\tau a_V^3}{\gamma_V} (1-\alpha)^2 \left(1 - (\alpha\beta)^2 \right) \right) \\
& = -\gamma_V \frac{v_V}{a_V} \varepsilon(\gamma_V) \\
& \overset{(4.4.1)(\mathbf{II})}{\geq} 0.
\end{aligned}
$$

It remains the case for

$$
\sqrt{\frac{a_V}{v_V} \frac{a_L}{v_L}} < p_V^* h(p_V^*, p_L^*) < \frac{a_L}{v_L}.
$$

In the subsequent Lemma 4.4.2 we will exclude this case and thus the proof of this Lemma is finished. □

Remark 4.4.1 (Assumptions on γ)**.** *In Lemma 4.4.1 we only consider cases where $\gamma_V \in (0, 1]$ for the vapor phase. As mentioned before the lower bound ensures hyperbolicity and thermodynamic stability. The upper bound is due to the fact, that we only consider pressures and temperatures* below *the critical point.*
To illustrate this we consider the isothermal compressibility κ_T *which is defined as follows*

$$
\kappa_T = -v \left(\frac{\partial v}{\partial p} \right)_T.
$$

For real *gases κ_T can be expressed in terms of the pressure and the* compressibility *or* gas deviation factor $\mathcal{Z}$ *(not to confuse with the mass flux z used in this work), i.e.*

$$
\kappa_T = \frac{1}{p} - \frac{1}{\mathcal{Z}} \left(\frac{\partial \mathcal{Z}}{\partial p} \right)_T.
$$

Below the critical point the second term is negative for most gases and hence

$$
\kappa_T > \frac{1}{p} \quad \Leftrightarrow \quad \gamma_V = \frac{1}{p \kappa_T} < 1.
$$

This property is reflected by nonlinear EOS such as the van der Waals *or* Dieterici *EOS. For an ideal gas the second term vanishes and we obtain $\gamma_V = 1$.*

Lemma 4.4.2. *Consider two phases such that the requirements (4.3.6) are fulfilled. Then there exists a maximal mass flux z_{max} such that for every admissible solution $f(p_V^*, p_L^*) = 0$ the following upper bound holds*

$$z_{max} \leq \sqrt{\frac{a_V}{v_V}\frac{a_L}{v_L}}.$$

Proof. Since $z(p_V) = 0$ if and only if $p_V = p_0$ and further $z(p_0)' < 0$ we can focus on vapor pressures smaller than p_0. We assume that

$$z_{max} > \sqrt{\frac{a_V}{v_V}\frac{a_L}{v_L}}.$$

Hence there exists a $\tilde{p} \in (0, p_0)$ such that

$$z(\tilde{p}) = \tilde{p}h(\tilde{p}, \varphi(\tilde{p})) = \sqrt{\frac{a_V}{v_V}\frac{a_L}{v_L}} \text{ and } z'(\tilde{p}) \leq 0.$$

This gives

$$\begin{aligned}
0 \geq z'(\tilde{p}) &= \frac{1}{\tilde{p}}\sqrt{\frac{a_V}{v_V}\frac{a_L}{v_L}} + \tilde{p}\left(\partial_{p_V} h(\tilde{p}, \varphi(\tilde{p})) + \partial_{p_L} h(\tilde{p}, \varphi(\tilde{p}))\varphi'(\tilde{p})\right) \\
&= \frac{1}{\tilde{p}}\sqrt{\frac{a_V}{v_V}\frac{a_L}{v_L}} + \frac{\tau\tilde{p}}{2}[\![v]\!]\left(1 - \frac{a_L}{a_V}\frac{v_V}{v_L} + \left(1 - \frac{a_V}{a_L}\frac{v_L}{v_V}\right)\varphi'(\tilde{p})\right) \\
&= \underbrace{\frac{1}{\tilde{p}}\sqrt{\frac{a_V}{v_V}\frac{a_L}{v_L}}}_{>0} + \underbrace{\frac{\tau\tilde{p}}{2}[\![v]\!]\left(1 - \frac{a_V}{a_L}\frac{v_L}{v_V}\right)}_{<0}\left(\varphi'(\tilde{p}) - \frac{a_L}{a_V}\frac{v_V}{v_L}\right) \\
&\Rightarrow \xi := \varphi'(\tilde{p}) > \frac{a_L}{a_V}\frac{v_V}{v_L} \geq \frac{1}{\alpha\beta} \overset{(4.3.6)_2}{>} 1.
\end{aligned}$$

Using the definition of $\varphi'(p_V)$ we obtain

$$\begin{aligned}
&-\partial_{p_V} f(\tilde{p}, \varphi(\tilde{p})) = \partial_{p_L} f(\tilde{p}, \varphi(\tilde{p}))\xi \\
&\Leftrightarrow \\
&1 - 2\sqrt{\frac{a_V}{v_V}\frac{a_L}{v_L}}\left(\frac{1}{\tilde{p}}\sqrt{\frac{a_V}{v_V}\frac{a_L}{v_L}} + \tilde{p}\partial_{p_V} h(\tilde{p}, \varphi(\tilde{p}))\right)[\![v]\!] - \frac{a_L}{v_L}\frac{v_V}{a_V} \\
&= \xi\left(1 + 2\sqrt{\frac{a_V}{v_V}\frac{a_L}{v_L}}\tilde{p}\partial_{p_L} h(\tilde{p}, \varphi(\tilde{p}))[\![v]\!] - \frac{a_V}{v_V}\frac{v_L}{a_L}\right) \\
&\Leftrightarrow \\
&1 - \xi + \frac{a_V}{v_V}\frac{a_L}{v_L}\left(\xi\frac{v_L^2}{a_L^2} - \frac{v_V^2}{a_V^2}\right) = \dots \\
&= 2\sqrt{\frac{a_V}{v_V}\frac{a_L}{v_L}}[\![v]\!]\left(\frac{1}{\tilde{p}}\sqrt{\frac{a_V}{v_V}\frac{a_L}{v_L}} + \tilde{p}(\partial_{p_V} h(\tilde{p}, \varphi(\tilde{p})) + \xi\partial_{p_L} h(\tilde{p}, \varphi(\tilde{p})))\right).
\end{aligned} \tag{4.4.4}$$

For the right hand side of (4.4.4) we easily see

$$2\sqrt{\frac{a_V}{v_V}\frac{a_L}{v_L}}[\![v]\!]\left(\frac{1}{\tilde{p}}\sqrt{\frac{a_V}{v_V}\frac{a_L}{v_L}} + \tilde{p}(\partial_{p_V} h + \xi\partial_{p_L} h)\right) = 2\sqrt{\frac{a_V}{v_V}\frac{a_L}{v_L}}[\![v]\!]z'(\tilde{p}) \geq 0.$$

If we consider the left hand side of (4.4.4) as a function of ξ we get

$$\frac{\mathrm{d}}{\mathrm{d}\xi}\left(1 - \xi + \frac{a_V}{v_V}\frac{a_L}{v_L}\left(\xi\frac{v_L^2}{a_L^2} - \frac{v_V^2}{a_V^2}\right)\right) = -1 + \frac{a_V}{a_L}\frac{v_L}{v_V} \leq -1 + \alpha\beta < 0.$$

Thus the left hand side of (4.4.4) is strictly decreasing in ξ and we have

$$1 - \xi + \frac{a_V}{v_V}\frac{a_L}{v_L}\left(\xi\frac{v_L^2}{a_L^2} - \frac{v_V^2}{a_V^2}\right) \overset{\xi=1}{=} \frac{a_V}{v_V}\frac{a_L}{v_L}[\![\frac{v^2}{c^2}]\!] < 0.$$

Since $\xi > 1$ the left hand side of (4.4.4) is negative and hence contradicts the positive right hand side. Therefore the assumption for z_{max} is wrong. □

Remark 4.4.2. *Lemma 4.4.2 is a direct improvement of Corollary 4.3.1 obtained during the proof of Theorem 4.3.1. There we stated that the upper bound a_L/v_L for the mass flux z is always fulfilled.*

Now we consider two phase flows, where we initially have the vapor phase on the left ($x < 0$) and the liquid phase on the right side ($x > 0$). The different phases are described using the corresponding *EOS*. The considered Riemann initial data is

$$\rho(x,0) = \begin{cases} \rho_V,\ x < 0 \\ \rho_L,\ x > 0 \end{cases} \quad \text{and} \quad u(x,0) = \begin{cases} u_V,\ x < 0 \\ u_L,\ x > 0 \end{cases}. \tag{4.4.5}$$

The solution consists of two classical waves and the phase boundary separating four constant states. Hence there are three possible wave patterns, see Figure 4.2.

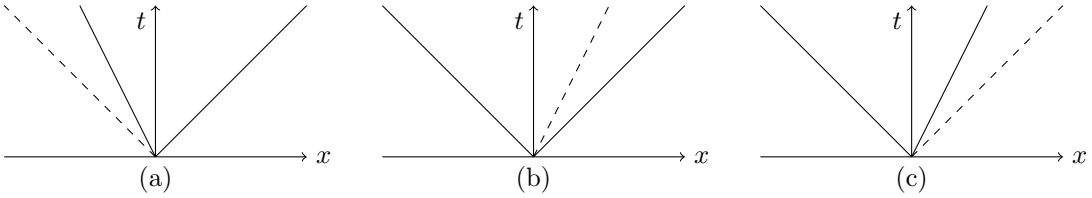

Figure 4.2: Wave patterns. Solid line: classical waves. Dashed line: phase boundary

4.4.1 1^{st} Case: Two Phase Flow without Phase Transition

At first we want to deal with the case where phase transition is excluded, i.e. $z = 0$. Let us consider a wave pattern of type (b), see Figure 4.2. The four constant states are denoted as follows

$$\mathbf{W}_V = \begin{pmatrix} \rho_V \\ u_V \end{pmatrix}, \quad \mathbf{W}_V^* = \begin{pmatrix} \rho_V^* \\ u_V^* \end{pmatrix}, \quad \mathbf{W}_L^* = \begin{pmatrix} \rho_L^* \\ u_L^* \end{pmatrix}, \quad \mathbf{W}_L = \begin{pmatrix} \rho_L \\ u_L \end{pmatrix}.$$

As in Section 4.2.2 we want to derive a single function such that the single root p is the solution for the pressure p_V^*. This procedure again uses the constancy of pressure and velocity across the phase boundary, $u_V^* = u_L^*$ and $p_V^* = p_L^*$, which is because of $z = 0$. For the solution we use the results obtained in Section 4.2.

Theorem 4.4.1 (Solution without Phase Transition)**.** *Let $f(p, \mathbf{W}_V, \mathbf{W}_L)$ be given as*

$$f(p, \mathbf{W}_V, \mathbf{W}_L) = f_V(p, \mathbf{W}_V) + f_L(p, \mathbf{W}_L) + \Delta u,\ \Delta u = u_L - u_V,$$

with the functions f_V andf_L given by

$$f_K(p, \mathbf{W}_K) = \begin{cases} \sqrt{-[\![p]\!][\![v_K]\!]},\ p > p_K\ \textit{(Shock)} \\ \displaystyle\int_{p_K}^{p} \frac{v_K(\zeta)}{a_K(\zeta)}\,\mathrm{d}\zeta,\ p \le p_K\ \textit{(Rarefaction)} \end{cases}, \quad K \in \{V, L\}.$$

If there is a root $f(p^*, \mathbf{W}_V, \mathbf{W}_L) = 0$ with $0 < p^* \le \tilde{p}$, then this root is unique. Here $\tilde{p}$ is given as in Definition 4.2.2. Further this is the unique solution for the pressure p_V^* of the Riemann problem (4.2.1)-(4.2.2), (4.4.5). The velocity $u^* := u_V^* = u_L^*$ is given by

$$u^* = \frac{1}{2}(u_L + u_V) + \frac{1}{2}(f_L(p^*, \mathbf{W}_V) - f_V(p^*, \mathbf{W}_L)).$$

Proof. The function f is strictly monotone increasing in p due to the inequalities (4.2.27), (4.2.28) and Lemma 4.4.1. Furthermore we have $f(p, \mathbf{W}_V, \mathbf{W}_L) \to -\infty$ for $p \to 0$. Hence f has at most one unique root, which is by construction the solution for the pressure p_V^*. The statement for the velocity u^* follows immediately from the results in Section 4.2. □

Note that one has to choose the corresponding *EOS* to calculate the pressure depending quantities according to the index $K \in \{L, V\}$.

Theorem 4.4.2 (Sufficient Condition for Solvability)**.** *Consider the Riemann problem (4.2.1)-(4.2.2), (4.4.5). We have two cases.*

(i) For $p_L < p_V = \tilde{p}$ the considered Riemann problem is solvable if and only if

$$\begin{aligned} &f(\tilde{p}, \mathbf{W}_V, \mathbf{W}_L) = \dots \\ &= \sqrt{-(\tilde{p} - p_V)(v_V(\tilde{p}) - v_V(p_V))} + \sqrt{-(p_L - \tilde{p})(v_L(p_L) - v_L(\tilde{p}))} + \Delta u \geq 0. \end{aligned}$$

(ii) For $p_L \geq \tilde{p}$ the considered Riemann problem is solvable if and only if

$$f(\tilde{p}, \mathbf{W}_V, \mathbf{W}_L) = \sqrt{-(\tilde{p} - p_V)(v_V(\tilde{p}) - v_V(p_V))} + \int_{p_L}^{\tilde{p}} \frac{v_L(\zeta)}{a_L(\zeta)} \, \mathrm{d}\zeta + \Delta u \geq 0.$$

Proof. As seen before in the proof of Theorem 4.4.1, f is strictly monotone increasing in p with $f(p, \mathbf{W}_V, \mathbf{W}_L) \to -\infty$ for $p \to 0$. Accordingly f has a unique root if and only if $f(p, \mathbf{W}_V, \mathbf{W}_L) \geq 0$ for $p \to \tilde{p}$. □

So far we discussed the case that the solution is of type (b). The following result deals with the cases (a) and (c).

Lemma 4.4.3. *There exists no solution of wave pattern types (a) and (c). This includes the coincidence of a classical wave and the phase boundary.*

Proof. Let us first discuss case (c). For the notation see Figure 4.3. Since $z = 0$ we have $w = u_L = u_V^*$

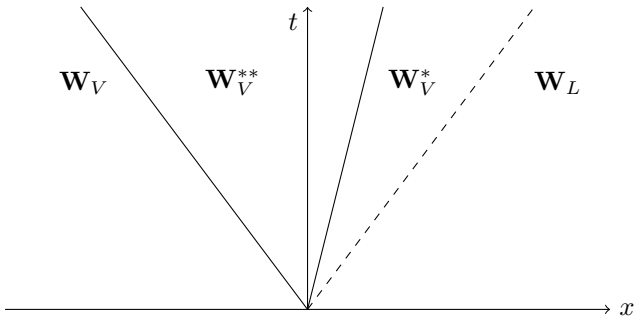

Figure 4.3: Wave pattern of type (c) with notation

for the velocity of the interface. Further we assume, that the right classical wave is a shock moving with speed S. It is obvious that $w \geq S$ must hold. For the case of a right shock we have $p_V^{**} > p_V^*$ and hence we obtain from the entropy inequality $Q < 0$, see Subsection 4.2.2.1. Now we make use of the continuity of the mass flux across a shock wave and obtain

$$Q = \rho_V^*(u_V^* - S) \quad \Leftrightarrow \quad u_V^* - S = \frac{Q}{\rho_V^*} \quad \overset{u_V^* = w}{\Leftrightarrow} \quad S = w - \frac{Q}{\rho_V^*} > w.$$

This contradicts the condition $w \geq S$. If, on the other hand, the right classical wave is a rarefaction wave we have for the head speed $u_V^* + a_V$, see Subsection 4.2.2.2. Again this contradicts $w = u_L = u_V^* \geq u_V^* + a_V$. In case that the phase boundary lies inside the rarefaction wave, we obtain similar contradictions in the wave speeds. For wave pattern type (a) the arguments are analogue. □

4.4.2 2^{nd} Case: Two Phase Flow with Phase Transition

Now we want to take phase transition into account, i.e. $z \neq 0$. As before we first want to discuss the wave pattern of type (b), see Figure 4.2. In order to determine the solution we again construct a function analogue to Subsection 4.4.1. For the left and right classical waves we use

$$u_V^* = u_V - f_V(p_V^*, \mathbf{W}_V) \quad \text{and} \quad u_L^* = u_L + f_L(p_L^*, \mathbf{W}_L). \tag{4.4.6}$$

Across the phase boundary we make use of the jump conditions and obtain as in Subsection 4.2.2.1

$$[\![u]\!] = u_L^* - u_V^* = z[\![v]\!] = z(v_L(p_L^*) - v_V(p_V^*)). \tag{4.4.7}$$

Finally we use the results obtained in Section 4.3, especially Theorem 4.3.1, to express the liquid pressure at the interface as a function of the interface vapor pressure $p_L = \varphi(p_V)$. Combining these considerations we end up with the following theorem.

Theorem 4.4.3 (Solution with Phase Transition)**.** *Let $f_z(p, \mathbf{W}_V, \mathbf{W}_L)$ be given as*

$$f_z(p, \mathbf{W}_V, \mathbf{W}_L) = f_V(p, \mathbf{W}_V) + f_L(\varphi(p), \mathbf{W}_L) + z[\![v]\!] + \Delta u, \ \Delta u = u_L - u_V,$$

with the functions f_V andf_L given by

$$f_V(p, \mathbf{W}_V) = \begin{cases} \sqrt{-[\![p]\!][\![v]\!]}, & p > p_V \ \textit{(Shock)} \\ \displaystyle\int_{p_V}^{p} \frac{v_V(\zeta)}{a_V(\zeta)} \, \mathrm{d}\zeta, & p \leq p_V \ \textit{(Rarefaction)} \end{cases},$$

$$f_L(\varphi(p), \mathbf{W}_L) = \begin{cases} \sqrt{-[\![p]\!][\![v]\!]}, & \varphi(p) > p_L \ \textit{(Shock)} \\ \displaystyle\int_{p_L}^{\varphi(p)} \frac{v_L(\zeta)}{a_L(\zeta)} \, \mathrm{d}\zeta, & \varphi(p) \leq p_L \ \textit{(Rarefaction)} \end{cases}.$$

The function $\varphi(p)$ is implicitly defined by (4.3.5) and the mass flux is given by (4.3.4). If there is a root $f_z(p^*, \mathbf{W}_V, \mathbf{W}_L) = 0$ with $0 < p^* \leq \tilde{p}$, this root is unique. If further

$$p^* > p_V \quad \textit{we must have} \quad z > -\frac{a_V(\bar{p})}{v_V(\bar{p})} \quad \textit{for} \quad \bar{p} \in (p_V, p^*). \tag{4.4.8}$$

Then p^* is the unique solution for the pressure p_V^* of a (b)-type solution of the Riemann problem (4.2.1)-(4.2.2), (4.4.5) with phase transition. If there is no root or condition (4.4.8) is not satisfied, then there is no solution to the mentioned Riemann problem.

Proof. Due to (4.2.27), (4.2.28), Corollary 4.3.2 and Lemma 4.4.1 we get that the function f_z is strictly monotone increasing in p. Furthermore we have $f(p, \mathbf{W}_V, \mathbf{W}_L) \to -\infty$ for $p \to 0$. Hence f has at most one unique root, which is by construction the solution for the pressure p_V^*. Theorem 4.3.1 then uniquely defines the liquid pressure $p_L^* = \varphi(p_V^*)$ and the mass flux z at the interface. The remaining quantities can be calculated using the *EOS* and (4.4.6). □

Remark 4.4.3. *Condition (4.4.8) is needed in the case of a shock wave in the vapor phase to guarantee that $w > S$. Where w denotes the velocity of the interface and S of the shock respectively. This can be obtained as follows*

$$u_V^* - S = v_V(p_V^*)Q_S \quad \textit{and} \quad u_V^* - w = -v_V(p_V^*)z \quad \Leftrightarrow \quad w - S = v_V(p_V^*)(Q_S + z)$$
$$\Rightarrow \quad S < w \quad \Leftrightarrow \quad z > -Q_S = -\frac{a_V(\bar{p})}{v_V(\bar{p})}.$$

For the last equality we used the Lax condition for S together with the monotonicity of $a(p)/v(p)$. If this condition is not satisfied by the root $f_z(p^*, \mathbf{W}_V, \mathbf{W}_L) = 0$, the root is meaningless.

Theorem 4.4.4 (Sufficient Condition for Solvability I)**.** *If the Riemann problem (4.2.1)-(4.2.2), (4.4.5) is solvable without phase transition, see Subsection 4.4.1, then the same Riemann problem is also solvable taking into account phase transition according to the kinetic relation (4.3.4).*

Proof. **First Case $f(p^*, \mathbf{W}_V, \mathbf{W}_L) = 0$ with $p^* = p_0$:** In view of Section 4.3 we have $p_0 = \varphi(p^*)$, $z = 0$ and hence $f_z(p^*, \mathbf{W}_V, \mathbf{W}_L) = 0$.

Second Case $f(p^*, \mathbf{W}_V, \mathbf{W}_L) = 0$ with $p^* > p_0$: From that we have

$$\varphi(p^*) \overset{4.3.1}{>} p^* > p_0 \quad \text{and} \quad z(p^*) = p^* h(p^*, \varphi(p^*)) < 0.$$

This gives

$$f_z(p^*, \mathbf{W}_V, \mathbf{W}_L) > f(p^*, \mathbf{W}_V, \mathbf{W}_L) = 0.$$

So there exists a $p_V^* < p^*$ such that $f_z(p_V^*, \mathbf{W}_V, \mathbf{W}_L) = 0$.

Third Case $f(p^*, \mathbf{W}_V, \mathbf{W}_L) = 0$ with $p^* < p_0$: In this situation we obtain

$$0 = f(p^*, \mathbf{W}_V, \mathbf{W}_L) \overset{p^* < p_0}{<} f(p_0, \mathbf{W}_V, \mathbf{W}_L) \overset{\varphi(p_0) = p_0, z = 0}{=} f_z(p_0, \mathbf{W}_V, \mathbf{W}_L)$$

Hence there exists a $p_V^* < p_0$ such that $f_z(p_V^*, \mathbf{W}_V, \mathbf{W}_L) = 0$. □

Corollary 4.4.1. *Consider the Riemann problem (4.2.1)-(4.2.2), (4.4.5) without phase transition and let p^* be the solution for the pressure. Then we have for the same Riemann problem with phase transition and the corresponding solutions p_V^* and $p_L^* = \varphi(p_V^*)$ the following relations:*

(1) $p^* = p_0$ implies $p_V^* = p_L^* = p_0$, i.e. equilibrium.

(2) $p^* > p_0$ implies $p_0 < p_V^* < p^*$, i.e. condensation.

(3) $p^* < p_0$ implies $p^* < p_L^* < p_0$, i.e. evaporation.

Proof. The equilibrium case is obvious. The inequality $p_V^* < p^*$ in the second was obtained in the second part in the proof of Theorem 4.4.4. It remains to show that $p_0 < p_V^*$. Assume that $p_V^* \leq p_0$, this gives

$$\begin{aligned} 0 = f_z(p_V^*, \mathbf{W}_V, \mathbf{W}_L) &\leq f_z(p_0, \mathbf{W}_V, \mathbf{W}_L) \\ &= f(p_0, \mathbf{W}_V, \mathbf{W}_L) \overset{p_0 < p^*}{<} f(p^*, \mathbf{W}_V, \mathbf{W}_L) = 0. \end{aligned}$$

For the evaporation case the inequality $p_L^* < p_0$ is a consequence of the third part in the proof of Theorem 4.4.4. There we obtained $p_V^* < p_0$ and this gives, together with Theorem 4.3.1, the second inequality. Finally we want to prove the first inequality $p^* < p_L^*$. Again using Theorem 4.3.1 gives $p_V^* > p_0$ if we assume $p_L^* > p_0$. By an analogous argument as for the second case this leads to a contradiction. Thus we have $p_L^* < p_0$. □

Theorem 4.4.5 (Sufficient Condition for Solvability II)**.** *Consider the Riemann problem (4.2.1)-(4.2.2), (4.4.5) with phase transition. This Riemann problem is solvable by a (b)-type solution if and only if condition (4.4.8) holds and*

$$f_z(\tilde{p}, \mathbf{W}_V, \mathbf{W}_L) \geq 0.$$

Proof. The statement is obvious, since it guarantees a root for f_z. □

As in Subsection 4.4.1 we want to discuss wave patterns of type (a) and (c) for the Riemann problem (4.2.1)-(4.2.2), (4.4.5) with phase transition. The results are given in the subsequent three lemmata.

Lemma 4.4.4. *There is no solution with a wave pattern of type (a).*

Proof. Assume there is a solution of type (a) as in Figure 4.4. In this case we observe condensation and according to Corollary 4.3.3 we have

$$z < 0 \quad \text{and} \quad p_0 < p_V^* < p_L^*.$$

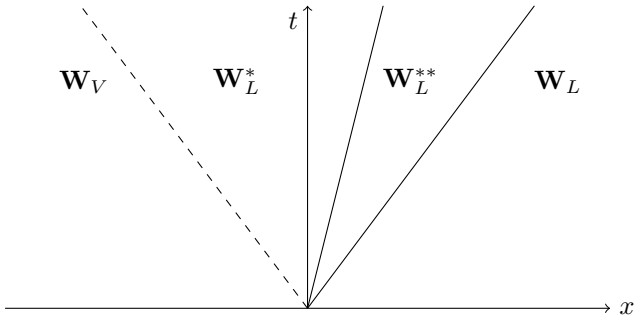

Figure 4.4: Wave pattern of type (a) with notation

Let us first assume that the left classical wave is a rarefaction wave. The head speed is given by $S = u_L^* - a_L(p_L^*)$ and we obtain

$$w = v_L(p_L^*)z + u_L^* \overset{(a)}{\leq} S = u_L^* - a_L(p_L^*) \quad \Leftrightarrow \quad z \leq -\frac{a_L(p_L^*)}{v_L(p_L^*)} \overset{(4.4.1)}{<} -\frac{a_V}{v_V}$$

This is a contradiction and thus we can exclude this case. Given a shock instead of a rarefaction wave we have using (4.2.19) and the Lax condition

$$u_L^* - a_L(p_L^*) > S = u_L^* - v_L(p_L^*)Q_S > u_L^{**} - a_L(p_L^{**}) \text{ with } Q_S = \frac{a_L(\bar{p}_L)}{v_L(\bar{p}_L)},\ \bar{p}_L \in (p_L^*, p_L^{**}).$$

Hence we yield

$$w < S \quad \Leftrightarrow \quad z < -Q_S = -\frac{a_L(\bar{p}_L)}{v_L(\bar{p}_L)} \overset{p_L^* < \bar{p}_L}{<} -\frac{a_L(p_L^*)}{v_L(p_L^*)} \overset{(4.4.1)}{<} -\frac{a_V}{v_V}.$$

Therefore we can also exclude this case and the proof is finished. □

Lemma 4.4.5. *For the considered Riemann problem with phase transition exists no solution of type (c) with $p_L \geq p_0$.*

Proof. A solution of type (c) implies an evaporation process which requires $p_L < p_0$. □

Lemma 4.4.6. *For $p_L \in (\hat{p}_L, p_0]$ exists no solution of type (c) of the considered Riemann problem with phase transition.*

Proof. Assume we have a wave pattern of type (c) as in Figure 4.3. Hence we have evaporation and according to Corollary 4.3.3 we have

$$z > 0 \quad \text{and} \quad p_V^* < p_L^* < p_0.$$

Let us first assume that the right classical wave is a rarefaction wave. The head speed is given by $S = u_V^* + a_V(p_V^*)$ and we obtain

$$w = v_V(p_V^*)z + u_V^* \overset{(c)}{\geq} S = u_V^* - a_V(p_V^*) \quad \Leftrightarrow \quad z \geq \frac{a_V(p_V^*)}{v_V(p_V^*)}.$$

For a right shock ($Q_S < 0$) we have using (4.2.19) and the Lax condition

$$u_V^{**} + a_V(p_V^{**}) > S = u_V^* - v_V(p_V^*)Q_S > u_V^* + a_V(p_V^*)$$
$$\text{with} \quad Q_S = \frac{a_V(\bar{p}_V)}{v_V(\bar{p}_V)}, \quad \bar{p}_V \in (p_V^*, p_V^{**}).$$

Hence we yield

$$w > S \quad \Leftrightarrow \quad z > -Q_S = \frac{a_V(\bar{p}_V)}{v_V(\bar{p}_V)} \overset{\bar{p}_V > p_V^*}{>} \frac{a_V(p_V^*)}{v_V(p_V^*)}.$$

Due to Lemma 4.4.2 we have an upper bound for the mass flux that does not initially exclude the conditions derived above for the rarefaction and shock wave. But the two cases are excluded if $z < a_V(p_V^*)/v_V(p_V^*)$. Indeed we have due to the monotonicity of z and a/v that

$$\exists\, \hat{p}_V < p_0 \quad \text{such that} \quad \forall p_V \in (\hat{p}_V, p_0] : z(p_V) < \frac{a_V(p_V)}{v_V(p_V)}.$$

Due to the strict monotonicity of $p_L^* = \varphi(p_V^*)$, see Theorem 4.3.1, the proof is complete. □

4.5 Phase Creation in Single Phase Flows

4.5.1 Condensation by Compression

Let us consider the following Riemann initial data with $\rho_{V^\pm} \in (0, \tilde{\rho}]$

$$\rho(x,0) = \begin{cases} \rho_{V^-},\ x < 0 \\ \rho_{V^+},\ x > 0 \end{cases} \quad \text{and} \quad u(x,0) = \begin{cases} u_{V^-},\ x < 0 \\ u_{V^+},\ x > 0 \end{cases}. \tag{4.5.1}$$

Hence initially we have a Riemann problem for a single vapor phase and therefore we can directly apply the results obtained in subsection 4.2.2.

Theorem 4.5.1 (Solution of Isothermal Euler Equations for a Single Vapor Phase)**.** *Let $f(p, \mathbf{W}_{V^-}, \mathbf{W}_{V^+})$ be given as*

$$f(p, \mathbf{W}_{V^-}, \mathbf{W}_{V^+}) = f_-(p, \mathbf{W}_{V^-}) + f_+(p, \mathbf{W}_{V^+}) + \Delta u,\ \Delta u = u_{V^+} - u_{V^-},$$

with the functions f_- andf_+ given by

$$f_\pm(p, \mathbf{W}_{V^\pm}) = \begin{cases} \sqrt{-[\![p]\!][\![v]\!]},\ p > p_{V^\pm}\ \textit{(Shock)} \\ \displaystyle\int_{p_{V^\pm}}^{p} \frac{v_V(\zeta)}{a_V(\zeta)}\,\mathrm{d}\zeta,\ p \le p_{V^\pm}\ \textit{(Rarefaction)} \end{cases}.$$

If there is a root $f(p^*, \mathbf{W}_{V^-}, \mathbf{W}_{V^+}) = 0$ with $0 < p^* \le \tilde{p}$, then this root is unique. Further this is the unique solution for the pressure p_V^* of the Riemann problem (4.2.1)-(4.2.2), (4.5.1). The velocity u_V^* is given by

$$u_V^* = \frac{1}{2}(u_{V^+} + u_{V^-}) + \frac{1}{2}(f_+(p^*, \mathbf{W}_{V^+}) - f_-(p^*, \mathbf{W}_{V^-})).$$

This is no new result and therefore it is well known, cf. Toro [31]. Usually one looks for a pressure p^* that solves $f(p, \mathbf{W}_{V^-}, \mathbf{W}_{V^+}) = 0$. Due to the asymptotic behavior there is always a solution. Nevertheless a solution with an unreasonable large vapor pressure is physically not meaningful, since a sufficiently high pressure in a gas will lead to a phase transition to a liquid or even solid phase. According to [12] we also only consider solutions which satisfy $0 < p^* \le \tilde{p}$, where $\tilde{p}$ again denotes the maximal gas pressure. This being said, we can find Riemann initial data without a solution. In this case proceed as follows.

Definition 4.5.1 (Nucleation Criterion)**.** *If there is no solution of the Riemann problem (4.2.1)-(4.2.2), (4.5.1) according to Theorem 4.5.1, then nucleation occurs.*

If this criterion is fulfilled, we search a solution consisting of two classical waves and two phase boundaries. In the following we will again discuss several wave patterns.

Lemma 4.5.1. *If there is a solution of the Riemann problem (4.2.1)-(4.2.2), (4.5.1) with two classical waves and two phase boundaries, then no wave is propagating inside the liquid phase. Hence classical waves may only occur in the vapor phase.*

Proof. Assume a left going classical wave is propagating through the liquid phase. We denote the liquid states left and right to this wave by $\mathbf{W}_L^*$ and $\mathbf{W}_L^{**}$. Further left to this classical wave there is a phase boundary moving with speed w_1. The vapor state left to this phase boundary is denoted by $\mathbf{W}_V^*$. Obviously this must be a condensation process and accordingly $p^* > p_0$ and $p_L^* > p_0$. This configuration is excluded by Lemma 4.4.4. Analogously we can discuss the case of a right going classical wave. □

As a consequence of the above result classical waves only propagate through the vapor phase. Hence we further have to discuss the following three patterns, see Figure 4.5.

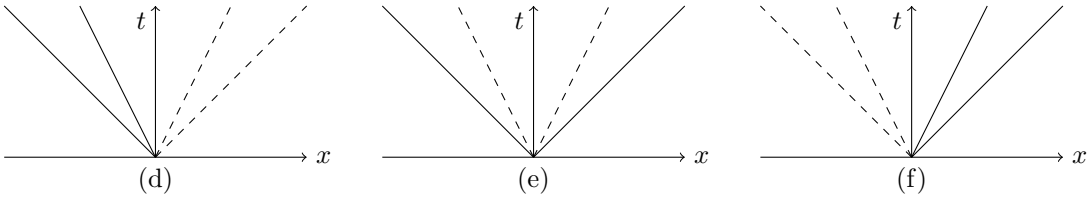

Figure 4.5: Wave patterns. Solid line: classical wave. Dashed line: phase boundary

Lemma 4.5.2. *There are no solutions of wave pattern types (d) and (f).*

Proof. A solution with type (d) wave pattern corresponds to wave pattern type (c) in the previous Subsection 4.4.2, see Figure 4.3. Thus by Lemma 4.4.5 and Lemma 4.4.6 we know that this is only possible for sufficiently small pressures and therefore implies evaporation. Since we have a condensation process wave pattern type (d) can be excluded. Analogously we discuss a type (f) solution. This corresponds to a type (a) solution in Subsection 4.4.2, see Figure 4.4. Hence due to Lemma 4.4.4 a solution of wave pattern type (f) is also impossible. □

Consequently the only possible wave pattern in this case is of type (e), see Figure 4.6.

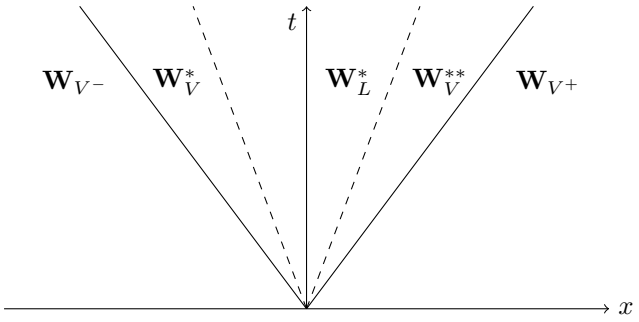

Figure 4.6: Wave pattern of type (e) with notation

Lemma 4.5.3. *For a solution of wave pattern type (e) the equality $p_V^* = p_V^{**}$ holds.*

Proof. Across the left phase boundary the liquid pressure p_L^* is uniquely defined by the vapor pressure p_V^* using Theorem 4.3.1. So far we assumed the vapor left of the liquid phase. For the right phase boundary the opposite is the case and thus we have to use the kinetic relation (4.3.2). Nevertheless the results of the previous section remain unchanged and hence we obtain the same function to determine the liquid pressure

$$p_L^* = \varphi(p_V^*) = \varphi(p_V^{**}).$$

Hence the vapor pressures are equal. □

Taking into account that there are two phase boundaries and using the results obtained in the previous sections we can state the following theorem.

Theorem 4.5.2 (Solution of Isothermal Euler Equations for Two Vapor States with Phase Transition)**.** *Consider the Riemann problem (4.2.1)-(4.2.2), (4.5.1) and assume the nucleation criterion is satisfied. Let $f_z(p, \mathbf{W}_{V^-}, \mathbf{W}_{V^+})$ be given as*

$$f_z(p, \mathbf{W}_{V^-}, \mathbf{W}_{V^+}) = f_-(p, \mathbf{W}_{V^-}) + f_+(p, \mathbf{W}_{V^+}) + 2z[\![v]\!] + \Delta u,\ \Delta u = u_{V^+} - u_{V^-},$$

with the functions f_- andf_+ given by

$$f_\pm(p, \mathbf{W}_{V^\pm}) = \begin{cases} \sqrt{-[\![p]\!][\![v]\!]},\ p > p_{V^\pm}\ \textit{(Shock)} \\ \displaystyle\int_{p_{V^\pm}}^{p} \frac{v_V(\zeta)}{a_V(\zeta)}\,\mathrm{d}\zeta,\ p \le p_{V^\pm}\ \textit{(Rarefaction)} \end{cases}.$$

Here z is given by (4.3.1) and $[\![v]\!] = v_L(\varphi(p)) - v_V(p)$. The function φ is implicitly defined by (4.3.5). If there is a root $f_z(p^*, \mathbf{W}_{V^-}, \mathbf{W}_{V^+}) = 0$ with $p_0 < p^* \le \tilde{p}$, then this root is the only one. Further this is the unique solution for the vapor pressures $p_V^* = p_V^{**}$ of the Riemann problem (4.2.1)-(4.2.2), (4.5.1). The liquid velocity u_L^* is given by

$$u_L^* = \frac{1}{2}(u_{V^+} + u_{V^-}) + \frac{1}{2}(f_+(p^*, \mathbf{W}_{V^+}) - f_-(p^*, \mathbf{W}_{V^-})).$$

By the previous results it is obvious that f_z has at most one root. By construction this root is the solution for the vapor pressure in the two star regions, see Figure 4.6. The following results are completely analogue to those obtained before for the two phase case.

Remark 4.5.1. *Note that $u_V^* \neq u_V^{**}$ with $u_V^* + u_V^{**} = 2u_L^*$.*

Theorem 4.5.3 (Sufficient Condition for Solvability I)**.** *Consider the Riemann problem (4.2.1)-(4.2.2), (4.5.1). This problem is solvable without phase transition if and only if*

$$f(\tilde{p}, \mathbf{W}_{V^-}, \mathbf{W}_{V^+}) \ge 0.$$

Here f is given as in Theorem 4.5.1.

Proof. This statement is obvious due to the monotonicity of f. □

Theorem 4.5.4 (Sufficient Condition for Solvability II)**.** *Consider the Riemann problem (4.2.1)-(4.2.2), (4.5.1) and assume the nucleation criterion is satisfied. Accounting for phase transition, this problem is solvable if and only if*

$$f_z(\tilde{p}, \mathbf{W}_{V^-}, \mathbf{W}_{V^+}) \ge 0.$$

The function f_z is defined as in Theorem 4.5.2.

Proof. Again the statement is obvious due to the monotonicity of f_z. □

4.5.2 Evaporation by Expansion

Now we consider the following Riemann initial data with $\rho_{L^\pm} \ge \rho_L^{min}$

$$\rho(x,0) = \begin{cases} \rho_{L^-},\ x < 0 \\ \rho_{L^+},\ x > 0 \end{cases} \quad \text{and} \quad u(x,0) = \begin{cases} u_{L^-},\ x < 0 \\ u_{L^+},\ x > 0 \end{cases}. \tag{4.5.2}$$

Hence initially we have a Riemann problem for a single liquid phase. We have seen so far that at a planar phase boundary the liquid pressure is always positive. However it is known that negative liquid pressures are possible, cf. Davitt et al. [6] for water. This gives rise to cavitation in the liquid phase. Again, in the liquid-vapor case a negative liquid pressure is forbidden, see (4.3.8). Nevertheless in the liquid-liquid case we may encounter negative liquid pressures. We define the smallest possible liquid pressure to be p_{min} and with this definition we obtain the following result.

Theorem 4.5.5 (Solution of Isothermal Euler Equations for a Single Liquid Phase)**.** *Let* $f(p, \mathbf{W}_{L^-}, \mathbf{W}_{L^+})$ *be given as*

$$f(p, \mathbf{W}_{L^-}, \mathbf{W}_{L^+}) = f_-(p, \mathbf{W}_{L^-}) + f_+(p, \mathbf{W}_{L^+}) + \Delta u,\ \Delta u = u_{L^+} - u_{L^-},$$

with the functions f_- *and* f_+ *given by*

$$f_\pm(p, \mathbf{W}_{L^\pm}) = \begin{cases} \sqrt{-[\![p]\!][\![v]\!]},\ p > p_{L^\pm}\ \textit{(Shock)} \\ \int_{p_{L^\pm}}^{p} \frac{v_L(\zeta)}{a_L(\zeta)}\,\mathrm{d}\zeta,\ p \le p_{L^\pm}\ \textit{(Rarefaction)} \end{cases}.$$

If there is a root $f(p^*, \mathbf{W}_{L^-}, \mathbf{W}_{L^+}) = 0$ *with* $p_{min} \le p^*$*, then this root is unique. Further this is the unique solution for the pressure* p_L^* *of the Riemann problem (4.2.1)-(4.2.2), (4.5.2). The velocity* u_L^* *is given by*

$$u_L^* = \frac{1}{2}(u_{L^+} + u_{L^-}) + \frac{1}{2}(f_+(p^*, \mathbf{W}_{L^+}) - f_-(p^*, \mathbf{W}_{L^-})).$$

Remark 4.5.2. *For simplicity we choose* $p_{min} = 0$ *but lower values are possible and the theoretical results do not depend on the specific value of* p_{min}*.*

Analogously to the case of nucleation we define the following.

Definition 4.5.2 (Cavitation Criterion)**.** *If there is no solution of the Riemann problem (4.2.1)-(4.2.2), (4.5.2) according to Theorem 4.5.5, then cavitation may occur.*

If this criterion is fulfilled, we look for a solution involving a vapor phase, two phase boundaries and two classical waves. Again we discuss the possible patterns.

Lemma 4.5.4. *Assume there is a solution of the Riemann problem (4.2.1)-(4.2.2), (4.5.2) consisting of two classical waves and two phase boundaries. If the pressures* p_{L^-}, p_{L^+} *are sufficiently large then no wave travels through the vapor.*

The proof is analogue to the one of Lemma 4.4.6.

Lemma 4.5.5. *There is no solution of type (d) or (f); see Figure 4.5.*

The proof of this lemma is analogue to the one of Lemma 4.5.2. Accordingly we construct solutions of type (e), see Figure 4.7.

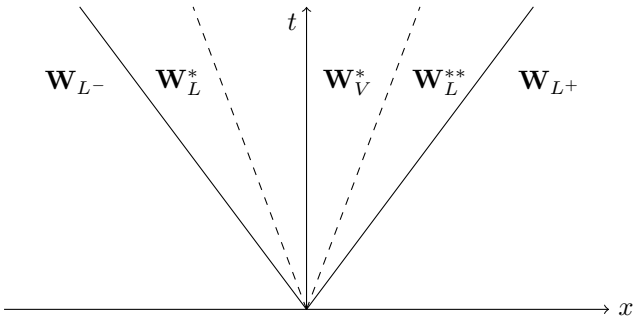

Figure 4.7: Wave pattern of type (e) with notation for the liquid case

Theorem 4.5.6 (Solution of Isothermal Euler Equations for Two Liquid States with Phase Transition)**.** *Consider the Riemann problem (4.2.1)-(4.2.2), (4.5.2) and assume the cavitation criterion is satisfied. Let* $f_z(p, \mathbf{W}_{L^-}, \mathbf{W}_{L^+})$ *be given as*

$$f_z(p, \mathbf{W}_{L^-}, \mathbf{W}_{L^+}) = f_-(p, \mathbf{W}_{L^-}) + f_+(p, \mathbf{W}_{L^+}) + 2z[\![v]\!] + \Delta u,\ \Delta u = u_{L^+} - u_{L^-},$$

with the functions f_- and f_+ given by

$$f_\pm(p, \mathbf{W}_{L^\pm}) = \begin{cases} \sqrt{-[\![p]\!][\![v]\!]}, & \varphi(p) > p_{L^\pm} \text{ (Shock)} \\ \displaystyle\int_{p_{L^\pm}}^{\varphi(p)} \frac{v_L(\zeta)}{a_L(\zeta)} \,\mathrm{d}\zeta, & \varphi(p) \le p_{L^\pm} \text{ (Rarefaction)} \end{cases}.$$

Here z is given by (4.3.1) and $[\![v]\!] = v_L(\varphi(p)) - v_V(p)$. The function φ is implicitly defined by (4.3.5). If there is a root $f_z(p^*, \mathbf{W}_{L^-}, \mathbf{W}_{L^+}) = 0$ with $p_{min} \le p^*$, then this root is unique. Further this is the unique solution for the vapor pressures p_V^* of the Riemann problem (4.2.1)-(4.2.2), (4.5.2). The vapor velocity u_V^* is given by

$$u_V^* = \frac{1}{2}(u_{L^+} + u_{L^-}) + \frac{1}{2}(f_+(p^*, \mathbf{W}_{L^+}) - f_-(p^*, \mathbf{W}_{L^-})).$$

Proof. Due to the previous results, the function f_z has at most one root. This root is by construction the solution for the vapor pressure in the star region. □

Completely analogue to the condensation case, see Subsection 4.5.1, we have the following results.

Theorem 4.5.7 (Sufficient Condition for Solvability I)**.** *Consider the Riemann problem (4.2.1)-(4.2.2), (4.5.2). This problem is solvable without phase transition if and only if*

$$f(p_{min}, \mathbf{W}_{L^-}, \mathbf{W}_{L^+}) \le 0.$$

Here f is given as in Theorem 4.5.5.

Proof. The statement is easily verified due to the monotonicity of f. □

Theorem 4.5.8 (Sufficient Condition for Solvability II)**.** *Consider the Riemann problem (4.2.1)-(4.2.2), (4.5.2) and assume the cavitation criterion is satisfied. If we admit phase transition, this problem is always solvable.*

Proof. This statement is obvious due to the fact that $z[\![v]\!] \to -\infty$ for $p_V^* \to 0$. □

4.6 Conclusion

4.6.1 Discussion of the Assumptions

In this part we now want to discuss the assumptions previously made to solve the problem. Basically we have three types of requirements. First there are the ones due to the underlying thermodynamics, in particular the first and second law of thermodynamics. Second there are conditions, one needs to solve the single phase Riemann problem for the Euler equations. The third type concerns the assumptions imposed to solve the two phase problem. Note that the assumptions are sufficient, from a mathematical point of view, to obtain the results presented throughout this work.

From a thermodynamic point of view we have first and foremost to satisfy the first and second law of thermodynamics including the requirement of thermodynamic stability (4.2.7). This is obtained by deriving the pressure law from a suited thermodynamic potential.
The conditions imposed on the EOS in order to solve the (single phase) Riemann problem for the Euler equations are

$$\gamma > 0, \quad \mathcal{G} > 0, \quad v(p) \overset{p\to\infty}{\to} 0, \quad \text{and} \quad v(p) \overset{p\to 0}{\to} \infty$$

That we require the single phase Riemann problem to be solvable is of course reasonable, since otherwise any further discussion would be unnecessary. The conditions above are completely analogue to those stated in [21]. Note that for any EOS where the speed of sound is a constant (such as in [12]) we have $\mathcal{G} = 1$. We want to point out that the aforementioned requirements of type one and two are basically no new or additional assumptions since they are already needed to treat the single phase case.

Since we are concerned with discussing the case of two phases it is reasonable to assume that all single phase requirements are met and only a few new ones need to be added. In order to solve the two phase Riemann problem we need the additional assumptions (4.3.6) and (4.4.1).
The uniform upper bound for the quotient of the specific volumes basically tells us how close we can get to the critical point, where the volumes would become equal. The case of $\alpha = 1$, i.e. we include the critical point where the volumes become equal, is not considered here and has to be treated separately. The constant β bounds the quotient of the sound speeds and is only needed to be strict smaller than $1/\alpha$.
The assumption on the lower bound of γ_V in (4.3.6) is a rather technical one. Nevertheless if we assume τ to be as in (4.3.3) and consider the ideal gas EOS for the vapor phase we have

$$1 = \gamma_V > \tau a_V^3 (1-\alpha)^2 = \frac{1}{\sqrt{2\pi}} \left(\frac{m}{kT_0} \right)^{\frac{3}{2}} (1-\alpha)^2 a_V^3 = \frac{(1-\alpha)^2}{\sqrt{2\pi}}.$$

Hence this bound is easily satisfied. If the sound speed of the vapor phase would depend on the pressure one would have to check this requirement more carefully. We further want to emphasize that apart from $\tau > 0$ and $(4.3.6)_3$ we do not assume any particular shape or even magnitude of τ. This is a further key point that contributes to the generality of our result.
The last requirement in (4.3.6) is concerned with the maximum vapor pressure. Due to this bound the vapor is allowed to be compressed (depending on α) with more than the saturation pressure. This allows metastable states, which is reflected in the Maxwell construction. Here of course one has to make sure that the maximum vapor pressure $\tilde{p}$ defined in Definition 4.2.2 satisfies this bound. This can be guaranteed by choosing an appropriate temperature and also how the two EOS are connected by $\bar{v}(p)$ in Definition 4.2.2. Usually $\tilde{p}$ will only be slightly larger than the saturation pressure for a wide range of temperatures.

Now we want to comment assumptions (4.4.1). Let us first consider γ_L. Over wide temperature ranges we have $\gamma_L \geq 1$ for many substances. For example in Section 4.6.2 we consider the *linear* and *nonlinear Tait* EOS for liquid water and for this type of EOS modeling water this is true up to $636.165K$. A similar result can be obtained for the *van der Waals* EOS. Above that temperature it is not possible to use the ideal (polytropic) gas EOS together with such a liquid EOS, because it would contradict (4.4.1) (**II**).
Regarding case (**II**) we want to emphasize that for $1 > \gamma_L > \gamma_V$ the inequality including α is trivial. In fact in numerical studies we exemplary obtained that this property is also true for the van der Waals EOS up to $\approx 640K$.
Now we want to comment on $\varepsilon(\gamma_V)$ in (4.4.2). Using the ideal gas or the polytropic gas EOS gives $\gamma_V = 1$ and hence

$$\varepsilon_0 := \varepsilon(1) = -\tau a_V^3 (1-\alpha)^2 \left(1 - (\alpha\beta)^2\right) < 0.$$

We consider (4.4.1) (**II**) and have $1 + \varepsilon_0/\alpha < 0$ over large temperature ranges. Suppose this term becomes positive at high temperatures, it is however still smaller than one. Whereas at the same time γ_L approaches one. Hence this bound may be still valid. This of course has to be checked for any given EOS.

4.6.2 Examples

Now we want to present several examples of choices for the equations of state used to model the fluid under consideration, in this case water. First we will discuss the ideal gas EOS for the vapor phase and the (linear) Tait EOS for the liquid phase as in [12]. For the ideal gas we obtain

$$p_V(v_V) = \frac{kT_0}{m} \frac{1}{v_V}, \quad \gamma_V = 1, \quad \mathcal{G}_V = 1. \tag{4.6.1}$$

Here k is the Boltzmann constant, T_0 is the fixed temperature and m denotes the mass of a single water molecule. Considering the liquid phase we obtain

$$p_L(v_L) = p_0 + K_0 \left(\frac{v_0}{v_L} - 1 \right), \quad \gamma_L = \left(1 + \frac{v_L}{K_0 v_0} (p_0 - K_0) \right)^{-1} \overset{K_0 \geq p_0}{\geq} 1, \quad \mathcal{G}_L = 1. \tag{4.6.2}$$

The quantities with index zero are calculated at the saturation state corresponding to T_0. We further have the saturation pressure p_0, the modulus of compression K_0 and the specific liquid volume v_0, cf. [34]. Note that the relation $K_0 \geq p_0$ breaks down for temperatures *above* $636.165K$ ($T_c = 647.096K$).
Both EOS are linear functions of the mass density and thus it is reasonable to connect them with a linear function $\bar{p}$. Hence we obtain the specific volume of the vapor phase corresponding to the maximum vapor pressure $\tilde{p}$ according to Definition 4.2.2 as the solution of the following equation

$$0 = K_0 v_0 \ln \frac{v_0}{v_{min}} + \frac{\tilde{v}}{v_{min} - \tilde{v}} \frac{kT_0}{m} \ln \frac{\tilde{v}}{v_{min}} + \frac{kT_0}{m} \ln \frac{v_V(p_0)}{v_{min}}. \tag{4.6.3}$$

Here v_m is chosen such that

$$v_m = \begin{cases} v_0 \left(1 - \dfrac{p_0}{K_0}\right)^{-1}, T_0 \leq 620K, \\ v_0 \left(1 + \dfrac{T_c - T_0}{T_c}\right), T_0 > 620K. \end{cases}$$

Using (4.6.3) we can calculate the quotient $v_m/\tilde{v}$ for every reasonable temperature and thus obtain α and also β. Now we can check the assumptions given in (4.3.6), (4.4.1). We have for temperatures up to $636.165K$ the following

$$\alpha \lesssim 0.1949, \quad \alpha\beta \lesssim 0.5419, \quad \frac{1}{\gamma_L} - \left(1 + \frac{\varepsilon_0}{\alpha}\right) \gtrsim 0.7484 \quad \text{and} \quad \tilde{p} \lesssim 1.4825 p_0.$$

Thus all requirements are met as expected and the limiting factor here are not the assumptions but the choice of the EOS.

Remark 4.6.1. *Note that in the isothermal case the linear Tait EOS is equivalent to the stiffend gas EOS*

$$p_L(v_L) = C(\gamma - 1)\frac{T_0}{v_L} - p_c \quad \textit{with} \quad C(\gamma - 1) = \frac{K_0 v_0}{T_0} \quad \textit{and} \quad p_c = K_0 - p_0.$$

As a second example we want to use the nonlinear Tait EOS instead of the linear one, i.e.

$$p_L(v_L) = p_0 + K_0 \left(\left(\frac{v_0}{v_L}\right)^{\eta} - 1\right), \ \eta > 1. \tag{4.6.4}$$

Again we use the ideal gas EOS for the vapor phase. We obtain for the nonlinear Tait EOS

$$\gamma_L = \eta \left(1 + \left(\frac{v_L}{v_0}\right)^{\eta} \left(\frac{p_0}{K_0} - 1\right)\right)^{-1} > 1, \quad \mathcal{G}_L = \frac{\eta + 1}{2}$$

and

$$v_m = \begin{cases} v_0 \left(1 - \dfrac{p_0}{K_0}\right)^{-\frac{1}{\eta}}, T_0 \leq 620K, \\ v_0 \left(1 + \dfrac{T_c - T_0}{T_c}\right), T_0 > 620K. \end{cases}$$

Next with an approach analogue to the previous case we obtain $\tilde{v}$ as solution of the following equation and then calculate $\tilde{p}$

$$\begin{aligned} 0 = (p_0 - K_0)v_m + K_0 v_0 + \frac{K_0 v_0^{\eta}}{1 - \eta} \left(\frac{1}{v_m^{\eta - 1}} - \frac{1}{v_0^{\eta - 1}}\right) \\ + \frac{v_m}{v_m - \tilde{v}} \frac{kT_0}{m} \ln \frac{\tilde{v}}{v_m} + \frac{kT_0}{m} \ln \frac{v_V(p_0)}{\tilde{v}}. \end{aligned} \tag{4.6.5}$$

We can use (4.6.5) to calculate the quotient $v_m/\tilde{v}$ for every reasonable temperature and thus obtain α and also β. Here we use $\eta = 7$ as in [29]. We again check the assumptions given in (4.3.6), (4.4.1) and obtain for temperatures up to $636.165K$ the following

$$\alpha \lesssim 0.1645, \quad \alpha\beta \lesssim 0.1818, \quad \frac{1}{\gamma_L} - \left(1 + \frac{\varepsilon_0}{\alpha}\right) \gtrsim 0.7795 \quad \text{and} \quad \tilde{p} \lesssim 1.2511 p_0.$$

Hence this choice of EOS is also suitable for solving this problem for temperatures from $273.15K$ up to $636.165K$. Again the limiting factor here are not the assumptions but the choice of the EOS.

4.6.3 Conclusion

The aim of the present work was to investigate the Riemann problem for the isothermal Euler equations when liquid and vapor phases are present which may condensate or evaporate. We proved that there exist unique solutions under the given assumptions.To this end we allow any EOS which satisfies these assumptions, especially nonlinear ones. This is a huge improvement to the previous work [12] where only two specific linear EOS were chosen to solve this problem. In contrast to this we for example allow the speed of sound to depend on the pressure or volume instead of being constant. Furthermore allow phase transitions where the pressures are not in equilibrium as for example in [9]. Additionally we can treat nucleation an cavitation. In view of the work by Hantke, T. [14] the last point has to be emphasized. To our knowledge this is the most general result concerning Riemann problems for isothermal two phase flows.

References

[1] R. Abeyaratne and J. K. Knowles. Kinetic relations and the propagation of phase boundaries in solids, *Arch. Rational Mech. Anal.*, **114** (1991), pp. 119-154.

[2] M. Bartelmann, B. Feuerbacher, T. Krüger, D. Lüst, A. Rebhan, and A. Wipf,. *Theoretische Physik*, Springer Spektrum 2015.

[3] D. Bedeaux and S. Kjelstrup. Irreversible thermodynamicsa tool to describe phase transitions far from global equilibrium , *Chemical Engineering Science* , **59** (2004), pp. 109 - 118.

[4] M. Bond and H. Struchtrup. Mean evaporation and condensation coefficients based on energy dependent condensation probability, *Phys. Rev. E.*, **70** (2004) 061605.

[5] C. M. Dafermos. *Hyperbolic Conservation Laws in Continuum Physics,* Springer-Verlag, Berlin - Heidelberg, 2010.

[6] K. Davitt, E. Rolley, F. Caupin, A. Arvengas, and S. Balibar. Equation of state of water under negative pressure, *Journal of Chemical Physics*, **133** (2010), pp. 1745071 - 1745078,

[7] W. Dreyer. On jump conditions at phase boundaries for ordered and disordered phases, *WIAS Preprint*, **869** (2003).

[8] W. Dreyer, F. Duderstadt, M. Hantke, and G. Warnecke. Bubbles in liquids with phase transition. Part 1. On phase change of a single vapor bubble in liquid water, *Contin. Mech. Thermodyn.*, **24** (2012), pp. 461–483,

[9] M. Dumbser, U. Iben, and C.-D. Munz. Efficient implementation of high order unstructured WENO schemes for cavitating flows, *Computers & Fluids*, **86** (2013), pp. 141 - 168.

[10] J.H. Dymond, and R. Malhotra. The Tait equation: 100 years on, *International Journal of Thermophysics*, **9** (1988), pp. 941-951,

[11] L.C. Evans. Entropy and Partial Differential Equations, Lecture Notes, http://math.berkeley.edu/ evans/entropy.and.PDE.pdf

[12] M. Hantke, W. Dreyer, and G. Warnecke. Exact solutions to the Riemann problem for compressible isothermal Euler equations for two phase flows with and without phase transition, *Quarterly of Applied Mathematics*, **71** (2013), pp. 509 - 540.

[13] M. Hantke and F. Thein. Numerical solutions to the Riemann problem for compressible isothermal Euler equations for two phase flows with and without phase transition, in:*Hyperbolic Problems, Theory, Numerics, Applications*, 2014.

[14] M. Hantke and F. Thein. Why condensation by compression in pure water vapor cannot occur in an approach based on Euler equations, *Quarterly of Applied Mathematics*, **73** (2015), pp. 575-591.

[15] M.J. Ivings, D.M. Causon, and E.F. Toro. On Riemann solvers for compressible liquids, *International Journal for Numerical Methods in Fluids*, **28** (1998), pp. 395–418.

[16] David C. Johnston. *Thermodynamic Properties of the van der Waals Fluid*, 2014. http://arxiv.org/abs/1402.1205v1

[17] A.H. Koop *Numerical Simulation of Unsteady Three-Dimensional Sheet Cavitation*, PhD thesis, University of Twente, Enschede, 2008.

[18] L.D. Landau and E.M. Lific. *Lehrbuch der theoretischen Physik*, Bd.V Statistische Physik, Akad.-Verl., 1987.

[19] P.G. LeFloch, *Hyperbolic Systems of Conservation Laws: The Theory of Classical and Nonclassical Shock Waves*, Birkhäuser Verlag, 2002.

[20] M.N. Berberan-Santos, E.N. Bodunov, and L. Pogliani. The van der Waals equation: Analytical and approximate solutions, *Journal of Mathematical Chemistry*, **43** (2008), pp. 1437-1457.

[21] R. Menikoff and B. J. Plohr. The Riemann problem for fluid flow of real materials, *Rev. of mod. Phys.*, **61** (1989), pp. 75-104.

[22] C. Merkle. *Dynamical Phase Transitions in Compressible Media*, Doctoral Thesis, Univ. Freiburg, 2006.

[23] C. Merkle and C. Rohde. The sharp-interface approach for fluids with phase change: Riemann problems and ghost fluid techniques, *ESAIM: M2AN*, **41** (2007), pp. 1089-1123.

[24] I. Müller. *Thermodynamics*, Pitman, 1985.

[25] I. Müller and W. Müller. *Fundamentals of Thermodynamics and Applications*, Springer-Verlag, Berlin, 2009.

[26] S. Müller and A. Voss. The Riemann Problem for the Euler equations with nonconvex and nonsmooth equation of state: Construction of wave curves, *SIAM J. Sci. Comput.*, **28** (2006), pp. 651-681.

[27] N.R. Nannan, A. Guardone, and P. Colonna. On the fundamental derivative of gas dynamics in the vaporliquid critical region of single-component typical fluids, *Fluid Phase Equilibria*, **337** (2013), pp. 259 - 273.

[28] E. Rebhan. *Theoretische Physik: Thermodynamik und Statistik*, Spektrum Akademischer Verlag, 2010.

[29] R. Saurel, P. Cocchi, P.B. and Butler. Numerical Study of Cavitation in the Wake of a Hypervelocity Underwater Projectile, *Journal of Propulsion and Power*, **15** (1999), pp. 513-522.

[30] E.F. Toro, M. Spruce, and W. Speares. Restoration of the contact surface in the HLL-Riemann solver, *Shock Waves*, **4** (1994), pp. 25-34.

[31] E. F. Toro. *Riemann Solvers and Numerical Methods for Fluid Dynamics*, Springer-Verlag, Berlin - Heidelberg, 1999.

[32] A. Voss. *Exact Riemann Solution for the Euler Equations with Nonconvex and Nonsmooth Equation of state*, Doctoral Thesis, RWTH Aachen 2005.

[33] W. Wagner and H.-J. Kretzschmar. *International Steam Tables*, Springer-Verlag, Berlin - Heidelberg, 2008.

[34] W. Wagner A. and Kruse. *Properties of water and steam: the industrial standard IAPWS-IF97 for the thermodynamic properties and supplementary equations for other properties : tables based on these equations*, Springer-Verlag, 1998.

[35] A. Zein. *Numerical methods for multiphase mixture conservation laws with phase transition*, Doctoral Thesis, Univ. Magdeburg, 2010.

Chapter 5

Singular and selfsimilar solutions for Euler equations

Bibliographic note: The content of this chapter is published in [H14]: F. Thein and M. Hantke. Singular and selfsimilar solutions for Euler equations with phase transitions, *Bulletin of the Brazilian Mathematical Society*, New Series 47 (2), (2016), 779-786.

Abstract: Riemann problems for the full set of Euler equations for two phases with phase transition are considered. Based on the assumptions across the phase boundary kinetic relations to describe the mass transfer between the phase are derived from the second law of thermodynamics. Self-similar as well as singular solutions can be constructed. For both cases the structure of the solution is discussed.

5.1 Introduction

Multiphase flows appear everywhere in nature and are of great importance in industrial applications. Usually phase transition effects play a significant role. For the modeling of phase transitions often continuum mechanics equations, derived using averaging or homogenization techniques, were used, see for instance Zein et. al [9]. For these models a large number of equations is used, one set of balances for each phase or component. In many cases additional differential terms appearing in the systems prevent them from being in divergence or conservative form. Exact expressions for the transfer terms are usually unknown. In fact, there is a lack of theory for these models and their numerical solutions require a big numerical effort.

On the other hand one can use only one set of balance equations to describe the flow. An additional kinetic relation describes the exchange of mass between the phases. This concept was introduced by Abeyaratne and Knowles [1]. The main advantage of this type of modeling is the smaller number of equations. Moreover, due to the explicit character of the kinetic relation it may be possible to construct exact solutions for Riemann initial data. For example, for the system of isothermal Euler equations equipped with a kinetic relation exact solutions for Riemann problems were constructed by Hantke et. al [6]. Also existence and uniqueness of the solution was proven. Riemann solutions are the basis to construct efficient Riemann solvers.

In the following we consider Riemann problems for the full system of Euler equations for liquid-vapor flows. Depending on the assumptions across the phase boundaries different kinetic relations can be derived from the second law of thermodynamics. These assumptions influence the structure of the solutions. Self-similar as well as singular solutions can be found. For both cases we discuss the structure of the solution and give an appropriate choice of a kinetic relation.

5.2 Balance laws and entropy inequality

The physical fields are assumed to depend on time $t \in \mathbb{R}_{\geq 0}$ and space $x \in \mathbb{R}$. In regular points of the bulk phases we have the local balances for mass (5.2.1), momentum (5.2.2) and energy (5.2.3)

$$\frac{\partial \rho}{\partial t} + \frac{\partial(\rho v)}{\partial x} = 0\,, \tag{5.2.1}$$

$$\frac{\partial(\rho v)}{\partial t} + \frac{\partial(\rho v^2 + p)}{\partial x} = 0\,, \tag{5.2.2}$$

$$\frac{\partial(\rho E)}{\partial t} + \frac{\partial(\rho E v + p v)}{\partial x} = 0\,, \tag{5.2.3}$$

where ρ, v, E denote the *density*, the *velocity* and the *specific total energy*, resp. The *specific internal energy* is related to the total energy by $E = e + \frac{1}{2}v^2$, whereas the *pressure* p is related to the density and the internal energy by an equation of state $p = p(\rho, e)$. For the *specific Gibbs free energy* g it holds

$$g = e - Th + \frac{p}{\rho}\,, \tag{5.2.4}$$

where $T = T(\rho, p)$ and $h = h(e, p)$ are the *temperature* and the *specific entropy*.

Using the notation

$$[\![\Psi]\!] = \Psi^+ - \Psi^-\,,$$

where $'+'$ and $'-'$ denote the right and left sided limits for any quantity Ψ, we give the mass (5.2.5), momentum (5.2.6) and energy balances (5.2.7) across any discontinuity in one dimension in their most general form

$$\frac{d}{dt}(\rho_s) - [\![\dot{m}]\!] = 0\,, \tag{5.2.5}$$

$$\frac{d}{dt}(\rho_s w) - [\![v\dot{m}]\!] + [\![p]\!] = 0\,, \tag{5.2.6}$$

$$\frac{d}{dt}(e_s + \rho_s \frac{w^2}{2}) - [\![(e + \frac{1}{2}v^2)\dot{m}]\!] + [\![q + pv]\!] = 0\,, \tag{5.2.7}$$

where q denotes the *heat flux*. The discontinuity, which can be a shock, a contact wave or a phase boundary, propagates with velocity w. The *singular mass* and the *singular internal energy* of the discontinuity are denoted by ρ_s and e_s, for more details see Dreyer [3]. Note, that the energy e_s is not proportional to the singular mass density ρ_s. This is in agreement with Dreyer [3]. In the following we always assume, that for waves propagating through the bulk phase (shock, contact) $e_s = 0$ and $\rho_s = 0$, whereas we also consider more general assumptions for phase interfaces. The mass flux $\dot{m} = -\rho^{\pm}(v^{\pm} - w)$ across the phase boundary has to be specified by an additional kinetic relation, which has to satisfy the *second law of thermodynamics*

$$\frac{d}{dt}h_s - [\![h\dot{m} - \frac{1}{T}q]\!] = \zeta_s \geq 0\,, \tag{5.2.8}$$

the *entropy production* ζ_s has to be nonnegative. The *interface temperature* T_s and the *Gibbs free energy of the phase boundary* g_s are defined by

$$\frac{1}{T_s} := \frac{\partial h_s}{\partial e_s} \qquad \text{and} \qquad \frac{g_s}{T_s} := -\frac{\partial h_s}{\partial \rho_s}\,. \tag{5.2.9}$$

In the following no heat conduction is taken into account, this means that we have $q = 0$. Finally we give Riemann initial data. Assuming that at $t = 0$ the phase boundary is located at $x = 0$ these data may be given by

$$(\rho, v, p)^T = \begin{cases} (\rho_L, v_L, p_L)^T & x < 0 \\ (\rho_R, v_R, p_R)^T & x > 0\,. \end{cases} \tag{5.2.10}$$

The construction of Rieman solution will be done analogously to Hantke et al. [6] and follows the ideas in the book of Toro [7]. The discussion of rarefaction, shock and contact waves is classical and will not be carried out in this paper. Instead we restrict ourselves to the discussion of phase boundaries.

5.3 Selfsimilar solutions

All relations are presented in its most general form. In order to construct self-similar solutions we make the following simplifying assumptions

$$\rho_s \equiv 0 \qquad \text{and} \qquad e_s \equiv 0 \tag{5.3.1}$$

to remove the derivative terms in the interface balance equations. This means that the interface has no mass and no energy. As a consequence we have

$$\frac{d}{dt} h_s = 0 \,.$$

Moreover the mass flux across the phase boundary is continuous, this means that

$$[\![\dot{m}]\!] = 0 \,.$$

Accordingly the entropy inequality (5.2.8) becomes

$$-\dot{m}[\![h]\!] = \zeta_s \geq 0 \,. \tag{5.3.2}$$

This inequality directly implies that the mass flux $\dot{m}$ is a function of the differences of the specific entropies h of the phases, i.e.

$$\dot{m} \sim -[\![h]\!] \,. \tag{5.3.3}$$

The mass flux is driven by the difference of the specific entropies of the phases.

To derive an explicit kinetic relation we follow the ideas in Dreyer et al. [5] and make a linear ansatz for the kinetic relation in the following form

$$\dot{m} = B_I [\![h]\!] \,.$$

The *interface mobility* B_I is a positive factor. In [5] B_I results from the Maxwell distribution, see [4], or rather from the classical Hertz-Knudsen theory, see Bond and Struchtrup [2]. With an analogous choice for the mobility we end up with

$$\dot{m} = \frac{p_V T_s}{\sqrt{2\pi}} \left(\frac{m}{k T_s} \right)^{\frac{3}{2}} [\![h]\!] \,, \tag{5.3.4}$$

where k denotes the Boltzmann constant, m the mass of a single molecule of the considered substance and p_V the pressure of the gas phase. For more details see [5].

Corresponding solutions of the considered Riemann problem consist of five constant states that are separated by four waves see Figure 5.1. The left and the right wave are classical shocks or rarefactions,

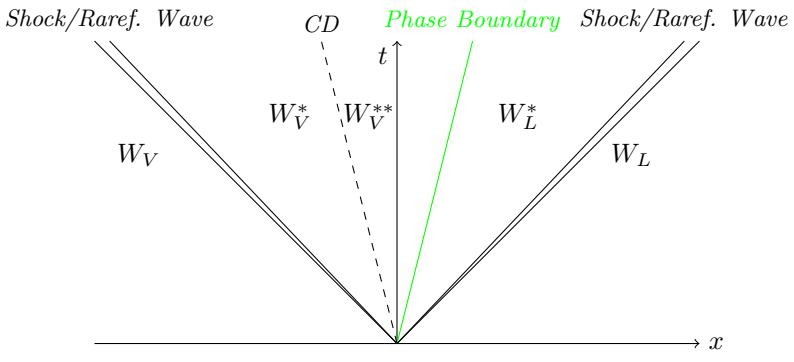

Figure 5.1: Solution structure for (5.3.1), $W = (\rho, \rho v, \rho E)^T$

that propagate through the bulk phases. In addition the solution has a classical contact wave and a phase boundary, which can be characterized as a non-classical discontinuity. Let us assume the vapor phase is on the left hand side. For temperatures lower than the critical temperature the specific entropy

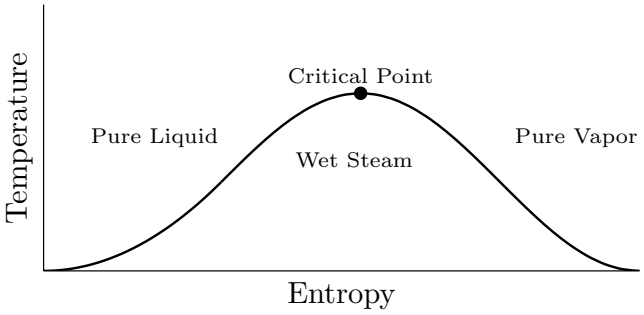

Figure 5.2: Schematic Entropy-Temperature Diagram

of the vapor phase is always larger than the specific entropy of the liquid phase of the same substance, see Figure 5.2.

Accordingly we have

$$\dot{m} \sim -[\![h]\!] > 0\,.$$

This implies that only evaporation processes can take place. In other words, for the simplifying assumptions (5.3.1) no thermal equilibrium may occur. Further, one can easily obtain that for the above assumption the phase boundary propagates faster than the bulk phases, which implies, that the contact wave always propagates through the vapor phase.

To overcome this phenomenon there are two possibilities. On the one hand heat conduction can be taken into account. On the other hand one can weaken the simplifying assumptions (5.3.1), which leads to singular solutions.

Remark 5.3.1. *We want to point out, that the wave structure as well as the non-existence of thermal equilibrium solutions are a direct consequence of the entropy principle (5.3.2). These phenomena occur for any appropriate choice for a kinetic relation.*

5.4 Singular solutions

As discussed in the previous section we now use weaker simplifying assumptions. As before we neglect surface density, i.a. $\rho_s \equiv 0$, but we take into account surface energy. The interface mass and momentum balances (5.2.5), (5.2.6) reduce to

$$[\![\dot{m}]\!] = 0 \tag{5.4.1}$$

$$-\dot{m}[\![v]\!] + [\![p]\!] = 0\,. \tag{5.4.2}$$

Using (5.4.1) and (5.4.2) we rewrite (5.2.7) and obtain the interface energy balance equation

$$\frac{d}{dt}e_s - \dot{m}[\![e + \frac{p}{\rho} + \frac{1}{2}(v-w)^2]\!] = 0\,. \tag{5.4.3}$$

The entropy production ζ_s is now given by

$$\zeta_s = \dot{m}[\![\frac{1}{T_s}(g + \frac{1}{2}(v-w)^2) + h(\frac{T}{T_s} - 1)]\!]\,, \tag{5.4.4}$$

which implies

$$\dot{m} \sim [\![\frac{1}{T_s}(g + \frac{1}{2}(v-w)^2) + h(\frac{T}{T_s} - 1)]\!]\,. \tag{5.4.5}$$

Due to the derivative in (5.4.3) the solution of the considered Riemann problem is not self-similar. Instead we follow the ideas of Yang [8] and construct solutions in the sense of measures, where a discontinuity appears on the phase interface.

Like Yang we assume a delta-shock, propagating with velocity w and located at $x(t) = wt$, where the singular value of the surface energy is described by $e_s(t) = e_0 t$.

The solution consists of five constant states, separated by four waves. As before, the right and left waves are classical shocks or rarefactions. The order of the two middle waves, the contact and the phase boundary, depends on the situation under consideration. With the same arguments as in the previous section we find, if evaporation occurs, the contact propagates through the vapor phase, otherwise through the liquid. Accordingly for the evaporation case we have the same wave structure as before, see Figure 5.1. For the condensation case see Figure 5.3. Note, that in contrast to the solutions of Section 5.3 the

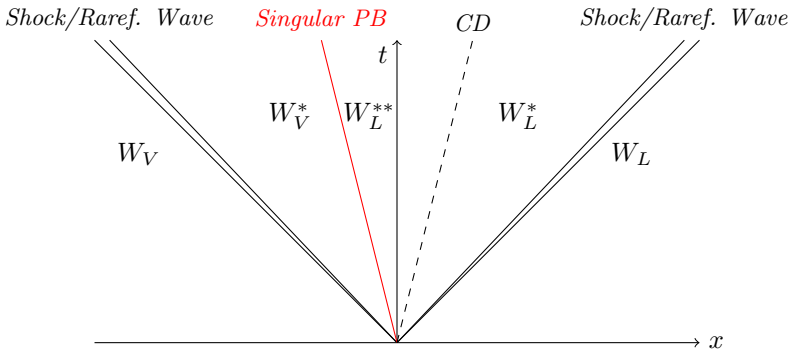

Figure 5.3: Solution structure for the condensation case with a singularity on the phase boundary, $W = (\rho, \rho v, \rho E)^T$

interface is now equipped with energy and forms a singularity and hence the solution is not self-similar anymore.

Assume, the solution considered describes a condensation process, where two shock waves propagate through the bulk phases with velocities S_L and S_R, then the solution at time t is of the following form

$$(\rho, \rho v, \rho E)^T(t,x) = \begin{cases} (\rho_V, \rho_V v_V, \rho_V E_V)^T & -\infty < x \leq S_L t \\ (\rho_V^*, \rho_V^* v_V^*, \rho_V^* E_V^*)^T & S_L t < x < wt \\ (0, 0, e_0 \delta(x - x(t))t)^T & x = wt \\ (\rho_L^{**}, \rho_L^{**} v_L^{**}, \rho_L^{**} E_L^{**})^T & wt < x < St \\ (\rho_L^*, \rho_L^* v_L^*, \rho_L^* E_L^*)^T & St \leq x < S_R t \\ (\rho_L, \rho_L v_L, \rho_L E_L)^T & S_R t \leq x < \infty\,, \end{cases} \tag{5.4.6}$$

where S denotes the speed of the contact. For solutions with rarefactions or with evaporation states one may find a similar structure.

Analogously to the previous case with the assumptions $\rho_s \equiv 0$ and $e_s(t) = e_0 \cdot t$ one can treat the following two cases

$$\rho_s(t) = \rho_0 \cdot t \qquad \text{and} \qquad e_s \equiv 0 \tag{5.4.7}$$

and

$$\rho_s(t) = \rho_0 \cdot t \qquad \text{and} \qquad e_s(t) = e_0 \cdot t\,. \tag{5.4.8}$$

In both cases a singularity will form on the phase interface. The structure of the solution is the same as before, but in contrast to the case before, one obtains singular values for all three components $(\rho, \rho v, \rho E)^T$. For a non-linear ansatz for $\rho_s(t)$ or $e_s(t)$ the solution structure becomes more complicated.

References

[1] R. Abeyaratne and J. K. Knowles. Kinetic relations and the propagation of phase boundaries in solids, *Arch. Rational Mech. Anal.*, **114** (1991), pp. 119-154.

[2] M. Bond and H. Struchtrup. Mean evaporation and condensation coefficients based on energy dependent condensation probability, *Phys. Rev. E.*, **70** (2004) 061605.

[3] W. Dreyer. On jump conditions at phase boundaries for ordered and disordered phases, *WIAS Preprint*, **869** (2003).

[4] W. Dreyer and F. Duderstadt. On the Becker/Döring theory of nucleation of liquid droplets in solids. *J. Stat. Phys.* **123** (2006), 55–87.

[5] W. Dreyer, F. Duderstadt, M. Hantke, and G. Warnecke. Bubbles in liquids with phase transition. Part 1: On phase change of a vapor bubble in liquid water, *Cont. Mech. Thermodyn.* (2011), DOI 10.1007/s00161-011-0225-6.

[6] M. Hantke, W. Dreyer, and G. Warnecke. Exact solutions to the Riemann problem for compressible isothermal Euler equations for two phase flows with and without phase transitions, *Quarterly of Applied Mathematics*, vol. LXXI **3** (2013), pp. 509–540.

[7] E.F. Toro. *Riemann Solvers and Numerical Methods for Fluid Dynamics*. Springer-Verlag, Berlin - Heidelberg, 1999.

[8] H. Yang. Riemann problems for a class of coupled hyperbolic systems of conservation laws. *J. Diff. Equ.* **159** (1999), 447–484.

[9] A. Zein, M. Hantke, and G. Warnecke. Modeling phase transition for compressible two-phase flows applied to metastable liquids. *J. Comput. Phys.*, **229** (2010), 2964-2998.

Chapter 6

A non-existence result

Bibliographic note: The content of this chapter is published in [H12]: Maren Hantke and Ferdinand Thein. Why condensation by compression in pure water vapor cannot occur in an approach based on Euler equations, *Quarterly of Applied Mathematics* 73 (2015), 575-591.

Abstract: Phase transitions are in the focus of the modeling of multiphase flows. A large number of models is available to describe such processes. We consider several different two phase models that are based on the Euler equations of compressible fluid flows and which take into account phase transitions between a liquid phase and its vapor. Especially we consider the flow of liquid water and water vapor. We give a mathematical proof, that all these models are not able to describe the process of condensation by compression. This behavior is in agreement with observations in experiments, that simulate adiabatic flows, and shows that the Euler equations give a fairly good description of the process. The mathematical proof is valid for the official standard *IAPWS-IF97* for water and for any other good equation of state. Also the opposite case of expanding the liquid phase will be discussed.

6.1 Introduction

Compressible two and multi phase flows occur in nature as well as in numerous industrial applications. In many cases phase transitions between the fluids are of major importance. Examples are the formation of clouds or the phenomenon of cavitation that for instance appears in liquid water flows around ship propellers.

The modeling of such processes is a challenge. The description of the interfaces between the fluids as well as their interaction is of high complexity. Therefore in the spotlight of the methods is the treatment of the interfaces. Many numerical simulations are based on the Euler equations of compressible fluid flow. We will direct our attention to two phase models of this type that take into account mass transfer between the fluids.

Very famous are the models of Baer-Nunziato type. Here both phases are described by their own set of Euler equations. An additional equation for the volume fractions of the phases is considered, see Section 6.4.3. The original model of Baer and Nunziato [2], that does not include the effect of mass exchange between the phases, was modified by Saurel and Abgrall in [18] by introducing relaxation terms for pressures and velocities of the phases. Later in [19] a similar idea allowed the description of phase transition by using relaxation terms for the temperatures and chemical potentials. This idea was picked up for instance by Petitpas et al. in [17] or by Zein et al. in [25].

Another type of modeling of two phase flows is to use only one set of Euler equations. Each phase has its own equation of state. Phase transitions can be described by a further equation that is called kinetic relation. See for instance the well reputed article of Abeyaratne and Knowles [1] that deals with solid- solid interfaces, the papers of Merkle [14] or Hantke et al. [6] on the isothermal Euler equations.

Finally we want to refer to a recent paper of Dumbser et al. [5]. In their work also only one set of equations is used. Phase transitions take place only in thermal equilibrium, no kinetic relation is used. Surprisingly this type of modeling is closely related to the Baer-Nunziato type modeling mentioned above including relaxation terms to describe mass transfer. We come back to this and the abovementioned models later in Section 6.4.3.

One can find an extensive literature on cavitating flows, but the opposite question of the creation of a liquid phase by a strong compression is discussed only in rare cases. In the following we consider pure water vapor, that will be highly compressed. This can be realized by a steam filled tube with a flexible piston, see Figure 6.2. If there is no heat exchange with the neighbourhood of the tube, the process is nearly an adiabatic flow. Therefore it can be fairly described by the compressible Euler equations. One may expect, that it is possible to compress the vapor phase such that the vapor will condensate. This means that a liquid phase is created. In fact, it turns out this is impossible in a non-isothermal approach based on Euler equations, which is in agreement with observations from experiments. The main focus of our work is to give a **mathematical proof for this phenomenon**.

In the case of expanding a liquid under the same boundary conditions, see Figure 6.6 the situation is more complex. Nevertheless, also for the cavitation case we can prove some theoretical results. For detailed discussions of cavitation models we refer to Iben [7] and [9].

The paper is organized as follows. In Section 6.2 we introduce the compressible Euler equations and briefly recall some well-known analytical results on the Riemann problem. Afterwards in Section 6.3 we give some equations of state to close the system and provide some physical background. Section 6.4 deals with compressed water vapor. First in Section 6.4.1 we explain the idea for the proof of our statement. In Section 6.4.2 we show for a special choice of equations of state for the phases, that condensation by compression cannot occur. After that in Section 6.4.3 we show, that this idea is also applicable to Baer-Nunziato type models with relaxation terms as in Saurel et al. [19], Zein et al. [25]. Thereafter, in Section 6.5 we generalize the proof to the *real equation of state for water*. Finally we consider the opposite case of cavitation by expansion in Section 6.6. We end up with some closing remarks in Section 6.7.

6.2 The Euler model

The compressible Euler equations in one space dimension are given by the following system

$$\frac{\partial}{\partial t}\rho + \frac{\partial}{\partial x}\rho u = 0\,, \tag{6.2.1}$$

$$\frac{\partial}{\partial t}\rho u + \frac{\partial}{\partial x}(\rho u^2 + p) = 0\,, \tag{6.2.2}$$

$$\frac{\partial}{\partial t}\rho(e + \frac{1}{2}u^2) + \frac{\partial}{\partial x}\big[\rho(e + \frac{1}{2}u^2) + p\big]u = 0\,, \tag{6.2.3}$$

where the variables ρ, u and e denote the *mass density*, the *velocity* and the *internal energy*, resp. The further quantity p describes the *pressure*. It is related to the mass density ρ and the internal energy e by an *equation of state*, see Section 6.3. All physical fields depend on time $t \in \mathbb{R}_{\geq 0}$ and on space $x \in \mathbb{R}$.

Here we consider Riemann problems for the Euler equations, that are given by the above balance equations (6.2.1)-(6.2.3), an equation of state and the corresponding *Riemann initial data*

$$\rho(0,x) = \begin{cases} \rho_- \\ \rho_+ \end{cases}, \quad u(0,x) = \begin{cases} u_- \\ u_+ \end{cases}, \quad e(0,x) = \begin{cases} e_- \text{ for } x < 0 \\ e_+ \text{ for } x \geq 0\,. \end{cases} \tag{6.2.4}$$

This is the simplest choice of initial conditions with piecewise constant data. It is possible and conventional to give initial states for (ρ, u, p) or (p, u, T) instead of initial states for (ρ, u, e). Also other choices are imaginable.

The Riemann problem is very helpful in the context of hyperbolic partial differential systems, because it exhibits all phenomena as shock or rarefaction waves. It is a basic problem in the theory of hyperbolic systems. In numerics Riemann problems appear in finite volume methods for systems of conservation laws due to the discreteness of the grid.

For the Riemann problem for the compressible Euler equations equipped with an appropriate equation of state one can construct the exact solution. The solution is selfsimilar. It consists of constant states, that are separated by shock and rarefaction waves and a contact discontinuity. Details can be found in several textbooks. For basics on conservation laws see the books of Toro [21], Lax [11], LeVeque [13], Smoller [20], Kröner [10], Dafermos [4], and others.

6.3 Equation of state

As mentioned in the previous section we need an equation of state to close the system (6.2.1)-(6.2.3). Several commonly accepted equations of state are available like the van der Waals equation of state or the Tait's equation. A collective problem is that for any choice of parameters all these equations at the best only locally give a good approximation of the thermodynamic properties of water vapor or liquid water.

On the other hand, the real equation of state for water to the official standard *IAPWS-IF97* based on the standard formulation of Wagner et al. [23], [24], [22] is too complex for analytical consideration. In the following this equation of state is called *real equation of state*.

For the moment we use a modified form of the stiffened gas equation of state, see [19]. It is given by the following relations

$$e_k(p_k, \rho_k) = \frac{p_k + \gamma_k \pi_k}{\rho_k(\gamma_k - 1)} + q_k \,, \tag{6.3.1}$$

$$T_k(p_k, \rho_k) = \frac{p_k + \pi_k}{C_k \rho_k(\gamma_k - 1)} \,, \tag{6.3.2}$$

$$a_k(p_k, \rho_k) = \sqrt{\frac{\gamma_k(p_k + \pi_k)}{\rho_k}} \,, \tag{6.3.3}$$

$$s_k(p_k, T_k) = C_k \ln \frac{T_k^{\gamma_k}}{(p_k + \pi_k)^{(\gamma_k - 1)}} + q_k' \,. \tag{6.3.4}$$

Here T and s denote the *temperature* and the *specific entropy* of the fluid. The speed of sound is given by a. The index $k = V, L$ indicates the fluid under consideration, vapor or liquid. The parameters γ, π, q, q' and C will be specified later. Note, that for the special choice of $\pi = 0$ and $q = 0$ the equation of state reduces to the ideal gas law.

For the physical background of the following considerations and more details on thermodynamics we refer to the books of Müller and Müller [15] and Müller [16].

The *specific Gibbs free energy* of the phases is given by

$$g_k = e_k + \frac{p_k}{\rho_k} - T_k s_k \,. \tag{6.3.5}$$

If the vapor and the liquid phase are in thermodynamic equilibrium the Gibbs free energies equal each other, this means that

$$g_V = g_L \,. \tag{6.3.6}$$

Using the relations (6.3.1)-(6.3.4) the Gibbs free energy of each phase can be expressed as a function of the temperature and the pressure

$$g_k = g_k(p_k, T_k) \,.$$

Then the equilibrium condition (6.3.6) gives a direct relation between the temperature and the corresponding equilibrium pressure or *saturation pressure*

$$p_{sat} = p_{sat}(T) \,. \tag{6.3.7}$$

This relation gives the *saturation line* in the (T, p)-phase space. Sometimes it is useful to inversly express the temperature as a function of the pressure

$$T_{sat} = T_{sat}(p) \,. \tag{6.3.8}$$

For admissible pressures we obtain the corresponding *saturation temperature*.

For the moment we use the same parameters as Saurel et al. [19]. These parameters are given in Table 6.1. For this special choice of parameters we obtain the saturation curve given by the solid line in Figure 6.1. Here Region 1 belongs to the liquid water phase, whereas Region 2 belongs to the water vapor. The dashed line marks the real saturation line. Obviously the precise shape of the saturation line directly depends on the choice for the equations of state and the parameters therein.

Note that for a thermodynamic consistent equation of state the following relations hold

$$\frac{\partial g(p,T)}{\partial p} = \frac{1}{\rho} \qquad \text{and} \qquad \frac{\partial g(p,T)}{\partial T} = -s \,. \tag{6.3.9}$$

These relations will be used for the proof of our statement.

k	γ	π [Pa]	C [J/kg/K]	q [J/kg]	q' [J/kg/K]
vapor	1.43	0	1040	2030000	-23000
liquid	2.35	10^9	1816	-1167000	0

Table 6.1: Parameters for water vapor and liquid water, [19]

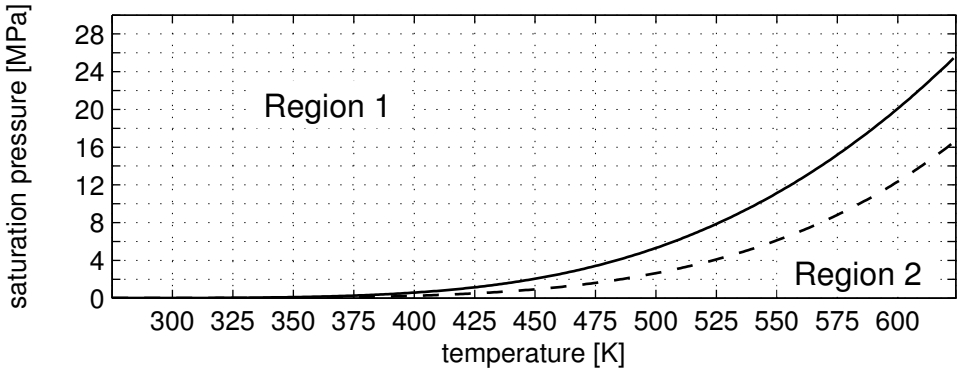

Figure 6.1: Solid line: saturation curve $p_{sat(T)}$ for parameters given in Table 6.1, dashed line: real saturation curve

6.4 Condensation by compression

6.4.1 Wave curve in the (p, T)-phase space

At first we consider the case of the compression of water vapor. This case can be simulated by a steam filled tube equipped with a flexible piston, which is highly sped up to compress the vapor phase, see Figure 6.2. The compression of water vapor will lead to an increase of the pressure and the density of

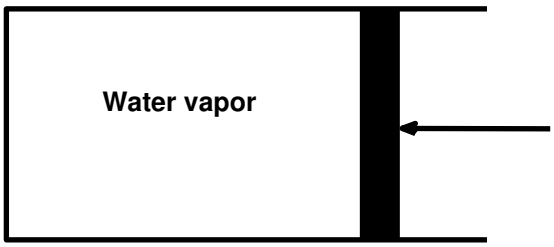

Figure 6.2: Compression of water vapor

the vapor phase. From the theory of the Euler equations we know, that a shock wave will propagate through the vapor phase.

Assume that the state ahead of the shock is given by $(\hat{\rho}, \hat{u}, \hat{p})$. The state behind the shock is denoted by (ρ_*, u_*, p_*). Then we have the following relationship for the density and the pressure

$$\frac{\rho_*}{\hat{\rho}} = \frac{\left(\frac{p_*}{\hat{p}}\right) + \left(\frac{\gamma-1}{\gamma+1}\right) + \frac{2\gamma\pi}{\hat{p}(\gamma+1)}}{\left(\frac{\gamma-1}{\gamma+1}\right)\left(\frac{p_*}{\hat{p}}\right) + 1 + \frac{2\gamma\pi}{\hat{p}(\gamma+1)}}. \tag{6.4.1}$$

For details of the derivation of relation (6.4.1) we recommend the book of Toro [21], Section 3.1. Note, that this relation holds only for the generalized stiffened gas law (6.3.1)-(6.3.4). Using the equation of

state (6.3.2) we easily obtain an analogous relation for the pressure and the temperature, which is given by

$$\frac{\hat{T}}{T_*} = \frac{\hat{p}+\pi}{p_*+\pi} \cdot \frac{p_*(\gamma+1)+\hat{p}(\gamma-1)+2\gamma\pi}{\hat{p}(\gamma+1)+p_*(\gamma-1)+2\gamma\pi\frac{\hat{p}}{p_*}}\,. \tag{6.4.2}$$

From Equation (6.4.2) we find the wave curve $T_*(p_*;\hat{p},\hat{T})$ in the (p,T)-phase space, that denotes all states (p_*,T_*) that can be connected to the initial state $(\hat{p},\hat{T})$ by a shock wave.

Assume that the vapor phase with initial pressure and temperature $(\hat{p},\hat{T})$ is compressed sufficiently such that a liquid phase is created, then the corresponding wave curve $T_*(p_*;\hat{p},\hat{T})$ must have an intersection point with the saturation line, see the sketch in Figure 6.3. We want to prove that this is impossible.

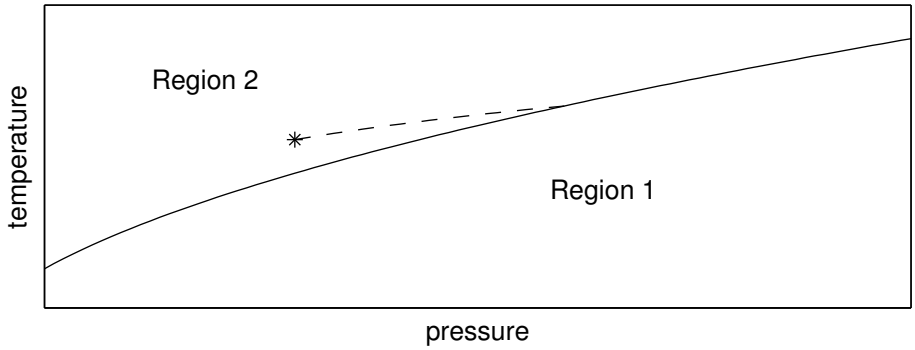

Figure 6.3: Solid line: saturation curve $T_{sat}(p)$, dashed line: wave curve, star: initial state

For the proof we assume the existence of the intersection point and derive a contradiction.

6.4.2 Proof of the statement for a particular equation of state

Assume, the intersection point of the wave curve and the saturation line is given by (p_*,T_*). Then the function

$$\hat{T}(\hat{p};p_*,T_*) = T_* \cdot \frac{\hat{p}}{p_*} \cdot \frac{p_*(\gamma_V+1)+\hat{p}(\gamma_V-1)}{\hat{p}(\gamma_V+1)+p_*(\gamma_V-1)} \tag{6.4.3}$$

denotes all admissible initial states $(\hat{p},\hat{T})$. Here we already used the fact that for the vapor phase we have $\pi = 0$. Let $'$ denote the derivative of the temperature functions with respect to the pressure. At the intersection point the following relation must hold

$$\hat{T}'(p_*) \le T'_{sat}(p_*)\,. \tag{6.4.4}$$

By a simple calculation we find

$$\hat{T}'(p_*;p_*,T_*) = \frac{T_*}{p_*} \cdot \frac{\gamma_V-1}{\gamma_V}\,. \tag{6.4.5}$$

To find $T'_{sat}(p_*)$ we start with the equilibrium condition (6.3.6) and express the Gibbs free energies of the phases as functions of p and T. We obtain

$$g_k(p,T) = C_k T\gamma_k + q_k - C_k T \ln\frac{T^{\gamma_k}}{(p+\pi_k)^{\gamma_k-1}} - Tq'_k \tag{6.4.6}$$

with $k = L,V$. From

$$f(p,T_{sat}(p)) = g_V(p,T) - g_L(p,T) = 0 \tag{6.4.7}$$

we derive by using the implicit function theorem

$$\begin{aligned}
\frac{\partial f}{\partial p} &= C_V(\gamma_V-1)\frac{T_{sat}}{p} - C_L(\gamma_L-1)\frac{T_{sat}}{p+\pi_L}\,,\\
\frac{\partial f}{\partial T_{sat}} &= -C_V \ln\frac{T_{sat}^{\gamma_V}}{(p)^{\gamma_V-1}} - q'_V + C_L \ln\frac{T_{sat}^{\gamma_L}}{(p+\pi_L)^{\gamma_L-1}}\\
&= C_L\gamma_L - C_V\gamma_V + \frac{q_L-q_V}{T_{sat}}
\end{aligned}$$

and finally

$$T'_{sat}(p_*;T_*) = T_* \cdot \frac{\frac{C_V(\gamma_V-1)}{p_*} - \frac{C_L(\gamma_L-1)}{p_*+\pi_L}}{C_V\gamma_V - C_L\gamma_L + \frac{q_V-q_L}{T_*}} < T_* \cdot \frac{\frac{C_V(\gamma_V-1)}{p_*}}{C_V\gamma_V}\,. \tag{6.4.8}$$

This is clear because

$$-\frac{C_L(\gamma_L-1)}{p_*+\pi_L} < 0 \qquad \text{and} \qquad -C_L\gamma_L + \frac{q_V-q_L}{T_*} > 0\,.$$

Obviously (6.4.8) implies

$$T'_{sat}(p_*;T_*) < \frac{T_*}{p_*} \cdot \frac{\gamma_V-1}{\gamma_V} = \hat{T}'(p_*;p_*,T_*)\,. \tag{6.4.9}$$

This is a contradiction, see (6.4.4). Accordingly we have

Theorem 6.4.1. *Using the equations of state (6.3.1)-(6.3.4) and the parameters given in Table 6.1 condensation by compression of pure water vapor cannot occur.*

6.4.3 Short discussion of different phase transition models

In the following paragraph we explain, why the proof of our statement given in Section 6.4.2 resp. in Section 6.5 is applicable for all considered models based on Euler equations.

A pure water vapor phase can be described by a single set of Euler equations. The compression leads to an increase of the density and the pressure as already mentioned in the previous section. One may assume that for sufficiently strong compression the vapor phase starts to condensate. This means, that a liquid phase is created.

Of course, for any state (p,T) which is in the interior of Region 2 (water vapor), the vapor phase is situated in a stable state. In order that phase condensation can happen, there must be a mechanism for phase transition. Therefore, it is clear that in the case of condensation the wave curve, see the next to last section, must have an intersection point with the saturation line. For this it doesn't matter, whether phase transition is modeled by a kinetic relation [6], [14] or by using an equilibrium assumption as done in [5].

Using a kinetic relation, a nucleation criterion is used, see [6]. Here a critical state is reached, in which the vapor phase starts to condensate, which implies the intersection point.

In Dumbser et al. [5] phase transition is modeled by an equilibrium assumption. For any given temperature T and $p < p_{sat}(T)$ the pair (T,p) describes some vapor state. Analogously (T,p) with $p > p_{sat}(T)$ describes the fluid in the liquid state. For $p = p_{sat}(T)$ one may have water vapor or liquid water as well as a mixture of both fluids. The fluid at the saturation state is defined by its temperature and the mass fraction or equivalently by its pressure and the mass fraction of the vapor/liquid phase. All corresponding states in the (p,T)-phase plane are located at the saturation line. For more details see Iben et al. [8]. Nevertheless, for condensation a wave curve must have an intersection point with the saturation line.

The Euler equations are only valid for pure fluids or homogeneous mixtures in the thermodynamic equilibrium. For models that use only one set of Euler equations as discussed before pure fluid are present. On the other hand in literatur often models of Baer-Nunziato type are used to describe the situation considered. The generalized Baer-Nunziato model is given by a two phase model using two sets of Euler equations

$$\begin{aligned}
\frac{\partial}{\partial t}\alpha_k\rho_k + \frac{\partial}{\partial x}\alpha_k\rho_k u_k &= \pm\dot{m}\,,\\
\frac{\partial}{\partial t}\alpha_k\rho_k u_k + \frac{\partial}{\partial x}\alpha_k(\rho_k u_k^2 + p_k) &= \pm P\frac{\partial}{\partial x}\alpha_k \pm M\,,\\
\frac{\partial}{\partial t}\alpha_k\rho_k(e_k + \frac{1}{2}u_k^2) + \frac{\partial}{\partial x}\big[\rho_k(e_k + \frac{1}{2}u_k^2) + p_k\big]u_k &= \mp P\frac{\partial}{\partial t}\alpha_k \pm E\,,
\end{aligned}$$

$k = 1,2$ and a further equation to describe the volume fractions of the phases

$$\frac{\partial}{\partial t}\alpha_1 + U\frac{\partial}{\partial x}\alpha_k = A$$

with the same notations as before. Further, α_k denotes the volumefraction of phase k. The sources $A, \dot{m}, M, E$ on the right hand side of the equations describe the exchange of mass, momentum and energy. They include relaxation terms for velocity, pressure, temperature and Gibbs free energy of the phases, that guarantee, that both phases relax to thermodynamic equilibrium. The pressure P und the velocity U have to be defined by some closure law, see [18], [19] or [25].

Again we start with a pure vapor phase, that will be compressed. For numerical reasons the volume fraction of the pure phase is assumed to be $1 - \varepsilon$, whereas the volume fraction of the absent phase is assumed to be ε. Typically one uses $\varepsilon = 10^{-8}$, see for instance Saurel and Abgrall [18].

Mass transfer is described by the Gibbs free energy relaxation term. Condensation will occur only in the case, that the specific Gibbs free energy of the vapor phase is larger than the specific Gibbs free energy of the (artificial) liquid phase. This is not the case for any set of initial data that describes a pure water vapor phase. Therefore there is no contribution by the relaxation terms as long as (T, p) is in the interior of Region 2 (vapor phase).

In regions of constant volume fractions the system decouples. The solution for each phase can be determined separately. This implies that the relations of the single phase Euler equations are also valid for the Baer Nunziato model in the case considered. In order that condensation can occur the vapor phase must be compressed in such a manner that the specific Gibbs free energy of the vapor phase is larger than the specific Gibbs free energy of the (artificial) liquid phase. This implies an intersection point of the wave curve with the saturation line.

6.5 Extension to the real equation of state for water

In the previous Section 6.4 we have proved, that condensation by compression can not occur for the chosen equations of state with parameters given in Table 6.1. On the other hand, in Figure 6.1 we can see, that this choice gives a very bad approximation of the real saturation curve for higher temperatures. We now generalize our statement using the results from the last section. We want to show, that for the *real equation of state* and for *good* approximations of the real equation of state condensation by compression cannot occur. The proof uses the same arguments as before.

We start with an arbitrary initial state in the vapor region and we consider the corresponding wave curve. Assume, (p_*, T_*) is the intersection point of the curve $\hat{T}(\hat{p}; p_*, T_*)$ of all admissible initial states in the (p, T)-phase space with the real saturation line $T_{sat}(p)$. We compare the derivatives and find the contradiction.

6.5.1 Approximation of the real equation of state

For our purpose it is sufficient to find a good approximation of the real equation of state in a small neighborhood of the saturation line. In the following we show how to find suitable parameters, coming from the intersection point (p_*, T_*). This is an improvement of the method of Le Metayer et al. [12], which is a modification of the idea introduced by Barberon and Helluy [3].

6.5.1.1 Vapor phase

For any temperature T_* the corresponding (real) saturation pressure is known by the real formulas given by Wagner [24], [22]. The same is true for the corresponding vapor density ρ_{V*}, the speed of sound a_{V*}, the entropy s_{V*} and the internal energy e_{V*}. For simplicity we choose $\pi_V = 0$. Then from (6.3.3) we directly obtain γ_V. Next we calculate q_V from (6.3.1), C_V from (6.3.2) and q'_V from (6.3.4). The results are given in Figure 6.4.

6.5.1.2 Liquid phase

For the liquid phase we disclaim the simplifying assumption for the parameter π. Accordingly we are looking for 5 parameters. Therefore beside the relations (6.3.1) - (6.3.4) we can use a further relation. From thermodynamics it is known, that

$$T \frac{\partial s(T, p)}{\partial T} = C^p$$

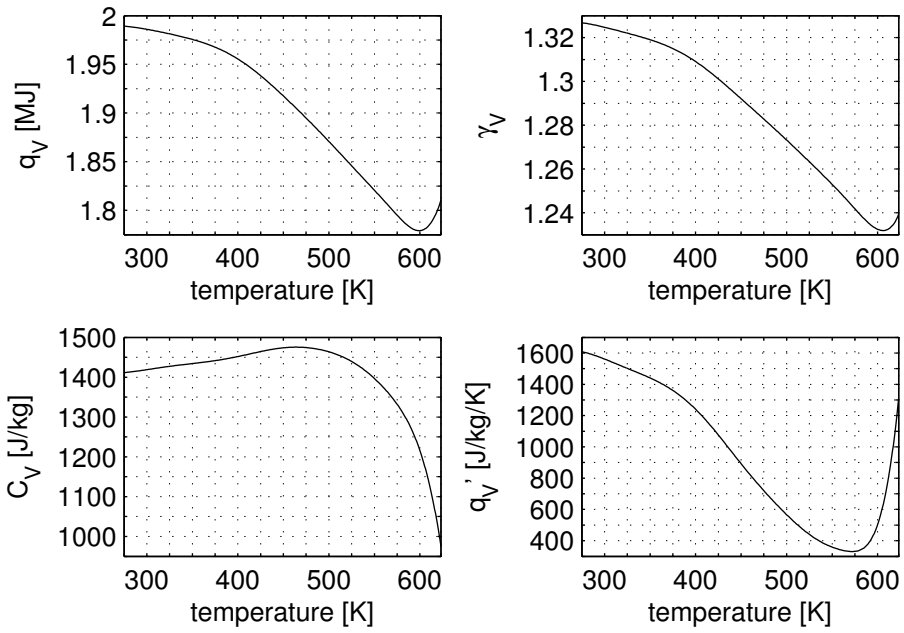

Figure 6.4: Local optimal parameters for the vapor phase

with the *specific heat capacity at constant pressure*. Using (6.3.4), (6.3.2) and (6.3.1) we find that

$$\begin{aligned} C_L^p = T_L \frac{\partial s_L(T_L, p_L)}{\partial T_L} &= C_L \gamma_L \\ &= \frac{1}{T_L}\left(\frac{p_L + \gamma_L \pi_L}{\rho_L(\gamma_L - 1)} + \frac{\gamma_L p_L - p_L}{\rho_L(\gamma_L - 1)}\right) \\ &= \frac{1}{T_L}\left(e_L - q_L + \frac{p_L}{\rho_L}\right). \end{aligned}$$

This gives us the further relation

$$e_L = C_L^p T - \frac{p_L}{\rho_L} + q_L\,, \tag{6.5.1}$$

where C_L^p denotes the specific heat capacity at constant pressure of the liquid phase. Again we use the real equation of state to obtain the liquid density ρ_{L*}, the speed of sound a_{L*}, the entropy s_{L*}, the internal energy e_{L*} as well as the specific heat capacity C_{L*}^p. Then from (6.5.1) we find q_L. After that we calculate π_L and γ_L from (6.3.1) and (6.3.3). Finally we obtain C_L from equation (6.3.2) and q_L' from equation (6.3.4). The results are given in Figure 6.5.

Using the parameters $\pi_V, \pi_L, \gamma_V, \gamma_L, C_V, C_L, q_V, q_L, q_V', q_L'$ obtained in Sections 6.5.1.1 and 6.5.1.2 the equations of state (6.3.1)-(6.3.4) give the exact values for the densities, the internal energies, the entropies and the sound speeds at saturation state (p_*, T_*). Also we obtain the exact values for the Gibbs free energies and the enthalpies. From equations $(6.3.9)_1$ and $(6.3.9)_2$ as well as equation (6.4.7) and the implicit function theorem we see, that we also find the exact value

$$T'_{sat}(p_*; T_*)\,. \tag{6.5.2}$$

Due to the smoothness of all expressions for any given tolerance $\varepsilon > 0$ we find a sufficiently small neighborhood of the saturation state (p_*, T_*) such that all relevant physical states $\rho_k, e_k, s_k, a_k, g_k$ are approximated with a deviation less then ε.

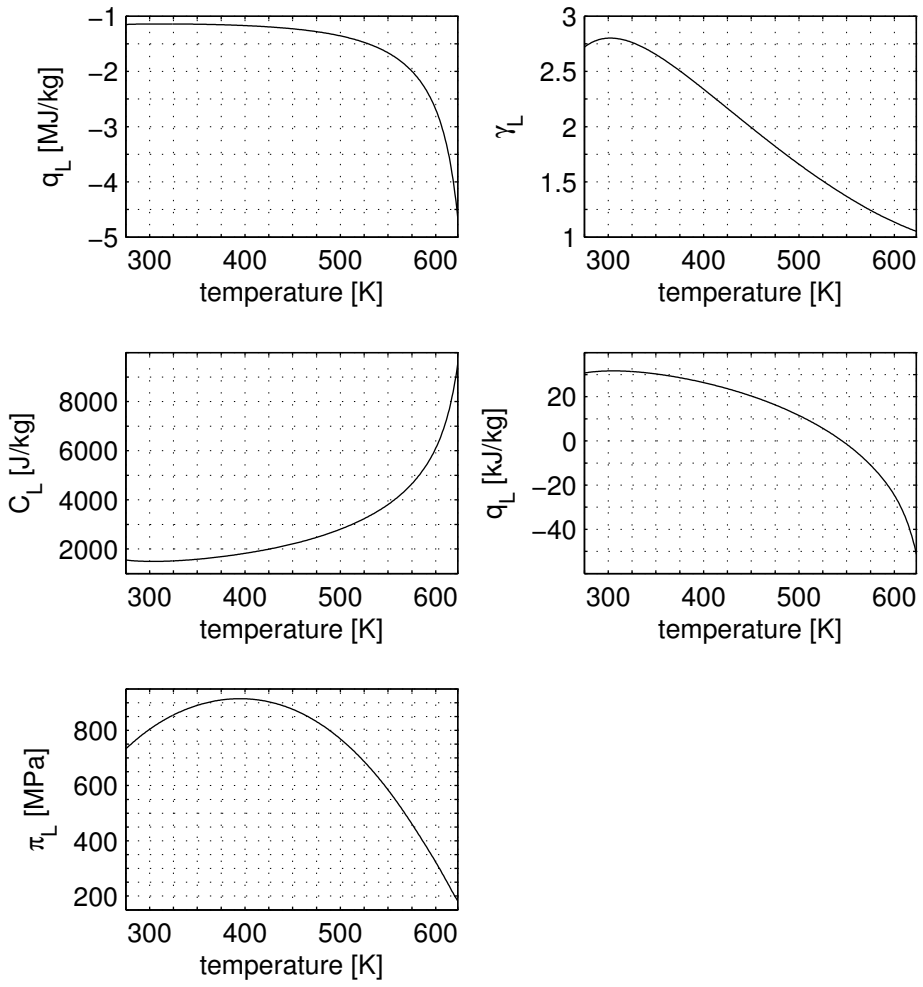

Figure 6.5: Local optimal parameters for the liquid phase

6.5.2 Proof of the statement for the real equation of state

Assume, for any initial state in the vapor region, that is close to the saturation line, the corresponding wave curve in the $(p.T)$-phase space and the (real) saturation line have the intersection point (p_*, T_*). Assume further, that we used the optimal parameters $\pi_V, \pi_L, \gamma_V, \gamma_L, C_V, C_L, q_V, q_L, q'_V, q'_L$, such that the equations of state (6.3.1)-(6.3.4) give the exact values for $\rho_k, e_k, s_k, a_k, g_k$ for both phases at saturation state (p_*, T_*). Then the following relation must hold at the intersection point

$$\hat{T}'(p_*) \leq T'_{sat}(p_*)\,. \tag{6.5.3}$$

As before $\hat{T}(\hat{p}; p_*, T_*)$ denotes all admissible initial states $(\hat{p}, \hat{T})$ in the vapor region, in a sufficiently small neighborhood of (p_*, T_*). For the derivative we have

$$\hat{T}'(p_*; p_*, T_*) = \frac{T_*}{p_*} \cdot \frac{\gamma_V - 1}{\gamma_V}\,. \tag{6.5.4}$$

Moreover, we have

$$T'_{sat}(p_*; T_*) = T_* \cdot \frac{\frac{C_V(\gamma_V-1)}{p_*} - \frac{C_L(\gamma_L-1)}{p_*+\pi_L}}{C_V\gamma_V - C_L\gamma_L + \frac{q_V-q_L}{T_*}}\,. \tag{6.5.5}$$

In both equations (6.5.4) and (6.5.5) we used the local optimal parameters. As already explained at the end of Section 6.5.1, equation (6.5.5) gives the exact value for the derivative. Simple estimations show, that

$$\hat{T}'(p_*) > T'_{sat}(p_*)\,. \tag{6.5.6}$$

Accordingly, there is no such intersection point. Due to the smoothness of all expressions and the exactness of (6.5.5) this statement is true for the real equation of state and for all sufficiently good approximations of the real equation of state. If there is any set of parameters $\pi_V, \pi_L, \gamma_V, \gamma_L, C_V, C_L, q_V, q_L, q'_V, q'_L$ such that (6.5.6) is not satisfied, then the parameters obviously give a coarse approximation of the saturation line and the result is not meaningful. The same is true for any other choice of equations of state for the liquid and the vapor phase. We summarize

Theorem 6.5.1. *Using the real equations of state [23] or any good approximation of the real equation of state nucleation by compression cannot occur.*

6.6 Cavitation by expansion

After the discussion of condensation by compression one may ask for the opposite case of cavitation by expansion. We will see, that this process is more complicated and we will distinguish between two cases. The liquid phase will be expanded in a manner that phase transition will occur. This case corresponds to a cavitation tube, which is a tube filled with liquid water and a flexible piston, see Figure 6.6. To

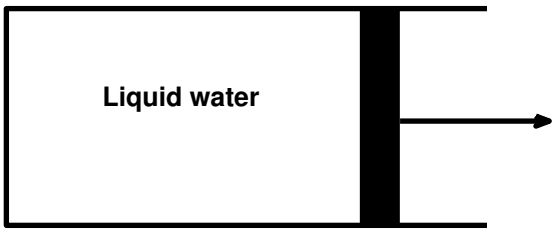

Figure 6.6: Expansion of liquid water

illustrate the physics we give the s-$T-$diagram in Figure 6.7, where the path (1) corresponds to the process considered. We have seen, that the Baer Nunziato type relaxation model allows the coexistence of both the vapor and the liquid phase in the same point of the physical domain at the saturation state. The same is true for the Eulerian model used by Dumbser et al. [5]. Here the phase transition is modeled

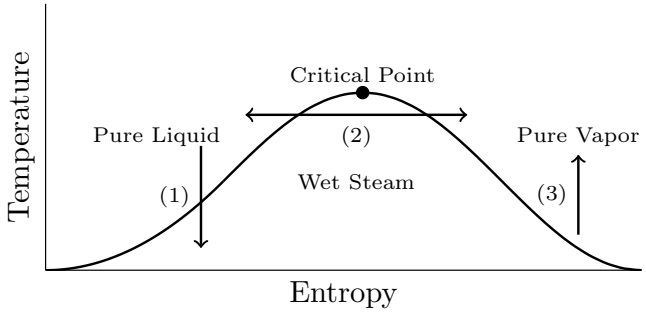

Figure 6.7: Entropy temperature diagram: (1) isentropic expansion - rarefaction wave, (2) isothermal path, (3) isentropic compression, see Iben [7]

by an equilibrium assumption. The mixture is called *wet steam*. An expansion process such that a mixture of water vapor and liquid water (wet steam) is created, we call the process **weak cavitation**. On the other hand, if pure water vapor is created, we call this process **strong cavitation**.

6.6.1 Cavitation in the weak sense

If the liquid phase is expanded, a rarefaction wave will propagate through the liquid phase. In analogy to the condensation case we start with an arbitrary set of initial data in the liquid phase (Region 1). We construct the wave curve, that connects the initial state to all possible states behind the rarefaction wave. If (weak) cavitation, by sufficiently strong expansion, can occur this wave curve must have an intersection point with the saturation line. It is not surprising, that this is usually the case. Numerous examples can be found in the literature, see for instance the example *cavitation by strong rarefaction* using one set of Euler equations and the equilibrium assumption in Dumbser et al. [5]. See further the *expansion tube problem* in Zein et al. [25] using the Baer Nunziato type relaxation model.

6.6.2 Cavitation in the strong sense

For the moment we restrict ourselves to the two model types, that allow the coexistence of vapor and liquid, [25], [5]. Models, using a kinetic relation will be discussed later.

One may assume that for sufficiently strong expansions one may create pure water vapor. To illustrate that situation we refer to Figure 6.8. Because Region 3, the wet steam region, reduces to a single line in

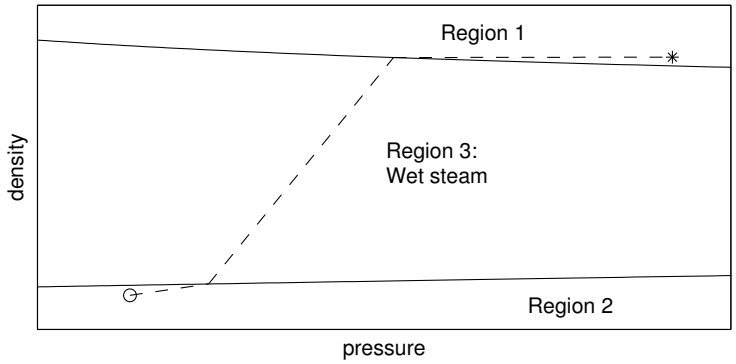

Figure 6.8: Solid line: saturation curves $\rho_V(p_{sat})$, $\rho_L(p_{sat})$, dashed line: wave curve, star: initial state, circle: pure water vapor state

the (p,T) phase plan, we now plot all the data in the more descriptive (p,ρ) phase plane. The wet steam region is bounded by the saturation (solid) lines. Assume, there is any initial liquid state, marked by the star and assume further, the liquid is expanded in a manner that pure water vapor is created. This state is indicated by the circle. Then there is a rarefaction wave curve, connecting the star and the circle state. This wave curve crosses the two curves $\rho_k(p_{sat})$. The same situation in the (p,T) phase plane is given in Figure 6.9. In the following we will show, that strong cavitation for the models considered cannot occur. The argument is similar to the argument in the condensation case. Assume, the circle state exists. This implies the existence of a rarefaction wave curve that connects both the circle and the star state. The intersection point of the wave curve and the saturation curve $T_{sat}(p)$ in the (p,T) phase plane is called (p_*,T_*). Let us consider that part of the wave curve, that is located in the vapor in Region 2. We denote this curve by $\hat{T}(p;p_*,T_*)$. As before for the intersection point we must have

$$\hat{T}'(p_*;p_*,T_*) \leq T'_{sat}(p_*)\,.$$

The wave curve is found to be

$$\hat{T}(p;p_*,T_*) = T_*\left(\frac{p}{p_*}\right)^{\frac{\gamma_V-1}{\gamma_V}}\,. \tag{6.6.1}$$

This directly follows from Equation (6.3.4) and the fact, that the entropy is constant across a rarefaction wave. Equation (6.6.1) implies

$$\hat{T}(p_*;p_*,T_*) = \frac{T_*}{p_*}\cdot\frac{\gamma_V-1}{\gamma_V}\,. \tag{6.6.2}$$

This gives a contradiction, see (6.5.4) and (6.5.6).

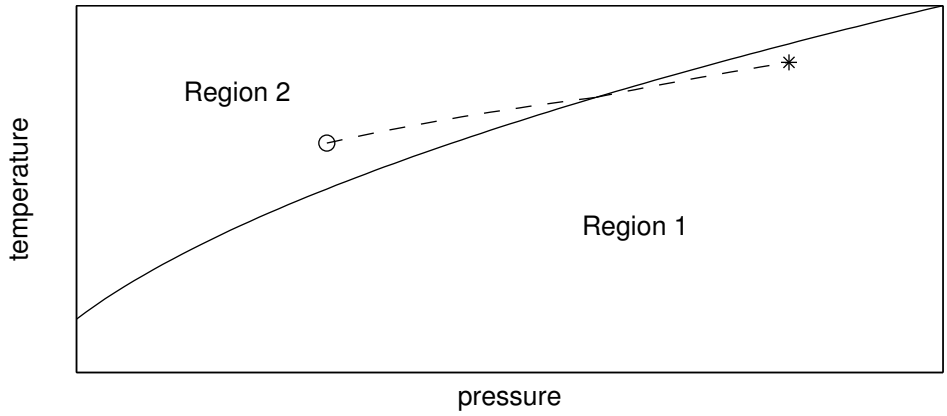

Figure 6.9: Solid line: saturation curve, dashed line: wave curve, star: initial state, circle: pure water vapor state

Theorem 6.6.1. *Using the real equation of state or any good approximation of the real equation of state strong cavitation by expansion cannot occur in an approach based on Euler equations and an equilibrium assumption, [5], [25].*

There is an alternative, very simple argument to show, that a pure liquid state and a pure water vapor state cannot be connected by a rarefaction wave. As already mentioned it is a well known fact, that the entropy is constant across a rarefaction wave. But it is also known, that for any temperature between triple point temperature and critical temperature $T_{tripel} = 273.16K < T < T_{crit} = 647.096K$ the entropies satisfy the inequalities

$$s_L < s_{crit} \qquad \text{and} \qquad s_{crit} < s_V \,. \tag{6.6.3}$$

Obviously there are no liquid and vapor states with the same entropy. This also can be seen in Figure 6.7.

Using an Eulerian approach like Dumbser et al. [5] one can obtain only weak cavitation. Wet steam is created, which is a mixture of water vapor and liquid water at saturation state. For the entropy one has

$$s_{mix} = \mu s_V + (1-\mu) s_L \tag{6.6.4}$$

where $\mu \in [0,1]$ denotes the vapor mass fraction, see [5]. Due to Equation (6.6.3) the value μ is bounded for cavitation starting from pure liquid water. Using the steam tables of Wagner [22] we find

$$\mu \leq 0.5 \,. \tag{6.6.5}$$

In contrast to the equilibrium models discussed in the first part of Section 6.6.2 models using a kinetic relation are able to produce strong cavitation. This is clear by Section 6.6.1. A rarefaction wave curve in the liquid Region 1 can have an intersection point with the saturation line. Here a critical state is reached. A cavitation criterion can be used, see Hantke et al. [6]. The liquid phase starts to evaporate and a pure vapor phase is created. An important difference to the previous models is, that the solution is nonsmooth and entropy production by phase transition is allowed. Therefore there is no contradiction to previous results.

6.7 Conclusions

We have seen, that condensation by compression cannot occur in an Eulerian approach. Due to the compression of the water vapor not only the pressure but also the temperature is increasing. Because of the temperature rise the saturation pressure is increasing. The key point is, that the saturation pressure increases much faster than the pressure inside the vapor phase. Therefore phase transition cannot take place. From observations of nearly adiabatic flows, see Figure 6.6, 6.2 this phenomenon is known.

- The Euler equations correctly reflect this behavior. We gave a mathematical proof for this.
- Adiabatic compression of vapor does not lead to liquid phase, see Figure 6.7, path (1). To reach this state, negative heat flow has to be used. This is equivalent to the use of isothermal Euler equations such as done by Hantke et. al [6]. This corresponds to path (1) in Figure 6.7.

This effect comes up in much weaker form in the case of cavitation. The reason may be that the temperature changes due to the expansion are much smaller.

- It is not possible to evaporate a pure liquid by a rarefaction wave completely, only with external supply of energy see again Figure 6.7. This is also equivalent to the use of isothermal Euler equations [6], see Figure 6.7, path (2).
- We gave a mathematical proof for this.

On the other hand this shows, that heat flow plays an important role in cavitating processes or in condensation processes caused by compression. Eulerian models are not appropriate to describe such effects.

References

[1] R. Abeyaratne, J.K. Knowles, Kinetic relations and the propagation of phase boundaries in solids, Aech. Rat. Mech. Anal., 114 (1991), 119–154.

[2] M.R. Baer, J.W. Nunziato, A two-phase mixture theory of the deflagration-to-detonation transition (DDT) in reactive granular materials, Int. J. Multiphase Flows, 12 (1986), 861–889.

[3] T. Barberon, P. Helluy, Finite volume simulations of cavitating flows, Computers & Fluids, 34 (2005), 832–858.

[4] C. M. Dafermos, *Hyperbolic Conservation Laws in Continuum Physics,* Springer-Verlag, Berlin - Heidelberg, 2010.

[5] M. Dumbser, U. Iben, and C.-D. Munz. Efficient implementation of high order unstructured WENO schemes for cavitating flows, *Computers & Fluids*, **86** (2013), pp. 141 - 168.

[6] M. Hantke, W. Dreyer, G. Warnecke, Exact solution to the Riemann problem for compressible isothermal Euler equations for two phase flows with and without phase transition.

[7] U. Iben, Modelling of cavitation, Systems Analysis Modelling Simulation, 42:9 (2002), 1283–1307.

[8] U. Iben, F. Wrona, C.D. Munz, M. Beck, Cavitation in hydraulic tools based on thermodynamic properties of liquid and gas, Journal of Fluids Engeneering - Transaction of the ASME, 124 (2002), 1011–1017.

[9] U. Iben, Entwicklung und Untersuchung von Kavitationsmodellen im Zusammenhang mit transienten Leitungsströmungen, Fortschritt-Berichte VDI, reihe 7, Strömngstechnik, VDI Verlag, 2004.

[10] D. Kröner, *Numerical schemes for conservation laws*, John Wiley and Sons, Chichester, 1997.

[11] P. Lax, *Hyperbolic Systems of Conservation Laws and the Mathematical Theory of Shock Waves*, Society for Industrial and Applied Mathematics, Philadelphia, 1990.

[12] O. Le Metayer, J. Massoni, R. Saurel, Elaborating equations of state of a liquid and its vapor for two phase flow models (in french), Int. J. Thermal Sci., 43(3) (2004), 265–276.

[13] R. LeVeque, *Numerical Methods for Conservation Laws*, Lectures in Mathematics ETH Zürich Birkhäuser Verlag, Basel - Boston - Berlin, 1990.

[14] C. Merkle, Dynamical Phase Transitions in Compressible Media, Doctoral Thesis, Univ. Freiburg, 2006.

[15] I. Müller and W. Müller, *Fundamentals of Thermodynamics and Applications*, Springer-Verlag, Berlin, 2009.

[16] I. Müller, *Thermodynamics*, Pitman, London, 1985.

[17] F. Petitpas, J. Massoni, R. Saurel, E. Lapebie, L. Munier, Diffuse interface models for high speed cavitating underwater systems, Int. J. Multiphase Flows, 35 (2009), 747–759.

[18] R. Saurel, R. Abgrall, A multiphase Godunov method for compressible multifluid and multiphase flows, J. Comput. Phys., 150(2) (1999), 425–467.

[19] R. Saurel, F. Petitpas, R. Abgrall, Modelling phase transition in metastable liquids: Application to cavitating and flashing flows, J. Fluid. Mech., 607 (2008), 313–350.

[20] J. Smoller, *Shock Waves and Reaction-Diffusion Equations*, Springer-Verlag, New York, 1994.

[21] E. F. Toro, *Riemann Solvers and Numerical Methods for Fluid Dynamics*, Springer-Verlag, Berlin - Heidelberg, 1999.

[22] W. Wagner, H.-J. Kretzschmar, *International Steam Tables*, Springer-Verlag, Berlin - Heidelberg, 2008.

[23] W. Wagner, A. Kruse, Properties of Water and Steam - The Industrial Standard IAPWS-IF97 / Zustandsgrößen von Wasser und Wasserdampf - Der Industriestandard IAPWS-IF97, Springer-Verlag, Berlin, 1998.

[24] W. Wagner et al., The IAPWS Industrial Formulation 1997 for the Thermodynamic Properties of Water and Steam, Journal of Engeneering for Gas, Turbines and Power, 122 (2000), 150–182.

[25] A. Zein, M. Hantke, G. Warnecke, Modeling phase transition for compressible two-phase flows applied to metastable liquids, J. Comput. Phys., 229(8) (2010), 2964–2998.

Part II

Diffusive Interface models

Chapter 7

Modeling Phase Transition for Two Phase Flows

Bibliographic note: The content of this chapter is published in [H3]: Ali Zein, Maren Hantke, and Gerald Warnecke. Modeling phase transition for compressible two-phase flows applied to metastable liquids, *Journal of Computational Physics*, 229 (2010), pp. 2964-2998.

Abstract: The seven-equation model for two-phase flows is a full non-equilibrium model, each phase has its own pressure, velocity, temperature, etc. A single value for each property, an equilibrium value, can be achieved by relaxation methods. This model has better features than other reduced models of equilibrium pressure for the numerical approximations in the presence of non-conservative terms. In this paper we modify this model to include the heat and mass transfer. We insert the heat and mass transfer through temperature and Gibbs free energy relaxation effects. New relaxation terms are modeled and new procedures for the instantaneous temperature and Gibbs free energy relaxation toward equilibrium is proposed. For modeling such relaxation terms, our idea is to make use of the assumptions that the mechanical properties, the pressure and the velocity, relax much faster than the thermal properties, the temperature and the Gibbs free energy, and the ratio of the Gibbs free energy relaxation time to the temperature relaxation time is extremely high. All relaxation processes are assumed to be instantaneous, i.e. the relaxation times are very close to zero. The temperature and the Gibbs free energy relaxation are used only at the interfaces. By these modifications we get a new model which is able to deal with transition fronts, evaporation fronts, where heat and mass transfer occur. These fronts appear as extra waves in the system. We use the same test problems on metastable liquids as in Saurel et al. [R. Saurel, F. Petitpas and R. Abgrall, Modeling phase transition in metastable liquids: application to cavitating and flashing flows, *J. Fluid Mech.*, 607, 313-350 (2008)]. We have almost similar results. Computed results are compared to the experimental ones of Simões-Moreira and Shepherd [J.R. Simões-Moreira and J.E. Shepherd, Evaporation waves in superheated dodecane, *J. Fluid Mech.*, 382, 63-86 (1999)]. A reasonable agreement is achieved. In addition we consider the six-equation model with a single velocity which is obtained from the seven-equation model in the asymptotic limit of zero velocity relaxation time. The same procedure for the heat and mass transfer is used with the six-equation model and a comparison is made between the results of this model with the results of the seven-equation model.

7.1 Introduction

In the last two decades, considerable research has been devoted to the modeling and simulation of compressible two-phase flows. Most of the models used are typically derived by using averaging procedures [9, 10, 14]. Both the mathematical modeling and numerical computation have certain inherent difficulties.

The difficulties in modeling concern the physical transfer processes taking place across the interface such as mass, momentum and heat transfer. Using averaging techniques of the single phase equations results in additional terms, which describe these transfer processes. The exact expressions for the transfer terms are usually unknown [9]. Also there appear differential terms that are extracted from the transfer

terms that prevent the system from being in divergence form. Therefore, they are referred to as the non-conservative terms and they are responsible for numerical difficulties.

The most general two-phase flow model consists of seven partial differential equations, the evolution equation for the volume fraction of one of the phases together with balance equations for mass, momentum and energy for each phase. The seven-equation model is a full non-equilibrium model, each phase has its own pressure, velocity, temperature, etc. Several authors considered such type of models, Baer and Nunziato [4], Embid and Baer [11] as well as Saurel and Abgrall [27]. Saurel and Abgrall [27] proposed a Godunov-type method for the solution of this model. Also they proposed instantaneous relaxation procedures for the pressure and the velocity that make the pressures and velocities of phases relax to common values. The main disadvantage of this model is the large number of waves.

Several authors have considered a five-equation reduced model which is obtained in the asymptotic limit of the seven-equation model, see Kapila et al. [15], Murrone and Guillard [23], Petitpas et al. [24] and Saurel et al. [33]. This model satisfies the mechanical equilibrium, it has a single pressure and a single velocity. It is composed of two mass equations, a mixture momentum equation and a mixture energy equation. These equations are written in conservative formulation, while the fifth equation of this model is a non-conservative equation for the volume fraction which contains a non-conservative term involving the divergence of the velocity.

Even though the five-equation model is reduced it has severe numerical difficulties. These difficulties include:

- Shock computational difficulties due to the non-conservative character of the model.
- Maintaining volume fraction positivity due to the difficulties in the approximation of the non-conservative term involving the divergence of the velocity.
- Non-monotonic behavior of the mixture sound speed, that obeys the Wood formula, with respect to the volume fraction, see [34]. This behavior may cause inaccurate wave transmission across diffuse interfaces.

The above difficulties are detailed in Saurel et. al. [34] and Petitpas et al. [24]. It is noted that the conventional Godunov-type schemes are not suitable for the resolution of this model [24]. To circumvent these difficulties, the Riemann problem is solved by the help of shock and Riemann invariant relations that were derived by Saurel et al. [32]. And a specific relaxation projection method is used instead of the conventional Godunov method, see Saurel et al. [29] and Petitpas et al. [24]. Moreover, Saurel et al. [33] modified this model to take into account phase transition by including temperature and chemical potential relaxation effects.

From the computational point of view the seven-equation model has several advantages over the five-equation model:

- Preserving the positivity of the volume fraction is easier.
- The mixture sound speed has a monotonic behavior, see Petitpas et al. [24].

According to the attractive advantages of the seven-equation model we aim in this paper to modify this model to include the heat and mass transfer and to present numerical investigations for the resulting model compared with some previously known results. Our attention is devoted to the evaporation that appears in cavitating flows. Thus we can compare our results with the results of [33] for metastable liquids, i.e. liquids with temperature higher than the saturation temperature.

We use the seven-equation model of Saurel and Abgrall [27] which is a modified form of the Baer-Nunziato model [4]. For the solution of the hyperbolic part of the model a modified Godunov-type scheme is used. For the mechanical relaxation, the instantaneous velocity and pressure relaxation procedures of Saurel and Abgrall [27] are taken.

We insert the heat and mass transfer through relaxation effects. New terms associated with the heat and mass transfer are modeled, these terms are given in terms of the temperature difference for the heat transfer and in terms of the Gibbs free energy difference for the mass transfer. Also we propose new procedures for the instantaneous temperature and Gibbs free energy relaxation toward equilibrium. These procedures are used at each time step after the mechanical relaxations. They are used only at specific locations, i.e at evaporation fronts.

Since the exact expressions for the transfer terms are unknown, our idea to model them is to refer to some general physical observations besides the second law of thermodynamics. In particular we assume that the mechanical properties relax much faster than the thermal properties. Also we assume that the relaxation time for the temperature is much smaller than that of the Gibbs free energy. In fact these assumptions agree with physical evidence in a large number of situations, see [5, 13, 15, 22]. In the book of Müller et al. [22] some similar assumption is used in the analysis of the equilibrium conditions for droplets and bubbles, see Chapter 11 there. In Kapila et al. [15] there are some estimates given for the time scales of the relaxation of the velocity, pressure and temperature in granular materials. These estimations show that the relaxation time for the temperature is significantly larger than relaxation times for both the velocity and the pressure. Also other estimations for detonation applications show that the time scale of the velocity relaxation and pressure relaxation are of the same order of magnitude while the temperature relaxation time is much greater than that for the velocity and pressure, see [7, 26]. More discussion of this point is given in Section 7.3.2.

By our modifications of the seven-equation model we get a new model which is able to deal with transition fronts, specifically here evaporation fronts, where heat and mass transfer occur. These fronts appear as extra waves in the system, see Le Metayer et al. [21] and Saurel et al. [33].

Moreover we consider the six-equation model with a single velocity which is obtained from the seven-equation model in the asymptotic limit of zero velocity relaxation time. This model consists of the volume fraction equation of one of the phases, two mass balance equations, a mixture momentum equation and two energy equations. As with the seven- equation model this model has better features for numerical computations than the five-equation model. In fact the major difficulty in the numerics of the five-equation model comes from the equilibrium of the pressure. For more details concerning the six-equation model without phase transition you can see [34].

We model the heat and mass transfer for the six-equation model by using our procedure that is proposed for the seven- equation model under the same assumptions.

We use the same test problems of reference [33] for metastable liquids. We see in our results the extra waves that appear due to the phase transition. Also our results are in a good agreement with the results of [33].

Computed results are compared to the experimental data of Simões-Moreira and Shepherd [36]. Indeed, the computed front velocities of the evaporation waves are compared to the measured ones at several initial temperatures. There is a reasonable agreement with the experimental data.

A comparison between the results of the two models is made. There is no significant difference between the results of both models under the same conditions, but there is a significant difference in the CPU time consumed by both models, this makes the six-equation model less expensive.

This paper is organized as follows. In Section 7.2 we present the mathematical model and its closure relations. Also we deduce phasic entropy equations that will be used in later sections. Section 7.3 is devoted to the numerical method, in particular, we present a modified Godunov-type scheme with the HLLC-type Riemann solver [38] for the seven-equation model. In Section 7.4 we model the heat and mass transfer through the temperature and the Gibbs free energy relaxation effects. Our modeled terms keep the mechanical equilibrium during the temperature relaxation, also they keep the mechanical equilibrium and the temperature equilibrium during the Gibbs free energy relaxation. Mathematical procedures are introduced for the instantaneous relaxation of the temperature and the Gibbs free energy that are used at each time step after the velocity and the pressure relaxation. In Section 7.5 we consider the six-equation model with a single velocity, we apply the same ideas proposed for the heat and mass transfer in the seven-equation model on this case too. Finally, in Section 7.6 we present some numerical results. Comparison with experimental data is made and comparisons between the results of the seven-equation model and the six-equation model are considered.

7.2 Mathematical model

The two-phase flow model of Saurel and Abgrall [27] without heat and mass transfer in one dimension can be written as:

$$\frac{\partial \alpha_1}{\partial t} + u_I \frac{\partial \alpha_1}{\partial x} = \mu(p_1 - p_2), \tag{7.2.1a}$$

$$\frac{\partial \alpha_1 \rho_1}{\partial t} + \frac{\partial(\alpha_1 \rho_1 u_1)}{\partial x} = 0, \tag{7.2.1b}$$

$$\frac{\partial \alpha_1 \rho_1 u_1}{\partial t} + \frac{\partial(\alpha_1 \rho_1 u_1^2 + \alpha_1 p_1)}{\partial x} = p_I \frac{\partial \alpha_1}{\partial x} + \lambda(u_2 - u_1), \tag{7.2.1c}$$

$$\frac{\partial \alpha_1 \rho_1 E_1}{\partial t} + \frac{\partial(\alpha_1(\rho_1 E_1 + p_1)u_1)}{\partial x} = p_I u_I \frac{\partial \alpha_1}{\partial x} + \mu p_I(p_2 - p_1) + \lambda u_I(u_2 - u_1), \tag{7.2.1d}$$

$$\frac{\partial \alpha_2 \rho_2}{\partial t} + \frac{\partial(\alpha_2 \rho_2 u_2)}{\partial x} = 0, \tag{7.2.1e}$$

$$\frac{\partial \alpha_2 \rho_2 u_2}{\partial t} + \frac{\partial(\alpha_2 \rho_2 u_2^2 + \alpha_2 p_2)}{\partial x} = -p_I \frac{\partial \alpha_1}{\partial x} - \lambda(u_2 - u_1), \tag{7.2.1f}$$

$$\frac{\partial \alpha_2 \rho_2 E_2}{\partial t} + \frac{\partial(\alpha_2(\rho_2 E_2 + p_2)u_2)}{\partial x} = -p_I u_I \frac{\partial \alpha_1}{\partial x} - \mu p_I(p_2 - p_1) - \lambda u_I(u_2 - u_1). \tag{7.2.1g}$$

The notations are classical: α_k is the *volume fraction*, ρ_k the *density*, u_k the *velocity*, p_k the *pressure* and $E_k = e_k + \frac{u_k^2}{2}$ the *total specific energy*, where e_k is the *specific internal energy*.

Equation (7.2.1a) is the evolution equation for the volume fraction of phase 1. The volume fractions for both phases are related by the saturation constraint, $\alpha_1 + \alpha_2 = 1$. The sets of equations (7.2.1b)-(7.2.1d) and (7.2.1e)-(7.2.1g) express the conservation of mass, momentum and energy for phase 1 and phase 2 respectively.

The terms p_I and u_I are the *interfacial pressure* and the *interfacial velocity* respectively. As in [27], the interfacial pressure is defined as the mixture pressure, while the interfacial velocity is defined as the velocity of the center of mass

$$p_I = \alpha_1 p_1 + \alpha_2 p_2, \qquad u_I = \frac{\alpha_1 \rho_1 u_1 + \alpha_2 \rho_2 u_2}{\alpha_1 \rho_1 + \alpha_2 \rho_2}. \tag{7.2.2}$$

Other closure relations for the interfacial terms are possible. One other choice is defined by Baer and Nunziato [4] as:

$$p_I = p_1, \qquad u_I = u_2.$$

Further closure relations were derived by Saurel et al. [30] and written as follows

$$p_I = \frac{Z_1 p_2 + Z_2 p_1}{Z_1 + Z_2} + \text{sign}\left(\frac{\partial \alpha_1}{\partial x}\right) \frac{(u_2 - u_1) Z_1 Z_2}{Z_1 + Z_2}, \tag{7.2.3}$$

$$u_I = \frac{Z_1 u_1 + Z_2 u_2}{Z_1 + Z_2} + \text{sign}\left(\frac{\partial \alpha_1}{\partial x}\right) \frac{p_2 - p_1}{Z_1 + Z_2},$$

where Z_k represents the *acoustic impedance*, $Z_k = \rho_k c_k$, where the *speed of sound* c_k is given as

$$c_k^2 = \frac{\frac{p_k}{\rho_k^2} - \left(\frac{\partial e_k}{\partial \rho_k}\right)_{p_k}}{\left(\frac{\partial e_k}{\partial p_k}\right)_{\rho_k}}, \quad k = 1, 2. \tag{7.2.4}$$

In this work for the model (7.2.1) we will use the relations that are given in (7.2.2).

The parameters λ and $\mu > 0$ that appear in the model are the relaxation parameters which determine the rates at which the velocities and pressures of the two phases relax to a common value. In this work we are interested in the instantaneous equilibrium for both the velocity and the pressure, thus the parameters λ and μ are assumed to be infinite.

The model (7.2.1) is a non-strictly hyperbolic system. For details of the mathematical properties of this model see 7.A.

7.2.1 Equations of state (EOS)

Equations of state are used to close the system of equations (7.2.1). Since this model will be modified to include the heat and mass transfer, appropriate EOS are required.

Most phase transition models use a cubic EOS, like the Van der Waals EOS. But using such an EOS produces negative squared sound speed in a certain zone of the two phase flow, the spinodal zone. This causes a loss of hyperbolicity and leads to computational failure [25, 33]. To overcome this problem each fluid obeys its own EOS as a pure material, also these EOS should satisfy certain convexity constraints [19, 25, 33].

In this paper we will use a modified form of the stiffened gas EOS (SG-EOS) with the same parameters for the dodecane and the water as in Saurel et al. [33] and Le Métayer et al. [20]. An essential i ssue is that the various parameters are linked to each other to fulfill some constraints to recover the phase diagram. This makes such a choice of EOS suitable for phase transitions [20, 33]. For $k = 1, 2$, they are expressed as

$$e_k(p_k, \rho_k) = \frac{p_k + \gamma_k \pi_k}{\rho_k(\gamma_k - 1)} + q_k, \tag{7.2.5a}$$

$$T_k(p_k, \rho_k) = \frac{p_k + \pi_k}{C_{vk}\rho_k(\gamma_k - 1)}, \tag{7.2.5b}$$

$$s(p_k, T_k) = C_{vk} \ln \frac{T_k^{\gamma_k}}{(p_k + \pi_k)^{(\gamma_k - 1)}} + q'_k, \tag{7.2.5c}$$

where T_k is the *temperature*, s_k the *specific entropy* and C_{vk} the *heat capacity at constant volume*. The parameters γ_k, π_k, q_k and q'_k are characteristic constants of the thermodynamic behavior of the fluid. All parameters of the SG-EOS are given in Table 7.2.1 for the water and in Table 7.2.1 for the dodecane.

Phase	γ	$\pi(Pa)$	$C_v(J/kg/K)$	$C_p(J/kg/K)$	$q(J/kg)$	$q'(J/kg/K)$
vapor	1.43	0	1.04×10^3	1.487×10^3	2030×10^3	-23×10^3
liquid	2.35	10^9	1.816×10^3	4.267×10^3	-1167×10^3	0

Table 7.1: EOS parameters for vapor and liquid water

Phase	γ	$\pi(Pa)$	$C_v(J/kg/K)$	$C_p(J/kg/K)$	$q(J/kg)$	$q'(J/kg/K)$
vapor	1.025	0	1.956×10^3	2.005×10^3	-237×10^3	-24×10^3
liquid	2.35	4×10^8	1.077×10^3	2.534×10^3	-755×10^3	0

Table 7.2: EOS parameters for vapor and liquid dodecane

7.2.2 Entropy equations

In this part we deduce the entropy equation for each phase. These equations will be used later. Denote the material derivative as

$$\frac{D_k(.)}{Dt} = \frac{\partial(.)}{\partial t} + u_k \frac{\partial(.)}{\partial x}, \quad k = 1, 2.$$

Using the continuity equation (7.2.1b) with the momentum equation (7.2.1c), we have

$$\alpha_1 \rho_1 \frac{D_1 u_1}{Dt} + \frac{\partial \alpha_1 p_1}{\partial x} = p_I \frac{\partial \alpha_1}{\partial x} + \lambda(u_2 - u_1).$$

Multiplying this equation by u_1, we get the following equation for the *kinetic energy*

$$\alpha_1\rho_1\frac{D_1(\frac{u_1^2}{2})}{Dt} + u_1\frac{\partial\alpha_1 p_1}{\partial x} = u_1 p_I\frac{\partial\alpha_1}{\partial x} + \lambda u_1(u_2-u_1).$$

Subtracting this equation from the total energy equation (7.2.1d), we obtain the *internal energy equation*

$$\alpha_1\rho_1\frac{D_1 e_1}{Dt} + \alpha_1 p_1\frac{\partial u_1}{\partial x} = p_I(u_I-u_1)\frac{\partial\alpha_1}{\partial x} + \mu p_I(p_2-p_1) + \lambda(u_I-u_1)(u_2-u_1). \tag{7.2.6}$$

From the volume fraction equation (7.2.1a) with the continuity equation (7.2.1b) we have

$$\alpha_1\frac{D_1\rho_1}{Dt} + \alpha_1\rho_1\frac{\partial u_1}{\partial x} = \rho_1(u_I-u_1)\frac{\partial\alpha_1}{\partial x} + \mu\rho_1(p_2-p_1). \tag{7.2.7}$$

To get an equation for the entropy we use the Gibbs relation

$$T_1 ds_1 = de_1 - \frac{p_1}{\rho_1^2}d\rho_1.$$

By taking the material derivative for this relation and multiplying by $\alpha_1\rho_1$, we obtain

$$\alpha_1\rho_1 T_1\frac{D_1 s_1}{Dt} = \alpha_1\rho_1\frac{D_1 e_1}{Dt} - \frac{\alpha_1 p_1}{\rho_1}\frac{D_1\rho_1}{Dt}. \tag{7.2.8}$$

Using (7.2.6) and (7.2.7) in (7.2.8), we have

$$\alpha_1\rho_1 T_1\frac{D_1 s_1}{Dt} = (p_I-p_1)(u_I-u_1)\frac{\partial\alpha_1}{\partial x} + \mu(p_I-p_1)(p_2-p_1) + \lambda(u_I-u_1)(u_2-u_1).$$

In a similar way we deduce the entropy equation for phase "2" which is given as

$$\alpha_2\rho_2 T_2\frac{D_2 s_2}{Dt} = (p_I-p_2)(u_I-u_2)\frac{\partial\alpha_2}{\partial x} - \mu(p_I-p_2)(p_2-p_1) - \lambda(u_I-u_2)(u_2-u_1).$$

7.3 Numerical method

The source terms of the system (7.2.1) consist of differential parts and non-differential parts. As in [27] to account for both parts we use the Strang splitting approach [37]. Let $L_h^{\Delta t}$ be the operator of numerical solution of the hyperbolic part of the system (7.2.1) over Δt and $L_s^{\frac{\Delta t}{2}}$ the operator of integration of the source and relaxation terms over half of the time interval, i.e. $\dfrac{\Delta t}{2}$. Thus the solution is obtained by the succession of operators.

$$\mathbf{U}_j^{n+1} = L_s^{\frac{\Delta t}{2}} L_h^{\Delta t} L_s^{\frac{\Delta t}{2}}\mathbf{U}_j^n, \tag{7.3.1}$$

where $\mathbf{U} = (\alpha_1, \alpha_1\rho_1, \alpha_1\rho_1 u_1, \alpha_1\rho_1 E_1, \alpha_2\rho_2, \alpha_2\rho_2 u_2, \alpha_2\rho_2 E_2)^T$.

7.3.1 Hyperbolic operator

Consider the hyperbolic part of the system (7.2.1)

$$\frac{\partial\alpha_1}{\partial t} + u_I\frac{\partial\alpha_1}{\partial x} = 0, \tag{7.3.2a}$$

$$\frac{\partial\mathbf{u}}{\partial t} + \frac{\partial\mathbf{f}(\mathbf{u},\alpha_1)}{\partial x} = \mathbf{h}(\mathbf{u},\alpha_1)\frac{\partial\alpha_1}{\partial x}, \tag{7.3.2b}$$

where

$$\mathbf{u} = \begin{bmatrix}\alpha_1\rho_1\\ \alpha_1\rho_1 u_1\\ \alpha_1\rho_1 E_1\\ \alpha_2\rho_2\\ \alpha_2\rho_2 u_2\\ \alpha_2\rho_2 E_2\end{bmatrix}, \quad \mathbf{f}(\mathbf{u},\alpha_1) = \begin{bmatrix}\alpha_1\rho_1 u_1\\ \alpha_1\rho_1 u_1^2 + \alpha_1 p_1\\ \alpha_1(\rho_1 E_1 + p_1)u_1\\ \alpha_2\rho_2 u_2\\ \alpha_2\rho_2 u_2^2 + \alpha_2 p_2\\ \alpha_2(\rho_2 E_2 + p_2)u_2\end{bmatrix}, \quad \mathbf{h}(\mathbf{u},\alpha_1) = \begin{bmatrix}0\\ p_I\\ p_I u_I\\ 0\\ -p_I\\ -p_I u_I\end{bmatrix}.$$

Following [27] a modified Godunov scheme is used to take into account the discretization of the non-conservative part of the system (7.3.2). Assume that we have some Godunov-type discretization for the system (7.3.2b) of the form

$$\mathbf{u}_j^{n+1} = \mathbf{u}_j^n - \frac{\Delta t}{\Delta x}[\mathbf{f}(\mathbf{u}^*(\mathbf{u}_j^n, \mathbf{u}_{j+1}^n)) - \mathbf{f}(\mathbf{u}^*(\mathbf{u}_{j-1}^n, \mathbf{u}_j^n))] + \Delta t \mathbf{h}_j \Delta_j, \tag{7.3.3}$$

where Δ_j is the discrete form of the term $\dfrac{\partial \alpha_1}{\partial x}$, which has to be determined, and $\mathbf{u}^*(\mathbf{u}_j^n, \mathbf{u}_{j+1}^n)$ is the value of $\mathbf{u}$ along the line $x = x_{j+\frac{1}{2}}$ for the Riemann problem with the states $\mathbf{u}_j^n, \mathbf{u}_{j+1}^n$.

The components of the system (7.3.3) for phase "1" can be written as

$$(\alpha\rho)_j^{n+1} = (\alpha\rho)_j^n - \frac{\Delta t}{\Delta x}[(\alpha\rho u)^*_{j+\frac{1}{2}} - (\alpha\rho u)^*_{j-\frac{1}{2}}], \tag{7.3.4a}$$

$$(\alpha\rho u)_j^{n+1} = (\alpha\rho u)_j^n - \frac{\Delta t}{\Delta x}[(\alpha\rho u^2 + \alpha p)^*_{j+\frac{1}{2}} - (\alpha\rho u^2 + \alpha p)^*_{j-\frac{1}{2}}] + \Delta t (p_I)_j^n \Delta_j, \tag{7.3.4b}$$

$$(\alpha\rho E)_j^{n+1} = (\alpha\rho E)_j^n - \frac{\Delta t}{\Delta x}[(\alpha\rho u E + \alpha p u)^*_{j+\frac{1}{2}} - (\alpha\rho u E + \alpha p u)^*_{j-\frac{1}{2}}] + \Delta t (p_I)_j^n (u_I)_j^n \Delta_j. \tag{7.3.4c}$$

The index "1" is omitted for simplicity.

In order to find an expression for Δ_j, the idea of Abgrall [1] is used, that a uniform pressure and velocity must remain uniform during time evolution, for more discussion about this idea see [28]. Assume p and u are a constant pressure and velocity everywhere at time t^n. Then according to the Abgrall principle we have

$$p_j^n = p_j^{n+1} = (p_I)_j^n = p^*_{j\pm\frac{1}{2}} = p, \tag{7.3.5}$$

$$u_j^n = u_j^{n+1} = (u_I)_j^n = u^*_{j\pm\frac{1}{2}} = u. \tag{7.3.6}$$

Multiplying (7.3.4a) by u and subtracting the result from (7.3.4b), we obtain

$$\Delta_j = \frac{1}{\Delta x}(\alpha^*_{j+\frac{1}{2}} - \alpha^*_{j-\frac{1}{2}}). \tag{7.3.7}$$

Using the definition of E and (7.3.7) in (7.3.4c), and using (7.3.4a), we have the following equation for internal energy

$$(\alpha\rho e)_j^{n+1} = (\alpha\rho e)_j^n - \frac{\Delta t}{\Delta x} u[(\alpha\rho e)^*_{j+\frac{1}{2}} - (\alpha\rho e)^*_{j-\frac{1}{2}}]. \tag{7.3.8}$$

Multiplying (7.3.4a) by the parameter q in the (7.2.5a) and subtracting the result from (7.3.8), we obtain

$$(\alpha\rho(e-q))_j^{n+1} = (\alpha\rho(e-q))_j^n - \frac{\Delta t}{\Delta x} u[(\alpha\rho(e-q))^*_{j+\frac{1}{2}} - (\alpha\rho(e-q))^*_{j-\frac{1}{2}}]. \tag{7.3.9}$$

From the EOS (7.2.5a) and uniformity of pressure (7.3.5), we see that

$$\rho(e-q) = \frac{p + \gamma\pi}{\gamma - 1} = const. \tag{7.3.10}$$

Thus from (7.3.9) with (7.3.10), we get by taking out the constant and using (7.3.6)

$$\alpha_j^{n+1} = \alpha_j^n - (u_I)_j^n \frac{\Delta t}{\Delta x}(\alpha^*_{j+\frac{1}{2}} - \alpha^*_{j-\frac{1}{2}}). \tag{7.3.11}$$

This equation provides a discretization for the volume fraction equation.

For the Riemann values the approximate solvers HLL, HLLC [38] and VFRoe [12] are used. For the seven-equation model (7.2.1) the HLL solver is introduced in [27] and the VFRoe solver is considered in [3]. In the following section we present the HLLC solver.

7.3.1.1 HLLC-type solver

The intercell flux of the HLLC Riemann solver is given by, see Toro [38]

$$\mathbf{F}^{HLLC}_{j+\frac{1}{2}} = \begin{cases} \mathbf{f}(\mathbf{u}_L), & 0 \le s_L \\ \mathbf{f}(\mathbf{u}_{*L}) = \mathbf{f}(\mathbf{u}_L) + s_L(\mathbf{u}_{*L} - \mathbf{u}_L), & s_L \le 0 \le s_* \\ \mathbf{f}(\mathbf{u}_{*R}) = \mathbf{f}(\mathbf{u}_R) + s_R(\mathbf{u}_{*R} - \mathbf{u}_R), & s_* \le 0 \le s_R \\ \mathbf{f}(\mathbf{u}_R), & 0 \ge s_R. \end{cases}$$

Where 'L' and 'R' refer to the left and right states of a cell boundary respectively.

Following the Davis estimates [8] the wave speeds can be taken as

$$s_L = \min\{u_{1L} - c_{1L}, u_{2L} - c_{2L}, u_{1R} - c_{1R}, u_{2R} - c_{2R}\},$$
$$s_R = \max\{u_{1L} + c_{1L}, u_{2L} + c_{2L}, u_{1R} + c_{1R}, u_{2R} + c_{2R}\}.$$

Following Toro [38] for a single phase, the vectors $\mathbf{u}_{*L}$ and $\mathbf{u}_{*R}$ can be given as

$$\mathbf{u}_{*K} = \begin{bmatrix} \alpha_{1K}\rho_{1K}\dfrac{s_K - u_{1K}}{s_K - s_*} \\ \alpha_{1K}\rho_{1K}\dfrac{s_K - u_{1K}}{s_K - s_*}s_* \\ \alpha_{1K}\rho_{1K}\dfrac{s_K - u_{1K}}{s_K - s_*}\left(E_{1K} + (s_* - u_{1K})(s_* + \dfrac{p_{1K}}{\rho_{1K}(s_K - u_{1K})})\right) \\ \alpha_{2K}\rho_{2K}\dfrac{s_K - u_{2K}}{s_K - s_*} \\ \alpha_{2K}\rho_{2K}\dfrac{s_K - u_{2K}}{s_K - s_*}s_* \\ \alpha_{2K}\rho_{2K}\dfrac{s_K - u_{2K}}{s_K - s_*}\left(E_{2K} + (s_* - u_{2K})(s_* + \dfrac{p_{2K}}{\rho_{2K}(s_K - u_{2K})})\right) \end{bmatrix}, \quad K = L, R.$$

We take the speed s_* as in [38] but with mixture values for pressure, velocity and density, i.e

$$s_* = \frac{p_R - p_L + \rho_L u_L(s_L - u_L) - \rho_R u_R(s_R - u_R)}{\rho_L(s_L - u_L) - \rho_R(s_R - u_R)}$$

where $\rho = \alpha_1\rho_1 + \alpha_2\rho_2$, $p = \alpha_1 p_1 + \alpha_2 p_2$ and $u = \dfrac{\alpha_1\rho_1 u_1 + \alpha_2\rho_2 u_2}{\rho}$.

We refer to the mathematical properties of the model (7.2.1) in 7.A Consider the eigenvectors (7.A.4) and (7.A.5) for the 2- to 7- fields. It is clear that the function $\varphi(\mathbf{W}) = \alpha_1$ is a Riemann invariant for all 2- to 7- characteristic fields. This means that α_1 is constant across all rarefaction waves of the 2- to 7- fields. Also note that the action of the non-conservative terms is reflected in the 1-field which corresponds to the eigenvalue $\lambda_1 = u_I$. Moreover, this eigenvalue comes from the evolutionary equation for α_1. Considering these observations we will assume that α_1 changes only across s_*, this means that

$$\alpha_{1*K} = \alpha_{1K}, \qquad K = L,\ R.$$

7.3.1.2 Extension to the second order

To achieve second order accuracy we use the MUSCL method, where MUSCL stands for Monotone Upstream-centered Scheme for Conservation Laws. In the following we will give a summary of this method, and for details we refer to Toro [38]. This method has three steps, they are

- *Data reconstruction:* The primitive variables on the cell boundary are extrapolated as

$$\mathbf{W}^-_{j+\frac{1}{2}} = \mathbf{W}^n_j + \frac{1}{2}\delta_j, \qquad \mathbf{W}^+_{j-\frac{1}{2}} = \mathbf{W}^n_j - \frac{1}{2}\delta_j.$$

  Performing this step in primitive variables ensures the preservation of uniformity of pressure and velocity, which is an essential issue in the discretization of the model.

The limited slope δ_j is taken as

$$\delta_j = \begin{cases} \max\{0, \min(\beta d_{j-\frac{1}{2}}, d_{j+\frac{1}{2}}), \min(d_{j-\frac{1}{2}}, \beta d_{j+\frac{1}{2}})\}, & d_{j+\frac{1}{2}} > 0 \\ \min\{0, \max(\beta d_{j-\frac{1}{2}}, d_{j+\frac{1}{2}}), \max(d_{j-\frac{1}{2}}, \beta d_{j+\frac{1}{2}})\}, & d_{j+\frac{1}{2}} < 0 \end{cases}$$

where

$$d_{j-\frac{1}{2}} = \mathbf{W}_j^n - \mathbf{W}_{j-1}^n, \qquad d_{j+\frac{1}{2}} = \mathbf{W}_{j+1}^n - \mathbf{W}_j^n.$$

For particular values of β, the value $\beta = 1$ corresponds to the minmod limiter and $\beta = 2$ corresponds to the superbee limiter.

- *Evolution*: Using (7.A.1) the values $\mathbf{W}_{j\mp\frac{1}{2}}^{\pm}$ are evolved by a time $\dfrac{\Delta t}{2}$ as

$$\widehat{\mathbf{W}}_{j-\frac{1}{2}}^{+} = \mathbf{W}_{j-\frac{1}{2}}^{+} - \frac{\Delta t}{2\Delta x}\mathbf{A}(\mathbf{W}_j)(\mathbf{W}_{j+\frac{1}{2}}^{-} - \mathbf{W}_{j-\frac{1}{2}}^{+}),$$

$$\widehat{\mathbf{W}}_{j+\frac{1}{2}}^{-} = \mathbf{W}_{j+\frac{1}{2}}^{-} - \frac{\Delta t}{2\Delta x}\mathbf{A}(\mathbf{W}_j)(\mathbf{W}_{j+\frac{1}{2}}^{-} - \mathbf{W}_{j-\frac{1}{2}}^{+}).$$

- *Solution of the Riemann problem:* We rewrite $\widehat{\mathbf{W}}_{j\pm\frac{1}{2}}^{\pm}$ in conservative form, and solve the Riemann problem with the piecewise constant data $(\widehat{\mathbf{U}}_{j+\frac{1}{2}}^{-}, \widehat{\mathbf{U}}_{j+\frac{1}{2}}^{+})$.

7.3.2 Source and relaxation operators

According to the Strang splitting (7.3.1), to take into account for source and relaxation terms we have to solve the following system of ordinary differential equations (ODE).

$$\frac{d\mathbf{U}}{dt} = \mathbf{S} \tag{7.3.12}$$

where $\mathbf{U} = (\alpha_1, \alpha_1\rho_1, \alpha_1\rho_1 u_1, \alpha_1\rho_1 E_1, \alpha_2\rho_2, \alpha_2\rho_2 u_2, \alpha_2\rho_2 E_2)^T$. The source vector $\mathbf{S}$ can be decomposed as the sum

$$\mathbf{S} = \mathbf{S}_V + \mathbf{S}_P + \mathbf{S}_{Thermal},$$

where $\mathbf{S}_V$ and $\mathbf{S}_P$ are associated with velocity and pressure relaxation terms respectively. The vector $\mathbf{S}_{Thermal}$ represents the thermal relaxation terms that include the temperature and Gibbs free energy relaxation terms that have to be modeled. The mechanical relaxation terms $\mathbf{S}_V$ and $\mathbf{S}_P$ are given by

$$\mathbf{S}_V = \begin{bmatrix} 0 \\ 0 \\ \lambda(u_2 - u_1) \\ \lambda u_I(u_2 - u_1) \\ 0 \\ -\lambda(u_2 - u_1) \\ -\lambda u_I(u_2 - u_1) \end{bmatrix}, \quad \text{and} \quad \mathbf{S}_P = \begin{bmatrix} \mu(p_1 - p_2) \\ 0 \\ 0 \\ \mu p_I(p_2 - p_1) \\ 0 \\ 0 \\ -\mu p_I(p_2 - p_1) \end{bmatrix}.$$

The system (7.3.12) is solved by successive integrations considering each one of the source vectors alone.

The relaxation time scales depend on many parameters of the fluids and also possibly on the process, i.e. evaporation, condensation combustion, etc. For example the rate of the pressure relaxation μ depends on the compressibility of each fluid besides the nature of each fluid and the two phase mixture topology [27, 31]. The velocity relaxation time may be greater than that required for the pressure relaxation, since the velocity relaxation depends on the fluid viscosity which has slow effects compared to others, also it depends on the pressure relaxation which is in general fast compared to the longitudinal wave propagation [27, 31]. The interface conditions, for the interface that separates two pure fluids, impose an equality for pressure and velocity. In many physical situations it is reasonable to assume that the pressure and velocity relax instantaneously. Such an assumption also fulfills the interface conditions. Some estimations in certain situations show that the time scale of the velocity relaxation and pressure relaxation are of the same order of magnitude [7, 26].

The temperature relaxation depends on the thermal conductivity of the fluids. Where this conduction occurs due to the collisions of the molecules of the fluids. To reach temperature equilibrium a large number of collisions is required. This in general has long characteristic time compared to the pressure and velocity relaxation.

The Gibbs free energy relaxation parameter depends on local chemical relaxation [33]. And this is a slow process compared with other processes that related to the pressure, velocity and temperature relaxation at the interfaces. Therefore the relaxation time of the Gibbs free energy relaxation is the longest compared to other relaxation times.

In this paper we assume that the relaxation times are very close to zero i.e. instantaneous relaxations. This assumption is justified for the pressure and the velocity in the entire flow field. For the temperature and the Gibbs free energy this assumption is considered only at the interface where the heat and mass transfer occur, indeed this assumption is standard at equilibrium interfaces when mass transfer occurs [33]. The assumption of instantaneous relaxations means that all relaxation parameters are taken to be infinite and this makes the model free of parameters.

Moreover we assume that the relaxation time of the mechanical variables is much smaller than that of the thermal variables. We assume that the mechanical variables relax very fast to equilibrium values, and they will stay in equilibrium during the thermal relaxation. Also we assume that the temperature relaxes much faster than the Gibbs free energy.

For the velocity and pressure relaxation we use the same procedures as Saurel and Abgrall [27], other procedures for pressure relaxation also are possible, see [17, 18, 31]. For the thermal relaxation terms we modeled them depending on the observation of the differences between relaxation times for various variables, they are the subject of the next section.

7.4 Thermal relaxation, modeling of heat and mass transfer

At each time step after the procedures for the velocity and pressure relaxations we have a two-phase mixture in mechanical equilibrium, but each phase has its own temperature and its own Gibbs free energy. In this section we will insert the effect of heat and mass transfer that take place at the interface.

To locate the interface we use the ideas of [33], that the cell is filled with pure fluid when its volume fraction is close to 1, say $(1-\epsilon)$, with $\epsilon = 10^{-6}$. The interface corresponds to mixture cells when the volume fraction ranges between $\bar{\epsilon}$ and $1-\bar{\epsilon}$, with $\bar{\epsilon} = 10^{-4}$. The value of $\bar{\epsilon}$ has to be chosen larger than the value of ϵ to ensure that phase transitions occur only in the interfacial zone, for a discussion on this point see [33]. Also mass transfer is allowed if the liquid is metastable, i.e. $T_l > T_{sat}(p_{equi})$. For the computation of the curve $T = T_{sat}(p_{equi})$ see 7.C.

According to our assumption that the mechanical relaxation time is very small compared with the thermal relaxation time we may also assume that the mechanical quantities will stay in equilibrium during the thermal relaxation. Therefore, our modeled terms will keep this assumption.

Also we assume that the temperature relaxes much faster than the Gibbs free energy. So we will split the thermal terms into two parts. One is related to the heat transfer $\mathbf{S}_Q$ and the other is related to the mass transfer $\mathbf{S}_m$, i.e.

$$\mathbf{S}_{Thermal} = \mathbf{S}_Q + \mathbf{S}_m.$$

The system of ODE (7.3.12) is solved for the temperature relaxation then for the Gibbs free energy relaxation. During the Gibbs free energy relaxation we assume that the temperature will stay in equilibrium, and our modeled terms will keep this condition.

7.4.1 Heat transfer and temperature relaxation

The heat transfer is added through the temperature relaxation terms. In the model (7.2.1) the heat transfer term Q initially appears in the energy equations. As the pressure equilibrium is maintained through the temperature relaxation we will modify the volume fraction equation to include the effect of the heat transfer in a way to be able to keep an equilibrium pressure during the temperature relaxation process. Therefore the heat source vector $\mathbf{S}_Q$ is modeled as

$$\mathbf{S}_Q = (\frac{Q}{\kappa}, 0, 0, Q, 0, 0, -Q)^T, \tag{7.4.1}$$

where the new variable κ has to be determined.

Then to take into account for the heat transfer we have to solve the following system of ODE

$$\frac{d\mathbf{U}}{dt} = \mathbf{S}_Q. \tag{7.4.2}$$

To find the expression for κ we will use the assumption that the pressure will stay in equilibrium, and to do that we assume

$$\frac{\partial p_1}{\partial t} = \frac{\partial p_2}{\partial t}. \tag{7.4.3}$$

7.4.1.1 Determination of κ

Consider the components of the system (7.4.2) for phase "1"

$$\frac{\partial \alpha_1}{\partial t} = \frac{Q}{\kappa}, \tag{7.4.4a}$$

$$\frac{\partial \alpha_1 \rho_1}{\partial t} = 0, \tag{7.4.4b}$$

$$\frac{\partial \alpha_1 \rho_1 u_1}{\partial t} = 0, \tag{7.4.4c}$$

$$\frac{\partial \alpha_1 \rho_1 E_1}{\partial t} = Q. \tag{7.4.4d}$$

From (7.4.4a) and (7.4.4d) we obtain

$$\frac{\partial \alpha_1 \rho_1 E_1}{\partial t} = \kappa \frac{\partial \alpha_1}{\partial t}. \tag{7.4.5}$$

Using the definition of E_1, (7.4.4b) and (7.4.4c) with (7.4.5) we have

$$\alpha_1 \rho_1 \frac{\partial e_1}{\partial t} = \kappa \frac{\partial \alpha_1}{\partial t}. \tag{7.4.6}$$

The internal energy e_1 is expressed in terms of p_1 and ρ_1, i.e. $e_1 = e_1(p_1, \rho_1)$. Differentiating it with respect to t and substituting the result in (7.4.6), we obtain

$$\alpha_1 \rho_1 \left(\frac{\partial e_1}{\partial p_1}\right)_{\rho_1} \frac{\partial p_1}{\partial t} + \alpha_1 \rho_1 \left(\frac{\partial e_1}{\partial \rho_1}\right)_{p_1} \frac{\partial \rho_1}{\partial t} = \kappa \frac{\partial \alpha_1}{\partial t}. \tag{7.4.7}$$

From (7.4.4b) we have $\alpha_1 \dfrac{\partial \rho_1}{\partial t} = -\rho_1 \dfrac{\partial \alpha_1}{\partial t}$. Using this in (7.4.7) we get

$$\alpha_1 \rho_1 \left(\frac{\partial e_1}{\partial p_1}\right)_{\rho_1} \frac{\partial p_1}{\partial t} - \rho_1^2 \left(\frac{\partial e_1}{\partial \rho_1}\right)_{p_1} \frac{\partial \alpha_1}{\partial t} = \kappa \frac{\partial \alpha_1}{\partial t},$$

or

$$\frac{\partial p_1}{\partial t} = \frac{\kappa + \rho_1^2 \left(\dfrac{\partial e_1}{\partial \rho_1}\right)_{p_1}}{\alpha_1 \rho_1 \left(\dfrac{\partial e_1}{\partial p_1}\right)_{\rho_1}} \frac{\partial \alpha_1}{\partial t}. \tag{7.4.8}$$

A similar equation can be attained for p_2

$$\frac{\partial p_2}{\partial t} = -\frac{\kappa + \rho_2^2 \left(\dfrac{\partial e_2}{\partial \rho_2}\right)_{p_2}}{\alpha_2 \rho_2 \left(\dfrac{\partial e_2}{\partial p_2}\right)_{\rho_2}} \frac{\partial \alpha_1}{\partial t}. \tag{7.4.9}$$

Using (7.4.8) and (7.4.9) in the condition (7.4.3) and after some manipulations we have the following expression for κ

$$\kappa = \frac{\dfrac{\rho_1 c_1^2}{\alpha_1} + \dfrac{\rho_2 c_2^2}{\alpha_2}}{\dfrac{\Gamma_1}{\alpha_1} + \dfrac{\Gamma_2}{\alpha_2}} - \frac{\dfrac{\Gamma_1}{\alpha_1} p_1 + \dfrac{\Gamma_2}{\alpha_2} p_2}{\dfrac{\Gamma_1}{\alpha_1} + \dfrac{\Gamma_2}{\alpha_2}}. \tag{7.4.10}$$

Here Γ_k denotes the Grüneisen coefficient of phase k which is given as

$$\Gamma_k = \frac{1}{\rho_k} \left(\frac{\partial p_k}{\partial e_k} \right)_{\rho_k}, \quad k = 1, 2. \tag{7.4.11}$$

Since the heat transfer relaxation is considered when pressure equilibrium is maintained, i.e. $p_1 = p_2 = p_{eq}$, the second term in the right hand side of (7.4.10) is equivalent to the equilibrium pressure. Thus we have

$$\kappa = \frac{\dfrac{\rho_1 c_1^2}{\alpha_1} + \dfrac{\rho_2 c_2^2}{\alpha_2}}{\dfrac{\Gamma_1}{\alpha_1} + \dfrac{\Gamma_2}{\alpha_2}} - p_{eq}. \tag{7.4.12}$$

It is interesting to note that the first term on the right hand side of (7.4.12) is exactly the same term that appears in a similar manner with heat transfer that is given in the model of Saurel et al. [33].

In the context of the SG-EOS (7.2.5), we have the following expression for κ

$$\kappa = \frac{\dfrac{p_1 + \gamma_1 \pi_1}{\alpha_1} + \dfrac{p_2 + \gamma_2 \pi_2}{\alpha_2}}{\dfrac{\gamma_1 - 1}{\alpha_1} + \dfrac{\gamma_2 - 1}{\alpha_2}}.$$

7.4.1.2 Mixture entropy

Now let us consider the equation of the mixture entropy. If we follow the same method in Section 7.2.2 for the model with new modifications, we have

$$\alpha_1 \rho_1 T_1 \frac{Ds_1}{Dt} = (1 + \frac{p_1}{\kappa}) Q, \tag{7.4.13a}$$

$$\alpha_2 \rho_2 T_2 \frac{Ds_2}{Dt} = -(1 + \frac{p_2}{\kappa}) Q. \tag{7.4.13b}$$

After the mechanical relaxation p_1 and p_2 are in equilibrium, so $p_1 = p_2 = p_{eq}$.

Combining the two equations in (7.4.13) we get the following equation for the mixture entropy

$$\frac{\partial \rho s}{\partial t} + \frac{\partial \rho s u}{\partial x} = (1 + \frac{p_{eq}}{\kappa}) Q \left(\frac{T_2 - T_1}{T_1 T_2} \right),$$

where $\rho s = \alpha_1 \rho_1 s_1 + \alpha_2 \rho_2 s_2$ and $u = u_1 = u_2$ is the equilibrium velocity.

The heat transfer Q is modeled as $Q = \theta(T_2 - T_1)$, where $\theta > 0$ is the temperature relaxation parameter. Since κ is always positive the mixture entropy satisfies the second law of thermodynamics, i.e.

$$\frac{\partial \rho s}{\partial t} + \frac{\partial \rho s u}{\partial x} = \theta (1 + \frac{p_{eq}}{\kappa}) \frac{(T_2 - T_1)^2}{T_1 T_2} \geq 0.$$

In this work the parameter θ is assumed to tend to infinity, i.e. the temperature relaxes to a common value instantaneously at any time. This assumption is considered at the interface only.

7.4.1.3 Temperature relaxation

Now to solve the system (7.4.4) with $\theta \to \infty$, we proceed as for the pressure relaxation in [27]. It is clear that $\alpha_1\rho_1$ and $\alpha_1\rho_1 u_1$, therefore also u_1 stay constant through the relaxation process.

From the system (7.4.4) we obtain (7.4.6) for the internal energy, which can be rewritten as

$$\frac{\partial e_1}{\partial t} = \frac{\kappa}{\alpha_1\rho_1}\frac{\partial \alpha_1}{\partial t}.$$

Integrating this equation, we obtain the following approximation

$$e_1^* = e_1^0 + \frac{\bar{\kappa}}{\alpha_1^0\rho_1^0}(\alpha_1^* - \alpha_1^0) \tag{7.4.14}$$

where '0' and '*' refer to the states before and after the relaxation process respectively and $\bar{\kappa}$ is the mean interfacial value between the states $(\alpha_1^0, \rho_1^0, e_1^0)$ and $(\alpha_1^*, \rho_1^*, e_1^*)$. Also, we can proceed in the same way to get a similar result for phase '2'.

We consider (7.4.14) as an equation for e_1 as a function of α_1, i.e. $e_1 = e_1^0 + \frac{\bar{\kappa}}{\alpha_1^0\rho_1^0}(\alpha_1 - \alpha_1^0)$, and from (7.4.4b) $\rho_1 = \frac{const}{\alpha_1}$. And analogously for the other phase, since $\alpha_2 = 1 - \alpha_1$ we have only one variable α_1 in the relation

$$f_T(\alpha_1) = T_2(e_2, \rho_2) - T_1(e_1, \rho_1) = 0. \tag{7.4.15}$$

Our aim now is to find an α_1 that satisfies the equilibrium condition (7.4.15). The variable $\bar{\kappa}$ can be approximated as $\bar{\kappa} = \frac{\tilde{\kappa} + \kappa^0}{2}$, where $\tilde{\kappa}$ is estimated at the new state resulting from iterative procedure for solving $f_T(\alpha_1) = 0$.

In this way we get the temperature equilibrium, while keeping the mechanical equilibrium.

7.4.2 Mass transfer and Gibbs free energy relaxation

Analogous to the heat transfer, the mass transfer is also modeled through relaxation terms. As mentioned we assume that the temperature relaxation time is very small compared with the Gibbs free energy relaxation time, and so we will consider that the mechanical equilibrium and the equilibrium of temperature will be satisfied through the Gibbs free energy relaxation.

To take into account the mass transfer we have to solve the following system of ODE

$$\frac{d\mathbf{U}}{dt} = \mathbf{S}_m. \tag{7.4.16}$$

Our aim now is to model the mass transfer source vector $\mathbf{S}_m$. The literature on averaging techniques shows that the mass transfer appears in the model as a mass rate in the interfacial momentum and in the interfacial energy, see [9, 10, 14]. But the expressions for these terms are unknown. Here we will insert these terms in the model as they appear by averaging, but we will use some assumptions to find certain expressions for these terms.

Let us assume that $\mathbf{S}_m$ is given in the model as

$$\frac{\partial \alpha_1}{\partial t} = \frac{\dot{m}}{\varrho}, \tag{7.4.17a}$$

$$\frac{\partial \alpha_1 \rho_1}{\partial t} = \dot{m}, \tag{7.4.17b}$$

$$\frac{\partial \alpha_1 \rho_1 u_1}{\partial t} = u_I \dot{m}, \tag{7.4.17c}$$

$$\frac{\partial \alpha_1 \rho_1 E_1}{\partial t} = (e_i + \frac{u_I^2}{2})\dot{m}, \tag{7.4.17d}$$

$$\frac{\partial \alpha_2 \rho_2}{\partial t} = -\dot{m}, \tag{7.4.17e}$$

$$\frac{\partial \alpha_2 \rho_2 u_2}{\partial t} = -u_I \dot{m}, \tag{7.4.17f}$$

$$\frac{\partial \alpha_2 \rho_2 E_2}{\partial t} = -(e_i + \frac{u_I^2}{2})\dot{m}. \tag{7.4.17g}$$

The new variables ϱ and e_i have to be determined. According to our assumption the relaxation time of the Gibbs free energy is much larger than other relaxation times, so during the Gibbs free energy relaxation process we will assume that the pressure and temperature stay in equilibrium. Thus to find the new variables we use the following assumptions

$$\frac{\partial p_1}{\partial t} = \frac{\partial p_2}{\partial t}, \tag{7.4.18a}$$

$$\frac{\partial T_1}{\partial t} = \frac{\partial T_2}{\partial t}. \tag{7.4.18b}$$

7.4.2.1 Determination of e_i and ϱ

Since the model (7.4.17) is solved after the mechanical relaxation we have $u_1 = u_2 = u_I$. From (7.4.17b) and (7.4.17c) the velocity u_1 is constant through the relaxation procedure, also from (7.4.17e) and (7.4.17f) the velocity u_2 is constant.

Using the equations (7.4.17a) - (7.4.17d) and the definition of E_1, we get

$$\alpha_1 \rho_1 \frac{\partial e_1}{\partial t} = (e_i - e_1)\dot{m}. \tag{7.4.19}$$

Differentiate $e_1(p_1, \rho_1)$ with respect to t and substitute the result in (7.4.19). We obtain

$$\alpha_1 \rho_1 \left(\frac{\partial e_1}{\partial p_1}\right)_{\rho_1} \frac{\partial p_1}{\partial t} + \alpha_1 \rho_1 \left(\frac{\partial e_1}{\partial \rho_1}\right)_{p_1} \frac{\partial \rho_1}{\partial t} = \varrho(e_i - e_1)\frac{\partial \alpha_1}{\partial t}. \tag{7.4.20}$$

From (7.4.17a) and (7.4.17b), we get

$$\alpha_1 \frac{\partial \rho_1}{\partial t} = (\varrho - \rho_1)\frac{\partial \alpha_1}{\partial t}. \tag{7.4.21}$$

Using this in (7.4.20), we have

$$\alpha_1 \rho_1 \left(\frac{\partial e_1}{\partial p_1}\right)_{\rho_1} \frac{\partial p_1}{\partial t} + \rho_1(\varrho - \rho_1) \left(\frac{\partial e_1}{\partial \rho_1}\right)_{p_1} \frac{\partial \alpha_1}{\partial t} = \varrho(e_i - e_1)\frac{\partial \alpha_1}{\partial t}. \tag{7.4.22}$$

This leads to

$$\frac{\partial p_1}{\partial t} = \frac{\Gamma_1}{\alpha_1}\left(-\rho_1(\varrho - \rho_1)\left(\frac{\partial e_1}{\partial \rho_1}\right)_{p_1} + \varrho(e_i - e_1)\right)\frac{\partial \alpha_1}{\partial t}. \tag{7.4.23}$$

In a similar way we have an equation for p_2

$$\frac{\partial p_2}{\partial t} = -\frac{\Gamma_2}{\alpha_2}\left(-\rho_2(\varrho-\rho_2)\left(\frac{\partial e_2}{\partial \rho_2}\right)_{p_2} + \varrho(e_i - e_2)\right)\frac{\partial \alpha_1}{\partial t}. \tag{7.4.24}$$

By the condition (7.4.18a) with (7.4.23) and (7.4.24), we obtain

$$\frac{\Gamma_1}{\alpha_1}\left(-\rho_1(\varrho-\rho_1)\left(\frac{\partial e_1}{\partial \rho_1}\right)_{p_1} + \varrho(e_i - e_1)\right) = -\frac{\Gamma_2}{\alpha_2}\left(-\rho_2(\varrho-\rho_2)\left(\frac{\partial e_2}{\partial \rho_2}\right)_{p_2} + \varrho(e_i - e_2)\right). \tag{7.4.25}$$

On the other hand, e_1 can be written in terms of T_1 and ρ_1, i.e. $e_1 = e_1(T_1, \rho_1)$. Differentiating it with respect to t, substituting the result in (7.4.19) and using (7.4.21), we get

$$\frac{\partial T_1}{\partial t} = \frac{1}{\alpha_1\rho_1\left(\dfrac{\partial e_1}{\partial T_1}\right)_{\rho_1}}\left(-\rho_1(\varrho-\rho_1)\left(\frac{\partial e_1}{\partial \rho_1}\right)_{T_1} + \varrho(e_i - e_1)\right)\frac{\partial \alpha_1}{\partial t}.$$

But $\left(\dfrac{\partial e_1}{\partial T_1}\right)_{\rho_1} = C_{v1}$, the specific heat at constant volume. Thus

$$\frac{\partial T_1}{\partial t} = \frac{1}{\alpha_1\rho_1 C_{v1}}\left(-\rho_1(\varrho-\rho_1)\left(\frac{\partial e_1}{\partial \rho_1}\right)_{T_1} + \varrho(e_i - e_1)\right)\frac{\partial \alpha_1}{\partial t}. \tag{7.4.26}$$

A similar equation can be attained for T_2

$$\frac{\partial T_2}{\partial t} = \frac{-1}{\alpha_2\rho_2 C_{v2}}\left(-\rho_2(\varrho-\rho_2)\left(\frac{\partial e_2}{\partial \rho_2}\right)_{T_2} + \varrho(e_i - e_2)\right)\frac{\partial \alpha_1}{\partial t}. \tag{7.4.27}$$

By the condition (7.4.18b) with (7.4.26) and (7.4.27), we get

$$\frac{1}{\alpha_1\rho_1 C_{v1}}\left(-\rho_1(\varrho-\rho_1)\left(\frac{\partial e_1}{\partial \rho_1}\right)_{T_1} + \varrho(e_i - e_1)\right) = \frac{-1}{\alpha_2\rho_2 C_{v2}}\left(-\rho_2(\varrho-\rho_2)\left(\frac{\partial e_2}{\partial \rho_2}\right)_{T_2} + \varrho(e_i - e_2)\right) \tag{7.4.28}$$

It is clear now that (7.4.25) and (7.4.28) are two equations for the two unknowns e_i and ϱ. After some manipulations, we get from these equations

$$\varrho = \frac{\phi\left(\dfrac{\rho_1 c_1^2}{\alpha_1} + \dfrac{\rho_2 c_2^2}{\alpha_2}\right) - \phi\left(\dfrac{\Gamma_1}{\alpha_1}p_1 + \dfrac{\Gamma_2}{\alpha_2}p_2\right) + \psi\left(\dfrac{\rho_1^2\left(\dfrac{\partial e_1}{\partial \rho_1}\right)_{T_1}}{\alpha_1\rho_1 C_{v1}} + \dfrac{\rho_2^2\left(\dfrac{\partial e_2}{\partial \rho_2}\right)_{T_2}}{\alpha_2\rho_2 C_{v2}}\right)}{\phi\left(\dfrac{c_1^2}{\alpha_1} + \dfrac{c_2^2}{\alpha_2}\right) - \phi\left(\dfrac{\Gamma_1}{\alpha_1}h_1 + \dfrac{\Gamma_2}{\alpha_2}h_2\right) + \psi\left(\dfrac{e_1 + \rho_1\left(\dfrac{\partial e_1}{\partial \rho_1}\right)_{T_1}}{\alpha_1\rho_1 C_{v1}} + \dfrac{e_2 + \rho_2\left(\dfrac{\partial e_2}{\partial \rho_2}\right)_{T_2}}{\alpha_2\rho_2 C_{v2}}\right)} \tag{7.4.29a}$$

$$e_i = \frac{\dfrac{e_1 + \rho_1\left(\dfrac{\partial e_1}{\partial \rho_1}\right)_{T_1}}{\alpha_1\rho_1 C_{v1}} + \dfrac{e_2 + \rho_2\left(\dfrac{\partial e_2}{\partial \rho_2}\right)_{T_2}}{\alpha_2\rho_2 C_{v2}}}{\phi} - \frac{\dfrac{\rho_1^2\left(\dfrac{\partial e_1}{\partial \rho_1}\right)_{T_1}}{\alpha_1\rho_1 C_{v1}} + \dfrac{\rho_2^2\left(\dfrac{\partial e_2}{\partial \rho_2}\right)_{T_2}}{\alpha_2\rho_2 C_{v2}}}{\varrho\phi} \tag{7.4.29b}$$

where $\phi = \dfrac{1}{\alpha_1\rho_1 C_{v1}} + \dfrac{1}{\alpha_2\rho_2 C_{v2}}$, $\psi = \dfrac{\Gamma_1}{\alpha_1} + \dfrac{\Gamma_2}{\alpha_2}$ and $h_k = e_k + \dfrac{p_k}{\rho_k}$ is the *enthalpy* for phase k.

Consider the expression of ϱ given by (7.4.29a), the terms that are multiplied by ψ come from the temperature equilibrium condition. While the terms that are multiplied by ϕ come from the pressure equilibrium condition. It is interesting to see that a similar expression is given in the Saurel et al. [33] by

$\rho_I = (\frac{\rho_1 c_1^2}{\alpha_1} + \frac{\rho_2 c_2^2}{\alpha_2})/(\frac{c_1^2}{\alpha_1} + \frac{c_2^2}{\alpha_2})$, see relation (5.9) in [33]. The term ρ_I in [33] appears with the volume fraction equation in the same way as our variable ϱ, see volume fraction equation (7.4.17a). It is obvious that all terms of ρ_I appear in the expression of ϱ. Note also that the terms are related to the equilibrium of the temperature in the variable ϱ do not appear in the variable ρ_I, this is due to the fact that ρ_I uses the pressure equilibrium with other assumptions, but it does not use the temperature equilibrium condition.

In the context of the SG-EOS we have the following expressions for ϱ and e_i,

$$\varrho = \frac{\phi\left(\frac{p_1+\gamma_1\pi_1}{\alpha_1} + \frac{p_2+\gamma_2\pi_2}{\alpha_2}\right) - \psi\left(\frac{\pi_1}{\alpha_1\rho_1 C_{v1}} + \frac{\pi_2}{\alpha_2\rho_2 C_{v2}}\right)}{-\phi\left(\frac{(\gamma_1-1)q_1}{\alpha_1} + \frac{(\gamma_2-1)q_2}{\alpha_2}\right) + \psi\left(\frac{e_1-\frac{\pi_1}{\rho_1}}{\alpha_1\rho_1 C_{v1}} + \frac{e_2-\frac{\pi_2}{\rho_2}}{\alpha_2\rho_2 C_{v2}}\right)},$$

$$e_i = \frac{\left(\frac{e_1-\frac{\pi_1}{\rho_1}}{\alpha_1\rho_1 C_{v1}} + \frac{e_2-\frac{\pi_2}{\rho_2}}{\alpha_2\rho_2 C_{v2}}\right)}{\phi} + \frac{\left(\frac{\pi_1}{\alpha_1\rho_1 C_{v1}} + \frac{\pi_2}{\alpha_2\rho_2 C_{v2}}\right)}{\varrho\phi}.$$

Note that $\Gamma_k = \gamma_k - 1$, $k = 1, 2$, for the SG-EOS.

7.4.2.2 Mixture entropy

Now we consider the equation of mixture entropy. If we follow the same argument as in Section 7.2.2, under the mechanical equilibrium and temperature equilibrium, we have

$$\alpha_1\rho_1 T_1 \frac{Ds_1}{Dt} = (e_i + \frac{p_1}{\varrho})\dot{m} - (e_1 + \frac{p_{eq}}{\rho_1})\dot{m}, \tag{7.4.31a}$$

$$\alpha_2\rho_2 T_2 \frac{Ds_2}{Dt} = -(e_i + \frac{p_2}{\varrho})\dot{m} + (e_2 + \frac{p_{eq}}{\rho_2})\dot{m}. \tag{7.4.31b}$$

Using the mass equations (7.4.17b) and (7.4.17e) with system (7.4.31), we have

$$T_1(\frac{\partial\alpha_1\rho_1 s_1}{\partial t} + \frac{\partial\alpha_1\rho_1 s_1 u_1}{\partial x}) = (e_i + \frac{p_{eq}}{\varrho})\dot{m} - (e_1 + \frac{p_1}{\rho_1} - T_1 s_1)\dot{m}, \tag{7.4.32a}$$

$$T_2(\frac{\partial\alpha_2\rho_2 s_2}{\partial t} + \frac{\partial\alpha_2\rho_2 s_2 u_2}{\partial x}) = -(e_i + \frac{p_{eq}}{\varrho})\dot{m} + (e_2 + \frac{p_2}{\rho_2} - T_2 s_2)\dot{m}. \tag{7.4.32b}$$

Note that the quantity $e_k + \frac{p_k}{\rho_k} - T_k s_k$, $k = 1, 2$ is the Gibbs free energy. Let us denote g_k for the Gibbs free energy.

Add the two entropy equations in (7.4.32) after division by temperatures, we obtain

$$\frac{\partial\rho s}{\partial t} + \frac{\partial\rho s u}{\partial x} = (e_i + \frac{p_{eq}}{\varrho})\dot{m}\left(\frac{T_2 - T_1}{T_1 T_2}\right) + \dot{m}\left(\frac{g_2}{T_2} - \frac{g_1}{T_1}\right). \tag{7.4.33}$$

Since the temperatures are in equilibrium by the temperature relaxation the first term in the right hand side of (7.4.33) vanishes and the mass transfer is modeled as $\dot{m} = \eta(g_2 - g_1)$, where $\eta > 0$ is the relaxation parameter of the Gibbs free energy. Thus the mixture entropy satisfies the second law of thermodynamics, i.e.

$$\frac{\partial\rho s}{\partial t} + \frac{\partial\rho s u}{\partial x} = \eta\frac{(g_2 - g_1)^2}{T_{eq}} \geq 0, \tag{7.4.34}$$

where T_{eq} is the equilibrium temperature, $T_1 = T_2 = T_{eq}$.

In this work we assume that the parameter η tends to infinity. This means that the Gibbs free energy relaxes instantaneously to equilibrium. This is considered at the interface only.

7.4.2.3 Free Gibbs energy relaxation, procedure I

Now, we will solve the system (7.4.17) when $\eta \to \infty$, this means that the mass transfer occurs until the Gibbs free energies reach equilibrium. Thus we have to find the value of $\dot{m}$ that makes the difference of the Gibbs free energies at the end of the time step is zero. To do that we use the equations for the rate of change of Gibbs free energies in terms of $\dot{m}$. Assume that

$$\frac{\partial g_1}{\partial t} = A\dot{m}, \quad \text{and} \quad \frac{\partial g_2}{\partial t} = B\dot{m}. \tag{7.4.35}$$

Using the SG-EOS, A and B can be given as

$$\begin{aligned} A = &\frac{\gamma_1 C_{v1} - C_{v1} - s_1}{\alpha_1 \rho_1 \varrho C_{v1}} \left[(e_1 - q_1)(\varrho - \rho_1) + \varrho(e_i - e_1)\right] \\ &+ \left[T_1(s_1 + \gamma_1 C_{v1}) - \frac{p_1}{\rho_1} - (e_1 - q_1)\right] \frac{(\varrho - \rho_1)}{\alpha_1 \rho_1 \varrho}, \\ B = &-\frac{\gamma_2 C_{v2} - C_{v2} - s_2}{\alpha_2 \rho_2 \varrho C_{v2}} \left[(e_2 - q_2)(\varrho - \rho_2) + \varrho(e_i - e_2)\right] \\ &- \left[T_2(s_2 + \gamma_2 C_{v2}) - \frac{p_2}{\rho_2} - (e_2 - q_2)\right] \frac{(\varrho - \rho_2)}{\alpha_2 \rho_2 \varrho}. \end{aligned}$$

From (7.4.35) we get

$$\frac{\partial \Delta g}{\partial t} = \frac{\partial (g_1 - g_2)}{\partial t} = (A - B)\dot{m}.$$

The simplest numerical approximation of this equation is

$$\frac{(\Delta g)^{n+1} - (\Delta g)^n}{\Delta t} = (A - B)^n (\dot{m})^n.$$

To satisfy the equilibrium condition for the Gibbs free energies we require $(\Delta g)^{n+1} = 0$. Thus the mass transfer can be approximated as

$$(\dot{m})^n = \frac{-(\Delta g)^n}{\Delta t (A - B)^n}.$$

Using this approximation for $(\dot{m})^n$ we can integrate the system (7.4.17). But we may face the problem of loosing the positivity of the volume fraction. Therefore a limitation on the value $\dot{m}/\varrho$ must be used. We take the following procedure from [33] which we cite for the sake of completeness. Assume that $S_{\alpha_1} = \dot{m}/\varrho$. Then the maximum admissible source term for the volume fraction evolution in order to presereve the positivity is given as

$$S_{\max,\ \alpha_1} = \begin{cases} \dfrac{1 - \alpha_1}{\Delta t}, & S_{\alpha_1} > 0 \\ -\dfrac{\alpha_1}{\Delta t}, & \text{otherwise.} \end{cases} \tag{7.4.36}$$

Then, if $|S_{\max,\ \alpha_1}| > |S_{\alpha_1}|$, the numerical integration for the system (7.4.17) can be done with the hydrodynamics time step which is restricted by the CFL number. Otherwise, the integration time step has to be reduced. The ratio $R_{\alpha_1} = S_{\max,\ \alpha_1}/S_{\alpha_1}$ is computed and the system (7.4.17) is integrated over a fraction of the time step, typically $\Delta t_m = R_{\alpha_1} \Delta t/2$. Successive point integrations are done to cover the complete hydrodynamic step.

The above procedure is cheap, fast and easy to implement. But this procedure is not an instantaneous one. This means that the equilibrium of the Gibbs free energy is reached very fast after a very short time but not instantaneously. Hereafter we propose another method for the Gibbs free energy relaxation which is an instantaneous relaxation procedure.

7.4.2.4 Free Gibbs energy relaxation, procedure II

By considering (7.4.17b) and (7.4.17c) with the fact that the velocities are in equilibrium we get $\frac{\partial u_1}{\partial t} = 0$. Using this with (7.4.17c) and (7.4.17d) we get

$$\frac{\partial \alpha_1 \rho_1 e_1}{\partial t} = e_i \dot{m}. \tag{7.4.37}$$

From (7.4.37) with (7.4.17a) we have

$$\frac{\partial \alpha_1 \rho_1 e_1}{\partial t} = \varrho e_i \frac{\partial \alpha_1}{\partial t}. \tag{7.4.38}$$

Integrating (7.4.38) we get the following approximation

$$(\alpha_1 \rho_1 e_1)^* = (\alpha_1 \rho_1 e_1)^0 + \overline{\varrho e}_i (\alpha_1^* - \alpha_1^0), \tag{7.4.39}$$

where $\overline{\varrho e}_i$ is the mean interfacial value between the states $(\alpha_1^0, \rho_1^0, e_1^0)$ and $(\alpha_1^*, \rho_1^*, e_1^*)$.

From (7.4.17a) and (7.4.17b) we have

$$\frac{\partial \alpha_1 \rho_1}{\partial t} = \varrho \frac{\partial \alpha_1}{\partial t}.$$

Integrating this equation we get

$$(\alpha_1 \rho_1)^* = (\alpha_1 \rho_1)^0 + \bar{\varrho}(\alpha_1^* - \alpha_1^0), \tag{7.4.40}$$

where $\bar{\varrho}$ is the mean interfacial value between the states $(\alpha_1^0, \rho_1^0, e_1^0)$ and $(\alpha_1^*, \rho_1^*, e_1^*)$.

In the same way we have the following equations for phase '2'

$$(\alpha_2 \rho_2 e_2)^* = (\alpha_2 \rho_2 e_2)^0 - \overline{\varrho e}_i (\alpha_1^* - \alpha_1^0), \tag{7.4.41}$$

$$(\alpha_2 \rho_2)^* = (\alpha_2 \rho_2)^0 - \bar{\varrho}(\alpha_1^* - \alpha_1^0). \tag{7.4.42}$$

Equation (7.4.40) shows that the density ρ_1 is a function of α_1. Using this fact with (7.4.39) we conclude that e_1 is also a function of α_1. Analogously ρ_2 and e_2 are functions of α_1. We aim now to find the α_1 which satisfies the equilibrium condition

$$f_g(\alpha_1) = g_2(e_2, \rho_2) - g_1(e_1, \rho_1) = 0. \tag{7.4.43}$$

The equation (7.4.43) can be solved by any iterative procedure. In this way the Gibbs free energy equilibrium is reached instantaneously.

This procedure for the Gibbs free energy relaxation is more expensive since an iterative method is used, but this method has a better resolution than the previous procedure.

7.4.3 The final model

In result of this section, the full model with heat and mass transfer is given as

$$\frac{\partial \alpha_1}{\partial t} + u_I \frac{\partial \alpha_1}{\partial x} = \mu(p_1 - p_2) + \frac{Q}{\kappa} + \frac{\dot{m}}{\varrho}, \tag{7.4.44a}$$

$$\frac{\partial \alpha_1 \rho_1}{\partial t} + \frac{\partial (\alpha_1 \rho_1 u_1)}{\partial x} = \dot{m}, \tag{7.4.44b}$$

$$\frac{\partial \alpha_1 \rho_1 u_1}{\partial t} + \frac{\partial (\alpha_1 \rho_1 u_1^2 + \alpha_1 p_1)}{\partial x} = p_I \frac{\partial \alpha_1}{\partial x} + \lambda(u_2 - u_1) + u_I \dot{m}, \tag{7.4.44c}$$

$$\begin{aligned} \frac{\partial \alpha_1 \rho_1 E_1}{\partial t} + \frac{\partial (\alpha_1 (\rho_1 E_1 + p_1) u_1)}{\partial x} &= p_I u_I \frac{\partial \alpha_1}{\partial x} + \mu p_I (p_2 - p_1) \\ &+ \lambda u_I (u_2 - u_1) + Q + (e_i + \frac{u_I^2}{2}) \dot{m}, \end{aligned} \tag{7.4.44d}$$

$$\frac{\partial \alpha_2 \rho_2}{\partial t} + \frac{\partial (\alpha_2 \rho_2 u_2)}{\partial x} = -\dot{m}, \tag{7.4.44e}$$

$$\frac{\partial \alpha_2 \rho_2 u_2}{\partial t} + \frac{\partial (\alpha_2 \rho_2 u_2^2 + \alpha_2 p_2)}{\partial x} = -p_I \frac{\partial \alpha_1}{\partial x} - \lambda(u_2 - u_1) - u_I \dot{m}, \tag{7.4.44f}$$

$$\begin{aligned} \frac{\partial \alpha_2 \rho_2 E_2}{\partial t} + \frac{\partial (\alpha_2 (\rho_2 E_2 + p_2) u_2)}{\partial x} &= -p_I u_I \frac{\partial \alpha_1}{\partial x} - \mu p_I (p_2 - p_1) \\ &- \lambda u_I (u_2 - u_1) - Q - (e_i + \frac{u_I^2}{2}) \dot{m}, \end{aligned} \tag{7.4.44g}$$

where

$$Q = \theta(T_2 - T_1),$$

$$\dot{m} = \eta(g_2 - g_1).$$

The variables κ, ϱ and e_i are given in (7.4.10), (7.4.29a) and (7.4.29b) respectively. All relaxation parameters λ, μ, θ and η are assumed to be infinite. The model (7.4.44) is solved by the Strang splitting (7.3.1). The operator L_s approximates the solution of the ordinary differential system (7.3.12). This system is solved by successive integrations considering separately each one of the source vectors that are related to the relaxation of the velocity, pressure, temperature and Gibbs free energy. The order of the successive integrations are essential for our model. They are done firstly for the velocity relaxation, then for the pressure relaxation, after for the temperature relaxation and finally for the Gibbs free energy relaxation. The velocity and the pressure relaxation are performed for the entire flow field while the temperature and the Gibbs free energy relaxation are used at the interface only. For the hyperbolic operator L_h a Godunov-type scheme is used.

7.5 Modeling phase transition for the six-equation model

The six-equation model with a single velocity is obtained from the seven-equation model in the asymptotic limit of zero velocity relaxation time, see Kapila et al. [15]. This model, as the seven-equation model, has more attractive advantages over the five-equation model for the numerical computations. Also this model is less expensive than the seven-equation model.

In this section we will insert the heat and mass transfer in the six-equation model by the relaxation effects. The above assumptions and ideas for the seven-equation model will be used, i.e. we will assume that the pressure relaxes much faster than the thermal properties and the temperature relaxation time is much smaller than that of the Gibbs free energy.

The six-equation model without heat and mass transfer can be written as

$$\frac{\partial \alpha_1}{\partial t} + u\frac{\partial \alpha_1}{\partial x} = \mu(p_1 - p_2), \tag{7.5.1a}$$

$$\frac{\partial \alpha_1\rho_1}{\partial t} + \frac{\partial(\alpha_1\rho_1 u)}{\partial x} = 0, \tag{7.5.1b}$$

$$\frac{\partial \alpha_2\rho_2}{\partial t} + \frac{\partial(\alpha_2\rho_2 u)}{\partial x} = 0, \tag{7.5.1c}$$

$$\frac{\partial \rho u}{\partial t} + \frac{\partial(\rho u^2 + \alpha_1 p_1 + \alpha_2 p_2)}{\partial x} = 0, \tag{7.5.1d}$$

$$\frac{\partial \alpha_1\rho_1 e_1}{\partial t} + \frac{\partial \alpha_1\rho_1 e_1 u}{\partial x} + \alpha_1 p_1 \frac{\partial u}{\partial x} = \mu p_I(p_2 - p_1), \tag{7.5.1e}$$

$$\frac{\partial \alpha_2\rho_2 e_2}{\partial t} + \frac{\partial \alpha_2\rho_2 e_2 u}{\partial x} + \alpha_2 p_2 \frac{\partial u}{\partial x} = -\mu p_I(p_2 - p_1). \tag{7.5.1f}$$

In this section we use the relation (7.2.3) for the interfacial pressure p_I.

We apply the idea of Saurel et al. [34] that during the numerical computations we use the mixture energy equation to correct the thermodynamic state predicted by the two non-conservative internal energy equations. By summing the two internal energy equations and using the mass and momentum equations we obtain the mixture energy equation

$$\frac{\partial(\rho e + \frac{1}{2}\rho u^2)}{\partial t} + \frac{\partial u(\rho e + \frac{1}{2}\rho u^2 + \alpha_1 p_1 + \alpha_2 p_2)}{\partial x} = 0, \tag{7.5.2}$$

where $\rho = \alpha_1\rho_1 + \alpha_2\rho_2$ and $\rho e = \alpha_1\rho_1 e_1 + \alpha_2\rho_2 e_2$.

7.5.1 Mathematical properties of the six-equation model

In terms of the primitive variables $\mathbf{W} = (\alpha_1, \rho_1, \rho_2, u, p_1, p_2)$, the model (7.5.1) can be expressed as

$$\frac{\partial \mathbf{W}}{\partial t} + \mathbf{A}\frac{\partial \mathbf{W}}{\partial x} = \mathbf{S} \tag{7.5.3}$$

where the matrix $\mathbf{A}$ is given as

$$\mathbf{A} = \begin{bmatrix} u & 0 & 0 & 0 & 0 & 0 \\ 0 & u & 0 & \rho_1 & 0 & 0 \\ 0 & 0 & u & \rho_2 & 0 & 0 \\ \dfrac{p_1 - p_2}{\rho} & 0 & 0 & u & \dfrac{\alpha_1}{\rho} & \dfrac{1-\alpha_1}{\rho} \\ 0 & 0 & 0 & \rho_1 c_1^2 & u & 0 \\ 0 & 0 & 0 & \rho_2 c_2^2 & 0 & u \end{bmatrix}.$$

The matrix $\mathbf{A}$ has six eigenvalues, only three of them are distinct

$$\begin{aligned} \lambda_1 &= \lambda_2 = \lambda_3 = \lambda_4 = u, \\ \lambda_5 &= u + c, \\ \lambda_6 &= u - c. \end{aligned} \tag{7.5.4}$$

Here c is the *mixture sound speed* and is expressed as

$$c^2 = \frac{\alpha_1\rho_1}{\rho}c_1^2 + \frac{\alpha_2\rho_2}{\rho}c_2^2.$$

The sound speeds c_k, $k = 1, 2$, are defined by (7.2.4).

The corresponding right eigenvectors are

$$\mathbf{r}_1 = \begin{bmatrix} 0 \\ 0 \\ 0 \\ 0 \\ -\frac{\alpha_2}{\alpha_1} \\ 1 \end{bmatrix}, \quad \mathbf{r}_2 = \begin{bmatrix} 0 \\ 0 \\ 1 \\ 0 \\ 0 \\ 0 \end{bmatrix}, \quad \mathbf{r}_3 = \begin{bmatrix} 0 \\ 1 \\ 0 \\ 0 \\ 0 \\ 0 \end{bmatrix}, \quad \mathbf{r}_4 = \begin{bmatrix} 1 \\ 0 \\ 0 \\ 0 \\ \frac{p_2 - p_1}{\alpha_1} \\ 0 \end{bmatrix}, \quad \mathbf{r}_5 = \begin{bmatrix} 0 \\ 1 \\ \frac{\rho_2}{\rho_1} \\ \frac{c}{\rho_1} \\ c_1^2 \\ \frac{\rho_2}{\rho_1} c_2^2 \end{bmatrix}, \quad \mathbf{r}_6 = \begin{bmatrix} 0 \\ 1 \\ \frac{\rho_2}{\rho_1} \\ -\frac{c}{\rho_1} \\ c_1^2 \\ \frac{\rho_2}{\rho_1} c_2^2 \end{bmatrix}. \tag{7.5.5}$$

Therfore, the system (7.5.1) is hyperbolic, but not strictly hyperbolic.

7.5.2 Numerical method

To take into account the non-differential source terms the Strang splitting (7.3.1) is used. In this case the vector of conservative variables $\mathbf{U}$ is given as

$$\mathbf{U} = (\alpha_1, \alpha_1\rho_1, \alpha_2\rho_2, \rho u, \alpha_1\rho_1 e_1, \alpha_2\rho_2 e_2, \rho e + \frac{1}{2}\rho u^2)^T.$$

The last element in $\mathbf{U}$ corresponds to the redundant equation (7.5.2).

For the hyperbolic part of the system a Godunov-type scheme is used that takes into account the discretization of the non-conservative terms.

The source vector $\mathbf{S}$ is associated with the relaxation terms and is decomposed as

$$\mathbf{S} = \mathbf{S}_P + \mathbf{S}_Q + \mathbf{S}_m,$$

where $\mathbf{S}_P = (\mu(p_1 - p_2), 0, 0, 0, \mu p_I(p_2 - p_1), -\mu p_I(p_2 - p_1), 0)^T$ represents the pressure relaxation terms. The vectors $\mathbf{S}_Q$ and $\mathbf{S}_m$ are associated with the heat and mass transfer relaxation terms respectively, they will be considered in the next section.

The HLL, HLLC and VFRoe Riemann solvers can be used. For the HLL solver we refer to the book of Toro [38], it is detailed in the context of Euler equations there but it is easily modified to the six-equation model. The HLLC solver was introduced above in Section 7.3.1.1 for the seven-equation model and is detailed in [34] for the six-equation model. The VFRoe solver [12] is explained in the following section in the context of the six-equation model.

7.5.2.1 VFRoe-type solver

Consider the Riemann problem consists of the homogenous part of the system (7.5.3)

$$\frac{\partial \mathbf{W}}{\partial t} + \mathbf{A}\frac{\partial \mathbf{W}}{\partial x} = 0,$$

with the initial conditions

$$\mathbf{W}(x, 0) = \begin{cases} \mathbf{W}_L, & x < 0 \\ \mathbf{W}_R, & x > 0. \end{cases}$$

The Jacobian matrix $A(\overline{\mathbf{W}})$ is calculated in the average state

$$\overline{\mathbf{W}} = \frac{\mathbf{W}_L + \mathbf{W}_R}{2}.$$

The intermediate state in the solution of the Riemann problem is

$$\mathbf{W}^* = \mathbf{W}_L + \sum_{\lambda_i < 0} a_i \mathbf{r}_i,$$

where the eigenvalues λ_i and the corresponding eigenvectors $\mathbf{r}_i$ are given by (7.5.4) and (7.5.5)

The coefficients a_i are determined by

$$\mathbf{W}_R - \mathbf{W}_L = \sum_{i=1}^{6} a_i \mathbf{r}_i,$$

Indeed, they are given by the following expressions

$$\begin{aligned}
a_4 &= \Delta_1, \\
a_1 &= -\frac{\frac{\rho_2}{\rho_1}c_2^2\Delta_5 - c_1^2\Delta_6 - \frac{\rho_2 c_2^2 a_4(p_2-p_1)}{\alpha_1\rho_1}}{\frac{\alpha_2\rho_2}{\alpha_1\rho_1}c_2^2 + c_1^2}, \\
a_5 &= \frac{\rho_1\rho_2 c_2^2\Delta_4 + \rho_1 c\Delta_6 - \rho_1 c a_1}{2\rho_2 c c_2^2}, \\
a_6 &= a_5 - \frac{\rho_1}{c}\Delta_4, \\
a_2 &= \Delta_3 - \frac{\rho_2}{\rho_1}(a_5 + a_6), \\
a_3 &= \Delta_2 - a_5 - a_6,
\end{aligned}$$

where Δ_k is the *k-th* component of $\mathbf{W}_R - \mathbf{W}_L = (\Delta_1, ..., \Delta_6)^T$.

7.5.2.2 Godunov-type method

The equations that are written in a conservative form are discretized by the conventional Godunov scheme

$$\mathbf{u}_j^{n+1} = \mathbf{u}_j^n - \frac{\Delta t}{\Delta x}[\mathbf{f}(\mathbf{u}^*(\mathbf{u}_j^n, \mathbf{u}_{j+1}^n)) - \mathbf{f}(\mathbf{u}^*(\mathbf{u}_{j-1}^n, \mathbf{u}_j^n))],$$

where

$$\mathbf{u} = (\alpha_1\rho_1,\ \alpha_2\rho_2,\ \rho u,\ \rho e + \frac{1}{2}\rho u^2)^T$$

and

$$\mathbf{f(u)} = (\alpha_1\rho_1 u,\ \alpha_2\rho_2 u,\ \rho u^2 + \alpha_1 p_1 + \alpha_2 p_2,\ u(\rho e + \frac{1}{2}\rho u^2 + \alpha_1 p_1 + \alpha_2 p_2))^T$$

.

The volume fraction equation and the internal energy equations are discretized as, see [34],

$$\alpha_{1j}^{n+1} = \alpha_{1j}^n - \frac{\Delta t}{\Delta x}((u\alpha_1)^*_{j+\frac{1}{2}} - (u\alpha_1)^*_{j-\frac{1}{2}} - \alpha_{1j}^n(u^*_{j+\frac{1}{2}} - u^*_{j-\frac{1}{2}})),$$

$$(\alpha\rho e)_{kj}^{n+1} = (\alpha\rho e)_{kj}^n - \frac{\Delta t}{\Delta x}((\alpha\rho e u)^*_{k,j+\frac{1}{2}} - (\alpha\rho e u)^*_{k,j-\frac{1}{2}} + (\alpha p)_{kj}^n(u^*_{j+\frac{1}{2}} - u^*_{j-\frac{1}{2}})).$$

To achieve a second order accuracy we use the MUSCL method detailed in Section 7.3.1.2.

7.5.2.3 Pressure relaxation and the correction criterion

It is clear that the pressure relaxation procedure for the seven-equation model that is introduced in [27] can be easily used for the six-equation model. Also we refer to the relaxation procedure that is used in [34]. We see that there is no significant difference between the results of the two procedures in our numerical results.

To make the relaxed pressure in agreement with the mixture EOS a correction criterion of [34] is used. From the SG-EOS (7.2.5a) for each phase with the pressure equilibrium we obtain the following expression for the mixture EOS, see [33, 34]

$$p(\rho_1, \rho_2, e, \alpha_1) = \frac{\rho e - \alpha_1\rho_1 q_1 - \alpha_2\rho_2 q_2 - \left(\frac{\alpha_1\gamma_1\pi_1}{\gamma_1 - 1} + \frac{\alpha_2\gamma_2\pi_2}{\gamma_2 - 1}\right)}{\frac{\alpha_1}{\gamma_1 - 1} + \frac{\alpha_2}{\gamma_2 - 1}}. \tag{7.5.6}$$

The mixture pressure (7.5.6) is obtained from the evolution of the mixture total energy (7.5.2). This is expected to be accurate in the entire field flow since the equation (7.5.2) is written in the conservative formulation.

By using evolution of the mixture total energy (7.5.2) we can find the value of ρe. Using this value in (7.5.6) we can find the value of the mixture pressure. Other variables in the relation (7.5.6) are estimated by the relaxation step. In this way we determine the value of the mixture pressure that agrees with the mixture EOS, then we use this value with the SG-EOS for each phase to reset the values of the internal energies.

7.5.3 Modeling of the heat and mass transfer for the six-equation model

To take into account the heat and mass transfer we have to solve the following system of ODE at each time step after the pressure relaxation step

$$\frac{d\mathbf{U}}{dt} = \mathbf{S}_Q + \mathbf{S}_m. \tag{7.5.7}$$

The system (7.5.7) is solved by considering each one of the source vectors alone. According to our assumptions during the temperature relaxation the pressures will stay in equilibrium, i.e. the condition (7.4.3) holds. And during the Gibbs free energy relaxation the pressures and the temperatures will stay in equilibrium, i.e. the conditions (7.4.18) hold.

The heat source vector is modeled as

$$\mathbf{S}_Q = (\frac{Q}{\kappa}, 0, 0, 0, Q, -Q, 0)^T, \tag{7.5.8}$$

where $Q = \theta(T_2 - T_1)$. Note that the last element of $\mathbf{S}_Q$ corresponds to the redundant equation (7.5.2). It is clear that the value of κ (7.4.10) for the seven-equation model works also for the six-equation model and satisfies the condition (7.4.3). Also it is easy to see that the same method of temperature relaxation for the seven-equation model can be used for the six-equation model.

The vector $\mathbf{S}_m$ is modeled as

$$\mathbf{S}_m = (\frac{\dot{m}}{\varrho}, \dot{m}, -\dot{m}, 0, e_i\dot{m}, -e_i\dot{m}, 0), \tag{7.5.9}$$

where $\dot{m} = \eta(g_2 - g_1)$. The values of ϱ and e_i that satisfy the conditions (7.4.18) are given in (7.4.29). Also the Gibbs free energy relaxation procedures for the seven-equation model can be used directly here.

Thus the final six-equation model with heat and mass transfer is given as

$$\frac{\partial \alpha_1}{\partial t} + u\frac{\partial \alpha_1}{\partial x} = \mu(p_1 - p_2) + \frac{1}{\kappa}Q + \frac{1}{\varrho}\dot{m}, \tag{7.5.10a}$$

$$\frac{\partial \alpha_1\rho_1}{\partial t} + \frac{\partial(\alpha_1\rho_1 u)}{\partial x} = \dot{m}, \tag{7.5.10b}$$

$$\frac{\partial \alpha_2\rho_2}{\partial t} + \frac{\partial(\alpha_2\rho_2 u)}{\partial x} = -\dot{m}, \tag{7.5.10c}$$

$$\frac{\partial \rho u}{\partial t} + \frac{\partial(\rho u^2 + \alpha_1 p_1 + \alpha_2 p_2)}{\partial x} = 0, \tag{7.5.10d}$$

$$\frac{\partial \alpha_1\rho_1 e_1}{\partial t} + \frac{\partial \alpha_1\rho_1 e_1 u}{\partial x} + \alpha_1 p_1\frac{\partial u}{\partial x} = \mu p_I(p_2 - p_1) + Q + e_i\dot{m}, \tag{7.5.10e}$$

$$\frac{\partial \alpha_2\rho_2 e_2}{\partial t} + \frac{\partial \alpha_2\rho_2 e_2 u}{\partial x} + \alpha_2 p_2\frac{\partial u}{\partial x} = -\mu p_I(p_2 - p_1) - Q - e_i\dot{m}. \tag{7.5.10f}$$

On the other hand, the six-equation model with heat and mass transfer is obtained directly from the seven-equation model involving the heat and mass transfer by the limit of infinitely fast velocity relaxation. This is shown in the 7.B We apply the reduction method of Chen et al. [6] on the seven-equation model including the heat and mass transfer (7.4.44) assuming stiff velocity relaxation. The resulting model is the six-equation model (7.5.10).

7.6 Numerical results

The tests for metastable liquids in [33] are used.

7.6.1 Two phase shock tube

Consider a 1 m shock tube filled with liquid dodecane under high pressure at the left, and with the vapor dodecane at atmospheric pressure at the right. The initial discontinuity is set at 0.75 m, and the initial data are

Left: $p_l = 10^8$ Pa, $\rho_l = 500$ kg/m^3, $u_l = 0$ m/s
Right: $p_v = 10^5$ Pa, $\rho_v = 2$ kg/m^3, $u_v = 0$ m/s.

For numerical reasons, in each side of the shock tube we allow the presence of a small volume fraction of the other fluid, typically 10^{-6}.

All computations for this example were done with a CFL number of 0.6. They used the first Gibbs free energy relaxation procedure with a limitation on the source terms given by (7.4.36). The time step for the fluid motion is restricted by the CFL number, but we observed that the Gibbs free energy relaxation procedure may require smaller time to ensure the positivity of the volume fraction. This means that sometimes the equations (7.4.17) are stiff. Thus by using the limitation (7.4.36) a smaller time step is used for the Gibbs free energy relaxation procedure and successive point integrations are done to cover the complete hydrodynamic step that is restricted by the CFL number. In the presence of stiffness from the Gibbs free energy relaxation, the first Gibbs free energy relaxation procedure is more appropriate than the second relaxation procedure, this is due to the easy of imposition the limitation (7.4.36) on the source terms.

By using the seven-equation model the results are shown at time $t = 473\mu$s. Figure 7.1 gives the results without phase transition, while in Figure 7.2 we see the case when the phase transition is included.

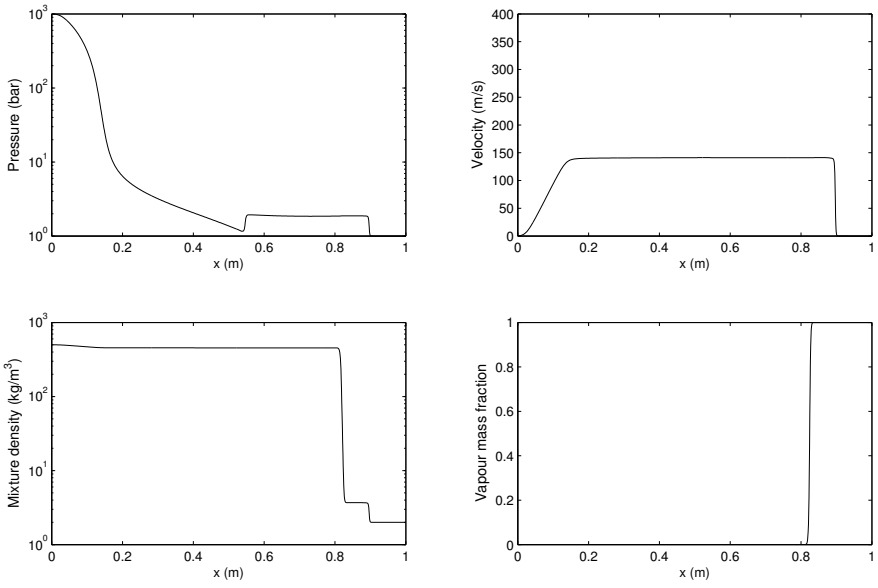

Figure 7.1: Dodecane liquid-vapor shock tube without phase transition, by using the 7-equation model. The mesh involves 1250 cells, the CPU time is 100.65 seconds and the number of time steps is 7197. The scale for the velocity graph is chosen in this way for a direct comparison with the velocity graph in Figure 7.2.

In comparison between the two figures, an extra wave appears between the rarefaction wave and the contact discontinuity which corresponds the evaporation front. Indeed, rarefaction waves propagate through the liquid producing a superheated liquid and evaporation has occurred. An extra wave representing the evaporation front propagates through the superheated liquid and produces a liquid vapor

mixture at thermodynamic equilibrium with a high velocity, for more details see [33].

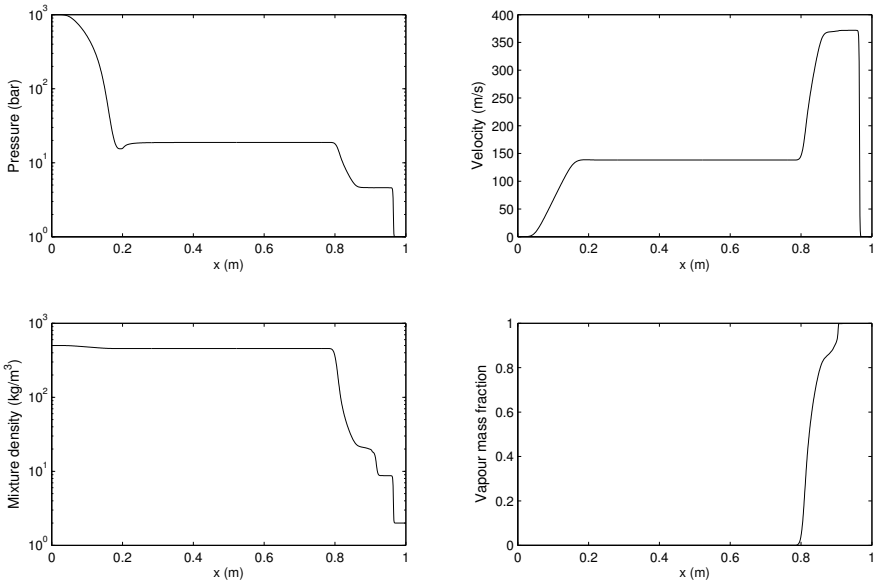

Figure 7.2: Dodecane liquid-vapor shock tube with phase transition, by using the 7-equation model. The mesh involves 1250 cells, the CPU time is 151.98 seconds and the number of time steps is 8828.

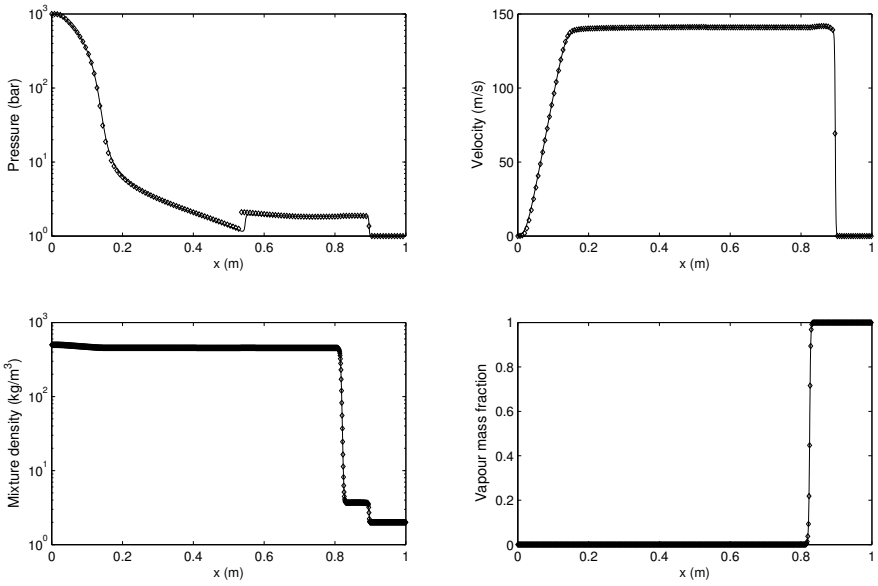

Figure 7.3: Dodecane liquid-vapor shock tube without phase transition, a comparison between the results of the 7-equation model (lines) and the 6-equation model results (symbols). The computations used 1250 cells. For the 7-equation model results: The CPU time is 100.65 seconds with 7197 time steps. For the 6-equation model results: The CPU time is 14.46 seconds with 1557 time steps.

A comparison between the results of the six-equation model and the seven-equation model is shown in Figures 7.3 - 7.6 by using the same number of cells and the same type of the Riemann solver. It is

clear that for both cases, with or without the phase transition, the results almost coincide. Just a very small difference appears at the left rarefaction in the curves of the pressure. Such a small difference has no significant numerical meaning. This small difference appears in both cases i.e. with or without the phase transition in the same manner, see the pressure profiles on logarithmic scales, Figures 7.4 and 7.5, the pressure profiles are drawn separately to be able to see the differences. Thus this small difference is not related to the treatment of the phase transition.

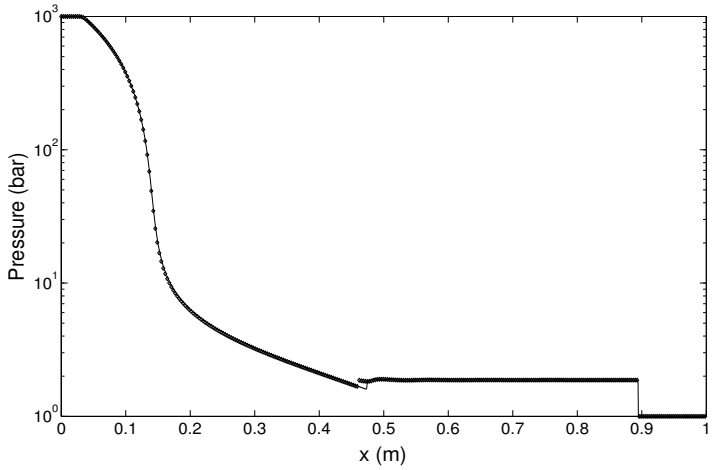

Figure 7.4: Dodecane liquid-vapor shock tube without phase transition. The pressure profile over (10000) cells, by the 7- equation model (lines) and the 6-equation model (symbols). For the 7-equation model: The CPU time is 8145.17 seconds taking 56749 time steps. For the 6-equation model: The CPU time is 1035.01 seconds with 12452 time steps.

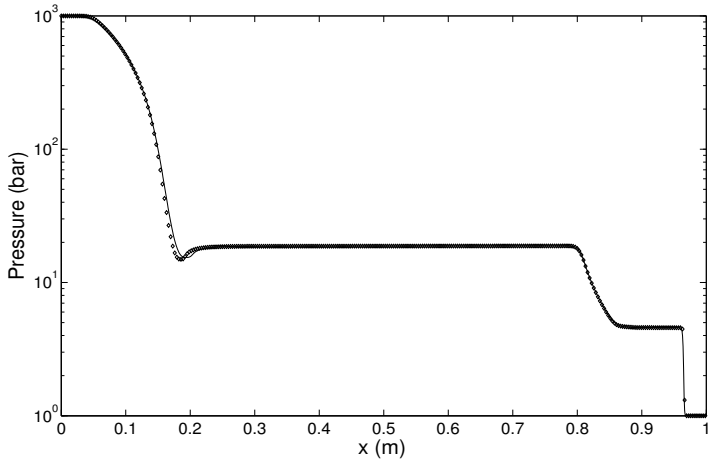

Figure 7.5: Dodecane liquid-vapor shock tube with phase transition. The pressure profile, a comparison between the results of the 7-equation model (lines) and the 6-equation model results (symbols). The computations were done with 1250 cells. For the 7-equation model: The CPU time is 151.98 seconds with 8828 time steps. For the 6-equation model: The CPU time is 19.87 seconds with 1556 time steps.

At the right face of the left rarefaction wave in the pressure profile in Figures 7.2 and 7.5 we can see a small distortion which does not appear in the results of [33] by using the five-equation model. We reran this test for higher number of cells for both models, seven-equation and six-equation, but observed no change. In fact we see the same feature on the curve of the pressure without phase transition, see Figure 7.4. The pressure curve is shown on logarithmic scale, 10000 cells were used in the computations

but this distortion still appears. Thus we conclude that this is not related to our new modifications for heat and mass transfer. This may come from the nature of the initial seven-equation or six-equation model or from the numerical method without phase transition. Moreover, such differences between the results of the seven-equation model and the five-equation model without phase transition appear also in the results of [23]. This requires further investigation.

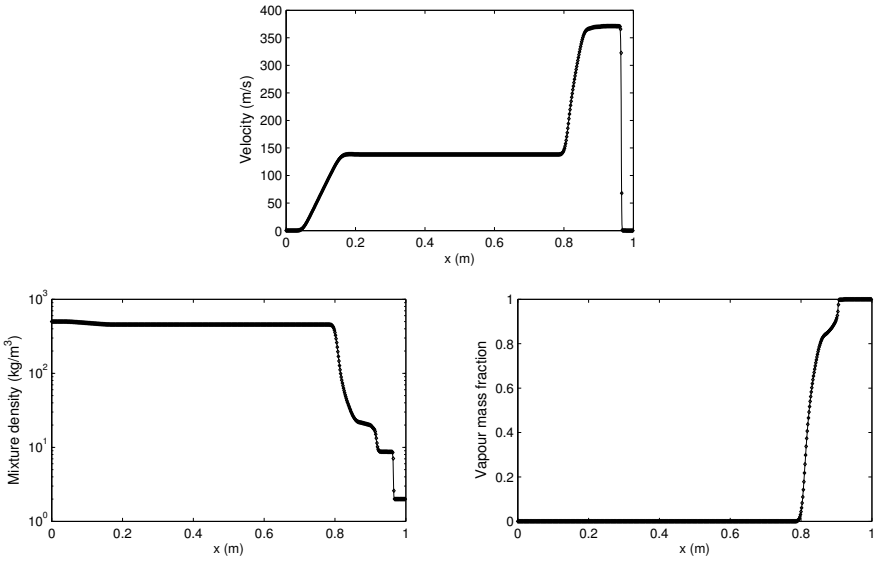

Figure 7.6: Dodecane liquid-vapor shock tube with phase transition, a comparison between the results of the 7-equation model (lines) and the 6-equation model results (symbols). The computations used 1250 cells. For the 7-equation model: The CPU time is 151.98 seconds with 8828 time steps. For the 6-equation model: The CPU time is 19.87 seconds with 1556 time steps.

In result, for this example, we see that there is no significant difference between the results of the 7-equation model and the 6-equation model and both models give similar results. But there is a significant difference in the required CPU time. The required time for the 6-equation model is much smaller ($\approx 13\%$) than that required for the 7-equation model.

7.6.2 Validation against shock tube experiments

Experimental results were obtained by Simões-Moreira and Shepherd [36]. Liquid dodecane in a tube was suddenly expanded into a low pressure chamber (1 mbar). An evaporation front or wave propagated into metastable liquid with a steady mean velocity. This velocity was measured for different initial temperatures of liquid dodecane. Also pressure data were obtained during the evaporation event before and after the evaporation wave, see [36] and for full details see the PhD thesis of Simões-Moreira [35].

At each temperature we compute the front velocity under conditions which are close to the experimental conditions with help of [21]. We consider a low pressure chamber (1 mbar) filled with gaseous dodecane at right side of the shock tube with density 10^{-4}kg/m^3. While a liquid dodecane is considered initially at the left side of the shock tube with a higher pressure. We adjust the initial pressure of the left hand side, so that the pressure in the state before the evaporation front is equal to the measured value. The density of the liquid is calculated from the equation of state (7.2.5b), as the initial temperature is known.

Table 3 shows the estimated initial pressure that we use for each temperature, column two. The columns three and four represent the experimental data for the pressure before the evaporation wave and the front velocity respectively [36]. The fifth column shows the computed values for the front velocity by present model.

As in [33] the front velocity is computed as a local wave speed, i.e. $U_F = ((\rho u)_i - (\rho u)_{i-1})/(\rho_i - \rho_{i-1})$, where i refers to the state after the evaporation wave. The computed values for the front velocity are calculated at several time ponits in the range between $200\mu s$ and $500\mu s$. Then an averaged value is taken. We see that for each case the computed values at different times are very close.

A comparison between our results with the experimental results and the results of Saurel et al. [33] is shown in Figure 7.7. It is clear that our results are more close to the experimental results. There is still not perfect agreement with the experimental data. This is related to several sources, like how realistic the equations of state we used are and how close we are to the real initial conditions of the experiments. However we have a reasonable agreement with the experimental data also in the tendency of the relation between the front velocity and the initial temperature, i.e. the front velocity increases if the temperature increases.

T_l (K)	p_l (bar)	p_B (bar)	U_F (m/s)(measured)	U_F (m/s)(computed)
453	1.5	0.24	0.253	0.147
473	2.2	0.33	0.309	0.240
489	3.0	0.44	0.390	0.328
503	3.9	0.59	0.472	0.441
523	5.0	0.83	0.648	0.576
543	7.5	1.19	0.837	0.888
563	11.0	1.91	1.381	1.337
573	13.0	2.12	1.578	1.620

Table 7.3: Estimated initial pressure, experimental results and the computed front velocity at several initial temperatures.

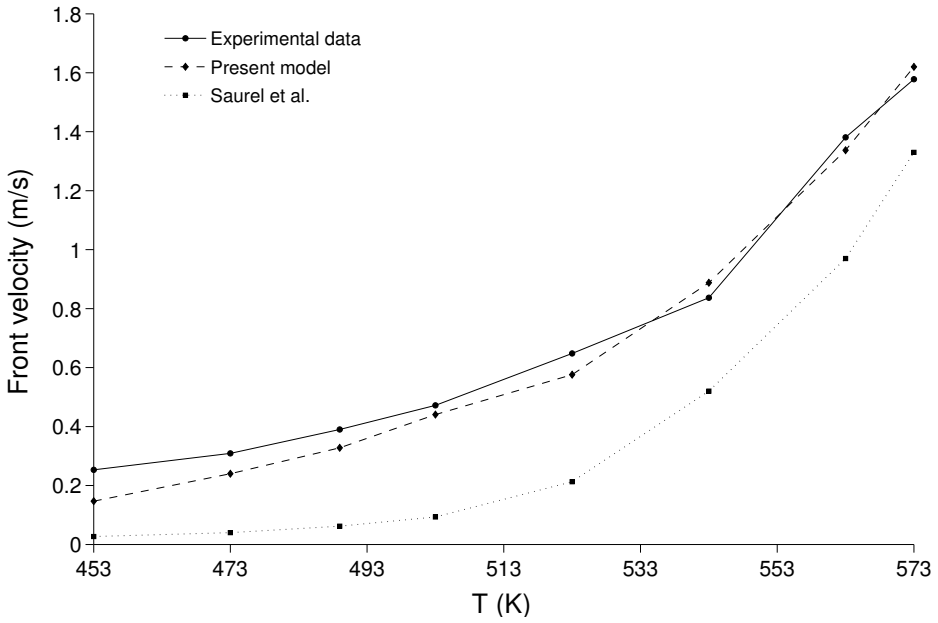

Figure 7.7: Evaporation front velocity versus initial temperature of liquid dodecane. Comparison between our results with the experimental results of Simões-Moreira and Shepherd [36] and the computed results of Saurel et al. [33].

7.6.3 Two phase expansion tube

This test consists of a 1 m long tube filled with liquid water at atmospheric pressure and with density $\rho_l = 1150$ kg/m^3. A weak volume fraction of vapor ($\alpha_v = 0.01$) is initially added to the liquid. The

initial discontinuity is set at 0.5 m, the left velocity is -2 m/s and the right velocity is 2 m/s.

In this test the water can not be treated as pure, and only the metastability condition is used to activate the phase transition, i.e. phase transition occurs if the liquid is metastable, i.e. if $T_l > T_{sat}(p_{equi})$. For the computation of $T_{sat}(p_{equi})$ see 7.C

This test case requires a small time step to obtain a stable solution (CFL$\approx$ 0.15). When the strong rarefaction are considered a smaller time step is required (CFL$\approx$ 0.03). Here for the sake of comparison we choose to do all computations with CFL=0.03. The small time here indicates that there is a stiffness coming from the relaxation procedures.

Both procedures of the Gibbs free energy relaxation give the same results, but we consider that the second procedure has a better resolution, thus it is adopted for this test case.

In Figure 7.8, we see the solution of this problem without phase transition at $t = 3.2$ ms. The results are obtained by the seven-equation model and are compared with those of the six-equation model, they are completely coinciding. The solution involves two expansion waves. The vapor volume fraction increases at the center of the domain due to the gas mechanical expansion present in small proportions [33].

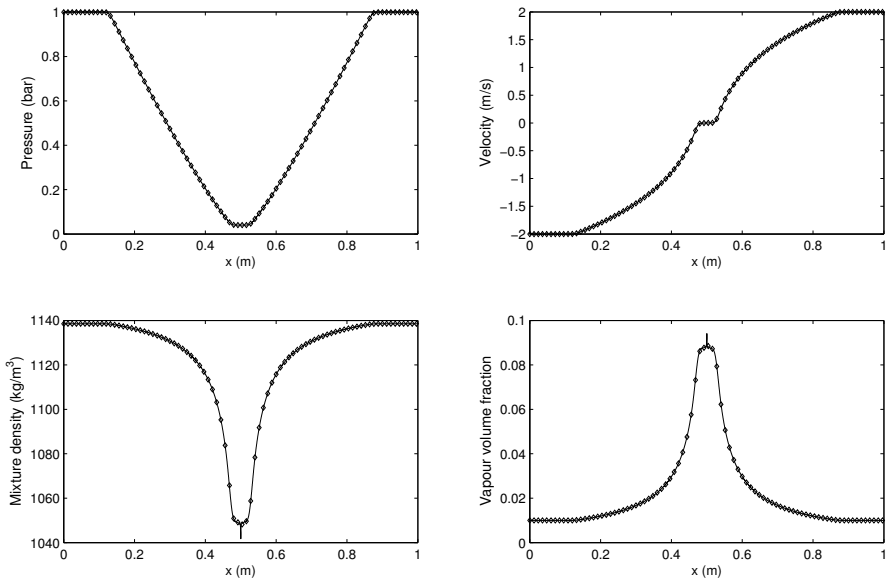

Figure 7.8: Water liquid-vapor expansion tube without phase transition, by using the 7-equation model (lines) and 6-equation model (symbols). The computations were done with 5000 cells. For the 7-equation model: The CPU time is 14.772 hours with 763550 time steps. For the 6-equation model: The CPU time is 7.305 hours with 763726 time steps.

The rarefaction waves make the liquid metastable and phase transition has to be added. Figure 7.9 presents the solution when the phase transition is involved and is compared with the solution without phase transition at $t = 3.2$ ms. Liquid water is expanded until the saturation pressure is reached (see the pressure graph) then evaporation appears and quite small of vapor is created, for details see [33]. In Figure 7.11 a comparison between the results of the seven-equation and the six-equation models is made at the same time, the curves are completely coinciding.

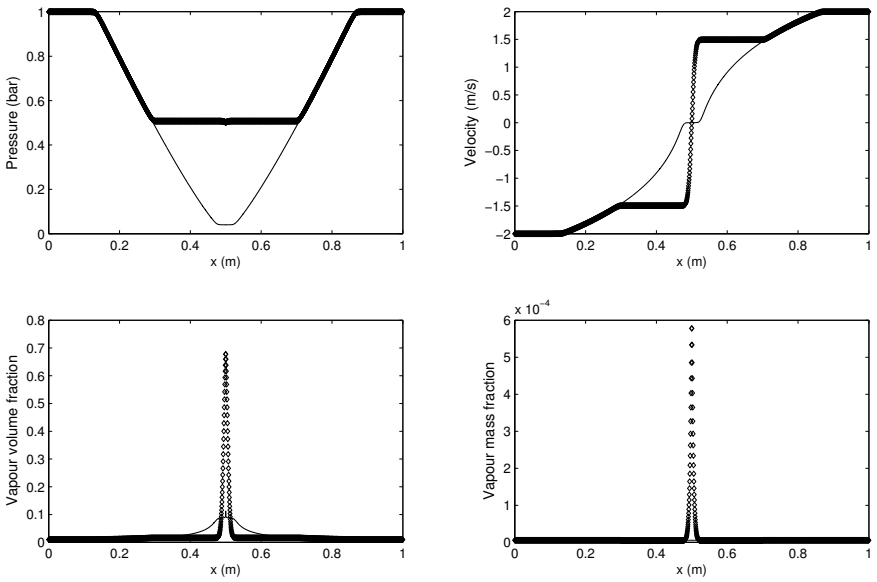

Figure 7.9: Water liquid-vapor expansion tube with phase transition at $t = 3.2$ ms, the computed results by the 7-equation model with phase transition (symbols) are compared with the results of the same model without phase transition (lines). The computations were done with 5000 cells. For the model without phase transition: The CPU time is 14.772 hours with 763550 time steps. when the phase transition is included: The CPU time is 18.838 hours with 763550 time steps.

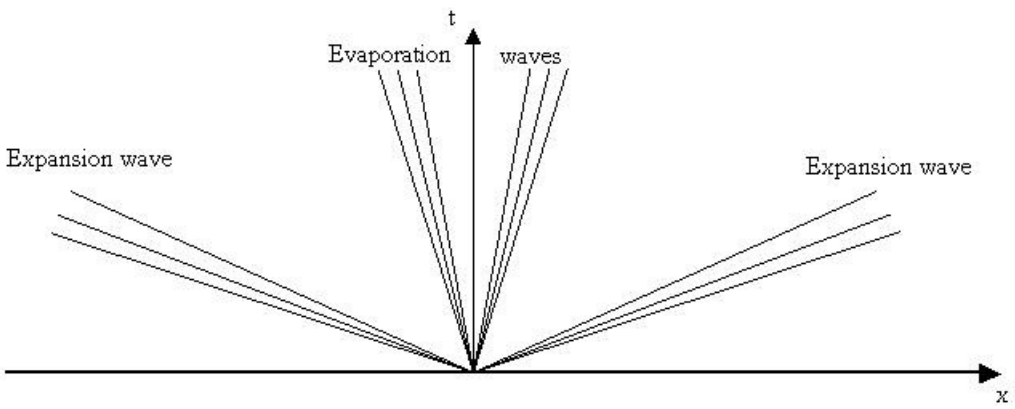

Figure 7.10: The waves pattern that correspond to the solutions in Figures 7.9 and 7.11. As shown the evaporation waves are expansion waves.

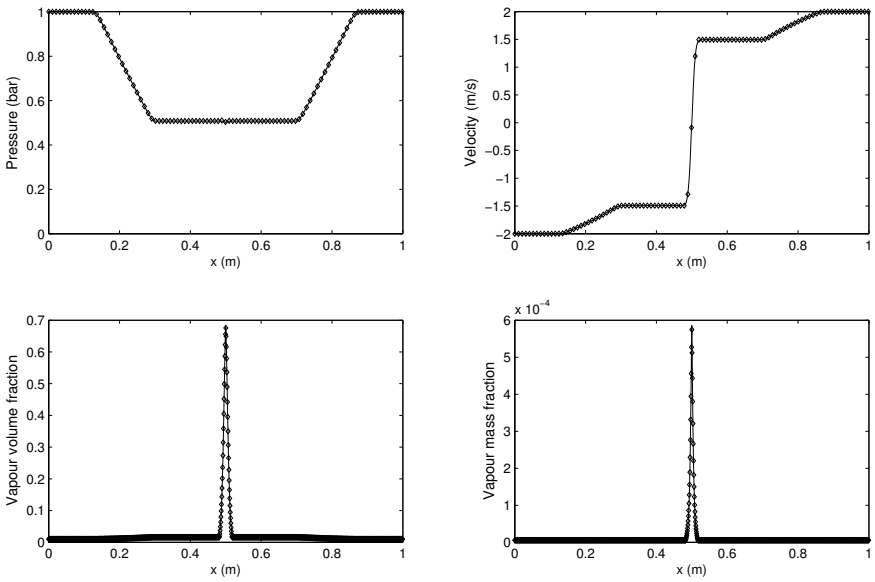

Figure 7.11: Water liquid-vapor expansion tube with phase transition at $t = 3.2$ ms. A comparison between the results of the 7-equation model (lines) and the 6-equation model (symbols). The computations used 5000 cells. For the 7-equation model model: The CPU time is 18.838 hours with 763550 time steps. For the 6-equation model: The CPU time is 9.447 hours with 764150 time steps.

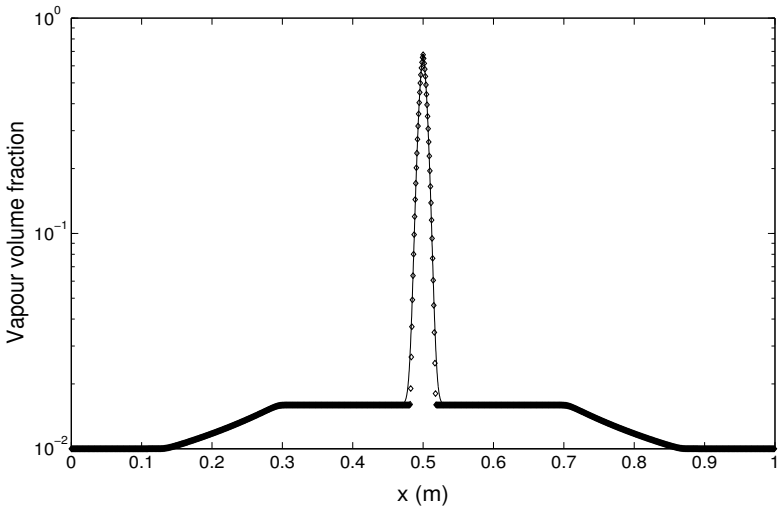

Figure 7.12: Water liquid-vapor expansion tube with phase transition at $t = 3.2$ ms, the vapor volume fraction profile on a logarithmic scale. By using the 7-equation model (lines) and 6-equation model (symbols).

The solution with phase transition, Figures 7.9 and 7.11, is composed of four expansion waves. This is clear if we consider the vapor volume fraction profile on a logarithmic scale as in Figure 7.12. Thus the wave pattern is as drawn in Figure 7.10. The extra two expansion waves correspond to the evaporation fronts.

If we consider the solution at later time, when $t = 59$ ms as in Figure 7.13, the two leading fast expansion waves leave the tube and the two slow evaporation waves are clearly visible. It is clear that these evaporation waves are expansion waves. Also it is clear that the results of the seven-equation model

and the six- equation model are completely coinciding.

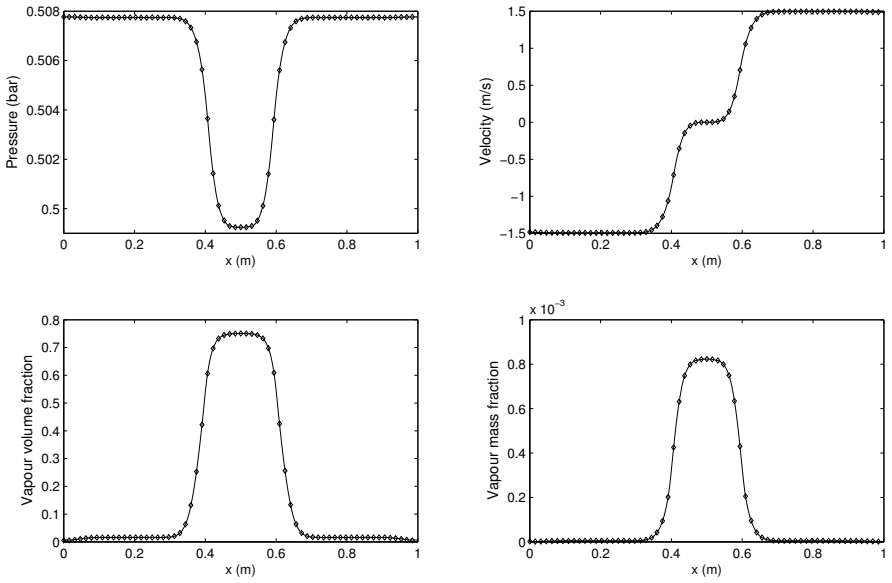

Figure 7.13: Water liquid-vapor expansion tube with phase transition at time $t = 59$ ms, by using the 7-equation model (lines) and 6-equation model (symbols). The two slow evaporation waves are visible. The computations were done with 3200 cells. For the 7-equation model: The CPU time is 116.078 hours with 8217444 time steps. For the 6-equation model: The CPU time is 99.406 hours with 8217444 time steps.

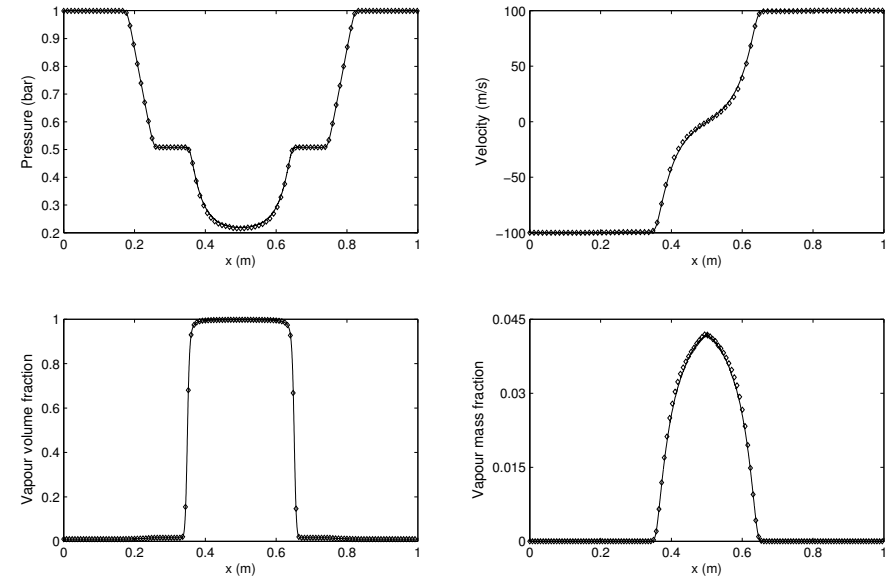

Figure 7.14: Water liquid-vapor expansion tube with phase transition and strong rarefaction effects (initial $|u| = 100$ m/s) at time $t = 1.5$ ms. The computations are done with 5000 cells. For the 7-equation model: The CPU time is 8.537 hours with 449836 time steps. For the 6-equation model: The CPU time is 5.700 hours with 381778 time steps.

To see the four expansion waves in one single graph we increase the value of the velocity which means an increase in the rarefaction effects. Under the same conditions except with a velocity -100 m/s on the left and 100 m/s on the right, the four waves are clearly visible as in Figure 7.14 at time $t = 1.5$ ms.

When the rarefaction effects become stronger we observe some difficulties. If the same conditions are maintained except the velocity is increased ($\gtrsim 200$m/s), we see that there are some differences between the results of both models. To consider such difficulty also for the sake of comparsion with the results of [33], we take the velocity -500 m/s on the left and 500 m/s on the right. The results are shown in Figure 7.15 at time $t = 0.58$ ms. There are some differences in the profiles of the pressure and the vapor mass fraction. Moreover there are some oscillations in the curve of the vapor mass fraction. We think that the differences in the results of both models may be related to the approximation of the non-conservative terms and to the fact that in seven-equation model an approximation is used in the velocity relaxation procedure. This may cause some deviation as the difference between the initial velocities is increased.

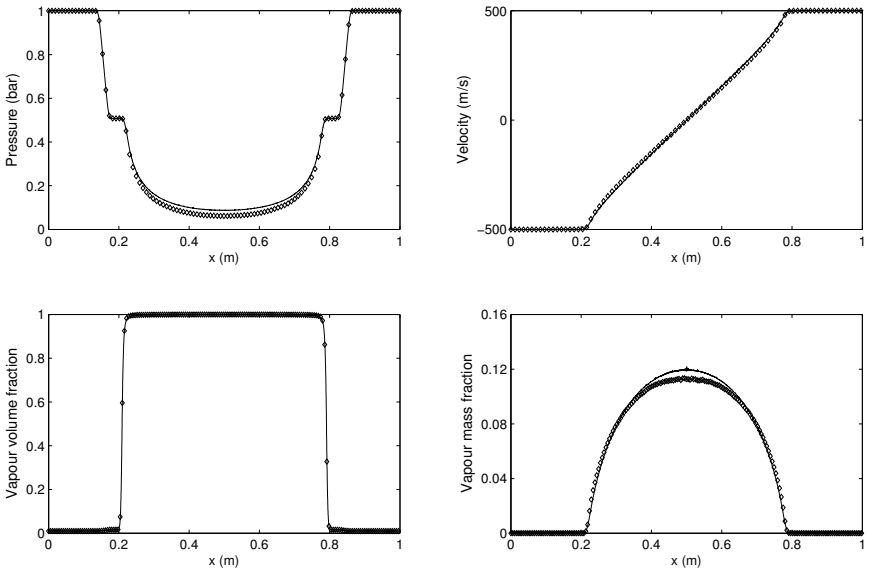

Figure 7.15: Water liquid-vapor expansion tube with phase transition and strong rarefaction effects (initial $|u| = 500$ m/s) at time $t = 0.58$ ms, by using the 7-equation model (lines) and 6-equation model (symbols). The computations used 5000 cells. For the 7-equation model: The CPU time is 4.947 hours with 218710 time steps. For the 6-equation model: The CPU time is 3.372 hours with 186601 time steps.

Under the grid refinement, the differences between the pressure profiles are decreased. They disappear with a very fine grid, as is shown in Figure 7.16. But the difference between the vapor mass fraction profiles remains, moreover the oscillations are more pronounced. To understand why the oscillations increase with grid refinement, we consider all variables that are related to the vapor mass fraction $Y_1 = \alpha_1\rho_1/\rho$. We see that as the number of the cells increases the mixture density decreases to a value very close to zero with small oscillations. Also the difference between the mixture density of the two models is reduced. But since the mixture density with low values lies in the denominator of the relation of Y_1, both of the differences and the oscillations in the curves of the vapor mass fraction will be more significant.

Again in this example it is noted that the required CPU time for the six-equation model is smaller than the CPU time that is required for the seven-equation model, in average it is about 66%. In all cases the results of both models coincide except when the difference between the initial velocities increase to a certain value, after that value is reached we observe a small deviation in the results of both models, also some oscillations appear. This problem is partially reduced under grid refinement.

As a result we think that since both models give the same results and also both of them may face similar problems under extreme initial conditions. We think that the six-equation model is to be

preferred for practical applications since it is less expensive. Moreover it is easier to modify this model to the multi-phase case.

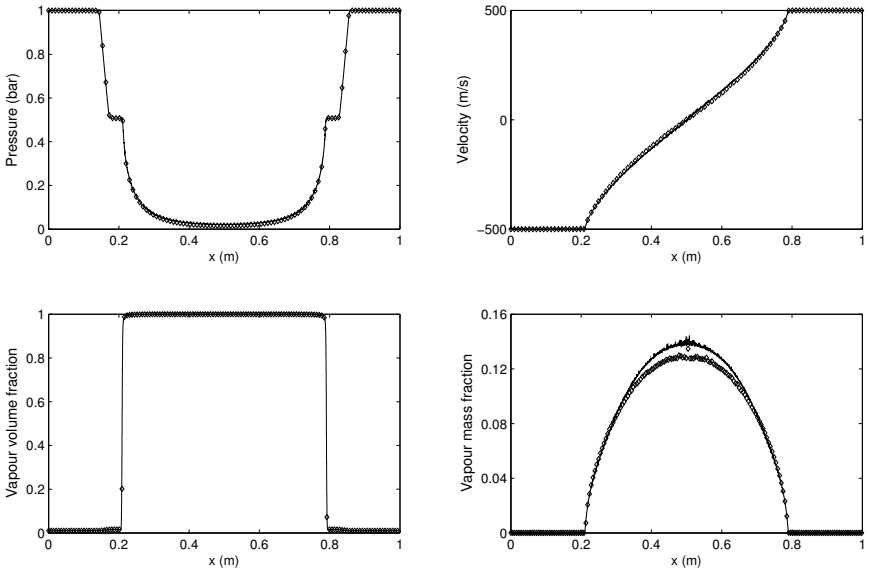

Figure 7.16: Water liquid-vapor expansion tube with phase transition and strong rarefaction effects (initial $|u| = 500$ m/s) at time $t = 0.58$ ms. By using the 7-equation model (lines) and 6-equation model (symbols). The computations are done with 25000 cells. For the 7-equation model: The CPU time is 112.393 hours with 1090545 time steps. For the 6-equation model: The CPU time is 85.4813 hours with 934593 time steps.

7.7 Conclusion

In this paper, we modified the seven-equation model for two-phase flows to include the heat and mass transfer through relaxation effects. Depending on the assumption that each property relaxes in a time is considerably different from the other characteristic times, we were able to model the effect of heat and mass transfer by using temperature and Gibbs free energy relaxations. The same ideas are also applied to the six-equation model with a single velocity, which is obtained from the seven equation-model in the limit of zero velocity relaxation time.

A modified Godunov-type method is used to solve the hyperbolic part of each model, while simple relaxation procedures are proposed for the temperature and Gibbs free energy relaxations.

We tested this model on the test problems of [33]. We were able to see also the extra expansion waves in our results which correspond to the evaporation fronts. Our results are similar to the results of [33] with few differences.

Computed front velocities in a shock tube at different initial temperatures are compared with experimental ones. A reasonable agreement is achieved.

A comparison between the results of the seven-equation model and the six-equation model was made. Both models almost give the same results, but the six-equation model is less expensive than the seven-equation model and easier to adopt to the multiphase case.

Due to the relaxation processes a stiffness may be encountered during the numerical computations. This requires a smaller time step than is needed for the hydrodynamic system. In particular, if the stiffness comes from the Gibbs free energy relaxation procedure it is possible to use a limitation on the source terms which can be used to find reduced time steps. Then a successive point integration is used to cover the complete hydrodynamic time step. Otherwise small CFL numbers would used and this consumes more computation time. In fact, this point still requires further efforts. For future work, the efficiency of the numerical method must be improved by using some adaptive discretizations. This will

be particularly important when the method is applied to two or three dimensional problems.

We observed that in mixtures under a high difference in the initial velocities there is a small deviation between the results of the seven-equation and six-equation models. This is reduced under grid refinement. We think this deviation is related to the approximation of the non-conservative terms and to some approximation used in velocity relaxation for the seven-equation model. However, to build a specific understanding for this point still more investigations are required. In fact, an extensive convergence study for both models would be very useful for this comparison and further insight into the models. This is a challenging issue for future work.

7.A Appendix: Mathematical properties of the seven-equation model

In order to investigate the mathematical properties of the model (7.2.1), we rewrite it in terms of primitive variables as

$$\frac{\partial \mathbf{W}}{\partial t} + \mathbf{A}\frac{\partial \mathbf{W}}{\partial x} = \mathbf{S} \tag{7.A.1}$$

where $\mathbf{W} = (\alpha_1, \rho_1, u_1, p_1, \rho_2, u_2, p_2)^T$, the source vector $\mathbf{S}$ represents the non-differential source terms and the matrix $\mathbf{A}$ is given as

$$\mathbf{A} = \begin{bmatrix} u_I & 0 & 0 & 0 & 0 & 0 & 0 \\ \frac{\rho_1}{\alpha_1}(u_1 - u_I) & u_1 & \rho_1 & 0 & 0 & 0 & 0 \\ \frac{p_1 - p_I}{\alpha_1 \rho_1} & 0 & u_1 & \frac{1}{\rho_1} & 0 & 0 & 0 \\ \frac{\rho_1 c_{I,1}^2}{\alpha_1}(u_1 - u_I) & 0 & \rho_1 c_1^2 & u_1 & 0 & 0 & 0 \\ -\frac{\rho_2}{\alpha_2}(u_2 - u_I) & 0 & 0 & 0 & u_2 & \rho_2 & 0 \\ -\frac{p_2 - p_I}{\alpha_2 \rho_2} & 0 & 0 & 0 & 0 & u_2 & \frac{1}{\rho_2} \\ -\frac{\rho_2 c_{I,2}^2}{\alpha_2}(u_2 - u_I) & 0 & 0 & 0 & 0 & \rho_2 c_2^2 & u_2 \end{bmatrix}.$$

Where the speed of sound c_k is given in (7.2.4) and $c_{I,k}$, *the speed of sound at interface*, is determined by

$$c_{I,k}^2 = \frac{\dfrac{p_I}{\rho_k^2} - \left(\dfrac{\partial e_k}{\partial \rho_k}\right)_{p_k}}{\left(\dfrac{\partial e_k}{\partial p_k}\right)_{\rho_k}}, \quad k = 1, 2. \tag{7.A.2}$$

The matrix $\mathbf{A}$ has real eigenvalues that are given by the following expressions

$$\begin{aligned} &\lambda_1 = u_I, \\ &\lambda_2 = u_1 - c_1, \qquad \lambda_3 = u_1, \qquad \lambda_4 = u_1 + c_1, \\ &\lambda_5 = u_2 - c_2, \qquad \lambda_6 = u_2, \qquad \lambda_7 = u_2 + c_2. \end{aligned}$$

The corresponding right eigenvectors are

$$\mathbf{r}_1 = \begin{bmatrix} \alpha_1\alpha_2\sigma_1\sigma_2 \\ -\alpha_2\sigma_2(\rho_1(\sigma_1 - c_{I,1}^2) + p_1 - p_I) \\ \alpha_2\sigma_2(u_1 - u_I)(p_1 - p_I - \rho_1 c_{I,1}^2)/\rho_1 \\ \alpha_2\sigma_2(\rho_1 c_{I,1}^2(u_1 - u_I)^2 - c_1^2(p_1 - p_I)) \\ -\alpha_1\sigma_1(\rho_2(c_{I,2}^2 - \sigma_2) - p_2 + p_I) \\ \alpha_1\sigma_1(u_2 - u_I)(-p_2 + p_I + \rho_2 c_{I,2}^2)/\rho_2 \\ \alpha_1\sigma_1(-\rho_2 c_{I,2}^2(u_2 - u_I)^2 + c_2^2(p_2 - p_I)) \end{bmatrix}, \tag{7.A.3}$$

$$\mathbf{r}_2 = \begin{bmatrix} 0 \\ \rho_1 \\ -c_1 \\ \rho_1 c_1^2 \\ 0 \\ 0 \\ 0 \end{bmatrix}, \qquad \mathbf{r}_3 = \begin{bmatrix} 0 \\ 1 \\ 0 \\ 0 \\ 0 \\ 0 \\ 0 \end{bmatrix}, \qquad \mathbf{r}_4 = \begin{bmatrix} 0 \\ \rho_1 \\ c_1 \\ \rho_1 c_1^2 \\ 0 \\ 0 \\ 0 \end{bmatrix} \tag{7.A.4}$$

$$\mathbf{r}_5 = \begin{bmatrix} 0 \\ 0 \\ 0 \\ 0 \\ \rho_2 \\ -c_2 \\ \rho_2 c_2^2 \end{bmatrix}, \qquad \mathbf{r}_6 = \begin{bmatrix} 0 \\ 0 \\ 0 \\ 0 \\ 1 \\ 0 \\ 0 \end{bmatrix}, \qquad \mathbf{r}_7 = \begin{bmatrix} 0 \\ 0 \\ 0 \\ 0 \\ \rho_2 \\ c_2 \\ \rho_2 c_2^2 \end{bmatrix}. \tag{7.A.5}$$

where

$$\sigma_1 = c_1^2 - (u_1 - u_I)^2, \qquad \sigma_2 = c_2^2 - (u_2 - u_I)^2.$$

Thus, the system (7.2.1) is strictly hyperbolic except when some of the eigenvalues coincide. Indeed the eigenvectors (7.A.3)-(7.A.5) become linearly dependent if any one of the conditions

$$\alpha_1 = 0, \qquad \alpha_2 = 0, \qquad \sigma_1 = 0, \qquad \sigma_2 = 0$$

holds. For more details see Andrianov [2].

Consider the Riemann problem for the system (7.A.1) which is the initial-value problem with initial data of the form

$$\mathbf{W}(x,0) = \begin{cases} \mathbf{W}_L, & x < 0 \\ \mathbf{W}_R, & x > 0. \end{cases}$$

One can show that the characteristic fields associated with λ_1, λ_3 and λ_6 are linearly degenerate, and the 2-, 4-, 5- and 7- fields are genuinely nonlinear. For a proof see Labois [16].

7.B Appendix: Derivation of the six-equation model from the seven-equation model

This appendix is devoted to the derivation of the six-equation model with heat and mass transfer (7.5.10) from the full seven-equation model with heat and mass transfer (7.4.44) by the asymptotic limit considering stiff velocity relaxation. We follow the method of Chen et al. [6]. This method is used by Murrone and Guillard [23] in the derivation of the five-equation model from the seven-equation model.

Firstly, we introduce briefly the method of reduction for a system of hyperbolic conservation laws in the presence of stiff relaxation terms using the notations of Murrone and Guillard [23] .

Consider a hyperbolic system with stiff source relaxation terms, i.e. consider the following system

$$\frac{\partial \mathbf{W}}{\partial t} + \mathbf{A}(\mathbf{W})\frac{\partial \mathbf{W}}{\partial x} = \frac{\mathbf{R}(\mathbf{W})}{\varepsilon} + \mathbf{S}(\mathbf{W}) \tag{7.B.1}$$

with $\varepsilon \to 0^+$. The vector $\mathbf{W}$ belongs to Ω, some open subset of $\mathbb{R}^N$.

As $\varepsilon \to 0^+$, the solution of the system (7.B.1) is expected to be close to the set $\Im \subset \mathbb{R}^N$, where

$$\Im = \{\mathbf{W} \in \mathbb{R}^N; \mathbf{R}(\mathbf{W}) = \mathbf{0}\}.$$

We make use of the following assumption, Murrone and Guillard [23]:

Assumption 1. *The set of equations $\boldsymbol{R}(\boldsymbol{W}) = 0$ defines a smooth manifold of dimension n, where $0 < n < N$. Moreover, for any $\boldsymbol{W} \in \Im$ we explicitly know the parameterization M from ω an open subset of $\mathbb{R}^n$ onto V a neighborhood of $\boldsymbol{W}$ in $\Im$, i.e.*

$$\begin{aligned} M : \omega \subset \mathbb{R}^n &\to V \subset \Im \subset \mathbb{R}^N, \\ \boldsymbol{w} &\to \boldsymbol{W} = M(\boldsymbol{w}). \end{aligned}$$

Under Assumption 1 the following holds. For any $\mathbf{w} \in \omega$ the Jacobian matrix $dM_{\mathbf{w}}$ is a full rank matrix. Also the column vectors of $dM_{\mathbf{w}}$ form a basis of $\ker(\mathbf{R}'(M(\mathbf{w})))$. For the proof see [23].

Let

$$\mathbf{C} = [dM^1_{\mathbf{w}}, ..., dM^n_{\mathbf{w}}, I^1, ..., I^{N-n}], \tag{7.B.2}$$

where $dM^1_{\mathbf{w}}, ..., dM^n_{\mathbf{w}}$ are the column vectors of $dM_{\mathbf{w}}$ and $I^1, ..., I^{N-n}$ are a basis of the range $\mathrm{rng}(\mathbf{R}'(M(\mathbf{w})))$ of $\mathbf{R}'(M(\mathbf{w}))$. The matrix (7.B.2) is invertible, let $\mathbf{B}$ be the matrix composed of the first n rows of the inverse of the matrix $\mathbf{C}$. Then we have the following results:

$$\mathbf{B} \cdot dM_{\mathbf{w}} = \mathbf{I}_{n\times n}, \text{ the identity matrix} \tag{7.B.3a}$$

$$\mathbf{B} \cdot \mathbf{R}'(M(\mathbf{w})) = 0. \tag{7.B.3b}$$

For proof see the same reference [23].

Decompose the state vector $\mathbf{W}$ as

$$\mathbf{W} = M(\mathbf{w}) + \varepsilon \mathbf{V}, \tag{7.B.4}$$

where $\mathbf{V}$ is a small perturbation around the state vector $M(\mathbf{w})$.

To obtain the reduced model we use the expression (7.B.4) in the system (7.B.1) and get

$$\frac{\partial M(\mathbf{w})}{\partial t} + \mathbf{A}(M(\mathbf{w}))\frac{\partial M(\mathbf{w})}{\partial x} - \mathbf{R}'(M(\mathbf{w})) \cdot \mathbf{V} = \mathbf{S}(M(\mathbf{w})) + O(\varepsilon). \tag{7.B.5}$$

Multiplying (7.B.5) by $\mathbf{B}$, using (7.B.3) and neglecting the terms of order ε, we obtain the reduced model of the system (7.B.1)

$$\frac{\partial \mathbf{w}}{\partial t} + \mathbf{B} \cdot \mathbf{A}(M(\mathbf{w})) \cdot dM_{\mathbf{w}} \frac{\partial \mathbf{w}}{\partial x} = \mathbf{B} \cdot \mathbf{S}(M(\mathbf{w})). \tag{7.B.6}$$

Now, we apply the above method for the reduction by using the asymptotic limit on the seven-equation model assuming a stiff velocity relaxation.

Take the vector of primitive variables as $\mathbf{W} = (\alpha_1, \rho_1, \rho_2, u_1, u_2, p_1, p_2)$, and write the seven-equation model (7.4.44) accompanied with all relaxation terms in the form (7.B.1). In this case, the source vector $\dfrac{\mathbf{R}(\mathbf{W})}{\varepsilon}$ consists of the velocity relaxation terms which is stiff, i.e. $\lambda = \dfrac{1}{\varepsilon}$, where $\varepsilon \to 0^+$. While the source vector $\mathbf{S}(\mathbf{W})$ is decomposed as

$$\mathbf{S}(\mathbf{W}) = \mathbf{S}_P(\mathbf{W}) + \mathbf{S}_Q(\mathbf{W}) + \mathbf{S}_m(\mathbf{W}).$$

The matrix $\mathbf{A}(\mathbf{W})$ and the source vectors can be given as

$$\mathbf{A}(\mathbf{W}) = \begin{bmatrix} u_I & 0 & 0 & 0 & 0 & 0 & 0 \\ -\frac{\rho_1}{\alpha_1}(u_I - u_1) & u_1 & 0 & \rho_1 & 0 & 0 & 0 \\ \frac{\rho_2}{\alpha_2}(u_I - u_2) & 0 & u_2 & 0 & \rho_2 & 0 & 0 \\ -\frac{p_I - p_1}{\alpha_1 \rho_1} & 0 & 0 & u_1 & 0 & \frac{1}{\rho_1} & 0 \\ \frac{p_I - p_2}{\alpha_2 \rho_2} & 0 & 0 & 0 & u_2 & 0 & \frac{1}{\rho_2} \\ -\frac{\Gamma_1}{\alpha_1}\left[p_I - \rho_1^2\left(\frac{\partial e_1}{\partial \rho_1}\right)_{p_1}\right](u_I - u_1) & 0 & 0 & \rho_1 c_1^2 & 0 & u_1 & 0 \\ \frac{\Gamma_2}{\alpha_2}\left[p_I - \rho_2^2\left(\frac{\partial e_2}{\partial \rho_2}\right)_{p_2}\right](u_I - u_2) & 0 & 0 & 0 & \rho_2 c_2^2 & 0 & u_2 \end{bmatrix},$$

$$\mathbf{R}(\mathbf{W}) = \begin{bmatrix} 0 \\ 0 \\ 0 \\ \frac{\lambda}{\alpha_1 \rho_1}(u_2 - u_1) \\ -\frac{\lambda}{\alpha_2 \rho_2}(u_2 - u_1) \\ \lambda \frac{\Gamma_1}{\alpha_1}(u_I - u_1)(u_2 - u_1) \\ -\lambda \frac{\Gamma_2}{\alpha_2}(u_I - u_2)(u_2 - u_1) \end{bmatrix},$$

$$\mathbf{S}_P(\mathbf{W}) = \begin{bmatrix} \mu(p_1 - p_2) \\ \mu \frac{\rho_1}{\alpha_1}(p_2 - p_1) \\ -\mu \frac{\rho_2}{\alpha_2}(p_2 - p_1) \\ 0 \\ 0 \\ \mu \frac{\Gamma_1}{\alpha_1}\left[p_I - \rho_1^2\left(\frac{\partial e_1}{\partial \rho_1}\right)_{p_1}\right](p_2 - p_1) \\ -\mu \frac{\Gamma_2}{\alpha_2}\left[p_I - \rho_2^2\left(\frac{\partial e_2}{\partial \rho_2}\right)_{p_2}\right](p_2 - p_1) \end{bmatrix}, \qquad \mathbf{S}_Q(\mathbf{W}) = \begin{bmatrix} \frac{1}{\kappa} Q \\ -\frac{\rho_1}{\alpha_1 \kappa} Q \\ \frac{\rho_2}{\alpha_2 \kappa} Q \\ 0 \\ 0 \\ -\frac{\rho_1 c_1^2}{\alpha_1 \kappa} Q + \frac{\Gamma_1}{\alpha_1}(1 + \frac{p_1}{\kappa}) Q \\ \frac{\rho_2 c_2^2}{\alpha_2 \kappa} Q - \frac{\Gamma_2}{\alpha_2}(1 + \frac{p_2}{\kappa}) Q \end{bmatrix},$$

$$\mathbf{S}_m(\mathbf{W}) = \begin{bmatrix} \frac{1}{\varrho}\dot{m} \\ \frac{1}{\alpha_1}(1-\frac{\rho_1}{\varrho})\dot{m} \\ -\frac{1}{\alpha_2}(1-\frac{\rho_2}{\varrho})\dot{m} \\ \frac{1}{\alpha_1\rho_1}(u_I-u_1)\dot{m} \\ -\frac{1}{\alpha_2\rho_2}(u_I-u_2)\dot{m} \\ \frac{c_1^2}{\alpha_1}(1-\frac{\rho_1}{\varrho})\dot{m} + \frac{\Gamma_1}{\alpha_1}\left[(e_i-e_1)+\frac{(u_I-u_1)^2}{2}-\frac{p_1}{\rho_1}(1-\frac{\rho_1}{\varrho})\right]\dot{m} \\ -\frac{c_2^2}{\alpha_2}(1-\frac{\rho_2}{\varrho})\dot{m} - \frac{\Gamma_2}{\alpha_2}\left[(e_i-e_2)+\frac{(u_I-u_2)^2}{2}-\frac{p_2}{\rho_2}(1-\frac{\rho_2}{\varrho})\right]\dot{m} \end{bmatrix},$$

where Γ_k is given in (7.4.11).

The limit of zero velocity relaxation time gives a single velocity, i.e. $u_1 = u_2 = u$. Thus the vector of the primitive variables for the reduced model is

$$\mathbf{w} = (\alpha_1, \rho_1, \rho_2, u, p_1, p_2)^T.$$

So $M(\mathbf{w})$ is defined as

$$M : \mathbf{w} \to M(\mathbf{w}) = (\alpha_1, \rho_1, \rho_2, u, u, p_1, p_2)^T. \tag{7.B.7}$$

Then the Jacobian matrix of the transformation (7.B.7) is given as

$$dM_{\mathbf{w}} = \begin{bmatrix} 1 & 0 & 0 & 0 & 0 & 0 \\ 0 & 1 & 0 & 0 & 0 & 0 \\ 0 & 0 & 1 & 0 & 0 & 0 \\ 0 & 0 & 0 & 1 & 0 & 0 \\ 0 & 0 & 0 & 1 & 0 & 0 \\ 0 & 0 & 0 & 0 & 1 & 0 \\ 0 & 0 & 0 & 0 & 0 & 1 \end{bmatrix}. \tag{7.B.8}$$

It is easy to see that the Jacobian matrix $\mathbf{R}'$ evaluated on the transformation is given as

$$\mathbf{R}'(M(\mathbf{w})) = \begin{bmatrix} 0 & 0 & 0 & 0 & 0 & 0 & 0 \\ 0 & 0 & 0 & 0 & 0 & 0 & 0 \\ 0 & 0 & 0 & 0 & 0 & 0 & 0 \\ 0 & 0 & 0 & -\frac{1}{\alpha_1\rho_1} & \frac{1}{\alpha_1\rho_1} & 0 & 0 \\ 0 & 0 & 0 & \frac{1}{\alpha_2\rho_2} & -\frac{1}{\alpha_2\rho_2} & 0 & 0 \\ 0 & 0 & 0 & 0 & 0 & 0 & 0 \\ 0 & 0 & 0 & 0 & 0 & 0 & 0 \end{bmatrix}.$$

Obviously, the basis of $\mathrm{rng}(\mathbf{R}'(M(\mathbf{w})))$ is

$$I^1 = \begin{bmatrix} 0 \\ 0 \\ 0 \\ -\frac{1}{\alpha_1\rho_1} \\ \frac{1}{\alpha_2\rho_2} \\ 0 \\ 0 \end{bmatrix}. \tag{7.B.9}$$

From (7.B.8) and (7.B.9) we can find the matrix $\mathbf{C}$, then we can find the matrix $\mathbf{B}$

$$\mathbf{B} = \begin{bmatrix} 1 & 0 & 0 & 0 & 0 & 0 & 0 \\ 0 & 1 & 0 & 0 & 0 & 0 & 0 \\ 0 & 0 & 1 & 0 & 0 & 0 & 0 \\ 0 & 0 & 0 & \frac{\alpha_1\rho_1}{\rho} & \frac{\alpha_2\rho_2}{\rho} & 0 & 0 \\ 0 & 0 & 0 & 0 & 0 & 1 & 0 \\ 0 & 0 & 0 & 0 & 0 & 0 & 1 \end{bmatrix}.$$

By using the matrix $\mathbf{B}$ together with the matrices we can find the reduced model as in (7.B.6). Thus the reduced model in primitive variables is given as

$$\frac{\partial \alpha_1}{\partial t} + u\frac{\partial \alpha_1}{\partial x} = \mu(p_1 - p_2) + \frac{1}{\kappa}Q + \frac{1}{\varrho}\dot{m}, \tag{7.B.10a}$$

$$\frac{\partial \rho_1}{\partial t} + u\frac{\partial \rho_1}{\partial x} + \rho_1\frac{\partial u}{\partial x} = \mu\frac{\rho_1}{\alpha_1}(p_2 - p_1) - \frac{\rho_1}{\alpha_1\kappa}Q + \frac{1}{\alpha_1}(1 - \frac{\rho_1}{\varrho})\dot{m}, \tag{7.B.10b}$$

$$\frac{\partial \rho_2}{\partial t} + u\frac{\partial \rho_2}{\partial x} + \rho_2\frac{\partial u}{\partial x} = -\mu\frac{\rho_2}{\alpha_2}(p_2 - p_1) + \frac{\rho_2}{\alpha_2\kappa}Q - \frac{1}{\alpha_2}(1 - \frac{\rho_2}{\varrho})\dot{m}, \tag{7.B.10c}$$

$$\frac{\partial u}{\partial t} + u\frac{\partial u}{\partial x} + \frac{(p_1 - p_2)}{\rho}\frac{\partial \alpha_1}{\partial x} + \frac{\alpha_1}{\rho}\frac{\partial p_1}{\partial x} + \frac{\alpha_2}{\rho}\frac{\partial p_2}{\partial x} = 0, \tag{7.B.10d}$$

$$\begin{aligned} \frac{\partial p_1}{\partial t} + u\frac{\partial p_1}{\partial x} + \rho_1 c_1^2\frac{\partial u}{\partial x} &= \mu\frac{\Gamma_1}{\alpha_1}\left[p_I - \rho_1^2\left(\frac{\partial e_1}{\partial \rho_1}\right)_{p_1}\right](p_2 - p_1) - \frac{\rho_1 c_1^2}{\alpha_1\kappa}Q \\ &+ \frac{\Gamma_1}{\alpha_1}(1 + \frac{p_1}{\kappa})Q + \frac{c_1^2}{\alpha_1}(1 - \frac{\rho_1}{\varrho})\dot{m} + \frac{\Gamma_1}{\alpha_1}\left[(e_i - e_1) - \frac{p_1}{\rho_1}(1 - \frac{\rho_1}{\varrho})\right]\dot{m}, \end{aligned} \tag{7.B.10e}$$

$$\begin{aligned} \frac{\partial p_2}{\partial t} + u\frac{\partial p_2}{\partial x} + \rho_2 c_2^2\frac{\partial u}{\partial x} &= -\mu\frac{\Gamma_2}{\alpha_2}\left[p_I - \rho_2^2\left(\frac{\partial e_2}{\partial \rho_2}\right)_{p_2}\right](p_2 - p_1) + \frac{\rho_2 c_2^2}{\alpha_2\kappa}Q \\ &- \frac{\Gamma_2}{\alpha_2}(1 + \frac{p_2}{\kappa})Q - \frac{c_2^2}{\alpha_2}(1 - \frac{\rho_2}{\varrho})\dot{m} - \frac{\Gamma_2}{\alpha_2}\left[(e_i - e_2) - \frac{p_2}{\rho_2}(1 - \frac{\rho_2}{\varrho})\right]\dot{m}, \end{aligned} \tag{7.B.10f}$$

where $\rho = \alpha_1\rho_1 + \alpha_2\rho_2$.

Using equations (7.B.10b) and (7.B.10c) with (7.B.10a), we obtain

$$\begin{aligned} \frac{\partial \alpha_1\rho_1}{\partial t} + \frac{\partial(\alpha_1\rho_1 u)}{\partial x} &= \dot{m}, \\ \frac{\partial \alpha_2\rho_2}{\partial t} + \frac{\partial(\alpha_2\rho_2 u)}{\partial x} &= -\dot{m}. \end{aligned}$$

Using these equations with (7.B.10d), we get

$$\frac{\partial \rho u}{\partial t} + \frac{\partial(\rho u^2 + \alpha_1 p_1 + \alpha_2 p_2)}{\partial x} = 0.$$

The internal energy of each phase can be written as a function of the phase density and pressure, i.e. $e_k = e_k(\rho_k, p_k)$, $k = 1, 2$. Then we obtain the following expression for the differential de_k

$$de_k = \left(\frac{\partial e_k}{\partial \rho_k}\right)_{p_k} d\rho_k + \left(\frac{\partial e_k}{\partial p_k}\right)_{\rho_k} dp_k. \tag{7.B.11}$$

With the help of this equation and with the equations of the system (7.B.10), we obtain the following equations for the internal energies

$$\frac{\partial \alpha_1\rho_1 e_1}{\partial t} + \frac{\partial \alpha_1\rho_1 e_1 u}{\partial x} + \alpha_1 p_1 \frac{\partial u}{\partial x} = \mu p_I(p_2 - p_1) + Q + e_i\dot{m},$$
$$\frac{\partial \alpha_2\rho_2 e_2}{\partial t} + \frac{\partial \alpha_2\rho_2 e_2 u}{\partial x} + \alpha_2 p_2 \frac{\partial u}{\partial x} = -\mu p_I(p_2 - p_1) - Q - e_i\dot{m}.$$

Thus the whole model can be written as in (7.5.10)

7.C Appendix: Determination of $T_{sat}(p_{equi})$

The metastable condition $T_k > T_{sat}(p_{equi})$ is used to activate the phase transition. In this appendix we consider the computation of the curve $T = T_{sat}(p)$.

Simply we use the same idea of [21, 33] that at thermodynamic equilibrium the Gibbs free energies are equal, and this equality provides a direct relation between the saturation pressure and temperature.

Using the SG-EOS (7.2.5) the Gibbs free energy g_k is expressed as

$$g_k = (\gamma_k C_{vk} - q'_k)T_k - T_k C_{vk} \ln \frac{T_k^{\gamma_k}}{(p_k + \pi_k)^{(\gamma_k - 1)}} + q_k.$$

At the saturation curve we have an equilibrium pressure p, an equilibrium temperature T and by the equality of the two Gibbs free energies g_1 and g_2 we have

$$(\gamma_1 C_{v1} - q'_1)T - TC_{v1} \ln \frac{T^{\gamma_1}}{(p + \pi_1)^{(\gamma_1 - 1)}} + q_1 =$$
$$(\gamma_2 C_{v2} - q'_2)T - TC_{v2} \ln \frac{T^{\gamma_2}}{(p + \pi_2)^{(\gamma_2 - 1)}} + q_2.$$

This equation is nonlinear and can be solved by any iterative technique to find the saturation temperature in terms of the saturation pressure.

References

[1] R. Abgrall, How to prevent pressure oscillations in multicomponent flow calculations: a quasi conservative approach, *Journal of Computational Physics*. 125 (1), 150-160 (1996).

[2] N. Andrianov, Analytical and numerical investigation of two-phase flows, PhD thesis, Otto-von-Guericke University, 2003.

[3] N. Andrianov, R. Saurel, G. Warnecke, A simple method for compressible multiphase mixtures and interfaces, *Int. J. Numer. Meth. Fluids*. 41, 109-131 (2003).

[4] M.R. Baer, J.W. Nunziato, A two-phase mixture theory for the deflagration-to-detonation transition (DDT) in reactive granular materials, *Int. J. Multiphase Flows*. 12, 861-889 (1986).

[5] Z. Bilicki, R. Kwidzinski, SA. Mohammadein, An estimation of a relaxation time of heat and mass exchange in the liquidvapour bubble flow, *Int. J. Heat Mass Transfer*. 39 (4), 753759 (1996).

[6] G.Q. Chen, C.D. Levermore, T.P.Liu, Hyperbolic conservation laws with stiff relaxation terms and entropy, *Comm. Pure. Appl. Math.* 47, 787-830 (1994).

[7] A. Chinnayya, E. Daniel, R. Saurel, Modelling detonation waves in heterogeneous energetic materials, *Journal of Computational Physics*. 196 (2), 490-538 (2004).

[8] S. F. Davis, Simplified second-order Godunov-type methods, *SIAM Journal on Scientific and Statistical Computing*. 9, 445-473 (1988).

[9] D.A. Drew, Mathematical modeling of two-phase flow, *Ann. Rev. Fluid Mech.* 15, 261-91 (1983).

[10] D. A. Drew; S. L. Passman, *Theory of multicomponent fluids* (Applied Mathematical Sciences, Vol. 135), Springer, New York, 1998.

[11] P. Embid and M. Baer, Mathematical analysis of a two-phase continuum mixture theory, *Continuum Mech. Thermodyn.* 4, 279-312 (1992).

[12] T. Gallouët and J. M. Masella, J.M.: Un schéma de Godunov approaché. Comptes Rendus Académie des Sciences Paris, Série I. 323, 7784 (1996).

[13] H. Guillard and M. Labois, Numerical modeling of compressible two-phase flows, European Conference on Computational Fluid Dynamics ECCOMAS CFD 2006, P. Wesseling and E. Onate and J. Priaux (Eds), 2006.

[14] M. Ishii and T. Hibiki, *Thermo fluid dynamics of two-phase flow*, Springer Science + Business Media, Inc., 2006.

[15] A.K. Kapila, R. Menikoff, J.B. Bdzil, S.F. Son, D.S. Stewart, Two-phase modelling of DDT in granular materials: reduced equations, *Phys. Fluid*. 13, 3002-3024 (2001).

[16] M. Labois, Modélisation des déséquilibres mécaniques pour les écoulements diphasiques: approches par relaxation et par modèle réduit, PhD thesis, Université de Provence - Aix-Marseille I, 2008.

[17] M. H. Lallemand, A. Chinnayya, O. Le Metayer, Pressure relaxation procedures for multiphase compressible flows, *Int. J. Numer. Meth. Fluids*. 49 (1), 1-56 (2005).

[18] M. H. Lallemand, R. Saurel, Pressure relaxation procedures for multi-phase compressible flows, Technical Report 4038, INRIA, 2000.

[19] R. Menikoff, B.J. Plohr, The Riemann problem for fluid flow of real materials, *Rev. Mod. Phys.* 61 (1), 75-130 (1989).

[20] Le Metayer O., Massoni J. and Saurel R., Elaborating equations of state of a liquid and its vapor for two-phase flow models (in French). Int. J. Thermal Sci. 43 (3), 265276 (2004).

[21] O. Le Metayer, J. Massoni, R. Saurel, Modelling evaporation fronts with reactive Riemann solvers, *Journal of Computational Physics*. 205, 567-610, (2005).

[22] I. Müller, W. H. Müller, *Fundamentals of Thermodynamics and Applications*: With Historical Annotations and Many Citations from Avogadro to Zermelo, Springer-Verlag Berlin Heidelberg, 2009.

[23] A. Murrone, H. Guillard, A five-equation reduced model for compressible two-phase flow problems, *Journal of Computational Physics*. 202 (2), 664 - 698 (2005).

[24] F. Petitpas, E. Franquet, R. Saurel and O. Le Metayer, A relaxation-projection method for compressible flows. Part II: Artificial heat exchanges for multiphase shocks, *Journal of Computational Physics archive*. 225 (2), 2214-2248 (2007).

[25] F. Petitpas, J. Massoni, R. Saurel, E. Lapebie, L. Munier, Diffuse interface models for high speed cavitating underwater systems. *Int. J. Multiphase Flows* 35 (8), 747759 (2009).

[26] F. Petitpas, R. Saurel, E. Franquet, A. Chinnayya, Modelling detonation waves in condensed materials: multiphase CJ conditions and multidimensional computations, *Shock waves*, 19, 377-401 (2009).

[27] R. Saurel, R. Abgrall, A multiphase Godunov method for compressbile multifluid and multiphase flows, *Journal of Computational Physics*, 150 (2), 425-467 (1999).

[28] R. Saurel and R. Abgrall, A simple method for compressible multifluid flows, *SIAM J. Sci. Comput.* 21, 1115-1145 (1999).

[29] R. Saurel, E. Franquet, E. Daniel, O. Le Metayer, A relaxation-projection method for compressible flows. Part I: The numerical equation of state for the Euler equations, *Journal of Computational Physics*, 223 (2), 822-845, (2007).

[30] R. Saurel, S. Gavrilyuk, F. Renaud, A multiphase model with internal degree of freedom, application to shock-bubble interaction, *J. Fluid. Mech.* 495, 283-321 (2003).

[31] R. Saurel and O. Le Metayer, A multiphase model for interfaces, shocks, detonation waves and cavitation, *J. Fluid Mech.* 431, 239-271 (2001).

[32] R. Saurel, O. Le Metayer, J. Massoni, S. Gavrilyuk, Shock jump relations for multiphase mixtures with stiff mechanical properties, *Shock waves*. 16, 209-232 (2007).

[33] R. Saurel, F. Petitpas and R. Abgrall, Modelling phase transition in metastable liquids: application to cavitating and flashing flows, *Journal of Fluid Mechanics*. 607, 313-350 (2008).

[34] R. Saurel, F. Petitpas, R. A. Berry, Simple and efficient relaxation methods for interfaces separating compressible fluids, cavitating flows and shocks in multiphase mixtures, *Journal of Computational Physics*. 228 (5), 1678-1712 (2009).

[35] J.R. Simões-Moreira, Adiabatic evaporation waves. PhD thesis, Rensselaer Polytechnic Institute, 1994.

[36] J.R. Simões-Moreira, J.E. Shepherd, Evaporation waves in superheated dodecane, *J. Fluid Mech.* 382, 63-86 (1999).

[37] G. Strang, On the construction and comparison of difference schemes, *SIAM J. Num. Anal.* 5, 506-517 (1968).

[38] E.F. Toro, *Riemann Solvers and Numerical Methods for Fluid Dynamics*, Springer, Berlin, 1999.

Chapter 8

A Laser-Induced Cavitation Bubble

Bibliographic note: The content of this chapter is published in [H10]: Ali Zein, Maren Hantke, and Gerald Warnecke. On the Modeling and Simulation of a Laser-Induced Cavitation Bubble, *Int. J. Num. Meth. Fluids*, Vol.73/2 (2013), pp. 172-203.

Abstract: Single cavitation bubbles exhibit severe modeling and simulation difficulties. This is due to the small scales of time and space as well as due to the involvement of different phenomena in the dynamics of the bubble. For example, the compressibility, phase transition and the existence of a non-condensable gas inside the bubble have strong effects on the dynamics of the bubble. Moreover, the collapse of the bubble involves the occurrence of critical conditions for the pressure and temperature. This adds extra difficulties to the choice of equations of state. Even though several models and simulations have been used to study the dynamics of the cavitation bubbles, many details are still not clearly accounted for.

Here, we present a numerical investigation for the collapse and rebound of a laser-induced cavitation bubble in liquid water. The compressibility of the liquid and vapor are involved. In addition, great focus is devoted to study the effects of phase transition and the existence of a non-condensable gas on the dynamics of the collapsing bubble. If the bubble contains vapor only we use the six-equation model for two-phase flows that was modified in our previous work [A. Zein, M. Hantke, and G. Warnecke, *J. Comput. Phys.*, 229(8):2964-2998, 2010]. This model is an extension to the six-equation model with a single velocity of Kapila et al. [*Phys. Fluid*, 13:3002-3024, 2001] taking into account the heat and mass transfer.

To study the effect of a non-condensable gas inside the bubble we add a third phase to the original model. In this case the phase transition is considered only at interfaces that separate the liquid and its vapor. The stiffened gas equations of state are used as closure relations. We use our own method to determine the parameters in order to obtain reasonable equations of state for a wide range of temperatures and make them suitable for the phase transition effects. We compare our results with experimental ones. Also our results confirm some expected physical phenomena.

8.1 Introduction

Cavitation is defined as the formation of vapor bubbles in a liquid due to the reduction of the pressure. The bubbles then collapse when they enter a region of higher pressure. The collapse of a cavitation bubble causes high pressure and high temperature. This increases the noise of the system and may cause material damage, cavitation erosion. This phenomenon may have destructive effects and it occurs in many engineering applications of hydrodynamics like pumps, piping systems and ship propellers [40]. Therefore, special attention has been devoted in the literature to study the mechanism of cavitation erosion [6, 20, 40, 62]. On the other hand, the cavitation can be advantageous in other applications, for example cavitation erosion is used to clean solid surfaces [53].

The dynamics of collapsing bubbles was studied first by Rayleigh [43] assuming that the surrounding liquid is incompressible and inviscid. Later the basic Rayleigh equation was modified by various authors to include the effects of viscosity and surface tension. The resulting equation after several modifications is known as Rayleigh-Plesset equation, see e.g. [5, 14]. A further modification was considered assuming

the surrounding liquid as slightly compressible, see Trilling [58], Keller and Kolodner [23] as well as Gilmore [16].

Hickling and Plesset [18] presented some numerical solutions to describe the bubble collapse and rebound by taking into account the liquid compressibility. They used the Gilmore model [16] for a Mach number smaller than 0.1 and the Lagrangian form of the Euler equations for higher values of Mach number. The results of Hickling and Plesset show the formation of pressure waves during the rebound of the bubble. Later several numerical algorithms were modified and several effects during the cavitation were studied like heat transfer, mass transfer and the existence of a non-condensable gas inside the bubble, see [15, 21, 24, 27, 35, 36, 41, 42, 52, 56, 60], in the book of Franc and Michel [14] one finds a good review for the development of the models.

Most of the above models are not suitable for periods of high Mach number flow, where the compressibility of the liquid plays an important role, especially at the end of the collapse. Indeed, a shock wave is emitted in the liquid at the final stage of the collapse [1, 51]. This phenomenon is confirmed by experiments, where some measurements for the strength of this shock wave were reported [1, 28]. This makes consideration of the compressibility of the surrounding water of great importance especially for a strong bubble collapse. But assuming compressibility introduces severe difficulties in the numerical simulations.

In recent investigations the full Euler equations were used to describe each fluid. For instance, Akhatov et al. [1] introduced two models to describe the collapse and rebound of a laser-induced cavitation bubble. One model for the low Mach number period which assumes an incompressible surrounding liquid, and the other model for the high Mach number period which consists of the Euler equations for each phase. The second model assumes compressibility for both the vapor and the liquid phases. It provides a detailed description for the behavior of both phases. Moreover, the effects of heat transfer, mass transfer and the existence of a non-condensable gas were studied. The Hertz-Knudsen-Langmuir model for evaporation and condensation was used. Regarding the model for the high Mach number period, the heat and mass transfer were modeled separately. Thus a coupling method was required to take into account these effects in the model. Even though this is not trivial it was unfortunately not detailed in [1]. This makes it difficult to compare their work with any other approach. In addition, the non-condensable gas was inserted in the energy equation through higher order terms. This adds extra difficulties to the solution of the model. For this some numerical simplifications were used in [1].

Müller et al. [32] investigated the problem of the laser-induced cavitation bubble by using recent models and numerical methods for compressible two-phase flows but without heat and mass transfer. Indeed, Müller et al. [32] presented numerical investigations using two different methods: The Saurel and Abgrall approach [44] and the real ghost fluid method of Wang et al. [59]. In both Akhatov et al. [1] as well as Müller et al. [32] some experimental issues were discussed and comparisons with experimental results were made.

In the last ten years a great progress has occurred in the modeling and simulation for compressible two-phase flows that is based on averaging techniques [11, 12, 19]. The most general model of this type consists of seven equations. This model is a full non-equilibrium model, i.e. each phase has its own pressure, velocity, temperature, etc. In Saurel and Abgrall [44] the solution of this model by a Godunov-type method was proposed. Also relaxation techniques were used to get equilibrium values for the velocity and the pressure.

Later, reduced models were derived from the general seven-equation model by the asymptotic analysis in the limit of zero relaxation time. A six-equation model which has a single velocity is deduced by assuming zero velocity relaxation time [22, 50]. Also a five-equation model with mechanical equilibrium, single velocity and single pressure, is deduced in the asymptotic limit of zero relaxation time for both the velocity and the pressure [22, 34, 38, 49]. More recently, these models were extended to include the effects of heat and mass transfer. The five-equation model was modified by Saurel et al. [49] to include the heat and mass transfer. Then it was extended to multiphase flows in Petitpas et al. [39]. The seven-equation model as well as the six-equation model were modified to take into account the heat and mass transfer by Zein et al. [61].

For the seven-equation and the six-equation models, the heat and mass transfer are modeled in the relaxation effects. A hierarchical model was built based on the assumptions that the pressure relaxes much faster than the temperature, and the temperature relaxes much faster than the Gibbs free energy. During the temperature relaxation it is assumed that the pressure stays in equilibrium and during the Gibbs free energy relaxation the pressure and temperature stay in equilibrium. The temperature and

Gibbs free energy relaxations toward the equilibrium are used at the interface where the heat and mass transfer occur. This fulfills the standard condition at equilibrium interfaces when the mass transfer occurs. For all details see Zein et al. [61].

In comparison with the latter models: the five equation model faces severe numerical difficulties that are the results of the equilibrium of the pressure. Some specific relaxation-projection procedures are used to circumvent these difficulties [38]. Both the seven-equation and six-equation models posses better features for the numerical approximations [50, 61]. But the six-equation model is less expensive and is easier to be modified for multiphase flows [61]. Thus it is adopted in this work to model the vapor bubble in liquid water.

It is expected that the bubble, besides the water vapor, contains a small mass of a non-condensable gas. This may be due to the plasma recombination during the bubble creation, see Akhatov et al. [1]. The effect of the existence of a non-condensable gas on the dynamics of the bubble was considered in Akhatov et al. [1] and Dreyer et al. [13]. The computational results in [1] show that a small amount of non-condensable gas inside the bubble greatly influences its dynamics. The authors of [13] proposed that the rebound of the bubble after the collapse is possible only if it contains a non-condensable gas.

In this work, the non-condensable gas is modeled as a third phase. Thus the whole model consists of nine equations. In this situation we use the ideas of Petitpas et al. [39] that the phase transition is considered only at the interface between the liquid and its vapor. But if the interface separates the liquid and the non-condensable gas the pressure relaxation is only used to fulfill the condition of the equilibrium of the pressure.

In the problem of the bubble collapse it is expected that the temperature inside the bubble will exceed the critical point. Thus the temperature range is very wide, i.e. it starts from low temperatures like the room temperature and exceeds the critical temperature. This makes the choice of the equations of state a difficult task. Moreover, including the phase transition requires further attention. In this work we use the stiffened gas equations of state which are the simplest formulation that contains the main physical properties of the pure fluid. We use our own method to estimate the parameters of the equations of state. These estimations respect the saturation curve. This idea was used by Barberon [3], Barberon and Helluy [4] as well as Le Metayer et al. [29]. This makes the equations of state appropriate if the phase transition is included in the model.

To test our results we use experimental data for the evolution of the bubble radius. These data were achieved by the group of Lauterborn in Göttingen, see [1, 32]. In the experiment a strong laser pulse is focused into liquid water. This generates a cavitation bubble, which expands to have a maximum radius, then it collapses to a non-zero minimum radius, then the bubble rebounds with a significant damping. The liquid temperature is kept fairly constant at room temperature during the experiment. Images of the bubble were taken during the experiment by using a high speed camera. These images were used to sketch the radius-time curve. For the details of the experiments see [1, 32].

Here we mainly adopt the experimental results that are shown in [32]. Where in this experiment the cuvette size is $50 \times 50 \times 50$ mm^3, the maximum radius $R_{max} = 747\ \mu\text{m} \pm 0.5\%$, the minimum radius $R_{min} < 12\ \mu$m and the time from the maximum expansion of the bubble to the first collapse is $69.3\mu s$. The surrounding water is kept at the atmospheric pressure with fairly constant temperature 20 °C.

In this work the computations start from the point of the maximal radius. But still the initial state inside the bubble is unknown. In fact there is no means until now to measure the physical quantities inside the bubble. Thus we have incomplete experimental data. Some authors introduced certain possibilities for the initial data inside the bubble. Hickling and Plesset [18] tested several initial pressures in the range $10^{-4} - 10^{-1}$ bar. Akhatov et al. [1] assumed the same liquid temperature inside the bubble with the corresponding saturation pressure for the initial pressure. In Müller et al. [32] the initial data were deduced from the experimental data by fitting of the computed bubble radius by the Keller-Miksis model [24] to the measured data. Another possibility for the initial data was taken by Dreyer et al. [13]. We test several initial conditions for comparison. These tests include the assumption of the saturation state inside the bubble, several tests with different pressures and one temperature, and several tests with one pressure and several temperatures. The aim of these tests is to try to understand the effect of the initial conditions on the evolution of the bubble radius.

To verify our results we compare the computed radius-time curve to the experimental one. Also we confirm some known and expected physical behaviors. Our results show that the pressure and the temperature at the center of the bubble increase to very high values at the collapse moment. Also the interface velocity goes to a high value at the final stage of the collapse.

When the phase transition is considered the results show that there is no rebound if the bubble contains vapor only. And inserting a non-condensable gas is responsible for the rebound. In fact this result confirms the idea that was proposed by Dreyer et al. [13]. Moreover, we see that the temperature and the pressure inside the bubble before the collapse point decreases if the mass transfer is included. This is due to the loss of energy in the mass transfer process.

This work is organized as follows. In Section 8.2 the mathematical models are introduced, a six-equation model for two phases and a nine-equation model for three phases. The first model is used if the bubble contains vapor only, while the latter model is used when the bubble contains a non-condensable gas besides the water vapor. Section 8.3 is devoted to the equations of state, previous criteria in the literature are recalled and our new criterion is introduced. In Section 8.4 the numerical method is introduced. Finally, Section 8.5 shows the numerical results and the discussion of the results.

8.2 Mathematical Model

If the bubble contains vapor only a two-phase model is used. One phase is the water vapor and the other phase is the liquid water. To consider the effect of a non-condensable gas inside the bubble a third phase is required, i.e. a three-phase model is used. The bubble is assumed to be perfectly spherical. Thus we consider the models in spherical coordinates. Also we assume rotational symmetry. In this section we recall the two-phase flow model of Zein et al. [61]. Then an extension of this model for three phases is introduced.

8.2.1 Two-phase flow model

The six-equation model of Zein et al. [61] including heat and mass transfer for two-phase flow is written as

$$\frac{\partial \alpha_1}{\partial t} + u\frac{\partial \alpha_1}{\partial r} = \mu(p_1 - p_2) + \frac{1}{\kappa}Q + \frac{1}{\varrho}\dot{m}, \tag{8.2.1a}$$

$$\frac{\partial \alpha_1\rho_1}{\partial t} + \frac{\partial(\alpha_1\rho_1 u)}{\partial r} = \dot{m} - \frac{2}{r}\alpha_1\rho_1 u, \tag{8.2.1b}$$

$$\frac{\partial \alpha_2\rho_2}{\partial t} + \frac{\partial(\alpha_2\rho_2 u)}{\partial r} = -\dot{m} - \frac{2}{r}\alpha_2\rho_2 u, \tag{8.2.1c}$$

$$\frac{\partial \rho u}{\partial t} + \frac{\partial(\rho u^2 + \alpha_1 p_1 + \alpha_2 p_2)}{\partial r} = -\frac{2}{r}\rho u^2, \tag{8.2.1d}$$

$$\frac{\partial \alpha_1\rho_1 e_1}{\partial t} + \frac{\partial \alpha_1\rho_1 e_1 u}{\partial r} + \alpha_1 p_1\frac{\partial u}{\partial r} = \mu p_I(p_2 - p_1) + Q + e_i\dot{m} - \frac{2}{r}\alpha_1\rho_1 e_1 u - \frac{2}{r}\alpha_1 p_1 u, \tag{8.2.1e}$$

$$\frac{\partial \alpha_2\rho_2 e_2}{\partial t} + \frac{\partial \alpha_2\rho_2 e_2 u}{\partial r} + \alpha_2 p_2\frac{\partial u}{\partial r} = -\mu p_I(p_2 - p_1) - Q - e_i\dot{m} - \frac{2}{r}\alpha_2\rho_2 e_2 u - \frac{2}{r}\alpha_2 p_2 u, \tag{8.2.1f}$$

where $Q = \theta(T_2 - T_1)$, $\dot{m} = \eta(g_2 - g_1)$ and $\rho = \alpha_1\rho_1 + \alpha_2\rho_2$.

Here α_k is the *volume fraction*, ρ_k the *density*, u is the *radial velocity*, p_k the *pressure*, e_k is the *specific internal energy*, T_k the *temperature*, g_k the *Gibbs free energy*, Q the *heat transfer* and $\dot{m}$ is the *mass transfer*. The volume fractions for both phases are related by the saturation constraint, $\alpha_1 + \alpha_2 = 1$.

The *interfacial pressure* p_I is assumed as in Saurel et al. [46] to be

$$p_I = \frac{Z_1 p_2 + Z_2 p_1}{Z_1 + Z_2}. \tag{8.2.2}$$

Here Z_k represents the *acoustic impedance*, $Z_k = \rho_k c_k$, where the *speed of sound* c_k is given as

$$c_k^2 = \frac{\dfrac{p_k}{\rho_k^2} - \left(\dfrac{\partial e_k}{\partial \rho_k}\right)_{p_k}}{\left(\dfrac{\partial e_k}{\partial p_k}\right)_{\rho_k}}, \quad k = 1, 2. \tag{8.2.3}$$

The parameters μ, θ and $\eta > 0$ are the relaxation parameters for the pressure, temperature and the Gibbs free energy respectively. In this work, the parameters μ and θ are assumed to be infinite, while η is assumed to be infinite at the interfaces and zero otherwise. Therefore, the model is free of parameters.

The combination of two internal energy equations with mass and momentum equations gives the quation for the mixture of the energy

$$\frac{\partial(\rho e + \frac{1}{2}\rho u^2)}{\partial t} + \frac{\partial u(\rho e + \frac{1}{2}\rho u^2 + \alpha_1 p_1 + \alpha_2 p_2)}{\partial r} = -\frac{2}{r}(\rho e + \frac{1}{2}\rho u^2 + \alpha_1 p_1 + \alpha_2 p_2)u,$$

where $\rho e = \alpha_1\rho_1 e_1 + \alpha_2\rho_2 e_2$. This extra equation is used during the computations to correct the thermodynamic states predicted by the two non-conservative internal energy equations [50].

The model (8.2.1a)-(8.2.1f) is a non-strictly hyperbolic model with eigenvalues u (four times), $u - c$, and $u + c$, with

$$c^2 = Y_1 c_1^2 + Y_2 c_2^2,$$

where c is the *mixture sound speed* and $Y_k = \alpha_k\rho_k/\rho$ is the *mass fraction*. For more information about the mathematical properties of this model you can see [50, 61].

The source terms in the model (8.2.1) are classified into four groups as follows

$$\mathbf{S} = \mathbf{S}_P + \mathbf{S}_Q + \mathbf{S}_m + \mathbf{S}_r, \tag{8.2.4}$$

where $\mathbf{S}_P$, $\mathbf{S}_Q$ and $\mathbf{S}_m$ are associated with the pressure, temperature and Gibbs free energy relaxation terms respectively and $\mathbf{S}_r$ represents the geometrical terms that come from the spherical coordinates in radial direction. These source vectors are given as

$$\begin{aligned}
\mathbf{S}_P &= (\mu(p_1 - p_2), 0, 0, 0, \mu p_I(p_2 - p_1), -\mu p_I(p_2 - p_1), 0)^T \\
\mathbf{S}_Q &= \left(\frac{Q}{\kappa}, 0, 0, 0, Q, -Q, 0\right)^T, \\
\mathbf{S}_m &= \left(\frac{\dot{m}}{\varrho}, \dot{m}, -\dot{m}, 0, e_i\dot{m}, -e_i\dot{m}, 0\right)^T, \\
\mathbf{S}_r &= -\frac{2}{r}(0, \alpha_1\rho_1 u, \alpha_2\rho_2 u, \rho u^2, (\alpha_1\rho_1 e_1 + \alpha_1 p_1)u, (\alpha_2\rho_2 e_2 + \alpha_2 p_2)u, \\
&\qquad (\rho e + \frac{1}{2}\rho u^2 + \alpha_1 p_1 + \alpha_2 p_2)u)^T.
\end{aligned} \tag{8.2.5}$$

We assume that the mechanical properties relax much faster than the thermal properties. Also we assume that the relaxation time for the temperature is much smaller than that of the Gibbs free energy. In fact, these assumptions agree with physical evidence in a large number of situations [61]. In particular, we assume that the pressures relax very fast to equilibrium and they will stay in equilibrium during the temperature relaxation. Moreover, the pressure and the temperature are assumed to maintain equilibrium states during the Gibbs free energy relaxation, for all details see Zein et al. [61]. These assumptions are used to find the expressions for the parameters κ, ϱ and e_i, see Section 8.4.2.

8.2.2 Extension to a three-phase flow model

To derive a multiphase flow model with a single velocity we start from the full non-equilibrium model for multiphase flows . The full non-equilibrium model for multiphase flows of Saurel-Abgrall type [44] without heat and mass transfer is written as

$$\begin{cases}
\dfrac{\partial \alpha_k}{\partial t} + \mathbf{u}_I \cdot \nabla\alpha_k = \mu(p_k - \hat{p}), \\
\dfrac{\partial \alpha_k\rho_k}{\partial t} + \nabla \cdot (\alpha_k\rho_k\mathbf{u}_k) = 0, \\
\dfrac{\partial \alpha_k\rho_k\mathbf{u}_k}{\partial t} + \nabla \cdot (\alpha_k\rho_k\mathbf{u}_k \otimes \mathbf{u}_k) + \nabla(\alpha_k p_k) = p_I\nabla\alpha_k + \lambda(\hat{\mathbf{u}} - \mathbf{u}_k), \\
\dfrac{\partial \alpha_k\rho_k E_k}{\partial t} + \nabla \cdot (\alpha_k(\rho_k E_k + p_k)\mathbf{u}_k) = p_I\mathbf{u}_I \cdot \nabla\alpha_k - \mu p_I(p_k - \hat{p}) + \lambda\mathbf{u}_I \cdot (\hat{\mathbf{u}} - \mathbf{u}_k),
\end{cases} \tag{8.2.6}$$

where $\mathbf{u}_I$ is the *interfacial velocity* and $E_k = e_k + \dfrac{\mathbf{u}_k \cdot \mathbf{u}_k}{2}$ is the *total specific energy* for phase k. Here $k = 1, 2, ..., N$, where N is the number of phases.

The summation over the phases of all relaxation terms for each type of balance is zero. Thus the mixture values $\hat{\mathbf{u}}$ and $\hat{p}$ are given as

$$\hat{\mathbf{u}} = \frac{\sum_{k=1}^{N} \mathbf{u}_k}{N}, \quad \hat{p} = \frac{\sum_{k=1}^{N} p_k}{N}.$$

Modeling the relaxation terms for the velocity and the pressure in the above way means that we assume that all velocities of different fluids have the same relaxation rate, also all pressures have the same relaxation rate. These terms can be modeled in different ways, for example see Hérard [17]. However, the above modeling is enough for our problem because we are interested in one velocity and one pressure in the whole domain of the flow.

To derive a single velocity model we use the method of Chen et al. [7]. This method was used by Murrone and Guillard [34] to derive a five-equation model with single velocity and single pressure from the seven-equation model by assuming stiff velocity and pressure relaxations. Also this method was used by Zein et al. [61] to derive the six-equation model of a single velocity from the full non-equilibrium seven-equation model by assuming stiff velocity relaxation.

Assume stiff velocity relaxation for the model (8.2.6), i.e. $\lambda = \dfrac{1}{\varepsilon}$ where $\varepsilon \to 0^+$. Then following the method of Chen et al. [7], we get the following reduced model

$$\begin{cases} \dfrac{\partial \alpha_k}{\partial t} + \mathbf{u} \cdot \nabla \alpha_k = \mu(p_k - \hat{p}), \\ \dfrac{\partial \alpha_k \rho_k}{\partial t} + \nabla \cdot (\alpha_k \rho_k \mathbf{u}) = 0, \\ \dfrac{\partial \rho \mathbf{u}}{\partial t} + \nabla \cdot (\rho \mathbf{u} \otimes \mathbf{u}) + \nabla p = 0, \\ \dfrac{\partial \alpha_k \rho_k e_k}{\partial t} + \nabla \cdot (\alpha_k \rho_k e_k \mathbf{u}) + \alpha_k p_k \nabla \cdot \mathbf{u} = -\mu p_I (p_k - \hat{p}), \end{cases} \tag{8.2.7}$$

where $\rho = \sum_{k=1}^{N} \alpha_k \rho_k$ and $p = \sum_{k=1}^{N} \alpha_k p_k$.

A model with three phases is enough to investigate the bubble containing vapor and a non-condensable gas with surrounding liquid water. Thus the model (8.2.7) for three phases in spherical coordinates assuming rotational symmetry is written as

$$\begin{cases} \dfrac{\partial \alpha_1}{\partial t} + u \dfrac{\partial \alpha_1}{\partial r} = \mu(p_1 - \hat{p}), \\ \dfrac{\partial \alpha_2}{\partial t} + u \dfrac{\partial \alpha_2}{\partial r} = \mu(p_2 - \hat{p}), \\ \dfrac{\partial \alpha_k \rho_k}{\partial t} + \dfrac{\partial (\alpha_k \rho_k u)}{\partial r} = -\dfrac{2}{r} \alpha_k \rho_k u, \\ \dfrac{\partial \rho u}{\partial t} + \dfrac{\partial (\rho u^2 + p)}{\partial r} = -\dfrac{2}{r} \rho u^2, \\ \dfrac{\partial \alpha_k \rho_k e_k}{\partial t} + \dfrac{\partial \alpha_k \rho_k e_k u}{\partial r} + \alpha_k p_k \dfrac{\partial u}{\partial r} = -\dfrac{2}{r} \alpha_k \rho_k e_k u - \dfrac{2}{r} \alpha_k p_k u - \mu p_I (p_k - \hat{p}), \\ \dfrac{\partial (\rho e + \frac{1}{2} \rho u^2)}{\partial t} + \dfrac{\partial u (\rho e + \frac{1}{2} \rho u^2 + p)}{\partial r} = -\dfrac{2}{r} (\rho e + \frac{1}{2} \rho u^2 + p) u, \end{cases} \tag{8.2.8}$$

where $k = 1, 2, 3$, and $\rho e = \sum_{k=1}^{3} \alpha_k \rho_k e_k$.

Here u is the radial velocity. The volume fractions for the three phases are connected by the saturation constraint, $\alpha_1 + \alpha_2 + \alpha_3 = 1$. Note that the model (8.2.8) consists of nine equations augmented with a redundant mixture energy equation.

The interfacial pressure in this model is taken as a generalization of the relation (8.2.2), i.e.

$$p_I = \frac{\sum_{k=1}^{3} \frac{p_k}{Z_k}}{\sum_{k=1}^{3} \frac{1}{Z_k}}.$$

The model (8.2.8) is a non-strictly hyperbolic model with eigenvalues u (seven fold), $u-c$ and $u+c$, with

$$c^2 = \sum_{k=1}^{3} Y_k c_k^2,$$

For more information about the mathematical properties of this model see 8.A.

After the pressure relaxation at each time step the heat and mass transfer are included through the temperature and the Gibbs free energy relaxations. Following Petitpas et al. [39] the heat and mass transfer are considered only if interface separates between the liquid and its vapor. When dealing with an interface between the liquid and the non-condensable gas the parameters of the temperature and Gibbs free energy relaxations are set to zero. Thus, the heat and mass transfer for the model (8.2.8) are included exactly as done in the previous section between the liquid and its vapor.

8.3 Equations of state (EOS)

In this paper we assume that each fluid obeys its own EOS as a pure material. Where in the present model equilibrium is achieved by relaxation processes.

The stiffened gas EOS (SG-EOS) is mostly used by authors for its simplicity [2, 8, 26, 44, 49]. This EOS reflects the main properties of the pure fluids, i.e. attractive and repulsive molecular effects [29, 49]. Moreover the SG-EOS satisfy the convexity constraints for stability that are discussed in [30]. The SG-EOS for each phase reads, see Le Metayer et al. [29]

$$e(p,v) = \frac{p+\gamma\pi}{(\gamma-1)}v + q, \tag{8.3.1a}$$

$$h(T) = C_p T + q, \tag{8.3.1b}$$

$$T(p,v) = \frac{p+\pi}{C_v(\gamma-1)}v, \tag{8.3.1c}$$

$$s(p,T) = C_v \ln \frac{T^\gamma}{(p+\pi)^{(\gamma-1)}} + q', \tag{8.3.1d}$$

$$g(p,T) = (\gamma C_v - q')T - C_v T \ln \frac{T^\gamma}{(p+\pi)^{(\gamma-1)}} + q, \tag{8.3.1e}$$

where $v = \frac{1}{\rho}$ is *the specific volume*, s the *specific entropy* and C_p the *specific heat capacity at constant pressure*. The constants γ, π, q and q' are characteristic constants of the thermodynamic behavior of the fluid.

The parameters of the SG-EOS are determined by using a reference curve. In the literature two types of curves are used: The Hugoniot curve and the saturation curve. Using the Hugoniot curve as a reference is the classical way used by authors for two-phase flow models to determine the parameters that appear in the internal energy equation (8.3.1a), see Cocchi et al. [9], Saurel and Abgrall [45]. Using the saturation curve as a reference seems to be more relevant to the phase transition. This idea was introduced by Barberon [3], Barberon and Helluy [4]. Then it was modified by Le Metayer et al. [29]. The main idea of this method is the following: Linking the two pure fluid EOS under thermodynamic equilibrium must be able to reproduce the liquid-vapor phase diagram. Therefore, the various parameters of the pure EOS are linked to each other to fulfill some constraints to recover the phase diagram [29].

The method of Le Metayer et al. [29] is summarized as:

- Choose two reference states, for example in [29] the chosen temperature range is $298-473\ K$. Then all experimental data that correspond to each temperature are taken from the saturation tables.
- From the linearity of the relation between the enthalpy and the temperature both C_p (the slope) and q (reference energy at a given state) are determined, see the relation (8.3.1b).
- Use the experimental curve $p = p_{sat}(T)$ in (8.3.1c), thus the specific volume is expressed in terms of temperature. Using the two known states with some manipulation the parameter π is determined, then C_v is also determined.
- Find γ by using $\gamma = C_p/C_v$.
- At thermodynamic equilibrium the Gibbs free energies are equal, i.e. $g_l = g_g$. By this equality with the definition (8.3.1e) we have

$$(\gamma_l C_{vl} - q'_l)T - C_{vl}T\ln\frac{T^{\gamma_l}}{(p+\pi_l)^{(\gamma_l-1)}} + q_l = (\gamma_g C_{vg} - q'_g)T - C_{vg}T\ln\frac{T^{\gamma_g}}{(p+\pi_g)^{(\gamma_g-1)}} + q_g. \tag{8.3.2}$$

  This equation is nonlinear and can be solved to find the saturation temperature in terms of the saturation pressure. But still the entropy constants q'_g and q'_l are unknown. The authors of [29] chose to set the parameter $q'_l = 0$ and chose the parameter q'_g that provides the best fit between the theoretical and experimental saturation curve.

The group of parameters were obtained by Le Metayer et al. [29], provides a good agreement between the theoretical and experimental curves for the saturation curve and the saturation enthalpies in the specified range of temperature, i.e. $298 - 473$ K, see the comparisons in [29]. Outside of this range the accuracy decreases. This is due to the fact that the saturation curves are nonlinear or may be considered as almost piecewise linear, while the SG-EOS provides a linear approximation in the (p, v)-plane. The above method mainly depends on the linearity of the relation between the enthalpy and temperature, but this linearity holds in limited ranges only. In fact, near the critical point the nonlinear feature appears strongly. Moreover, the choice of the entropy constants q'_k may lead to negative values for the entropy.

In the problem under consideration i.e. bubble collapse, the range of the temperature is very wide. It starts from the room temperature and exceeds the critical point. Thus choosing appropriate parameters for EOS is not an easy task. Moreover, including the heat and mass transfer requires more attention. In fact, finding EOS that cover very wide ranges of properties and provide the required stability for the solution of the hyperbolic system is a difficult issue.

In this work we adopt the SG-EOS (8.3.1). We use our own method for the determination of the parameters. In this method we keep the aim of the previous method that the various parameters of each EOS are linked to each other to recover the saturation curve. Since the range of the temperature is very wide it is impossible to obtain good agreements between the theoretical and the experimental curves by one group of parameters. Instead of that we aim to keep the physical properties of the quantities besides reasonable agreement with the tendency of the relations between the various quantities.

Now, we determine the parameters for water vapor then for liquid water.

8.3.1 Determination of the SG-EOS for the water vapor

For gases it is typical to set $\pi_g = 0$. For example, if we follow the method of Le Metayer et al. [29] for some short ranges of temperatures we find that π_g is either negative or has a small value. Thus we choose $\pi_g = 0$.

Using $\pi_g = 0$, it is easy to see from (8.3.1a) and (8.3.1c) that

$$e_g(T) = C_{vg}T + q_g. \tag{8.3.3}$$

This is a linear equation. In the literature we find several values that can be taken for the specific heat at constant volume for the water vapor, more precisely they are in the range $(1.04 - 1.4) \times 10^3$ J/kg/K, see [29, 54]. The choice depends on the range of the temperature. In our case we choose $C_{vg} = 1.2 \times 10^3$ J/kg/K. Then we choose q_g which gives a good fitting for the experimental relation between e_g and

T. For the experimental data we use the saturation tables, see [37, 54]. We found that the choice of $q_g = 1995 \times 10^3$ J/kg provides a good fitting for the experimental data, see Figure 8.1. Here we did not use any mathematical method to find the best linear fit. In fact, we are not interested in the best linear fit since the nonlinearity effect is continued to a small range. Instead of that we choose our line in order to be close to the experimental curve in the wide range of approximate linearity.

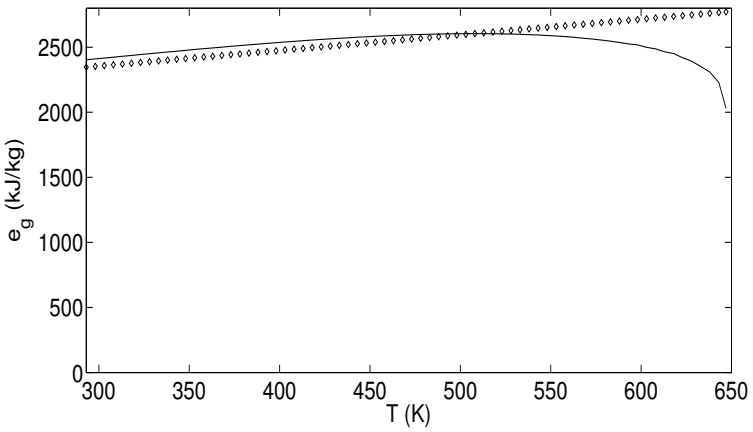

Figure 8.1: Saturation internal energy for the water vapor. Experimental curves are shown in lines and the SG-EOS approximation with symbols.

The relation (8.3.1c) can be reformulated as

$$v_g(T) = \frac{(\gamma_g - 1)C_{vg}T}{p_{sat}(T)}. \tag{8.3.4}$$

Then we choose the value of γ_g which provides a good fit between the theoretical and experimental curves of vg versus T. Indeed, the value of $\gamma_g = 1.327$ provides such a good fitting, see Figure 8.2.

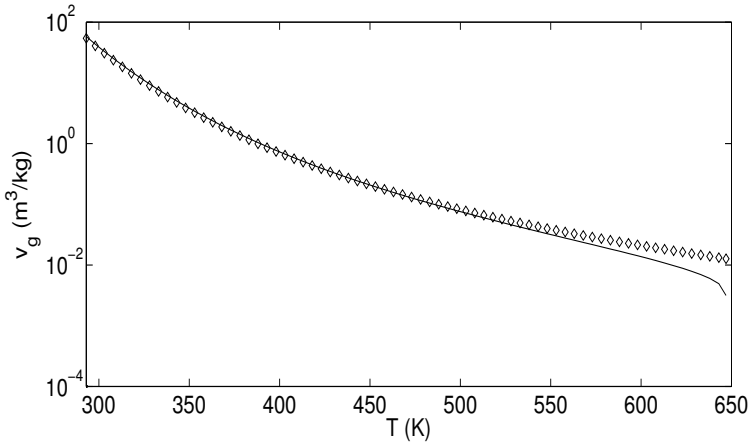

Figure 8.2: Saturation specific volume for the water vapor. Experimental curves are shown in lines and the SG-EOS approximation with symbols.

Still the parameter q'_g is unknown. We will postpone this untill after the presentation of the liquid water parameters.

8.3.2 Determination of the SG-EOS for the liquid water

For the liquid water the situation is more complicated and the nonlinear feature for the internal energy is stronger. From the thermodynamic approximations it is known that the internal energy and the specific

volume for the compressed water can be approximated by the saturated values, while the enthalpy of the compressed water is approximated by the saturated enthalpy by adding a correction, see e.g. Moran and Shapiro [31]. Moreover, the internal energy appears explicitly in the models. Thus we use the saturated values for the internal energy e and specific volume v in our method.

We start from the idea that the internal energy e is a convex function of the specific volume v. The relation between e and v is non linear, but the SG-EOS (8.3.1a) provides a linear approximation in the (p, v)- plane. Here, we choose two states from the saturation tables: The first state is the initial temperature of the liquid, i.e. the room temperature. The second state is chosen to be a little bit less than the critical temperature since near the critical temperature the quantities change dramatically. Indeed, we choose the first temperature $T_1 = 293$ K and the second temperature $T_2 = 623$ K. Note that the critical temperature is $T_{cr} = 647$ K.

The experimental data corresponding to T_1 and T_2 are, see [37, 54]:

$p_{sat}(T_1) = 2339$ Pa	$e_l(T_1) = 83.94 \times 10^3$ J/kg	$v_l(T_1) = 0.001002$ m^3/kg
$p_{sat}(T_2) = 16.514 \times 10^6$ Pa	$e_l(T_2) = 1641.81 \times 10^3$ J/kg	$v_l(T_2) = 0.00174$ m^3/kg

Substitute each group of the experimental data into the relation (8.3.1a). We obtain two equations

$$83.94 \times 10^3 = (0.001002)\frac{2339 + \gamma_l \pi_l}{\gamma_1 - 1} + q_l, \tag{8.3.5}$$

$$1641.81 \times 10^3 = (0.00174)\frac{16.514 \times 10^6 + \gamma_l \pi_l}{\gamma_l - 1} + q_l. \tag{8.3.6}$$

Equations (8.3.5) and (8.3.6) are two equations of three variables, so a third equation is required. For the third equation we use the expression of the sound speed (8.2.3). The sound speed in the liquid water is 1482 m/s at $T_1 = 293$ K. Thus we get the following equation

$$(1482)^2 = 0.001002\gamma_l(2339 + \pi_l). \tag{8.3.7}$$

We have three equations with three unknowns. Solving the equations (8.3.5)-(8.3.7), we obtain

$$\gamma_l = 2.057, \qquad \pi_l = 1.066 \times 10^9 \text{ Pa}, \qquad q_l = -1.994674 \times 10^6 \text{ J/kg}.$$

To determine C_v we use the temperature expression (8.3.1c) with one of the known states. In fact this will produce a big error. Indeed the expression (8.3.1c) itself is an approximation derived initially from a linear approximation in terms of v, see Le Metayer et al. [29]. But it is expected in the bubble collapse that the water will stay at the initial temperature during the whole process. Thus we choose to use the initial state to find C_v to reduce the error. Substituting the experimental data related to T_1 in (8.3.1c) we have $C_v = 3.449 \times 10^3$ J/kg/K.

From (8.3.1a) and (8.3.1c) we can write the internal energy in terms of v and T, i.e.

$$e_l(T, v) = C_v T + \pi_l v + q_l. \tag{8.3.8}$$

Also we can write the internal energy in terms of T and p as

$$e_l(T, p) = \frac{p + \gamma_l \pi}{p + \pi} C_v T + q_l,$$

or

$$e_l(T) = \frac{p_{sat}(T) + \gamma_l \pi_l}{p_{sat}(T) + \pi_l} C_v T + q_l. \tag{8.3.9}$$

To see the experimental curves versus the theoretical ones, we use the relation (8.3.8) and draw the internal energy versus the temperature. For v we use the values that are given in the saturation tables, see the left graph of Figure 8.3. Then we use the relation (8.3.9) and draw the internal energy versus the temperature, see the right graph of Figure 8.3.

In fact the relation (8.3.8) shows a reasonable agreement between the theoretical and experimental curves. But in this case the values of specific volume are taken directly from the tables. However this indicates that this relation provides a reliable description for the relation between the internal energy with T and v. But if the specific volume written in terms of the saturation temperature, i.e. the internal

energy is a function of temperature, then we see that the agreement between the experimental and theoretical curves is bad. This is due to the choice of the temperature expression (8.3.1c). In other words, there is a relatively big error in the relation between T and v. To reduce the effect of this error we give more attention to the initial state since it is expected that the water outside the bubble will keep the initial temperature throughout all of the collapse process as is explained above. However, we think that the expression (8.3.1c) for the temperature should be improved to give more realistic values.

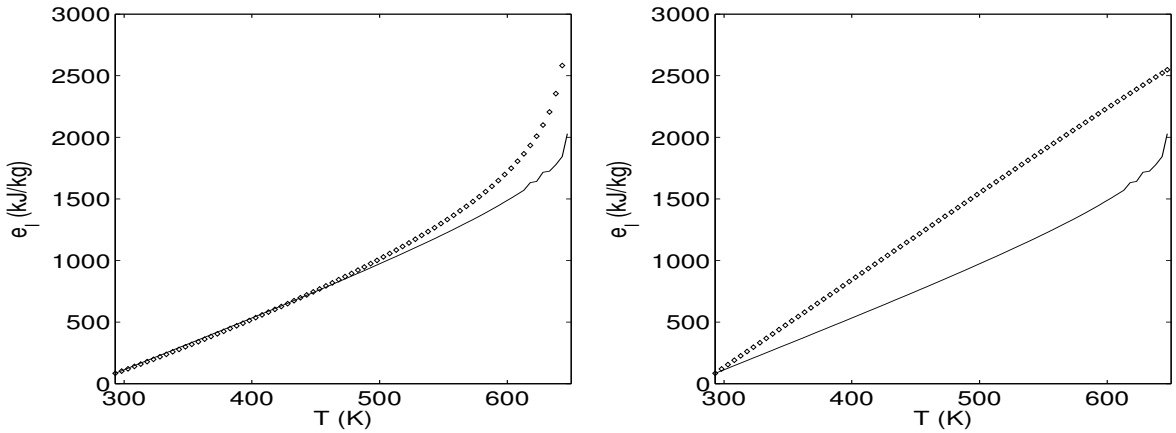

Figure 8.3: Saturation internal energy for the liquid water. Experimental curves are shown in lines and the SG-EOS approximation with symbols.

8.3.3 Determination of the entropy constants

To determine the entropy constants q_l' and q_g' we proceed as in Le Metayer et al. [29], i.e. at thermodynamic equilibrium the Gibbs free energies are equal, see equation (8.3.2). In our case we did not set any of the parameters to zero to avoid negative values for the entropy. Instead of that we take q_l' to satisfy the initial value of the entropy of the liquid. Then we choose q_g' in order to obtain a good fitting for the saturation curve.

The entropy of the liquid at $T_1 = 293$ K is $s_{l1} = 0.296$ kJ/kg/K. Using these data in (8.3.1d) we find $q_l' = 35.78$ kJ/kg/K. Using this value we can obtain a good agreement to the experimental saturation curve in the range $293 - 500$ K if we choose $q_g' = 2.41$ kJ/kg/K, see Figure 8.4. Out this range of temperature the agreement is bad. If the expected range of the temperature within the specified range then this choice is enough, but if the temperature can exceed 500 K an improvement is required.

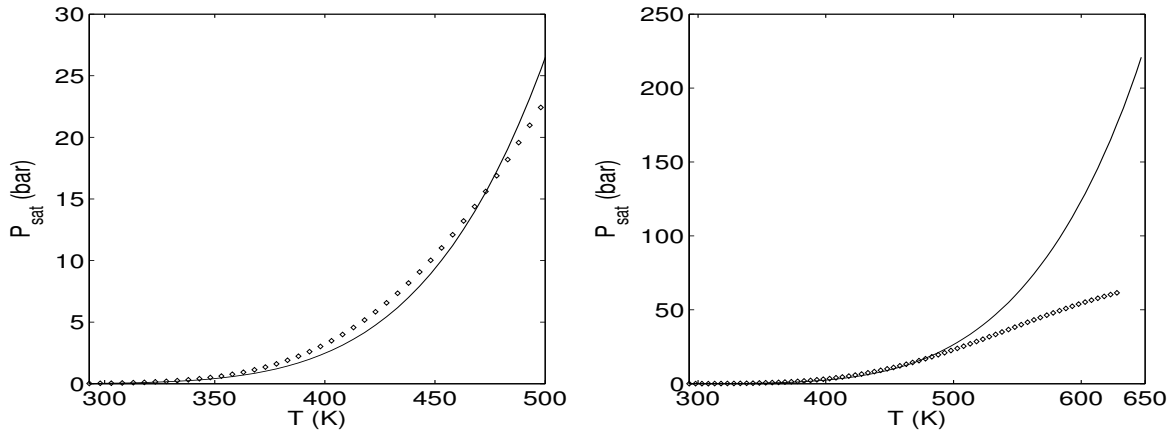

Figure 8.4: Saturation curve of the water. Experimental curves are shown in lines and the SG-EOS approximation with symbols.

In fact to obtain a good agreement to the experimental saturation curve with one choice of q'_g in the whole range is impossible. Instead of that we choose more than one value to q'_g regarding to the temperature range. For example, choose $q'_l = 35.64$ kJ/kg/K and

$$q'_g = \begin{cases} 2.41, & T < 573 \\ 2.51, & 573 \leq T \leq 593 \\ 2.57, & 593 \leq T \leq 613 \\ 2.61, & T > 613 \end{cases}, \tag{8.3.10}$$

where the unit of T is K and the unit of q'_g is kJ/kg/K. By these values the saturation curve is recovered for a wide range of temperatures, see Figure 8.5.

In the computations we observed that if the phase transition is included the interfacial temperature increases as the time evolves. After about 550 K the change of the temperature becomes very fast, then the bubble collapses. Thus, the several values of q'_g in (8.3.10) are used just for very short intervals of time with respect to the total time of the evolution. Thus for most time the computations were made with $q'_g = 2.41$ kJ/kg/K.

In Summary the parameters of the SG-EOS by this method are given in Table 2.

Phase	γ	$\pi(Pa)$	$C_v(J/kg/K)$	$q(J/kg)$	$q'(J/kg/K)$
vapor	1.327	0	1.2×10^3	1995×10^3	2.41×10^3
liquid	2.057	1.066×10^9	3.449×10^3	-1994.674×10^3	35.78×10^3

Table 8.1: EOS parameters for vapor and liquid water by the present method.

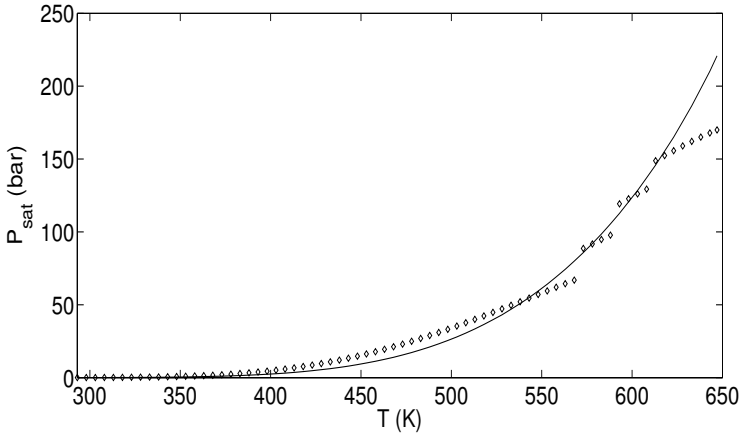

Figure 8.5: Saturation curve of the water. Experimental curves are shown in lines and the SG-EOS approximation with symbols.

8.4 Numerical method

To take into account the relaxation terms the Strang splitting [55] is used. Thus when a second-order numerical scheme is employed the solution of the systems (8.2.1) and (8.2.8) are obtained by the succession of operators

$$\mathbf{U}_j^{n+1} = L_{Rs}^{\frac{\Delta t}{2}} L_h^{\Delta t} L_{Rs}^{\frac{\Delta t}{2}} \mathbf{U}_j^n, \tag{8.4.1}$$

where

$$\mathbf{U} = (\alpha_1, \alpha_1\rho_1, \alpha_2\rho_2, \rho u, \alpha_1\rho_1 e_1, \alpha_2\rho_2 e_2, \rho e + \frac{1}{2}\rho u^2)^T,$$

or

$$\mathbf{U} = (\alpha_1, \alpha_2, \alpha_1\rho_1, \alpha_2\rho_2, \alpha_3\rho_3, \rho u, \alpha_1\rho_1 e_1, \alpha_2\rho_2 e_2, \alpha_3\rho_3 e_3, \rho e + \frac{1}{2}\rho u^2)^T,$$

for the systems (8.2.1) and (8.2.8) respectively.

Here L_{Rs} is the operator of integration of the relaxation terms over half of the time interval and L_h the operator of numerical solution of the hyperbolic part of the system accompanied by the geometrical source vector.

A Godunov-type method is used for the operator L_h while a successive relaxation processes are used for the operator L_{Rs} in order: The pressure relaxation, the temperature relaxation then the Gibbs free energy relaxation. Hereafter, we explain a Godunov-type method in the context of two phases, i.e the system (8.2.1), for simplicity. This method can directly be extended to the three-phase model (8.2.8). Then the relaxation step is detailed for the model (8.2.1).

8.4.1 Godunov-type method

The system (8.2.1) is discretized by a Godunov-type method. The equations of the system (8.2.1) that are written in a conservative form are discretized as

$$\mathbf{u}_j^{n+1} = \mathbf{u}_j^n - \frac{\Delta t}{\Delta r}[\mathbf{f}(\mathbf{u}^*(\mathbf{u}_j^n, \mathbf{u}_{j+1}^n)) - \mathbf{f}(\mathbf{u}^*(\mathbf{u}_{j-1}^n, \mathbf{u}_j^n))] + \Delta t \mathbf{S}_{rj}^n,$$

where

$$\mathbf{u} = (\alpha_1\rho_1,\ \alpha_2\rho_2,\ \rho u,\ \rho e + \frac{1}{2}\rho u^2)^T,$$

$$\mathbf{f(u)} = (\alpha_1\rho_1 u,\ \alpha_2\rho_2 u,\ \rho u^2 + \alpha_1 p_1 + \alpha_2 p_2,\ u(\rho e + \frac{1}{2}\rho u^2 + \alpha_1 p_1 + \alpha_2 p_2))^T,$$

and $\mathbf{u}^*(\mathbf{u}_j^n, \mathbf{u}_{j+1}^n)$ the value of $\mathbf{u}$ along the line $r = r_{j+\frac{1}{2}}$ for the Riemann problem with the states $\mathbf{u}_j^n, \mathbf{u}_{j+1}^n$. The numerical approximation $\mathbf{S}_{rj}^n$ of the geometrical source vector (8.2.5) is evaluated as the average between the left and right states $\mathbf{u}_j^n, \mathbf{u}_{j+1}^n$.

The volume fraction equation and the internal energy equations are discretized as, see [50],

$$\alpha_{1j}^{n+1} = \alpha_{1j}^n - \frac{\Delta t}{\Delta x}((u\alpha_1)^*_{j+\frac{1}{2}} - (u\alpha_1)^*_{j-\frac{1}{2}} - \alpha_{1j}^n(u^*_{j+\frac{1}{2}} - u^*_{j-\frac{1}{2}})),$$

$$(\alpha\rho e)_{kj}^{n+1} = (\alpha\rho e)_{kj}^n - \frac{\Delta t}{\Delta x}((\alpha\rho eu)^*_{k,j+\frac{1}{2}} - (\alpha\rho eu)^*_{k,j-\frac{1}{2}} + (\alpha p)_{kj}^n(u^*_{j+\frac{1}{2}} - u^*_{j-\frac{1}{2}})) - \frac{2}{r_j}(\alpha\rho eu + \alpha pu)_{kj}^n.$$

The geometrical term $\frac{2}{r_j}(\alpha\rho eu + \alpha pu)_{kj}^n$ is taken as the average between the left and right states.

To achieve a second order accuracy we use the MUSCL method [57]. For the Riemann values we use the HLLC-type Riemann solver that was proposed by Saurel et al. [50]. This solver uses the non-conventional shock relations that were derived in Saurel et al. [48].

8.4.2 Relaxation step

In the relaxation step, applying the Strang splitting on the model (8.2.1), we must solve the following system of ordinary differential equations (ODE)

$$\frac{d\mathbf{U}}{dt} = \mathbf{S}_P + \mathbf{S}_Q + \mathbf{S}_m.$$

This system is solved successively for each source vector alone.

The relaxation steps are performed in the following order: first pressure relaxation then temperature relaxation and at last Gibbs free energy relaxation. From one step to the other, what is relaxed stays relaxed. The variable κ is related to the heat transfer modeling and is determined in a way to keep the pressure equilibrium during the temperature relaxation. The variables ϱ and e_i are related to the mass transfer and are determined to keep the equilibrium of the pressure and temperature during the Gibbs

free energy relaxation. It is essential to emphasize that the model with new terms for the heat and mass transfer satisfies the second law of thermodynamics, for details see [61].

For numerical reasons, we allow the presence of a negligibly small amount of vapor outside the bubble, and a small amount of liquid inside the bubble, typically these values are $\epsilon = 10^{-6}$. Then to locate the interface we use the ideas of Saurel et al. [49]. We assume that the cell is filled with pure fluid when its volume fraction is close to 1, say $(1-\epsilon)$. The interface corresponds to mixture cells when the volume fraction ranges between $\bar{\epsilon}$ and $1-\bar{\epsilon}$, with $\bar{\epsilon} = 10^{-4}$. The value of $\bar{\epsilon}$ has to be chosen larger than the value of ϵ to ensure that phase transitions occur only in the interfacial zone, for a discussion on this point see [49].

It is expected that the small values of different volume fractions on each side have no significant effects. Indeed, by using pressure relaxation in the whole domain we keep a single value for the pressure. In addition, we use the temperature relaxation in the whole domain, so we have a single temperature. This seems to be better for the resolution of the physical variables. In fact, we observed just a small change in the results if we use the temperature relaxation at the interface only. The mass transfer is considered only at the interface, i.e. the Gibbs free energy relaxation is used only at the interface.

To perform the temperature relaxation we must solve the following ODE system

$$\frac{d\mathbf{U}}{dt} = \mathbf{S}_Q, \tag{8.4.2}$$

During the temperature relaxation the pressure is assumed to stay in equilibrium. To ensure this during the temperature relaxation process we assume that

$$\frac{\partial p_1}{\partial t} = \frac{\partial p_2}{\partial t}.$$

From this condition with system (8.4.2), we obtain

$$\kappa = \frac{\dfrac{\rho_1 c_1^2}{\alpha_1} + \dfrac{\rho_2 c_2^2}{\alpha_2}}{\dfrac{\Gamma_1}{\alpha_1} + \dfrac{\Gamma_2}{\alpha_2}} - \frac{\dfrac{\Gamma_1}{\alpha_1} p_1 + \dfrac{\Gamma_2}{\alpha_2} p_2}{\dfrac{\Gamma_1}{\alpha_1} + \dfrac{\Gamma_2}{\alpha_2}}. \tag{8.4.3}$$

Here Γ_k denotes the Grüneisen coefficient of phase k which is given as

$$\Gamma_k = \frac{1}{\rho_k} \left(\frac{\partial p_k}{\partial e_k} \right)_{\rho_k}, \quad k = 1, 2. \tag{8.4.4}$$

After the temperature relaxation the Gibbs free energy relaxation is performed by solving the system

$$\frac{d\mathbf{U}}{dt} = \mathbf{S}_m. \tag{8.4.5}$$

Through the process of the Gibbs free energy relaxation the pressure and the temperature are assumed to stay in equilibrium, i.e.

$$\begin{aligned} \frac{\partial p_1}{\partial t} &= \frac{\partial p_2}{\partial t}, \\ \frac{\partial T_1}{\partial t} &= \frac{\partial T_2}{\partial t}. \end{aligned}$$

Using these conditions with system (8.4.5) we obtain the following expressions for ϱ and e_i

$$\varrho = \frac{\phi\left(\frac{\rho_1 c_1^2}{\alpha_1} + \frac{\rho_2 c_2^2}{\alpha_2}\right) - \phi\left(\frac{\Gamma_1}{\alpha_1}p_1 + \frac{\Gamma_2}{\alpha_2}p_2\right) + \psi\left(\frac{\rho_1^2\left(\frac{\partial e_1}{\partial \rho_1}\right)_{T_1}}{\alpha_1\rho_1 C_{v1}} + \frac{\rho_2^2\left(\frac{\partial e_2}{\partial \rho_2}\right)_{T_2}}{\alpha_2\rho_2 C_{v2}}\right)}{\phi\left(\frac{c_1^2}{\alpha_1} + \frac{c_2^2}{\alpha_2}\right) - \phi\left(\frac{\Gamma_1}{\alpha_1}h_1 + \frac{\Gamma_2}{\alpha_2}h_2\right) + \psi\left(\frac{e_1 + \rho_1\left(\frac{\partial e_1}{\partial \rho_1}\right)_{T_1}}{\alpha_1\rho_1 C_{v1}} + \frac{e_2 + \rho_2\left(\frac{\partial e_2}{\partial \rho_2}\right)_{T_2}}{\alpha_2\rho_2 C_{v2}}\right)},$$

$$e_i = \frac{\frac{e_1 + \rho_1\left(\frac{\partial e_1}{\partial \rho_1}\right)_{T_1}}{\alpha_1\rho_1 C_{v1}} + \frac{e_2 + \rho_2\left(\frac{\partial e_2}{\partial \rho_2}\right)_{T_2}}{\alpha_2\rho_2 C_{v2}}}{\phi} - \frac{\frac{\rho_1^2\left(\frac{\partial e_1}{\partial \rho_1}\right)_{T_1}}{\alpha_1\rho_1 C_{v1}} + \frac{\rho_2^2\left(\frac{\partial e_2}{\partial \rho_2}\right)_{T_2}}{\alpha_2\rho_2 C_{v2}}}{\varrho\phi},$$

where C_{vk} is the *specific heat capacity at constant volume*, $\phi = \frac{1}{\alpha_1\rho_1 C_{v1}} + \frac{1}{\alpha_2\rho_2 C_{v2}}$, $\psi = \frac{\Gamma_1}{\alpha_1} + \frac{\Gamma_2}{\alpha_2}$ and $h_k = e_k + \frac{p_k}{\rho_k}$ is the *specific enthalpy* for phase k.

The relaxation procedures for the temperature and the Gibbs free energy were detailed in Zein et al. [61]. These procedures are used for the model (8.2.1). Also they are used directly for the model (8.2.8), since the heat and mass transfer is considered only at the interface between the liquid and its vapor. Several procedures are available for the pressure relaxation with model (8.2.1), see [25, 26, 44, 47, 50]. In this work we adopt the recent procedure of Saurel et al. [50]. This method is easily implemented and easily used for multiphase flows.

In addition a correction criterion of Saurel et al. [50] is used to make the relaxed pressure in agreement with the mixture EOS. It is based on the evolution of the total energy equation, see equation (8.2.1) in the system (8.2.1) and the last equation in system (8.2.8). This is expected to be accurate in the entire fluid flow since the equation is written in a conservative formulation.

In the presence of a non-condensable gas, i.e. in the three-phase model, the interface between the liquid and vapor is located as in Petitpas et al. [39] by using the volume fractions of both the vapor and liquid. Assume α_1 and α_2 to be the volume fractions of vapor and liquid respectively. Then the interface is located where

$$\bar{\epsilon} \leq \alpha_1 \leq (1 - \bar{\epsilon}) \quad \text{and} \quad \bar{\epsilon} \leq \alpha_2 \leq (1 - \bar{\epsilon}).$$

Note that in this case the bubble is identified by the summation of the vapor volume fraction and the non-condensable gas volume fraction.

The heat and mass transfer change the pressure of the vapor and liquid. But both stay in equilibrium. To keep one pressure in the system at each time step we also set the pressure of the non-condensable gas to the new pressure. This effect modifies the internal energy of the non-condensable gas.

8.5 Numerical Results

In this section, we provide numerical computations for the dynamics of a laser-induced bubble. The results are shown taking the six-equation model (8.2.1) for the two-phase flow if the bubble contains vapor only. While if the bubble contains a percentage of non-condensable gas also, then the three-phase model of nine equations (8.2.8) is used. In all computations the CFL number is fixed to 0.6 and a uniform grid is used.

For validation we take the experimental radius-time curve that appears in Müller et al. [32]. Thus for all computations, unless mentioned, the initial conditions are as follows: The radius of the bubble $R_{max} = .75$ mm. The surrounding water has a pressure $p_l = 1$ bar and temperature $T_l = 293$ K.

Since the initial state inside the bubble is unknown, we choose several possibilities to provide a description for the dynamics of the collapsing bubble with different initial conditions. The computational domain is taken to be suitably large compared to the bubble size to avoid boundary effects. In our computations the domain is chosen to be the interval $[0, 99]$ mm. The left boundary conditions, i.e. at the center of the bubble, are the symmetric conditions. For the right boundary conditions, i.e. at the

far wall of the domain, there are two choices in the literature. Müller et al. [32] assumed a reflected velocity at the far field wall. In Dreyer et al. [13] the velocity at the far wall is set to be zero. In our computations both choices were tested, there is no significant effect on the results. This may be due to the large size of the computational domain.

Since the grid is uniform and the computational domain is very large compared to the bubble radius, we introduce the number of cells N_I. This number N_I represents the number of cells inside the bubble from its center to its wall at the initial state, i.e. the number of cells that cover the maximum radius of the bubble at the initial state. In Table 3, the values of N_I are shown with the corresponding numbers of the cells in the whole domain.

N_I	250	500	750	1000
Total number of cells	33,000	66,000	99,000	132,000

Table 8.2: The concept of N_I.

For numerical reasons, we allow the presence of a small volume fraction of the liquid water inside the bubble and a small volume fraction of vapor outside the bubble, typically these small values are taken 10^{-6}.

For each numerical test the results are shown with respect to time for the radius of the bubble, the pressure and temperature at the center of the bubble and the velocity at the interface.

8.5.1 Tests for vapor bubble

This subsection deals with the case that the bubble contains vapor only. Assume that the initial state inside the bubble is the saturation state, i.e. $T_v = 293$ K and $p_v = 2339$ Pa. A comparison between results with and without mass tansfer are first considered. Then mesh refinement tests are addressed. After that tests for different initial temperatures and pressures are included.

8.5.1.1 Comparison between with and without mass transfer

The results without mass transfer are shown in Figure 8.6. If the mass transfer is included the results are shown in Figure 8.7. Following Akhatov et al. [1] and Dreyer et al. [13], the mass transfer is activated from the beginning of the evolution until the critical state is exceeded, the critical temperature of the water is $T_{cr} = 647$ K. If the interfacial temperature of the bubble exceeds the critical temperature the mass transfer is stopped. This is due to the fact that there is no difference between the phases at the bubble interface beyond the critical state. Then the mass transfer is activated again after the collapse when the temperature falls below the critical temperature. In the computations, we observe that in the case with no mass transfer the temperature inside the bubble after reaching 1500 K increases rapidly and then the collapse occurs. The temperature reaches almost immediately a very high value (> 6000 K). If the phase transition is included the temperature after reaching 515 K increases rapidly and then the collapse occurs. The temperature again becomes greater than 6000 K.

The radius-time curves before the collapsing point are coinciding and in an excellent agreement with the experimental data, see the radius graph in Figure 8.7. The collapse occurs slightly earlier if the mass transfer is included. Indeed, in this case the collapse occurs at time $t = 69.431$ μs, while if the mass transfer is excluded the collapse occurs at time $t = 69.743$ μs. Both values for the collapsing time are very close to the experimental value $t = 69.3$ μs.

In the computations, before the instant of the collapse, we observe that the temperature and the pressure inside the bubble, when the phase transition, is included is less than the corresponding values if the phase transition is not considered, see Figures 8.7 and 8.8. In Figure 8.8 the temperature and the pressure are shown before the collapse point. We think this behavior is physically correct, since a part of the energy inside the bubble is consumed by the phase transition.

At the collapse time, both the pressure and the temperature at the center of the bubble almost jump to very high values. These values are higher in the case of mass transfer than the case without mass transfer. This indicates that the collapse is more violent if the mass transfer is included and the bubble vanishes. In fact we cannot say more about the physics of this behavior. Moreover, there seems to be no way to check such comparisons experimentally.

It is clear from Figure 8.7 that there is no rebound if the phase transition is included. This occurs since most of the vapor mass leaves the bubble and there is no mechanism for a rebound. In real experiments this behavior is not observed. Always there is a rebound of the bubble. This motivates us to consider a percentage of non-condensable gas inside the bubble besides the water vapor, as is expected in real experiments. This will be investigated numerically in Subsection 8.5.2.

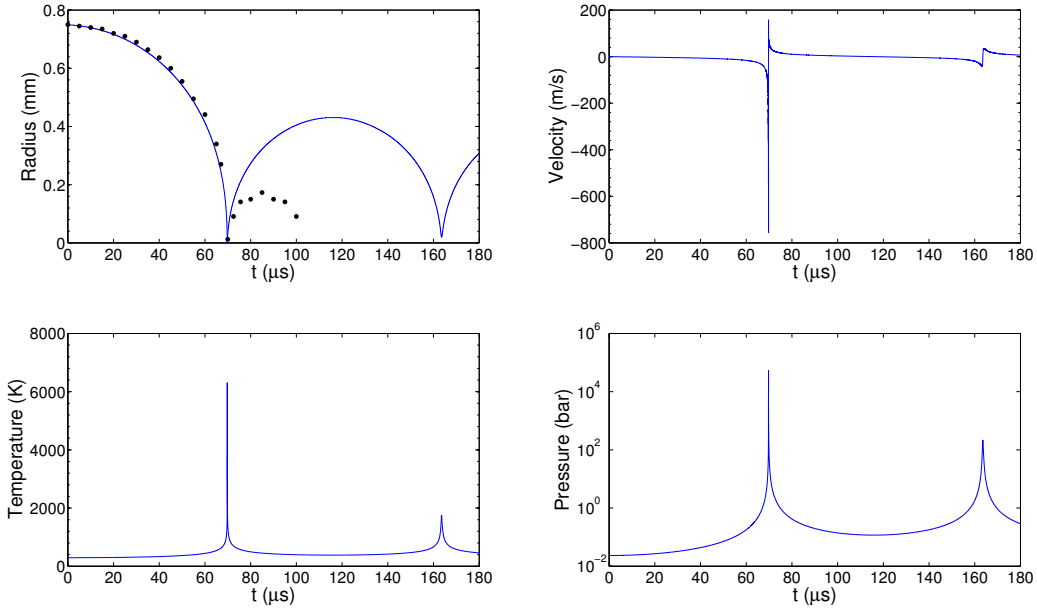

Figure 8.6: The collapse and rebound of the vapor bubble without mass transfer. The computed radius is compared with the experimental data (dots). $N_I = 500$ cells, $T_v = 293$ K and $p_v = 2339\ Pa$.

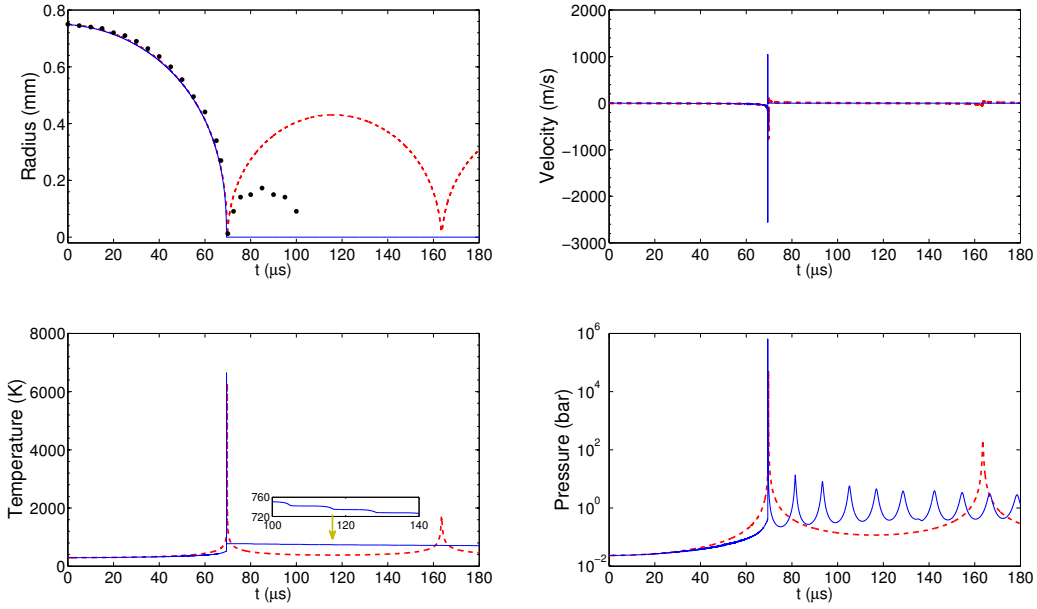

Figure 8.7: The collapsing vapor bubble results with mass transfer (solid line) compared to those without mass transfer (dashed line). The computed radii are compared with the experimental data (dots). $N_I = 500$ cells, $T_v = 293$ K and $p_v = 2339\ Pa$.

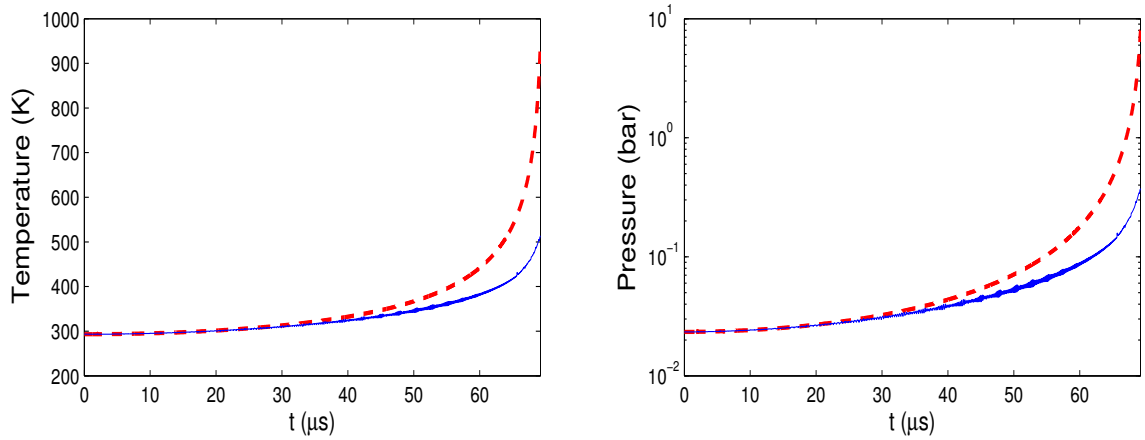

Figure 8.8: The center temperature and pressure of the bubble before the collapse instant. Results with mass transfer (solid line) compared to the ones without mass transfer (dashed line). With $N_I = 500$ cells, $T_v = 293$ K and $p_v = 2339$ Pa. The graphs here are some zoom of the temperature and pressure graphs in Figure 8.7.

In the case of phase transition after the collapse the bubble vanishes, so it is expected that after a certain time the pressure and the temperature in all of the domain will be like the values for the liquid water. From the pressure profile we see after the collapse point that there are some oscillations around the value of atmospheric pressure. From the temperature profile we see that the temperature remains quite high. In fact even though the bubble vanishes there still is a certain small remaining vapor concentration. This is shown in Figure 8.9. The left side graphs are shown for a very small domain while the right graphs are shown for the distance equal to the initial maximum radius. It is clear from the figure that there still is some concentration of vapor at the bubble center. Moreover, the oscillations of the pressure in Figure 8.7 have decreasing amplitudes in time, also the temperature decreases with time but very slowly.

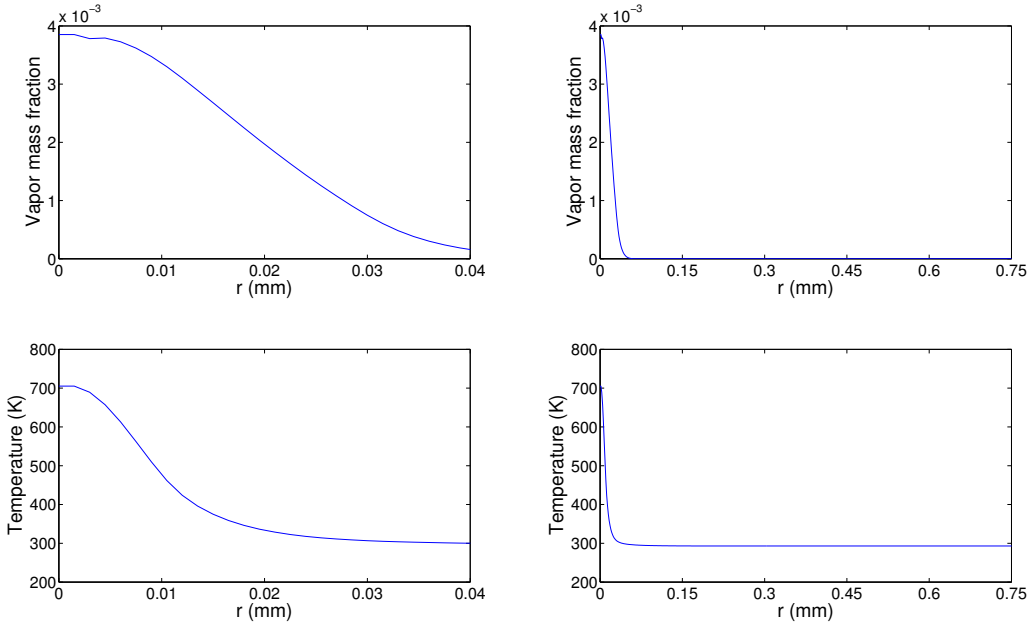

Figure 8.9: The vapor mass fraction and temperature versus radial direction if the phase transition is included at time $t = 180$ μs. With $N_I = 500$ cells, $T_v = 293$ K and $p_v = 2339$ Pa.

8.5.1.2 Mesh refinement tests

We repeat the same problem with a different number of cells, without mass transfer as shown in Figure 8.10 and with mass transfer as in Figure 8.12. A common feature is that before the instant of the collapse all curves are almost coinciding. In addition there is an excellent agreement with the experimental data.

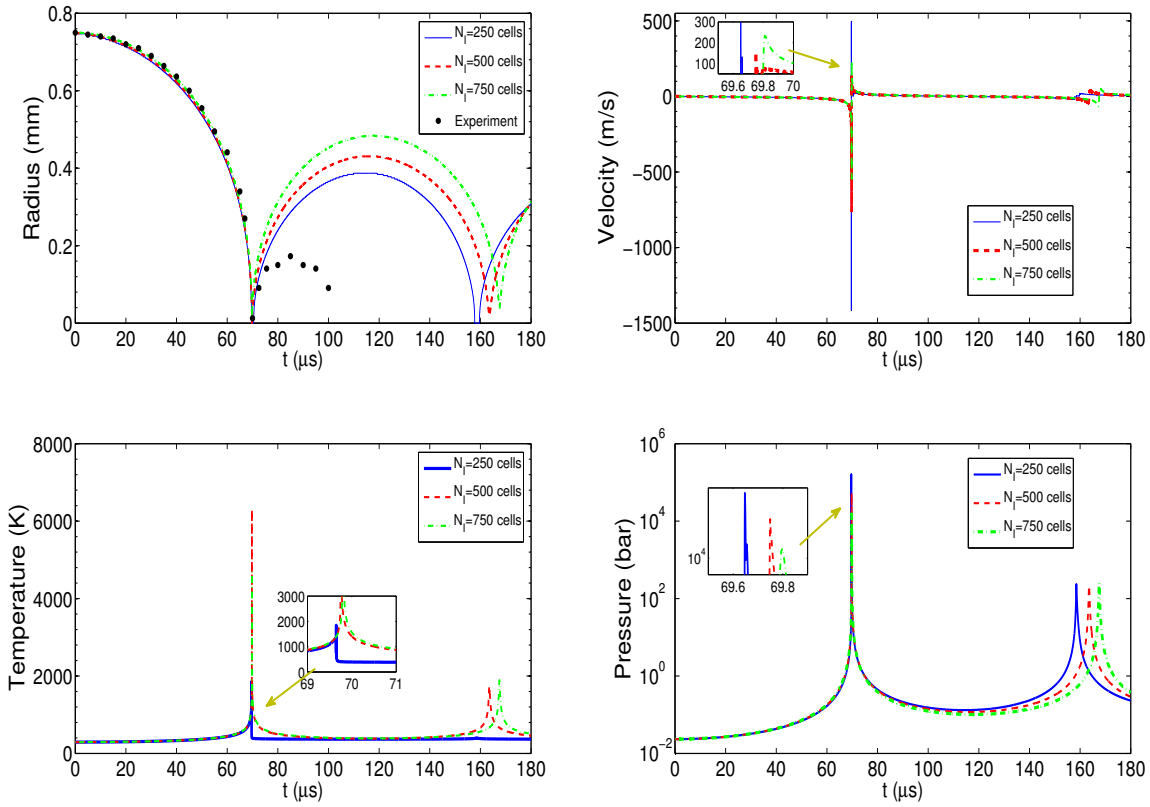

Figure 8.10: Vapor bubble without mass transfer, comparison using several grids. The computed radii are compared with the experimental data (dots). Initial values $T_v = 293$ K and $p_v = 2339$ Pa.

Figure 8.10 shows that there is a significant difference between the curves for a different number of cells after the collapse point. To understand the reasons we draw the volume fraction profiles at different instants of time, see Figure 8.11. It is clear that the interface diffusion is weaker if the number of cells is higher. Long before the time of collapse the diffusion in the curves is very small, thus the radius curves coincide, see graph (a), the results are shown at time $t = 50\ \mu s$. Around the time of collapse the curves start to diffuse. See graphs (b) and (c), where the diffusion now became more serious. Graphs (d) and (e) show the results after the collapse but still very close to the collapsing time. There is a big diffusion across the interface especially for $N_I = 250$ cells. The diffusion will be reduced again as the time evolves as in graph (f), but now the curves remain clearly distinct from each other. This produces the differences in the radii curves. Hence, we conclude that the diffusion of the curves increases around the collapse point. In addition, the pressure and temperature relaxations reduce some amount of the vapor inside the bubble, this is higher if the interface is more diffusive. Thus passing through the collapse point the diffusion has a significant effect which will continue to be observed after the collapse. So it is important to reduce the diffusion as much possible.

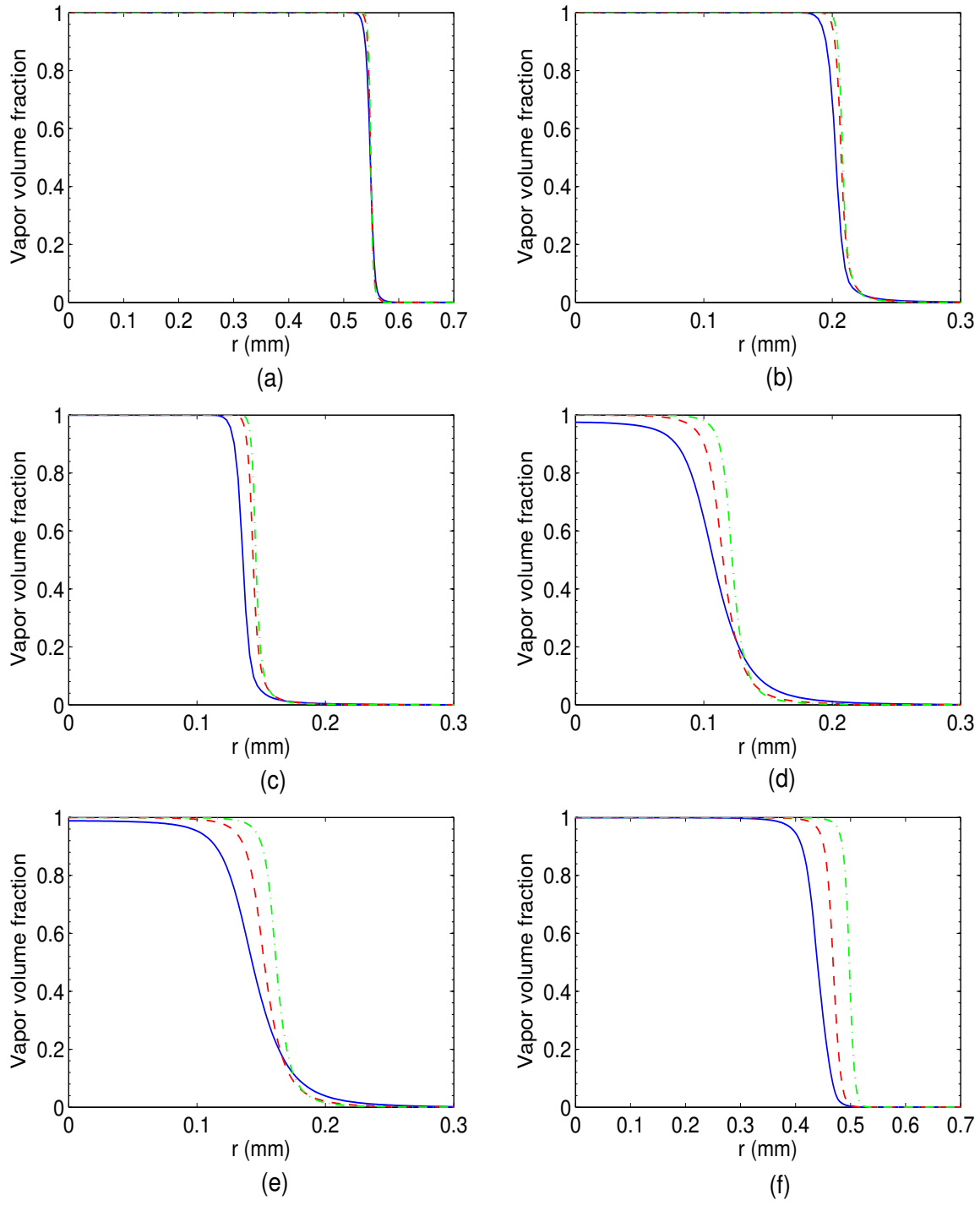

Figure 8.11: Vapor volume fraction profiles of the results in Figure 8.10, they are shown at times (a) $t = 50\ \mu s$ (b) $t = 68\ \mu s$ (c) $t = 69\ \mu s$ (d) $t = 71\ \mu s$ (e) $t = 72\ \mu s$ (f) $t = 120\ \mu s$. The computations are made with $N_I = 250$ cells (solid line), $N_I = 500$ cells (dashed line), and $N_I = 750$ cells (dashed-dotted line).

In the temperature profiles of Figure 8.10 one cannot conclude anything about the effect of the

number of cells on the direction of the maximal temperature at the collapse time. This may come from the larger diffusion for $N_I = 250$ cells.

In the case of phase transition as in Figure 8.12, it is clear that the bubble vanishes in all cases. There are noticeable differences in other values as the number of cells is increased. This is effected by the diffusion of the interface, where in the case of $N_I = 250$ cells the bubble vanishes before the others and the concentration of the mass fraction after the collapse times is lower.

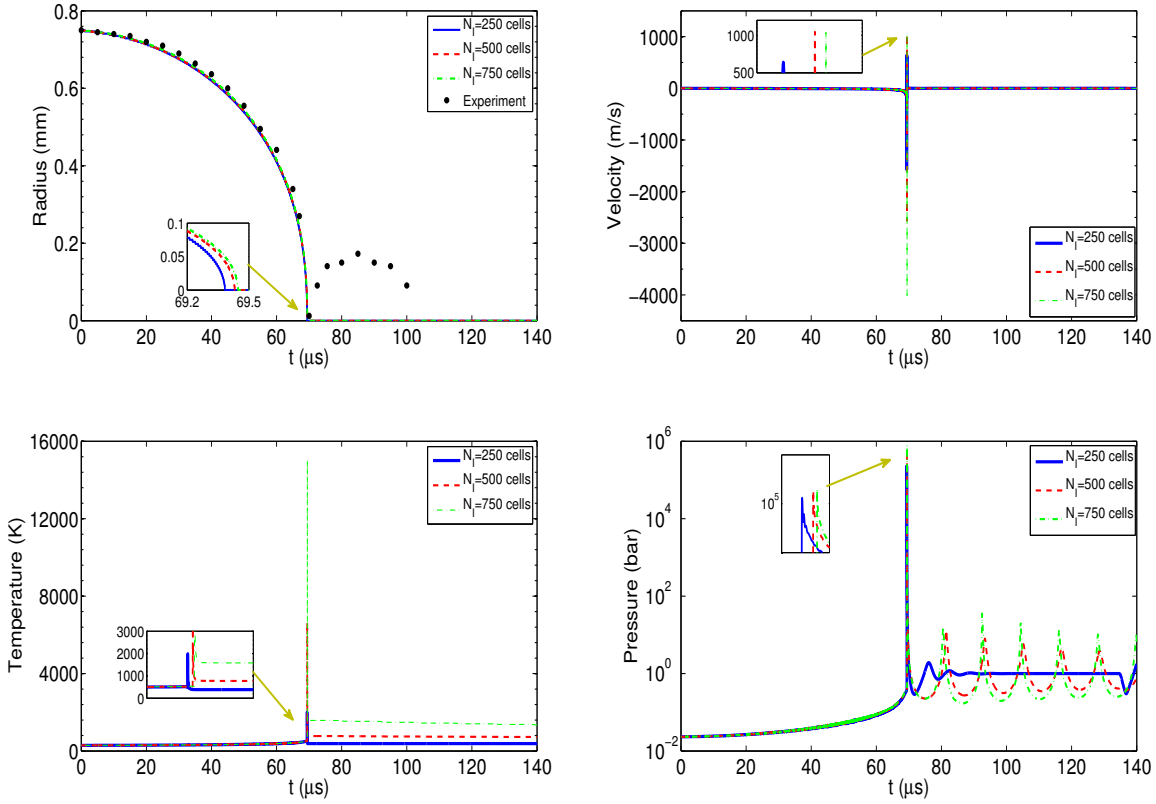

Figure 8.12: Vapor bubble with mass transfer, comparison between several grids. The computed radii are compared with the experimental data (dots). Initial values $T_v = 293$ K and $p_v = 2339$ Pa.

However, in both cases, i.e. with or without phase transition the diffusion of the interface has bad consequences on the results after the collapse point. A similar problem was also discussed in Müller et al. [32] for the Saurel and Abgrall model [44], i.e. the seven-equation model. In next tests to reduce the effects of diffusion we use a relatively high number of cells, we use $N_I = 500$ cells. In fact using high number of cells is expensive. Thus the issue of diffusion requires more investigation.

8.5.1.3 Effects of the initial values inside the bubble

Let us now study the effects of the initial values of the temperature and the pressure inside the bubble on its dynamics. First, we keep the temperature inside the bubble constant at $T_v = 293$ K and change the values of the pressure. The results for the case without mass transfer are shown in Figure 8.13. We see the following features in the results for the lower initial pressure: The collapse occurs earlier, the rebound is faster and more damped. Also the values of pressure, temperature and velocity are higher at the collapse point. If the phase transition is included the results are shown in Figure 8.14. For lower pressure the collapse occurs earlier with a higher temperature. The velocities and pressures are almost the same.

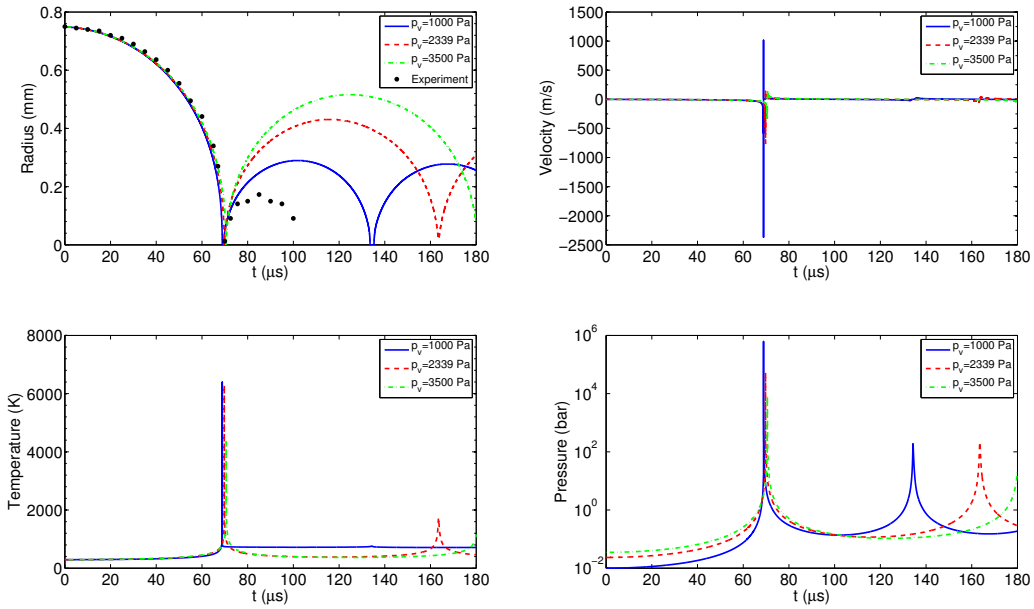

Figure 8.13: Vapor bubble without mass transfer, comparison between different initial bubble pressures at $T_v = 293$ K. The computed radii are compared with the experimental data (dots). The computations are made with $N_I = 500$ cells.

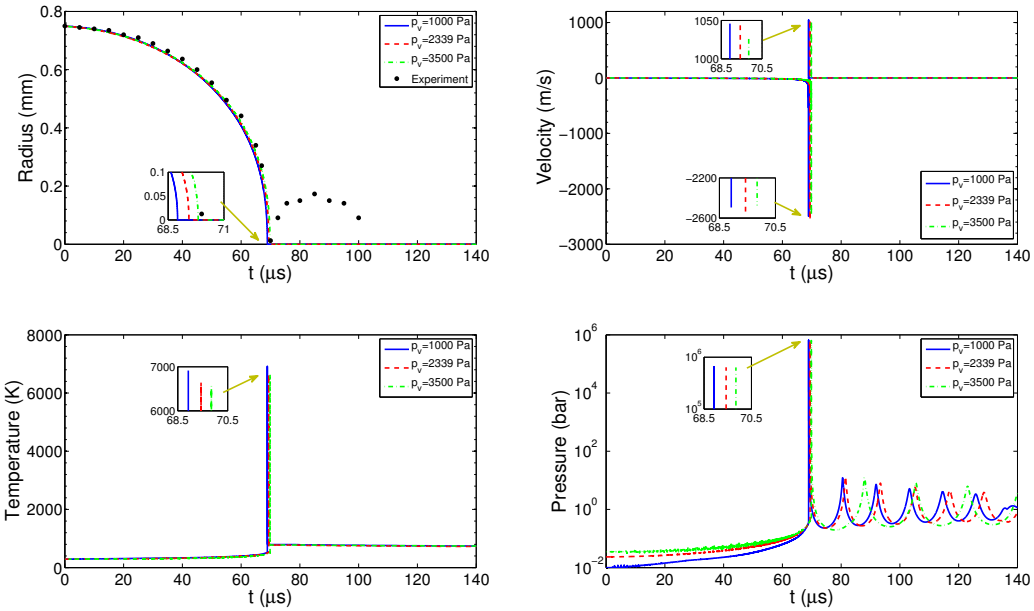

Figure 8.14: Vapor bubble with mass transfer, comparison between different initial bubble pressures at $T_v = 293$ K. The computed radii are compared with the experimental data (dots). The computations are made with $N_I = 500$ cells.

Second, we keep the initial pressure inside the bubble constant at $p_v = 2339$ Pa and change the temperature. The results are shown in Figure 8.15 with no mass transfer and in Figure 8.16 if the mass transfer is included. The differences between the curves in both figures are small. In both cases, it is noted that for the higher initial temperature the collapse is a little bit faster and the temperature at the center of the bubble at the collapse time is higher.

Whatever the initial state inside the bubble we can conclude the following results for the collapsing of the vapor bubble:

- There is no rebound of the bubble after the collapse if the mass transfer is included.
- In all cases at the collapse time the pressure and temperature at the bubble center jump to very high values. The high pressure shows the importance of considering compressibility for the surrounding water.
- Before the collapse time the curves for the radius of the bubble in all cases are coinciding. In addition, in this period there is a perfect agreement with the experimental data.
- The pressure and temperature inside the bubble before the collapse time when the mass transfer is included are less than those values with no mass transfer. This is due to the loss of energy by the phase transition process.
- In the cases of no mass transfer it is noted that the first collapse is much more violent than the second one.

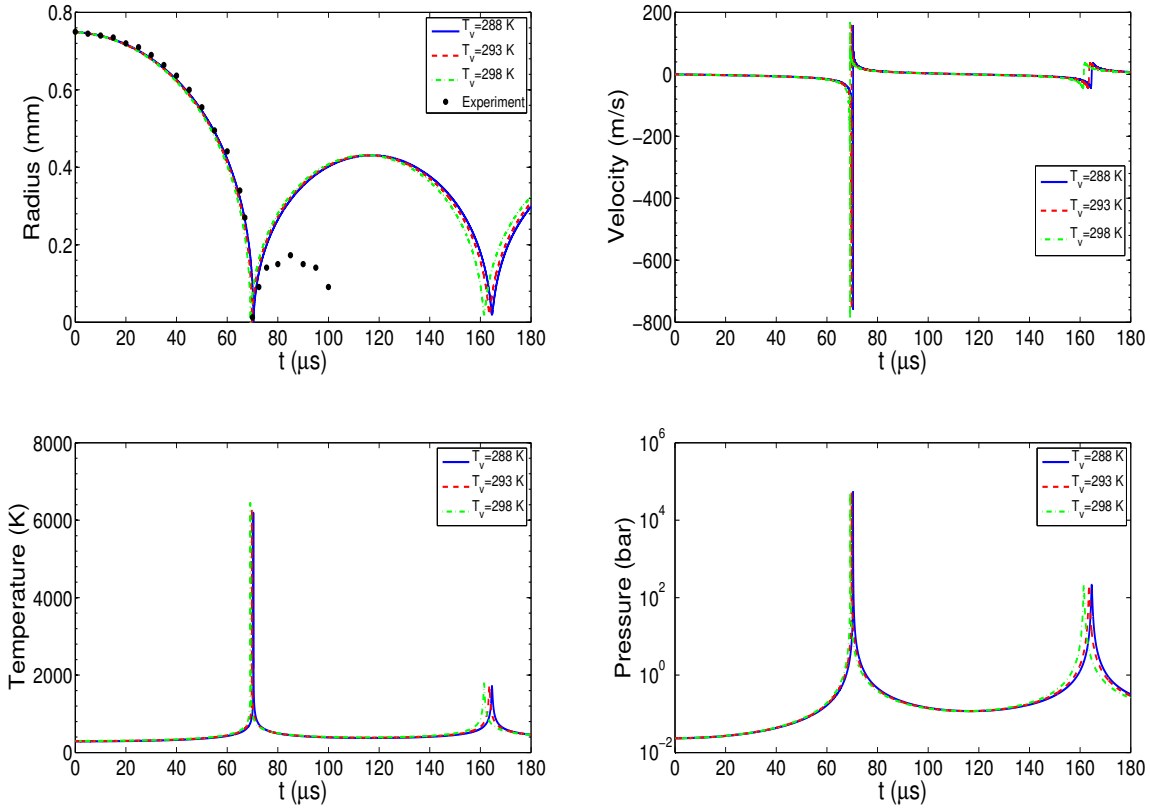

Figure 8.15: Vapor bubble without mass transfer, comparison between different initial bubble temperatures at $p_v = 2339$ Pa. The computed radii are compared with the experimental data (dots). The computations are made with $N_I = 500$ cells.

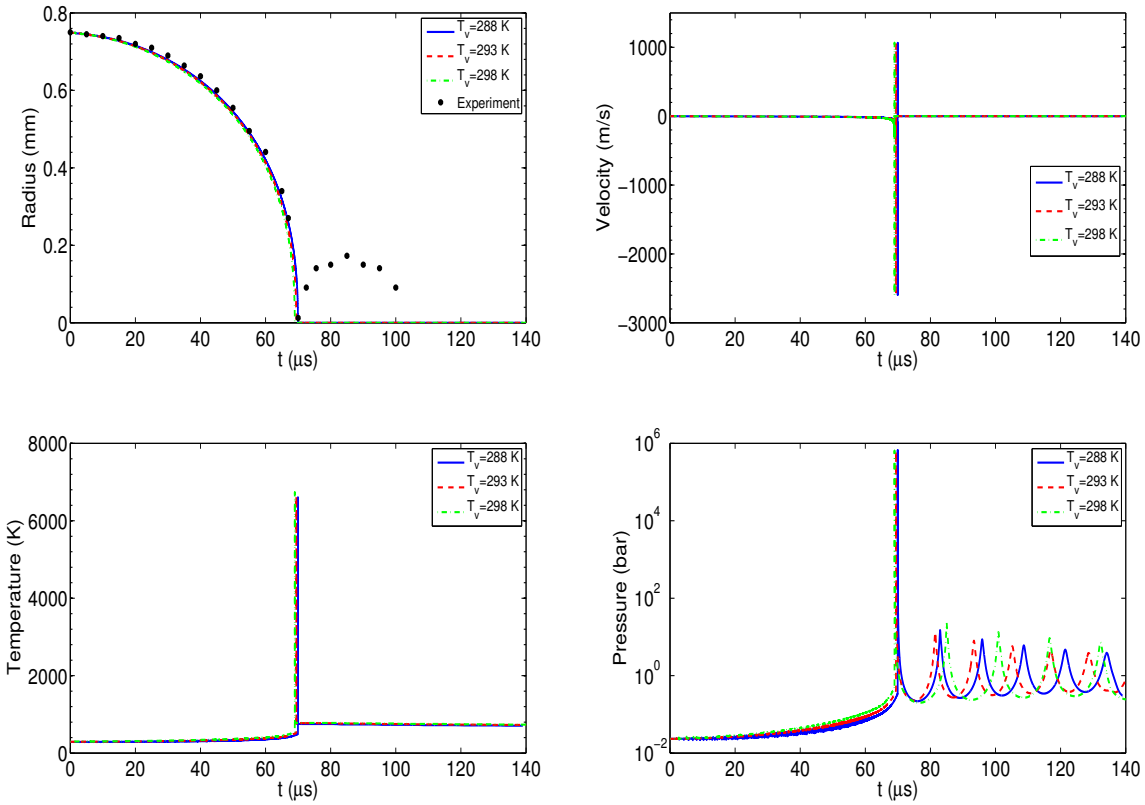

Figure 8.16: Vapor bubble with mass transfer, comparison between different initial bubble temperatures at $p_v = 2339$ Pa. The computed radii are compared with the experimental data (dots). The computations are made with $N_I = 500$ cells.

8.5.2 Tests for gas-vapor bubble

In the tests of this subsection, besides the vapor inside the bubble we assume a percentage of non-condensable gas. The existence of such a gas is justified physically, but its specific nature is not really known. As our aim is just to consider the general effect of the existence of such gas we use several assumptions. Following Dreyer et al. [13], Hydrogen H_2 and Oxygen O_2 are most probably present since they are the components of water and may be produced by the plasma due to the laser beam. Here we deal with both gases, i.e. Hydrogen or Oxygen.

We assume that the non-condensable gas obeys the SG-EOS, i.e. it obeys equations (8.3.1). For both Hydrogen and Oxygen we assume $\gamma = 1.4$, $\pi = 0$ and $q = 0$. For Hydrogen we use $C_v = 10.1$ kJ/kg/K. For Oxygen we take $C_v = 0.662$ kJ/kg/K.

8.5.2.1 A percentage of Hydrogen inside the bubble

Consider a saturation state inside the bubble at temperature $T = 293$ K, i.e. the pressure is $p = 2339$ Pa. Then, assume an initial 1% of Hydrogen mass inside the bubble. Always, for numerical reasons, we assume a small volume fraction of non-condensable gas outside the bubble, i.e. in the liquid water, typically 10^{-6}. The results with mass transfer are shown in Figure 8.17 for vapor and gas-vapor bubbles. The main feature of the results is that: *The bubble rebounds again after the collapse if it contains a non-condensable gas, whereas the bubble dies if it contains vapor only.* In fact, in the literature there are two different considerations of this experiment and the issue of rebound. For example, the numerical results of Akhatov et al. [1] show that the existence of non-condensable gas has a strong influence on the dynamics of the bubble. But in their results the rebound occurs even if the bubble contains vapor

only. A different consideration was proposed by Dreyer et al. [13]. It depends on some fundamental thermodynamic properties. Due to these the rebound of the bubble after the first collapse is possible only if there is a non-condensable gas inside the bubble. Our computational results confirm the ideas of Dreyer et al. [13]. However, this point requires more investigations.

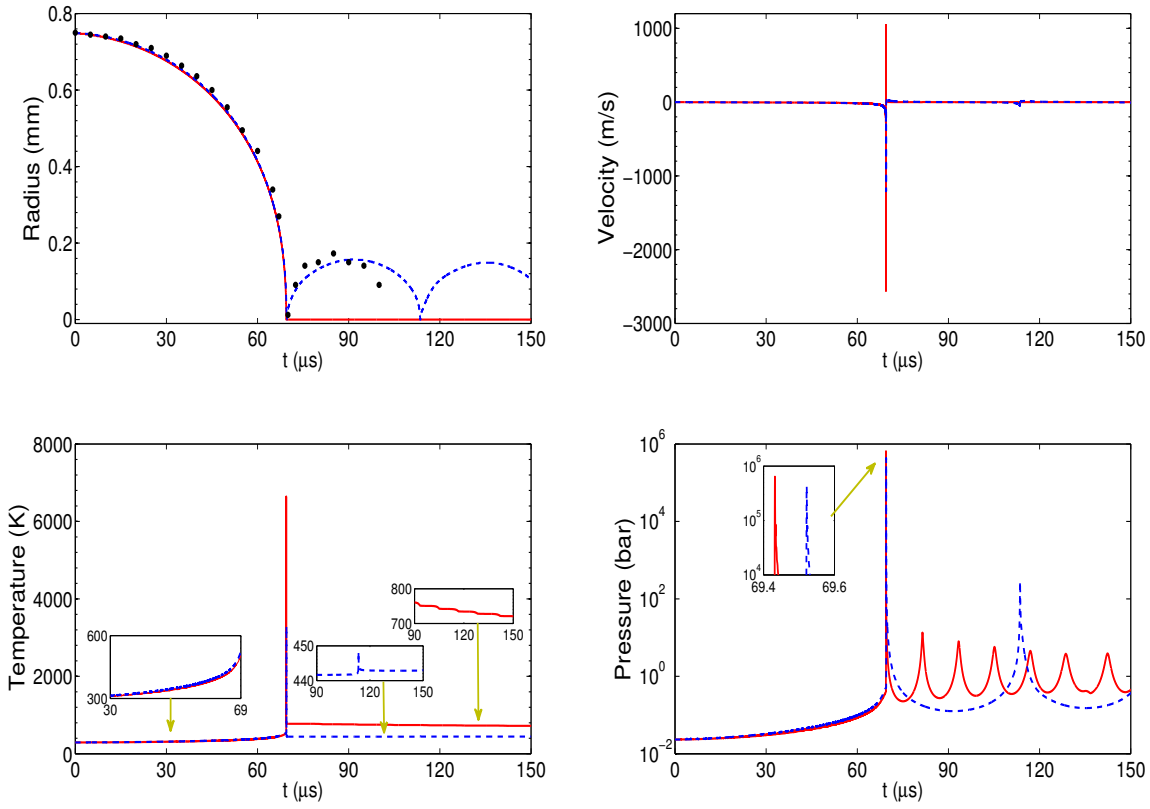

Figure 8.17: Bubble results with mass transfer, comparison between the results of vapor bubble (solid line) with gas-vapor bubble (dashed line). The computed radii are compared with the experimental data (dots). Computations are made with $N_I = 500$ cells, initial state inside the bubble: $T = 293$ K and $p = 2339$ Pa. The non-condensable gas is Hydrogen with a mass fraction of 1%.

It is clear from Figure 8.17 that the values of temperature, pressure and velocity are reduced for the gas-vapor bubble. Moreover, the temperature and pressure inside the bubble before the instant of collapse are smaller in the results of vapor bubble than those of gas-vapor bubble. Again we think this is physical since the action of the phase transition is stronger in the vapor bubble than in the gas-vapor bubble.

Figure 8.18 shows the results for a gas-vapor bubble using a different number of computational cells. The same previous conditions with a mass fraction of 1% of Hydrogen are used. We see in all cases that the bubble rebounds after the collapse. The differences in the curves are due to the diffusion of the interface especially through passing the collapse point, see the discussion in the previous subsection.

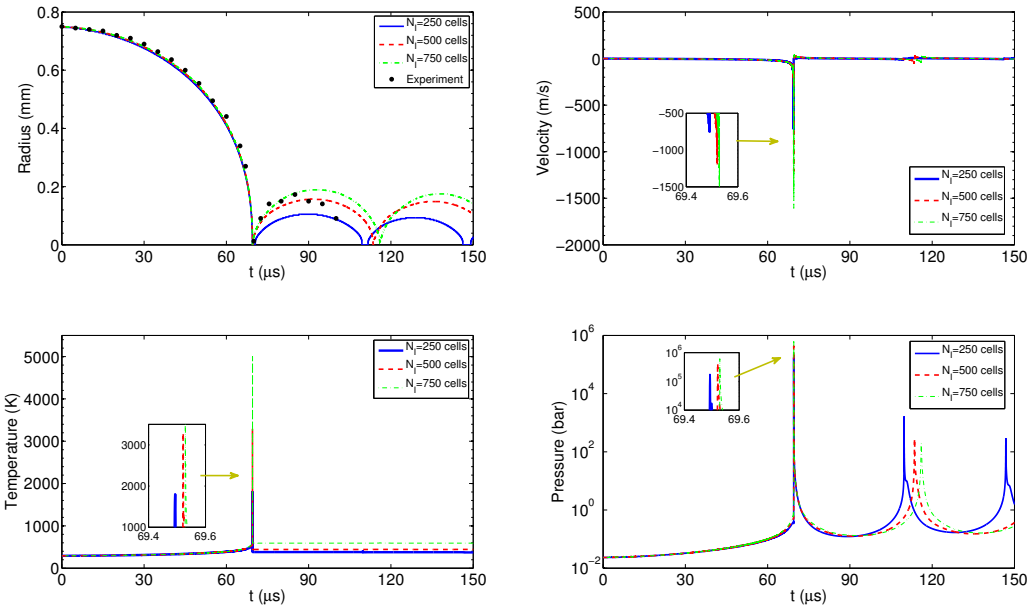

Figure 8.18: Gas-vapor bubble with mass transfer, comparison at different grids. The computed radii are compared with the experimental data (dots). Computations are made with $N_I = 500$ cells, initial state inside the bubble: $T = 293$ K and $p = 2339$ Pa. The non-condensable gas is Hydrogen with a mass fraction of 1%.

8.5.2.2 A percentage of Oxygen inside the bubble

For more validation consider the gas-vapor bubble with the same initial state except that instead of Hydrogen we assume Oxygen with a mass fraction of 2.2%. T

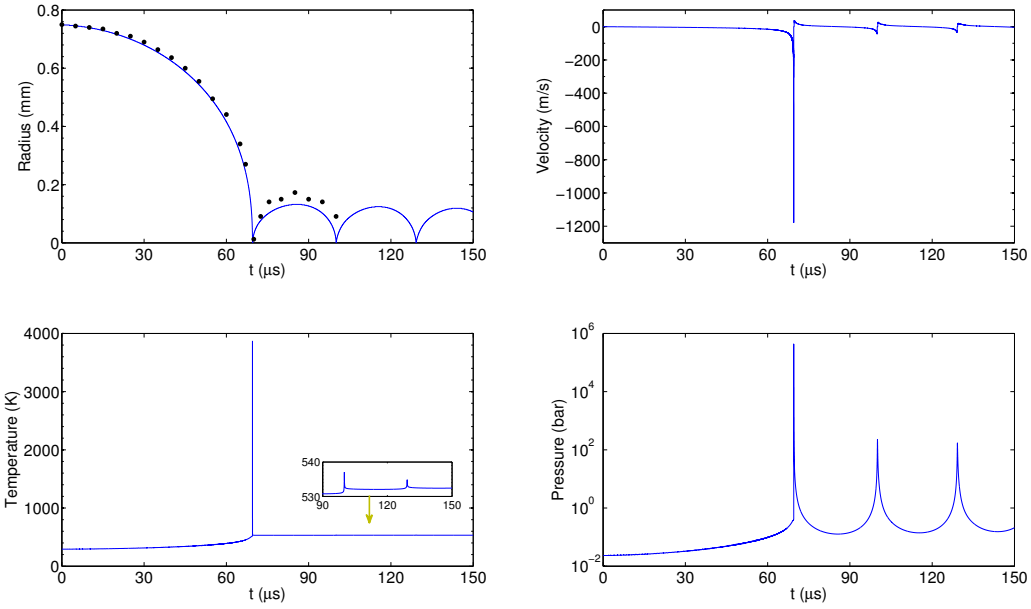

Figure 8.19: Gas-vapor bubble with mass transfer, the non-condensable gas is Oxygen with a mass fraction of 2.2%. The computed radii are compared with the experimental data (dots). Computations are made with $N_I = 500$ cells, initial state inside the bubble: $T = 293$ K and $p = 2339$ Pa.

he results are shown in Figure 8.19. To achieve this percentage we set the initial value of the volume fraction of the Oxygen to be 0.015. For the previous case of Hydrogen to get 1% of mass fraction we set the initial volume fraction to 0.1. These values depend on the values of heat capacity C_v since we keep the temperature constant.

Consider the same gas-vapor problem with Oxygen as a non-condensable gas with different percentages. This is shown in Figure 8.20. For the lower value of volume fraction we note that the maximum radius after the collapse is smaller and the center temperature is higher.

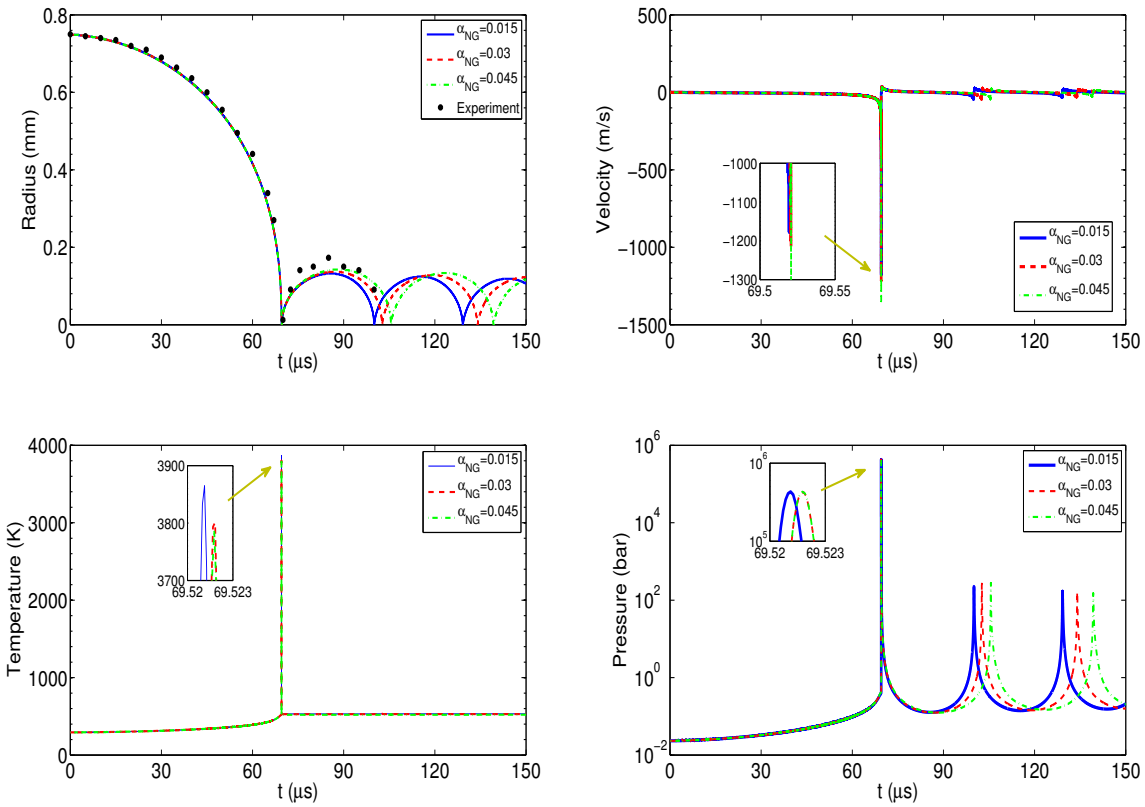

Figure 8.20: Gas-vapor bubble with mass transfer, the non-condensable gas is Oxygen with different percentages. The computed radii are compared with the experimental data (dots). Computations are made with $N_I = 500$ cells, initial state inside the bubble: $T = 293$ K and $p = 2339$ Pa. Note that NG stands for non-condensable gas.

8.5.2.3 More validation tests

In Figures 8.21 and 8.22 the solution of the problem is shown for different assumptions for the non-condensable gas, i.e. different values of the specific heat C_v. In Figure 8.21 the results are shown with an assumption of a 2% mass fraction for all gases. For Figure 8.22 the volume fraction is taken to be 0.045 for all gases. The results in Figure 8.22 are very close. Thus the equal initial volume fractions for different non-condensable gases give results not so far from each other. Moreover, we see during the computations that an assumption of a too small percentage for the non-condensable gas is insignificant for the rebound.

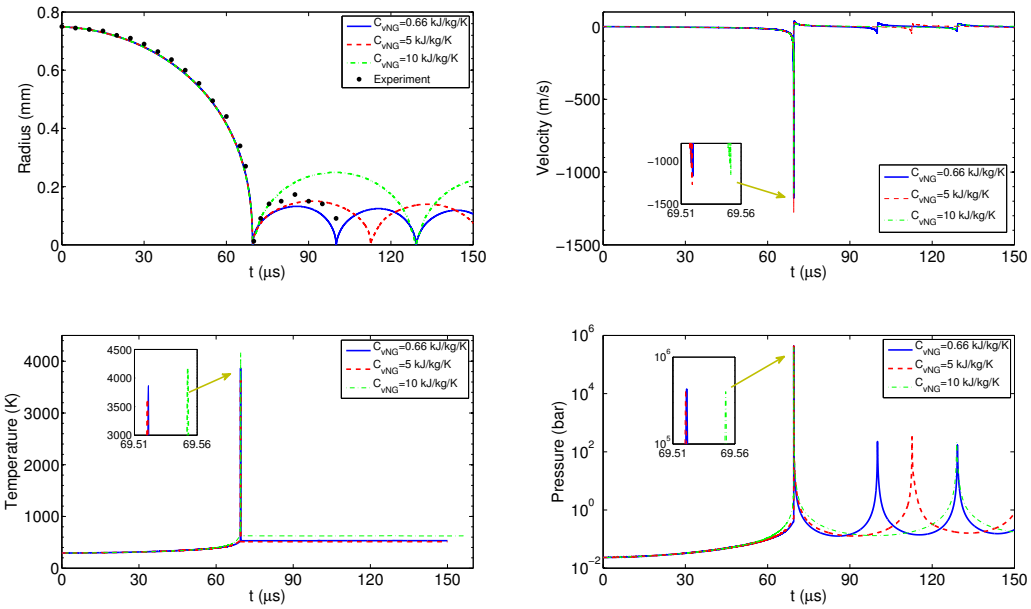

Figure 8.21: Gas-vapor bubble with mass transfer, different gases with percent 2% in mass. The computed radii are compared with the experimental data (dots). Computations are made with $N_I = 500$ cells, initial state inside the bubble: $T = 293$ K and $p = 2339$ Pa.

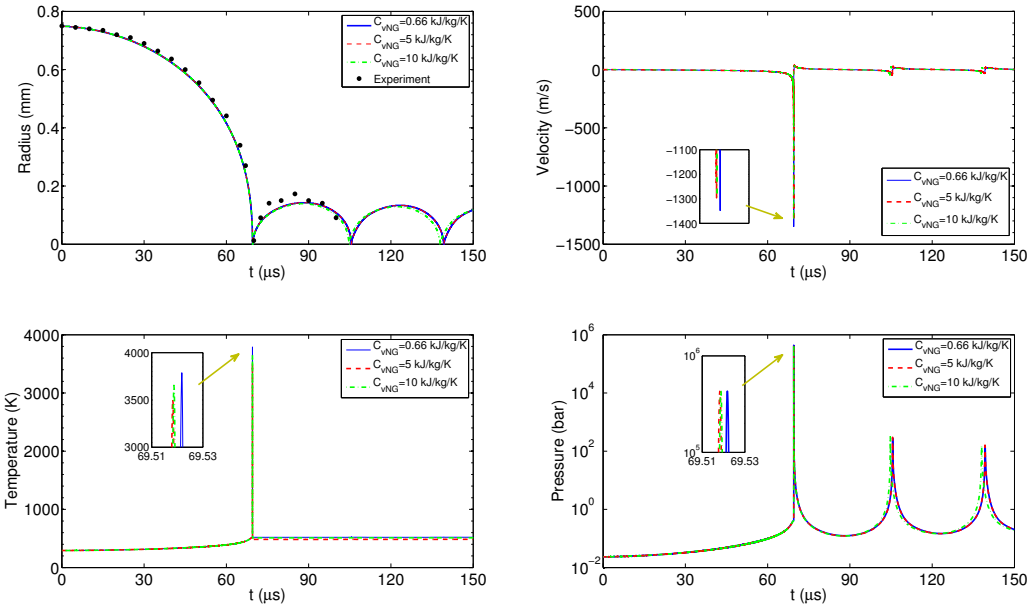

Figure 8.22: Gas-vapor bubble with mass transfer, different gases with initial volume fraction 0.045. The computed radii are compared with the experimental data (dots). Computations are made with $N_I = 500$ cells, initial state inside the bubble: $T = 293$ K and $p = 2339$ Pa.

We conclude the following results for the collapse of the gas-vapor bubble:

- The existence of sufficient amount of non-condensable gas is essential for the rebound after the collapse if the mass transfer is included.
- The behavior of the rebound depends on the percentage of the non-condensable gas and on the

nature of the gas.

For more validation we compute the maximum radius after the first collapse for several values of initial radius of the bubble. Then we compare these values with experimental data of Akhatov et al. [1]. For this test the initial temperature is assumed to be $T = 296$ K inside and outside the bubble with pressure inside the bubble $p = 2339$ Pa. For the non-condensable gas we assume $C_v = 5$ kJ/kg/K with 1.5% mass fraction. We choose this assumption for the heat capacity to be in the middle between the values of Hydrogen and Oxygen. The results are shown in Figure 8.23. It is clear that the computed results have the same tendency as the experimental ones. In Figure 8.24 detailed results for different initial radii are shown.

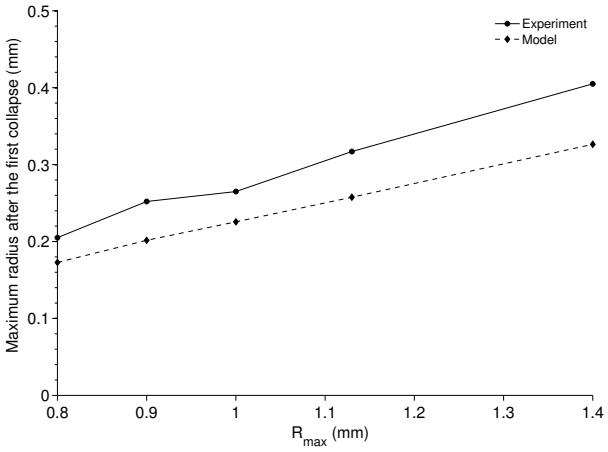

Figure 8.23: The initial bubble radius versus the maximum radius after the first collapse. Computations are made with uniform grid $\Delta r = 1.6 \times 10^{-6}$.

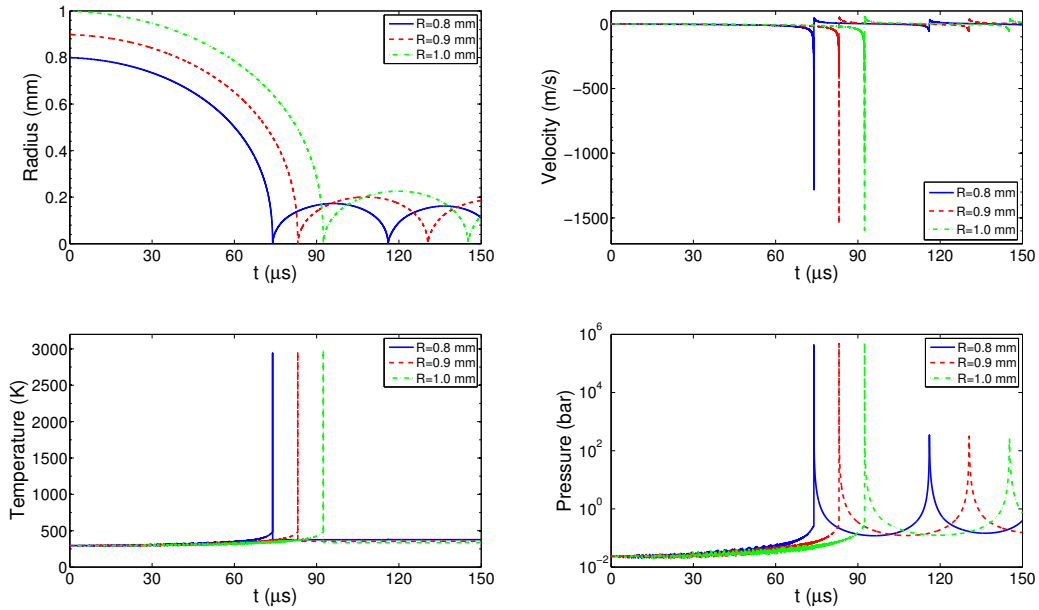

Figure 8.24: Gas-vapor bubble with mass transfer, different initial radii. Computations are made with uniform grid $\Delta r = 1.6 \times 10^{-6}$, initial state inside the bubble: $T = 296$ K and $p = 2339$ Pa.

8.6 Conclusion

A laser-induced cavitation bubble in liquid water has been investigated by using diffusive interface models. The vapor bubble is modeled by the six-equation model including heat and mass transfer which was modified in Zein et al. [61]. This model was extended in the paper to include the existence of a non-condensable gas inside the bubble, i.e. gas-vapor bubble.

To overcome the problem of negative squares of sound speed in computations, each fluid obeys its own equations of state as a pure fluid. The stiffened gas equations of state were used. We proposed new estimations for the parameters of these equations of state taking into account a wide range of temperature. These parameters are linked to each other in a way to recover the saturation curve.

The main result from the computations is that if the mass transfer is included then the rebound of the bubble after the collapse is only possible when a non-condensable gas presents inside the bubble.

The computations show a high pressure and temperature at the center of the bubble at the collapse. In addition, using phase transition reduces the pressure and temperature inside the bubble before the collapse point.

The diffusive interface may have bad effects on the results. This diffusion increases around the collapse point which has strong effects on the results after the collapse point. To avoid this problem in the computations we used a higher number of cells. For future work some adaptive discretization should be used to improve the capturing of the interface. Also, we plan to study the coupling between our approach here with the ideas of sharp interface modeling just around the collapse point. By this coupling we expect to collect the benefits of considering the phase transition as well as avoiding the problem of diffusion through the collapse.

In this paper we were interested in the general effect of the presence of a non-condensable gas. For future work the treatment using the non-condensable gas requires more investigation. Indeed, modeling the non-condensable gas with vapor as a mixture seems to be more physical.

8.A Appendix: Mathematical properties of the three-phase model

In order to investigate the mathematical properties of the model (8.2.8), without the redundant equation, we rewrite its hyperbolic part in terms of primitive variables as

$$\frac{\partial \mathbf{W}}{\partial t} + \mathbf{A}\frac{\partial \mathbf{W}}{\partial x} = 0, \tag{8.A.1}$$

where $\mathbf{W} = (\alpha_1, \alpha_2, \rho_1, \rho_2, \rho_3, u, p_1, p_2, p_3)$. The matrix $\mathbf{A}$ is given as

$$\mathbf{A} = \begin{bmatrix} u & 0 & 0 & 0 & 0 & 0 & 0 & 0 & 0 \\ 0 & u & 0 & 0 & 0 & 0 & 0 & 0 & 0 \\ 0 & 0 & u & 0 & 0 & \rho_1 & 0 & 0 & 0 \\ 0 & 0 & 0 & u & 0 & \rho_2 & 0 & 0 & 0 \\ 0 & 0 & 0 & 0 & u & \rho_3 & 0 & 0 & 0 \\ \frac{p_1-p_3}{\rho} & \frac{p_2-p_3}{\rho} & 0 & 0 & 0 & u & \frac{\alpha_1}{\rho} & \frac{\alpha_2}{\rho} & \frac{1-\alpha_1-\alpha_2}{\rho} \\ 0 & 0 & 0 & 0 & 0 & \rho_1 c_1^2 & u & 0 & 0 \\ 0 & 0 & 0 & 0 & 0 & \rho_2 c_2^2 & 0 & u & 0 \\ 0 & 0 & 0 & 0 & 0 & \rho_3 c_3^2 & 0 & 0 & u \end{bmatrix}.$$

The matrix $\mathbf{A}$ has real eigenvalues that are given by the following expressions

$$\begin{aligned} \lambda_1 &= \lambda_2 = ... = \lambda_7 = u, \\ \lambda_8 &= u + c, \\ \lambda_9 &= u - c. \end{aligned}$$

Here c is the mixture sound speed for the model and is expressed as

$$c^2 = \frac{\alpha_1\rho_1}{\rho}c_1^2 + \frac{\alpha_2\rho_2}{\rho}c_2^2 + \frac{\alpha_3\rho_3}{\rho}c_3^2.$$

The sound speeds c_k, $k = 1, 2, 3$, are defined by (8.2.3).

The corresponding right eigenvectors are

$$\mathbf{r}_1 = \begin{bmatrix} 0 \\ 0 \\ 0 \\ 0 \\ 0 \\ 0 \\ -\dfrac{\alpha_3}{\alpha_1} \\ 0 \\ 1 \end{bmatrix}, \quad \mathbf{r}_2 = \begin{bmatrix} 0 \\ 0 \\ 0 \\ 0 \\ 0 \\ 0 \\ -\dfrac{\alpha_2}{\alpha_1} \\ 1 \\ 0 \end{bmatrix}, \quad \mathbf{r}_3 = \begin{bmatrix} 0 \\ 0 \\ 0 \\ 0 \\ 1 \\ 0 \\ 0 \\ 0 \\ 0 \end{bmatrix}, \quad \mathbf{r}_4 = \begin{bmatrix} 0 \\ 0 \\ 0 \\ 1 \\ 0 \\ 0 \\ 0 \\ 0 \\ 0 \end{bmatrix}, \quad \mathbf{r}_5 = \begin{bmatrix} 0 \\ 0 \\ 1 \\ 0 \\ 0 \\ 0 \\ 0 \\ 0 \\ 0 \end{bmatrix}, \tag{8.A.2}$$

$$\mathbf{r}_6 = \begin{bmatrix} 0 \\ 1 \\ 0 \\ 0 \\ 0 \\ 0 \\ \dfrac{p_3 - p_2}{\alpha_1} \\ 0 \\ 0 \end{bmatrix}, \quad \mathbf{r}_7 = \begin{bmatrix} 1 \\ 0 \\ 0 \\ 0 \\ 0 \\ 0 \\ \dfrac{p_3 - p_1}{\alpha_1} \\ 0 \\ 0 \end{bmatrix}, \quad \mathbf{r}_8 = \begin{bmatrix} 0 \\ 0 \\ 1 \\ \rho_2/\rho_1 \\ \rho_3/\rho_1 \\ c/\rho_1 \\ c_1^2 \\ \rho_2 c_2^2/\rho_1 \\ \rho_3 c_3^2/\rho_1 \end{bmatrix}, \quad \mathbf{r}_9 = \begin{bmatrix} 0 \\ 0 \\ 1 \\ \rho_2/\rho_1 \\ \rho_3/\rho_1 \\ -c/\rho_1 \\ c_1^2 \\ \rho_2 c_2^2/\rho_1 \\ \rho_3 c_3^2/\rho_1 \end{bmatrix}, \tag{8.A.3}$$

Thus, the system (8.2.8) is non strictly hyperbolic.

References

[1] I. Akhatov, O. Lindau, A. Topolnikov, R. Mettin, N. Vakhitova, and W. Lauterborn. Collapse and rebound of a laser-induced cavitation bubble. *Phys. Fluids*, 13:2805-2819, 2003.

[2] N. Andrianov, R. Saurel, and G. Warnecke. A simple method for compressible multiphase mixtures and interfaces. *Int. J. Numer. Meth. Fluids*, 41:109-131, 2003.

[3] T. Barberon, Modélisation mathématique et numérique de la cavitation dans des écoulements multiphasiques compressibles, Ph.D. Thesis, Université de Toulon, 2002.

[4] T. Barberon and P. Helluy. Finite volume simulation of cavitating flows. Computers & Fluids 34:832-858, 2005.

[5] C. E. Brennen. *Cavitation and Bubble Dynamics*. Oxford University Press, 1995.

[6] E. A. Brujan, G. S. Keen, A. Vogel, and J. R. Blake. The final stage of the collapse of a cavitation bubble close to a rigid boundary. *Phys. fluids*, 14:85-92, 2002.

[7] G. Chen, C. Levermore, and T.P.Liu. Hyperbolic conservation laws with stiff? relaxation terms and entropy. *Comm. Pure. Appl. Math.*, 47:787-830, 1994.

[8] A. Chinnayya, E. Daniel, and R. Saurel. Modelling detonation waves in heterogeneous energetic materials. *J. Comput. Phys.*, 196(2):490-538, 2004.

[9] J. P. Cocchi, R. Saurel, and J. C. Loraud. Treatment of interface problems with Godunov-type schemes. *Shock Waves*, 5:347-357, 1996.

[10] S. F. Davis. Simplified second-order Godunov-type methods. *SIAM J. Sci. Statist. Comput.*,9:445-473, 1998.

[11] D. Drew. Mathematical modeling of two-phase flow. *Ann. Rev. Fluid Mech.*, 15:261-291, 1983.

[12] D. A. Drew and S. L. Passman. *Theory of multicomponent fluids*. Springer, 1998.

[13] W. Dreyer, F. Duderstadt, M. Hantke, and G. Warnecke. On phase change of a vapor bubble in liquid water. Technical report, WIAS Preprint No. 1424, 2009.

[14] J. P. Franc and J. M. Michel. *Fundamentals of Cavitation*. Springer Science and Business Media, Inc., 2005.

[15] S. Fujikawa and T. Akamatsu. Effects of the non-equilibrium condensation of vapor on the pressure wave produced by the collapse of a bubble in a liquid. *J. Fluid. Mech.*, 97:481-512, 1980.

[16] F. R. Gilmore. The growth or collapse of a spherical bubble in a viscous compressible liquid. Technical Report 26-4, Hydrodynamics Laboratory, California Institute of Technology, Pasadena, California, 1952.

[17] J. M. Hérard. An hyperbolic three phase flow model. CRAS Paris, I-342, 10:779-784, 2006.

[18] R. Hickling and M. Plesset. Collapse and rebound of a spherical bubble in water. *Phys. Fluids*, 7:7-14, 1964.

[19] M. Ishii and T. Hibiki. *Thermo fluid dynamics of two-phase flow*. Springer Science + Business Media, 2006.

[20] J. C. Isselin, A. P. Alloncle, and M. Autric. On laser induced single bubble near a solid boundary: Contribution to the understanding of erosion phenomena. *J. Appl. Phys.*, 84(10):5766-5771, 1998.

[21] V. Kamath and A. Prosperetti. Numerical integration methods in gas bubble dynamics. *J. Acoust. Soc. Am.*, 85:1538-1548, 1989.

[22] A. Kapila, R. Meniko?, J. Bdzil, S. Son, and D. Stewart. Two-phase modelling of DDT in granular materials: reduced equations. *Phys. Fluid*, 13:3002-3024, 2001.

[23] J. B. Keller and I. I. Kolodner. Damping of underwater explosion bubble oscillations. *J. Appl. Phys.*, 27:1152-1161, 1956.

[24] J. B. Keller and M. Miksis. Bubble oscillations of large amplitude. *J. Acoust. Soc. Am.*, 68:628-633, 1980.

[25] M. H. Lallemand, A. Chinnayya, and O. L. Metayer. Pressure relaxation procedures for multiphase compressible flows. *Int. J. Numer. Meth. Fluids*, 49(1):1-56, 2005.

[26] M. H. Lallemand and R. Saurel. Pressure relaxation procedures for multiphase compressible flows. Technical Report 4038, INRIA, 2000.

[27] W. Lauterborn. Numerical investigation of nonlinear oscillations of gas bubbles in liquids. *J. Acoust. Soc. Am.*, 59(2):283-293, 1976.

[28] W. Lauterborn, T. Kurz, C. Schencke, O. Lindau, and B. Wolfrum. Laser-induced bubbles in cavitation research. In Proceedings of the IUTAM Symposium on Free Surface Flows. Birmingham United Kingdom, 2000.

[29] O. Le Metayer, J. Massoni, and R. Saurel. Elaborating equations of state of a liquid and its vapor for two-phase flow models (in french). *Int. J. Thermal Sci.*, 43(3):265-276, 2004.

[30] R. Menikoff and B.J. Plohr, The Riemann problem for fluid flow of real materials. *Rev. Mod. Phys.*, 61(1):75-130, 1989.

[31] M. J. Moran and H. N. Shapiro. *Fundamentals of Engineering Thermodynamics*. John Wiley & sons, Inc., fourth edition, 2000.

[32] S. Müller, M. Bachmann, D. Kröninger, Th. Kurz and Ph. Helluy, Comparison and validation of compressible flow simulations of laser-induced cavitation bubbles, Computers & Fluids. 38:1850-1862, 2009.

[33] S. Müller, Ph. Helluy, J. Ballmann, Numerical Simulation of Cavitation Bubbles by Compressible Two-Phase Fluids. Int. J. Fluid Mech., 2009, doi:10.1002/fld.2033.

[34] A. Murrone and H. Guillard. A five-equation reduced model for compressible two-phase flow problems. *J. Comput. Phys.*, 202(2):664-698, 2005.

[35] R. I. Nigmatulin, I. S. Akhatov, N. K. Vakhitova, and R. T. Lahey. On the forced oscillations of a small gas bubble in a spherical liquid filled flask. *J. Fluid Mech.*, 414:47-73, 2000.

[36] R. I. Nigmatulin and N. S. Khabeev. Heat exchange between a gas bubble and a liquid. *rdquo Izv. Akad. Nauk SSSR, Mekh. Zhidk. Gaza*, 5, 1974.

[37] R. Oldendourg. *Properties of water and steam in SI-units*. Springer, 1989.

[38] F. Petitpas, E. Franquet, R. Saurel, and O. L. Metayer. A relaxation-projection method for compressible flows. Part II: Artificial heat exchanges for multiphase shocks. *J. Comput. Phys.*, 225(2):2214-2248, 2007.

[39] F. Petitpas, J. Massoni, R. Saurel, E. Lapebie, and L. Munier. Diffuse interface models for high speed cavitating underwater systems. *Int. J. Multiphase Flows*, 35(8):747-759, 2009.

[40] A. Philipp, W. Lauterborn, Cavitation erosion by single laser-produced bubbles, *J. Fluid. Mech.* 361, 75-116 (1998).

[41] A. Prosperetti, L. A. Crum, and K. W. Commander. Nonlinear bubble dynamics. *J. Acoust. Soc. Am.*, 83:502-514, 1988.

[42] A. Prosperetti and A. Lezzi. Bubble dynamics in a compressible liquid. part 1. first order theory. *J. Fluid Mech.*, 168:457-478, 1986.

[43] L. Rayleigh. On the pressure developed in a liquid during the collapse of a spherical cavity. *Phil. Mag.*, 34:94-98, 1917.

[44] R. Saurel and R. Abgrall. A multiphase Godunov method for compressbile multifluid and multiphase flows. *J. Comput. Phys.*, 150(2):425-467, 1999.

[45] R. Saurel and R. Abgrall. A simple method for compressible multifluid flows. *SIAM J. Sci. Comput.*, 21:1115-1145, 1999.

[46] R. Saurel, S. Gavrilyuk, and F. Renaud. A multiphase model with internal degree of freedom, application to shock-bubble interaction. *J. Fluid. Mech.*, 495:283-321, 2003.

[47] R. Saurel and O. Le Metayer. A multiphase model for interfaces, shocks, detonation waves and cavitation. *J. Fluid Mech.*, 431:239-271, 2001.

[48] R. Saurel, O. Le Metayer, J. Massoni, and S. Gavrilyuk. Shock jump relations for multiphase mixtures with stiff? mechanical properties. *Shock waves*, 16:209-232, 2007.

[49] R. Saurel, F. Petitpas, and R. Abgrall. Modelling phase transition in metastable liquids: application to cavitating and flashing flows. *J. Fluid. Mech.*, 607:313-350, 2008.

[50] R. Saurel, F. Petitpas, and R. A. Berry. Simple and efficient relaxation methods for interfaces separating compressible fluids, cavitating flows and shocks in multiphase mixtures. *J. Comput. Phys.*, 228(5):1678-1712, 2009.

[51] G. H. Schnerr, I. H. Sezal, and S. J. Schmidt. Numerical investigation of three dimensional cloud cavitation with special emphasis on collapse induced shock dynamics. *Phys. Fluids*, 20(4):040703, 2008.

[52] S. Sochard, A. Wilhem, and H. Delmas. Modeling of free radical production in a collapsing gas-vapour bubble. Ultrason. Sonochem, 4:77-84, 1997.

[53] W. D. Song, M. H. Hong, B. Lukyanchuk, and T. C. Chong. Laser-induced cavitation bubbles for cleaning of solid surfaces. *J. Appl. Phys.*, 95(6):2952-2956, 2004.

[54] R.E. Sonntag and C. Borgnakke, *Introduction to Engineering Thermodynamics*, John Wiley and Sons, Inc., 2001

[55] G. Strang. On the construction and comparison of difference schemes. *SIAM J. Num. Anal.*, 5:506-517, 1968.

[56] Y. Tomita and A. Shima. On the behavior of a spherical bubble and the impulse pressure in a viscous compressible liquid. Bull. JSME, 20:1453-1460, 1977.

[57] E.F. Toro, *Riemann solvers and numerical methods for fluid dynamics*, Springer, Berlin, 1999.

[58] L. Trilling. The collapse and rebound of a gas bubble. *J. Appl. Phys.*, 23:14-17, 1952.

[59] C. W. Wang, T. G. Liu, and B. C. Khoo. A real-ghost fluid method for the simulation of multi-medium compressible flow. *SIAM J. Sci. Computing*, 28:278-302, 2006.

[60] K. Yasui. Effects of thermal conduction on bubble dynamics near the sonoluminescence threshold. *J. Acoust. Soc. Amer.*, 98(5):2772-2782, 1995.

[61] A. Zein, M. Hantke, and G. Warnecke. Modeling phase transition for compressible two-phase flows applied to metastable liquids. *J. Comput. Phys.*, 229(8):2964-2998, 2010.

[62] R. Zhao, Z. c. Liang, R. q. Xu, J. Lu, and X. w Ni. Dynamics of laser-induced cavitation bubble near solid boundary. *Jpn. J. Appl. Phys.*, 47(7):5482-5485, 2008.

Chapter 9

Closure conditions for multi-component models

Bibliographic note: The content of this chapter is published in [H13]: Siegfried Müller, Maren Hantke, and Pascal Richter. Closure conditions for non-equilibrium multi-component models, *Continuum Mech. Thermodyn.* (2016). 28:1157.

Abstract: A class of non-equilibrium models for compressible multi-component fluids in multi-dimensions is investigated taking into account viscosity and heat conduction. These models are subject to the choice of interfacial pressures and interfacial velocity as well as relaxation terms for velocity, pressure, temperature and chemical potentials. Sufficient conditions are derived for these quantities that ensure meaningful physical properties such as a non-negative entropy production, thermodynamical stability, Galilean invariance as well as mathematical properties such as hyperbolicity, subcharacteristic property and existence of an entropy-entropy flux pair. For the relaxation of chemical potentials a two-component and a three-component model for vapor-water and gas-water-vapor, respectively, is considered.

9.1 Introduction

Flows of compressible multi-component fluids, where the single components may be in the liquid or the gas phase, respectively, have a wide range of applications. Difficulties in the modeling result from the interaction of the fluids, especially from the exchange of mass and energy across the phase interfaces. So the treatment of the phase interfaces is in the focus of the modeling.

Our particular interest is on a two-phase flow where we consider one liquid phase and one gaseous phase. The liquid phase is assumed to consist of one species. The gaseous phase may consist of $K-1$ species where one of these species is the same as in the liquid phase but in a different aggregate state. To model this flow we use a K component model where in each point all $K-1$ species are present with one species in both aggregate states. Only a species that is present in both aggregate states can undergo a phase change. Typical applications are evaporation and drying processes as can be observed in daily live, e.g. cooking pot or puddle, or formation of clouds. A technical application is the spherical collapse of a laser-induced bubble at elevated temperatures to investigate the influence of the amount of non-condensable gas inside the bubble, see [21, 42, 46].

In the literature several models are available that are distinguished in sharp interface and diffuse interface models. A detailed survey of these models can be found in Zein [44]. Here our interest is on multi-component fluids derived from an ensemble averaging procedure of Drew [12]. A comprehensive introduction to these models can be found in the classical book of Drew and Passman [13].

Baer and Nunziato [5] proposed a two-phase model for detonation waves in granular explosives. This model is a full non-equilibrium model, which means, each component has its own pressure, velocity and temperature and is governed by its own set of fluid equations. It was modified and generalized by several authors. For instance, Saurel and Abgrall [38] also included relaxation terms for the pressure and the velocities of the components. By instantaneous relaxation procedures equilibrium values for the pressure and the velocity can be found. Using further relaxation procedures to drive the temperatures and the

chemical potentials into equilibrium mass transfer between the phases can be modeled, see Abgrall et al. [36, 41] or Zein et al. [45].

There are simplified models available in the literature that can be derived from the above general model by assuming zero relaxation times, see [25]. Typically these are classified by the number of equations in case of *two* phases in *one* space dimension. For instance, a *six-equation model* with a single velocity is derived by assuming a zero velocity relaxation time. Assuming zero relaxation time for both the velocity and the pressure a *five-equation model* with mechanical equilibrium, i.e., single velocity and single pressure, is deduced in the asymptotic limit. The *four-equation model* has a single velocity, single pressure and also single temperature coinciding with the single-fluid reactive Euler equations. While the *three-equation model* is the system of Euler equations. It has single velocity, pressure, temperature, and also single chemical potential, i.e., it is in full equilibrium. A detailed discussion of these models is beyond the scope of this work. For this purpose the interested reader is referred to [44] and the references cited therein.

Typically reduced models suffer from some short-comings. For instance, conservation of energy might be violated or the system looses its hyperbolicity. Therefore we prefer a full non-equilibrium model taking into account viscosity and heat conduction. For this purpose we consider a general class of non-equilibrium models that is a generalization of the three-phase model investigated by Hérard, see Remark 7 in [23]. For instance, the Saurel-Abgrall approach [38] fits into this class.

Characteristic for models based on ensemble averaging is the problem to close the set of equations, i.e., find appropriate interfacial pressures and interfacial velocity as well as relaxation terms for velocity, pressure, temperature and chemical potentials. Since the closing procedure is not unique, there is some freedom left for modeling. However, a reasonable model that is acceptable from a physical point of view has to be consistent with the fundamental principles of thermodynamics, e.g., the second law of thermodynamics. Besides this there are also constraints from a mathematical point of view that are related to existence and uniqueness of solutions to the model, e.g., the existence of entropy-entropy flux pairs. When it comes to the numerical solution additional properties are helpful for the design of appropriate schemes, e.g., the hyperbolicity of the transport operator or the sub-characteristic condition. The objective of this paper is to derive constraints for the closing terms such that the aforementioned physical, analytical and numerical properties hold for the non-equilibrium multi-component model. Similar investigations have been performed in case of two-phase models [3, 16, 37, 44] and three-phase models [7, 23]. Here we do not confine ourselves to two and three components but on an arbitrary number of components. Drew and Passmann [13] consider multi-component fluids from a physical point of view but do not investigate analytical and numerical properties of the models.

The paper is organized as follows. In Section 9.2 we introduce the non-equilibrium multi-component model and derive the model for the mixture as well the model at equilibrium. Then we rewrite these models in terms of primitive quantities in Section 9.3. Neglecting viscosity and heat conduction some mathematical properties of the models are investigated. In particular, we verify hyperbolicity and the sub-characteristic condition, see Section 9.4. Furthermore, a physical meaningful model should be Galilean invariant. This is investigated in Section 9.5. In Section 9.6 we are concerned with the entropies corresponding to the non-equilibrium model and the mixture model. From the 2nd law of thermodynamics we derive constraints for the definition of the interfacial velocity and pressures. In Section 9.7 we introduce the relaxation terms for mechanical and thermal relaxation as well as relaxation of chemical potentials. In particular, we verify that they are in agreement with the 2nd law of thermodynamics.

9.2 Mathematical model

First of all, we describe the full non-equilibrium model and then derive from this the mixture model and the equilibrium model.

9.2.1 Non-equilibrium model

The multi-component flow is described by a non-equilibrium model where all components are present in each point of the space-time continuum. Each component $k = 1, \dots, K$ has density ρ_k, velocity $\boldsymbol{v}_k$ and pressure p_k, The amount of each component is determined by its volume fraction α_k. The volume

fractions are related by the saturation constraint

$$\sum_{k=1}^{K} \alpha_k = 1, \quad \alpha_k \in (0,1). \tag{9.2.1}$$

In analogy to the three-phase model of Hérard [23] the fluid equations for each component can be written as

$$\partial_t (\alpha_k \rho_k) + \nabla \cdot (\alpha_k \rho_k \boldsymbol{v}_k) = S_{\alpha\rho,k}, \tag{9.2.2}$$

$$\partial_t (\alpha_k \rho_k \boldsymbol{v}_k) + \nabla \cdot (\alpha_k \rho_k \boldsymbol{v}_k \boldsymbol{v}_k^T + \alpha_k p_k \boldsymbol{I}) = - \sum_{l=1}^{K} P_{k,l} \nabla \alpha_l + \nabla \cdot (\alpha_k \boldsymbol{T}_k) + \boldsymbol{S}_{\alpha\rho\boldsymbol{v},k}, \tag{9.2.3}$$

$$\partial_t (\alpha_k \rho_k E_k) + \nabla \cdot (\alpha_k \rho_k \boldsymbol{v}_k (E_k + p_k/\rho_k)) = - \sum_{l=1}^{K} P_{k,l} \boldsymbol{V}_I \cdot \nabla \alpha_l + \nabla \cdot (\alpha_k (\boldsymbol{v}_k \cdot \boldsymbol{T}_k - \boldsymbol{q}_k)) + S_{\alpha\rho E,k}, \tag{9.2.4}$$

taking into account viscosity and heat conduction via the stress tensor $\boldsymbol{T}_k$ and the heat flux $\boldsymbol{q}_k$, but neglecting effects due to surface tension and gravity. In our notation $E_k = e_k + \boldsymbol{v}_k^2/2$ is the total specific energy with e_k the specific internal energy of component k. There may be other contributions to be accounted for, see [13], p. 68 ff and 144 ff. In particular, the term $P_{k,l}$ accounts for different pressures at the phase interface. Without loss of generality we may assume

$$P_{k,k} = 0. \tag{9.2.5}$$

Otherwise we replace $P_{k,l}$ by $P_{k,l} - P_{k,k}$ due to the saturation condition (9.2.1). The interfacial velocity is denoted by $\boldsymbol{V}_I$. Obviously, the equations cannot be written in conservative form. Finally, the fluid equations are supplemented by an equation of state

$$p_k = p_k(\rho_k, e_k) \quad \text{resp.} \quad e_k = e_k(\rho_k, p_k) \tag{9.2.6}$$

for each of the components.

The evolution of the volume fractions is characterized by the non-conservative equation

$$\partial_t \alpha_k + \boldsymbol{V}_I \cdot \nabla \alpha_k = S_{\alpha,k}, \ k = 1, \ldots, K. \tag{9.2.7}$$

Due to the saturation condition (9.2.1) we only need $K-1$ equations. Without loss of generality we express α_K by the other volume fractions, i.e.,

$$\alpha_K = 1 - \sum_{k=1}^{K-1} \alpha_k, \ \nabla \alpha_K = - \sum_{k=1}^{K-1} \nabla \alpha_k, \ S_{\alpha,K} = - \sum_{k=1}^{K-1} S_{\alpha,k}. \tag{9.2.8}$$

The source terms $S_{\alpha,k}$, $S_{\rho,k}$, $\boldsymbol{S}_{\rho\boldsymbol{v},k}$ and $S_{\rho E,k}$ on the right-hand sides of (9.2.2), (9.2.3), (9.2.4) and (9.2.7) describe the relaxation process due to mass, momentum, energy transfer and volume fraction between the different components corresponding to the relaxation of velocity, pressure, temperature and chemical potentials, $\xi \in \{v, p, T, \mu\}$, i.e.,

$$S_{\alpha,k} := \sum_{\xi} S_{\alpha,k}^{\xi}, \ S_{\alpha\rho,k} := \sum_{\xi} S_{\alpha\rho,k}^{\xi}, \ \boldsymbol{S}_{\alpha\rho\boldsymbol{v},k} := \sum_{\xi} \boldsymbol{S}_{\alpha\rho\boldsymbol{v},k}^{\xi}, \ S_{\alpha\rho E,k} := \sum_{\xi} S_{\alpha\rho E,k}^{\xi}. \tag{9.2.9}$$

These depend on the specific components at hand discussed in Section 9.7.

So far, the model is not yet closed. For this purpose, we have to find closing conditions for the pressures $P_{k,l}$, the interfacial velocity $\boldsymbol{V}_I$ and the relaxation terms $S_{\alpha,k}$, $S_{\alpha\rho,k}$, $\boldsymbol{S}_{\alpha\rho\boldsymbol{v},k}$ and $S_{\alpha\rho E,k}$. In the following sections we will derive appropriate constraints. However, these will not specify a unique model but some options are still remaining for the choice of the interfacial velocity, the relaxation terms, the stress tensor and the heat conduction.

9.2.2 Mixture model

From the non-equilibrium model we can derive the equations for the mixture. For this purpose we introduce the mixture quantities

$$p := \sum_{k=1}^{K} \alpha_k \, p_k, \;\; \rho := \sum_{k=1}^{K} \alpha_k \, \rho_k, \;\; \boldsymbol{v} := \frac{1}{\rho} \sum_{k=1}^{K} \alpha_k \, \rho_k \, \boldsymbol{v}_k, \tag{9.2.10}$$

for pressure, density and velocity. Accordingly, we define the specific internal energy, the specific total energy and the specific total enthalpy of the mixture as

$$e := \frac{1}{\rho} \sum_{k=1}^{K} \alpha_k \, \rho_k \, e_k, \;\; E := \frac{1}{\rho} \sum_{k=1}^{K} \alpha_k \, \rho_k \, E_k, \;\; H := \frac{1}{\rho} \sum_{k=1}^{K} \alpha_k \, \rho_k H_k = E + \frac{p}{\rho} \tag{9.2.11}$$

with $H_k := E_k + p_k/\rho_k$ the total enthalpy of component k. The stress tensor and the heat flux of the mixture are determined by

$$\boldsymbol{T} := \sum_{k=1}^{K} \alpha_k \boldsymbol{T}_k, \;\; \boldsymbol{q} := \sum_{k=1}^{K} \alpha_k \boldsymbol{q}_k. \tag{9.2.12}$$

In order to ensure conservation of mass, momentum and energy of the mixture the relaxation terms (9.2.9) have to satisfy the conservation constraints

$$\sum_{k=1}^{K} S^{\xi}_{\alpha,k} = 0, \quad \sum_{k=1}^{K} S^{\xi}_{\alpha\rho,k} = 0, \quad \sum_{k=1}^{K} \boldsymbol{S}^{\xi}_{\alpha\rho\boldsymbol{v},k} = \boldsymbol{0}, \quad \sum_{k=1}^{K} S^{\xi}_{\alpha\rho E,k} = 0 \tag{9.2.13}$$

for each relaxation type $\xi \in \{v, p, T, \mu\}$. In addition, we need that the interfacial pressures satisfy

$$P_l := \sum_{k=1}^{K} P_{k,l} \equiv P = const \quad \forall l = 1, \ldots, K. \tag{9.2.14}$$

Then by summation of the single-component fluid equations (9.2.2), (9.2.3), (9.2.4) and employing the saturation constraint (9.2.1) as well as the conservation constraints (9.2.13) and (9.2.14) we obtain

$$\partial_t \, \rho + \nabla \cdot \, (\rho \, \boldsymbol{v}) = 0, \tag{9.2.15}$$

$$\partial_t \, (\rho \, \boldsymbol{v}) + \nabla \cdot \, (\rho \, \boldsymbol{v} \, \boldsymbol{v}^T + p \, \boldsymbol{I}) = \nabla \cdot \, \boldsymbol{T} - \nabla \cdot \left(\sum_{k=1}^{K} \alpha_k \, \rho_k \, (\boldsymbol{v} - \boldsymbol{v}_k) \, (\boldsymbol{v} - \boldsymbol{v}_k)^T \right), \tag{9.2.16}$$

$$\partial_t \, (\rho \, E) + \nabla \cdot \, (\rho \, \boldsymbol{v} \, (E + p/\rho)) = \nabla \cdot \, (\boldsymbol{v} \cdot \boldsymbol{T} - \boldsymbol{q}) - \nabla \cdot \left(\sum_{k=1}^{K} \alpha_k \, \boldsymbol{T}_k \, (\boldsymbol{v}_k - \boldsymbol{v}) \right) - \nabla \cdot \left(\sum_{k=1}^{K} \alpha_k \, \rho_k \, (H_k - H) \, (\boldsymbol{v}_k - \boldsymbol{v}) \right). \tag{9.2.17}$$

We note that there are contributions corresponding to the slip between the mixture velocity $\boldsymbol{v}$ and the velocities of the components $\boldsymbol{v}_k$. In the multi-component model of Drew and Passman these terms are added to the mixture stress tensor and the mixture heat flux, see [13], p. 82-83. In contrast to the non-equilibrium model, the mixture model is in conservative form if and only if the conditions (9.2.13) and (9.2.14) hold.

9.2.3 Equilibrium model

If the relaxation processes are much faster than the transport and dissipation effects, then the fluid can be considered to be at equilibrium. This state is characterized by vanishing relaxation terms, i.e.,

$$S_{\alpha,k} = 0, \;\; S_{\alpha\rho,k} = 0, \;\; \boldsymbol{S}_{\alpha\rho\boldsymbol{v},k} = \boldsymbol{0}, \;\; S_{\alpha\rho E,k} = 0. \tag{9.2.18}$$

At equilibrium the velocities, pressures and temperatures coincide, i.e.,

$$\boldsymbol{v}_1 = \ldots = \boldsymbol{v}_K = \boldsymbol{v},\ p_1 = \ldots = p_K = p,\ T_1 = \ldots = T_K = T, \tag{9.2.19}$$

and the chemical potentials of reacting components are equal. In particular, for the interfacial pressures and interfacial velocity it holds

$$P_{k,l} = p,\ k \neq l, \quad \boldsymbol{V}_I = \boldsymbol{v}. \tag{9.2.20}$$

Then the mixture model (9.2.15), (9.2.16) and (9.2.17) reduces to the the equilibrium model

$$\partial_t \rho + \nabla \cdot (\rho \boldsymbol{v}) = 0, \tag{9.2.21}$$
$$\partial_t (\rho \boldsymbol{v}) + \nabla \cdot (\rho \boldsymbol{v}\, \boldsymbol{v}^T + p\, \boldsymbol{I}) = \nabla \cdot \boldsymbol{T}, \tag{9.2.22}$$
$$\partial_t (\rho E) + \nabla \cdot (\rho \boldsymbol{v}\, (E + p/\rho)) = \nabla \cdot (\boldsymbol{v} \cdot \boldsymbol{T} - \boldsymbol{q}). \tag{9.2.23}$$

Note that by definition (9.2.10) and (9.2.12) the mixture pressure p, the mixture stress tensor $\boldsymbol{T}$ and the mixture heat flux $\boldsymbol{q}$ depend on the volume fractions α_k. These are determined by the algebraic conditions (9.2.18) and (9.2.19), e.g., [31, 45].

9.3 Primitive variables

For the verification of some physical and mathematical properties it will be helpful to rewrite the systems of equations for the non-equilibrium, mixture and the equilibrium model in terms of primitive quantities

9.3.1 Non-equilibrium model

By means of the system (9.2.2), (9.2.3), (9.2.4) and (9.2.7) we derive evolution equations for the density ρ_k, the velocity $\boldsymbol{v}_k$ and the pressure p_k for each component k. Inserting the evolution equation for the volume fraction (9.2.7) into the continuity equation (9.2.2) we obtain

$$\partial_t \rho_k + \frac{\rho_k}{\alpha_k} (\boldsymbol{v}_k - \boldsymbol{V}_I) \cdot \nabla \alpha_k + \boldsymbol{v}_k \cdot \nabla \rho_k + \rho_k \nabla \cdot \boldsymbol{v}_k = \frac{1}{\alpha_k} (S_{\alpha\rho,k} - \rho_k S_{\alpha,k}). \tag{9.3.1}$$

From the momentum equation (9.2.3) we deduce with (9.2.2) Cauchy's equation of motion

$$\begin{aligned} &\partial_t \boldsymbol{v}_k + (\nabla \boldsymbol{v}_k)\, \boldsymbol{v}_k + \frac{1}{\rho_k} \nabla p_k + \frac{p_k}{\alpha_k \rho_k} \nabla \alpha_k = \\ &\frac{1}{\alpha_k \rho_k} \left(- \sum_{l=1}^{K} P_{k,l} \nabla \alpha_l + \nabla \cdot (\alpha_k \boldsymbol{T}_k) \right) + \frac{1}{\alpha_k \rho_k} (\boldsymbol{S}_{\alpha\rho\boldsymbol{v},k} - S_{\alpha\rho,k} \boldsymbol{v}_k). \end{aligned} \tag{9.3.2}$$

Here the gradient of the velocity is defined as $\nabla \boldsymbol{v}_k = (\nabla v_{k,1}, \ldots, \nabla v_{k,d})^T$. Then we immediately obtain the evolution equation for the kinetic energy $u_k := \boldsymbol{v}_k^2/2$

$$\begin{aligned} &\partial_t u_k + \boldsymbol{v}_k \cdot (\nabla \boldsymbol{v}_k\, \boldsymbol{v}_k) + \frac{1}{\rho_k} \boldsymbol{v}_k \cdot \nabla p_k + \frac{p_k}{\alpha_k \rho_k} \boldsymbol{v}_k \cdot \nabla \alpha_k = \\ &\frac{1}{\alpha_k \rho_k} \boldsymbol{v}_k \cdot \left(- \sum_{l=1}^{K} P_{k,l} \nabla \alpha_l + \nabla \cdot (\alpha_k \boldsymbol{T}_k) \right) + \frac{1}{\alpha_k \rho_k} \boldsymbol{v}_k \cdot (\boldsymbol{S}_{\alpha\rho\boldsymbol{v},k} - S_{\alpha\rho,k} \boldsymbol{v}_k). \end{aligned} \tag{9.3.3}$$

Since the total energy is composed of the internal energy and the kinetic energy, we derive the evolution equation for the internal energy $e_k = E_k - u_k$ from the energy equation (9.2.4), where we employ (9.2.2) and (9.3.3). Finally we obtain

$$\begin{aligned} \partial_t e_k + \boldsymbol{v}_k \cdot (\nabla e_k) = &\frac{1}{\alpha_k \rho_k} \sum_{l=1}^{K} P_{k,l} (\boldsymbol{v}_k - \boldsymbol{V}_I) \cdot \nabla \alpha_l - \frac{p_k}{\rho_k} \nabla \cdot \boldsymbol{v}_k + \\ &\frac{1}{\rho_k} \sum_{i,l=1}^{d} \frac{\partial v_{k,l}}{\partial x_i} (\boldsymbol{T}_k)_{l,i} - \frac{1}{\alpha_k \rho_k} \nabla \cdot (\alpha_k \boldsymbol{q}_k) + \frac{1}{\alpha_k \rho_k} S_{e,k} \end{aligned} \tag{9.3.4}$$

with the relaxation term

$$S_{e,k} := S_{\alpha\rho E,k} - \boldsymbol{v}_k \cdot \boldsymbol{S}_{\alpha\rho\boldsymbol{v},k} + S_{\alpha\rho,k}(u_k - e_k). \tag{9.3.5}$$

Next we derive the evolution equation for the pressure p_k. For this purpose we first note that for any equation of state (9.2.6) the following relation holds

$$dp_k = (\partial p_k/\partial \rho_k)\, d\rho_k + (\partial p_k/\partial e_k)\, de_k. \tag{9.3.6}$$

By means of the continuity equation (9.3.1) and the energy equation (9.3.4) we then derive from (9.3.6)

$$\begin{aligned} &\partial_t p_k + \sum_{l=1,l\neq k}^{K} \frac{\rho_k}{\alpha_k} C_{k,l}^2 (\boldsymbol{v}_k - \boldsymbol{V}_I) \cdot \nabla \alpha_l + \boldsymbol{v}_k \cdot \nabla p_k + \rho_k c_k^2 \nabla \cdot \boldsymbol{v}_k = \\ &(\partial p_k/\partial e_k) \left(\frac{1}{\rho_k} \sum_{i,l=1}^{d} \frac{\partial v_{k,l}}{\partial x_i} (\boldsymbol{T}_k)_{l,i} - \frac{1}{\alpha_k \rho_k} \nabla \cdot (\alpha_k \boldsymbol{q}_k) \right) + \frac{1}{\alpha_k \rho_k} S_{p,k} \end{aligned} \tag{9.3.7}$$

with the relaxation term

$$S_{p,k} := \rho_k (\partial p_k/\partial \rho_k)\, (S_{\alpha\rho,k} - \rho_k S_{\alpha,k}) + (\partial p_k/\partial e_k)\, S_{e,k}. \tag{9.3.8}$$

Here the interfacial sound speed and the phase sound speed are defined as

$$C_{k,l}^2 := -\left((\partial p_k/\partial e_k) P_{k,l}/\rho_k^2 + (\partial p_k/\partial \rho_k) \right),\ c_k^2 := \partial p_k/\partial \rho_k + p_k/\rho_k^2 (\partial p_k/\partial e_k). \tag{9.3.9}$$

9.3.2 Mixture model

Similar to the non-equilibrium model we derive evolution equations for the mixture quantities ρ, $\boldsymbol{v}$, e and p defined by (9.2.10) and (9.2.11) from the evolution equations (9.2.15), (9.2.16) and (9.2.17). First of all, we determine Cauchy's equation of motion from the momentum equation (9.2.16) where we use the continuity equation (9.2.15) and the constraint (9.2.14):

$$\begin{aligned} &\partial_t \boldsymbol{v} + (\nabla \boldsymbol{v})\, \boldsymbol{v} + \frac{1}{\rho} \nabla p = \\ &\frac{1}{\rho} \nabla \cdot \boldsymbol{T} - \frac{1}{\rho} \sum_{l=1}^{K} P_l \nabla \alpha_l - \frac{1}{\rho} \nabla \cdot \sum_{k=1}^{K} \alpha_k \rho_k (\boldsymbol{v}_k - \boldsymbol{v})(\boldsymbol{v}_k - \boldsymbol{v})^T. \end{aligned} \tag{9.3.10}$$

Since definition (9.2.11) of the mixture energy e implies that $\rho e = \sum_{k=1}^{K} \alpha_k \rho_k e_k$, we obtain by (9.3.4) and (9.2.2) the evolution equation for the internal energy

$$\begin{aligned} &\partial_t e + \boldsymbol{v} \cdot \nabla e + \frac{1}{\rho} \sum_{k=1}^{K} \alpha_k p_k \nabla \cdot \boldsymbol{v}_k = \frac{1}{\rho} \sum_{l,k=1}^{K} P_{k,l} (\boldsymbol{v}_k - \boldsymbol{V}_I) \cdot \nabla \alpha_l \\ &-\frac{1}{\rho} \sum_{k=1}^{K} \alpha_k \rho_k e_k (\boldsymbol{v}_k - \boldsymbol{v}) + \frac{1}{\rho} \sum_{k=1}^{K} \sum_{i,l=1}^{d} \frac{\partial v_{k,l}}{\partial x_i} \alpha_k (\boldsymbol{T}_k)_{l,i} - \frac{1}{\rho} \nabla \cdot \boldsymbol{q} \\ &-\frac{1}{\rho} \sum_{k=1}^{K} (\boldsymbol{v}_k \cdot \boldsymbol{S}_{\alpha\rho\boldsymbol{v},k} - S_{\alpha\rho,k} u_k). \end{aligned} \tag{9.3.11}$$

Finally we determine the evolution equation for the mixture pressure p. Applying the time derivative to the definition (9.2.10) of p and using (9.2.7) and (9.3.7) we obtain

$$\begin{aligned} &\partial_t p + \boldsymbol{v} \cdot \nabla p + \rho c^2 \nabla \cdot \boldsymbol{v} = \\ &-\sum_{k=1}^{K} \rho_k \sum_{l=1,l\neq k}^{K} C_{k,l}^2 (\boldsymbol{v}_k - \boldsymbol{V}_I) \cdot \nabla \alpha_l - \sum_{k=1}^{K} \alpha_k (\boldsymbol{v} \cdot \nabla (p_k - p)) \\ &+(\boldsymbol{v}_k - \boldsymbol{v}) \cdot \nabla p_k - \sum_{k=1}^{K} \alpha_k \rho_k c_k^2 \nabla \cdot (\boldsymbol{v}_k - \boldsymbol{v}) + \sum_{k=1}^{K} \left(p_k S_{\alpha,k} + \frac{1}{\rho_k} S_{p,k} \right) \\ &+\sum_{k=1}^{K} \frac{1}{\rho_k} (\partial p_k/\partial e_k) \left(\alpha_k \sum_{i,l=1}^{d} \frac{\partial v_{k,l}}{\partial x_i} (\boldsymbol{T}_k)_{i,l} - \nabla \cdot (\alpha_k \boldsymbol{q}_k) \right). \end{aligned} \tag{9.3.12}$$

Here the sound speed of the mixture is defined as

$$c^2 := \frac{1}{\rho} \sum_{k=1}^{K} \alpha_k \, \rho_k \, c_k^2. \tag{9.3.13}$$

9.3.3 Equilibrium model

In case of the equilibrium model the evolution equations for the primitive variables can be directly determined from those of the mixture model where we make use of the equilibrium assumptions (9.2.18), (9.2.19) and (9.2.20) and the saturation condition (9.2.1). Then Cauchy's equation of motion reads

$$\partial_t \, \boldsymbol{v} + (\nabla \, \boldsymbol{v}) \, \boldsymbol{v} + \frac{1}{\rho} \nabla \, p = \frac{1}{\rho} \nabla \cdot \boldsymbol{T}. \tag{9.3.14}$$

The energy equation reduces to

$$\partial_t \, e + \boldsymbol{v} \cdot \nabla \, e + \frac{p}{\rho} \nabla \cdot \boldsymbol{v} = \frac{1}{\rho} \sum_{i,l=1}^{d} \frac{\partial \, v_l}{\partial \, x_i} (\boldsymbol{T})_{l,i} - \frac{1}{\rho} \nabla \cdot \boldsymbol{q}. \tag{9.3.15}$$

Finally the pressure equation becomes

$$\begin{aligned} &\partial_t \, p + \boldsymbol{v} \cdot \nabla \, p + \rho c^2 \nabla \cdot \boldsymbol{v} = \\ &\qquad \sum_{k=1}^{K} \frac{1}{\rho_k} (\partial p_k / \partial e_k) \left(\alpha_k \sum_{i,l=1}^{d} \frac{\partial \, v_l}{\partial \, x_i} (\boldsymbol{T}_k)_{i,l} - \nabla \cdot (\alpha_k \boldsymbol{q}_k) \right). \end{aligned} \tag{9.3.16}$$

9.4 Mathematical properties: hyperbolicity and sub-characteristic condition

Neglecting viscosity and heat conduction as well as relaxation processes in the fluid equations introduced in Section 9.2 the models reduce to first order systems describing transport effects only. Therefore these systems should be hyperbolic. This ensures that all wave speeds are finite and the system may be locally decoupled. From a mathematical point of view, this property is helpful in the construction of Riemann solvers. Therefore we determine the eigenvalues and eigenvectors corresponding to the non-equilibrium model. From a numerical point of view the relation between the eigenvalues of the non-equilibrium and the equilibrium model are of special interest. We conclude this section with a note on the symmetrization of the hyperbolic system.

9.4.1 Non-equilibrium model

Starting point are the evolution equations for the primitive variables (9.2.7), (9.3.1) , (9.3.2) and (9.3.7). The corresponding first order system then reads

$$\partial_t \, \alpha_k + \sum_{i=1}^{d} V_{I,i} \, \frac{\partial \, \alpha_k}{\partial \, x_i} = 0 \tag{9.4.1}$$

$$\partial_t \, \rho_k + \sum_{i=1}^{d} \left(\frac{\rho_k}{\alpha_k} \, (v_{k,i} - V_{I,i}) \, \frac{\partial \, \alpha_k}{\partial \, x_i} + v_{k,i} \, \frac{\partial \, \rho_k}{\partial \, x_i} + \rho_k \, \frac{\partial \, v_{k,i}}{\partial \, x_i} \right) = 0, \tag{9.4.2}$$

$$\partial_t \, \boldsymbol{v}_k + \sum_{i=1}^{d} \left(v_{k,i} \, \frac{\partial \, \boldsymbol{v}_k}{\partial \, x_i} + \sum_{l=1, l \neq k}^{K} \frac{1}{\alpha_k \, \rho_k} (P_{k,l} - p_k) \, \boldsymbol{e}_{i,d} \, \frac{\partial \, \alpha_l}{\partial \, x_i} + \frac{1}{\rho_k} \, \boldsymbol{e}_{i,d} \, \frac{\partial \, p_k}{\partial \, x_i} \right) = \boldsymbol{0}, \tag{9.4.3}$$

$$\partial_t \, p_k + \sum_{i=1}^{d} \left(v_{k,i} \, \frac{\partial \, p_k}{\partial \, x_i} + \sum_{l=1, l \neq k}^{K} \frac{\rho_k}{\alpha_k} \, C_{k,l}^2 \, (v_{k,i} - V_{I,i}) \, \frac{\partial \, \alpha_l}{\partial \, x_i} + \rho_k \, c_k^2 \, \frac{\partial \, v_{k,i}}{\partial \, x_i} \right) = 0, \tag{9.4.4}$$

where $\boldsymbol{e}_{i,d} \in \mathbb{R}^d$ denotes the unit vector in the ith coordinate direction. In order to characterize hyperbolicity of this system we consider its projection onto normal direction $\xi := \boldsymbol{x} \cdot \boldsymbol{n}$ for arbitrary unit direction $\boldsymbol{n} \in \mathbb{R}^d$. Introducing the vector of primitive variables

$$\boldsymbol{w} = (\alpha_1, \ldots, \alpha_{K-1}, \boldsymbol{w}_1^T, \ldots, \boldsymbol{w}_K^T)^T, \ \boldsymbol{w}_k = (\rho_k, \boldsymbol{v}_k^T, p_k)^T \tag{9.4.5}$$

the projected system can be written in quasi-conservative form as

$$\partial_t \boldsymbol{w} + \boldsymbol{B}_n(\boldsymbol{w}) \frac{\partial \boldsymbol{w}}{\partial \xi} = \boldsymbol{0}. \tag{9.4.6}$$

The matrix $\boldsymbol{B}_n$ is determined by the block matrix

$$\boldsymbol{B}_n := \sum_{i=1}^{d} \boldsymbol{B}_i \, n_i = \begin{pmatrix} V_{I,n} \, \boldsymbol{I}_{K-1} & & \\ \boldsymbol{A}_{1,n} & \boldsymbol{B}_{1,n} & \\ \vdots & & \ddots \\ \boldsymbol{A}_{K,n} & & \boldsymbol{B}_{K,n} \end{pmatrix}, \tag{9.4.7}$$

with the blocks defined as

$$\boldsymbol{A}_{k,n} := \begin{pmatrix} \frac{\rho_k}{\alpha_k} \, (v_{k,n} - V_{I,n}) \, (\boldsymbol{e}_{k,K-1}^T (1 - \delta_{k,K}) - \boldsymbol{1}_{K-1}^T \, \delta_{k,K}) \\ \boldsymbol{n} \boldsymbol{\beta}_k^T \\ \frac{\rho_k}{\alpha_k} \, (v_{k,n} - V_{I,n}) \, \boldsymbol{\gamma}_k^T \end{pmatrix}, \tag{9.4.8}$$

$$\boldsymbol{B}_{k,n} := \begin{pmatrix} v_{k,n} & \rho_k \, \boldsymbol{n}^T & 0 \\ \boldsymbol{0}_d & v_{k,n} \, \boldsymbol{I}_d & \frac{1}{\rho_k} \, \boldsymbol{n} \\ 0 & \rho_k \, c_k^2 \boldsymbol{n}^T & v_{k,n} \end{pmatrix}. \tag{9.4.9}$$

Here $\boldsymbol{e}_{k,K-1}$ is the kth unit vector in $\mathbb{R}^{K-1}$. In particular, we make the convention $\boldsymbol{e}_{K,K-1} = \boldsymbol{0}$. Furthermore, $\boldsymbol{I}_d$ and $\boldsymbol{I}_{K-1}$ are the unit matrices in $\mathbb{R}^{d \times d}$ and $\mathbb{R}^{(K-1)\times(K-1)}$, respectively, and $\boldsymbol{0}_d$ and $\boldsymbol{1}_{K-1}$ are vectors in $\mathbb{R}^d$ and $\mathbb{R}^{(K-1)}$ with value 0 or 1, respectively. The vectors $\boldsymbol{\beta}_k$ and $\boldsymbol{\gamma}_k$ are defined by their components $l = 1, \ldots, K-1$ as

$$\beta_{k,l} := \frac{1}{\alpha_k \rho_k} \left((P_{k,l} - p_k)(1 - \delta_{k,l}) - (P_{k,K} - p_k)(1 - \delta_{k,K}) \right), \tag{9.4.10}$$

$$\gamma_{k,l} := C_{k,l}^2 (1 - \delta_{k,l}) - C_{k,K}^2 (1 - \delta_{k,K}) \tag{9.4.11}$$

with $\delta_{k,l}$ the Kronecker symbol. The normal components of the velocities and the interfacial velocity are defined as

$$v_{k,n} := \boldsymbol{v}_k \cdot \boldsymbol{n}, \quad V_{I,n} := \boldsymbol{V}_I \cdot \boldsymbol{n}. \tag{9.4.12}$$

Obviously, the eigenvalues of the matrix (9.4.7) can now be easily computed where we employ the block structure:

$$\det(\boldsymbol{B}_n - \lambda \, \boldsymbol{I}) = \det(V_{n,I} \, \boldsymbol{I}_{K-1} - \lambda \, \boldsymbol{I}_{K-1}) \prod_{k=1}^{K} \det(\boldsymbol{B}_{k,n} - \lambda \, \boldsymbol{I}_{d+2}) = 0 \tag{9.4.13}$$

Since the matrices $\boldsymbol{B}_{k,n}$ coincide with those in case of a single-phase fluid, we then compute

$$\det(\boldsymbol{B}_{k,n} - \lambda \, \boldsymbol{I}_{d+2}) = (v_{k,n} - \lambda)^d \left((v_{k,n} - \lambda)^2 - c_k^2 \right) \tag{9.4.14}$$

Hence we obtain the following eigenvalues:

$$\lambda_{I,k} = V_{I,n}, \ k = 1, \ldots, K-1 \tag{9.4.15}$$

$$\lambda_{k,i} = v_{k,n}, \ k = 1, \ldots, K, \ i = 1, \ldots, d \tag{9.4.16}$$

$$\lambda_{k,\pm} = v_{k,n} \pm c_k, \ k = 1, \ldots, K. \tag{9.4.17}$$

Motivated by the block structure of the matrix $\boldsymbol{B}_n$ we make the following ansatz for computing the corresponding left and right eigenvectors

$$\boldsymbol{R}_n := \begin{pmatrix} \boldsymbol{R}^0_{I,n} & & & \\ \boldsymbol{R}^1_{I,n} & \boldsymbol{R}_{1,n} & & \\ \vdots & & \ddots & \\ \boldsymbol{R}^K_{I,n} & & & \boldsymbol{R}_{K,n} \end{pmatrix}, \quad \boldsymbol{L}_n := \begin{pmatrix} \boldsymbol{L}^0_{I,n} & & & \\ \boldsymbol{L}^1_{I,n} & \boldsymbol{L}_{1,n} & & \\ \vdots & & \ddots & \\ \boldsymbol{L}^K_{I,n} & & & \boldsymbol{L}_{K,n} \end{pmatrix} \tag{9.4.18}$$

with blocks

$$\begin{aligned} &\boldsymbol{R}^0_{I,n} := \kappa_0 \boldsymbol{I}_{K-1},\ \kappa_0 \in \mathbb{R},\ \boldsymbol{L}^0_{I,n} \in \mathbb{R}^{(K-1)\times(K-1)}, \\ &\boldsymbol{R}^k_{I,n}, \boldsymbol{L}^k_{I,n} \in \mathbb{R}^{(d+2)\times(K-1)}, \quad \boldsymbol{R}_{k,n}, \boldsymbol{L}_{k,n} \in \mathbb{R}^{(d+2)\times(d+2)},\ k = 1, \dots, K. \end{aligned}$$

Here the matrices $\boldsymbol{R}_n$ and $\boldsymbol{L}_n$ are composed of the right and left eigenvectors in their columns and rows, respectively. To determine the blocks $\boldsymbol{R}_{k,n}$ we note that $\lambda_{k,i}$ and $\lambda_{k,\pm}$ are also eigenvalues of the matrix $\boldsymbol{B}_{k,n}$ and the eigenvalue problem for $\boldsymbol{B}_n$ decouples into eigenvalue problems for the matrices $\boldsymbol{B}_{k,n}$ corresponding to a single component. In a first step, we therefore compute the eigenvectors to these sub-problems where we first determine an orthonormal basis $\{\boldsymbol{n}, \boldsymbol{t}_1, \dots, \boldsymbol{t}_{d-1}\}$ of $\mathbb{R}^d$ such that $\boldsymbol{t}_i \cdot \boldsymbol{t}_j = \delta_{i,j}$ and $\boldsymbol{t}_i \cdot \boldsymbol{n} = 0$. Then the right and left eigenvectors to the eigenvalues (9.4.16) and (9.4.17) are

$$\boldsymbol{r}_{k,d} = (1, \boldsymbol{0}_d^T, 0)^T,\ \boldsymbol{r}_{k,i} = (0, \boldsymbol{t}_i^T, 0)^T,\ \boldsymbol{r}_{k,\pm} = (1, \pm c_k/\rho_k \boldsymbol{n}^T, c_k^2)^T, \tag{9.4.19}$$

$$\boldsymbol{l}_{k,d} = (1, \boldsymbol{0}_d^T, -c_k^{-2})^T,\ \boldsymbol{l}_{k,i} = (0, \boldsymbol{t}_i^T, 0)^T,\ \boldsymbol{l}_{k,\pm} = 0.5 c_k^{-2} (1, \pm c_k \rho_k \boldsymbol{n}^T, 1)^T \tag{9.4.20}$$

for $i = 1, \dots, d-1$. Thus there exists an eigenvalue decomposition of the matrix $\boldsymbol{B}_{k,n}$, i.e.,

$$\boldsymbol{L}_{k,n} \boldsymbol{B}_{k,n} \boldsymbol{R}_{k,n} = \boldsymbol{\Lambda}_{k,n}, \tag{9.4.21}$$

where $\boldsymbol{L}_{k,n}$ and $\boldsymbol{R}_{k,n}$ are defined by the left and right eigenvectors and $\boldsymbol{\Lambda}_{k,n}$ is a diagonal matrix with eigenvalues on the diagonal

$$\boldsymbol{R}_{k,n} := \begin{pmatrix} 1 & 0 & \dots & 0 & 1 & 1 \\ -c_k/\rho_k \boldsymbol{n} & \boldsymbol{t}_1 & \dots & \boldsymbol{t}_{d-1} & \boldsymbol{0}_d & c_k/\rho_k \boldsymbol{n} \\ c_k^2 & 0 & \dots & 0 & 0 & c_k^2 \end{pmatrix}, \tag{9.4.22}$$

$$\boldsymbol{L}_{k,n} := \frac{1}{2c_k^2} \begin{pmatrix} 0 & 0 & \dots & 0 & 2c_k^2 & 0 \\ -c_k \rho_k \boldsymbol{n} & 2c_k^2 \boldsymbol{t}_1 & \dots & 2c_k^2 \boldsymbol{t}_{d-1} & \boldsymbol{0}_d & c_k \rho_k \boldsymbol{n} \\ 1 & 0 & \dots & 0 & -2 & 1 \end{pmatrix}^T, \tag{9.4.23}$$

$$\boldsymbol{\Lambda}_{k,n} := \begin{pmatrix} v_{k,n} - c_k & \boldsymbol{0}_d^T & 0 \\ \boldsymbol{0}_d & v_{k,n} \boldsymbol{I}_d & \boldsymbol{0}_d \\ 0 & \boldsymbol{0}_d^T & v_{k,n} + c_k \end{pmatrix}. \tag{9.4.24}$$

To calculate the eigenvectors to the multiple eigenvalue $\lambda_{I,i}$ we employ the knowledge of the matrices $\boldsymbol{R}_{k,n}$. According to the block structure of the matrix $\boldsymbol{R}_n$ the matrix of corresponding right eigenvectors needs to satisfy

$$(\boldsymbol{B}_n - \lambda_{I,i} \boldsymbol{I}) \boldsymbol{R}_n = \boldsymbol{0} \Leftrightarrow (\boldsymbol{B}_{k,n} - \lambda_{I,i} \boldsymbol{I}_{d+2}) \boldsymbol{R}^k_{I,n} = -\boldsymbol{A}_{k,n} \boldsymbol{R}^0_{I,n} = -\kappa_0 \boldsymbol{A}_{k,n}$$

for $k = 1, \dots, K$. Assuming that the eigenvalue $\lambda_{I,i}$ does not coincide with one of the eigenvalues $\lambda_{k,i}$ and $\lambda_{k,\pm}$, then $\boldsymbol{B}_{k,n} - \lambda_{I,i} \boldsymbol{I}_{d+2}$ is regular and there exists a unique solution for $\boldsymbol{R}^k_{I,n}$. For its representation we introduce

$$\kappa_0 := \prod_{l=1}^{K} \alpha_l \sigma_l,\ \kappa_k := \prod_{l=1, l\neq k}^{K} \alpha_l \sigma_l,\ k = 1, \dots, K$$

with $\delta_k^n := v_{k,n} - V_{I,n}$ and $\sigma_k := (\delta_k^n)^2 - c_k^2$. Then we obtain

$$\boldsymbol{R}^0_{I,n} := \kappa_0\, \boldsymbol{I}_{K-1}, \tag{9.4.25}$$

$$\boldsymbol{R}^k_{I,n} := \kappa_k\, \rho_k \begin{pmatrix} \alpha_k c_k^2 \boldsymbol{\beta}_k^T - (\delta_k^n)^2 \boldsymbol{\gamma}_k^T \\ -\boldsymbol{n}(\alpha_k \boldsymbol{\beta}_k^T - \boldsymbol{\gamma}_k^T) \delta_k^n/\rho_k \\ -\sigma_k (\boldsymbol{e}^T_{i,K-1}(1 - \delta_{k,K}) - \boldsymbol{1}^T_{K-1} \delta_{k,K}) + \alpha_k \boldsymbol{\beta}_k^T - \boldsymbol{\gamma}_k^T \end{pmatrix} \tag{9.4.26}$$

Since $\alpha_k \in (0,1)$ according to (9.2.1), these matrices are regular, i.e., the columns are linearly independent, if and only if

$$\sigma_k \neq 0 \quad \forall\, k = 1, \dots, K, \tag{9.4.27}$$

holds. This condition is referred to as the *non-resonance condition*, see [8] in case of a two-velocity-two-pressure model in two-phase flows. Thus the corresponding left eigenvectors are determined by the rows of the inverse of $\boldsymbol{R}_n$. Since $\boldsymbol{L}_n \boldsymbol{R}_n = \boldsymbol{I}$, the blocks turn out to be

$$\boldsymbol{L}_{k,n} = \boldsymbol{R}_{k,n}^{-1}, \ k = 1, \dots, K, \tag{9.4.28}$$

$$\boldsymbol{L}_{I,n}^0 = (\boldsymbol{R}_{I,n}^0)^{-1} = \kappa_0^{-1}\, \boldsymbol{I}_{K-1}, \tag{9.4.29}$$

$$\boldsymbol{L}_{I,n}^K = -\boldsymbol{L}_{k,n} \boldsymbol{R}_{I,n}^K (\boldsymbol{R}_{I,n}^0)^{-1} = -\kappa_0^{-1}\, \boldsymbol{L}_{k,n} \boldsymbol{R}_{I,n}^K, \ k = 1, \dots, K, \tag{9.4.30}$$

and we obtain for the right eigenvectors

$$\boldsymbol{r}_{I,l} := \kappa_0 \left((\overline{\boldsymbol{r}}_{I,l}^0)^T, (\overline{\boldsymbol{r}}_{I,l}^1)^T, \dots, (\overline{\boldsymbol{r}}_{I,l}^K)^T \right)^T, \ l = 1, \dots, K-1. \tag{9.4.31}$$

where $\overline{\boldsymbol{r}}_{I,l}^0 = \boldsymbol{e}_{l,K-1}$ and $\overline{\boldsymbol{r}}_{I,l}^k = (\overline{x}_{k,l}, \overline{\boldsymbol{y}}_{k,l}^T, \overline{z}_{k,l})^T$ is determined by the components

$$\overline{z}_{k,l} = \rho_k \left(\alpha_k c_k^2 \beta_{k,l} - (\delta_k^n)^2 \gamma_{k,l} \right) / (\alpha_k \sigma_k), \tag{9.4.32}$$

$$\overline{\boldsymbol{y}}_{k,l} = -\boldsymbol{n} \left(\alpha_k \beta_{k,l} - \gamma_{k,l} \right) \delta_k^n / (\alpha_k \sigma_k), \tag{9.4.33}$$

$$\overline{x}_{k,l} = \left(-\sigma_k (\delta_{k,l}(1 - \delta_{k,K}) - \delta_{k,K}) + \alpha_k \beta_{k,l} - \gamma_{k,l} \right) \rho_k / (\alpha_k \sigma_k). \tag{9.4.34}$$

These are well-defined also in case of $\alpha_k = 0$ or $\sigma_k = 0$. Similar to (9.4.31) the left eigenvectors are then given by

$$\boldsymbol{l}_{I,l} := \left((\boldsymbol{l}_{I,0}^1)^T, (\boldsymbol{l}_{I,l}^1)^T, \dots, (\boldsymbol{l}_{I,l}^K)^T \right)^T, \ l = 1, \dots, K-1. \tag{9.4.35}$$

with

$$\boldsymbol{l}_{I,l}^0 = \prod_{k=1}^{K} (\alpha_k \sigma_k)^{-1}\, \boldsymbol{e}_{l,K-1}, \quad \boldsymbol{l}_{I,l}^k = \frac{\rho_k}{2 c_k^2 \alpha_k \sigma_k} (a_k^l, 0, \dots, 0, b_k^l, c_k^l)^T$$

and

$$\begin{aligned}
a_k^l &:= -c_k (\alpha_k \beta_{k,l} - \gamma_{k,l}) \delta_k^n + \sigma_k (\delta_{k,l}(1 - \delta_{k,K}) - \delta_{k,K}) - \alpha_k \beta_{k,l} + \gamma_{k,l}, \\
b_k^l &:= 2 c_k^2 ((\delta_k^n)^2 \gamma_{k,l} - \alpha_k c_k^2 \beta_{k,l}) - 2 \sigma_k (\delta_{k,l}(1 - \delta_{k,K}) - \delta_{k,K}) \\
&\quad + 2 (\alpha_k \beta_{k,l} - \gamma_{k,l}), \\
c_k^l &:= c_k (\alpha_k \beta_{k,l} - \gamma_{k,l}) \delta_k^n + \sigma_k (\delta_{k,l}(1 - \delta_{k,K}) - \delta_{k,K}) - \alpha_k \beta_{k,l} + \gamma_{k,l}.
\end{aligned}$$

After having determined the eigenvalues and the corresponding linearly independent right and left eigenvectors we finally end up with the eigenvalue decomposition of the matrix $\boldsymbol{B}_n$

$$\boldsymbol{L}_n \boldsymbol{B}_n \boldsymbol{R}_n = \boldsymbol{\Lambda}_n \tag{9.4.36}$$

with the block-diagonal matrix $\boldsymbol{\Lambda}_n = \operatorname{diag}(\boldsymbol{\Lambda}_{0,n}, \boldsymbol{\Lambda}_{1,n}, \dots, \boldsymbol{\Lambda}_{K,n})$ and $\boldsymbol{\Lambda}_{0,n} := V_{I,n} \boldsymbol{I}_{K-1}$. To verify this decomposition we make use of the identity $\boldsymbol{B}_{k,n} \boldsymbol{R}_{I,n}^k = \boldsymbol{R}_{I,n}^k \boldsymbol{\Lambda}_{0,n} - \boldsymbol{A}_{k,n} \boldsymbol{R}_{I,n}^0$. To conclude the investigation on the hyperbolicity we summarize the findings in the following theorem.

Theorem 9.4.1. *(Hyperbolicity) Let the interfacial pressures satisfy the conditions (9.2.5) and (9.2.14). Let the interfacial velocity $\boldsymbol{V}_I$ be chosen such that for arbitrary normal direction $\boldsymbol{n}$ the normal interfacial velocity $v_{I,n}$ does not coincide with one of the eigenvalues $\lambda_{k,i}$ and $\lambda_{k,\pm}$ of $\boldsymbol{B}_n$, i.e., the non-resonance condition (9.4.27) is satisfied. Then the first order system (9.4.1), (9.4.2), (9.4.3) and (9.4.4) is hyperbolic, i.e., (i) the eigenvalues of the matrix (9.4.7) are all real but not necessarily distinct and (ii) there exists a system of linearly independent left and right eigenvectors with (9.4.36).*

This theorem holds true also for the non-equilibrium model (9.2.2), (9.2.3), (9.2.4) and (9.2.7) neglecting viscosity and heat conduction as well as relaxation processes, because eigenvalues are invariant under a regular, bijective change of variables and the corresponding eigenvectors can be determined by scaling of the original eigenvectors by the Jacobian of the transformation and its inverse, respectively.

Finally we want to remark that the eigenvectors coincide with the one given in [3, 44] in case of a 7-equation model in one space dimension ($K = 2$, $d = 1$).

9.4.2 Equilibrium model

Similar to the non-equilibrium case we can determine the eigenvalues of the equilibrium model. A starting point is the evolution equations (9.2.21), (9.2.22) and (9.2.23). The corresponding first order system then reads

$$\partial_t \rho + \sum_{i=1}^{d} \left(v_i \frac{\partial \rho}{\partial x_i} + \rho \frac{\partial v_i}{\partial x_i} \right) = 0, \tag{9.4.37}$$

$$\partial_t \boldsymbol{v} + \sum_{i=1}^{d} \left(v_i \frac{\partial \boldsymbol{v}}{\partial x_i} + \frac{1}{\rho} \boldsymbol{e}_i \frac{\partial p}{\partial x_i} \right) = \boldsymbol{0}, \tag{9.4.38}$$

$$\partial_t p + \sum_{i=1}^{d} \left(v_i \frac{\partial p}{\partial x_i} + \rho c^2 \frac{\partial v_i}{\partial x_i} \right) = 0, \tag{9.4.39}$$

Again we consider its projection onto normal direction $\xi := \boldsymbol{x} \cdot \boldsymbol{n}$ for arbitrary unit direction $\boldsymbol{n} \in \mathbb{R}^d$ that can be written in quasi-conservative form

$$\partial_t \boldsymbol{w} + \boldsymbol{B}_n(\boldsymbol{w}) \frac{\partial \boldsymbol{w}}{\partial \xi} = \boldsymbol{0} \tag{9.4.40}$$

with the vector of primitive variables $\boldsymbol{w} = (\rho, \boldsymbol{v}^T, p)^T$ and matrix

$$\boldsymbol{B}_n := \begin{pmatrix} v_n & \rho \boldsymbol{n}^T & 0 \\ \boldsymbol{0}_d & v_n \boldsymbol{I}_d & \frac{1}{\rho} \boldsymbol{n} \\ 0 & \rho c^2 \boldsymbol{n}^T & v_n \end{pmatrix}. \tag{9.4.41}$$

The normal component of the velocity is defined as

$$v_n := \boldsymbol{v} \cdot \boldsymbol{n}. \tag{9.4.42}$$

The eigenvalues of $\boldsymbol{B}_n$ are then characterized by the roots of the characteristic polynomial

$$\det(\boldsymbol{B}_n - \lambda \boldsymbol{I}_{d+2}) = (v_n - \lambda)^d \left((v_n - \lambda)^2 - c^2 \right).$$

Hence we obtain the following eigenvalues:

$$\lambda_\pm = v_n \pm c, \quad \lambda_i = v_n, \ i = 1, \ldots, d. \tag{9.4.43}$$

With regard to a stable numerical discretization of the non-equilibrium model in the limit of vanishing relaxation terms, the so-called sub-characteristic condition, see Whitham [43] and Liu [28], has to hold true. For this purpose we evaluate the eigenvalues (9.4.15), (9.4.16) and (9.4.17) with respect to an equilibrium state, i.e.,(9.2.18), (9.2.19) and (9.2.20) hold,

$$\overline{\lambda}_{I,k} = \overline{V}_{I,n} = \overline{\boldsymbol{v}}_I \cdot \boldsymbol{n} = \overline{\boldsymbol{v}} \cdot \boldsymbol{n} = \overline{v}_n, \ k = 1, \ldots, K-1 \tag{9.4.44}$$

$$\overline{\lambda}_{k,i} = \overline{v}_{k,n} = \overline{\boldsymbol{v}}_k \cdot \boldsymbol{n} = \overline{\boldsymbol{v}} \cdot \boldsymbol{n} = \overline{v}_n, \ k = 1, \ldots, K, \ i = 1, \ldots, d \tag{9.4.45}$$

$$\overline{\lambda}_{k,\pm} = \overline{v}_{k,n} \pm c_k = \overline{v}_n \pm c_k, \ k = 1, \ldots, K. \tag{9.4.46}$$

Here the bar indicates evaluation with respect to an equilibrium state. Then by definition (9.3.13) and (9.2.10) of the mixture sound speed and the mixture density we conclude from the positivity of the densities ρ_k and the volume fractions α_k

$$\overline{c} \in \left[\min_{k=1,\ldots,K} \overline{c}_k, \max_{k=1,\ldots,K} \overline{c}_k \right] =: [c_{min}, c_{max}].$$

A straight forward estimate gives

$$\min_{k=1,\ldots,K} \overline{\lambda}_{k,+} \leq \overline{\lambda}_+ \leq \max_{k=1,\ldots,K} \overline{\lambda}_{k,+},$$

$$\min_{k=1,\ldots,K} \overline{\lambda}_{k,-} \leq \overline{\lambda}_- \leq \max_{k=1,\ldots,K} \overline{\lambda}_{k,-}.$$

In the second estimate we use that

$$-\overline{c} \in \left[-\max_{k=1,\dots,K} \overline{c}_k, -\min_{k=1,\dots,K} \overline{c}_k, \right] = \left[\min_{k=1,\dots,K} -\overline{c}_k, \max_{k=1,\dots,K} -\overline{c}_k \right].$$

This immediately implies that the following theorem holds true.

Theorem 9.4.2. *(Sub-characteristic condition) Let α_k, ρ_k and c_k, $k = 1, \dots, K$, be non-negative. Then the eigenvalues (9.4.15), (9.4.16), (9.4.17) and (9.4.44), (9.4.45), (9.4.46) of the non-equilibrium model and the equilibrium model, respectively, evaluated with respect to an equilibrium state, i.e., (9.2.18), (9.2.19) and (9.2.20) hold, satisfy the sub-characteristic condition*

$$\overline{\lambda}_i \in \left[\min \left(\min_k \overline{\lambda}_{I,k}, \min_{k,i} \overline{\lambda}_{k,i} \right), \max \left(\max_k \overline{\lambda}_{I,k}, \max_{k,i} \overline{\lambda}_{k,i} \right) \right] = \{\overline{v}_n\},$$

$$\overline{\lambda}_\pm \in \left[\min_k \overline{\lambda}_{k,\pm}, \max_k \overline{\lambda}_{k,\pm} \right].$$

Note that similar results have been proven recently by Flatten and Lund [15] for a hierarchy of two-phase relaxation models.

9.4.3 Symmetrization

From Kato's theorem [26] it follows that there exists a local-in-time smooth solution to the Cauchy problem of the projected system (9.4.6), if the problem is symmetrizable, i.e., there exists a symmetric positive definite matrix $\boldsymbol{P}_n = \boldsymbol{P}_n(\boldsymbol{w})$ such that the matrix $\boldsymbol{P}_n \boldsymbol{B}_n$ is symmetric. To construct such a symmetrizer we first observe that the matrix

$$\boldsymbol{P}_k = \begin{pmatrix} 1 & \boldsymbol{0}_d^T & -1/c_k^2 \\ \boldsymbol{0}_d & 0.5(\rho_k/c_k)^2 \, \boldsymbol{I}_d & \boldsymbol{0}_d \\ -1/c_k^2 & \boldsymbol{0}_d^T & 1.5/c_k^4 \end{pmatrix}.$$

is a symmetrizer of the phasic problem

$$\partial_t \, \boldsymbol{w}_k + \boldsymbol{B}_{k,n}(\boldsymbol{w}_k) \, \frac{\partial \, \boldsymbol{w}_k}{\partial \, \xi} = \boldsymbol{0}.$$

We then make the following ansatz for a symmetrizer of (9.4.6):

$$\boldsymbol{P}_n = \begin{pmatrix} K \, P_{\alpha,n} \boldsymbol{I}_{K-1} & \boldsymbol{P}_{1,\alpha,n}^T & \cdots & \boldsymbol{P}_{K,\alpha,n}^T \\ \boldsymbol{P}_{1,\alpha,n} & \boldsymbol{P}_1 & & \\ \vdots & & \ddots & \\ \boldsymbol{P}_{K,\alpha,n} & & & \boldsymbol{P}_K \end{pmatrix},$$

where

$$\boldsymbol{P}_{k,\alpha,n} = \boldsymbol{L}_{k,n}^T \left(\boldsymbol{\Lambda}_{k,n} - V_{I,n} \boldsymbol{I}_{d+2} \right)^{-1} \boldsymbol{R}_{k,n} \boldsymbol{P}_k \boldsymbol{A}_{k,n}$$

with $\boldsymbol{A}_{k,n}$, $\boldsymbol{R}_{k,n}$, $\boldsymbol{L}_{k,n}$ and $\boldsymbol{\Lambda}_{k,n}$ defined by (9.4.8), (9.4.22), (9.4.23) and (9.4.24). Note that $\boldsymbol{P}_{k,\alpha,n}$ is well-defined if the non-resonance condition (9.4.27) holds true. Obviously, $\boldsymbol{P}_n$ is symmetric. It turns out that $\boldsymbol{P}_n \boldsymbol{B}_n$ is symmetric whenever $\boldsymbol{P}_{k,\alpha,n}^T \boldsymbol{A}_{k,n}$ is symmetric. The latter holds true provided that $\boldsymbol{P}_{k,n}^T \boldsymbol{R}_{k,n} = \boldsymbol{L}_{k,n}^T$. This condition is only satisfied in the one-dimensional case, i.e., $d = 1$. It remains to verify that $\boldsymbol{P}_n$ is positive definite. For this purpose we have to verify for any $\boldsymbol{a} = (\boldsymbol{a}_\alpha^T, \boldsymbol{a}_1^T, \dots, \boldsymbol{a}_K^T)^T \neq \boldsymbol{0}$ with $\boldsymbol{a}_\alpha \in \mathbb{R}^{K-1}$, $\boldsymbol{a}_k \in \mathbb{R}^{d+2}$, $k = 1, \dots, K$ that $\boldsymbol{a}^T \boldsymbol{P}_n \boldsymbol{a}$ is positive. A straightforward calculus yields

$$\boldsymbol{a}^T \boldsymbol{P}_n \boldsymbol{a} = P_{\alpha,n} \sum_{k=1}^{K-1} \sum_{i=1}^{K-1} \left(a_{\alpha,i} + (\boldsymbol{P}_{k,\alpha,n}^T \boldsymbol{a}_k)_i / P_{\alpha,n} \right)^2 + \sum_{k=1}^{K} P_{\alpha,n}^{-1} \boldsymbol{a}_k^T \boldsymbol{Q} \boldsymbol{a}_k$$

with $\boldsymbol{Q} := P_{\alpha,n} \boldsymbol{P}_k - \boldsymbol{P}_{k,\alpha,n} \boldsymbol{P}_{k,\alpha,n}^T$. Since $\boldsymbol{P}_k$ is symmetric positive definite, the Cholesky decomposition $\boldsymbol{P}_k = \boldsymbol{C}_k \boldsymbol{C}_k^T$ exists. Furthermore, the matrix $\boldsymbol{E}_k := \boldsymbol{C}_k^{-1} \boldsymbol{P}_{k,\alpha,n}^T \boldsymbol{P}_{k,\alpha,n} \boldsymbol{C}_k^T$ is symmetric and, thus, there

exists an orthogonal matrix $\boldsymbol{T}_k$ such that $\boldsymbol{T}_k \boldsymbol{E}_k \boldsymbol{T}_k^T = \boldsymbol{D}_k$ where $\boldsymbol{D}_k$ is a diagonal matrix with the eigenvalues μ_i^k of $\boldsymbol{E}_k$ as entries. Then we obtain

$$\boldsymbol{a}_k^T \boldsymbol{Q} \boldsymbol{a}_k = \boldsymbol{b}_k^T (P_{\alpha,n} \boldsymbol{I}_{d+2} - \boldsymbol{D}_k) \boldsymbol{b}_k = \sum_{i=1}^{d+2} b_{k,i}^2 \left(P_{\alpha,n} - \mu_i^k\right)$$

with $\boldsymbol{b}_k := \boldsymbol{T}_k^T \boldsymbol{C}_k^T \boldsymbol{a}_k$. Choosing $P_{\alpha,n} > \max_{i,k} \left\{|\mu_i^k|\right\} > 0$ the term $\boldsymbol{a}_k^T \boldsymbol{Q} \boldsymbol{a}_k$ is non-negative and is positive for $\boldsymbol{a}_k \neq \boldsymbol{0}$. Thus, we have finally verified that in the one-dimensional case the matrix $\boldsymbol{P}_n$ is a symmetrizer of (9.4.6) provided the non-resonance condition (9.4.27) holds true. This generalizes the result in [8] for a two-phase model.

9.5 Frame invariance, objectivity and Galilean transformation

Since the results of an experiment should be independent of the observer's position in the Euclidean space, a physical meaningful model should reflect this behavior. This property is referred to as frame indifference and objectivity in the literature, cf. [13], p. 31 ff, and [29]: performing the general Euclidean change of frame

$$t^* = t + a, \quad \boldsymbol{x}^* = \boldsymbol{x}_0^*(t) + \boldsymbol{Q}(t)(\boldsymbol{x} - \boldsymbol{x}_0), \tag{9.5.1}$$

with constant values a and $\boldsymbol{x}_0$ and $\boldsymbol{Q}$ an orthogonal matrix, i.e.,

$$\boldsymbol{Q}\boldsymbol{Q}^T = \boldsymbol{Q}\boldsymbol{Q}^T = \boldsymbol{I}, \tag{9.5.2}$$

then a scalar f, a vector $\boldsymbol{u}$ and a tensor $\boldsymbol{T}$ are called objective, if

$$f^*(t^*, \boldsymbol{x}^*) = f(t, x), \ \boldsymbol{u}^*(t^*, \boldsymbol{x}^*) = \boldsymbol{Q}(t)\boldsymbol{u}(t, x), \ \boldsymbol{T}^*(t^*, \boldsymbol{x}^*) = \boldsymbol{Q}(t)\boldsymbol{T}(t, x)\boldsymbol{Q}^T(t). \tag{9.5.3}$$

To rewrite the fluid equations in terms of the general Euclidean change of frame we introduce the change of variables

$$f(t, \boldsymbol{x}) = f(t^* - a, \boldsymbol{x}_0 + \boldsymbol{Q}^T(t)(\boldsymbol{x}^* - \boldsymbol{x}_0^*(t)), \tag{9.5.4}$$
$$\boldsymbol{u}(t, \boldsymbol{x}) = \boldsymbol{u}(t^* - a, \boldsymbol{x}_0 + \boldsymbol{Q}^T(t)(\boldsymbol{x}^* - \boldsymbol{x}_0^*(t)), \tag{9.5.5}$$
$$\boldsymbol{T}(t, \boldsymbol{x}) = \boldsymbol{T}(t^* - a, \boldsymbol{x}_0 + \boldsymbol{Q}^T(t)(\boldsymbol{x}^* - \boldsymbol{x}_0^*(t)). \tag{9.5.6}$$

It is well-known that the fluid equations for a single phase are not invariant under a general Euclidean frame of change. For instance, Coriolis forces enter in case of a time-dependent rotation. However, the fluid equations are invariant under a Galilean transformation where we choose

$$\dot{\boldsymbol{x}}_0 = 0, \ \dot{\boldsymbol{Q}} = \boldsymbol{0} \quad \text{equiv.} \quad \boldsymbol{Q} = const, \quad \boldsymbol{x}_0^*(t) = \boldsymbol{c}_0 + \boldsymbol{c}_1 t, \ \boldsymbol{c}_1, \boldsymbol{c}_2 = const \tag{9.5.7}$$

in (9.5.1). For this transformation the velocity vector is still not objective but the acceleration and the rotation tensor are objective.

In the following we will confine ourselves to a Galilean transformation and derive constraints for the source terms $S_{\alpha,k}$, $S_{\alpha\rho,k}$, $S_{\alpha\rho\boldsymbol{v},k}$ and $S_{\alpha\rho E,k}$. For this purpose we apply a Galilean frame of change to the fluid equations (9.2.2), (9.2.3), (9.2.4) and (9.2.7). A detailed derivation can be found in [34]. Here we will confine ourselves to the main results. First of all, we derive from the evolution equation (9.2.7) of the volume fractions assuming that the volume fractions are objective, i.e., $\alpha_k^* = \alpha_k$,

$$\partial_{t^*} \alpha_k^* + \boldsymbol{V}_I^* \cdot \nabla_{\boldsymbol{x}^*} \alpha_k^* = S_{\alpha^*,k}^*, \ k = 1, \ldots, K, \tag{9.5.8}$$

where the interfacial velocity and the source term are given as

$$\boldsymbol{V}_I^* := \dot{\boldsymbol{x}}_0^* + \boldsymbol{Q}\boldsymbol{V}_I + \dot{\boldsymbol{Q}}(\boldsymbol{x} - \boldsymbol{x}_0) = \dot{\boldsymbol{x}}_0^* + \boldsymbol{Q}\boldsymbol{V}_I = \boldsymbol{c}_1 + \boldsymbol{Q}\boldsymbol{V}_I, \tag{9.5.9}$$
$$S_{\alpha^*,k}^* := S_{\alpha,k}. \tag{9.5.10}$$

Next we consider the evolution of mass. Assuming that the mass is objective, i.e., $\rho_k^* = \rho_k$, we derive from (9.2.3)

$$\partial_{t^*} (\alpha_k^* \rho_k^*) + \nabla_{\boldsymbol{x}^*} \cdot (\alpha_k^* \rho_k^* \boldsymbol{v}_k^*) = S_{\alpha^*\rho^*,k}^*, \tag{9.5.11}$$

with source term

$$S^*_{\alpha^*\rho^*,k} := S_{\alpha\rho,k}. \tag{9.5.12}$$

Note that (9.5.8) and (9.5.11) hold true for a general Euclidean change of frame (9.5.1). The transformation of the momentum equation (9.2.3) is cumbersome. It significantly simplifies in case of a Galilean transformation. Starting from (9.2.3) one has to incorporate (9.5.11). Assuming that the pressures p_k and $P_{k,l}$ and the stress tensors $\boldsymbol{T}_k$ are objective, i.e., $p^*_k = p_k$, $P^*_{k,l} = P_{k,l}$ and $\boldsymbol{T}^*_k = \boldsymbol{Q}\boldsymbol{T}_k\boldsymbol{Q}^T$, we obtain

$$\begin{aligned}\partial_{t^*}(\alpha^*_k\,\rho^*_k\,\boldsymbol{v}^*_k) + \nabla_{\boldsymbol{x}^*}\cdot(\alpha^*_k\,\rho^*_k\,\boldsymbol{v}_k{}^*\,\boldsymbol{v}^{*T}_k + \alpha^*_k\,p^*_k\,\boldsymbol{I}) = \\ -\sum_{l=1}^{K} P^*_{k,l}\,\nabla_{\boldsymbol{x}^*}\,\alpha^*_l + \nabla_{\boldsymbol{x}^*}\cdot(\alpha^*_k\,\boldsymbol{T}^*_k) + \boldsymbol{S}^*_{\alpha^*\rho^*\boldsymbol{v}^*,k},\end{aligned} \tag{9.5.13}$$

with source term

$$\boldsymbol{S}^*_{\alpha^*\rho^*\boldsymbol{v}^*,k} := S_{\alpha\rho,k}\,\dot{\boldsymbol{x}}^*_0 + \boldsymbol{Q}\,\boldsymbol{S}_{\alpha\rho\boldsymbol{v},k}. \tag{9.5.14}$$

Finally we apply the Galilean transformation to the energy equation (9.2.4). Since the velocity is not an objective vector, the kinetic energy in the Galilean frame becomes

$$e^*_{kin,k} = e_{kin,k} + \dot{\boldsymbol{x}}^*_0\cdot\boldsymbol{v}^*_k - \frac{1}{2}(\dot{\boldsymbol{x}}^*_0)^2, \quad e_{kin,k} := \frac{1}{2}\boldsymbol{v}^2_k. \tag{9.5.15}$$

Thus the total energy and the total enthalpy are

$$E_k := e_k + \frac{1}{2}\boldsymbol{v}^2_k = E^*_k - \dot{\boldsymbol{x}}^*_0\cdot\boldsymbol{v}^*_k + \frac{1}{2}(\dot{\boldsymbol{x}}^*_0)^2, \quad E^*_k := e^*_k + \frac{1}{2}(\boldsymbol{v}^*_k)^2, \tag{9.5.16}$$

$$H_k := E_k + \frac{p_k}{\rho_k} = H^*_k - \dot{\boldsymbol{x}}^*_0\cdot\boldsymbol{v}^*_k + \frac{1}{2}(\dot{\boldsymbol{x}}^*_0)^2, \quad H^*_k := E^*_k + \frac{p^*_k}{\rho^*_k}, \tag{9.5.17}$$

where we also assume objectivity of the internal energy, i.e., $e^*_k = e_k$. Again, after some tedious work of calculus using (9.5.2) and incorporating (9.5.11), (9.5.13), the energy equation (9.2.4) in the Galilean frame becomes

$$\begin{aligned}\partial_{t^*}(\alpha^*_k\,\rho^*_k\,E^*_k) + \nabla_{\boldsymbol{x}^*}\cdot(\alpha^*_k\,\rho^*_k\,\boldsymbol{v}^*_k\,(E^*_k + p^*_k/\rho^*_k)) = \\ -\sum_{l=1}^{K} P^*_{k,l}\,\boldsymbol{V}^*_I\cdot\nabla_{\boldsymbol{x}^*}\,\alpha^*_l + \nabla_{\boldsymbol{x}^*}\cdot(\alpha^*_k\,(\boldsymbol{v}^*_k\cdot\boldsymbol{T}^*_k - \boldsymbol{q}^*_k)) + S^*_{\alpha^*\rho^*E^*,k},\end{aligned} \tag{9.5.18}$$

with source term

$$S^*_{\alpha^*\rho^*E^*,k} := S_{\alpha\rho E,k} + \boldsymbol{Q}\boldsymbol{S}_{\alpha\rho\boldsymbol{v},k}\cdot\dot{\boldsymbol{x}}^*_0 + \frac{1}{2}\,(\dot{\boldsymbol{x}}^*_0)^2 S_{\alpha\rho,k}. \tag{9.5.19}$$

Here we again assume objectivity of the pressure $P_{k,l}$ and the heat flux $\boldsymbol{q}_k$, i.e., $P^*_{k,l} = P_{k,l}$ and $\boldsymbol{q}^*_k = \boldsymbol{Q}\boldsymbol{q}_k$.

Finally, we conclude with summarizing our findings in the following

Theorem 9.5.1. *(Galilean Invariance) Let the following assumptions hold true*

1. *α_k, ρ_k, p_k, e_k and $P_{k,l}$ are objective scalars,*
2. *$\boldsymbol{q}_k$, $\boldsymbol{T}_k$ are objective vectors and tensors, respectively,*
3. *all material parameters, e.g., the viscosity coefficient $\overline{\mu}_k$, the heat conduction coefficient $\overline{\lambda}_k$ introduced in Section 9.6.3.1, are objective,*
4. *the source terms (9.5.10), (9.5.12), (9.5.14), (9.5.19) are invariant under a Galilean transformation, i.e.,*

$$S^*_{\alpha^*,k} = S_{\alpha^*,k},\ S^*_{(\alpha\rho)^*,k} = S_{(\alpha\rho)^*,k},\ \boldsymbol{S}^*_{(\alpha\rho\boldsymbol{v})^*,k} = \boldsymbol{S}_{(\alpha\rho\boldsymbol{v})^*,k},\ S^*_{(\alpha\rho E)^*,k} = S_{(\alpha\rho E)^*,k}. \tag{9.5.20}$$

Then the non-equilibrium model (9.2.2), (9.2.3), (9.2.4) and (9.2.7) with velocity $\boldsymbol{v}^*_k = \dot{\boldsymbol{x}}^*_0 + \boldsymbol{Q}\boldsymbol{v}_k$, interfacial velocity velocity $\dot{\boldsymbol{x}}^*_0 + \boldsymbol{Q}\boldsymbol{V}_I$ and total energy (9.5.16) is Galilean invariant. This also holds true for the system without the source term terms as well as for the mixture model and the equilibrium model because the latter are derived from the non-equilibrium model by summation.

9.6 Thermodynamical properties: 2nd law of thermodynamics

From a physical point of view, a model is admissible if it is in agreement with the principles of thermodynamics. For this purpose we first derive the entropy law for the non-equilibrium model. Then we determine the entropy production terms of the mixture. To be consistent with the 2nd law of thermodynamics we have to check the sign of the entropy production terms. This will provide us with admissibility criteria for the interfacial pressures and velocity as well as the relaxation terms.

9.6.1 Entropy

In order to investigate thermodynamical properties of the non-equilibrium model (9.2.2), (9.2.3), (9.2.4) and (9.2.7), we assume that the entropy of each component satisfies

$$de_k = T_k ds_k - p_k d\tau_k, \tag{9.6.1}$$

where $\tau_k := 1/\rho_k$ is the specific volume of component k. Thus the pressure and the temperature are the partial derivatives of $e_k(\tau_k, s_k)$ that are assumed to be positive, i.e.,

$$p_k(\tau_k, s_k) = -\frac{\partial e_k}{\partial \tau_k}(\tau_k, s_k) \geq 0, \quad T_k(\tau_k, s_k) = \frac{\partial e_k}{\partial s_k}(\tau_k, s_k) \geq 0.$$

Furthermore, to ensure thermodynamical stability we assume that the Hessian of e_k is a convex function with respect to τ_k and s_k, i.e.,

$$\begin{aligned} &\frac{\partial^2 e_k}{\partial^2 \tau_k}(\tau_k, s_k) \geq 0, \ \frac{\partial^2 e_k}{\partial^2 s_k}(\tau_k, s_k) \geq 0, \\ &\frac{\partial^2 e_k}{\partial^2 \tau_k}(\tau_k, s_k)\frac{\partial^2 e_k}{\partial^2 s_k}(\tau_k, s_k) \geq \left(\frac{\partial^2 e_k}{\partial \tau_k \partial s_k}(\tau_k, s_k)\right)^2. \end{aligned}$$

Finally, the third law of thermodynamics implies

$$\tau_k \geq 0, \quad s_k \geq 0.$$

Assuming that p_k and T_k are strictly positive, then e_k becomes a monotone function in τ_k and s_k and we may change variables, i.e., $s_k = s_k(\tau_k, e_k)$ satisfying

$$T_k ds_k = de_k + p_k d\tau_k \tag{9.6.2}$$

with partial derivatives

$$\frac{\partial s_k}{\partial \tau_k}(\tau_k, e_k) = \frac{p_k}{T_k} > 0, \quad \frac{\partial s_k}{\partial e_k}(\tau_k, e_k) = \frac{1}{T_k} > 0. \tag{9.6.3}$$

It is well-known that $s_k = s_k(\tau_k, e_k)$ is a concave function, i.e., the Hessian is negative-definite

$$\begin{aligned} &\frac{\partial^2 s_k}{\partial^2 \tau_k}(\tau_k, e_k) \leq 0, \ \frac{\partial^2 s_k}{\partial^2 e_k}(\tau_k, e_k) \leq 0, \\ &\frac{\partial^2 s_k}{\partial^2 \tau_k}(\tau_k, e_k)\frac{\partial^2 s_k}{\partial^2 e_k}(\tau_k, e_k) \geq \left(\frac{\partial^2 e_k}{\partial \tau_k \partial e_k}(\tau_k, e_k)\right)^2, \end{aligned} \tag{9.6.4}$$

if and only if $e_k(\tau_k, s_k)$ is a convex function, i.e., thermodynamic stability holds.

9.6.2 Entropy equation

In order to derive the entropy equation we rewrite (9.6.2) as

$$T_k ds_k = de_k - \frac{p_k}{\rho_k^2} d\rho_k. \tag{9.6.5}$$

By means of the evolution equations (9.3.1) and (9.3.4) for the density and the internal energy we then deduce the entropy law

$$\partial_t s_k + \boldsymbol{v}_k \cdot \nabla s_k = \frac{1}{\alpha_k \rho_k T_k} \left(\sum_{l=1}^{K} P_{k,l} \left(\boldsymbol{v}_k - \boldsymbol{V}_I \right) \cdot \nabla \alpha_l + p_k (\boldsymbol{v}_k - \boldsymbol{V}_I) \cdot \nabla \alpha_k \right.$$
$$\left. + \alpha_k \sum_{i,l=1}^{d} \frac{\partial v_{k,l}}{\partial x_i} (\boldsymbol{T}_k)_{l,i} - \nabla \cdot \left(\alpha_k \boldsymbol{q}_k \right) + S_{s,k} \right) \tag{9.6.6}$$

with the relaxation term

$$S_{s,k} := S_{e,k} - \frac{p_k}{\rho_k} S_{\alpha\rho,k} + p_k S_{\alpha,k}. \tag{9.6.7}$$

For the volume specific entropy we then obtain together with (9.2.2)

$$\partial_t \left(\alpha_k \rho_k s_k \right) + \nabla \cdot \left(\alpha_k \rho_k s_k \boldsymbol{v}_k \right) + \nabla \cdot \left(\frac{1}{T_k} \alpha_k \boldsymbol{q}_k \right) = \frac{1}{T_k} \left(\sum_{l=1}^{K} P_{k,l} \left(\boldsymbol{v}_k - \boldsymbol{V}_I \right) \cdot \nabla \alpha_l \right.$$
$$\left. + p_k (\boldsymbol{v}_k - \boldsymbol{V}_I) \cdot \nabla \alpha_k + \alpha_k \sum_{i,l=1}^{d} \frac{\partial v_{k,l}}{\partial x_i} (\boldsymbol{T}_k)_{l,i} - \alpha_k \frac{1}{T_k} \boldsymbol{q}_k \cdot \nabla T_k \right) + S_{\alpha\rho s,k} \tag{9.6.8}$$

with the relaxation term

$$S_{\alpha\rho s,k} := \frac{1}{T_k} S_{s,k} + s_k S_{\alpha\rho,k}. \tag{9.6.9}$$

Introducing the entropy of the components of the mixture

$$\rho s := \sum_{k=1}^{K} \alpha_k \rho_k s_k \tag{9.6.10}$$

we finally obtain with (9.2.12) the entropy law of the mixture

$$\partial_t \left(\rho s \right) + \nabla \cdot \left(\sum_{k=1}^{K} \alpha_k \rho_k s_k \boldsymbol{v}_k \right) + \nabla \cdot \left(\sum_{k=1}^{K} \frac{1}{T_k} \alpha_k \boldsymbol{q}_k \right) = \tag{9.6.11}$$
$$\sum_{k=1}^{K} (\alpha_k \Sigma_k + \alpha_k \Delta_k + \Pi_k + S_{\alpha\rho s,k}),$$

where the production terms are defined as

$$\Pi_k := \frac{1}{T_k} \left(\sum_{l=1}^{K} P_{k,l} \left(\boldsymbol{v}_k - \boldsymbol{V}_I \right) \cdot \nabla \alpha_l + p_k (\boldsymbol{v}_k - \boldsymbol{V}_I) \cdot \nabla \alpha_k \right), \tag{9.6.12}$$

$$\Sigma_k := \frac{1}{T_k} \sum_{i,l=1}^{d} \frac{\partial v_{k,l}}{\partial x_i} (\boldsymbol{T}_k)_{l,i}, \tag{9.6.13}$$

$$\Delta_k := -\frac{1}{T_k^2} \boldsymbol{q}_k \cdot \nabla T_k. \tag{9.6.14}$$

Note that the total entropy of a homogeneous mixture is determined by the sum of ρs and the non-negative mixture entropy, [32], p. 320. We discuss the mixture entropy in the context of the relaxation terms for chemical potentials for a three-component mixture, see Section 9.7.3.2.

9.6.3 Entropy production

According to the 2nd law of thermodynamics the production terms (9.6.12), (9.6.13) and (9.6.14) have to be non-negative. In the subsequent sections we will derive sufficient conditions that ensure thermodynamical compatibility.

9.6.3.1 Entropy production due to viscosity and heat conduction

In order to verify the physically admissible sign of the entropy production term Σ_k we have to specify the viscous stress tensor $\boldsymbol{T}_k$ for each component. For an isotropic Newtonian fluid the stress tensor reads

$$\boldsymbol{T}_k = \overline{\mu}_k \left(\nabla \boldsymbol{v}_k + \nabla \boldsymbol{v}_k{}^T - \frac{2}{3}(\nabla \cdot \boldsymbol{v}_k)\boldsymbol{I} \right), \tag{9.6.15}$$

where $\overline{\mu}_k$ denotes the viscosity coefficient of component k. Thus the components of this symmetric tensor are

$$(\boldsymbol{T}_k)_{l,i} = \overline{\mu}_k \left(\frac{\partial v_{k,l}}{\partial x_i} + \frac{\partial v_{k,i}}{\partial x_l} - \frac{2}{3} \sum_{j=1}^{d} \frac{\partial v_{k,j}}{\partial x_j} \delta_{l,i} \right) = (\boldsymbol{T}_k)_{i,l}.$$

Then we compute for the entropy production term (9.6.13)

$$\frac{T_k}{\overline{\mu}_k} \Sigma_k = 2 \sum_{i=1}^{d} \sum_{l=1}^{i-1} \left(\frac{\partial v_{k,l}}{\partial x_i} + \frac{\partial v_{k,i}}{\partial x_l} \right)^2 + \frac{2}{3} \Gamma$$

with

$$\begin{aligned} \Gamma &:= \sum_{i=1}^{d} \left(2 \left(\frac{\partial v_{k,i}}{\partial x_i} \right)^2 - \sum_{j=1, j \neq i}^{d} \frac{\partial v_{k,j}}{\partial x_j} \frac{\partial v_{k,i}}{\partial x_i} \right) \\ &= \begin{cases} 2 \left(\frac{\partial v_{k,1}}{\partial x_1} \right)^2 & , d = 1 \\ \left(\frac{\partial v_{k,1}}{\partial x_1} \right)^2 + \left(\frac{\partial v_{k,2}}{\partial x_2} \right)^2 + \left(\frac{\partial v_{k,1}}{\partial x_1} - \frac{\partial v_{k,2}}{\partial x_2} \right)^2 & , d = 2 \\ \left(\frac{\partial v_{k,1}}{\partial x_1} - \frac{\partial v_{k,2}}{\partial x_2} \right)^2 + \left(\frac{\partial v_{k,2}}{\partial x_2} - \frac{\partial v_{k,3}}{\partial x_3} \right)^2 + \left(\frac{\partial v_{k,1}}{\partial x_1} - \frac{\partial v_{k,3}}{\partial x_3} \right)^2 & , d = 3 \end{cases}. \end{aligned}$$

Obviously, the following theorem holds true.

Theorem 9.6.1. *(Entropy production due to viscosity) The viscous stress tensors are determined by (9.6.15). Let the temperatures T_k and the viscosity coefficients $\overline{\mu}_k$, $k = 1, \ldots, K$, be non-negative. Then the production terms (9.6.13) are non-negative. In addition, assuming the saturation condition (9.2.1), then the entropy production due to viscosity $\sum_{k=1}^{K} \alpha_k \Sigma_k$ is non-negative.*

The heat fluxes are modeled by Fourier's law of heat conduction for a fluid with isotropic material property

$$\boldsymbol{q}_k = -\overline{\lambda}_k \nabla T_k, \tag{9.6.16}$$

where $\overline{\lambda}_k$ denotes the heat conduction coefficient of component k.

Then the entropy production term (9.6.14) reads

$$\Delta_k = \frac{1}{T_k^2} \overline{\lambda}_k \nabla T_k \cdot \nabla T_k.$$

From this we directly conclude

Theorem 9.6.2. *(Entropy production due to heat conduction) The heat fluxes are determined by (9.6.16). Let the temperatures T_k and the heat conduction coefficients $\overline{\lambda}_k$, $k = 1, \ldots, K$, be non-negative. Then the production terms (9.6.14) are non-negative. In addition, assuming the saturation condition (9.2.1), the entropy production due to heat conduction $\sum_{k=1}^{K} \alpha_k \Delta_k$ is non-negative.*

Note that Theorems 9.6.1 and 9.6.2 are counterparts of the results of Guillemaud [20] in case of a two-component model.

9.6.3.2 Interfacial velocity and pressure

To investigate the admissibility of the production terms Π_k we first make use of the assumptions (9.2.5) and (9.2.14) for the interfacial pressures. Then these terms become

$$\Pi_k = \frac{1}{T_k} \sum_{l=1, l\neq k}^{K} (P_{k,l} - p_k)\ (\boldsymbol{v}_k - \boldsymbol{V}_I) \cdot \nabla\, \alpha_l.$$

Obviously, we cannot control the sign of Π_k. According to the conservation constraints (9.2.14) all $P_{k,l}$, $k \neq l$, are coupled. Therefore we determine the interfacial pressures $P_{k,l}$ and the interfacial velocity $\boldsymbol{V}_I$ such that the sum $\Pi := \sum_{k=1}^{K} \Pi_k$ vanishes. For this purpose we substitute $\nabla\, \alpha_K$ by the other gradients using (9.2.8). According to the saturation condition (9.2.1) the gradients $\nabla\, \alpha_k$, $k = 1, \ldots, K-1$, are linearly independent. Thus rearranging the terms in Π with respect to the $K-1$ gradients of α_k the coefficients in front of these gradients must be zero when Π vanishes. This yields the following $K-1$ conditions

$$\sum_{k=1, k\neq l}^{K-1} \frac{1}{T_k} \left((P_{k,l} - p_k) - (P_{k,K} - p_k)\right) (\boldsymbol{v}_k - \boldsymbol{V}_I) + \frac{1}{T_K} (P_{K,l} - p_K)(\boldsymbol{v}_K - \boldsymbol{V}_I) = \boldsymbol{0} \tag{9.6.17}$$

for $l = 1, \ldots, K-1$. Next we assume that the interfacial velocity is a convex combination of the single component velocities $\boldsymbol{v}_k$, i.e.,

$$\boldsymbol{V}_I = \sum_{k=1}^{K} \beta_k \boldsymbol{v}_k, \quad \beta_k \in [0,1], \quad \sum_{k=1}^{K} \beta_k = 1. \tag{9.6.18}$$

This is motivated by Gallouët et al. [16] and Hérard [23] for a two-phase and a three-phase model, respectively. Then we may rewrite the velocity differences in (9.6.17) as

$$\boldsymbol{v}_K - \boldsymbol{V}_I = \sum_{i=1}^{k-1} \sum_{j=1}^{i} (-\beta_j)\, (\boldsymbol{v}_i - \boldsymbol{v}_{i+1}) + \sum_{i=k}^{K-1} \sum_{j=i+1}^{K} \beta_j\, (\boldsymbol{v}_i - \boldsymbol{v}_{i+1}).$$

Rearranging (9.6.17) in terms of the independent differences $\boldsymbol{v}_i - \boldsymbol{v}_{i+1}$, $i = 1, \ldots, K-1$, we obtain the following conditions

$$\begin{aligned} &\sum_{k=1}^{i} \frac{1}{T_k} \left((P_{k,l} - p_k)(1 - \delta_{l,k}) - (P_{k,K} - p_k)\right) \sum_{j=i+1}^{K} \beta_j + \\ &\left(\sum_{k=i+1}^{K-1} \frac{1}{T_k} \left((P_{k,l} - p_k)(1 - \delta_{l,k}) - (P_{k,K} - p_k)\right) + \frac{1}{T_K} (P_{K,l} - p_K) \right) \sum_{j=1}^{i} (-\beta_j) = 0 \end{aligned} \tag{9.6.19}$$

or, equivalently,

$$\begin{aligned} &\sum_{k=1, \neq l}^{i} \left(\frac{1}{T_k} \sum_{j=i+1}^{K} \beta_j \right) P_{k,l} - \sum_{k=1}^{i} \left(\frac{1}{T_k} \sum_{j=i+1}^{K} \beta_j \right) P_{k,K} - \\ &\sum_{k=i+1, \neq l}^{K-1} \left(\frac{1}{T_k} \sum_{j=1}^{i} \beta_j \right) P_{k,l} + \sum_{k=i+1}^{K-1} \left(\frac{1}{T_k} \sum_{j=1}^{i} \beta_j \right) P_{k,K} - \frac{1}{T_K} \sum_{j=1}^{i} \beta_j P_{K,l} = \\ &- \sum_{k=1}^{i} \frac{1}{T_k} p_k \delta_{l,k} \sum_{j=i+1}^{K} \beta_j + \left(\sum_{k=i+1}^{K-1} \frac{1}{T_k} p_k \delta_{l,k} - \frac{1}{T_K} p_K \right) \sum_{j=1}^{i} \beta_j \end{aligned} \tag{9.6.20}$$

for $l, i = 1, \ldots, K-1$. This gives $(K-1)^2$ equations for $(K-1)K$ unknowns $P_{k,l}$, $k, l = 1, \ldots, K$, $k \neq l$. Thus we need additional $K-1$ equations to ensure uniqueness for fixed parameters $\beta_1, \ldots, \beta_K$. These equations are determined by the conservation constraints (9.2.14) that read

$$\sum_{k=1, k\neq l}^{K} P_{k,l} = P_I = const, \quad l = 1, \ldots, K. \tag{9.6.21}$$

These equations are equivalent to

$$\sum_{k=1,k\neq l}^{K} P_{k,l} - \sum_{k=1}^{K-1} P_{k,K} = 0, \quad l = 1,\dots,K-1, \tag{9.6.22}$$

Then (9.6.20) and (9.6.22) form a linear system for the interfacial pressures. To solve the system it is convenient to rewrite it in blockwise form

$$\boldsymbol{A}_l\boldsymbol{\Lambda}_l\boldsymbol{P}_l + \boldsymbol{B}\boldsymbol{\Lambda}_K\boldsymbol{P}_K = \boldsymbol{d}_l, \quad l = 1,\dots,K-1 \tag{9.6.23}$$

for the unknowns $\boldsymbol{P}_l := (P_{1,l},\dots,P_{l-1,l},P_{l+1,l},\dots,P_{1,K})^T$, $l = 1,\dots,K$ with matrix $\boldsymbol{\Lambda}_l = \mathrm{diag}(T_1^{-1},\dots,T_{l-1}^{-1},T_{l+1}^{-1},\dots,T$ assuming positive temperatures T_k, and $\boldsymbol{A}_l = (\boldsymbol{a}^1,\dots,\boldsymbol{a}^{l-1},\boldsymbol{a}^{l+1},\dots,\boldsymbol{a}^K)$ and $\boldsymbol{B} = (\boldsymbol{b}^1,\dots,\boldsymbol{b}^{K-1})$ in $\mathbb{R}^{K\times(K-1)}$ defined by the columns

$$\begin{aligned}\boldsymbol{a}^k &= (-c_1,\dots,-c_{k-1},c^k,\dots,c^{K-1},T_k)^T \in \mathbb{R}^K, \quad k = 1,\dots,K,\\ \boldsymbol{b}^k &= (c_1,\dots,c_{k-1},-c^k,\dots,-c^{K-1},T_k)^T \in \mathbb{R}^K, \quad k = 1,\dots,K-1\end{aligned}$$

and right-hand side $d_{l,i} = c_i(p_l/T_l - P_K/T_K)$, $1 \le i \le l-1$ and $d_{l,i} = c_i(p_l/T_l - P_K/T_K) - p_l/T_l$, $l \le i \le K-1$. Here we define $c_k := \sum_{j=1}^{k}\beta_j$, $c^k := \sum_{j=k+1}^{K}\beta_j$. Note that by the convexity assumption (9.6.18) it holds $c_k + c^k = 1$, $k = 1,\dots,K$. Manipulating the rows and columns of (9.6.23) we obtain the equivalent system $\overline{\boldsymbol{A}}\,\overline{\boldsymbol{P}} = \overline{\boldsymbol{d}}$ with

$$\overline{\boldsymbol{A}} = \begin{pmatrix} \overline{\boldsymbol{A}}_1 & & & \overline{\boldsymbol{B}} \\ & \overline{\boldsymbol{A}}_2 & & \overline{\boldsymbol{B}} \\ & & \ddots & \vdots \\ & & \overline{\boldsymbol{A}}_{K-1} & \overline{\boldsymbol{B}} \end{pmatrix} \overline{\boldsymbol{S}}, \quad \overline{\boldsymbol{P}} = \overline{\boldsymbol{S}}^{-1}\begin{pmatrix} \boldsymbol{S}^{-1}\overline{\boldsymbol{P}}_1 \\ \boldsymbol{S}^{-1}\overline{\boldsymbol{P}}_2 \\ \vdots \\ \boldsymbol{S}^{-1}\overline{\boldsymbol{P}}_K \end{pmatrix}, \quad \overline{\boldsymbol{r}} = \begin{pmatrix} \boldsymbol{L}\boldsymbol{d}_1 \\ \boldsymbol{L}\boldsymbol{d}_2 \\ \vdots \\ \boldsymbol{L}\boldsymbol{d}_{K-1} \end{pmatrix}$$

with $\overline{\boldsymbol{A}}_l = \boldsymbol{L}\boldsymbol{A}_l\boldsymbol{\Lambda}_l\boldsymbol{S}$, $\boldsymbol{B} = \boldsymbol{L}\boldsymbol{B}\boldsymbol{\Lambda}_K\boldsymbol{S}$ and Frobenius matrices

$$\boldsymbol{S} = \boldsymbol{I}_{K-1} - \sum_{j=1}^{K-2}\boldsymbol{e}_{j+1}\otimes\boldsymbol{e}_j, \quad \boldsymbol{L} = \boldsymbol{I}_K + \sum_{j=1}^{K-1}(T_{j+1}-T_j)\boldsymbol{e}_j\otimes\boldsymbol{e}_K$$

and the transpose of a Frobenius matrix

$$\overline{\boldsymbol{S}} = \boldsymbol{I}_{(K-1)K} + \sum_{k=1}^{K-1}\left(\sum_{j=1}^{k-2}\boldsymbol{e}_{j'(k,j)}\otimes\boldsymbol{e}_{j'(K,j)} + \sum_{j=k}^{K-2}\boldsymbol{e}_{j'(k,j)}\otimes\boldsymbol{e}_{j'(K,j+1)} + \boldsymbol{e}_{j'(k,K-1)}\otimes\boldsymbol{e}_{j'(K,K-1)}\right)$$

with indices $j'(k,j) = j + (k-1)(K-1)$. Here we make the convention that in case of $K = 2$ empty sums in $\overline{\boldsymbol{S}}$ and $\boldsymbol{S}$ correspond to zero matrices. Since the determinant of Frobenius matrices is one, it follows that $\det(\overline{\boldsymbol{A}}) = \left(\hat{T}/\prod_{k=1}^{K}T_k\right)^{K-1}$ with $\hat{T} = \sum_{k=1}^{K}\beta_k T_k$. Thus, the system has a unique solution. This can be determined by successively solving the subsystems $\check{\boldsymbol{A}}_l\check{\boldsymbol{P}}_l = \check{\boldsymbol{r}}_l$, $l = 1,\dots,L-1$ with $\check{\boldsymbol{A}}_l = (\check{\boldsymbol{a}}_1^l,\dots,\check{\boldsymbol{a}}_{K-1}^l,\check{\boldsymbol{b}}_l)^T$ with $\check{\boldsymbol{a}}_k^l = \boldsymbol{e}_k$, $k = 1,\dots,l-2$, $\check{\boldsymbol{a}}_{l-1}^l = \boldsymbol{e}_{l-1}+\boldsymbol{e}_l$, $\check{\boldsymbol{a}}_k^l = \boldsymbol{e}_{k+1}$, $k = l,\dots,K-2$, $\check{\boldsymbol{a}}_{K-1}^l = (-c_1,\dots,-c_{K-1},\hat{T})^T$ and $\check{\boldsymbol{b}}_k^l = -\boldsymbol{e}_k$, $k = l-1,l$ and $\check{\boldsymbol{b}}_k^l = \boldsymbol{0}$ otherwise. The right-hand side is determined by $\check{\boldsymbol{r}}_l = \overline{\boldsymbol{r}}_l + \boldsymbol{e}_{l-1}\overline{P}_{l-1+(K-2)K}$. A tedious calculation finally gives the unique solution to the system (9.6.20) and (9.6.22) and we conclude with the following

Theorem 9.6.3. *(Entropy production due to interfacial states) Let the assumptions (9.2.5) and (9.2.14) hold true. If the temperatures T_k are all positive, then for any convex combination (9.6.18) for the interfacial velocity $\boldsymbol{V}_I$ there uniquely exist interfacial pressures*

$$P_{k,l} = \frac{1}{\hat{T}}\left(\beta_k p_l T_k + p_k\sum_{j=1,\neq k}^{K}\beta_j T_j\right), \quad \hat{T} := \sum_{k=1}^{K}\beta_k T_k \tag{9.6.24}$$

solving the linear system (9.6.20) and (9.6.22) and, thus, the production term $\Pi = \sum_{k=1}^{K} \Pi_k$ *vanishes. In particular, the interfacial pressures are all positive and it holds*

$$P_I = \sum_{k=1}^{K} p_k \sum_{j=1,\neq k}^{K} \beta_j T_j / \hat{T}. \tag{9.6.25}$$

.

Since by means of the linear system (9.6.20) and (9.6.22) the interfacial pressures $P_{k,l}$ depend on the convex combination (9.6.18) for the interfacial velocity $\boldsymbol{V}_I$, the 2nd law of thermodynamics does not uniquely characterize interfacial velocity. There are several options discussed in the literature for two-component and three-component models, cf. [16, 23, 37]. We comment on this in Section 9.7.4.

9.6.3.3 Entropy production due to relaxation

According to the entropy law (9.6.8) of a single component the entropy production due to the relaxation processes is determined by

$$S_{\alpha\rho s,k} = \frac{1}{T_k} \left(p_k S_{\alpha,k} + (u_k - g_k) S_{\alpha\rho,k} - \boldsymbol{v}_k \cdot \boldsymbol{S}_{\alpha\rho\boldsymbol{v},k} + S_{\alpha\rho E,k} \right), \tag{9.6.26}$$

where we plug (9.6.7) and (9.3.5) into (9.6.9). Here the Gibbs free energy of component k is defined as

$$g_k = e_k + p_k/\rho_k - T_k s_k \tag{9.6.27}$$

In addition to the conservation constraints (9.2.13) the relaxation terms (9.2.9) have to satisfy

$$S_{\rho s,k} \geq 0, \;\; k = 1, \ldots, K \text{ or } \sum_{k=1}^{K} S_{\alpha\rho s,k} \geq 0. \tag{9.6.28}$$

to ensure that the mixture is consistent with the 2nd law of thermodynamics.

9.6.4 Thermodynamic stability

According to Menikoff and Plohr [30] thermodynamic stability of a single component k requires that e_k is a convex function of the specific volume τ_k and the specific entropy s_k, see also Section 9.6.1. In [19], p. 99 ff, it is proven that this holds true, if the entropy $U_k := -\rho_k s_k$ is a convex function of $\boldsymbol{u}_k := (\rho_k, \rho_k \boldsymbol{v}_k^T, \rho_k E_k)^T$. In the following we will verify that

$$U(\boldsymbol{u}) := -\sum_{k=1}^{K} \alpha_k \rho_k s_k = -\rho s \tag{9.6.29}$$

is a convex function of the quantities $\boldsymbol{u} := (\boldsymbol{\alpha}, \alpha_1 \boldsymbol{u}_1^T, \ldots, \alpha_K \boldsymbol{u}_K^T)^T$ with $\boldsymbol{\alpha} := (\alpha_1, \ldots, \alpha_{K-1})^T$. For this purpose we extend the proof in [37], Appendix A, for a two-phase model to our K-component model.

To verify the convexity of U we need to prove that the Hessian is positive semi-definite. First of all, we note that by (9.2.1)

$$\frac{\partial \alpha_k}{\partial \alpha_l} = \delta_{k,l} - \delta_{k,K}, \quad \frac{\partial \boldsymbol{u}_k}{\partial \alpha_l} = -\frac{1}{\alpha_k} \boldsymbol{u}_k (\delta_{k,l} - \delta_{k,K}), \;\; \frac{\partial \boldsymbol{u}_k}{\partial \alpha_l \boldsymbol{u}_l} = \frac{1}{\alpha_k} \delta_{k,l} \boldsymbol{I}_{d+2}$$

holds for $k = 1, \ldots, K, \;\; l = 1, \ldots, K-1$. Then it follows for the gradient of U:

$$\frac{\partial U}{\partial \alpha_l}(\boldsymbol{u}) = U_l(\boldsymbol{u}_l) - U_K(\boldsymbol{u}_K) - \frac{\partial U_l}{\partial \boldsymbol{u}_l}(\boldsymbol{u}_l) \cdot \boldsymbol{u}_l + \frac{\partial U_K}{\partial \boldsymbol{u}_K}(\boldsymbol{u}_K) \cdot \boldsymbol{u}_K, \;\; \frac{\partial U}{\partial \alpha_l \boldsymbol{u}_l}(\boldsymbol{u}) = \frac{\partial U_l}{\partial \boldsymbol{u}_l}(\boldsymbol{u}_l). \tag{9.6.30}$$

The Hessian of U is determined by the second order derivatives

$$\begin{aligned}
\frac{\partial^2 U}{\partial \alpha_k \partial \alpha_l}(\boldsymbol{u}) &= \delta_{k,l} \frac{1}{\alpha_l} \boldsymbol{u}_l^T \frac{\partial^2 U_l}{\partial^2 \boldsymbol{u}_l}(\boldsymbol{u}_l) \boldsymbol{u}_l + \frac{1}{\alpha_K} \boldsymbol{u}_K^T \frac{\partial^2 U_K}{\partial^2 \boldsymbol{u}_K}(\boldsymbol{u}_K) \boldsymbol{u}_K, \;\; k, l = 1, \ldots, K, \\
\frac{\partial^2 U}{\partial \alpha_k \partial \alpha_l \boldsymbol{u}_l}(\boldsymbol{u}) &= -\frac{1}{\alpha_l} (\delta_{k,l} - \delta_{K,l}) \frac{\partial^2 U_l}{\partial^2 \boldsymbol{u}_l}(\boldsymbol{u}_l) \boldsymbol{u}_l, l = 1, \ldots, K, \;\; k = 1, \ldots, K-1, \\
\frac{\partial^2 U}{\partial \alpha_k \boldsymbol{u}_k \partial \alpha_l \boldsymbol{u}_l}(\boldsymbol{u}) &= \frac{1}{\alpha_l} \delta_{k,l} \frac{\partial^2 U_l}{\partial^2 \boldsymbol{u}_l}(\boldsymbol{u}_l), \;\; k, l = 1, \ldots, K.
\end{aligned}$$

For a compact representation of the Hessian we introduce the notation

$$\begin{aligned}
\boldsymbol{U}_{\boldsymbol{\alpha},\boldsymbol{\alpha}} &:= \left(\frac{\partial^2 U}{\partial\alpha_k\partial\alpha_l}(\boldsymbol{u})\right)_{l,k=1,\dots,K-1} \in \mathbb{R}^{(K-1)\times(K-1)},\\
\boldsymbol{U}_{\alpha_k\boldsymbol{u_k},\alpha_k\boldsymbol{u_k}} &:= \frac{\partial^2 U}{\partial\alpha_k\boldsymbol{u}_k\partial\alpha_k\boldsymbol{u}_k}(\boldsymbol{u}) \in \mathbb{R}^{(d+2)\times(d+2)},\\
\boldsymbol{U}_{\alpha_k\boldsymbol{u_k},\boldsymbol{\alpha}} &:= \left(\frac{\partial^2 U}{\partial\alpha_k\boldsymbol{u}_k\partial\alpha_1}(\boldsymbol{u}),\dots,\frac{\partial^2 U}{\partial\alpha_k\boldsymbol{u}_k\partial\alpha_{K-1}}(\boldsymbol{u})\right) \in \mathbb{R}^{(d+2)\times(K-1)}.
\end{aligned}$$

According to the above second order derivatives these are determined by

$$\boldsymbol{U}_{\boldsymbol{\alpha},\boldsymbol{\alpha}} = \frac{1}{\alpha_K}\boldsymbol{u}_K^T\boldsymbol{U}_K''\boldsymbol{u}_K\mathbf{1}_{K-1} + \operatorname{diag}\left(\left(\frac{1}{\alpha_k}\boldsymbol{u}_k^T\boldsymbol{U}_k''\boldsymbol{u}_k\right)_{k=1,\dots,K-1}\right), \tag{9.6.31}$$

$$\boldsymbol{U}_{\alpha_k\boldsymbol{u_k},\alpha_k\boldsymbol{u_k}} = \frac{1}{\alpha_k}\boldsymbol{U}_k'', \tag{9.6.32}$$

$$\boldsymbol{U}_{\alpha_k\boldsymbol{u_k},\boldsymbol{\alpha}} = \left(-\frac{1}{\alpha_k}(\delta_{k,l}-\delta_{K,k})\boldsymbol{U}_k''\boldsymbol{u}_k\right)_{l=1,\dots,K-1} = \boldsymbol{U}_{\boldsymbol{\alpha},\alpha_k\boldsymbol{u}_k}^T, \tag{9.6.33}$$

where $\boldsymbol{U}_k''$ denotes the Hessian of the entropy $U_k = U_k(\boldsymbol{u}_k)$ of component k. Then the Hessian can be represented as block-matrix

$$\boldsymbol{U}''(\boldsymbol{u}) = \begin{pmatrix} \boldsymbol{U}_{\boldsymbol{\alpha},\boldsymbol{\alpha}} & \boldsymbol{U}_{\boldsymbol{\alpha},\alpha_1\boldsymbol{u_1}} & \cdots & \boldsymbol{U}_{\boldsymbol{\alpha},\alpha_1\boldsymbol{u_K}} \\ \boldsymbol{U}_{\alpha_1\boldsymbol{u_1},\boldsymbol{\alpha}} & \boldsymbol{U}_{\alpha_1\boldsymbol{u_1},\alpha_1\boldsymbol{u_1}} & & \\ \vdots & & \ddots & \\ \boldsymbol{U}_{\alpha_K\boldsymbol{u_K},\boldsymbol{\alpha}} & & & \boldsymbol{U}_{\alpha_1\boldsymbol{u_K},\alpha_K\boldsymbol{u_K}} \end{pmatrix}. \tag{9.6.34}$$

To verify positive semi-definiteness of the Hessian we introduce the vector $\boldsymbol{x} = (\boldsymbol{a}^T, \boldsymbol{b}_1^T, \dots, \boldsymbol{b}_K^T)^T$ with $\boldsymbol{a} \in \mathbb{R}^{K-1}$ and $\boldsymbol{b}_k \in \mathbb{R}^{d+2}$, $k = 1,\dots,K$. Then we obtain by the block-structure (9.6.34) of the Hessian

$$\boldsymbol{x}^T\boldsymbol{U}''\boldsymbol{x} = \boldsymbol{a}^T\boldsymbol{U}_{\boldsymbol{\alpha},\boldsymbol{\alpha}}\boldsymbol{a} + \sum_{k=1}^K \boldsymbol{a}^T\boldsymbol{U}_{\boldsymbol{\alpha},\alpha_k\boldsymbol{u_k}}\boldsymbol{b}_k + \sum_{k=1}^K \boldsymbol{b}_k^T\left(\boldsymbol{U}_{\alpha_k\boldsymbol{u_k},\boldsymbol{\alpha}}\boldsymbol{a} + \boldsymbol{U}_{\alpha_k\boldsymbol{u_k},\alpha_k\boldsymbol{u_k}}\boldsymbol{b}_k\right). \tag{9.6.35}$$

By means of (9.6.31), (9.6.32) and (9.6.33) we determine

$$\begin{aligned}
\boldsymbol{a}^T\boldsymbol{U}_{\boldsymbol{\alpha},\boldsymbol{\alpha}}\boldsymbol{a} &= \frac{1}{\alpha_K}(a\boldsymbol{u}_K)^T\boldsymbol{U}_K''(a\boldsymbol{u}_K) + \sum_{k=1}^{K-1}\frac{1}{\alpha_k}(a_k\boldsymbol{u}_k)^T\boldsymbol{U}_k''(a_k\boldsymbol{u}_k),\ a := \sum_{l=1}^{K-1} a_l,\\
\boldsymbol{a}^T\boldsymbol{U}_{\boldsymbol{\alpha},\alpha_k\boldsymbol{u_k}}\boldsymbol{b}_k &= -\sum_{l=1}^{K-1}\frac{1}{\alpha_k}(\delta_{k,l}-\delta_{k,K})\boldsymbol{b}_k^T\boldsymbol{U}_k''(a_l\boldsymbol{u}_k),\\
\boldsymbol{b}_k^T\boldsymbol{U}_{\boldsymbol{\alpha},\alpha_k\boldsymbol{u_k}}\boldsymbol{a} &= \frac{1}{\alpha_K}\delta_{k,K}\boldsymbol{b}_K^T\boldsymbol{U}_K''(a\boldsymbol{u}_K) - \frac{1}{\alpha_k}(1-\delta_{k,K})\boldsymbol{b}_k^T\boldsymbol{U}_k''(a_k\boldsymbol{u}_k),\\
\boldsymbol{b}_k^T\boldsymbol{U}_{\alpha_k\boldsymbol{u_k},\alpha_k\boldsymbol{u_k}}\boldsymbol{b}_k &= \frac{1}{\alpha_k}\boldsymbol{b}_k^T\boldsymbol{U}_k''\boldsymbol{b}_k.
\end{aligned}$$

Incorporating this into (9.6.35) we finally conclude after some calculus with

$$\begin{aligned}
\boldsymbol{x}^T\boldsymbol{U}''\boldsymbol{x} = &\sum_{k=1}^{K-1}\frac{1}{\alpha_k}(\boldsymbol{b}_k - a_k\boldsymbol{u}_k)^T\boldsymbol{U}_k''(\boldsymbol{b}_k - a_k\boldsymbol{u}_k)\\
&+\frac{1}{\alpha_K}(\boldsymbol{b}_K - a\boldsymbol{u}_K)^T\boldsymbol{U}_K''(\boldsymbol{b}_K - a\boldsymbol{u}_K) \ge 0,
\end{aligned}$$

because the Hessians $\boldsymbol{U}_k''$ are assumed to be positive semi-definite. Note that for $\boldsymbol{x} \neq \boldsymbol{0}$ we cannot ensure $\boldsymbol{x}^T\boldsymbol{U}''\boldsymbol{x}$ to be positive even if $\boldsymbol{U}_k''$ is strictly convex because all the terms $\boldsymbol{b}_k - a_k\boldsymbol{u}_k$, $k = 1,\dots,K-1$, and $\boldsymbol{b}_K - a\boldsymbol{u}_K$ may vanish at the same time. Thus we have proven the following

Theorem 9.6.4. *(Convexity of entropy function) Let e_k be a convex function of (τ_k, s_k), $k = 1,\dots,K$. Then the entropy U is a convex function of $\boldsymbol{u}$, i.e, the Hessian of U is positive semi-definite.*

9.6.5 Remarks on entropy-entropy flux pairs

From a mathematical point of view, the concept of entropy-entropy flux pairs, cf. [18], has been introduced to characterize a unique weak solution of an initial (boundary) value problem of (inhomogeneous) conservation laws that in quasi-conservative form reads

$$\partial_t \boldsymbol{u} + \sum_{i=1}^{d} \boldsymbol{A}_i(\boldsymbol{u}) \partial_{x_i} \boldsymbol{u} = \boldsymbol{S}(\boldsymbol{u}), \quad \boldsymbol{A}_i(\boldsymbol{u}) := \frac{\partial \boldsymbol{f}_i}{\partial \boldsymbol{u}}(\boldsymbol{u}) \tag{9.6.36}$$

where $\boldsymbol{u} : \mathbb{R}_+ \times \Omega \to D \subset \mathbb{R}^m$ with $\Omega \subset \mathbb{R}^d$, $\boldsymbol{f}_i : D \to \mathbb{R}^m$, $i = 1, \ldots, d$ and $\boldsymbol{S} : D \to \mathbb{R}^m$, denote the vector of m conserved quantities, the fluxes in the ith coordinate direction, $i = 1, \ldots, d$, and the source function, respectively. Motivated by thermodynamics, the entropy inequality

$$\partial_t U(\boldsymbol{u}) + \sum_{i=1}^{d} \partial_{x_i} \boldsymbol{F}_i(\boldsymbol{u}) \leq 0 \tag{9.6.37}$$

has to hold in a weak sense for any convex function $U : D \to \mathbb{R}$ and functions $F_i : D \to \mathbb{R}$, $i = 1, \ldots, d$, referred to as entropy and entropy flux, that satisfy the compatibility conditions

$$\nabla_{\boldsymbol{u}} U(\boldsymbol{u})^T \boldsymbol{A}_i(\boldsymbol{u}) = \nabla_{\boldsymbol{u}} F_i(\boldsymbol{u})^T, \ i = 1, \ldots, d. \tag{9.6.38}$$

Due to these conditions we infer for smooth solutions of (9.6.36) the entropy equation

$$\partial_t U(\boldsymbol{u}) + \sum_{i=1}^{d} \partial_{x_i} F_i(\boldsymbol{u}) = \nabla_{\boldsymbol{u}} U(\boldsymbol{u})^T \boldsymbol{S}(\boldsymbol{u}), \tag{9.6.39}$$

Obviously, the entropy inequality (9.6.37) holds if and only if the entropy production is negative, i.e.,

$$\nabla_{\boldsymbol{u}} U(\boldsymbol{u})^T \boldsymbol{S}(\boldsymbol{u}) \leq 0. \tag{9.6.40}$$

Motivated by the entropy equation (9.6.11) a candidate for an entropy-entropy flux pair for our non-equilibrium model (9.2.2), (9.2.3), (9.2.4) and (9.2.7) neglecting viscosity and heat conduction is

$$U(\boldsymbol{u}) := -\sum_{k=1}^{K} \alpha_k \rho_k s_k = -\rho s, \quad F_i(\boldsymbol{u}) := -\sum_{k=1}^{K} \alpha_k \rho_k s_k v_{k,i}, \ i = 1, \ldots, d. \tag{9.6.41}$$

In [34] it has been proven that the entropy-entropy flux pairs (U, F_i) satisfies the compatibility conditions (9.6.38), if the conditions (9.6.17) hold. Furthermore, it was shown that inequality (9.6.40) is equivalent to $S_{\rho s} \geq 0$ provided that the entropies $s_k = s_k(\tau_k, e_k)$, $k = 1, \ldots, K$, are concave functions, i.e., (9.6.4) holds.

9.7 Relaxation model

The non-equilibrium model presented in Section 9.2.1 allows for different values for velocities, pressures, temperatures as well as chemical potentials at the same point. Therefore one has to introduce a relaxation mechanism, that drives all these quantities into equilibrium. Typically it is distinguished between mechanical and thermal relaxation processes that relax either pressures and velocities or temperatures and chemical potentials to equilibrium.

The relaxation terms are of major importance when dealing with interface problems, see for instance Saurel and Abgrall [38] or Lallemand et al. [27] for mechanical relaxation terms and Métayer et al. [31] for pressure, temperature and Gibbs free energy relaxation terms. Typically, it is assumed that pressure and velocity relax instantaneously, see [38], whereas the thermal relaxation and the relaxation of chemical potentials are much slower, see Zein [44]. For particular applications the orders of the relaxation times can be precised, for instance in the barotropic case, cf. [2].

Note that in the equilibrium model the equilibrium state is characterized by vanishing relaxation terms rather than the transient relaxation process itself. Since the equilibrium state does not depend on the order of relaxation, the relaxation times have not to be known explicitly.

In the subsequent sections we present the relaxation terms for mechanical, thermal and chemical potential relaxation. For each relaxation process we verify the constraints due to conservation (9.2.13) and entropy production (9.6.28). Note that for all relaxation processes the corresponding source terms satisfy the constraint (9.5.20) due to Galilean invariance.

9.7.1 Mechanical relaxation

The *pressure relaxation* implies volume variations, that induce energy variations due to the interfacial pressure work. Here we extend the pressure relaxation vector given in [38] for a two-phase model according to [44] by introducing a pressure average that we choose as the mixture pressure. The pressure relaxation terms then read

$$S^p_{\alpha,k} := \theta_p\,\alpha_k\,(p_k - p),\;\; S^p_{\alpha\rho,k} := 0,\;\; \boldsymbol{S}^p_{\alpha\rho\boldsymbol{v},k} := \boldsymbol{0},\;\; S^p_{\alpha\rho E,k} := \theta_p\,\alpha_k\,p(p - p_k). \tag{9.7.1}$$

Here θ_p denotes the pressure relaxation parameter. Similarly the *velocity relaxation* terms read

$$S^v_{\alpha,k} = S^v_{\alpha\rho,k} := 0,\;\; \boldsymbol{S}^v_{\alpha\rho\boldsymbol{v},k} := \theta_v\,\alpha_k\,\rho_k\,(\boldsymbol{v} - \boldsymbol{v}_k),\;\; S^v_{\alpha\rho E,k} := \theta_v\,\alpha_k\,\rho_k\,\boldsymbol{v}\cdot(\boldsymbol{v} - \boldsymbol{v}_k) \tag{9.7.2}$$

with the velocity relaxation parameter θ_v. For more details on mechanical relaxation see Baer and Nunziato [5] or Baer [14] for two-phase models.

Obviously, the mechanical relaxation terms (9.7.1) and (9.7.2) satisfy the conservation constraints (9.2.13) as can be validated by the definition of the mixture pressure and the mixture velocity (9.2.10) and the saturation condition (9.2.1). Furthermore we determine by (9.6.26) and (9.7.1), (9.7.2) the entropy production terms

$$S^v_{\alpha\rho s,k} = \theta_v\frac{\alpha_k\rho_k}{T_k}(\boldsymbol{v} - \boldsymbol{v}_k)^2, \quad S^p_{\alpha\rho s,k} = \theta_p\frac{\alpha_k}{T_k}(p - p_k)^2. \tag{9.7.3}$$

This immediately implies

Theorem 9.7.1. *(Entropy production due to mechanical relaxation) Let $\rho_k \geq 0$, $T_k > 0$ and the relaxation parameters θ_p, $\theta_v \geq 0$. Then the entropy production due to mechanical relaxation is non-negative, i.e.,*

$$S^{p,v}_{\alpha\rho s,k} \geq 0,\;\; k = 1,\ldots,K \quad \textit{and} \quad \sum_{k=1}^{K} S^{p,v}_{\alpha\rho s,k} \geq 0. \tag{9.7.4}$$

9.7.2 Thermal relaxation

For the modeling of *temperature relaxation* we follow in principal Zein [44]. First of all, we introduce a general class of temperature relaxation models

$$S^T_{\alpha,k} := \theta_T\frac{Q_k}{\kappa_k},\;\; S^T_{\alpha\rho,k} := 0,\;\; \boldsymbol{S}^T_{\alpha\rho\boldsymbol{v},k} := \boldsymbol{0},\;\; S^T_{\alpha\rho E,k} := \theta_T\,Q_k, \tag{9.7.5}$$

with the relaxation parameter θ_T and

$$Q_k = \gamma_k(\hat{T} - T_k). \tag{9.7.6}$$

According to the conservation constraint (9.2.13) the terms Q_k have to satisfy

$$\sum_{k=1}^{K} Q_k = 0 \qquad \text{and} \qquad \sum_{k=1}^{K}\frac{Q_k}{\kappa_k} = 0. \tag{9.7.7}$$

In order to guarantee the first constraint, we choose for $\hat{T}$ the following expression

$$\hat{T} = \sum_{k=1}^{K}\beta^T_k T_k \tag{9.7.8}$$

with coefficients

$$\beta^T_k = \gamma_k/\gamma, \quad \gamma := \sum_{k=1}^{K}\gamma_k. \tag{9.7.9}$$

Obviously, $\hat{T}$ is a convex combination of the temperatures T_k because

$$\sum_{k=1}^{K}\beta^T_k = 1. \tag{9.7.10}$$

For instance, we may choose (a) $\gamma_k = \alpha_k$. Then $\beta_k^T = \alpha_k$ and $\hat{T}$ coincides with the mixture temperature (9.6.10). In case of (b) $\gamma_k = 1$ or (c) $\gamma_k = K$ we compute $\beta_k^T = 1/K$ and $\hat{T}$ is given as the averaged mixture $\hat{T} = \sum_{k=1}^K T_k/K$. For these three cases we obtain (a) $Q_k = \alpha_k(\hat{T} - T_k)$, (b) $Q_k = (\hat{T} - T_k)$ and (c) $Q_k = \sum_{l=1}^K (T_l - T_k)$, respectively.

Next we determine by (9.6.26) and (9.7.5) the entropy production term

$$S_{\rho s,k}^T = \theta_T \frac{1}{T_k} Q_k \left(\frac{p_k}{\kappa_k} + 1 \right). \tag{9.7.11}$$

Thus the entropy production due to thermal relaxation becomes

$$S_{\rho s}^T := \sum_{k=1}^K S_{\alpha\rho s,k}^T = \theta_T \sum_{k=1}^K \frac{1}{T_k} Q_k \left(\frac{p_k}{\kappa_k} + 1 \right) = \theta_T \sum_{k=1}^K \frac{1}{T_k} Q_k + \theta_T \sum_{k=1}^K \frac{p_k}{T_k \kappa_k} Q_k. \tag{9.7.12}$$

We note that by the definitions (9.7.6) and (9.7.9) of Q_k and β_k, respectively, the relation

$$\sum_{k=1}^K \frac{1}{T_k} Q_k = \gamma \sum_{k,l=1}^K \frac{1}{T_k} \beta_k^T \beta_l^T (T_l - T_k)$$

holds. Here we employ (9.7.8) and (9.7.10) to compute the difference $\hat{T} - T_k = \sum_{l=1}^K \beta_l^T (T_l - T_k)$. Furthermore we observe that for any b_k and $a_{k,l} = -a_{l,k}$, $l, k = 1, \dots, k$ we have

$$\sum_{k,l=1}^K b_k a_{k,l} = \sum_{k=2}^K b_k \sum_{l=1}^{k-1} a_{k,l} + \sum_{k=1}^{K-1} b_k \sum_{l=k+1}^K a_{k,l} = \sum_{k=1}^{K-1} \sum_{l=k+1}^K (b_k - b_l) a_{k,l}.$$

Choosing $b_k = 1/T_k$ and $a_{k,l} = \beta_k^T \beta_l^T (T_l - T_k)$ we thus conclude with

$$\sum_{k=1}^K \frac{1}{T_k} Q_k = \gamma \sum_{k=1}^{K-1} \sum_{l=k+1}^K \beta_k^T \beta_l^T \frac{(T_k - T_l)^2}{T_k T_l}.$$

Obviously, the sum is non-negative whenever the temperatures are positive. Thus the first term on the right-hand side of (9.7.12) is non-negative. To ensure that the second term is also non-negative, we rewrite the sum by means of the conservation constraints (9.7.7) as

$$\sum_{k=1}^K \frac{p_k}{T_k \kappa_k} Q_k = \sum_{k=1}^{K-1} \left(\frac{p_k}{T_k} - \frac{p_K}{T_K} \right) \frac{1}{\kappa_k} Q_k.$$

and choose κ_k such that

$$\left(\frac{p_k}{T_k} - \frac{p_K}{T_K} \right) \frac{1}{\kappa_k} = a_k Q_k, \quad k = 1, \dots, K-1$$

holds for some positive parameters a_k, i.e.,

$$\kappa_k = \frac{T_K p_k - T_k p_K}{a_k T_k T_K Q_k}, \quad k = 1, \dots, K-1. \tag{9.7.13}$$

The missing parameter κ_K is determined by the conservation constrains (9.7.7) as

$$\kappa_K = -Q_K \left(\sum_{k=1}^{K-1} \frac{Q_k}{\kappa_k} \right)^{-1}. \tag{9.7.14}$$

Finally we summarize our results in the following

Theorem 9.7.2. *(Entropy production due to thermal relaxation) Let the temperatures and the relaxation parameter be strictly positive, i.e., $T_k > 0$ and $\theta_T > 0$. Let Q_k satisfy (9.7.6) where $\hat{T}$ is defined as convex*

combination (9.7.8) of the temperatures T_k with coefficients β_k satisfying (9.7.9) and (9.7.10). Then the mixture entropy production due to thermal relaxation is non-negative, i.e.,

$$S_{\rho s}^T = \theta_T \sum_{k=1}^{K} \frac{1}{T_k} Q_k \left(\frac{p_k}{\kappa_k} + 1 \right) \geq 0, \tag{9.7.15}$$

provided that the condition

$$\sum_{k=1}^{K} \frac{p_k}{T_k \kappa_k} Q_k \geq 0$$

holds. In particular, this condition holds for the parameters κ_k determined by (9.7.13) and (9.7.14) with non-negative coefficients a_k. It also holds in case of pressure equilibrium, i.e., $p_1 = \ldots = p_K = p$, and constant parameters $\kappa_1 = \ldots = \kappa_K = \kappa$.

When the temperature relaxation approaches thermal equilibrium, the parameters κ_k, $k = 1, \ldots, K-1$, tend to $\kappa_k = p/(a_k \gamma_k T^2)$ provided that the pressure relaxes faster to its equilibrium state. If the pressure is not at equilibrium when thermal equilibrium is reached, then $\kappa_k = \infty$, i.e., $S_{\alpha,k}^T = 0$. However, it is widely accepted that the mechanical relaxation proceeds faster than the thermal relaxation.

Finally we conclude with some remarks on existing relaxation models. In [44] a constant parameter $\kappa_k = \kappa$ is chosen such that pressure stays at equilibrium during the temperature relaxation. More details on its definition in case of a two-phase and a three-phase model can be found in Zein [44] and Zein et al. [45], respectively. Note that the coefficient κ in [44] results in a non-negative entropy production if the pressures are at equilibrium. In the non-equilibrium case (9.7.15) cannot be proven to hold.

In the thermal relaxation model considered by Saleh [37] there is no relaxation term accounted for in the evolution equations for the volume fractions, i.e., $S_{\alpha,k}^T = 0$. This fits into our model when choosing $a_k = 0$, i.e., $\kappa_k = \infty$, for $k = 1, \ldots, K$. Then the investigation of the entropy production simplifies because the second term on the right-hand side in (9.7.12) does not exist.

9.7.3 Chemical potential relaxation

Mass transfer between different phases of the same substance occurs, whenever these phases are not in chemical equilibrium. This physical matter of fact is the decisive factor for the idea to model the mass transfer by relaxation of the chemical potentials. The mass transfer is driven by the difference of the chemical potentials. It is obvious, that from now on it is necessary to identify the phases.

9.7.3.1 Chemical potential relaxation for two-component mixtures

For a two-component mixture ($K = 2$) the relaxation of chemical potentials is modeled according to [44] by

$$\begin{aligned} &S_{\alpha,1}^\mu := \theta_\mu \frac{\dot{m}}{\varrho}, \; S_{\alpha\rho,1}^\mu := \theta_\mu \dot{m}, \; \boldsymbol{S}_{\alpha\rho\boldsymbol{v},1}^\mu := \theta_\mu \dot{m} \hat{\boldsymbol{v}}, \; S_{\alpha\rho E,1}^\mu := \theta_\mu \dot{m} \left(\epsilon + \frac{\hat{\boldsymbol{v}}^2}{2} \right), \\ &S_{\alpha,2}^\mu := -S_{\alpha,1}^\mu, \; S_{\alpha\rho,2}^\mu := -S_{\alpha\rho,1}^\mu, \; \boldsymbol{S}_{\alpha\rho\boldsymbol{v},2}^\mu := -\boldsymbol{S}_{\alpha\rho\boldsymbol{v},1}^\mu, \; S_{\alpha\rho E,2}^\mu := -S_{\alpha\rho E,1}^\mu, \end{aligned} \tag{9.7.16}$$

with the relaxation parameter θ_μ. Similar to the interfacial velocity (9.6.18) we choose for the velocity $\hat{\boldsymbol{v}}$ a convex combination

$$\hat{\boldsymbol{v}} = \sum_{k=1}^{K} \beta_k^v \boldsymbol{v}_k, \quad \beta_k^v \in [0,1], \quad \sum_{k=1}^{K} \beta_k^v = 1. \tag{9.7.17}$$

Since for a two-component mixture the Gibbs free energy coincides with the chemical potential, chemical equilibrium is achieved, if the Gibbs free energies of the two components coincide, i.e., $g_1 = g_2$.

Obviously, the conservation constraints (9.2.13) are satisfied. Note that due to these constraints we are not allowed to introduce ϵ_k and ϱ_k differently for each component $k = 1, 2$. Furthermore, the entropy production terms are determined by (9.6.26) and (9.7.16) as

$$S_{\alpha\rho s,k}^\mu = (-1)^{k+1} \theta_\mu \dot{m} \frac{1}{T_k} \left(\epsilon + \frac{1}{2} (\hat{\boldsymbol{v}} - \boldsymbol{v}_k)^2 - g_k + \frac{p_k}{\varrho} \right), \quad k = 1, 2. \tag{9.7.18}$$

These terms may become negative also when θ_μ, $\dot{m}$ and T_k are positive. However, for an appropriate choice of ϵ, ϱ and $\hat{\boldsymbol{v}}$ the entropy production due to the sum of the phasic entropies

$$S^\mu_{\rho s} = \theta_\mu \dot{m} \sum_{k=1}^{2} (-1)^{k+1} \frac{1}{T_k} \left(\epsilon + \frac{1}{2}(\hat{\boldsymbol{v}} - \boldsymbol{v}_k)^2 - g_k + \frac{p_k}{\varrho} \right) \tag{9.7.19}$$

can be verified to be non-negative. For this purpose, we first note that in case of mechanical and thermal equilibrium, i.e.,

$$\boldsymbol{v}_1 = \ldots = \boldsymbol{v}_K = \boldsymbol{v}, \quad p_1 = \ldots = p_K = p, \quad T_1 = \ldots = T_K = T, \tag{9.7.20}$$

the entropy production term becomes

$$S^\mu_{\rho s} = \frac{1}{T} \dot{m} \, \theta_\mu \, (g_2 - g_1)$$

as was already proven in [44]. Obviously this term is non-negative if

$$\dot{m} = a(g_2 - g_1) \tag{9.7.21}$$

with $a \geq 0$. This is an agreement with the kinetic relation in [11].

At mechanical and thermal non-equilibrium we may enforce a non-negative entropy production by choosing the parameters ϵ and ϱ such that

$$\sum_{k=1}^{2} (-1)^{k+1} \frac{1}{T_k} \left(\epsilon + \frac{1}{2}(\hat{\boldsymbol{v}} - \boldsymbol{v}_k)^2 - g_k + \frac{p_k}{\varrho} \right) = b \, (g_2 - g_1) \tag{9.7.22}$$

for some non-negative b. Note that for the parameters ϵ and ϱ in [44] this condition does not hold true. To verify (9.7.22) we proceed in three steps to determine $\hat{\boldsymbol{v}}$, ϵ and ϱ:

1. The velocity $\hat{\boldsymbol{v}}$ is chosen in such a way, that the velocity terms in (9.7.19) vanish:

$$\frac{1}{T_1}(\hat{\boldsymbol{v}} - \boldsymbol{v}_1)^2 - \frac{1}{T_2}(\hat{\boldsymbol{v}} - \boldsymbol{v}_2)^2 = 0. \tag{9.7.23}$$

   This is reasonable because the entropy production (9.7.19) should be a product of the relaxed mass flux $\theta_\mu \dot{m}$ and an interfacial entropy s_I that should not depend on any velocity. Because the velocity $\hat{\boldsymbol{v}}$ is assumed to be a convex combination of the single component velocities, i.e. $\hat{\boldsymbol{v}} = \beta^v_1 \boldsymbol{v}_1 + \beta^v_2 \boldsymbol{v}_2$ with $\beta^v_2 = 1 - \beta^v_1$ according to (9.7.17), we derive from (9.7.23)

$$\beta^v_1 := \frac{\sqrt{T_2}}{\sqrt{T_1} + \sqrt{T_2}}, \quad \beta^v_2 := \frac{\sqrt{T_1}}{\sqrt{T_1} + \sqrt{T_2}}. \tag{9.7.24}$$

2. In the next step we determine ϵ such that

$$\frac{1}{T_1}(\epsilon - c\, g_1) - \frac{1}{T_2}(\epsilon - c\, g_2) = b_\epsilon (g_2 - g_1), \quad \text{with} \quad b_\epsilon = \frac{2c}{T_1 + T_2}$$

   resulting in

$$\epsilon = c \frac{g_2 T_1 + g_1 T_2}{T_1 + T_2}.$$

3. Finally we determine ϱ such that

$$\frac{1}{T_1}\left(\frac{p_1}{\varrho} - d g_1\right) - \frac{1}{T_2}\left(\frac{p_2}{\varrho} - d g_2\right) = b_\varrho (g_2 - g_1), \quad \text{with} \quad b_\varrho = \frac{2d}{T_1 + T_2}$$

   resulting in

$$\varrho = \frac{1}{d} \frac{T_1 + T_2}{g_2 T_1 + g_1 T_2} \frac{p_2 T_1 - p_1 T_2}{T_1 - T_2}.$$

Choosing

$$d = \frac{1}{2}\text{sign}\left(\frac{p_2T_1 - p_1T_2}{T_1 - T_2}\right), \qquad c = 1 - d, \tag{9.7.25}$$

then with the above choice of $\hat{\boldsymbol{v}}$, ϵ and ϱ we obtain (9.7.22) with $b = b_\epsilon + b_\varrho = ((T_1 + T_2)/2)^{-1}$ the reciprocal of the mean temperature of the components. Note that in the equilibrium case ϵ and ϱ tend to $g/2$ and $2p/g$, respectively, assuming that the pressure relaxes faster than the Gibbs free energy.

Again we conclude with the following

Theorem 9.7.3. *(Entropy production due to relaxation of Gibbs free energies) At mechanical and thermal equilibrium, i.e., (9.7.20) holds, the mixture entropy production due to relaxation of Gibbs free energies is non-negative, i.e.,*

$$S^\mu_{\rho s} \geq 0, \tag{9.7.26}$$

if the mass flux is chosen as the kinetic relation (9.7.21) and the relaxation parameter θ_μ as well as the equilibrium temperature T are positive. In the non-equilibrium case, the entropy production is non-negative, if the parameters ϵ and ϱ are chosen such that (9.7.22) holds.

9.7.3.2 Chemical potential relaxation for three-component mixtures

Exemplarily, we consider three components, i.e., $K = 3$, with water vapor ($k = 1$), liquid water ($k = 2$) and inert gas ($k = 3$). Then the vector for relaxation of chemical potentials is given by

$$\begin{aligned}
&S^\mu_{\alpha,1} := \theta_\mu \frac{\dot{m}}{\varrho_1},\ S^\mu_{\alpha\rho,1} := \theta_\mu \dot{m},\ \boldsymbol{S}^\mu_{\alpha\rho\boldsymbol{v},1} := \theta_\mu \dot{m}\,\hat{\boldsymbol{v}},\ S^\mu_{\alpha\rho E,1} := \theta_\mu \dot{m}\left(\epsilon_1 + \frac{\hat{\boldsymbol{v}}^2}{2}\right),\\
&S^\mu_{\alpha,2} := \theta_\mu \frac{\dot{m}}{\varrho_2},\ S^\mu_{\alpha\rho,2} := -\theta_\mu \dot{m},\ \boldsymbol{S}^\mu_{\alpha\rho\boldsymbol{v},2} := -\theta_\mu \dot{m}\,\hat{\boldsymbol{v}},\ S^\mu_{\alpha\rho E,2} := -\theta_\mu \dot{m}\left(\epsilon_2 + \frac{\hat{\boldsymbol{v}}^2}{2}\right),\\
&S^\mu_{\alpha,3} := -\theta_\mu \dot{m}\left(\frac{1}{\varrho_1} + \frac{1}{\varrho_2}\right),\ S^\mu_{\alpha\rho,3} := 0,\ \boldsymbol{S}^\mu_{\alpha\rho\boldsymbol{v},3} := \boldsymbol{0},\ S^\mu_{\alpha\rho E,3} := \theta_\mu \dot{m}\,(\epsilon_2 - \epsilon_1),
\end{aligned} \tag{9.7.27}$$

with the relaxation parameter θ_μ and $\hat{\boldsymbol{v}}$ given by (9.7.17). For details on the physics see the book of Müller and Müller [33]. Again we note that the conservation constraints (9.2.13) are satisfied. Furthermore the entropy production terms can be determined by (9.6.26) and (9.7.16)

$$\begin{aligned}
S^\mu_{\alpha\rho s,1} &= \theta_\mu \dot{m}\frac{1}{T_1}\left(\epsilon_1 + \frac{1}{2}(\hat{\boldsymbol{v}} - \boldsymbol{v}_1)^2 - g_1 + \frac{p_1}{\varrho_1}\right),\\
S^\mu_{\alpha\rho s,2} &= -\theta_\mu \dot{m}\frac{1}{T_2}\left(\epsilon_2 + \frac{1}{2}(\hat{\boldsymbol{v}} - \boldsymbol{v}_2)^2 - g_2 - \frac{p_2}{\varrho_2}\right),\\
S^\mu_{\alpha\rho s,3} &= \theta_\mu \dot{m}\frac{1}{T_3}\left(\epsilon_2 - \epsilon_1 - p_3(\frac{1}{\varrho_1} + \frac{1}{\varrho_2})\right).
\end{aligned} \tag{9.7.28}$$

These terms may become negative also when θ_μ, $\dot{m}$ and T_k are non-negative. For the sum of the phasic entropy production $S^\mu_{\rho s} = S^\mu_{\rho s,1} + S^\mu_{\rho s,2} + S^\mu_{\rho s,3}$ we obtain

$$\begin{aligned}
S^\mu_{\rho s} = \dot{m}\,\theta_\mu \Bigg(\sum_{k=1}^{2} \frac{(-1)^{k+1}}{T_k}\Bigg(\epsilon_k + \frac{1}{2}(\hat{\boldsymbol{v}} - \boldsymbol{v}_k)^2 - g_k - (-1)^k\frac{p_k}{\varrho_k}\Bigg)\\
+\frac{1}{T_3}\left(\epsilon_2 - \epsilon_1 - p_3\left(\frac{1}{\varrho_1} + \frac{1}{\varrho_2}\right)\right)\Bigg).
\end{aligned} \tag{9.7.29}$$

In the following we distinguish between a non-homogeneous and a homogeneous mixture, respectively.

Non-homogeneous mixture. In a non-homogeneous mixture velocity, pressure and temperature are not necessarily in equilibrium. Therefore we need not to account for the mixture entropy. Thus, the chemical potentials and the Gibbs free energies of water vapor and liquid water, respectively, coincide, i.e., $g_k = \mu_k$, $k = 1, 2$, and the mass flux is proportional to the difference in the Gibbs free energies, i.e.,

(9.7.21) holds. Similar to the two- component case, see Section (9.7.3.1), we may enforce a non-negative entropy production by choosing the parameters ϵ_k and ϱ_k such that the condition

$$\sum_{k=1}^{2} \frac{(-1)^{k+1}}{T_k} \left(\epsilon_k + \frac{1}{2}(\boldsymbol{V}_I - \boldsymbol{v}_k)^2 - g_k - (-1)^k \frac{p_k}{\varrho_k} \right) + \frac{1}{T_3} \left(\epsilon_2 - \epsilon_1 - p_3 \left(\frac{1}{\varrho_1} + \frac{1}{\varrho_2} \right) \right) = b\,(g_2 - g_1) \tag{9.7.30}$$

holds for some non-negative b analogously to (9.7.22). Note that the parameters ϵ_k and ϱ_k in [44,46] do not satisfy this condition.

As already assumed in the two-component mixture, we expect that the entropy production of the three-component mixture (9.7.28) should not depend on any velocity. This assumption gives us a condition for the velocity $\hat{\boldsymbol{v}}$ and delivers us the same result as above (9.7.24):

$$\beta_1^v := \frac{\sqrt{T_2}}{\sqrt{T_1} + \sqrt{T_2}}, \quad \beta_2^v := \frac{\sqrt{T_1}}{\sqrt{T_1} + \sqrt{T_2}}, \quad \beta_3^v := 0. \tag{9.7.31}$$

The remaining parameters ϵ_k, ϱ_k, $k = 1, 2$, can be determined similar to the two-component case. We omit details here.

Homogeneous mixture. In a homogeneous mixture velocity, pressure and temperature are in equilibrium. Therefore, as already mentioned in Section 9.6.2, in the total entropy we also have to account for the mixture entropy given by

$$S_M = -\sum_{k=1,3} \alpha_k \rho_k \frac{\kappa_b}{m_k} \ln\left(\frac{\alpha_k}{\alpha_1 + \alpha_3} \right), \tag{9.7.32}$$

with κ_b the Boltzmann constant and m_k the mass of a single molecule of component k, see [32], p. 54, 298, 320. Moreover, the chemical potential of the vapor phase is now given by

$$\mu_1 = g_1 + \frac{\kappa_b T}{m_1} \ln\left(\frac{\alpha_1}{\alpha_1 + \alpha_3} \right) \tag{9.7.33}$$

i.e., it does not coincide with its Gibbs free energy. Note that for vanishing third component, i.e., $\alpha_3 = 0$, the chemical potential of the vapor phase reduces to the vapor Gibbs free energy. Again, the chemical potential of the liquid phase equals its Gibbs free energy, i.e., $\mu_2 = g_2$. In chemical equilibrium the chemical potentials of the vapor and the liquid phase equal each other. Accordingly, the mass flux is now a function of $\mu_2 - \mu_1$, i.e.,

$$\dot{m} = a(\mu_2 - \mu_1) \tag{9.7.34}$$

with $a \geq 0$ that again is an agreement with the kinetic relation in [11].

For a homogeneous mixture the entropy production (9.7.29) reduces to

$$S_{\rho s}^{\mu} = \frac{1}{T} \dot{m}\, \theta_\mu\, (g_2 - g_1) = \frac{1}{T} \dot{m}\, \theta_\mu \left(\mu_2 - \mu_1 + \frac{\kappa_b T}{m_1} \ln\left(\frac{\alpha_1}{\alpha_1 + \alpha_3} \right) \right).$$

Analogously to Section 9.6.2, we determine the entropy production of the mixture entropy S_M

$$S_{S_M}^{\mu} = -\frac{1}{T} \dot{m}\, \theta_\mu \frac{\kappa_b T}{m_1} \ln\left(\frac{\alpha_1}{\alpha_1 + \alpha_3} \right). \tag{9.7.35}$$

Then the total entropy production is given by

$$S_{\rho s}^{\mu} + S_{S_M}^{\mu} = \frac{1}{T} \dot{m}\, \theta_\mu\, (\mu_2 - \mu_1). \tag{9.7.36}$$

Thus we conclude with the following theorem.

Theorem 9.7.4. *(Entropy production due to relaxation of chemical potentials) For a homogeneous mixture the total entropy production is non-negative, i.e.,*

$$S_{\rho s}^{\mu} + S_{S_M}^{\mu} \geq 0, \tag{9.7.37}$$

if the relaxation parameter θ_μ as well as the equilibrium temperature T are positive.

Finally we would like to remark that the above procedure for a particular three-component mixture can be extended to a multi-component mixture.

9.7.4 Remarks on the closure of the interfacial velocity

According to the ansatz (9.6.18) for the interfacial velocity we have some freedom in the choice of the parameters β_k. One option might be the velocity $\hat{\boldsymbol{v}}$ determined in Section 9.7.3. However, these are state-dependent, i.e., $\beta_k^v = \beta_k^v(\boldsymbol{w})$, see (9.7.24) and (9.7.31). As a consequence the linear field associated with the eigenvalue $\lambda_{I,i}$, $i = 1, \dots, K-1$, will not be linearly degenerated, i.e.,

$$\boldsymbol{r}_{I,i} \cdot \nabla_{\boldsymbol{w}} \lambda_{I,i} = \kappa_0 \left(\frac{\partial V_{I,n}}{\partial \alpha_i} + \sum_{k=1}^{K} \left(\overline{x}_{k,i} \frac{\partial V_{I,n}}{\partial \rho_k} + \overline{\boldsymbol{y}}_{k,i} \cdot \nabla_{\boldsymbol{v}_k} V_{I,n} + \overline{z}_{k,i} \frac{\partial V_{I,n}}{\partial p_k} \right) \right) \neq 0.$$

Since the non-equilibrium model contains non-conservative products in the phasic momentum and energy equations, see eqns. (9.2.3) and (9.2.4), there is no way to cope with these terms in case of genuinely nonlinear fields. If fields associated to the non-conservative products only occur in linearly degenerated fields, then Riemann invariants of the associated field can be enforced and, thus, the exact solution of the Riemann problem exists as has been verified for Baer-Nunziato type models in [17]. Therefore, it is suggested in [16] and [23] to determine the interfacial velocity such that the associated field is linearly degenerated. Obviously, at mechanical and thermal equilibrium this field is linearly degenerate for arbitrary convex combinations (9.6.18) provided that $\beta_k \neq \beta_k(\alpha)$ because $\overline{\boldsymbol{y}}_{k,i} = \boldsymbol{0}$, $\overline{x}_{k,i} = \overline{z}_{k,i} = \partial \beta_k / \partial \alpha_i = 0$. At non-equilibrium this no longer holds true.

To derive appropriate closing conditions in this case we extend the ansatz of Saleh [37], eqn. (4.3.40), in case of a two-phase mixture. For this purpose we introduce another arbitrary but fixed convex combination $\sum_{k=1}^{K} c_k = 1$ with constant coefficients $c_k \in [0,1]$. Then we define the coefficients β_k in (9.6.18) as

$$\beta_k := \frac{c_k \alpha_k \rho_k}{\hat{\rho}}, \quad \hat{\rho} := \sum_{k=1}^{K} c_k \alpha_k \rho_k.$$

By a straightforward calculation using (9.4.32), (9.4.33) and (9.4.34) we can verify that $\boldsymbol{r}_{I,i} \cdot \nabla_{\boldsymbol{w}} \lambda_{I,i}$ vanishes. Then the interfacial pressure and velocity are given by

$$P_I = \sum_{k=1}^{K} p_k (1 - c_k \alpha_k \rho_k T_k / (\hat{\rho} \hat{T})), \quad \boldsymbol{V}_I = \sum_{i=1}^{K} c_i \alpha_i \rho_i \boldsymbol{v}_i \Big/ \sum_{k=1}^{K} c_k \alpha_k \rho_k. \tag{9.7.38}$$

For special choices of $\boldsymbol{c} \in [0,1]^K$ these interfacial values coincide with those in the literature in case of two and three components. For instance, choosing $\boldsymbol{c} = \boldsymbol{e}_i$ for some $i \in \{1, \dots, K\}$ we obtain

$$P_I = \sum_{k=1, \neq i}^{K} p_k, \quad \boldsymbol{V}_I = \boldsymbol{v}_i. \tag{9.7.39}$$

For $i = 1$ these coincide with those given in [16] and [23] for $K = 2$ and $K = 3$, respectively. In case of uniform coefficients $c_k = 1/K$, $k = 1, \dots, K$, the interfacial pressure and velocity are given by

$$P_I = \sum_{k=1}^{K} p_k (1 - \alpha_k \rho_k T_k / (\rho \hat{T})), \quad \boldsymbol{V}_I = \sum_{i=1}^{K} \alpha_i \rho_i \boldsymbol{v}_i \Big/ \sum_{k=1}^{K} \alpha_k \rho_k = \boldsymbol{v}. \tag{9.7.40}$$

where ρ and $\boldsymbol{v}$ are the density and the velocity of the mixture, see (9.2.10), respectively.

Obviously, the interfacial states (9.7.38) do not satisfy (9.7.23) for an arbitrary non-equilibrium state meaning that (9.7.26) and (9.7.37) might not hold in general, i.e., the 2nd law of thermodynamics might be violated. To overcome this contradiction, it is recommended in [24] to use different interfacial velocities for the convective system and the relaxation terms. This is admissible because the conservation constraint (9.2.13) is satisfied for any convex combination (9.6.18). Moreover, the source term cannot be derived from the ensemble averaging procedure, see [13], Chapter 11, but the averaged model has to be closed by modeling these terms appropriately. Therefore, we are free to choose another velocity in the chemical relaxation model. Note that in the Drew-Passman model different interfacial velocities have been introduced in the evolution equations for volume fraction, momentum and energy, see [13], formulae (11.8), (11.39) and (11.41).

9.8 Conclusion

In the present work we discussed some properties of a non-equilibrium multi-component model of Baer-Nunziato type taking into account viscosity and heat conduction. This model is non-conservative due to exchange terms between different components. However, these terms vanish in the mixture model derived from the non-equilibrium model by averaging over all components and the resulting equilibrium model, i.e., the mixture model as well as the equilibrium model are conservative. Furthermore, the first order model, i.e., neglecting viscosity and heat conduction, could be verified to be hyperbolic, i.e., all eigenvalues are real and there exists a family of linearly independent eigenvectors provided that the non-resonance condition is satisfied and none of the components of the mixture vanishes. This holds true for both the non-equilibrium and the equilibrium model. In particular, the corresponding eigenvalues satisfy the sub-characteristic condition.

The main interest was on the derivation of closure conditions for the relaxation model as well as the interfacial pressures and the interfacial velocity. These were set up by verifying the second law of thermodynamics. It turned out that the pressures and the interfacial velocity can be chosen such that their contribution in the entropy law of the mixture vanishes. However, this does not characterize a unique choice for the interfacial pressures and the interfacial velocity because a physically reasonable choice of the interfacial velocities could not be derived so far in the general case of $K > 2$ components. The entropy production due to mechanical relaxation could be proven to be non-negative. The entropy production due to thermal and chemical relaxation is non-negative when assuming mechanical and thermal equilibrium, respectively. In the non-equilibrium case, sufficient conditions are given that pose constraints on the relaxation parameters to ensure a non-negative entropy production. Finally, we obtained constraints for the relaxation terms to ensure Galilean invariance.

We conclude with some remarks on the numerical discretization of the multi-component model. The main difficulty arises from the non-conservative products in the momentum equation (9.2.3) and the energy equation (9.2.4) as well as the evolution equation for the volume fractions (9.2.7). A popular approach to deal with those products is based upon so-called path-conservative schemes, see [35]. However, it was verified by Abgrall and Karni [1] that path-conservative schemes may not be able, in general, to compute correctly the solution of non-conservative hyperbolic problems. In case of a stiffened gas equation of state for the single components one may employ the Saurel-Abgrall trick [38] that couples the discretization of the evolution equations of the volume fractions with the discretization of the fluid equations of the components resulting in a non-conservative finite volume discretization. Numerical results for inviscid computations have been reported in [45] and [21,46] for two-phase fluids and three-phase fluids. There are many other publications available in the literature using different discretizations, see the aforementioned publications and citations therein.

References

[1] R. Abgrall and S. Karni. A comment on the computation of non-conservative products, *J. Comput. Phys.*, 229 (2010), 2759–2763.

[2] A. Ambroso, C. Chalons, F. Coquel, T. Galie, E. Godlewski, P. Raviart, and N. Seguin. The drift-flux asymptotic limit of barotropic two-phase two-pressure models. *Commun. Math.* Sci. 6(2), 521–529 (2008).

[3] N. Andrianov. *Analytical and numerical investigation of two-phase flows*, PhD thesis, Otto-von-Guericke University, Magdeburg, 2003.

[4] N. Andrianov, R. Saurel, and G. Warnecke. A simple method for compressible multiphase mixtures and interfaces, *Int. J. Numer. Meth. Fluids*, 41 (2003), 109–131.

[5] M.R. Baer and J.W. Nunziato. A two-phase mixture theory of the deflagration-to-detonation transition (DDT) in reactive granular materials, *Int. J. Multiphase Flows*, 12 (1986), 861–889.

[6] R.A. Berry, R. Saurel, and F. Petitpas. A simple and efficient diffuse interface method for compressible two-phase flows, *2009 International Conference on Mathyematics, Computational Methods & Reactor Physics*, Preprint, 2009.

[7] F. Coquel, T. Gallouet, P. Helluy, J.M. Herard, O. Hurisse, N. Seguin. Modelling compressible multiphase ows. *ESAIM: PROCEEDINGS* 40, 34–50 (2013).

[8] F. Coquel, J.-M. Hérard, K. Saleh, and N. Seguin. Two properties of two-velocity two-pressure models for two-phase flows, *Communications in Mathematical Sciences*, 12(3) (2014), 593–600.

[9] J. Dalton. *A new System of Chemical Philosophy*, 3 vols, Manchester 1808.

[10] J. Dalton, A new System of Chemical Philosophy, in: *Ostwalds Klassiker der Exacten Wissenschaften*, Band 3, Leipzig 1889.

[11] W. Dreyer, F. Duderstadt, M. Hantke, and G. Warnecke. Bubbles in liquids with phase transition. Part 1: On phase change of a single vapor bubble in liquid water, *Continuum Mechanics and Thermodynamics*, 24 (2012), 461–483.

[12] D. Drew. Mathematical modeling of two-phase flow, *Ann. Rev. Fluid Mech.*, 15 (1983), 261–291.

[13] D.A. Drew and S.L. Passman. Theory of Multicomponent Fluids, *Applied Mathematical Sciences*, Vol. 135, Springer, 1999.

[14] P. Embid and M. Baer. Mathematical analysis of a two-phase continuum mixture theory, *Contin. Mech. Thermodyn.*, 4 (1992), 279–312.

[15] T. Flåtten and H. Lund. Relaxation two-phase flow models and the subcharacteristic condition, *Mathematical Models and Methods in Applied Sciences*, 21(12) (2011), 2379–2407.

[16] T. Gallouët, J.-M. Hérard, and N. Seguin. Numerical modelling of two-phase flows using the two-fluid two-pressure approach, *Math. Models Methods Appl. Sci.*, 14(5) (2004), 663–700.

[17] P. Goatin and P. LeFloch. The Riemann problem for a class of resonant hyperbolic systems of balance laws. *Annales Inst. Henri Poincare* 21(6), 881–902 (2004).

[18] E. Godlewski and P.-A. Raviart. Hyperbolic systems of conservation laws, *Mathématiques & Applications* (Paris), 3-4, Paris: Ellipses, 1991.

[19] E. Godlewski and P.-A. Raviart. *Numerical approximation of hyperbolic systems of conservation laws*, New York, NY: Springer, 1996

[20] V. Guillemaud. *Modelisation et simulation numerique des eqoulements diphasiques par une approche bifluide a deux pressions.* Ph.D. thesis, Aix Marseille Universite (2007). https://tel.archives-ouvertes.fr/tel-0169178

[21] Ee Han, M. Hantke, and S. Müeller. Modeling of multi-component ows with phase transition and application to collapsing bubbles. *IGPM Preprint* 409, RWTH Aachen University (2014).

[22] F. Harlow and A. Amsden,. Fluid dynamics, *Technical Report*, LA-4700, Los Alamos National Laboratory, 1971.

[23] J.-M. Hérard. A three-phase flow model, *Mathematical and Computer Modelling*, 45 (2007), 732–755.

[24] J.M. Herard, O. Hurisse. A fractional step method to compute gas-liquid ows. *Computers and Fluids* 55, 57–69 (2012).

[25] A. Kapila, R. Menikoff, J. Bdzil, S. Son, and D. Stewart. Two-phase modelling of DDT in granular materials: Reduced equations, *Phys. Fluid*, 13 (2001), 3002–3024.

[26] T. Kato. The cauchy problem for quasi-linear symmetric hyperbolic systems. *Arch. Rational Mech. Anal.* 58(3), 181–205 (1975).

[27] M.H. Lallemand, A. Chinnayya, and . Le Metayer. Pressure relaxation procedures for multi-phase compressible flows, *International Journal for Numerical Methods in Fluids*, 49(1) (2005), 1–56.

[28] T.-P. Liu. Hyperbolic conservation laws with relaxation, *Commun. Math. Phys.*, 108 (1987), 153–175.

[29] I. Liu and R. Sampaio. On objectivity and the principle of material frame-indifference, *Mecánica Computacional* Vol XXXI, 1553–1569, A. Cardona, P.H. Kohan, R.D. Quinteros, M.A. Storti (Eds.) Salta, Argentina, 13-16 November 2012.

[30] R. Menikoff, B.J. Plohr, The Riemann problem for fluid flow of real materials, *Rev. Mod. Phys.* 61 (1), 75-130 (1989).

[31] O.L. Metayer, J. Massoni, and R. Saurel. Dynamic relaxation processes in compressible multiphase flows. application to evaporation phenomena. *ESAIM: PROCEEDINGS* 40, 103–123 (2013).

[32] I. Müller, *Thermodynamics*, Pitman, London, 1985.

[33] I. Müller and W. Müller. *Fundamentals of Thermodynamics and Applications*, Springer-Verlag, Berlin, 2009.

[34] S. Müller, M. Hantke, and P. Richter. Closure conditions for non-equilibrium multi-component models. *IGPM Preprint 414*, RWTH Aachen University (2014).

[35] C. Pares. Numerical methods for nonconservative hyperbolic systems: A theoretical framework, *SIAM Journal on Numerical Analysis* 44(1), 300–321 (2006).

[36] M.G. Rodio and R. Abgrall. An innovative phase transition modeling for reproducing cavitation. Part 1: Formulation of a 5-equations model and theoretical generalization to six and seven-equations models, preprint submitted to International Journal of Heat and Mass Transfer, September 6, 2014.

[37] K. Saleh. *Analyse et Simulation Numérique par Relaxation d'Écoulements Diphasiques Compressibles*, PhD thesis, Université Pierre et Marie Curie, Paris, 2012.

[38] R. Saurel and R. Abgrall. A multiphase Godunov method for compressible multifluid and multiphase flows, *J. Comput. Phys.*, 150(2) (1999), 425–467.

[39] R. Saurel and R. Abgrall. A simple method for compressible multifluid flows, *SIAM J. Sci. Comput.*, **21**, No. 3 (1999), 1115-1145.

[40] R. Saurel and O. LeMetayer. A multiphase flow model for compressible flows with interfaces, shocks, detonation waves and cavitation, *J. Fluid Mech.*, 43 (2001), 239–271.

[41] R. Saurel, F. Petitpas, and R. Abgrall. Modelling phase transition in metastable liquids: Application to cavitation and flashing flows, *J. Fluid. Mech.*, 607 (2008), 313–350.

[42] H. Söhnholz and Th. Kurz,. Thermal Effects upon Collapse of Laser-induced Cavitation Bubbles, DOI:10.3850/978-981-07-2826-7_137, *Proceedings of 8th International Symposium on Cavitation*, Singapore, 13–16 August 2012.

[43] G. Whitham. *Linear and Nonlinear Waves*, John Wiley & Sons Inc. (1974)

[44] A. Zein. *Numerical methods for multiphase mixture conservation laws with phase transition*, PhD thesis, Otto-von-Guericke University, Magdeburg, 2010.

[45] A. Zein, M. Hantke, and G. Warnecke. Modeling phase transition for compressible two-phase flows applied to metastable liquids, *J. Comput. Phys.*, 229(8) (2010), 2964–2998.

[46] A. Zein, M. Hantke, and G. Warnecke. On the Modelling and Simulation of a Laser-Induced Cavitation Bubble, *Int. J. Num. Meth. Fluids.*, 73(2) (2013), 172-203.

Chapter 10

Efficient and robust relaxation procedures

Bibliographic note: The content of this chapter is published in [H15]: Ee Han, Maren Hantke, and Siegfried Müller. Efficient and robust relaxation procedures for multi-component mixtures including phase transition, *Journal of Computational Physics*, Vol. 338 (2017), pp. 217-239.

Abstract: We consider a thermodynamic consistent multi-component model in multi dimensions that is a generalization of the classical two-phase flow model of Baer and Nunziato. The exchange of mass, momentum and energy between the phases is described by additional source terms. Typically these terms are handled by relaxation procedures. Available relaxation procedures suffer from efficiency and robustness resulting in very costly computations that in general only allow for one-dimensional computations. Therefore we focus on the development of new efficient and robust numerical methods for relaxation processes. We derive exact procedures to determine mechanical and thermal equilibrium states. Further we introduce a novel iterative method to treat the mass transfer for a three component mixture. All new procedures can be extended to an arbitrary number of inert ideal gases. We prove existence, uniqueness and physical admissibility of the resulting states and convergence of our new procedures. Efficiency and robustness of the procedures is verified by means of numerical computations in one and two space dimensions.

10.1 Introduction

Flows of compressible multi-component fluids, where the single components may be in the liquid or the gas phase, respectively, have a wide range of applications. Difficulties in the modeling result from the interaction of the fluids, especially from the exchange of mass and energy across the phase interfaces. In the literature several models are available that are distinguished in sharp interface and diffuse interface models. A detailed survey of these models can be found in Zein [40].

In our work we focus on models of Baer-Nunziato type derived from an ensemble averaging procedure of Drew [12]. A comprehensive introduction to these models can be found in the classical book of Drew and Passman [13].

Saurel and Abgrall modified the original two-phase non-equilibrium model of Baer and Nunziato [5] by including relaxation terms for the pressure and the velocities of the components. By additional relaxation processes for the temperatures and the chemical potentials the transfer of thermal energy and mass between the components and phases, respectively, can be modeled, see Saurel et al. [36] or Zein et al. [41]. By instantaneous relaxation procedures equilibrium values for pressures, velocities, temperatures and chemical potentials can be found.

Typically the relaxation procedures are based on iterative algorithms that are very much time-consuming, see Zein et al. [42]. Thus multi-dimensional applications are only feasible in acceptable computational time on massive parallel architectures. In order to reduce the high computational cost we need highly efficient and robust relaxation procedures. In the literature there are three contributions in this context. In [42] Zein et al. consider a third inert component. Here the Gibbs free energies are

relaxed to model phase transition between the vapor and the liquid phase instead of relaxing the chemical potentials. Thus, for a three component mixture a physically incorrect equilibrium state is determined. Pelanti and Shyue [30] improved one of the relaxation procedures. In particular, they modified the relaxation procedure for Gibbs free energies presented in [42] in case of a two component mixture. However, this is not sufficient because the assumption of pure phases is no longer justified apart from laboratory conditions. Moreover, they restrict their investigations to a six-equation model assuming velocity equilibrium. Also Le Métayer et al. [23] consider an inert component. As in Zein et al. [42] a physically incorrect equilibrium state is determined due to relaxing Gibbs free energies. Beside this Le Métayer et al. suggest a simultaneous temperature-pressure relaxation but do not give any details on the iterative procedures used. In particular, they cannot guarantee existence and uniqueness of an equilibrium state or positivity of the equilibrium temperature.

Our main objective is to improve *all* the relaxation procedures where, in particular, we account for a third inert component. Thus, the main focus of this work is the development of new relaxation procedures. Starting from the ideas of Zein et al. [42] we enhance the simulations in several aspects: (1) First of all, we simplify the relaxation procedures for pressure and temperature for multi-component mixtures. (2) Furthermore, we prove existence and uniqueness results and physical admissibility of the equilibrium states. (3) Opposite to [42] we avoid the calculation of model parameters that allows us to find the relaxed pressures and temperatures directly *without* performing an iterative procedure. (4) Instead of Gibbs free energies we relax the chemical potentials. Therefore we may take into account additional components in the phases by considering the mixture entropy and, thus, the model becomes physically correct. (5) A new procedure for the chemical relaxation is developed that performs significantly better than available procedures. (6) Furthermore, we avoid the artificial definition of an interfacial region. This allows us to simulate *physical* cavitation, which means that we can start from a pure liquid phase. The vapor phase will be created by expansion. In previous work it was necessary to start with an appreciable amount of vapor, for instance 1% in [41] and also in [30]. Nevertheless in our simulations we avoid *unphysical* nucleation or *unphysical* cavitation. We will give evidence for this by numerical examples. (7) Another essential difference to [41] is that we do not restrict mass transfer to metastable states with liquid temperature larger than the saturation temperature. Typically, condensation processes are not considered due to this restriction, cf. [41] and [30], whereas we are able to deal with these processes. (8) Moreover, we perform temperature relaxation also when no mass transfer occurs. This is physically reasonable as it may occur, for instance, in gas mixtures. (9) Furthermore, we improve the efficiency of the relaxation procedure where we perform pressure and temperature relaxation simultaneously resulting in explicit formulae for the equilibrium state rather than an iterative procedure as in Le Métayer et al. [23]. By this we avoid the approximate pressure relaxation procedure, see [21] or [40], that may cause numerical instabilities and, thus, very small time steps. (10) In contrast to Le Métayer et al. [23] we prove existence and uniqueness of the equilibrium states as well as physical admissibility, e.g. positivity of the equilibrium temperature.

The new relaxation procedures in combination with efficient discretization techniques using multiresolution-based grid adaptation, see Müller [27, 28], allow for highly efficient multi-dimensional computations. To illustrate the efficiency and robustness of our enhanced relaxation procedures we investigate the interaction of a collapsing bubble with a planar shock wave. This genuinely two-dimensional application is motivated by lithotripter shock wave experiments, see [1]. Here we perform computations where the bubble is filled with vapor and non-condensable gas. In addition we make several comparisons with the literature.

The paper is organized as follows. In Section 10.2 we introduce the non-equilibrium multi-component model. The main part of the present work is Section 10.3 where we develop and investigate new procedures for mechanical, temperature and chemical relaxation. Details of the algorithms are given. In Section 10.4 we discretize the model by an operator splitting. Finally in Section 10.5 we give numerical results. We discuss several test cases in one and two space dimensions to underline the robustness and efficiency of our new procedures. Furthermore we investigate physical cavitation. We conclude with a brief summary.

10.2 Mathematical formulation of the model

In the literature there are numerous simplified two-phase models available, e.g., see [40] and the references cited therein. Reduced models may suffer from some short-comings. For instance, conservation of energy might be violated or the system looses its hyperbolicity. There exist reduced models that preserve hyperbolicity as well as conservation of mass, momentum and energy. For instance, see the four equations model in [34] where both phases are in mechanical and thermal equilibria or the model in [22] corresponding to the homogeneous Euler equations combined with the vapor pressure function as equation of state. The aforementioned reduced models do not suffer from short-comings and may be solved efficiently and robustly when using appropriate numerical schemes. However, their domain of validity is restricted due to the equilibria hypothesis.

Therefore we prefer a full non-equilibrium model, where each component has its own pressure, velocity and temperature and is governed by its own set of fluid equations. For this generalized model closure conditions have been derived ensuring thermodynamically consistency, see [29]. In the following we first describe the full non-equilibrium model, see Section 10.2.1. To close the model we specify the equations of state in Section 10.2.2 and the source terms in Section 10.2.3.

10.2.1 Non-equilibrium multi-component model

For the multi-component model we use the Saurel-Abgrall approach [32] that is derived by the ensemble averaging procedure of Drew [12] and neglecting all dissipative terms everywhere except at the interfaces. It can be considered as a modified form of the Baer and Nunziato model [5].

Thus the multi-component flow is described by a non-equilibrium model where all components are present in each point of the space-time continuum. Each component $k = 1, \dots, K$ has density ρ_k, velocity $\boldsymbol{v}_k$ and pressure p_k. The amount of each component is determined by its volume fraction α_k. The volume fractions are related by the saturation constraint

$$\sum_{k=1}^{K} \alpha_k = 1, \quad \alpha_k \in [0,1]. \tag{10.2.1}$$

In analogy to the two-phase model of Saurel and Abgrall [32] the fluid equations for each component can be written as

$$\partial_t (\alpha_k \rho_k) + \nabla \cdot (\alpha_k \rho_k \boldsymbol{v}_k) = S_{\rho,k}, \tag{10.2.2}$$
$$\partial_t (\alpha_k \rho_k \boldsymbol{v}_k) + \nabla \cdot (\alpha_k \rho_k \boldsymbol{v}_k \boldsymbol{v}_k^T + \alpha_k p_k \boldsymbol{I}) = P_I \nabla \alpha_k + \boldsymbol{S}_{\rho \boldsymbol{v},k}, \tag{10.2.3}$$
$$\partial_t (\alpha_k \rho_k E_k) + \nabla \cdot (\alpha_k \rho_k \boldsymbol{v}_k (E_k + p_k/\rho_k)) = P_I \boldsymbol{V}_I \cdot \nabla \alpha_k + S_{\rho E,k}, \tag{10.2.4}$$

where we neglect effects due to viscosity, heat conduction, surface tension and gravity. Nevertheless, due to the thermal relaxation procedures we account for heat exchange between the components. In our notation $E_k = e_k + \boldsymbol{v}_k^2/2$ is the total specific energy with e_k the specific internal energy of component k. The terms P_I and $\boldsymbol{V}_I$ are the interfacial pressure and velocity, respectively. The fluid equations are supplemented by an equation of state

$$p_k = p_k(\rho_k, e_k) \quad \text{resp.} \quad e_k = e_k(\rho_k, p_k) \tag{10.2.5}$$

for each of the components, see Section 10.2.2 for the specific choice. The evolution of the volume fractions is characterized by the non-conservative equations

$$\partial_t \alpha_k + \boldsymbol{V}_I \cdot \nabla \alpha_k = S_{\alpha,k}, \ k = 1, \dots, K. \tag{10.2.6}$$

Due to the saturation condition (10.2.1) we only need $K-1$ equations. Without loss of generality we express α_K by the other volume fractions, i.e.,

$$\alpha_K = 1 - \sum_{k=1}^{K-1} \alpha_k, \ \nabla \alpha_K = -\sum_{k=1}^{K-1} \nabla \alpha_k, \ S_{\alpha,K} = -\sum_{k=1}^{K-1} S_{\alpha,k}. \tag{10.2.7}$$

The source terms $S_{\alpha,k}$, $S_{\rho,k}$, $\boldsymbol{S}_{\rho \boldsymbol{v},k}$ and $S_{\rho E,k}$ on the right-hand sides of (10.2.2), (10.2.3), (10.2.4) and (10.2.6) describe the interaction of the components corresponding to mass, momentum and energy

transfer via the relaxation of velocity, pressure, temperature and chemical potentials, $\xi \in \{v, p, T, \mu\}$, i.e.,

$$S_{\alpha,k} := \sum_{\xi} S^{\xi}_{\alpha,k}, \;\; S_{\rho,k} := \sum_{\xi} S^{\xi}_{\rho,k}, \;\; \boldsymbol{S}_{\rho\boldsymbol{v},k} := \sum_{\xi} \boldsymbol{S}^{\xi}_{\rho\boldsymbol{v},k}, \;\; S_{\rho E,k} := \sum_{\xi} S^{\xi}_{\rho E,k}.$$

These depend on the specific components at hand that will be discussed in Section 10.2.3. Due to conservation of mass, momentum and energy these terms satisfy the conservation constraints

$$\sum_{k=1}^{K} S^{\xi}_{\alpha,k} = 0, \quad \sum_{k=1}^{K} S^{\xi}_{\rho,k} = 0, \quad \sum_{k=1}^{K} \boldsymbol{S}^{\xi}_{\rho\boldsymbol{v},k} = \boldsymbol{0}, \quad \sum_{k=1}^{K} S^{\xi}_{\rho E,k} = 0 \tag{10.2.8}$$

for each relaxation type $\xi \in \{v, p, T, \mu\}$.

It remains to define the interfacial pressure P_I and the interfacial velocity $\boldsymbol{V}_I$. We choose

$$P_I := \sum_{k=2}^{K} p_k \quad \text{and} \quad \boldsymbol{V}_I := \boldsymbol{v}_1 \,. \tag{10.2.9}$$

In [29] it has been proven that this is an admissible choice which is in agreement with the 2nd law of thermodynamics. A different numbering of the components would not affect the results due to relaxing towards equilibrium.

10.2.2 Equation of state

Each component is complemented by its own equation of state (EOS) as a pure material. Here we choose the stiffened gas model that was introduced by Harlow and Amsden [18]. It can be considered as a combination of the perfect gas law and the barotropic Tait equation supplemented with an appropriate energy law [37]. The corresponding thermal and caloric EOS read

$$p_k(\rho_k, e_k) = (\gamma_k - 1)\,\rho_k\,(e_k - q_k) - \gamma_k\,\pi_k, \tag{10.2.10}$$
$$T_k(\rho_k, e_k) = (e_k - q_k - \pi_k/\rho_k)/c_{v,k}, \tag{10.2.11}$$

where T_k is the temperature and the material parameters are the ratio of specific heats γ_k, the specific heat at constant volume $c_{v,k}$, the minimal pressure π_k and the heat of formation q_k. Equivalently, these equations can be rewritten as

$$e_k(\rho_k, p_k) = \frac{p_k + \gamma_k \pi_k}{\rho_k\,(\gamma_k - 1)} + q_k, \tag{10.2.12}$$
$$T_k(\rho_k, p_k) = \frac{p_k + \pi_k}{c_{v,k}\,\rho_k\,(\gamma_k - 1)}. \tag{10.2.13}$$

From the equation of states we conclude by

$$T_k ds_k = de_k - \frac{p_k}{\rho_k^2} d\rho_k \tag{10.2.14}$$

from equilibrium thermodynamics for the specific entropy s_k and the Gibbs free energy g_k

$$s_k(p_k, T_k) = c_{v,k}\,\ln\left(\frac{T_k^{\gamma_k}}{(p_k + \pi_k)^{\gamma_k - 1}}\right) + q_k', \tag{10.2.15}$$
$$g_k(p_k, T_k) = e_k + p_k/\rho_k - T_k s_k. \tag{10.2.16}$$

Here q_k' is another material parameter. Furthermore the speed of sound is given by

$$c_k^2 := \left.\frac{\partial p_k}{\partial \rho_k}\right|_{s_k = const} = \frac{p_k}{\rho_k^2}\left.\frac{\partial p_k}{\partial e_k}\right|_{\rho_k = const} + \left.\frac{\partial p_k}{\partial \rho_k}\right|_{e_k = const} = \frac{(p_k + \pi_k)\gamma_k}{\rho_k}. \tag{10.2.17}$$

Note that the stiffened gas EOS allows for negative pressures while $p_k + \pi_k$ remains positive, i.e., the system is hyperbolic.

component	γ	π [Pa]	c_v [J/kg/K]	q [J/kg]	q' [J/kg/K]
vapor (1)	1.327	0	1200	1.995000×10^6	2.410×10^3
water (2)	2.057	1.066×10^9	3449	-1.994674×10^6	3.578×10^4
gas (3)	1.4	0	10100	0	0

Table 10.1: Material parameters for three component simulations, taken from [40].

component	γ	π [Pa]	c_v [J/kg/K]	q [J/kg]	q' [J/kg/K]
vapor (1)	1.43	0	1040	2.03×10^6	0
water (2)	2.35	10^9	1816	-1.167×10^6	-2.3×10^4

Table 10.2: Material parameters for two component simulations, taken from [40].

In particular, we are interested in the three-component model, i.e., $K = 3$, with water vapor ($k = 1$), liquid water ($k = 2$) and inert gas ($k = 3$).

The corresponding material parameters used for the two-component and the three-component simulations are listed in Table 10.1 and 10.2, respectively.

The source terms describing the mass transfer depend on the chemical potentials of the vapor and the liquid. In the model under consideration the gas is a mixture of water vapor and some other constituent, where both components are modeled as an ideal gas. Accordingly the chemical potential of the vapor is given by

$$\mu_1 = g_1 + (\gamma_1 - 1)c_{v,1}T_1 \ln\left(\frac{\alpha_1 p_1}{\alpha_1 p_1 + \alpha_3 p_3}\right). \tag{10.2.18}$$

In the special case of vanishing third component, i.e., $\alpha_3 = 0$, the chemical potential of the vapor reduces to the vapor Gibbs free energy. The chemical potential μ_2 of the liquid equals its Gibbs free energy g_2, i.e.,

$$\mu_2 = g_2\,.$$

In chemical equilibrium the chemical potentials of the vapor and the liquid equal each other. For details see the book of Müller and Müller [26], Section 8.2.4.

10.2.3 Relaxation terms

The non-equilibrium model without relaxation terms allows for different values for velocities, pressures, temperatures as well as chemical potentials at the same point. The relaxation mechanism described by the source terms drives all these quantities into equilibrium. Typically it is distinguished between mechanical and thermal relaxation processes that relax either pressures and velocities or temperatures and chemical potentials to equilibrium.

Mechanical relaxation. The *pressure relaxation* implies volume variations that induce energy variations due to the interfacial pressure work. The pressure relaxation terms read

$$S^p_{\alpha,k} := \theta_p\,\alpha_k\,(p_k - p),\;\; S^p_{\rho,k} := 0,\;\; \boldsymbol{S}^p_{\rho\boldsymbol{v},k} := \boldsymbol{0},\;\; S^p_{\rho E,k} := \theta_p\,\alpha_k\,p(p - p_k)\,, \tag{10.2.19}$$

see [40] or [32] for a two-component model. By θ_p we denote the pressure relaxation parameter. Similarly the *velocity relaxation* terms read

$$S^v_{\alpha,k} = S^v_{\rho,k} := 0,\;\; \boldsymbol{S}^v_{\rho\boldsymbol{v},k} := \theta_v\,\alpha_k\,\rho_k\,(\boldsymbol{v} - \boldsymbol{v}_k),\;\; S^v_{\rho E,k} := \theta_v\,\alpha_k\,\rho_k\,\boldsymbol{v}\cdot(\boldsymbol{v} - \boldsymbol{v}_k) \tag{10.2.20}$$

with the velocity relaxation parameter θ_v. Performing velocity and pressure relaxation the fluid mixture is in mechanical equilibrium, i.e., $p_k = p^\infty$ and $\boldsymbol{v}_k = \boldsymbol{v}^\infty$, $k = 1, \dots, K$. Using the definition

$$p := \sum_{k=1}^{K} \alpha_k\,p_k,\;\; \rho\boldsymbol{v} := \sum_{k=1}^{K} \alpha_k\,\rho_k\,\boldsymbol{v}_k \tag{10.2.21}$$

for the mixture pressure and mixture velocity it is obvious, that the conservation constraints (10.2.8) are satisfied. In this context we further define the mixture density as well as the mixture total energy by

$$\rho := \sum_{k=1}^{K} \alpha_k \, \rho_k, \;\; \rho E := \sum_{k=1}^{K} \alpha_k \, \rho_k \, E_k \, . \tag{10.2.22}$$

Thermal relaxation. The source terms corresponding to the temperature relaxation are given by

$$S^T_{\alpha,k} := \frac{\theta_T}{\kappa_k} \, \alpha_k \, (\hat{T} - T_k), \;\; S^T_{\rho,k} := 0, \;\; \boldsymbol{S}^T_{\rho \boldsymbol{v},k} := \boldsymbol{0}, \;\; S^T_{\rho E,k} := \theta_T \, \alpha_k \, (\hat{T} - T_k), \tag{10.2.23}$$

where θ_T denotes the temperature relaxation parameter and the mean of the temperature is defined as

$$\hat{T} := \sum_{k=1}^{K} \alpha_k \, T_k.$$

By the definition of $\hat{T}$ the conservation constraints (10.2.8) are satisfied and at temperature equilibrium, i.e., $T_k = T^\infty$, $k = 1, \ldots, K$, it coincides with the equilibrium temperature, i.e., $\hat{T} = T^\infty$. Note, that $\hat{T}$ has no physical meaning and other choices for $\hat{T}$ are possible. The quantity $\hat{T}$ is a technical one. Its choice does not affect the equilibrium state, but the relaxation path.

The relaxation parameters κ_k were introduced in Zein [40] and Zein et al. [41] in case of a two-component and a three-component model, respectively, to ensure the pressure keeping equilibrium during the temperature relaxation.

However, in our new thermal relaxation procedure these parameters do not enter explicitly the computation of the equilibrium state, cf. [30] and, thus, are not given here.

Chemical potential relaxation. Mass transfer between different phases of the same substance occurs, whenever these phases are not in thermal equilibrium. This physical fact is the key idea to model the mass transfer by relaxation of the chemical potentials. It is obvious, that from now on it is necessary to identify the components. The gas phase is assumed to be a mixture of water vapor and some further gas. Here we only consider three components, i.e., $K = 3$, with water vapor ($k = 1$), liquid water ($k = 2$) and inert gas ($k = 3$). Thermal equilibrium is achieved, if the chemical potential of the water vapor phase equals the Gibbs free energy of the liquid water phase. In the limit case of no inert gas the expression of the chemical potential of the water vapor phase reduces to the Gibbs free energy, see (10.2.18). The mass flux $\dot{m}$ between the liquid and the vapor phase is driven by the difference of their chemical potentials, i.e., $\dot{m} = \dot{m}(\mu_1 - \mu_2)$. In particular, the mass flux vanishes if and only if the difference of the chemical potentials is zero, i.e., $\mu_1 = \mu_2$.

The relaxation terms of chemical potentials are given by

$$\begin{aligned}
&S^\mu_{\alpha,1} := \theta_\mu \, \frac{\dot{m}}{\varrho_1}, \;\; S^\mu_{\rho,1} := \theta_\mu \, \dot{m}, \;\; \boldsymbol{S}^\mu_{\rho \boldsymbol{v},1} := \theta_\mu \, \dot{m} \, \boldsymbol{V}_I, \;\; S^\mu_{\rho E,1} := \theta_\mu \, \dot{m} \, \left(\epsilon_1 + \frac{\boldsymbol{V}_I^2}{2} \right), \\
&S^\mu_{\alpha,2} := \theta_\mu \, \frac{\dot{m}}{\varrho_2}, \;\; S^\mu_{\rho,2} := -\theta_\mu \, \dot{m}, \;\; \boldsymbol{S}^\mu_{\rho \boldsymbol{v},2} := -\theta_\mu \, \dot{m} \, \boldsymbol{V}_I, \;\; S^\mu_{\rho E,2} := -\theta_\mu \, \dot{m} \, \left(\epsilon_2 + \frac{\boldsymbol{V}_I^2}{2} \right), \\
&S^\mu_{\alpha,3} := -\theta_\mu \, \dot{m} \, \left(\frac{1}{\varrho_1} + \frac{1}{\varrho_2} \right), \;\; S^\mu_{\rho,3} := 0, \;\; \boldsymbol{S}^\mu_{\rho \boldsymbol{v},3} := \boldsymbol{0}, \;\; S^\mu_{\rho E,3} := \theta_\mu \, \dot{m} \, (\epsilon_2 - \epsilon_1),
\end{aligned} \tag{10.2.24}$$

with the relaxation parameter θ_μ. Formulas for the parameters $\varrho_1, \varrho_2, \epsilon_1, \epsilon_2$ can be found in [40, 42]. For details on the physics see the book of Müller and Müller [26].

The relaxation terms (10.2.19), (10.2.20), (10.2.23), (10.2.24) are of major importance when dealing with interface problems, see for instance Saurel and Abgrall [32] or Lallemand and Saurel [21] for mechanical relaxation terms. Typically, it is assumed that pressure and velocity relax instantaneously, see [32], whereas the thermal relaxation and the relaxation of chemical potentials are much slower, see Zein [40]. Here we are interested only in the equilibrium state that is characterized by vanishing relaxation terms rather than the transient relaxation process itself. Since the equilibrium state does not depend on the

order of relaxation, the relaxation parameters θ_ξ, $\xi \in \{p, v, T, \mu\}$, drop out and have not to be known explicitly.

As already mentioned and as will be explained later on in Section 10.3 in our new procedure to determine the thermal equilibrium state the parameters κ_k and ε_k, ϱ_k, $k = 1, 2$, respectively, do not enter explicitly and, thus, are not given here. This is an important improvement to the approach proposed in [40, 42], since we avoid an additional iteration process in the relaxation procedure.
Furthermore, our modeling of the mass transfer is physically correct because we take into account chemical potentials instead of Gibbs free energies. In [40, 42] the Gibbs free energy is relaxed, which neglects the effect of mixture entropy in cases of impure substances. The expression for the chemical potential is based on the assumption that the vapor phase is modeled as an ideal gas.

10.3 Relaxation procedures

The main objective of our work is to develop new, efficient and robust relaxation procedures. For this purpose we split the relaxation process from the fluid motion by formally performing an operator splitting. Since the relaxation times differ for the different relaxation types, we solve the initial value problem

$$\frac{d\,\boldsymbol{w}(t)}{d\,t} = \boldsymbol{S}^\xi(\boldsymbol{w}(t)), \quad t \in [t_n, t_{n+1}], \qquad \boldsymbol{w}(t_n) = \boldsymbol{w}^0 \tag{10.3.1}$$

with $\boldsymbol{S}^\xi = ((S^\xi_{\alpha_k})_{k=1,\dots,K-1}, (S^\xi_{\rho,k}, \boldsymbol{S}^\xi_{\rho\boldsymbol{v},k}, S^\xi_{\rho E,k})_{k=1,\dots,K})^T$ separately for each relaxation type $\xi \in \{v, p, T, \mu\}$. To avoid the explicit computation of the relaxation times θ_ξ in (10.2.19), (10.2.20), (10.2.23) and (10.2.24), we may perform the change of variables $\bar{t} := (t_n - t)\theta_\xi$ and $\overline{\boldsymbol{w}}(\bar{t}) := \boldsymbol{w}(t)$ in (10.3.1), i.e.,

$$\frac{d\,\overline{\boldsymbol{w}}(\bar{t})}{d\,\bar{t}} = \frac{1}{\theta^\xi}\boldsymbol{S}^\xi(\overline{\boldsymbol{w}}(\bar{t})), \quad \bar{t} \in [0, \Delta t\theta_\xi], \qquad \overline{\boldsymbol{w}}(0) = \overline{\boldsymbol{w}}^0. \tag{10.3.2}$$

Then by definition of the relaxation terms, the relaxation parameter cancels on the right-hand side of (10.3.2). Since for all relaxation processes the conservation constraints (10.2.8) are satisfied we conclude from (10.3.1) that

$$\sum_{k=1}^{K} \frac{d\,\overline{\alpha}_k(\bar{t})}{d\,\bar{t}} = 0, \quad \frac{d\,\overline{\rho}(\bar{t})}{d\,\bar{t}} = 0, \quad \frac{d\,(\overline{\rho}\,\overline{\boldsymbol{v}})(\bar{t})}{d\,\bar{t}} = \boldsymbol{0}, \quad \frac{d\,(\overline{\rho E})(\bar{t})}{d\,\bar{t}} = 0. \tag{10.3.3}$$

Hence, the bulk quantities for mixture density, momentum and energy as well as the saturation condition (10.2.1) remain constant during the relaxation process and it holds

$$\sum_{k=1}^{K} \alpha_k^\infty = \sum_{k=1}^{K} \alpha_k^0 = 1, \ \rho^\infty = \rho^0, \ (\rho\,\boldsymbol{v})^\infty = (\rho\,\boldsymbol{v})^0, \ (\rho E)^\infty = (\rho E)^0. \tag{10.3.4}$$

Furthermore, the conservation of bulk mass and momentum imply that the bulk velocity remains constant

$$\frac{d\,\overline{\boldsymbol{v}}}{d\,\bar{t}} = \boldsymbol{0} \tag{10.3.5}$$

and, thus, it holds

$$\boldsymbol{v}^\infty = \boldsymbol{v}^0. \tag{10.3.6}$$

As already discussed in Section 10.2.3 we are only interested in the equilibrium state rather the transient relaxation behavior. Therefore we assume that the relaxation process is infinitely fast, i.e., $\theta_\xi \to \infty$ and we do not need to determine the relaxation parameters. To compute the equilibrium state, where the source terms (10.2.19), (10.2.20), (10.2.23) and (10.2.24) vanish, we perform integration of the ODE system to infinity. This results in a system of algebraic equations for the equilibrium state that will be derived and solved in the subsequent sections. For ease of notation we will use $\boldsymbol{w}$ instead of $\overline{\boldsymbol{w}}$ in (10.3.2). In the following we consider one by one the different relaxation processes to equilibrium. Note that the equilibrium state is independent of the order of the relaxation procedures.

10.3.1 Velocity relaxation

In order to determine the equilibrium state of the velocity relaxation process we proceed similar to Saurel and Le Métayer in [35]. The equilibrium state of the velocity relaxation process is determined by solving the system of ODEs

$$\frac{d\,\alpha_k}{d\,\bar{t}} = 0, \tag{10.3.7}$$

$$\frac{d\,\alpha_k\,\rho_k}{d\,\bar{t}} = 0, \tag{10.3.8}$$

$$\frac{d\,\alpha_k\,\rho_k\,\boldsymbol{v}_k}{d\,\bar{t}} = \alpha_k\,\rho_k(\boldsymbol{v} - \boldsymbol{v}_k), \tag{10.3.9}$$

$$\frac{d\,\alpha_k\,\rho_k\,E_k}{d\,\bar{t}} = \alpha_k\,\rho_k\,\boldsymbol{v}\cdot(\boldsymbol{v} - \boldsymbol{v}_k) \tag{10.3.10}$$

resulting from (10.3.2) with the source terms (10.2.20). Since we assume that the relaxation process is infinitely fast, the solution of the system of ODEs converges towards the equilibrium state where the right-hand side vanishes. This holds true for

$$\boldsymbol{v}_k = \boldsymbol{v}^\infty, \quad \bar{t} \to \infty. \tag{10.3.11}$$

Integration of (10.3.7), (10.3.8) over $[0, \infty]$ then results in the algebraic equations

$$\alpha_k^\infty = \alpha_k^0, \tag{10.3.12}$$

$$\alpha_k^\infty\,\rho_k^\infty = \alpha_k^0\,\rho_k^0 \quad \text{equiv.} \quad \rho_k^\infty = \rho_k^0. \tag{10.3.13}$$

From the equilibrium condition (10.3.11) and (10.3.6) we conclude that

$$\boldsymbol{v}_k^\infty = \boldsymbol{v}^\infty = \boldsymbol{v}^0. \tag{10.3.14}$$

To determine the energy at equilibrium we first observe that by (10.3.9) and (10.3.10)

$$\frac{d\,\alpha_k\,\rho_k\,E_k}{d\,\bar{t}} = \boldsymbol{v}\frac{d\,\alpha_k\,\rho_k\,\boldsymbol{v}_k}{d\,\bar{t}}. \tag{10.3.15}$$

Since the bulk velocity remains constant according to (10.3.5), we obtain by integration of (10.3.15) over $[0, \infty]$ and (10.3.14)

$$\alpha_k^\infty\,\rho_k^\infty\,E_k^\infty = \alpha_k^0\,\rho_k^0\,E_k^0 + \alpha_k^0\,\rho_k^0\,\boldsymbol{v}^0\cdot(\boldsymbol{v}^0 - \boldsymbol{v}_k^0) \tag{10.3.16}$$

or, equivalently by (10.3.13),

$$E_k^\infty = E_k^0 + \boldsymbol{v}^0\cdot(\boldsymbol{v}^0 - \boldsymbol{v}_k^0). \tag{10.3.17}$$

Finally, we end up with the algebraic system (10.3.6), (10.3.12), (10.3.13), (10.3.14) and (10.3.17) by which we determine the velocity equilibrium state. The procedure is summarized in the following algorithm.

Algorithmus 10.3.1 (Velocity Relaxation Procedure)**.**

1. *Compute the equilibrium mixture velocity according to (10.2.21) as*

$$\boldsymbol{v}^\infty = \sum_{k=1}^{K}\alpha_k^0\rho_k^0\boldsymbol{v}_k^0 \Big/ \sum_{k=1}^{K}\alpha_k^0\rho_k^0; \tag{10.3.18}$$

2. *Update the velocities of the components using (10.3.14);*

3. *Update the specific total energies of the components using (10.3.17).*

The equilibrium state coincides with the results of Saurel and Le Métayer in [35] for the two-phase model although the derivation is slightly different considering e instead of E.

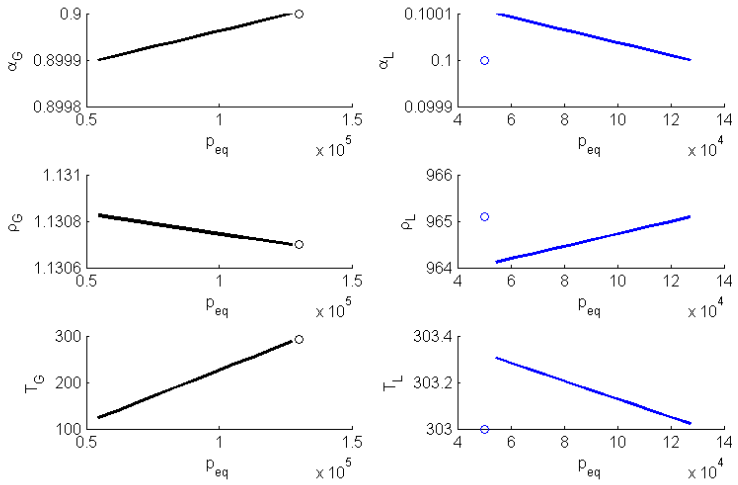

Figure 10.1: Equilibrium states.

10.3.2 Pressure relaxation

For the pressure relaxation we may proceed similarly to [21] for two- and multi-component models. Lallemand et al. [21] give eight different procedures based on a closure of the interfacial pressure that become physically non-admissible for more than two components, see [29]. These procedures predict different values for the equilibrium pressure.

The equilibrium pressure is path-depending and accordingly non-unique. In fact, there are infinitely many equilibrium states that can be obtained by conservative pressure relaxation procedures. This can be seen clearly in Figure 10.1 where all possible equilibrium states for the following set of initial data are given

$$\alpha_G = 0.9, \quad p_G = 130000, \quad T_G = 293, \quad p_L = 50000, \quad T_L = 303.$$

Obviously small differences in the equilibrium volume fractions cause appreciable changes in the corresponding equilibrium pressure and significant variations in the phase temperatures. Note in particular the temperature of the vapor phase.

One of the eight approaches given in [21] is based on the following approximation of the intermediate interfacial pressure state

$$\bar{p} \approx \frac{p^0 + p^\infty}{2}. \tag{10.3.19}$$

In [17] we give a procedure in case of a K component mixture using a physically admissible closure of the interfacial pressure resulting in a polynomial of degree K. However, for large pressure differences between the initial pressure and the equilibrium pressure the approximation (10.3.19) may cause stability problems resulting in very small CFL numbers. These instabilities are induced by the non-uniqueness of the equilibrium state. Small differences in the equilibrium pressure and in the corresponding volume fractions may cause large variations of the phase temperatures.

Alternatively, uniqueness can be enforced by the additional condition of temperature equilibrium. For this purpose we suggest to simultaneously relax pressure and temperature and, thus, determine a unique equilibrium pressure by avoiding iteration processes. This results in an efficient and stable procedure.

10.3.3 Simultaneous pressure-temperature relaxation

For the pressure-temperature relaxation process we have to solve the system of ODEs

$$\frac{d\,\alpha_k}{d\,\bar{t}} = \frac{\theta_T}{\theta_p}\,\alpha_k\,(p_k - p) + \frac{\alpha_k}{\kappa_k}(\hat{T} - T_k), \tag{10.3.20}$$

$$\frac{d\,\alpha_k\,\rho_k}{d\,\bar{t}} = 0, \tag{10.3.21}$$

$$\frac{d\,\alpha_k\,\rho_k\,\boldsymbol{v}_k}{d\,\bar{t}} = 0, \tag{10.3.22}$$

$$\frac{d\,\alpha_k\,\rho_k\,E_k}{d\,\bar{t}} = \frac{\theta_T}{\theta_p}\,\alpha_k\,p(p - p_k) + \alpha_k\,(\hat{T} - T_k), \tag{10.3.23}$$

resulting from (10.3.2) with the source terms (10.2.23). Since we assume that the relaxation process is infinitely fast, the solution of the system of ODEs converges towards the equilibrium state where the right-hand side vanishes. This holds true for

$$p_k^\infty = p^\infty, \quad T_k^\infty = T^\infty, \qquad \bar{t} \to \infty. \tag{10.3.24}$$

Note that we *also* impose pressure equilibrium.

Again, equations (10.3.21), (10.3.22) and (10.3.23) entail conservation of mass, momentum and bulk energy, i.e.,

$$\alpha_k^\infty\,\rho_k^\infty = \alpha_k^0\rho_k^0, \tag{10.3.25}$$

$$\boldsymbol{v}_k^\infty = \boldsymbol{v}_k^0, \tag{10.3.26}$$

$$\sum_{k=1}^{K}(\alpha_k\rho_k e_k)^\infty = \sum_{k=1}^{K}(\alpha_k\rho_k e_k)^0. \tag{10.3.27}$$

Due to the mass conservation (10.3.25) and the equation of state (10.2.12) the latter is equivalent to

$$\sum_{k=1}^{K}\alpha_k^\infty\frac{p_k^\infty + \gamma_k\pi_k}{(\gamma_k - 1)} = \sum_{k=1}^{K}\alpha_k^0\frac{p_k^0 + \gamma_k\pi_k}{(\gamma_k - 1)} =: \Lambda. \tag{10.3.28}$$

The temperature equilibrium (10.3.24) implies $T_k^\infty = T_{k_0}^\infty$ for all phases k, where we fix an arbitrary phase k_0 to be specified below. Since we also assume pressure equilibrium, i.e., $p_k^\infty = p^\infty$, we conclude together with the equation of state (10.2.13) that

$$\alpha_k^\infty = \alpha_{k_0}^\infty\frac{a_k}{a_{k_0}}\frac{p^\infty + \pi_{k_0}}{p^\infty + \pi_k} \quad \text{with} \quad a_k := c_{v,k}(\gamma_k - 1)\alpha_k^0\rho_k^0. \tag{10.3.29}$$

Then the saturation condition (10.2.1) yields

$$\alpha_{k_0}^\infty = \left(\sum_{k=1}^{K}\frac{a_k}{a_{k_0}}\frac{p^\infty + \pi_{k_0}}{p^\infty + \pi_k}\right)^{-1} \tag{10.3.30}$$

We now substitute α_k^∞ in (10.3.28) by (10.3.29) and replace $\alpha_{k_0}^\infty$ by (10.3.30). For ease of representation we introduce the sets

$$\mathcal{E} := \{k\,:\,\pi_k = \pi_{k_0},\ k \in \{1,\dots,K\}\}, \quad \mathcal{N} := \{k\,:\,\pi_k \neq \pi_{k_0},\ k \in \{1,\dots,K\}\}. \tag{10.3.31}$$

Together with the assumption of pressure equilibrium (10.3.24) we finally obtain after some algebraic manipulations

$$\begin{aligned}&\sum_{k\in\mathcal{E}}\frac{a_k}{a_{k_0}}\left(\frac{p^\infty + \gamma_k\pi_k}{\gamma_k - 1} - \Lambda\right)\prod_{l\in\mathcal{N}}(p^\infty + \pi_l) + \\ &\sum_{k\in\mathcal{N}}\frac{a_k}{a_{k_0}}\left(\frac{p^\infty + \gamma_k\pi_k}{\gamma_k - 1} - \Lambda\right)(p^\infty + \pi_{k_0})\prod_{l\in\mathcal{N},l\neq k}(p^\infty + \pi_l) = 0.\end{aligned} \tag{10.3.32}$$

Hence, the equilibrium pressure p^∞ is characterized as the root of a polynomial of degree $\#\mathcal{N}+1$. By the conditions $\alpha_k^\infty \in (0,1)$ and $p^\infty > 0$ we may single out the unique physically admissible solution as we will do for some models at the end of this section. To reduce the number of roots we therefore recommend that the index k_0 should be chosen such that the cardinality of $\mathcal{N}$ is smallest. In particular, if all π_k coincide, then we may compute p^∞ directly as

$$p^\infty = \sum_{k=1}^{K} \frac{a_k}{a_{k_0}} \left(\Lambda - \frac{\gamma_k \pi_k}{\gamma_k - 1} \right) \left(\sum_{k=1}^{K} \frac{a_k}{a_{k_0}} \frac{1}{\gamma_k - 1} \right)^{-1}. \tag{10.3.33}$$

Another special case is the three-component model composed of water vapor, liquid water and gas, see Section 10.2.3 and Table 10.1 where in particular $\pi_1 = \pi_3 \equiv \pi_{1,3}$ and, thus, equation (10.3.32) becomes a quadratic rather than a cubic polynomial in p^∞. Choosing $k_0 = 1$ and multiplying (10.3.32) by $a_{k_0} = a_1$ we obtain

$$A\,(p^\infty)^2 + B\,p^\infty + C = 0, \tag{10.3.34}$$

where the coefficients are determined by

$$\begin{aligned}
A &:= \sum_{k=1}^{3} \frac{a_k}{\gamma_k - 1}, \\
B &:= a_1 \left(\frac{\gamma_1 \pi_{1,3} + \pi_2}{\gamma_1 - 1} - \Lambda \right) + a_2 \left(\frac{\gamma_2 \pi_2 + \pi_{1,3}}{\gamma_2 - 1} - \Lambda \right) + a_3 \left(\frac{\gamma_3 \pi_{1,3} + \pi_2}{\gamma_3 - 1} - \Lambda \right), \\
C &:= a_1 \pi_2 \left(\frac{\gamma_1 \pi_{1,3}}{\gamma_1 - 1} - \Lambda \right) + a_2 \pi_{1,3} \left(\frac{\gamma_2 \pi_2}{\gamma_2 - 1} - \Lambda \right) + a_3 \pi_2 \left(\frac{\gamma_3 \pi_{1,3}}{\gamma_3 - 1} - \Lambda \right).
\end{aligned}$$

Note that the equilibrium temperature T^∞ may be directly computed from the equilibrium pressure. Starting from the equation of state (10.2.13) we first employ mass conservation (10.3.25) and replace α_k^∞ by (10.3.29) and (10.3.30). Finally we obtain together with (10.3.30)

$$T_k^\infty = \left(\sum_{l=1}^{K} \frac{a_l}{p^\infty + \pi_l} \right)^{-1} = T^\infty \tag{10.3.35}$$

After having determined p^∞, the volume fractions $\alpha_{k_0}^\infty$ and α_k^∞, $k \neq k_0$, can be computed by (10.3.30) and (10.3.29), respectively. Then the mass conservation (10.3.25) provides us with ρ_k^∞. Finally we compute the internal energies e_k^∞ according to the equation of state (10.2.12).

For convenience of the reader we summarize the relaxation procedure in the following algorithm.

Algorithmus 10.3.2 (Pressure and Temperature Relaxation Procedure)**.**
Determine the index k_0 such that the cardinality of the set $\mathcal{N}$ is smallest.

1. *Compute Λ and a_k^∞, $k = 1, \ldots, K$, by (10.3.28) and (10.3.29), respectively;*
2. *Determine the roots of the polynomial (10.3.32);*
3. *For each root $i = 1, \ldots, \#\mathcal{N}+1$ determine $\alpha_k^{\infty,i}$, $k = 1, \ldots, K$, from (10.3.30) and (10.3.29);*
4. *Single out the unique physically admissible solution by verifying the conditions $\alpha_k^{\infty,i} \in (0,1)$ and $p^{\infty,i} > 0$ for all $k = 1, \ldots, K$;*
5. *By means of this solution compute the equilibrium temperature using (10.3.35);*
6. *Update the partial densities ρ_k^∞ and partial energies e_k^∞ using (10.3.25) and (10.2.12), respectively.*

For special cases we can prove the existence and uniqueness of admissible equilibrium states, see Step 4 in the above algorithm.

Theorem 10.3.1 (Positivity of equilibrium pressure and temperature)**.**
For all of the three cases (1) two components with $\pi_2 \neq \pi_1 = 0$, (2) three components with $\pi_1 = \pi_2 \neq \pi_3$ and (3) K components with $\pi_1 = \ldots = \pi_K$ there exist unique equilibrium pressure and equilibrium temperature with $p^\infty > 0$ and $T^\infty > 0$.

Proof:
Case 1: In this case $\pi_2 \neq \pi_1 = 0$. There exist two roots of (10.3.34) with $a_3 = 0$ because $A = a_1/(\gamma_1 - 1) + a_2/(\gamma_2 - 1) > 0$ and $C = -a_1 \Lambda \pi_2 < 0$. The only admissible solution is

$$p^\infty = -\frac{B}{2A} + \sqrt{\frac{B^2}{4A^2} - \frac{C}{A}} > 0. \tag{10.3.36}$$

From (10.3.30) and (10.3.35) we then conclude

$$\alpha_1^\infty = \frac{a_1(p^\infty + \pi_2)}{(a_1 + a_2)p^\infty + a_1\pi_2} = 1 - \alpha_1^\infty \in [0,1], \quad T^\infty = \frac{p^\infty(p^\infty + \pi_2)}{(a_1 + a_2)p^\infty + a_1\pi_2} > 0.$$

Case 2: In this case we assume that $\pi_1 = \pi_2 \neq \pi_3$. Then we observe that again $A > 0$ and $C < 0$ in (10.3.34) and thus (10.3.36) is the only admissible root. From (10.3.30), (10.3.29) and (10.3.35) we then conclude $\alpha_1 \in [0,1]$, $\alpha_2, \alpha_2 > 0$ and $T^\infty > 0$.

Case 3: In this case there only exists one root of (10.3.32) given by (10.3.33). Equations (10.3.28) and (10.3.29) imply that the equilibrium pressure is positive. Accordingly, the equilibrium temperature given by (10.3.35) is positive. □

It is worthwhile mentioning that in [23] Le Métayer et al. also develop a simultaneous pressure-temperature relaxation. However, their relaxation requires an iterative procedure to determine the pressure-temperature equilibrium whereas we derive an explicit expression for the equilibrium state. Moreover, they do not prove existence and uniqueness of the equilibrium state as well as physical admissibility. To the best of our knowledge no positivity results have been reported so far in the literature for the equilibrium temperature.

10.3.4 Relaxation of chemical potentials

The equilibrium state of the chemical potential relaxation process is determined by solving the system of ODEs

$$\frac{d\,\alpha_k}{d\,\bar{t}} = \frac{\dot{m}}{\varrho_k}, \; k = 1,2, \quad \frac{d\,\alpha_3}{d\,\bar{t}} = -\dot{m}\left(\frac{1}{\varrho_1} + \frac{1}{\varrho_2}\right), \tag{10.3.37}$$

$$\frac{d\,\alpha_k\,\rho_k}{d\,\bar{t}} = (-1)^{k+1}\dot{m}, \; k = 1,2, \quad \frac{d\,\alpha_3\,\rho_3}{d\,\bar{t}} = 0, \tag{10.3.38}$$

$$\frac{d\,\alpha_k\,\rho_k\,\boldsymbol{v}_k}{d\,\bar{t}} = (-1)^{k+1}\dot{m}\,\boldsymbol{V}_I, \; k = 1,2, \quad \frac{d\,\alpha_3\,\rho_3\,\boldsymbol{v}_3}{d\,\bar{t}} = \boldsymbol{0}, \tag{10.3.39}$$

$$\frac{d\,\alpha_k\,\rho_k\,E_k}{d\,\bar{t}} = (-1)^{k+1}\dot{m}\left(\epsilon_k + \frac{\boldsymbol{V}_I^2}{2}\right), \; k = 1,2, \quad \frac{d\,\alpha_3\,\rho_3\,E_3}{d\,\bar{t}} = \dot{m}\,(\epsilon_2 - \epsilon_1) \tag{10.3.40}$$

resulting from (10.3.2) with the source terms (10.2.24). Again we assume that the relaxation process is infinitely fast such that the solution of the system of ODEs converges towards the equilibrium state, where the right-hand side vanishes. According to [40, 42] this holds true for

$$p_1^\infty = p_2^\infty = p_3^\infty = p^\infty, \quad \bar{t} \to \infty, \tag{10.3.41}$$

$$T_1^\infty = T_2^\infty = T_3^\infty = T^\infty, \quad \bar{t} \to \infty, \tag{10.3.42}$$

$$\mu_1^\infty = g_2^\infty, \quad \bar{t} \to \infty. \tag{10.3.43}$$

Note that due to these equilibrium conditions the muss flux $\dot{m}$ vanishes at equilibrium and, thus, the right-hand sides in (10.3.37), (10.3.38), (10.3.39) and (10.3.40) become zero. Obviously, the equations (10.3.37) are in agreement with the saturation condition (10.2.1), i.e.,

$$\alpha_1^\infty + \alpha_2^\infty + \alpha_3^\infty = 1. \tag{10.3.44}$$

In the following we start with relaxed values for velocity, pressure and temperature obtained by the previous mechanical and thermal relaxation procedures described in Section 10.3.1 and 10.3.3 and, thus, it holds

$$p_1^0 = p_2^0 = p_3^0, \quad T_1^0 = T_2^0 = T_3^0, \quad \boldsymbol{v}_1^0 = \boldsymbol{v}_2^0 = \boldsymbol{v}_3^0. \tag{10.3.45}$$

During the chemical relaxation procedure we now assume that mechanical and thermal equilibrium is maintained but the corresponding equilibrium values may change. Due to conservation of total mass and total momentum it is obvious that the equilibrium velocity does not change, i.e.,

$$\boldsymbol{v}^\infty = \boldsymbol{v}_k^\infty = \boldsymbol{v}_k^0 = \boldsymbol{v}^0, \quad k = 1, 2, 3. \tag{10.3.46}$$

The mass equations (10.3.38) induce

$$\alpha_3^\infty \rho_3^\infty = \alpha_3^0 \rho_3^0, \tag{10.3.47}$$

$$\alpha_1^\infty \rho_1^\infty + \alpha_2^\infty \rho_2^\infty = \alpha_1^0 \rho_1^0 + \alpha_2^0 \rho_2^0 =: W\,. \tag{10.3.48}$$

Then we conclude with (10.3.40) that

$$\sum_{k=1}^{3} \alpha_k^\infty \rho_k^\infty e_k^\infty = \sum_{k=1}^{3} \alpha_k^0 \rho_k^0 e_k^0 =: E\,. \tag{10.3.49}$$

Motivated by the equilibrium condition (10.3.43) the aim is now to derive a function

$$f_\mu(\alpha_1\rho_1) := \mu_1^\infty(\alpha_1\rho_1) - g_2^\infty(\alpha_1\rho_1) \tag{10.3.50}$$

depending only on the product $\alpha_1\rho_1$ such that the root $\alpha_1^\infty\rho_1^\infty$ is the solution for the relaxed mass density for the first component. For this purpose we have to express α_1^∞, α_2^∞, T^∞ and p^∞ in terms of $\alpha_1^\infty\rho_1^\infty$. Then the chemical potential for water vapor μ_2 and the Gibbs free energies g_k, $k = 1, 2$, see Section 10.2.2, can be written as

$$\mu_1^\infty(\alpha_1\rho_1) = g_1^\infty(\alpha_1\rho_1) + (\gamma_1 - 1)c_{v,1}T^\infty(\alpha_1\rho_1)\ln\left(\frac{\alpha_1(\alpha_1\rho_1)}{1-\alpha_2(\alpha_1\rho_1)}\right), \tag{10.3.51}$$

$$\begin{aligned} g_k^\infty(\alpha_1\rho_1) = {} & (c_{v,k}\gamma_k - q_k')T^\infty(\alpha_1\rho_1) - c_{v,k}\gamma_k T^\infty(\alpha_1\rho_1)\ln(T^\infty(\alpha_1\rho_1)) + \\ & T^\infty(\alpha_1\rho_1)c_{v,k}(\gamma_k - 1)\ln(p^\infty(\alpha_1\rho_1) + \pi_k) + q_k. \end{aligned} \tag{10.3.52}$$

Note that a root of (10.3.50) may not exist. Beside the existence of an equilibrium solution the water vapor may completely condensate or the liquid water may completely evaporate. Therefore in a first step one has to figure out, which of the four cases occurs:

(i-a) condensation process with equilibrium solution,

(i-b) total condensation,

(ii-a) evaporation process with equilibrium solution,

(ii-b) total evaporation.

In case (i-b) and (ii-b) the result can be directly obtained. In the cases (i-a) and (ii-a) a bisection method is provided to find the equilibrium state. Due to the fact that the pressure-temperature relaxation method is simple and always gives a unique, physical solution, we base the bisection method to find the equilibrium state on the temperature relaxation procedure.

According to thermodynamics a condensation process and an evaporation process are characterized by a positive or negative sign of $\mu_1 - g_2$, respectively. Thus, using the data from the pressure-temperature relaxation procedure we may identify condensation and evaporation processes.

Condensation. If a condensation process is identified by $\mu_1 - g_2 > 0$ the expression $\alpha_1^0\rho_1^0$ is too large and $\alpha_1\rho_1$ has to decrease. The smallest admissible value for this expression is $\alpha_1^*\rho_1^* = tol > 0$. This means that all water vapor has condensated except a small amount due to numerical reasons. Using the pressure-temperature relaxation procedure according to Section 10.3.3 with $\alpha_1^*\rho_1^*$ instead of $\alpha_1^0\rho_1^0$ we determine the corresponding values for all variables of the phases. Using these data one has to check the sign of the difference of the chemical potentials. If still $\mu_1 - g_2 \geq 0$ holds, then total condensation will occur. We keep $\alpha_1^*\rho_1^* = tol > 0$ and the corresponding data. Otherwise the interval $[\alpha_1^*\rho_1^* = tol, \alpha_1^0\rho_1^0]$ is admissible for the bisection method.

Evaporation. If an evaporation process is identified by $\mu_1 - g_2 < 0$ the expression $\alpha_1^0\rho_1^0$ is too small and $\alpha_1\rho_1$ has to increase. Because of (10.3.48) we have the bound $\alpha_1^*\rho_1^* \leq W$. Moreover, we have to guarantee that

$$E - \alpha_1\rho_1 q_1 - W q_2 + \alpha_1\rho_1 q_2 = \sum_{k=1}^{3} \alpha_k \frac{p + \gamma_k \pi_k}{\gamma_k - 1} \geq 0\,.$$

Here the left-hand side is derived from (10.3.49) where we plug in (10.3.48) and (10.2.12) and use $\pi_1 = 0$ and $q_3 = 0$. Thus we conclude

$$\alpha_1^*\rho_1^* = \min\left\{W - tol, \frac{E - W q_2}{q_1 - q_2}\right\}\,.$$

Again using the pressure-temperature relaxation procedure according to Section 10.3.3 with $\alpha_1^*\rho_1^*$ instead of $\alpha_1^0\rho_1^0$ we find the corresponding values for all variables of the phases. Using these data one has to check the sign of the difference of the chemical potentials. If still $\mu_1 - g_2 \leq 0$ holds, then total evaporation will occur. We keep $\alpha_1^*\rho_1^* = tol > 0$ and the corresponding data. Otherwise the interval $[\alpha_1^0\rho_1^0, \alpha_1^*\rho_1^*]$ is admissible for the bisection method.

Again, we summarize the relaxation procedure in the following algorithm.

Algorithmus 10.3.3 (Chemical Relaxation Procedure)**.**

1. *Identify condensation or evaporation processes (i) or (ii) by the sign of* $\mu_1 - g_2$*;*
2. *Check, whether an equilibrium solution exists; this leads to four possible cases (i-a), (i-b), (ii-a), (ii-b):*
   - *if (i-a): Apply the bisection method to find the root* $\overline{\alpha_1\rho_1}$ *of (10.3.50) in the interval* $[\alpha_1^*\rho_1^* = tol, \alpha_1^0\rho_1^0]$ *and perform pressure-temperature relaxation with* $\overline{\alpha_1\rho_1}$*, see Alg. 10.3.2;*
   - *if (i-b): Apply the pressure-temperature relaxation procedure, see Alg. 10.3.2, to* $\alpha_1^*\rho_1^* = tol$*;*
   - *if (ii-a): Apply the bisection method to find the root* $\overline{\alpha_1\rho_1}$ *of (10.3.50) in the interval* $[\alpha_1^0\rho_1^0, \alpha_1^*\rho_1^*]$ *with* $\alpha_1^*\rho_1^* = \min\left\{W - tol, \frac{E - W q_2}{q_1 - q_2}\right\}$ *and perform pressure-temperature relaxation, see Alg. 10.3.2, with* $\overline{\alpha_1\rho_1}$*;*
   - *if (ii-b): Apply the pressure-temperature relaxation procedure, see Alg. 10.3.2, to* $\alpha_1^*\rho_1^* = W - tol$*.*

A direct consequence of the algorithm is the following theorem.

Theorem 10.3.2. *The chemical relaxation procedure given by Alg. 10.3.3 provides a unique solution. In particular, the resulting states for the equilibrium pressure and equilibrium temperature are positive.*

The above relaxation procedure can be considered as an essential improvement of the original one presented in [40, 42] due to the following aspects: In the original procedure the Gibbs free energies are relaxed, i.e., the influence of the mixture entropy, which is described by the difference of the chemical potential and the Gibbs free energy of the vapor phase, is neglected. This extra term cancels in pure phases. Moreover, in the original procedure a nested iteration method was used. We now reduce the numerical costs significantly by simplifying the equilibrium system to a *scalar* equation depending only on $\alpha_1\rho_1$ that has to be solved by a *single* iteration process. Thus, the computational costs are significantly reduced, see Section 10.5.

Finally we point out that in complete analogy the above procedure can also be applied to mixtures with an arbitrary number of additional inert ideal gases.

10.3.5 Application of relaxation procedures

We conclude the section on the relaxation to equilibrium by some remarks on (i) the order of performing the relaxation procedures and (ii) where to apply them.

From a physical point of view the equilibrium state should not depend on the order of the relaxation processes. For instance, performing relaxation of the chemical potentials does not require to perform

mechanical and thermal relaxation before. According to (10.3.41) and (10.3.42) pressures and temperatures are relaxed to equilibrium together with the mass. On the other hand, the equilibrium velocity is not changed by neither of the other relaxation procedures and vice versa as becomes obvious from the definition (10.2.19), (10.2.20), (10.2.23) and (10.2.24) of the relaxation terms. However, from a numerical point of view performing the latter relaxation procedures will provide a better initial guess for the bisection method involved in performing the mass transfer.
For the same reasons we do not have to perform pressure relaxation first when performing temperature relaxation without accounting for mass transfer, see Section 10.3.3, because the pressures are relaxed simultaneously to equilibrium together with the temperatures according to (10.3.24).

Since by both the thermal and the chemical relaxation procedure we also relax the pressures simultaneously there is no need to perform the pressure relaxation, see Section 10.3.2. The advantage is twofold: First of all, for our three-component model we do not have to compute the roots of a cubic polynomial but the quadratic polynomial (10.3.34) where the admissible root can be singled out a priori. Furthermore, we avoid the approximation step (10.3.19) as usually performed, cf. [23,30,41,42], that can cause instabilities in case of strong non-equilibrium, i.e., the differences $p_k^0 - p^\infty$ are large. In particular, we observe that by the pressure relaxation small oscillations may be triggered that spoil significantly the performance of locally adaptive computations due to denser grids. Consequently, the computational costs of our computations could be significantly reduced.

Furthermore we strongly recommend that temperature relaxation should always be accounted for in the computations. We performed investigations for a spherical bubble collapse not reported here. It turned out that without temperature relaxation unphysically high temperatures for water vapor and inert gas may occur in the order of 100000 K. This caused high sound speeds that triggered very small time steps due to the CFL number restriction. When performing the same computation with temperature relaxation, the equilibrium temperatures stayed in a physically admissible range and the computations run much faster because the CFL number was moderate and the time steps did not become as small as before.

Finally, we note that after each evolution step the phases may be in non-equilibrium. Therefore the relaxation procedures have to be performed in *each* cell of the computational domain, see Section 10.4. In [40] an interfacial region or a mixture zone has been introduced to avoid *unphysical* nucleation or cavitation. In Section 10.5.2 we will verify that these do not occur in our model due to the sign of the difference of the chemical potentials. On the other hand, the model is able to describe *physical* cavitation by expansion. For this reason we avoid introducing an artificial interfacial region to avoid numerical instabilities.

10.4 Discretization

For a condensed presentation of the discretization it is convenient to rewrite the system (10.2.2), (10.2.3), (10.2.4) and (10.2.6) in matrix-vector representation

$$\partial_t \alpha_k + \boldsymbol{V}_I \cdot \nabla \alpha_k = S_{\alpha,k}(\boldsymbol{w}),\ k = 1, \dots, K-1, \tag{10.4.1}$$

$$\partial_t \boldsymbol{u}_k + \nabla \cdot (\boldsymbol{f}_k(\alpha_k, \boldsymbol{u}_k)) = \boldsymbol{H}(\boldsymbol{w}) \nabla \alpha_k + \boldsymbol{S}_{\boldsymbol{u},k}(\boldsymbol{w}),\ k = 1, \dots, K, \tag{10.4.2}$$

where we make use of the convention (10.2.7). This forms a coupled system for the volume fractions $\boldsymbol{\alpha} := (\alpha_1, \dots, \alpha_{K-1})^T$ and the vectors $\boldsymbol{u}_k$ of the conserved quantities of phase $k = 1, \dots, K$. These are condensed in the vector $\boldsymbol{w} := (\boldsymbol{\alpha}^T, \boldsymbol{u}_1^T, \dots, \boldsymbol{u}_K^T)^T$, where the field $\boldsymbol{f}_k := (\boldsymbol{f}_{k,1}, \dots, \boldsymbol{f}_{k,d})$ of the fluxes in the *ith* coordinate direction and the vector of relaxation terms $\boldsymbol{S}_{\boldsymbol{u},k}$ corresponding to $\boldsymbol{u}_k$ as well as the matrices $\boldsymbol{H}$ are defined by

$$\boldsymbol{u}_k := \begin{pmatrix} \alpha_k \rho_k \\ \alpha_k \rho_k \boldsymbol{v}_k \\ \alpha_k \rho_k E_k \end{pmatrix},\ \boldsymbol{f}_{k,i} := \begin{pmatrix} \alpha_k \rho_k v_{k,i} \\ \alpha_k \rho_k v_{k,i} \boldsymbol{v}_k + \alpha_k p_k \boldsymbol{e}_i \\ \alpha_k \rho_k v_{k,i} (E_k + p_k/\rho_k) \end{pmatrix}, \tag{10.4.3}$$

$$\boldsymbol{H} := \begin{pmatrix} \boldsymbol{0}^T \\ P_I \boldsymbol{I}_{d\times d} \\ P_I \boldsymbol{V}_I^T \end{pmatrix},\ \boldsymbol{S}_{\boldsymbol{u},k} := \begin{pmatrix} S_{\rho,k} \\ \boldsymbol{S}_{\rho\boldsymbol{v},k} \\ S_{\rho E,k} \end{pmatrix}. \tag{10.4.4}$$

Here $\boldsymbol{e}_i \in \mathbb{R}^d$ and $\boldsymbol{I}_{d\times d} \in \mathbb{R}^{d\times d}$ denote the *ith* unit vector and the identity matrix in $\mathbb{R}^d$ and $\mathbb{R}^{d\times d}$, respectively. Note that because of the choice (10.2.9) of the interfacial pressure P_I and interfacial velocity $\boldsymbol{V}_I$, the fluid equations of *all* phases are coupled, i.e., $P_I = P_I(\boldsymbol{w})$, $\boldsymbol{V}_I = \boldsymbol{V}_I(\boldsymbol{w})$, whereas the left-hand side of (10.4.2) only depends on $\boldsymbol{w}_k := (\alpha_k, \boldsymbol{u}_k^T)^T$. Again note that for $k = K$ we make use of the convention (10.2.7).

Following [32] we do not discretize the coupled system (10.4.1) and (10.4.2) but perform an operator splitting according to Godunov or Strang, see [38,39], resulting in the system of equations of fluid motion

$$\partial_t \alpha_k + \boldsymbol{V}_I \cdot \nabla \alpha_k = \boldsymbol{0}, \ k = 1, \dots, K-1, \tag{10.4.5}$$
$$\partial_t \boldsymbol{u}_k + \nabla \cdot (\boldsymbol{f}_k(\alpha_k, \boldsymbol{u}_k)) = \boldsymbol{H}(\boldsymbol{w}) \nabla \alpha_k, \ k = 1, \dots, K, \tag{10.4.6}$$

and the system of relaxation

$$\frac{d\,\alpha_k}{d\,t} = S_{\alpha,k}(\boldsymbol{w}), \ k = 1, \dots, K-1, \tag{10.4.7}$$
$$\frac{d\,\boldsymbol{u}_k}{d\,t} = \boldsymbol{S}_{\boldsymbol{u},k}(\boldsymbol{w}), \ k = 1, \dots, K. \tag{10.4.8}$$

Note that the differential equation (10.4.5), (10.4.6) describes a variation in time and space, whereas the system (10.4.7), (10.4.8) is an evolution in time only although the state $\boldsymbol{w}$ depends on both time and space. Therefore we use different symbols for the differentiation.

In each time step we thus perform alternately the evolution of the fluid and the new relaxation process. Since our interest is in equilibrium processes we replace the transient relaxation procedure (10.4.7) and (10.4.8) by the relaxation procedures introduced in Section 10.3. The discretization of the fluid system (10.4.5) and (10.4.6) is briefly summarized for the convenience of the reader.

A finite volume scheme is applied to the fluid equations (10.4.6). Due to the non-conservative term on the right-hand side this discretization is linked to the discretization of the non-conservative evolution equation (10.4.5) for the volume fractions. In order to avoid oscillations in the pressures and velocities at the phase interface Saurel and Abgrall [32] suggest to use a special upwind discretization of (10.4.5) that preserves homogeneous pressure and velocity fields. Let be $\{V_i\}_i$ the spatial discretization of the computational domain $\Omega \subset \mathbb{R}^d$ and $\{t_n\}_{n\geq 0}$ the temporal discretization which for ease of representation is assumed to be uniform, i.e., $t_{n+1} = t_n + \Delta t$. Then the resulting scheme reads

$$(\alpha_k)_i^{n+1} = (\alpha_k)_i^n - \frac{\Delta t}{|V_i|} \sum_{j\in N(i)} |\Gamma_{ij}| \, (\overline{\boldsymbol{V}}_I)_{ij} \cdot (\nabla \alpha_k)_{ij}^n, \tag{10.4.9}$$
$$(\boldsymbol{u}_k)_i^{n+1} = (\boldsymbol{u}_k)_i^n - \frac{\Delta t}{|V_i|} \sum_{j\in N(i)} |\Gamma_{ij}| \, \boldsymbol{G}_{ij}^n, \tag{10.4.10}$$

where the fluxes $\boldsymbol{G}_{ij}^n$ and the gradients of the volume fractions in normal direction are determined by

$$\boldsymbol{G}_{ij}^n := \boldsymbol{F}_k(\boldsymbol{w}_{ij}^n, \boldsymbol{w}_{ji}^n, \boldsymbol{n}_{ij}) - \boldsymbol{H}(\overline{\boldsymbol{w}}_{ij})(\nabla \alpha_k)_{ij}^n, \tag{10.4.11}$$
$$(\nabla \alpha_k)_{ij}^n := ((\overline{\alpha}_k)_{ij} - (\alpha_k)_i^n) \, \boldsymbol{n}_{ij}, \tag{10.4.12}$$

and $|V_i|$ and $|\Gamma_{ij}|$ denote the volume and the interface area of the cell V_i and the cell interface Γ_{ij}, respectively. Here the quantities $(\overline{\alpha}_l)_{ij}$, $(\overline{\boldsymbol{V}}_I)_{ij}$ and $\overline{\boldsymbol{w}}_{ij}$ are determined by the solution of a Riemann problem at the cell interface Γ_{ij} evaluated $|\Gamma|$ from the interior of the cell V_i. For details on the derivation we refer to Appendix A in [17].

At each cell interface Γ_{ij} of cell V_i with a neighbor cell V_j, $j \in N(i)$, a numerical flux in outer normal direction $\boldsymbol{n}_{ij}$ to the cell interface is computed in two steps:

(i) In each of the two neighboring cells a quasi-one-dimensional $2nd$ order ENO reconstruction of the primitive variables $(\rho_k, \boldsymbol{v}_k, p_k)$ with van Leer limiter and the volume fractions α_k is computed for *all* components to determine two states $\boldsymbol{w}_{ij}^n$, $\boldsymbol{w}_{ji}^n$ left and right of the cell interface. Note that for the volume fractions we switch to $1st$ order reconstruction whenever the higher order reconstruction of the volume fractions lies outside a tolerance range $[\alpha_{Tol}, 1 - \alpha_{Tol}]$ with $\alpha_{Tol} = 10^{-18}$ in our computations.

(ii) A multi-phase multi-component Riemann problem determined by $\boldsymbol{w}_{ij}^n$, $\boldsymbol{w}_{ji}^n$ is approximately solved using an HLLC-type Riemann solver, see Appendix B in [17], providing us with an intermediate state $\overline{\boldsymbol{w}} := (\overline{\boldsymbol{\alpha}}^T, \overline{\boldsymbol{u}}_1^T, \dots, \overline{\boldsymbol{u}}_k^T)^T$ at the cell interface by which we evaluate the flux at the cell interface in normal direction $\boldsymbol{n}$, i.e,

$$\boldsymbol{F}_k(\boldsymbol{w}_{ij}^n, \boldsymbol{w}_{ji}^n, \boldsymbol{n}_{ij}) := \sum_{l=1}^{d} \boldsymbol{f}_{k,l}(\overline{\boldsymbol{w}}(\boldsymbol{w}_{ij}^n, \boldsymbol{w}_{ji}^n))\,(\boldsymbol{n}_{ij})_l. \tag{10.4.13}$$

Note that the intermediate state also enters the approximation (10.4.9) of the volume fractions and their gradients (10.4.12). In principle, any numerical flux is admissible that is consistent with the flux, i.e.,

$$\boldsymbol{F}_k(\boldsymbol{w}, \boldsymbol{w}, \boldsymbol{n}) = \sum_{i=1}^{d} \boldsymbol{f}_{k,i}(\alpha_k, \boldsymbol{u}_k)\, n_i, \ \forall\, \boldsymbol{w} = (\boldsymbol{\alpha}^T, \boldsymbol{u}_1^T, \dots, \boldsymbol{u}_K^T)^T, \tag{10.4.14}$$

$$\sum_{j \in N(i)} |\Gamma_{ij}|\, \boldsymbol{n}_{ij} = \boldsymbol{0}. \tag{10.4.15}$$

Finally, we remark that in order to use the multi-component model also in absence of one or several components, the fluid must be modeled as a mixture of *all* components in the *entire* computational domain. Therefore the fluid contains at least a negligible amount of each fluid. Thus we require $\alpha_k \geq \varepsilon$ for the initial data. This is common practice, see for instance [3, 7, 21, 32]. In [7] ε is chosen to be 10^{-6}, in [3] $\varepsilon = 10^{-8}$. In our computation we mostly choose $\varepsilon = 10^{-8}$, see also Section 10.3.4.

During the computation α_k may become smaller. In that case α_k often is set to ε. However, this leads to the violation of conservation of mass, momentum and energy. We avoid this by allowing smaller values for α_k. To guarantee that α_k always stays positive, we terminate the computation whenever α_k drops below a tolerance value of 10^{-18} that never happened in our computations.

Finally, the efficiency of the scheme is improved by local grid adaption where we employ the multi-resolution concept based on biorthogonal wavelets. The key idea is to perform a multi-resolution analysis on a sequence of nested grids providing a decomposition of the data on a coarse scale and a sequence of details that encode the difference of approximations on subsequent resolution levels. The detail coefficients become small when the underlying data are locally smooth and, hence, can be discarded when dropping below a threshold value ε_{thresh}. By means of the thresholded sequence a new, locally refined grid is determined. Details on this concept can be found in [27, 28].

10.5 Numerical results

By means of several numerical computations using our new relaxation procedures we want to (i) validate their reliability, the efficiency and robustness, (ii) verify that they can deal with physical cavitation and (iii) apply them for the investigation of complex 2D problems.

10.5.1 Validation

For the validation we consider different configurations summarized in the following.

Test case C1: water liquid–vapor expansion tube problem. This configuration is a benchmark problem taken from Zein [40] that has been originally proposed in [36]. It is a two-component 1d-Riemann problem given by the initial data summarized in Table 10.3. Note that the vapor density has not been given in [36, 40]. Here we choose the vapor density determined by the pressure and temperature of the liquid. For this problem we use the material parameters given in Table 10.2. The computations for this configuration are performed with velocity and temperature relaxation.

Test case C2: Vapor–liquid–gas expansion and compression problem. To investigate cavitation phenomena we consider two 1d-Riemann problems: an expansion problem (C2a) and a compression problem (C2b) for a three-component fluid. The data are listed in Table 10.4 with material parameters given in Table 10.1. The computations for these configurations are performed with all relaxation processes: velocity, temperature and chemical relaxation.

α_{vapor}	ρ_{vapor}	ρ_{water}	p [bar]	v_{left} [m/s]	v_{right} [m/s]
0.01	0.63	1150	100000	-2	+2

Table 10.3: Initial data for Riemann problem: water liquid–vapor expansion tube problem (C1).

	α_{vapor}	α_{water}	p [bar]	T [K]	v_{left} [m/s]	v_{right} [m/s]
C2a	ε	$1-2\varepsilon$	1	293	-10	+10
C2b	ε	$1-2\varepsilon$	1	293	+10	-10

Table 10.4: Initial data for Riemann problems: vapor–liquid–gas expansion problem (C2a) and compression problem (C2b) with $\varepsilon = 10^{-8}$.

Grid convergence. Due to the lack of exact solutions we present here a grid convergence study for the validation of our code. For this purpose we consider the water liquid – vapor expansion tube problem (C1). The solution has been computed at time $t = 3.2ms$ on the domain $\Omega = [0,1]$ discretized by 5×2^L cells performing $L = 6, \ldots, 12$ uniform refinements and time discretization using a CFL number of 0.9. The performance of the computations is listed in Table 10.5 (left). In Figure 10.2 we show

L	CPU (sec)	# cells	# steps
6	6	320	1629
7	20	640	3258
8	82	1280	6516
9	331	2560	13031
10	1274	5120	26062
11	5029	10240	52123
12	20493	20480	104245

L	CPU (sec)	# cells	# steps	speed up
6	3	184	1628	1.7
7	7	248	3255	2.8
8	20	340	6509	4.0
9	50	527	13017	6.7
10	137	742	26029	9.3
11	382	964	52053	13.2
12	3193	1514	104101	20.0

Table 10.5: Water liquid–vapor expansion tube problem (C1): performance for computations with temperature relaxation for uniform (left) and adaptive ($\varepsilon_{thresh} = 10^{-4}$) (right) discretization.

the convergence behavior for the mixture pressure, the mixture velocity, the mixture density and the vapor volume fraction. We observe that with increasing resolution the leading and trailing front of the rarefaction fans become less smeared and finally a sharp kink is reproduced. The solution is in agreement with the one presented in Zein [40], Figure 3.7.

For the vapor–liquid–gas expansion problem (C2a) we perform a similar grid convergence study. The solution has been computed at time $t = 0.2ms$ on the domain $\Omega = [0,1]$ discretized by 5×2^L cells performing $L = 6, \ldots, 12$ uniform refinements and time discretization using a CFL number of 0.9. The performance of the computations is listed in Table 10.6 (left). In Figure 10.3 we show the convergence behavior for the mixture pressure, the mixture velocity, the mixture density and the vapor volume fraction. The convergence behavior is similar to the test case (C1).

Robustness and efficiency of temperature relaxation. For the water liquid–vapor expansion tube problem (C1) computational times are given in [40]: the CPU time was 14.772 hours (4 core AMD Opteron(tm) 2218, 2.6 GHz, 32 GB Ram) for performing 763,550 time steps were performed on a uniform grid with 5000 cells. In comparison to our uniform computation (4 core AMD Opteron 8356, 2.3 GHz, 256 GB Ram) for $L = 10$ (5120 cells) this is a speed up of 41.7. The number of time steps is reduced by 29.3. Note that the AMD Opteron 8356 is 4–5 times faster than the AMD Opteron(tm) 2218. There are mainly two reasons for the significant speed up:

(i) It is mentioned in [40], p. 74, that "...this test case requires a small time step to obtain a stable solution ... indicating that there is a stiffness coming from the relaxation". Therefore he used a CFL number of 0.03 that is 30 times smaller than we used for our computations. This clearly indicates that our new temperature relaxation procedure is significantly more robust.

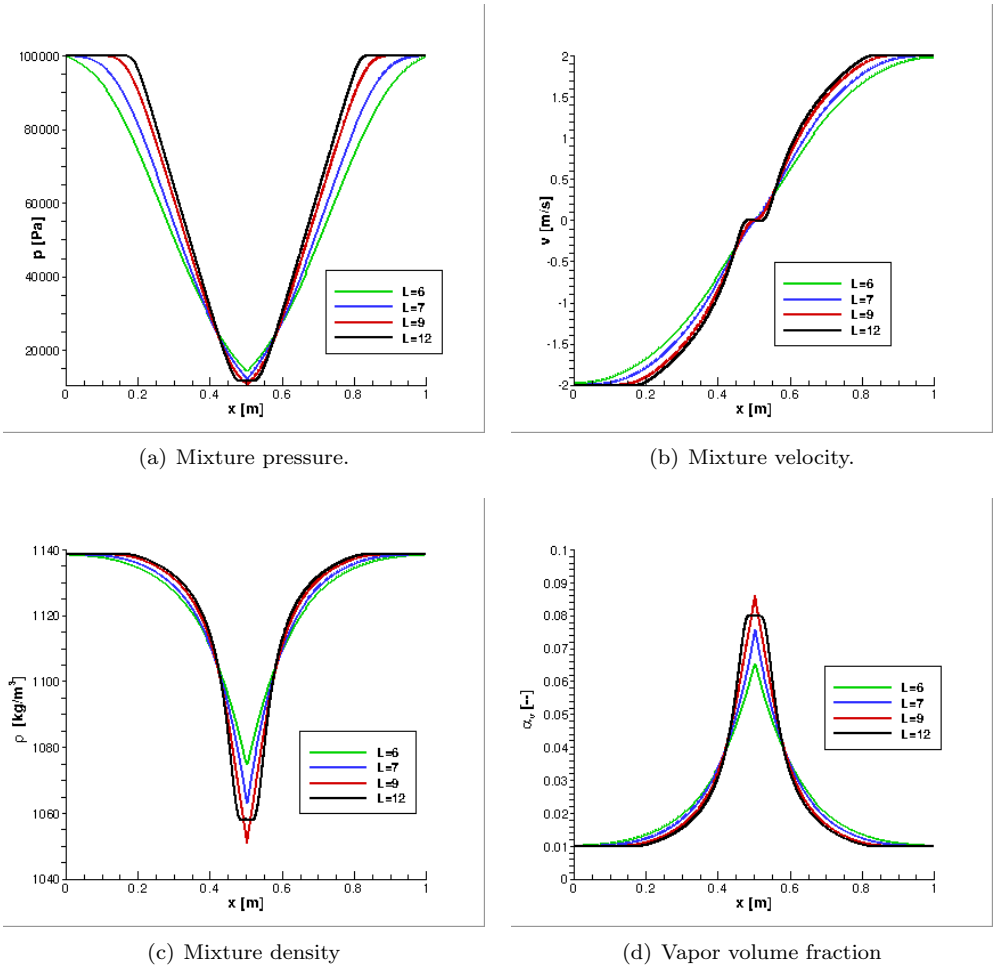

(a) Mixture pressure.

(b) Mixture velocity.

(c) Mixture density

(d) Vapor volume fraction

Figure 10.2: Water liquid–vapor expansion tube problem (C1): convergence study.

(ii) In our new temperature relaxation procedure we avoid an iterative process. Instead we perform an explicit computation of the equilibrium state. We point out that we perform temperature relaxation in all cells whereas Zein applies the temperature relaxation only at the phase interface.

Furthermore, the computations are significantly accelerated using local grid adaptation. For this purpose we also performed the parameter study with multi-resolution based adaptation using a constant threshold value of 10^{-4}, see Table 10.5 (right). As can be observed in Table 10.5 the speed up between uniform and adaptive computation is increasing with higher number of refinement level L. For configuration (C2a) the grid adaptation does not perform as good and the speed up of about 4 is moderate, see Table 10.6.

Robustness and efficiency of chemical relaxation. The most important speedup is achieved by our new relaxation procedure driving the chemical potentials into equilibrium. To our knowledge the only numerical results accounting for chemical relaxation in a three-component model have been reported in [42]. There a spherically symmetric cavitation bubble is considered with initial radius $R = 0.75mm$. The initial data are summarized in Table 10.7. Due to the high computational cost Zein et al. used reduced models to simulate three-component flows, see [42]. Nevertheless, the simulation of a collapsing cavitation bubble ($t = 150\mu s$, 66000 cells) took about two months on the system 4 core AMD Opteron(tm) 2218, 2.6 GHz, 32 GB Ram. Using our improved numerical method including the new relaxation procedures and local grid adaptation the computational time is reduced to at most 60 CPU hours on the system 84 core AMD Opteron 8356, 2.3 GHz, 256 GB Ram, although the full model is considered and the

L	CPU (sec)	# cells	# steps
6	1	320	107
7	5	640	213
8	19	1280	425
9	73	5120	849
10	293	5120	1698
11	1109	10240	3396
12	4374	20480	6792

L	CPU (sec)	# cells	# steps	speed up
6	1	214	107	1.6
7	2	342	213	2.4
8	7	604	425	2.7
9	24	1234	849	3.0
10	86	2256	1698	3.4
11	290	4068	3396	3.8
12	1017	7674	6792	4.3

Table 10.6: Vapor–liquid–gas expansion problem (C2a): performance for computations with temperature relaxation for uniform (left) and adaptive ($\varepsilon_{thresh} = 10^{-4}$) (right) discretization.

	α_{vapor}	α_{gas}	T	p	v
inside the bubble	$1 - \varepsilon_I - \alpha_{gas}$	0.1	293	2339	0
outside	ε_O	ε_O	293	100000	0

Table 10.7: Initial data for cavitation bubble with $\varepsilon_I = 10^{-8}$, $\varepsilon_O = 10^{-6}$

.

computations have been performed on a four times larger computational domain for a longer time period ($t = 240\mu s$) with higher local resolution. For details on the numerical discretization see [17]. Note, that the simplification in [42] of relaxing Gibbs free energies leads to slightly different (physically wrong) equilibrium states, what is also avoided in our new procedure.

10.5.2 Physical cavitation

Cavitation induced by expansion is a frequently investigated problem in the literature. For instance, in [41] an expansion tube filled with liquid water is investigated. For numerical reasons it is necessary that some amount of vapor exists initially. In [41] a large initial vapor volume fraction, $\alpha_{vapor} = 0.01$, was necessary due to the definition of an interfacial region and the constraints for the thermal relaxation procedures. Here we use $\alpha_{vapor} = 10^{-8}$. Although the vapor volume fraction may decrease during the computation it always stays positive. This also holds true for all phases that may be initialized by a small value. Furthermore, we avoid to introduce technical parameters, e.g., the definition of an interfacial region or a tolerance range $[\bar{\epsilon}, 1-\bar{\epsilon}]$ for the volume fractions. These may trigger oscillations and unphysical phenomena in the solution, e.g. wave splitting. In the worst case these effects lead to a breakdown of the simulation. Nevertheless, we are able to simulate cavitation *without* causing unphysical cavitation. For illustration we consider two symmetric examples where the pressure, velocity and temperature of each component is in equilibrium. The volume fractions as well as the pressure and the velocity are constant, whereas the velocity exhibits a discontinuity. The fluid consists of almost pure liquid water perturbed by a small amount $\varepsilon = 10^{-8}$ of the other components. The parameters are listed in Table 10.4.

For all our computations, the computational domain is $\Omega = [0, 1]$ m, where for boundary conditions we set the initial left and right state, respectively. The initial jump is located at $x = 0.5$ m. The domain is discretized by $N_0 = 5$ cells on coarsest level and successively refined using $L = 10$ refinement levels. The threshold value is set to $\varepsilon_{thresh} = 10^{-4}$. The temporal discretization is adjusted during the computation by a fixed CFL number of 0.5. The computations terminate at the final time $T = 2 \times 10^{-4}$ s.

In test case (C2a) the almost pure liquid water phase is expanded and the pressure drops. This leads to cavitation, i.e., water vapor is created due to the phase transition where mass is transferred from liquid water to water vapor, see Figure 10.4. Thus we can simulate cavitation *without* having initialized a significant amount of water vapor.

Next we present the results for test case (C2b), see Figure 10.5. The liquid phase is now compressed. The water volume fraction remains constant, i.e., no unphysical cavitation occurs. This confirms that we do not have to introduce an interfacial region but may perform relaxation of chemical potentials throughout the computational domain.

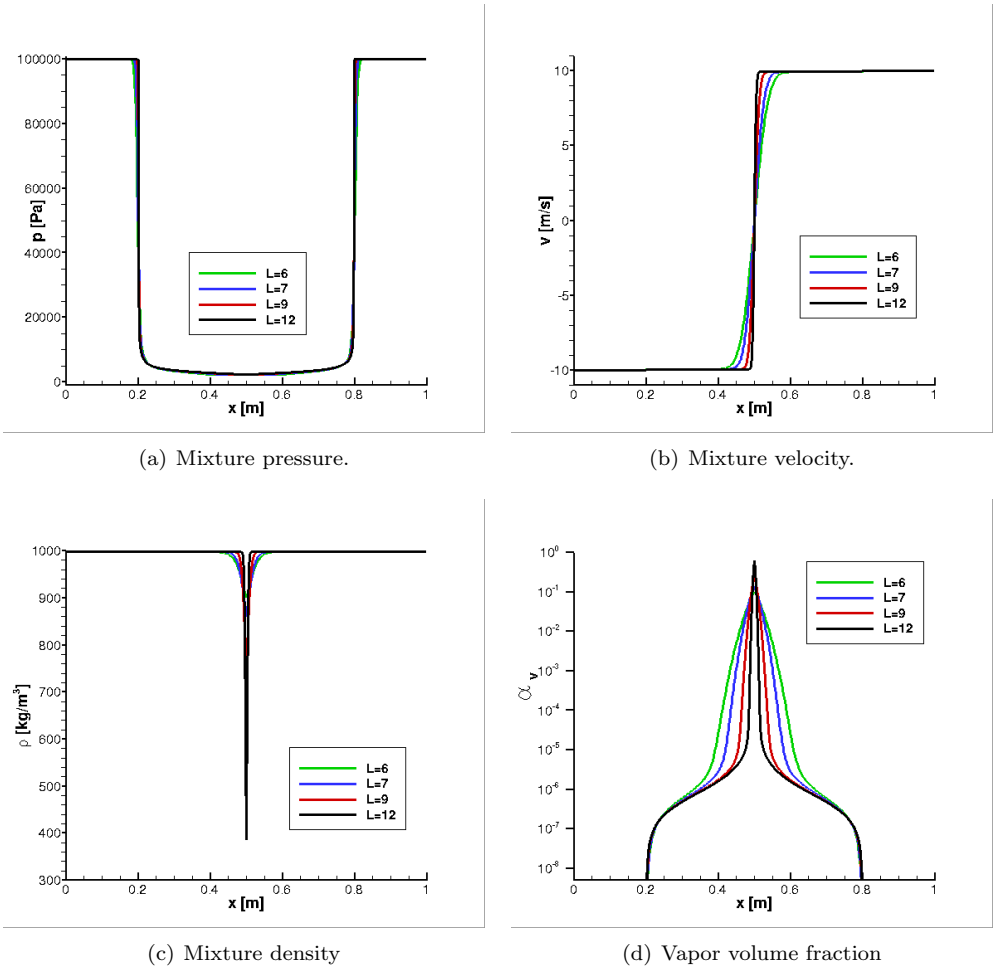

(a) Mixture pressure.

(b) Mixture velocity.

(c) Mixture density

(d) Vapor volume fraction

Figure 10.3: Vapor–liquid–gas expansion problem (C2a): convergence study.

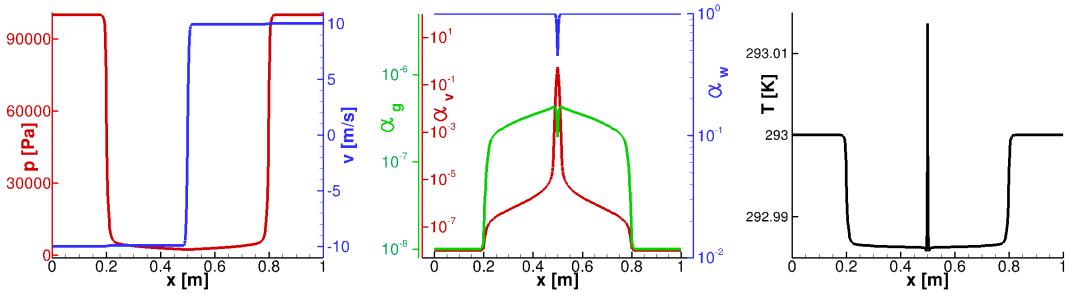

Figure 10.4: Test case (C2a): Pressure and velocity (left), volume fractions (middle) and temperature (right).

10.5.3 Application: 2d-shock-bubble interaction

For a multi-dimensional application we consider the interaction of a collapsing bubble with a planar shock wave. This problem is important for medical applications such as shock wave lithotripsy, as well as from a more fundamental point of view because bubbles in a cloud are exposed to the collapse shock waves of neighboring bubbles. This problem has been investigated both by so-called lithotripter

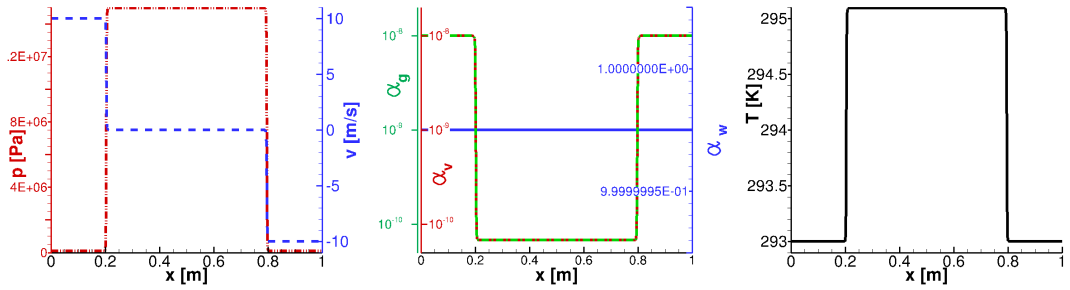

Figure 10.5: Test case (C2b): Pressure and velocity (left), volume fractions (middle) and temperature (right).

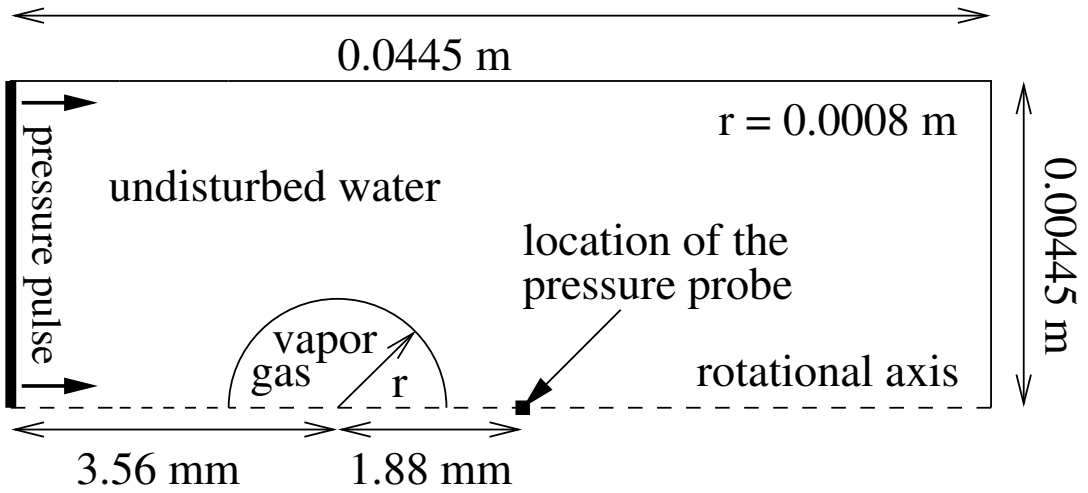

Figure 10.6: Computational setup.

shock wave (LSW) experiments and numerical simulations. For a detailed review we refer to [1, 4] and references cited therein. Since in this paper the main objective is on the feasibility of multi-dimensional multi-component simulations the focus is on the numerical simulation rather than the comparison with experiments, we therefore confine ourselves to a simplified quasi-two-dimensional computational setting employing rotational symmetry as sketched in Figure 10.6.

Note that a quantitative comparison with the experiments is not feasible due to significant uncertainties in the numerical setup. For instance, the initial data cannot be depicted from the experiment but has to be guessed. Furthermore, measurement techniques only provide qualitative results using high-speed cameras that do not allow for quantitative data inside the bubble.

Computational setup. The computation is initialized with a bubble of radius 0.8 mm filled with liquid vapor and non-condensable gas. Since the state inside the bubble cannot be observed experimentally, we assume that the state is homogeneous and at rest with temperature 293 K and corresponding saturation pressure 2339 Pa referred to as state S_b. The bubble is embedded in water at rest where the ambient state S_0 is chosen to be the atmospheric pressure 1 bar at temperature 293 K. The computation is first started without perturbation in the water. Then at time $T_0 = 37.45\,\mu$s a pressure pulse with pressure condition S_p of 80 MPa starts propagating from the left boundary. The pressure pulse lasts $0.23\,\mu$s before recovering the initial water state at rest S_0. The boundary conditions at the left boundary are thus given by

$$S(t) = \begin{cases} S_0, & t < T_0 \text{ or } t > T_1 \\ S_p, & T_0 \le t \le T_1 \end{cases} \tag{10.5.1}$$

with $T_1 = 37.68\,\mu$s. The initial conditions are recorded in Table 10.8.

		S_b	S_0	S_p
p	$[Pa]$	2339	1×10^5	8×10^7
T	$[K]$	293	293	293
$\boldsymbol{v}$	$[m/s]$	$\mathbf{0}$	$\mathbf{0}$	$\mathbf{0}$
α_{vapor}		$0.1 - \epsilon_2$	ϵ_1	ϵ_1
α_{water}		ϵ_2	$1 - 2\epsilon_1$	$1 - 2\epsilon_1$
α_{gas}		0.9	ϵ_1	ϵ_1

Table 10.8: Initial data with $\epsilon_1 = 10^{-4}$ and $\epsilon_2 = 10^{-8}$. The state inside the bubble S_b, the ambient water state S_0 and the pressure pulse S_p are assumed to be in equilibrium.

Discretization. Since the problem is inherently two-dimensional due to rotational symmetry, we perform quasi-two-dimensional computations where we have to take the change of metric into account in the fluid discretization (10.4.9) and (10.4.10). For a structured grid in a two-dimensional space with longitudinal coordinate z and radial coordinate r, i.e., $V_{\boldsymbol{i}} = [z_{i-\frac{1}{2}}, z_{i+\frac{1}{2}}] \times [r_{j-\frac{1}{2}}, r_{j+\frac{1}{2}}]$ with $\boldsymbol{i} = (i, j)$, the resulting scheme can be written as

$$(\alpha_k)_{\boldsymbol{i}}^{n+1} = (\alpha_k)_{\boldsymbol{i}}^{n} - \frac{\Delta t}{\|V_{\boldsymbol{i}}\|} \sum_{\boldsymbol{j} \in N(\boldsymbol{i})} \|\Gamma_{\boldsymbol{ij}}\| \, (\overline{\boldsymbol{V}}_I)_{\boldsymbol{ij}} \cdot (\nabla \alpha_k)_{\boldsymbol{ij}}^{n}, \tag{10.5.2}$$

$$(\boldsymbol{u}_k)_{\boldsymbol{i}}^{n+1} = (\boldsymbol{u}_k)_{\boldsymbol{i}}^{n} - \frac{\Delta t}{\|V_{\boldsymbol{i}}\|} \sum_{\boldsymbol{j} \in N(\boldsymbol{i})} \|\Gamma_{\boldsymbol{ij}}\| \, \boldsymbol{G}_{\boldsymbol{ij}}^{n} + \frac{\Delta t |V_{ij}|}{\|V_{ij}\|} \boldsymbol{S}_{ij}^{n}, \tag{10.5.3}$$

with the volumes $|V_{(i,j)}| := \Delta z_i \, \Delta r_j = (z_{i+\frac{1}{2}} - z_{i-\frac{1}{2}})\,(r_{j+\frac{1}{2}} - r_{j-\frac{1}{2}})$, $\|V_{(ij)}\| := r_j \Delta r_j \Delta z_i$, $r_j := (r_{j+\frac{1}{2}} + r_{j-\frac{1}{2}})/2$ and the interface areas $\|\Gamma_{(i,j),(i,j\pm1)}\| := \Delta z_i \, r_{j\pm\frac{1}{2}}$ and $\|\Gamma_{(i,j),(i\pm1,j)}\| := r_j \, \Delta r_j$. Here the fluxes and the derivatives of the volume fractions are given by (10.4.11) and (10.4.12), respectively. Note that $\boldsymbol{u}_k = \alpha_k(\rho_k, \rho_k(v_z)_k, \rho_k(v_r)_k, E_k)^T$ is now composed of the density, the momentum in longitudinal and radial direction and total energy of component k. The additional metric term is defined by $\boldsymbol{S}_k(\boldsymbol{w}) = (0, \alpha_k p_k, 0, 0)^T$. This quasi-two-dimensional scheme can be derived from the three-dimensional discretization applied to a special grid similar to [6] and, in more details, in [4], Appendix A. For our problem we choose the computational domain as $\Omega = [0, 0.0445] \times [0, 0.00445]$ m^2 to avoid unphysical reflections from the right boundary and a short distance between the pressure pulse and the bubble at the left boundary. The domain is discretized by 50×5 cells on the coarsest level using $L = 7$ refinement levels. The threshold value is chosen as $\epsilon_{thresh} = 10^{-3}$. We perform 120000 time steps with CFL number 0.5. The computation is performed with mass transfer.

Numerical results. The initial phase of the computation is characterized by a rarefaction wave and a shock wave both emanating from the bubble interface and running into the liquid and towards the bubble center, respectively, see Fig. 10.7(a). The shock wave is focusing in the bubble center where it is reflected. The reflected shock wave is then interacting with the bubble interface where it is partially transmitted into the liquid and partially reflected. Thus the shock wave is bouncing between the bubble center and the bubble interface. Due to the interactions the bubble starts shrinking.

The second phase starts at time $t = T_0$ where the pressure pulse enters the computational domain at the left boundary, see Fig. 10.7(b). It hits the bubble at about $t = 39.5$ μs with the bubble at a radius of approximately 0.59 mm, see Fig. 10.8. The LSW is partially transmitted and reflected at the interface, see Figs. 10.7(c) and 10.7(d). The reflected LSW causes a significant pressure drop in the water causing vaporization, see Fig. 10.7(e). With advancing time the pressure raises again and the vapor condensates again causing pressure waves, see Fig. 10.7(f).

In a final phase the bubble interface is significantly accelerated due to the interaction with the LSW and the bubble collapses, see Fig. 10.7(f). When the bubble collapses at about $t = 44.32$ μs shock waves are emanated into the liquid, see Fig. 10.8.

An overview of the wave dynamics is given in Fig. 10.8 where we extract data on the symmetry axis every 50 time steps. The pressure gradient magnitude shows very well the collapse of the bubble and the emanated shock waves.

Finally we present in Fig. 10.9 a pressure probe taken on the symmetry axis at a distance of 1.88 mm behind the initial bubble center, see probe location in Fig. 10.6. The first peak is the pressure

measurement of the LSW and the second one is shock-induced by the collapse.

10.6 Conclusion

A generalized multi-component fluid model has been introduced. This model is thermodynamically consistent as proven in [29]. It accounts for relaxation of velocity, pressure, temperature, and chemical potentials.

Opposite to previous work, cf. [30,41], pressure and temperature are relaxed simultaneously. Typically pressure relaxation relies on an approximation process that can cause numerical instabilities in case of strong pressure non-equilibrium, cf. [21]. Alternatively, iterative procedures can be used that make computations very expensive, in particular in multi-dimensions. This is avoided in our new pressure-temperature relaxation procedure. In particular, we have proven that for particular mixtures the unique equilibrium state exists such that the equilibrium temperature as well as the equilibrium pressure are positive and the volume fractions are in the admissible range.

Instead of relaxing Gibbs free energies as in [23, 42] we perform relaxation of the chemical potentials in case of three or more components. Exemplarily for a three-component model consisting of water vapor, liquid water and inert gas we have verified that either a unique equilibrium state exists or one phase vanishes. This model is consistent with the two-component model if the inert gas is not present. We emphasize that determining the equilibrium state only requires a single iteration procedure whereas in [42] an additional internal iteration is needed. This significantly speeds up the computation.

This model is solved numerically by applying an operator splitting where the evolution of the fluid and the relaxation to equilibrium are separated in each time step. For the solution of the homogenized fluid equations we apply a second order finite volume solver based on ENO reconstruction and the HLLC Riemann solver. Computations are performed on a locally refined grid where grid adaptation is triggered by advanced multi-scale techniques, cf. [27, 28]. We emphasize that local grid adaptation is a key ingredient to perform the computations in affordable time. Moreover, we apply thermal and chemical relaxation throughout the computational domain instead of an artificial interface region near the phase boundary as done for instance in [30, 42].

By means of parameter studies for several 1d-Riemann problems we have validated the robustness and efficiency of the new relaxation procedures. Moreover, we have verified that multi-dimensional computations are feasible for the model at hand. For this purpose we have considered the interaction of a collapsing bubble with a planar shock wave. This problem is important for medical applications such as shock wave lithotripsy. To our knowledge this is one of the first 2D-computations presented using this type of model besides the two-component simulations in [30]. However, we emphasize that our computations are more complex due to three components and taking into account also chemical potentials, but are more efficient and robust due to grid adaptation and enhanced relaxation procedures, respectively.

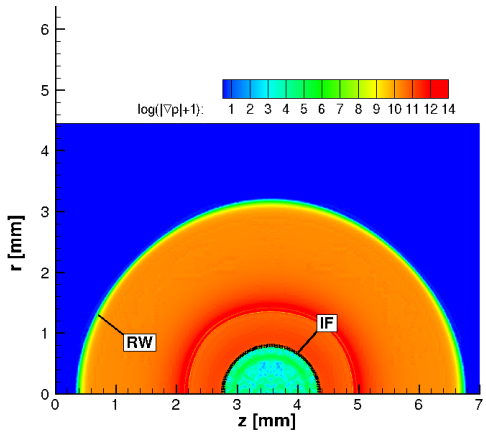

(a) 3.50 μs

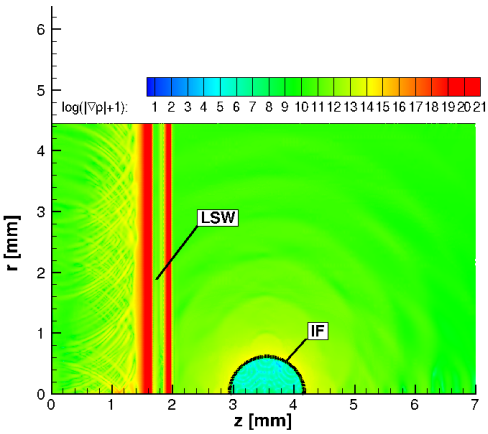

(b) 38.74 μs

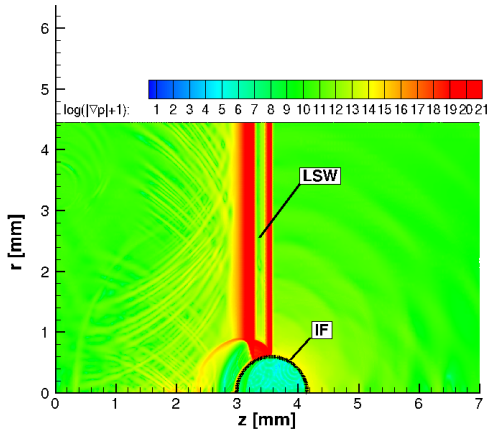

(c) 39.80 μs

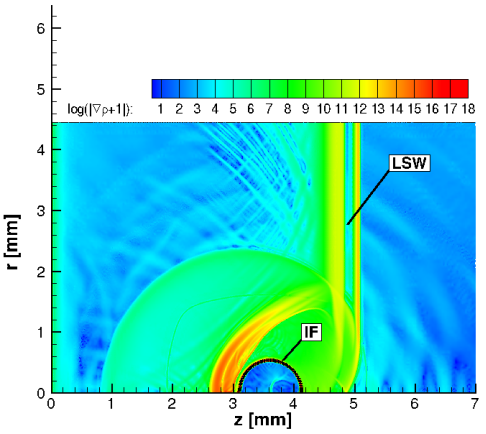

(d) 40.80 μs

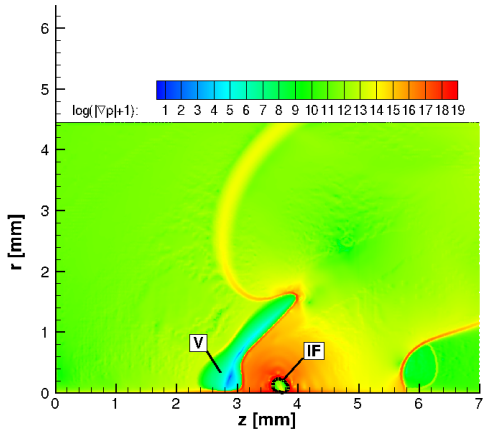

(e) 44.39 μs

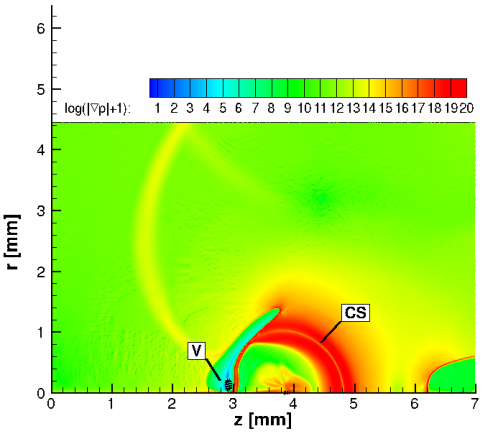

(f) 45.40 μs

Figure 10.7: Pressure gradient magnitude with bubble interface IF identified by $\alpha_{water} = 0.5$, rarefaction wave RW, lithotripter shock wave LSW, vaporization region V and collapse shock CS.

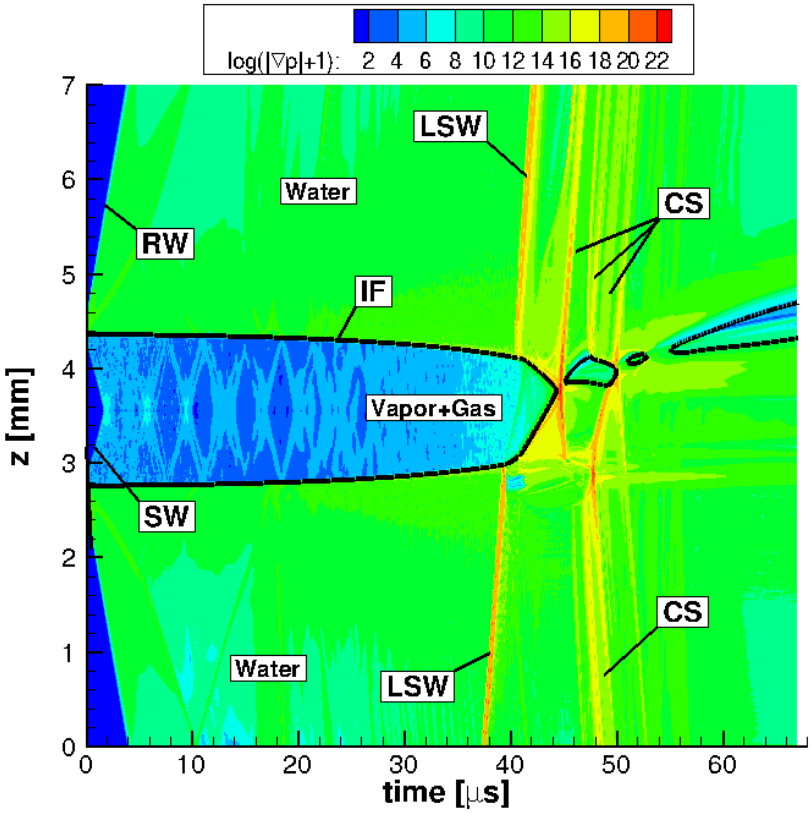

Figure 10.8: Pressure gradient magnitude with bubble interface IF identified by $\alpha_{water} = 0.5$, rarefaction wave RW, shock wave SW, lithotripter shock wave LSW and collapsing shock waves CS.

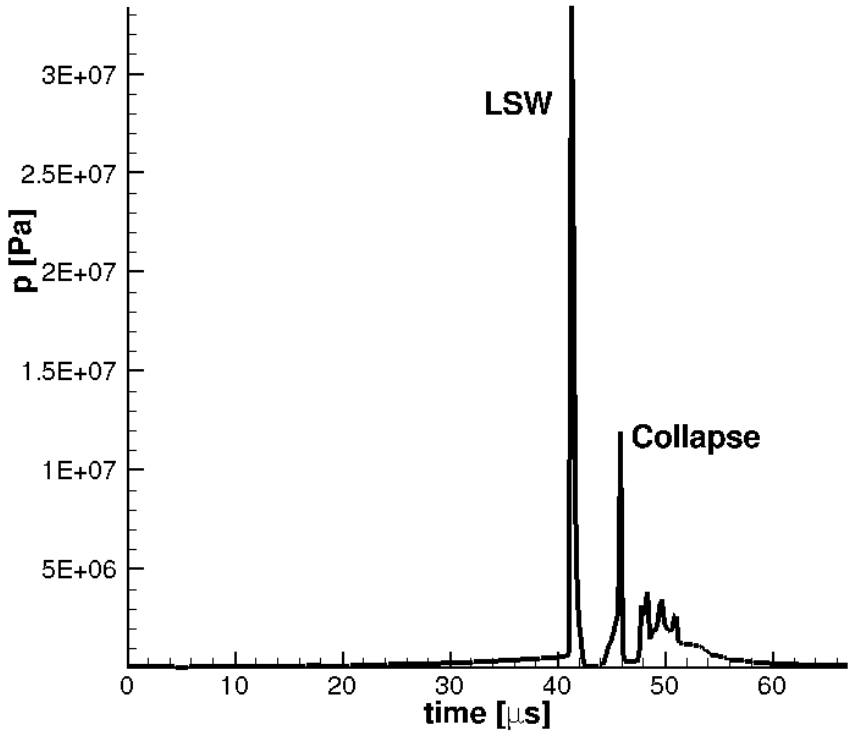

Figure 10.9: Pressure probe.

References

[1] M. Alizadeh, Experimental investigation of shock wave-bubble interaction, Phd thesis, Drittes Physikalisches Institut, Göttingen, 2010.

[2] N. Andrianov, Analytical and numerical investigation of two-phase flows, PhD thesis, Otto-von-Guericke University, Magdeburg, 2003.

[3] N. Andrianov, R. Saurel, G. Warnecke, A simple method for compressible multiphase mixtures and interfaces, Int. J. Numer. Meth. Fluids, 41 (2003), 109–131.

[4] M. Bachmann, Dynamics of cavitation bubbles in compressible two-phase fluid flow, PhD thesis, RWTH Aachen, http://darwin.bth.rwth-aachen.de/opus3/volltexte/2013/4554/pdf/4554.pdf, 2013.

[5] M.R. Baer, J.W. Nunziato, A two-phase mixture theory of the deflagration-to-detonation transition (DDT) in reactive granular materials, Int. J. Multiphase Flows, 12 (1986), 861–889.

[6] T. Barberon, Ph. Helluy, S. Rouy, Practical computation of axisymmetrical multifluid flows, International Journal of Finite Volumes, 1(1) (2003), 1–34.

[7] R.A. Berry, R. Saurel, F. Petitpas, A simple and efficient diffuse interface method for compressible two-phase flows, 2009 International Conference on Mathematics, Computational Methods & Reactor Physics, Preprint, 2009.

[8] J. Dalton, A new System of Chemical Philosophy, 3 vols, Manchester 1808.

[9] J. Dalton, A new System of Chemical Philosophy, in: Ostwalds Klassiker der Exacten Wissenschaften, Band 3, Leipzig 1889.

[10] W. Dreyer, F. Duderstadt, M. Hantke, G. Warnecke, Bubbles in liquids with phase transition. Part 1: On phase change of a single vapor bubble in liquid water, Continuum Mechanics and Thermodynamics, 24 (2012), 461–483.

[11] S.F. Davis, Simplified second-order Godunov-type methods, SIAM J. Sci. Stat. Comput., 9(3) (1988), 445–473.

[12] D. Drew, Mathematical modeling of two-phase flow, Ann. Rev. Fluid Mech., 15 (1983), 261–291.

[13] D.A. Drew, S.L. Passman, Theory of Multicomponent Fluids, Applied Mathematical Sciences, Vol. 135, Springer, 1999.

[14] P. Embid, M. Baer, Mathematical analysis of a two-phase continuum mixture theory, Contin. Mech. Thermodyn., 4 (1992), 279–312.

[15] T. Flåtten, H. Lund, Relaxation two-phase flow models and the subcharacteristic condition, Mathematical Models and Methods in Applied Sciences, 21(12) (2012), 2379–2407.

[16] T. Gallouët, J.-M. Hérard, N. Seguin, Numerical modelling of two-phase flows using the two-fluid two-pressure approach, Math. Models Methods Appl. Sci., 14(5) (2004), 663–700.

[17] E. Han, M. Hantke, S. Müller, Modeling of multi-component flows with phase transition and application to collapsing bubbles, IGPM Report No. 409, RWTH Aachen, 2014.

[18] F. Harlow, A. Amsden, Fluid dynamics, Technical Report, LA-4700, Los Alamos National Laboratory, 1971.

[19] J.-M. Hérard, A three-phase flow model, Mathematical and Computer Modelling, 45 (2007), 732–755.

[20] A. Kapila, R. Menikoff, J. Bdzil, S. Son, D. Stewart, Two-phase modelling of DDT in granular materials: Reduced equations, Phys. Fluid, 13 (2001), 3002–3024.

[21] M.H. Lallemand, A. Cinnayya, O. Le Métayer, Pressure relaxation procedures for multi-phase compressible flows, Int. J. Numer. Meth. Fluids, 49(1) (2005), 1–56.

[22] S. LeMartelot, R. Saurel, O. Le Métayer, Steady one-dimensional nozzle ow solutions of liquid-gas mixtures, J. Fluid Mechanics, 737 (2013), 146–175.

[23] O. Le Métayer, J. Massoni, R. Saurel, Dynamic relaxation processes in compressible multiphase flows. Application to evaporation phenomena. ESAIM: Proceedings, 40 (2013), 103–123.

[24] T.-P. Liu, Hyperbolic conservation laws with relaxation, Commun. Math. Phys, 108 (1987), 153–175.

[25] I. Müller, Thermodynamics, Pitman, London, 1985.

[26] I. Müller, W. Müller, Fundamentals of Thermodynamics and Applications, Springer-Verlag, Berlin, 2009.

[27] S. Müller, Adaptive multiscale schemes for conservation laws, Lecture Notes in Computational Science and Engineering, 27, Berlin: Springer, 2003.

[28] S. Müller, Multiresolution schemes for conservation laws, R. DeVore, A. Kunoth (eds.), Multiscale, nonlinear and adaptive approximation. Dedicated to Wolfgang Dahmen on the occasion of his 60th birthday. Berlin: Springer, 379–408, 2009.

[29] S. Müller, M. Hantke, P. Richter, Closure conditions for non-equilibrium multi-component models, Continuum Mechanics and Thermodynamics, 28(4) (2016), 1157–1189.

[30] M. Pelanti, K.-M. Shyue. A mixture-energy-consistent six-equation two-phase numerical model for fluids with interfaces, cavitation and evaporation waves, J. Comput. Phys., 259 (2014), 331–357.

[31] K. Saleh, Analyse et Simulation Numérique par Relaxation d'Écoulements Diphasiques Compressibles, PhD thesis, Université Pierre et Marie Curie, Paris, 2012.

[32] R. Saurel, R. Abgrall, A multiphase Godunov method for compressible multifluid and multiphase flows, J. Comput. Phys., 150(2) (1999), 425–467.

[33] R. Saurel, R. Abgrall, A simple method for compressible multifluid flows, SIAM J. Sci. Comput., 21(3) (1999), 1115-1145.

[34] R. Saurel, P. Boivin, O. Le Métayer, A general formulation for cavitating, boiling and evaporating ows, Computers and Fluids, 128 (2016), 53–64.

[35] R. Saurel, O. Le Métayer, A multiphase flow model for compressible flows with interfaces, shocks, detonation waves and cavitation, J. Fluid Mech., 43 (2001), 239–271.

[36] R. Saurel, F. Petitpas, R. Abgrall, Modelling phase transition in metastable liquids: Application to cavitation and flashing flows, J. Fluid. Mech., 607 (2008), 313–350.

[37] U. Specht, Numerical Simulation of Mechanical Waves at Fluid-Solid-Interfaces, PhD thesis, RWTH Aachen, 2000 (in German).

[38] G. Strang, On the construction and comparison of difference schemes, SIAM J. Numer. Anal., 5 (1968) 506-517.

[39] E. F. Toro, Riemann solvers and numerical methods for fluid dynamics: A practical introduction, Berlin: Springer, 1997.

[40] A. Zein, Numerical methods for multiphase mixture conservation laws with phase transition, PhD thesis, Otto-von-Guericke University, Magdeburg, 2010.

[41] A. Zein, M. Hantke, G. Warnecke, Modeling phase transition for compressible two-phase flows applied to metastable liquids, J. Comput. Phys., 229(8) (2010), 2964–2998.

[42] A. Zein, M. Hantke, G. Warnecke, On the Modelling and Simulation of a Laser-Induced Cavitation Bubble, Int. J. Num. Meth. Fluids, 73(2) (2013), 172-203.

Part III

Particle flows

Chapter 11

Bubble evolution models

Bibliographic note: The content of this chapter is published in [H5]: Wolfgang Dreyer, Frank Duderstadt, Maren Hantke, and Gerald Warnecke. On phase change of a single vapor bubble in liquid water, *Continuum mechanics and thermodynamics* 24 (2012), pp. 461-483.

Abstract: In the forthcoming second part of this paper a system of balance laws for a multi-phase mixture with many dispersed bubbles in liquid is derived where phase transition is taken into account. The exchange terms for mass, momentum and energy explicitely depend on evolution laws for total mass, radius and temperature of single bubbles.

Therefore in the current paper we consider the dynamics of a single fully developed bubble of vapor and inert gas surrounded by the corresponding liquid phase. The creation of bubbles, e.g. by nucleation, is not taken into account. We study the behavior of this bubble due to condensation and evaporation at the interface. The aim is to find evolution laws for total mass, radius and temperature of the bubble, which should be as simple as possible but consider all relevant physical effects.

Special attention is given to the effects of surface tension and heat production on the bubble dynamics as well as the propagation of acoustic elastic waves by including slight compressibility of the liquid phase. Separately we study the influence of the three phenomena heat conduction, elastic waves, and phase transition on the evolution of the bubble.

We find ordinary differential equations that describe the bubble dynamics.

It turns out that the elastic waves in the liquid are of greatest importance to the dynamics of the bubble radius. The phase transition has a strong influence on the evolution of the temperature, in particular at the interface. Furthermore the phase transition leads to a drastic change of the water content in the bubble. It is shown that a rebounding bubble is only possible, if it contains in addition an inert gas.

In Part 2 of the current paper the equations derived are sought in order to close the system of equations for multi-phase mixture balance laws for dispersed bubbles in liquids involving phase change.

11.1 Introduction

Mathematical modeling of fluid flow with phase change between liquid water and its vapor has many applications in science and technology, such as the study of cloud formation, of bubbles in boiling water, spray cooling in metal production or damage of ship propellers due to cavitation. For numerical computations of such flows, via mathematical equations describing the balances of mass, momentum and energy, one needs appropriate terms modeling the transfer of these physical quantities between the phases. It is a commonly found situation that one phase is dispersed in the other. Normally we do not have pure substances but mixtures, for instance in cloud formation or spray cooling we have mixtures of water vapor and air. Therefore in this paper we also take into account further phases, in particular we consider vapor bubbles containing some additional inert gas in liquid water.

The subproblem concerning the precise modelling of the evolution of a single bubble is a challenge, because various different phenomena are involved and strongly couple with each other. For example, here we meet heat conduction, elastic waves, phase transitions and diffusion.

The theoretical study of a spherical bubble surrounded by liquid has quite a long history. Much of the literature is an extension of the 1917 paper of Rayleigh [27] on the pressure during collapse of a spherical bubble. He considered a constant outer pressure and basically integrated the equations of motion, under the assumption of complete radial symmetry, of an incompressible, inviscid liquid. The work was then extended 1949 by Plesset [23] in a study on cavitation considering the case of a non-constant *external pressure* $P(t)$ leading to a bubble which grows and then collapses. This was observed in the cavitation experiments he discussed. Let us consider the *density* ρ of the liquid and the *pressure of the liquid at the interface* $p(R)$. In his paper he derived the second order nonlinear ordinary differential equation for the time dependent bubble radius R

$$R\ddot{R} + \frac{3}{2}\dot{R}^2 + \frac{P(t) - p(R)}{\rho} = 0 \tag{11.1.1}$$

which has become known as the *Rayleigh-Plesset equation* of bubble dynamics, see also [10], [30], [13], [11] for further early studies on this topic.

The latter occurs if the initial bubble is created by a laser beam, see e.g. Akhatov et al. [1] and especially Müller et al. [20], so that the bubble might contain inert gas, i.e. most probably hydrogen and oxygen, in the vapor due to the high temperature during the bubble creation process. Experimental results were obtained by the group of Lauterborn in Göttingen, see Müller et al. [20]. We will refer to this as the Göttingen experiment in this paper. In the experiment one observes a collapsing and rebounding bubble. In fact, the bubble radius increases to a maximum, then decreases to a non-zero minimum, and hereafter the cycle is repeated, however, an apparent damping is observed. Müller et al. investigate two different discretizations to describe the dynamics of the laser induced cavitation bubble without taking into account phase transitions.

In Akhatov et al. [1] the problem is treated numerically by a full system of coupled partial differential equations, which obviously is the correct description. However, the objective of our paper is to explore if a description by a much simpler system of equations than in [1] and [20] is possible with respect to total mass and radius of the bubble as well as its temperature. The creation of bubbles by nucleation is not investigated.

The aim of our work is to find evolution laws for the quantities mentioned above. The laws should be as simple as possible, but should consider all relevant physical effects. The evolution laws obtained will be used in the forthcoming second part of this paper to close a system of partial differential equations describing a finite number of well separated bubbles in liquid, taking into account phase transitions.

To this end it is important to determine the influence of the various participating phenomena on the observed evolution. Thus we describe the problem by a hierarchy of model systems of increasing complexity. We start out with the model of the undamped oscillation of a bubble immersed in an incompressible liquid at constant temperature without phase transition, given by the Rayleigh-Plesset equation [23], [17], [4], [7]. Hereafter we take the liquid-vapor phase transition into account. Next we consider in addition heat conduction. Finally elastic waves due to the compressibility of the liquid are incorporated.

In the Göttingen experiment a laser pulse is focussed inside a vessel of water. This leads to the formation of a plasma and creation of a vapor bubble that collapses and rebounds. If a liquid-vapor phase transition is allowed, the latter effect is only possible when an inert gas is present in the bubble. A pure water vapor phase cannot persist beyond the first collapse since the vapor phase is unstable under the conditions of the experiment. Currently it is not known by measurements what constitutes the inert gas. The most likely seem to be oxygen and hydrogen. So for this paper we are assuming this to be the case. We are considering the data described in Müller et al. [20]. Earlier experimental work on this topic is described in Akhatov et al. [1, 2] and Kurz et al. [15].

Later extensions were summarized by Lauterborn [16] and studied numerically. Next Keller and Miksis [14] were interested in the acoustics of oscillating bubbles and included the effect of acoustic radiation by considering compressibility. Also they carried the viscosity term with *viscosity* μ through the derivation. Further their derivation involved the *speed of sound* c in the liquid and the *pressure inside the bubble* $p_b(R)$. They considered a pressure at infinity perturbed by an incoming sound wave $P(t) = p_\infty - P\sin\omega\left(t + \frac{R}{c}\right)$. Assuming that the interface velocity is equal to the liquid velocity at the interface, i.e. the phase transition is ignored, this leads to the *Keller-Miksis equation* [14, (3.9)], [26]

which in our notation is

$$\ddot{R}\left(\frac{4\mu}{\rho}-R(\dot{R}-c)\right)=\frac{1}{2}\dot{R}^3+\dot{R}\frac{p_b(R)-p_\infty}{\rho}-c\left(\frac{3}{2}\dot{R}^2+\frac{4\mu\dot{R}}{\rho R}+\frac{2\sigma}{\rho R}-\frac{p_b(R)-p_\infty}{\rho}\right)$$
$$+R\frac{\dot{p}_b(R)}{\rho}+\left(1+\frac{\dot{R}}{c}\right)\frac{cP}{\rho}\sin\omega\left(t+\frac{R}{c}\right).$$

This equation is only valid for small Mach numbers. We simplyfy the equation by setting $\mu=0$. Then we divide by c and use the *Laplace-Young relation* $p_b(R)=p(R)+\frac{2\sigma}{R}$ to obtain

$$R\ddot{R}\left(1-\frac{\dot{R}}{c}\right)=\frac{3}{2}\dot{R}^2\left(\frac{\dot{R}}{3c}-1\right)+\dot{R}\frac{p_b(R)-P(t)}{\rho c}-\left(\frac{P(t)-p(R)}{\rho}\right)+R\frac{\dot{p}_b(R)}{\rho c}. \tag{11.1.2}$$

Taking the limit $c\to\infty$ reduces this equation to the Rayleigh-Plesset equation (11.1.1). Prosperetti and Lezzi [26] have generalized these equations even further using singular perturbation methods. Wu and Roberts [31] considered a version of this equation coupled to radially symmetric Euler equations in order to study sonoluminescence. In Akhatov et al. [1] a model for the laser induced bubble experiment ist introduced. Near the recollapse of the bubble the bubble radius velocity becomes very high, so the Euler equations of gas dynamics are used to simulate this part of the bubble dynamics. The paper [1] includes quite extensive citations of the relevant literature.

As a result of our considerations we obtain a hierarchy of models consisting of a system of ordinary and partial differential equations describing the evolution of the bubble with the main objective to identify the various driving forces involved. From the numerical computations we can clearly see that the elastic waves in the liquid are of greatest importance to the evolution of the bubble radius in comparison with the experiment. Phase transition and heat conduction play no significant role for movement of the bubble radius. The phase transition has an enormous influence on the evolution of the temperature, in particular at the interface. Furthermore the phase transition leads to a drastic change of the water content in the bubble, so that a rebounding bubble is only possible, if it contains in addition an inert gas. For further investigations we refer to [22], [24], [29], [8], [25], [32], [21], [33].

After this introduction we have organized the paper as follows. In Section 11.2 we first start with the balances of mass, momentum and internal energy for an inviscid compressible fluid in Subsection 11.2.2, including the jump relations that describe the conservation properties at moving interfaces. Appropriate constitutive relations for mixtures are introduced in Subsection 11.2.3 and complemented by the entropy principle in the bulk and in Subsection 11.2.4 at liquid-vapor interfaces. The entropy principle is exploited in Subsection 11.2.5 to introduce the interfacial mobility. In Subsection 11.2.6 the constitutive relations for a vapor phase containing water vapor and oxygen as well as hydrogen as inert gases are formulated. Next we derive in Subsection 11.2.7 a kinetic equation for the evolution of the bubble mass under phase transition. The condensation rate may be taken from well established kinetic considerations. An important point is that the evaporation rate at the interface is derived in a thermodynamically consistent way. In Section 11.3 we recall the data from the laser induced bubble experiment that we are modelling.

The central part of the paper is Section 11.4 in which we give a hierarchy of models for radially symmetric bubbles in order to study numerically which physical effects are important to explain the experimentally observed dynamics of laser induced bubbles. Starting point is the well known second order Rayleigh-Plesset equation in Subsection 11.4.3. In Subsection 11.4.4 the mass dynamics due to phase transition is introduced to give a system of implicit first order ordinary differential equations. Then we add in Subsection 11.4.5 the heat conduction in the liquid. Finally a wave equation for acoustic waves is coupled to the other phenomena. The details of the derivations of these models are given in Section 11.5. In Section 11.6 we present some of our numerical computations within the setting of these models. We will present numerical results using four different models in order to give an indication which terms are important. A comparison of the observed evolution of a bubble with a model is a subtle problem, because the initial states of all physical quantities involved cannot be precisely measured experimentally. At this time we have to work with very incomplete experimental data. The paper ends with a short summary of the main conclusions.

11.2 Variables, equations of balance and local entropy principle

11.2.1 Basic variables and constitutive quantities

As a starting point we take a spherical bubble $B = B_R(0) = \{x \in \mathbb{R}^3 | \, |x| < R(t)\}$ of vapor sitting at the origin surrounded by the liquid. Here t is time and R the time dependent radius of the bubble. However, later on we also will treat the case of a bounded planar interface between liquid and vapor. For the case of the bubble we will work in radial coordinates assuming that all physical quantities depend on time and distance from the origin. All vector fields are then assumed to be radial.

We have one vapor bubble in a closed, very large control volume. One could assume either that the control volume is subject to a given constant *outer pressure* p_0 or that the volume in the control volume remains constant in time. Note that the physics of phase transition depends considerably on whether the pressure or the volume is held constant in the control volume. In the first case the phases cannot coexist in equilibrium, whereas in the second case they may coexist. In nature the gas phase usually consists of a mixture of several constituents, for example vapor, oxygen, and nitrogen. This again changes the physics of the phase transition, allowing for fog in the pressure controlled situation found in nature.

In this paper we do not consider the case of constant volume. We only consider the case that the outer pressure p_0 of the global control volume is held constant, e.g. in a container with a moveable piston that is controled by the outer pressure.

11.2.2 Equations of balance in regular and singular points

Here we exclusively consider the gas and the liquid phase as inviscid heat conducting fluids. The gas consists of water vapor, oxygen, and hydrogen. The appearance of oxygen and hydrogen is due to the fact that a bubble is created by a focussed laser beam in water. This initially leads to a high temperature so that some of the water vapor dissociates into O_2 and H_2. In the following we will only consider temperatures under which no further chemical reactions take place. Futhermore, we study short time bubble evolutions during which hydrogen and in particular oxygen cannot leave the bubble into the liquid. Consequently the liquid consists of pure water only, thus we describe the liquid by 5 variables which are the mass density ρ, velocity $\mathbf{v}$, and temperature T. In the gas we have as variables three partial mass densities ρ_a, with $a = W, H, O$ for water, hydrogen, and oxygen. Further, there are the velocity of the mixture $\mathbf{v}$ and the temperature T. Unless stated otherwise, physical fields are assumed to depend on the time variable $t \in \mathbb{R}$ and space variable $x \in \mathbb{R}^3$.

The determination of the variables relies on the local conservation laws for mass and momentum, as well as the balance law for internal energy. In regular points of the liquid phase these are

$$\frac{\partial \rho}{\partial t} + \operatorname{div}(\rho \mathbf{v}) = 0 \tag{11.2.1}$$

$$\frac{\partial \rho \mathbf{v}}{\partial t} + \operatorname{div}(\rho \mathbf{v} \otimes \mathbf{v} + p\,\mathbf{1}) = 0 \tag{11.2.2}$$

$$\frac{\partial \rho u}{\partial t} + \operatorname{div}(\rho u \mathbf{v} + \mathbf{q}) = -p\,\mathbf{1} \cdot \operatorname{grad}\mathbf{v}\,. \tag{11.2.3}$$

Here we use the second order tensor $\mathbf{1} = (\delta_{ij})_{1 \le i,j \le 3}$ with $\delta_{ij} = 1$ for $i = j$ and $= 0$ for $i \neq j$, the tensor product of vectors $\otimes$ giving a second order tensor. The divergence of a second order tensor is the vector of divergences of each row and the product $\cdot$ of two such tensors is the scalar obtained by double contraction.

In these equations there are further quantities which are not among the basic variables. We call them constitutive quantities, and these are the internal energy density u, the heat flux $\mathbf{q}$ and the pressure p. The constitutive quantities are related to the basic variables in a material dependent manner, which will be given in Section 11.2.6.

In the gas phase, the equations for momentum and energy of the mixture have the same structure as (11.2.2) and (11.2.3). However here we have to consider 3 conservation laws for the partial mass densities

$$\frac{\partial \rho_a}{\partial t} + \operatorname{div}(\rho_a \mathbf{v}_a) = 0. \tag{11.2.4}$$

The partial mass densities are defined so that they sum up to the mass density of the mixture, and the weighted sum of partial velocities gives the (barycentric) velocity of the mixture, i.e.

$$\rho = \sum_a \rho_a, \qquad \mathbf{v} = \sum_a \frac{\rho_a}{\rho}\mathbf{v}_a \qquad \text{which implies with (11.2.4)} \qquad \frac{\partial \rho}{\partial t} + \operatorname{div}(\rho \mathbf{v}) = 0.$$

The constitutive quantities are pressure p, internal energy e, and heat flux $\mathbf{q}$, as before, and the partial velocities $\mathbf{v}_a$, but these are usually substituted by the diffusion fluxes $\mathbf{J}_a = \rho_a(\mathbf{v}_a - \mathbf{v})$.

We will use the superscripts L, V and the subscript I to specify physical quantities Ψ in the liquid, the vapor, and on the interface respectively. The combination of the subscript I with one of the superscripts denotes the one sided limit $\Psi_I^{L,V}(t, x_I) = \lim_{x^{L,V} \to x_I} \Psi(t, x)$ of the quantity in the respective bulk fluid at the interface. The superscript η together with I denotes the scalar obtained by projection of a vector on the chosen normal vector $\boldsymbol{\eta}$ on the surface. We denote vectors, except for the spatial coordinate vector of a point, and higher order tensors in boldface.

Along the singular surface I between the phases we consider the normal vector $\boldsymbol{\eta}$ pointing into the liquid region. It is moving with normal speed w^η. Across this interface we use the jump bracket $[\![\Psi]\!] = \Psi_I^L - \Psi_I^V$ for any physical quantity Ψ. We have the following relations

$$[\![\rho_a(v_a^\eta - w^\eta)]\!] = 0 \tag{11.2.5}$$

$$\rho(v^\eta - w^\eta)[\![\mathbf{v}]\!] + [\![p\,\boldsymbol{\eta}]\!] = 2\sigma k_m \boldsymbol{\eta} \tag{11.2.6}$$

$$\rho(v^\eta - w^\eta)[\![u + \frac{p}{\rho} + \frac{1}{2}(\mathbf{v} - \mathbf{w})^2]\!] + [\![q^\eta]\!] = 0\,. \tag{11.2.7}$$

Here the interface is exclusively equipped with *surface tension* σ. This is the term appearing on the right hand side of the momentum balance. We ignore for example tangential heat and diffusion fluxes. Additionally we assume that the interface has no mass and no inertia, and in particular we ignore the dependence of the surface tension on the concentration of the constituents of the gas and the temperature. The complete interface relations may be found in Dreyer [5, Sections 5-14] and Müller [19, Section 2.2.2, Chapter 3]. The term k_m is the *mean curvature* of the surface, with $k_m = -\frac{1}{R}$ for a sphere and $k_m = 0$ for a plane.

The assumption that there is no oxygen and hydrogen in the liquid phase implies that the equations (11.2.5) can be written as

$$v_O^\eta = v_H^\eta = w^\eta \qquad \text{and} \qquad [\![\rho_W(v_W^\eta - w^\eta)]\!] = 0\,. \tag{11.2.8}$$

In contrast to the need of partial mass balances, even for a mixture we only have to take a single energy balance, as it was given above, because there is only one temperature of the mixture. However, for a reduction of the necessary numerical data, which are needed to evaluate the energy balance, it is useful to decompose the internal energy density, the pressure, and the heat flux of the mixture into the corresponding quantities of the constituents, according to the detailed description in [19] without quadratic terms of the diffusion fluxes we have

$$\rho u = \sum_{a\in\{W,H,O\}} \rho_a u_a, \qquad p = \sum_{a\in\{W,H,O\}} p_a, \quad \text{and} \quad \mathbf{q} = \sum_{a\in\{W,H,O\}} \left(\mathbf{q}_a + \left(u_a + \frac{p_a}{\rho_a}\right)\mathbf{J}_a\right). \tag{11.2.9}$$

In terms of these quantities the balance of internal energy (11.2.3) in the gas phase now reads

$$\sum_{a\in\{W,H,O\}} \left(\rho_a \dot{u}_a + \operatorname{div}(\mathbf{q}_a + \mathbf{J}_a \frac{p_a}{\rho_a})\right) = \frac{p}{\rho}\dot{\rho}\,, \tag{11.2.10}$$

where $(\,)^{\cdot} = \frac{\partial}{\partial t}(\,) + v\operatorname{grad}(\,)$ denotes the material time derivative. Across the interface the internal energy balance (11.2.7) assumes the form

$$q_L^\eta - \sum_{a\in\{W,H,O\}} q_a^\eta = \rho^L(u^L + \frac{p^L}{\rho^L})(v_L^\eta - w^\eta) - \sum_{a\in\{W,H,O\}} \rho_a(u_a + \frac{p_a}{\rho_a})(v_a^\eta - w^\eta)\,. \tag{11.2.11}$$

11.2.3 General constitutive model and local entropy principle for the bulk phases of the two phase system

The general constitutive model for the system under consideration relies on two functions for the *specific Helmholtz free energy*

$$\psi = u - Ts \tag{11.2.12}$$

that is a combination of specific internal energy u and *specific entropy* s. We assume that we have in the liquid resp. the vapor phase

$$\psi^L = \widehat{\psi}^L(T, \rho^L) \qquad \text{and} \qquad \psi^V = \widehat{\psi}^V(T, \rho_W, \rho_H, \rho_O) = \widetilde{\psi}^V(T, \rho^V, X_W, X_H),$$

where the *mole fractions* are defined by $X_a = \frac{\rho_a/m_a}{\sum_b \rho_b/m_b}$. The knowledge of the specific free energy allows in combination with the local entropy principle for the bulk phases to calculate the pressure p, the specific entropy s, the specific *Gibbs free energy* g, and the chemical potentials μ_a, see Müller [19],

$$p = \rho^2 \frac{\partial \widehat{\psi}}{\partial \rho}\,, \qquad s = -\frac{\partial \widehat{\psi}}{\partial T}\,, \qquad g = \psi + \frac{p}{\rho}\,, \qquad \mu_a = \frac{\partial \rho \widetilde{\psi}}{\partial \rho_a}\,. \tag{11.2.13}$$

Moreover the Gibbs-Duhem equation for the two phases, viz.

$$g^L = \mu_W^L\,, \qquad g^V = \frac{\sum_{a=W,H,O} \mu_a^V \rho_a}{\rho} \tag{11.2.14}$$

is likewise a consequence of the entropy principle, which also gives the entropy flux ϕ, and an inequality that controls the flow of heat

$$\boldsymbol{\phi}^L = \frac{\mathbf{q}^L}{T}\,, \qquad \boldsymbol{\phi}^V = \frac{\mathbf{q}^V}{T} - \frac{\sum_{a=W,H,O} \mu_a \mathbf{J}_a}{T}\,, \qquad \mathbf{q} \cdot \operatorname{grad} \frac{1}{T} \geq 0. \tag{11.2.15}$$

11.2.4 The local entropy principle across the liquid-vapor interface

The entropy principle holds point wise in a given body, thus we also must have an entropy principle at the interface. In the current study that principle relies on two basic assumptions: (i) There is no tangential entropy flux within the surface, (ii) the tangential velocities of the bulk phases at the interface are zero.

In this case the entropy principle at the interface consists of two parts

$$[\![T]\!] = 0 \qquad \rho(v^\eta - w^\eta)[\![s]\!] + [\![\phi^\eta]\!] \geq 0\,. \tag{11.2.16}$$

The continuous temperature at the interface is denoted by T_I. In equilibrium the equality sign holds, whereas in nonequilibrium the left hand side of the inequality in (11.2.16) must be greater than zero. The axiom of continuous temperature across the interface can be given up. However, in this case the subsequent treatment of the problem becomes very involved.

Remark 11.2.1. *The energy balance (11.2.7) as well as the entropy balance (11.2.16) also contain contributions due to the liquid/vapor interface. However, due to two assumptions and a consequence of the exploitation of the interfacial entropy inequality, the interface contributions drop out. The inequality implies here that the interfacial free energy density is equal to the surface tension. The two assumptions are: (i) radial symmetry, (ii) the surface tension is a constant, i.e. it does not depend on temperature or concentrations of the constituents.*

11.2.5 Exploitation of the entropy principle

We introduce the jump of the *specific kinetic energy* at the interface $[\![e_{kin}]\!] = [\![\frac{1}{2}(\mathbf{v}-\mathbf{w})^2]\!] = [\![\frac{1}{2}(v^\eta - w^\eta)^2]\!]$. Next we multiply the entropy inequality (11.2.16) by T, subtract the result from the energy equation at the interface (11.2.7), and use (11.2.13) to obtain

$$\rho(v^\eta - w^\eta)[\![g + e_{kin}]\!] + [\![\sum_{a=W,H,O} \mu_a \mathbf{J}_a]\!] \leq 0\,. \tag{11.2.17}$$

Now we assume that oxygen and hydrogen cannot cross the interface from the bubble into the liquid, i.e. $v_O^\eta = v_H^\eta = w^\eta$. In this case the inequality (11.2.17), using $g^L = \mu_W^L$, can be reduced to

$$\rho_W(v_W^\eta - w^\eta)[\![\mu_W + e_{kin}]\!] \le 0. \tag{11.2.18}$$

In nonequilibrium the flux $\rho_W(v_W^\eta - w^\eta)$ of mass across the interface is driven by $[\![\mu_W + e_{kin}]\!]$. For this reason that factor is called the driving force. The left hand side of (11.2.18) is of the form *flux* $\times$ *driving force*.

In thermodynamics it can be shown that in equilibrium the driving force must be zero. Thus the product assumes its maximum in equilibrium. We now assume that there is a relation between the flux and the driving force in non-equilibrium which usually is called *kinetic relation*. A consequence of the existence of the kinetic relation is that

$$[\![\mu_W + e_{kin}]\!] = 0 \qquad \Longleftrightarrow \qquad \rho_W(v_W^\eta - w^\eta) = 0\,, \tag{11.2.19}$$

see [12].

The simplest ansatz to satisfy the inequality in nonequilibrium is to assume that the two factors of the product are positively proportional to each other. We write

$$-4\pi R^2 \rho_W(v_W^\eta - w^\eta) = 4\pi R^2 B_I [\![\mu_W + e_{kin}]\!] \qquad \text{with} \qquad B_I > 0\,, \tag{11.2.20}$$

the quantity B_I is called *interfacial mobility* which must be measured or calculated from an underlying model. Such a model will be discussed in Section 11.2.7. The sign in (11.2.20) is due to (11.2.18).

11.2.6 Special constitutive model for the two phase system

The vapor phase consists of the three constituents water vapor, hydrogen and oxygen. These are described by the ideal thermal and the caloric equations of state for the partial pressures and for the partial internal energies, for details see Müller and Müller [18]. These are for $a \in \{W, H, O\}$

$$p_a(T, \rho_a) = \rho_a \frac{kT}{m_a} \qquad \text{and} \qquad u_a(T) = z_a \frac{k}{m_a}(T - T_*) + u_a(T_*) \tag{11.2.21}$$

with

$$z_a = \begin{cases} 3/2 \text{ for a monoatomic,} \\ 5/2 \quad '' \quad \text{diatomic,} \\ 3 \quad '' \quad \text{polyatomic gas.} \end{cases}$$

The *Boltzmann constant* is denoted by k, the *molecular mass* of constituent a is m_a. We use the symbol $*$ to denote arbitrary reference values.

The constitutive laws for the partial specific entropies are also needed here

$$s_a(T, \rho_a) = z_a \frac{k}{m_a} \log \frac{T}{T_*} - \frac{k}{m_a} \log \frac{\rho_a}{\rho_a^*} + s_a(T_*, \rho_a^*)\,. \tag{11.2.22}$$

Likewise to (11.2.9) the *entropy density* ρs for the mixture is given by

$$\rho s = \sum_{a \in \{W,H,O\}} \rho_a s_a\,. \tag{11.2.23}$$

We have already assumed that the vapor mixture is inviscid but we allow heat conduction. From now on we exclusively consider a bubble with homogenous distributions of matter. Note that this does not mean that the bubble is homogeneous. For example, a simple integration of the continuity equation leads for a time dependent $\rho(t)$ to a velocity field that depends on the radius. Due to this homogeneity assumption in the bubble we do not need the constitutive law for the heat flux $\mathbf{q}$.

The liquid phase consists only of water which is modeled as a compressible inviscid liquid. We use the following constitutive laws for the liquid pressure and energy

$$p^L = p_* + K\left(\frac{\rho}{\rho_*} - 1\right) \tag{11.2.24}$$

and

$$u^L(T,\rho) = c(T-T_*) + (p_* - K)\left(\frac{1}{\rho_*} - \frac{1}{\rho}\right) + \frac{K}{\rho_*}\ln\frac{\rho}{\rho_*} + u^L(T_*,\rho_*)\,. \tag{11.2.25}$$

The pressure is related to the density variation by a linear law, and additionally we ignore thermal expansion and the temperature dependence of the *modulus of compression* K. Thus the pressure is assumed to be independent of temperature. For the specific heat capacities we have $c_p = c_v = c$. This implies that the specific entropy of the liquid does not depend on the mass density, and we have

$$s^L(T) = c\log\frac{T}{T_*} + s^L(T_*)\,.$$

The constitutive law for the heat flux in the liquid is given by Fourier's law, i.e.

$$\mathbf{q}^L = -\kappa^L \operatorname{grad} T \qquad \text{with} \qquad \kappa^L > 0\,. \tag{11.2.26}$$

The liquid *heat conductivity* κ^L is assumed to be constant.

From the above constitutive equations for the vapor we obtain

$$\mu_a^V(T,p,X_a) = g_a(T,p) + \frac{kT}{m_a}\ln X_a\,, \tag{11.2.27}$$

where the terms have been combined, s.t. the chemical potential of constituent a can be written as the specific Gibbs free energy for the pure substance a under the total pressure of the mixture p^V plus the so called entropy of mixing. Thus $g_a(T,p)$ is defined by

$$g_a(T,p) = g_a(T_*,p_a^*) + \frac{kT}{m_a}\ln\left(\frac{p}{p_a^*}\right) + (z_a+1)\frac{k}{m_a}\left[T - T_* - T\ln\left(\frac{T}{T_*}\right)\right] - (T-T_*)s_a(T_*)\,. \tag{11.2.28}$$

Recall that the liquid consists of the single substance water. Its specific Gibbs free energy can easily be calculated and reads

$$g^L(T,p) = g^L(T_*,p_*) + \frac{K}{\rho_*}\ln\left(1+\frac{p-p_*}{K}\right) + c\left[T - T_* - T\ln\left(\frac{T}{T_*}\right)\right] - (T-T_*)s^L(T_*)\,. \tag{11.2.29}$$

The incompressible liquid is included here as the limiting case $K \to \infty$ that gives

$$g^L(T,p) = g^L(T_*,p_*) + \frac{1}{\rho_*}(p-p_*) + c\left[T - T_* - T\ln\left(\frac{T}{T_*}\right)\right] - (T-T_*)s^L(T_*)\,. \tag{11.2.30}$$

11.2.7 Simple kinetic model for the evolution of a single bubble

In this section we introduce a kinetic model for the case at hand. To this end we consider a bubble with radius $R(t)$ filled with the vapor mixture from above. The bubble is immersed in the liquid, and the evolution $\dot m$ of the total bubble mass is given by

$$\frac{dm}{dt} = \frac{d}{dt}\int_{\Omega^V}\rho^V\,dx = -\oint_{\partial\Omega^V}\rho^V(v^\eta - w^\eta)\,dS = -4\pi R^2\rho^V(v^\eta - w^\eta)\,, \tag{11.2.31}$$

where we have used the continuity equation (11.2.1) and Reynolds transport theorem [28]. Now we calculate $\dot m$ by a simple kinetic model. We start from the representation

$$\dot m = m_W(\gamma^E - \gamma^C) \tag{11.2.32}$$

where γ^E and γ^C are the *evaporation* respectively the *condensation rate*. The latter results from the encounters of the gas molecules with the interface of the bubble. We assume that each incoming water molecule leads to condensation, and furthermore we assume that the two other constituents remain in the bubble. In this case the kinetic theory of ideal gases gives the condensation rate by the expression

$$\gamma^C(R,T_I,p_W) = 4\pi R^2\sqrt{\frac{kT_I}{2\pi m_W}}\frac{\rho_W}{m_W} = 4\pi R^2\frac{p_W}{\sqrt{2\pi m_W kT_I}}\,. \tag{11.2.33}$$

This expression is well-known. It results from the Maxwell distribution, see Dreyer and Duderstadt [6].

The relation (11.2.32) is usually called *kinetic relation*, but it is also known as the classical Hertz-Knudsen-theory, see Struchtrup [3].

Next we calculate the evaporation rate γ^E. At first we calculate γ^E in equilibrium, and according to (10.3.43) and (11.2.31) we have here $\dot{m} = 0$. As stated in (11.2.32) this is equivalent to $\tilde{\gamma}^E = \tilde{\gamma}^C$, where $\tilde{}$ indicates an equilibrium state.

The necessary condition can be read from $(10.3.43)_1$ with $e_{kin} = 0$. At the interface it states that $\mu_W^L(T_I, p_I^L, X^L) = \mu_W^V(T_I, p^V, X_W)$. In the liquid we have $X^L = 1$. For the vapor we insert into (11.2.27) the relation $X_W = p_W/p^V$, which holds for ideal gases. Thus we obtain from (11.2.28) that $g^L(T_I, p_I^L) = g_W(T, p_W)$. Thus for given T_I and p_I^L we may solve this condition for $p_W = \tilde{p}(T_I, p_I^L)$, so that the condensation rate in equilibrium can be written as

$$\tilde{\gamma}^C = \gamma^C(R, T_I, \tilde{p}(T_I, p_I^L)) = 4\pi R^2 \frac{\tilde{p}(T_I, p_I^L)}{\sqrt{2\pi m_W k T_I}}\,. \tag{11.2.34}$$

Next we introduce a trick to represent the function $p_W = \tilde{p}(T_I, p_I^L)$ by a form that does not explicitly refer to equilibrium. To this end we introduce the saturation pressure $\bar{p}$, which denotes the equilibrium pressure at a planar interface between the vapor and the liquid phase of pure water. In such a situation the equation $g^L(T_I, p) = g_W(T_I, p)$ holds for the equilibrium pressure $\bar{p}$. Consequently for a given T_I we have $p = \bar{p}(T_I)$.

Using (11.2.28) we calculate $g_W(T_I, \tilde{p})$ and $g_W(T_I, \bar{p})$ to obtain the difference

$$g_W(T_I, \tilde{p}) - g_W(T_I, \bar{p}) = \frac{kT}{m_W} \ln \frac{\tilde{p}}{\bar{p}}\,. \tag{11.2.35}$$

From $g^L(T_I, p_I^L) = g_W(T_I, \tilde{p})$ we conclude

$$g^L(T_I, p_I^L) = g_W(T_I, \bar{p}(T_I)) + \frac{kT}{m_W} \ln \frac{\tilde{p}}{\bar{p}}\,, \tag{11.2.36}$$

thus we get

$$\tilde{p} = \bar{p} \exp\left(m_W \frac{g^L(T_I, p_I^L) - g_W(T_I, \bar{p})}{kT} \right)\,. \tag{11.2.37}$$

In equilibrium we have $\tilde{\gamma}^E = \tilde{\gamma}^C$, so using (11.2.37) the evaporation rate in equilibrium can be calculated according to

$$\tilde{\gamma}^E = \tilde{\gamma}^C = 4\pi R^2 \frac{\tilde{p}}{\sqrt{2\pi m_W k T_I}} = 4\pi R^2 \frac{\bar{p}(T_I)}{\sqrt{2\pi m_W k T_I}} \exp\left(m_W \frac{g^L(T_I, p_I^L) - g_W(T_I, \bar{p}(T_I))}{kT_I} \right)\,. \tag{11.2.38}$$

Analogously to (11.2.35) we obtain from (11.2.28)

$$g_W(T_I, \bar{p}) = g_W(T_I, p_W) - \frac{kT}{m_W} \ln \frac{p_W}{\bar{p}}\,. \tag{11.2.39}$$

Using this expression the equilibrium evaporation rate can be given in the following form

$$\tilde{\gamma}^E = 4\pi R^2 \frac{p_W}{\sqrt{2\pi m_W k T_I}} \exp\left(m_W \frac{g^L(T_I, p_I^L) - g_W(T_I, p_W)}{kT_I} \right)\,. \tag{11.2.40}$$

Finally, due to $g^L(T_I, p_L) = \mu^L(T_I, p_L, 1)$ and $g_W^V(T, p_W^V) = \mu_W^V(T, p_V, X_W)$ using (11.2.33) we obtain

$$\tilde{\gamma}^E = \gamma^C \exp\left(\frac{m_W}{kT_I} [\![\mu_W]\!] \right)\,. \tag{11.2.41}$$

It is important to note that the equilibrium evaporation rate is now given in terms of non-equilibrium quantities. This fact motivates to assume that the condensation rate γ^E in non-equilibrium is given by the same expression as $\tilde{\gamma}^E$. However, the presented motivation has ignored the contribution of the kinetic energy to the chemical potential. A more careful study leads to

$$\gamma^E = \gamma^C \exp\left(\frac{m_W}{kT_I} [\![\mu_W + e_{kin}]\!] \right)\,. \tag{11.2.42}$$

For small deviations from equilibrium the expression

$$\gamma^E = \gamma^C \left(1 + \frac{m_W}{kT_I}[\![\mu_W + e_{kin}]\!]\right) \tag{11.2.43}$$

gives a good approximation. A comparison with the phenomenological ansatz (11.2.20) identifies the mobility B_I as

$$B_I = m_W \frac{p_W}{\sqrt{2\pi m_W kT_I}} \frac{m_W}{kT_I} \,. \tag{11.2.44}$$

As the final result we use

$$\dot{m} = 4\pi R^2 m_W \frac{p_W}{\sqrt{2\pi m_W kT_I}} \frac{m_W}{kT_I}[\![\mu_W + e_{kin}]\!] \,. \tag{11.2.45}$$

Here we would like to make two remarks. (i) If the liquid were incompressible, a case that we do not consider here, the relation (11.2.42) can be derived without the assumption from above. (ii) If we were to ignore the kinetic energy the same result can also be obtained by the *principle of detailed balance*. However, that principle must be handled with care. An important counterexample is given by Dreyer and Duderstadt in [6].

11.3 The Göttingen laser induced bubble experiment

Our objective is to apply the developed model to a single spherical bubble that is produced by laser pulses. The bubble is created in a cuvette filled with clean destilled water. The temperature and the pressure far from the bubble are kept constant at $20°C$ and 1 *bar*. Everything that is seriously known from the experiment can be read of from the Figure 11.1 that gives the bubble radius versus the time.

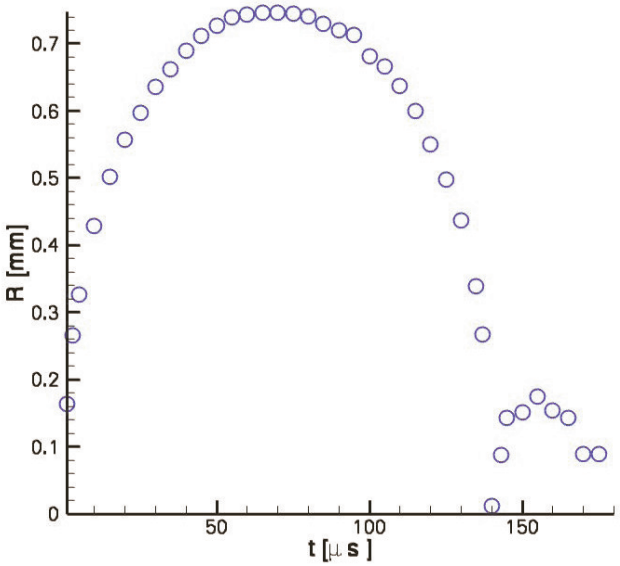

Figure 11.1: Evolution of bubble radius, experimental data from [20].

Aparently there is a growing bubble that reaches its maximum radius $R_{\max} = 7.469 \cdot 10^{-3}\, m$ at 70.7 μs and collapses hereafter to a minimal radius $R_{\min} = 12.467\, \mu m$ which is assumed at $140\, \mu s$. Hereafter the bubble starts to grow again, however, the new maximal radius is very much smaller than the first one, so that one may conclude that a large damping mechanism accompanies the observed process. The experimental researchers in Göttingen report that the second cycle is followed by further cycles that almost show no damping. It is also reported that presumably there is plasma in the bubble, which is created by the laser, which has completely recombined at time $t = 0$. Further observations and in particular data, that give information on the thermodynamic state of bubble and liquid, are not available.

Obviously, on this slim data basis a serious simulation of the described process is not possible without further speculations. We do not describe here speculations that are given in [20]. Instead from now on we present our point of view to formulate at least the necessary initial conditions. For simplification we start the simulation at the first maximum radius so that we need to know the thermodynamic state of the bubble-liquid system at that instant.

According to our point of view the main assumption to reach coincidence between measured and simulated data concern the permanent existence of an inert gas in the bubble. We believe that oxygen and hydrogen molecules have survived the dramatic period that followed the bubble creation by the laser, and we properly adjust their amount at the first maximal radius of the bubble, so that the first subsequent minimal radius is met. Thus the initial data for our simulation are given by

$$T = 293.15\,K \quad N_W = 7.5 \cdot 10^{15} \quad N_O = 2.5 \cdot 10^{13} \quad \text{implying} \quad N_H = 2N_O \quad p_V(t=0) = 17350\,Pa$$

The temperature is assumed to be homogeneous in the bubble-liquid system at $t = 0$ and is equal to the liquid temperature far away from the bubble. Initially we take $R(0) = R_{\max}$ and $v^L = 0$.

We already mention here that agreement with the experimental data can only be achieved if the bubble-liquid system enters a single phase state for a finite period of the evolution. This happens if the interfacial temperature T_I exceeds the critical temperature. In the above model the single phase region is characterized by $\dot{m} = 0$.

11.4 Special cases

11.4.1 Introduction of special cases

The evolution of the bubble radius is accompanied by three damping mechanisms which are due to: phase transition, heat conduction and generation of waves in the liquid. In order to see their influence on the damping of the bubble radius we separately consider the three phenomena.

In this section we give only the main results for the bubble dynamics. The detailed derivation of the formulas is given in Section 11.5.

11.4.2 Spherical symmetry and homogeneous bubble

We consider exclusively a bubble-liquid system with spherical symmetry which implies that the conservation laws assume in the bubble as well as in the liquid the following form

$$\frac{\partial \rho}{\partial t} + \frac{1}{r^2}\frac{\partial (r^2 \rho v)}{\partial r} = 0 \tag{11.4.1}$$

$$\frac{\partial \rho v}{\partial t} + \frac{1}{r^2}\frac{\partial (r^2 \rho v^2)}{\partial r} + \frac{\partial p}{\partial r} = 0 \tag{11.4.2}$$

$$\frac{\partial \rho u}{\partial t} + \frac{1}{r^2}\frac{\partial (r^2 \rho u v)}{\partial r} + \frac{1}{r^2}\frac{\partial (r^2 q)}{\partial r} = -\frac{p}{r^2}\frac{\partial (r^2 v)}{\partial r}\,. \tag{11.4.3}$$

The corresponding constitutive equations will be separately inserted for the various special cases.

The interfacial conservation laws (3.2.3), (11.2.6) and (11.2.7) in spherical coordinates are with $w^\eta = \dot{R}$

$$v_I^H(t) = v_I^O(t) = \dot{R}(t) \qquad \text{and} \qquad [\![\rho_W (v_W - \dot{R})]\!] = 0, \tag{11.4.4}$$

$$\rho(v_I - \dot{R})[\![v]\!] + [\![p]\!] = -\frac{2\sigma}{R}\,, \tag{11.4.5}$$

$$-\rho(v - \dot{R})[\![u + \frac{p}{\rho} + \frac{1}{2}(v - \dot{R})^2]\!] + [\![q]\!] = 0\,. \tag{11.4.6}$$

The total mass of the spherical bubble B is given by $m(t) = 4\pi \int_0^{R(t)} r^2 \rho^V(t,r)dr$. From now on we exclusively consider a homogeneous bubble, thus we have

$$m(t) = \frac{4}{3}\pi R(t)^3 \rho^V(t) \qquad \text{implying} \qquad \dot{m} = 4\pi R^2 \dot{R}\rho^V + \frac{4}{3}\pi R^3 \dot{\rho}^V\,. \tag{11.4.7}$$

We eliminate $\dot{m}$ by means of the mass balance (11.2.31) and obtain

$$\dot{\rho}^V = -\frac{3\rho^V v_I^V}{R}\,, \tag{11.4.8}$$

so that $(11.4.7)_2$ can be written as

$$\dot{m} = 4\pi R^2 \rho^V (\dot{R} - v_I^V) = 4\pi R^2 \rho_I^L (\dot{R} - v_I^L)\,. \tag{11.4.9}$$

Now $(11.4.9)_2$ is used to calculate the liquid velocity at the interface

$$v_I^L = \dot{R} - \frac{\dot{m}}{4\pi R^2 \rho_I^L}\,. \tag{11.4.10}$$

The assumption of a homogeneous gas phase means, that the processes of diffusion and heat conduction are much faster than the adjustment to mechanical equilibrium. In the homogeneous case from $(3.3.2)_1$ and $(11.2.23)_1$ we obtain

$$p_I^V(t) = \frac{3N(t)kT}{4\pi R(t)^3}\,, \tag{11.4.11}$$

where the quantity $N(t) = N_W(t) + N_H + N_O$ gives the total number of particles in the bubble. With

$$m(t) = N_W(t) m_W + N_H m_H + N_O m_O \tag{11.4.12}$$

we have

$$\dot{m} = m_W \dot{N}\,. \tag{11.4.13}$$

11.4.3 Case 1: The undamped oscillation of a bubble immersed in an incompressible liquid at constant temperature without phase transition

In this case the evolution law for the bubble radius can be reduced to a single ODE that reads

$$\ddot{R} + \frac{3\dot{R}^2}{2R} + \frac{1}{\rho^L R}\left(p_0 - \frac{3NkT}{4\pi R^3} + \frac{2\sigma}{R}\right) = 0\,, \tag{11.4.14}$$

which is known as the Rayleigh-Plesset equation. The total number of particles in the bubble N is constant, because in this case the number of water molecules in the bubble does not change. The equation describes an undamped periodic oscillation around the equilibrium radius R_{eq} with $p_0 + \frac{2\sigma}{R_{eq}} = \frac{3NkT}{4\pi R_{eq}^3}$. With the initial conditions $R(0) = R_0 > 0$ and $\dot{R}(0) = \dot{R}_0$ integration of (11.4.14) leads to two solutions for the interfacial velocity

$$\dot{R} = \pm\frac{1}{R^{3/2}}\sqrt{\dot{R}_0^2 R_0^3 - \frac{1}{\rho^L}\left(\frac{2}{3}p_0(R^3 - R_0^3) - \frac{3NkT}{2\pi}\ln\frac{R}{R_0} + 2\sigma(R^2 - R_0^2)\right)}\,, \tag{11.4.15}$$

which describe a closed curve, see Subsection 11.5.1.

11.4.4 Case 2: The oscillation of a bubble immersed in an incompressible liquid at constant temperature with damping due to phase transition

Next we take into account phase transition, that means $\dot{N} \neq 0$. This case can be described by three ordinary first order differential equations

$$\dot{N} = \frac{4\pi R^2 p_W}{\sqrt{2\pi m_W kT}}\frac{m_W}{kT}\left[\frac{1}{\rho^L}(p_I^L - \bar{p}) - \frac{kT}{m_W}\ln\frac{p_W}{\bar{p}} + \frac{1}{2}\left(\frac{1}{(\rho^L)^2} - \frac{1}{(\rho^V)^2}\right)\left(\frac{m_W\dot{N}}{4\pi R^2}\right)^2\right] \tag{11.4.16}$$

$$\dot{R} = \frac{F}{R^2} + \frac{m_W\dot{N}}{4\pi R^2\rho^L} \tag{11.4.17}$$

$$\dot{F} = \frac{F^2}{2R^3} - \frac{R}{\rho^L}(p_0 - p_I^L)\,, \tag{11.4.18}$$

where the explicit representations of p^W, p_I^L, ρ^V are given in Subsection 11.5.2. The resulting system describes a damped oscillation.

The system is implicit with respect to $\dot{N}$. We are interested in solutions that lie in the domain of positive R and N_W, i.e. $(R, N_W, F) \in]0,\infty[\times]0,\infty[\times \mathbb{R}$. The system is solveable for the initial conditions $R(0) = R_0$, $\dot{R}(0) = \dot{R}_0$ and $N(0) = N_0$.

Case 1 is included here by replacing equation (11.4.16) with $\dot{N} = 0$.

11.4.5 Case 3: The oscillation of a bubble immersed in an incompressible liquid with damping due to phase transition and heat conduction

In contrast to the previous cases the temperature field is unknown and controlled by heat conduction. Therefore we now have to consider the energy balance equations.

The resulting ODE system is almost the same as before but coupled to the energy balance equation in the liquid and to the corresponding interfacial boundary condition

$$\begin{aligned}
\dot{N} = \frac{4\pi R^2 p_W}{\sqrt{2\pi m_W k T_I}} \frac{m_W}{k T_I} \Bigg[& \frac{1}{\rho^L(T_0)}(p_I^L - \bar{p}(T_0)) - \frac{kT_I}{m_W} \ln \frac{p_W}{\bar{p}(T_0)} \\
& + \frac{1}{2}\left(\frac{1}{(\rho^L(T_0))^2} - \frac{1}{(\rho^V)^2}\right)\left(\frac{m_W \dot{N}}{4\pi R^2}\right)^2 \\
& + (c^L - c_W)(T_I - T_0 - T_I \ln \frac{T_I}{T_0}) - (s^L - s_W)(T_I - T_0) \Bigg] \qquad (11.4.19)
\end{aligned}$$

$$\dot{R} = \frac{F}{R^2} + \frac{m_W \dot{N}}{4\pi R^2 \rho^L(T_0)} \qquad (11.4.20)$$

$$\dot{F} = \frac{F^2}{2R^3} - \frac{R}{\rho^L(T_0)}(p_0 - p_I^L) \qquad (11.4.21)$$

$$\left.\frac{\partial T}{\partial r}\right|_{r=R} = \frac{k\dot{T}}{4\pi R^2 \kappa^L} \sum_{a \in \{W,H,O\}} N_a z_a + \frac{\dot{R} p}{\kappa^L} - \frac{kT\dot{N}}{4\pi R^2 \kappa^L} + \frac{\lambda m_W \dot{N}}{4\pi R^2 \kappa^L} \qquad (11.4.22)$$

$$\frac{\partial T}{\partial t} = a^L \left(\frac{\partial^2 T}{\partial r^2} + \frac{2}{r}\frac{\partial T}{\partial r}\right) - \frac{F}{r^2}\frac{\partial T}{\partial r}\,. \qquad (11.4.23)$$

In addition to $R(0) = R_0$, $\dot{R}(0) = \dot{R}_0$ and $N(0) = N_0$ we need for the temperature the initial condition $T^L(0, r) = T_0^L(r)$ and at the outer boundary $r = R_a$ we choose $\frac{\partial T}{\partial r} = 0$ for R_a sufficiently large.

11.4.6 Case 4: The oscillation of a bubble immersed in a weakly compressible liquid with damping due to phase transition, heat conduction and acoustic waves

In the previous cases the liquid was assumed to be incompressible. This assumption is too restrictive for the experiment at hand. Thus now we take weak compressibility of the liquid into account. The

necessary modifications lead to the following system

$$\dot{N} = \frac{4\pi R^2 p_W}{\sqrt{2\pi m_W k T_I}} \frac{m_W}{k T_I} \left[\frac{K}{\rho^L(T_0)} \ln\left(1 + \frac{p_I^L - \bar{p}(T_0)}{K}\right) - \frac{k T_I}{m_W} \ln \frac{p_W}{\bar{p}(T_0)} + \frac{1}{2}\left(\frac{1}{(\rho^L(T_0))^2} - \frac{1}{(\rho^V)^2}\right)\left(\frac{m_W \dot{N}}{4\pi R^2}\right)^2 + (c^L - c_W)(T_I - T_0 - T_I \ln \frac{T_I}{T_0}) - (s^L - s_W)(T_I - T_0)\right] \tag{11.4.24}$$

$$\dot{R} = \frac{\phi(2R_a - R - c_0 t) - \phi(R - c_0 t)}{R^2} + \frac{\phi'(2R_a - R - c_0 t) + \phi'(R - c_0 t)}{R} + \frac{m_W \dot{N}}{4\pi R^2 \rho_L(T_0)} \tag{11.4.25}$$

$$\frac{R}{\rho^L(T_0) c_0}(p_I^L - p_0) = \phi'(R - c_0 t) - \phi'(2R_a - R - c_0 t) \tag{11.4.26}$$

$$\left.\frac{\partial T}{\partial r}\right|_{r=R} = \frac{k\dot{T}}{4\pi R^2 \kappa^L} \sum_{a \in \{W,H,O\}} N_a z_a + \frac{\dot{R} p}{\kappa^L} - \frac{k T \dot{N}}{4\pi R^2 \kappa^L} + \frac{\lambda m_W \dot{N}}{4\pi R^2 \kappa^L} \tag{11.4.27}$$

$$\frac{\partial T}{\partial t} = a^L \left(\frac{\partial^2 T}{\partial r^2} + \frac{2}{r}\frac{\partial T}{\partial r}\right) - v^L \frac{\partial T}{\partial r}\,. \tag{11.4.28}$$

The newly introduced function ϕ describes in- and outgoing waves.

11.5 Detailed derivations

11.5.1 Case 1: A bubble immersed in an incompressible liquid at constant temperature without phase transition

In the isothermal case the temperature T is given and considered to be constant. Therefore we do not need the energy balance equation, we merely have to solve the mass and momentum balance equations. The liquid is assumed to be incompressible, i.e. we require that the liquid mass density ρ^L does not depend on pressure. Then mass conservation of the liquid (11.4.1) simplifies to

$$\frac{\partial (r^2 v^L)}{\partial r} = 0 \tag{11.5.1}$$

and leads to the liquid velocity

$$v^L(t, r) = \frac{F(t)}{r^2} \tag{11.5.2}$$

with the time dependent function F. For an incompressible liquid the momentum balance equation (11.4.2) reduces to

$$\frac{\partial v^L}{\partial t} + \frac{\partial}{\partial r}\left(\frac{(v^L)^2}{2}\right) = -\frac{1}{\rho^L}\frac{\partial p^L}{\partial r}\,. \tag{11.5.3}$$

Using (11.5.2) we replace v^L in the time derivative and obtain

$$\frac{\dot{F}}{r^2} + \frac{\partial}{\partial r}\left(\frac{(v^L)^2}{2}\right) = -\frac{1}{\rho^L}\frac{\partial p^L}{\partial r}\,.$$

We integrate the equation over $[R(t), \infty[$ assuming the velocity v^L to vanish at infinity and here the pressure p becomes the outer pressure. The result is

$$\dot{F} = \frac{F^2}{2R^3} - \frac{R}{\rho^L}(p_0 - p_I^L)\,. \tag{11.5.4}$$

Without phase transition the mass balance $(11.4.4)_2$ at the interface I simplifies to

$$v_I^L(t) = v_I^V(t) = \dot{R}(t)\,. \tag{11.5.5}$$

This implies

$$v_I^L(t) = v^L(t, R(t)) = \frac{F(t)}{R(t)^2} = \dot{R}(t) \qquad \text{i.e.} \qquad F = \dot{R}R^2\,. \tag{11.5.6}$$

The velocity field in the liquid domain is given by

$$v^L(t,r) = \dot{R}(t)\left(\frac{R(t)}{r}\right)^2\,. \tag{11.5.7}$$

Using (11.5.6) in (11.5.4) we end up with

$$\ddot{R}R + \frac{3}{2}\dot{R}^2 = -\frac{1}{\rho^L}(p_0 - p_I^L)\,. \tag{11.5.8}$$

The momentum balance (11.4.5) at the interface can be written as

$$p_I^L(t) = p_I^V(t) - \frac{2\sigma}{R(t)} = \frac{3NkT}{4\pi R(t)^3} - \frac{2\sigma}{R(t)}\,. \tag{11.5.9}$$

We replace p_I^L in (11.5.8) and obtain the oscillation equation

$$\ddot{R}R^3 + \frac{3R^2\dot{R}^2}{2} + \frac{1}{\rho^L}\left(p_0R^2 - \frac{3NkT}{4\pi R} + 2\sigma R\right) = 0\,. \tag{11.5.10}$$

This ordinary second order differential equation describes an oscillation around the stationary radius R_{stat}, that solves the equation $p_0R^3 + 2\sigma R^2 = \frac{3NkT}{4\pi}$. The left hand side of this equation is monotone increasing in R and it is zero for $R = 0$. The right hand side of the equation is positive. Thus there is a only one real positive solution R_{stat}.

Obviously we have

$$\left(\ddot{R}R^3 + \frac{3R^2\dot{R}^2}{2}\right)\dot{R} = \frac{1}{2}(\dot{R}^2R^3)^{\cdot}\,, \tag{11.5.11}$$

and by integration of (11.5.10) we derive

$$\frac{1}{2}(\dot{R}^2R^3 - \dot{R}_0^2R_0^3) + \frac{1}{\rho^L}\left(\frac{1}{3}p_0(R^3 - R_0^3) - \frac{3NkT}{4\pi}\ln\frac{R}{R_0} + \sigma(R^2 - R_0^2)\right) = 0\,, \tag{11.5.12}$$

where the integration constant is determined by the initial condition. This is a quadratic equation in $\dot{R}$ with two solutions (11.4.16), which only depend on R and the initial conditions R_0, $\dot{R}_0$. Together these solutions describe a closed curve. We conclude, that (11.5.10) describes an undamped oscillation.

11.5.2 Case 2: A bubble immersed in an incompressible liquid at constant temperature with phase transition

In the case of phase transition we have to make some modifications in the interfacial mass and momentum balance. We already derived the formula $v_I^L = F/R^2$ in Subsection 11.5.1. Using the mass balance equation (11.4.10) at the interface and $\dot{m} = m_W\dot{N}$ we obtain

$$F = R^2\dot{R} - \frac{m_W\dot{N}}{4\pi\rho^L}\,. \tag{11.5.13}$$

The momentum balance equation (11.4.5) at the interface gives

$$p_I^L = \frac{3NkT}{4\pi R^3} - \frac{2\sigma}{R} - \left(\frac{1}{\rho^L} - \frac{1}{\rho^V}\right)\left(\frac{m_W\dot{N}}{4\pi R^2}\right)^2\,. \tag{11.5.14}$$

For convenience we define the number of particles of the inert gas $N_i := N_H + N_O$ and the corresponding mass $m_i := N_H \cdot m_H + N_O \cdot m_O$. This notation allows to apply all the formulas to any arbitrary inert gas. Then the density of the gas phase assumes the following form

$$\rho^V = \frac{3(m_W \cdot (N - N_i) + m_i)}{4\pi R^3}\,. \tag{11.5.15}$$

We replace p_I^L in (11.5.4) and obtain

$$\dot{F} = \frac{F^2}{2R^3} - \frac{R}{\rho^L}\left(p_0 - \frac{3NkT}{4\pi R^3} + \frac{2\sigma}{R} + \left(\frac{1}{\rho^L} - \frac{4\pi R^3}{3(m_W\cdot(N-N_i)+m_i)}\right)\left(\frac{m_W\dot{N}}{4\pi R^2}\right)^2\right). \tag{11.5.16}$$

The evolution of the water particles in the bubble is described by (11.2.45). Here we replace $\dot{m} = m_W\dot{N}$, choose $T^* = T$ and calculate $[\![\mu_W + e_{kin}]\!]$ using (11.2.27), (11.2.28), (11.2.30) and (11.4.4). The partial pressure p_W is given by

$$p_W = \frac{3(N-N_i)kT}{4\pi R^3}.$$

Finally we have to replace the liquid pressure at the interface p_I^L and the vapor density ρ^V as in the previous subsection, using (11.5.14) and (11.5.15). We thus obtain

$$\begin{aligned}\dot{N} = \frac{3(N-N_i)m_W}{R\sqrt{2\pi m_W kT}}\Bigg(&\frac{1}{\rho^L}\left(\frac{3NkT}{4\pi R^3} - \frac{2\sigma}{R} - \left(\frac{1}{\rho^L} - \frac{4\pi R^3}{3(m_W\cdot(N-N_i)+m_i)}\right)\left(\frac{m_W\dot{N}}{4\pi R^2}\right)^2 - \bar{p}\right)\\ &- \frac{kT}{m_W}\ln\left(\frac{3(N-N_i)kT}{4\pi R^3\bar{p}}\right) + \frac{1}{2}\left(\left(\frac{1}{\rho^L}\right)^2 - \left(\frac{4\pi R^3}{3(m_W\cdot(N-N_i)+m_i)}\right)^2\right)\left(\frac{m_W\dot{N}}{4\pi R^2}\right)^2\Bigg),\end{aligned}$$

which can be simplified to

$$\begin{aligned}\dot{N} = \frac{3(N-N_i)m_W}{R\sqrt{2\pi m_W kT}}\Bigg(&\frac{1}{\rho^L}\left(\frac{3NkT}{4\pi R^3} - \frac{2\sigma}{R} - \bar{p}\right) - \frac{kT}{m_W}\ln\left(\frac{3(N-N_i)kT}{4\pi R^3\bar{p}}\right)\\ &- \frac{1}{2}\left(\frac{1}{\rho^L} - \frac{4\pi R^3}{3(m_W\cdot(N-N_i)+m_i)}\right)^2\left(\frac{m_W\dot{N}}{4\pi R^2}\right)^2\Bigg).\end{aligned} \tag{11.5.17}$$

This equation together with (11.5.13) and (11.5.16) gives the resulting system in the considered case.

11.5.3 Case 3: A bubble immersed in an incompressible liquid with phase transition and heat conduction

Now we take heat conduction into account, so that the temperature field is determined by the energy balance equations of the phases and at the interface.

The energy balance of the phases can be written in the general form

$$\rho\left(\frac{\partial u}{\partial t} + \mathbf{v}\,\mathrm{grad}\,u\right) + \mathrm{div}\,\mathbf{q} = \frac{p}{\rho}\left(\frac{\partial\rho}{\partial t} + \mathbf{v}\,\mathrm{grad}\rho\right). \tag{11.5.18}$$

In the liquid phase this can be reduced, with temperature independent compressibility K and using (11.2.12), $(11.2.13)_1$ as well as $(11.2.13)_2$, to

$$\rho^L c^L\left(\frac{\partial T^L}{\partial t} + \mathbf{v}^L\,\mathrm{grad}\,T^L\right) + \mathrm{div}\,\mathbf{q}^L = 0,$$

which holds for the incompressible as for the compressible case. Here q^L is determined by Fourier's law (11.2.26) and with the thermal conductivity $a^L = \kappa^L/(\rho^L c^L)$ the heat conduction equation reads

$$\frac{\partial T^L}{\partial t} + v^L\frac{\partial T^L}{\partial r} = a^L\left(\frac{\partial^2 T^L}{\partial r^2} + \frac{2}{r}\frac{\partial T^L}{\partial r}\right). \tag{11.5.19}$$

In the gas phase we also start from (11.5.18) and replace the internal energy respectively the pressure by the constitutive laws (3.3.2) and (11.2.23) and after some rearrangements of terms we obtain

$$\sum_{a\in\{W,H,O\}}\rho_a\left(\frac{\partial u_a}{\partial t} + \mathbf{v}_a\,\mathrm{grad}\,u_a\right) + \mathrm{div}\sum_{a\in\{W,H,O\}}(\mathbf{q}_a + (\mathbf{v}_a - \mathbf{v})p_a) = \frac{p}{\rho}\left(\frac{\partial\rho}{\partial t} + \mathbf{v}\,\mathrm{grad}\rho\right). \tag{11.5.20}$$

We use $(3.3.2)_2$ to substitue $\frac{\partial u_a}{\partial t} + \mathbf{v}_a \operatorname{grad} u_a$, integrate (11.5.20) and get

$$\sum_{a\in\{W,H,O\}} q_a^I = -\frac{k\dot{T}}{4\pi R^2} \sum_{a\in\{W,H,O\}} N_a z_a - \dot{R}p + \frac{kT\dot{N}}{4\pi R^2}\,. \tag{11.5.21}$$

From the balance of internal energy at the interface we obtain

$$q_I^L - \sum_{a\in\{W,H,O\}} q_a^I = -\frac{\lambda m_W \dot{N}}{4\pi R^2}\,. \tag{11.5.22}$$

We use Fouriers law (11.2.26) on the liquid side of the interface to get

$$\frac{\partial T}{\partial r} = \frac{k\dot{T}}{4\pi R^2\kappa} \sum_{a\in\{W,H,O\}} N_a z_a + \frac{\dot{R}p}{\kappa} - \frac{kT\dot{N}}{4\pi R^2\kappa} + \frac{\lambda m_W \dot{N}}{4\pi R^2\kappa}\,. \tag{11.5.23}$$

The equations (11.5.13) and (11.5.16) remain the same as before, when we ignored heat conduction. In the equation (11.5.17), which describes the mass transfer across the interface, the temperature dependent function $\mu(T) = (c^L - c_{pw})(T - T_0 - T\ln\frac{T}{T_0}) - (s^L - s_W)(T - T_0)$ does not drop out any longer here, and we set therein the reference temperature $T^* = T_0$. This leads to

$$\begin{aligned}\dot{N} = \frac{3(N-N_f)m_W}{R\sqrt{2\pi m_W kT}} \Bigg(&\frac{1}{\rho^L}\left(\frac{3NkT}{4\pi R^3} - \frac{2\sigma}{R} - \bar{p}\right) - \frac{kT}{m_W}\ln\left(\frac{3(N-N_f)kT}{4\pi R^3\bar{p}}\right) \\ &-\frac{1}{2}\left(\frac{1}{\rho^L} - \frac{4\pi R^3}{3(m_W\cdot(N-N_f)+m_f)}\right)^2\left(\frac{m_W\dot{N}}{4\pi R^2}\right)^2 \\ &+(c^L - c_{pw})(T - T_0 - T\ln\frac{T}{T_0}) - (s^L - s_W)(T-T_0)\Bigg)\,.\end{aligned} \tag{11.5.24}$$

Finally we couple the system (11.5.13), (11.5.16), (11.5.24) with the energy balance equation (11.5.19) and (11.5.23). In (11.5.19) we substitute $v^L(t,r)$ by (11.5.2) and get

$$\frac{\partial T^L}{\partial t} + \frac{F}{r^2}\frac{\partial T^L}{\partial r} = a^L\left(\frac{\partial^2 T^L}{\partial r^2} + \frac{2}{r}\frac{\partial T^L}{\partial r}\right)\,. \tag{11.5.25}$$

11.5.4 Case 4: A bubble immersed in a weakly compressible liquid with phase transition and heat conduction

The model from the previous subsection leads to a damping of the bubble oscillations that is not sufficiently strong to describe the experimental data. A further damping effect is related to the propagation of waves in the liquid, which are induced by the motion of the bubble. In this case we must skip the assumption of an incompressible liquid. For this reason we now consider a weak compressible liquid and in order to avoid extreme difficulties we linearize the mass conservation law and the momentum balance, which then read

$$\frac{\partial \rho}{\partial t} + \rho_0\frac{\partial v}{\partial r} = 0 \tag{11.5.26}$$

$$\rho_0\frac{\partial v}{\partial t} + \frac{\partial p}{\partial r} = 0\,. \tag{11.5.27}$$

With the definition $v := \frac{\partial f}{\partial r}$ and $\frac{\partial p}{\partial \rho} = c_0^2$ we can rewrite these equations in the following form

$$\frac{1}{c_0^2}\frac{\partial p}{\partial t} + \rho_0\Delta f = 0 \tag{11.5.28}$$

$$\frac{\partial}{\partial r}\left(\rho_0\frac{\partial f}{\partial t} + p\right) = 0\,. \tag{11.5.29}$$

Integration of (11.5.29) leads to

$$p - p_0 = -\rho_0\frac{\partial f}{\partial t}\,. \tag{11.5.30}$$

Thus for the potential f we obtain the wave equation

$$\frac{1}{c_0^2}\frac{\partial^2 f}{\partial t^2} = \Delta f\,. \tag{11.5.31}$$

For radial symmetry its general solution is known to be

$$f(t,r) = \frac{\phi(r-c_0t)}{r} + \frac{\varphi(r+c_0t)}{r}\,, \tag{11.5.32}$$

where ϕ and φ describe outgoing respectively ingoing waves. We consider $p = p_0$ at the outer boundary $r = R_a$. This leads to the reflection condition $\varphi(r+c_0t) = -\phi(r+c_0t-2(R_a-r)) = -\phi(2R_a-r-c_0t)$. We calculate

$$p(t,r) = p_0 + \rho_0 c_0 \frac{\phi'(r-c_0t)}{r} - \rho_0 c_0 \frac{\phi'(2R_a-r-c_0t)}{r} \qquad \text{and} \tag{11.5.33}$$

$$v(t,r) = -\frac{\phi(r-c_0t)}{r^2} + \frac{\phi'(r-c_0t)}{r} + \frac{\phi(2R_a-r-c_0t)}{r^2} + \frac{\phi'(2R_a-r-c_0t)}{r}\,. \tag{11.5.34}$$

Using the balance of mass at the interface we end up with

$$\frac{\phi(2R_a-R-c_0t)-\phi(R-c_0t)}{R^2} + \frac{\phi'(2R_a-R-c_0t)+\phi'(R-c_0t)}{R} = \dot R - \frac{m_W\dot N}{4\pi R^2\rho_0} \tag{11.5.35}$$

$$\text{and} \qquad p_I^L = p_0 + \rho_0 c_0 \frac{\phi'(R-c_0t)-\phi'(2R_a-R-c_0t)}{R}\,. \tag{11.5.36}$$

Unlike (11.5.13) and (11.5.16) we now get two differential equations including the unknown function ϕ which depends on time explicitely and on the unknown time dependent bubble radius R.

The consideration of weak compressibility leads to a small modification in the derivation of the equation to describe the mass transfer. In contrast to the previous cases in Subsection 11.5.2 and 11.5.3 we have to use (11.2.29) instaed of (11.2.30) to calculate $[\![\mu_W + e_{kin}]\!]$. Equation (11.5.24) modifies to

$$\begin{aligned}\dot N = \frac{3(N-N_f)m_W}{R\sqrt{2\pi m_W kT}}\Bigg(\frac{K}{\rho^L}\ln\Bigg(1+\Bigg(\frac{3NkT}{4\pi R^3} - \frac{2\sigma}{R} - \Big(\frac{1}{\rho^L}-\frac{1}{\rho^V}\Big)\Big(\frac{m_W\dot N}{4\pi R^2}\Big)^2 - \bar p\Bigg)/K\Bigg)\\ -\frac{kT}{m_W}\ln\Big(\frac{3(N-N_f)kT}{4\pi R^3\bar p}\Big) - \frac{1}{2}\Big(\frac{1}{\rho^L} - \frac{4\pi R^3}{3(m_W\cdot(N-N_f)+m_f)}\Big)^2\Big(\frac{m_W\dot N}{4\pi R^2}\Big)^2\\ +(c^L - cp_W)(T-T_0-T\ln\frac{T}{T_0}) - (s^L-s_W)(T-T_0)\Bigg)\,.\end{aligned} \tag{11.5.37}$$

The now more complicated resulting system consists of the ordinary differential equation (11.5.37), the delay equations (11.5.35) and (11.5.36) which are coupled to the partial differential equation

$$\frac{\partial T^L}{\partial t} + v^L\frac{\partial T^L}{\partial r} = a^L\Big(\frac{\partial^2 T^L}{\partial r^2} + \frac{2}{r}\frac{\partial T^L}{\partial r}\Big)\,. \tag{11.5.38}$$

and to the corresponding interfacial boundary condition (11.5.23). The liquid velocity v^L in (11.5.38) can be calculated with (11.5.34).

11.6 Numerical results

In this section we will discuss the four described cases on the basis of the numerical computations for the corresponding systems of equations.

For all computations we choose the external pressure $p_0 = 101300Pa$, initial radius $R_0 = 0.00075m$, initial interface velocity $\dot R = 0$, initial particle numbers $N_O = 2.5\cdot 10^{13}$, $N_H = 5\cdot 10^{13}$, $N_W = 7.5\cdot 10^{15}$, and initial temperature $T = 293.15K$.

The cases 1 and 2 are concerned with isothermal evolution, i.e. the temperature does not change. However the given initial value determines the reference values for those quantities that are listed in the

table below. Such values may be found in Grigull et. al. [9]. The composition of the gas in the bubble plays no role in the dynamics of the first case. The sum of the three particle numbers is used in order to determine the initial pressure.

Case 1: A bubble immersed in an incompressible liquid at constant temperature without phase transition.

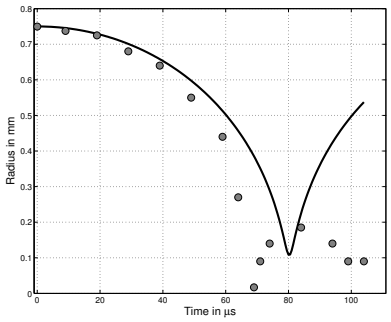

Figure 11.2: Calculated bubble radius according to Case 1. Dots: Experimental data, solid line: Computation.

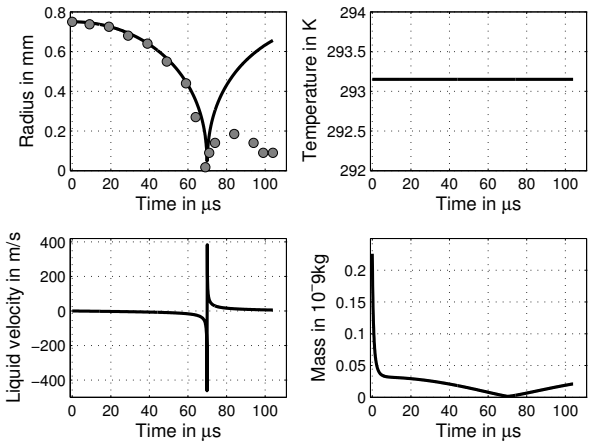

Figure 11.3: Calculated bubble radius, bubble mass, liquid velocity and temperature at the interface according to Case 2. Dots: Experimental data, solid line: Computation.

The numerical solution of the second order ordinary differential equation is obtained by solving the corresponding first order system with one of the second order Runge Kutta methods.

As was shown above, the bubble radius oscillates without damping in this case. This result is compared in Figure 11.2 with experimental data. We observe that computational oscillation period is longer than the experimental one.

Case 2: A bubble immersed in an incompressible liquid at constant temperature with phase transition. Again a second order Runge Kutta method is used for the system of three ordinary first order equations, including a standard step size control. Due to stability restrictions on the numerical scheme this is needed in the vicinity of the minimal radius.

The incorporation of the phase transition leads to a damping, that however is too small to describe the experimental observations. Moreover the comparison of this case with the experimental data in Figure 11.3. The computational oscillation period is smaller now than in Case 1.

Case 3: A bubble immersed in an incompressible liquid with phase transition and heat conduction. The non-isothermal evolution is described by a system of three first order ordinary differential equations that are coupled now to the partial differential equation for the evolution of the temperature. The latter

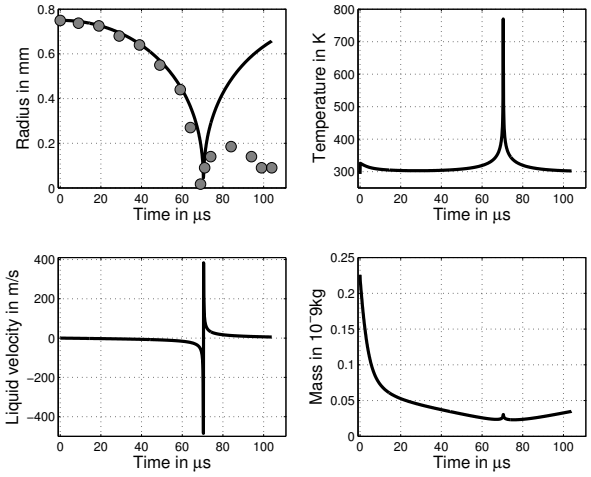

Figure 11.4: Calculated bubble radius, bubble mass, liquid velocity and temperature at the interface according to Case 3. Dots: Experimental data, solid line: Computation.

equation is solved numerically by the method of lines. The resulting large system of ordinary differential equations is again solved with a second order Runge Kutta method. For the spatial discretization finite differences of second order are used.

In this case we observe an enormous variation of the temperature. However its influence on the evolution of the bubble radius can be ignored, in particular there is only a small additional damping in comparison to Case 2, see Figure 11.4 and Figure 11.3 for comparison.

The temperature variation has large impact on the phase transition. At the minimal radius there is a large increase of temperature that leads to a change of the gas-liquid phase transition. In fact, we observe here evaporation leading for some time to a reduction of the released latent heat. During that period where the temperature exceeds the critical temperature we turn off the phase transition, by setting $\dot{N} = 0$. Note, that in addition to the initial data from above we start here with $v = 0$ at $t = 0$ in the whole liquid domain.

Case 4: A bubble immersed in a weakly compressible liquid with phase transition and heat conduction. Recall that in the cases 1 - 3 the momentum balance is reduced to an ordinary differential equation. This is not possible anymore if the compressibility of the liquid is taken into account. In order to reduce numerical complexity we restrict here to the case where the momentum balance becomes a linear wave equation, that is now coupled to a modified version of the equations of Case 3. The wave equation is solved by means of in- and outgoing waves and the resulting system of two delay equations is likewise solved with a second order Runge-Kutta method. Note, that we meet a free boundary here, and in Case 3, i.e. at constant cell number we have a variable spatial mesh size.

Figure 11.5 reveals a sufficiently strong damping now, so that we can observe good agreement with the experimental data. On the other hand the oscillation period is slightly smaller than in the experiment.

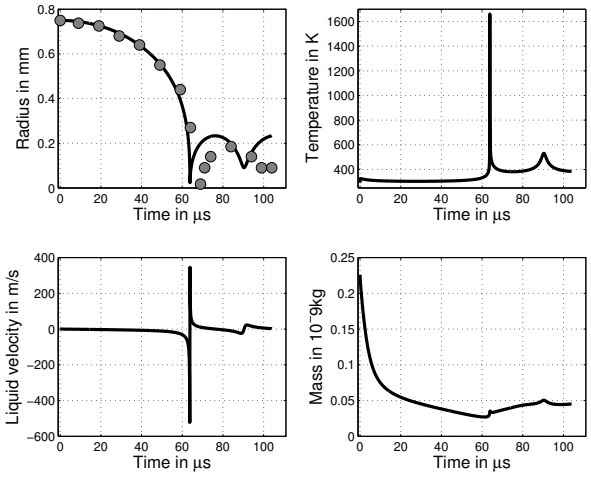

Figure 11.5: Calculated bubble radius, bubble mass, liquid velocity and temperature at the interface according to Case 4. Dots: Experimental data, solid line: Computation.

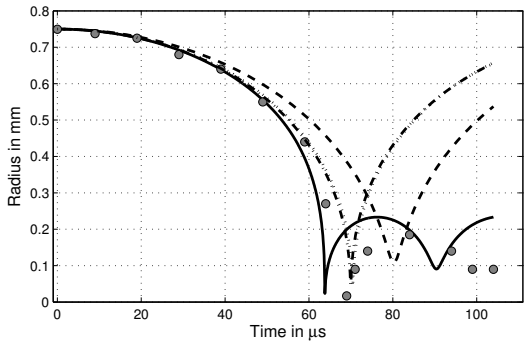

Figure 11.6: Calculated bubble radii according to Cases 1 - 4. Dots: Experimental data, dashed line: Case 1, dash-dotted line: Case 2, dotted line: Case 3, solid line: Case 4. (Remark: Case 2 and Case 3 are nearly the same.)

$\sigma = 0.07274N/m$	surfacial tension
$\bar{p} = 2330Pa$	saturation pressure
$\rho = 998.2kg/m^3$	liquid density
$c_p^L = 4183J/kg/K$	specific heat capacity of liquid water at constant pressure
$c_{p_W} = 1882J/kg/K$	specific heat capacity of water vapor at constant pressure
$s^L = 296J/kg/K$	specific entropy of liquid water
$s_W = 8665J/kg/K$	specific entropy of water vapor
$r = 2453300J/kg$	specific heat of evaporation
$\lambda = 0.5984W/m/K$	heat conductivity
$c = 1482m/s$	speed of sound in liquid water
$m_H = 2 \cdot 1.0079g/mol$	molecular weight of hydrogen
$m_O = 2 \cdot 15.9994g/mol$	molecular weight of oxygen

Table 11.1: Thermodynamic data at reference pressure $p_0 = 101300Pa$ and at reference temperature $T = 293.15K$

11.7 Conclusions

The main conclusions of this study concern the evolution of a laser induced bubble as it is described in Section 3, and can be summarized in five statements.

- Isothermal treatment of liquid-vapor phase transitions is not appropriate if the two phase system is exposed to atmospheric pressure.
- The modelling of the liquid as an incompressible body ignores the crucial effect that controls the damping of the bubble oscillation.
- The exclusive description of the evolution of the bubble radius, as it is done in the framework of Keller-Miksis type approximation like (11.1.2), where the phase transition is ignored, is possible. However, if the obtained data are used we calculate presssures and temperatures in the bubble as well as in the liquid, one observes unplausible values for those quantities. This is related to the fact, that the Keller-Miksis approximation relies on a small Mach number expansion, that becomes unrealistic in the region of minimal bubble radius.
- If a liquid-vapor phase transition is allowed, the rebound of the bubble is only possible when an inert gas is present in the bubble. A pure water vapor phase cannot persist beyond the first collapse since the vapor phase is unstable under the conditions of the experiment.
- Surprisingly, the non-isothermal treatment including phase transition has no large impact on the evolution of the bubble radius but on the other variables of the thermodynamic states of the bubble-liquid system. However, the bubble radius is the only quantity, that currently can easily be measured.

Finally we have collected the evolutions of the bubble radius corresponding to the four cases considered in a common plot, see Figure 11.6.

In the second part of this paper, which is in progress, we will use the models developed in this paper for the derivation of two-phase mixture conservation laws with phase transition. These are obtained using averaging procedures.

References

[1] Akhatov, I., Lindau, O., Topolnikov, A., Mettin, R., Vakhitova, N., Lauterborn, W.: Collapse and rebound of a laser-induced cavitation bubble. *Phys. Fluids* **13** (2001) 2805-2819.

[2] Akhatov, I., Vakhitova, N., Topolnikov, A., Zakirov, K., Wolfrum, B., Kurz, T., Lindau, O., Mettin, R., Lauterborn, W.: Dynamics of laser-induced cavitation bubbles, Exper. Thermal and Fluid Sci. **26**, 731–737 (2002).

[3] Bond, M., Struchtrup, H.: Mean evaporation and condensation coefficients based on energy dependent condensation probability, Phys. Rev. E **70**, 061605 (2004).

[4] Brennen, C. E.: Cavitation and Bubble Dynamics. Oxford Univ. Press, New York 1995.

[5] Dreyer, W.: On jump conditions at phase boundaries for ordered and disordered phases, WIAS Preprint **869**, (2003). [http://www.wias-berlin.de/main/publications/wias-publ/]

[6] Dreyer, W., Duderstadt, F.: On the Becker/Döring theory of nucleation of liquid droplets in solids, *J. Stat. Phys.* **123**, 55–87 (2006).

[7] Franc, J. P., Michel, J. M.: Fundamentals of Cavitation. Springer Sience and Business Media, Inc., 2005.

[8] Fujikawa, S., Akamatsu, T., Effects of the non-equilibrium condensation of vapor on the pressure wave produced by the collapse of a bubble in a liquid, J. Fluid Mech. **97**, 481–512 (1980).

[9] Grigull, U., Straub, S., Schiebener, P.: Steam Tables in SI-Units, Wasserdampftafeln. Springer-Verlag, Berlin 1990.

[10] Gilmore, F. R.: The growth or collapse of a spherical bubble in a viscous compressible liquid, Technical Report 26-4, Hydrodynamics Laboratory, California Institue of Technology, Pasadena, California 1952.

[11] Hickling, R., Plesset, M.: Collapse and rebound of a spherical bubble in water, Phys. Fluids **7**, 7–14 (1964).

[12] Gurtin, M. E.: Thermomechanics of moving phase boundaries in the plane. Oxford University Press, Oxford 1993.

[13] Keller, J. B., Kolodner, I. I.: Damping of underwater explosion bubble oscillations, J. Appl. Phys. **27**, 1152–1161 (1956).

[14] Keller, J. B., Miksis, M.: Bubble oscillations of large amplitude, J. Acoust. Soc. Am. **68**, 628–633 (1980).

[15] Kurz, T., Kröninger, D., Geisler, R., Lauterborn, W.: Optic cavitation in an ultrasonic field. Phys. Rev. E, 066307 (2006).

[16] Lauterborn, W.: Numerical investigation of nonlinear oscillations of gas bubbles in liquids, J. Acoust. Soc. Am. **59**, 283–293 (1976).

[17] Leighton, T. G.: The acoustic bubble. Academic Press, London 1994.

[18] Müller, I., Müller, W.: Fundamentals of Thermodynamics and Applications. Springer-Verlag, Berlin 2009.

[19] Müller, I.: Thermodynamics. Pitman, London 1985.

[20] Müller, S., Bachmann, M., Kröninger, D., Kurz, T., Helluy, P.: Comparison and Validation of Compressible Flow Simulations of Laser-Induced Cavitation Bubbles, Computers and Fluids, DOI: 10.1016/j.compfluid.2009.04.004, (2009).

[21] Nigmatulin, R. I., Akhatov, I. S., Vakhitova, N. K., Lahey, R. T.: On the forced oscillations of a small gas bubble in a spherical liquid filled flask, J. Fluid Mech. **414**, 47–73 (2000).

[22] Nigmatulin, R. I., Khabeev, N. S.: Heat exchange between a gas bubble and a liquid, rdquo Izv. Akad. Nauk SSSR, Mekh. Zhidk. Gaza bf 5, (1974).

[23] Plesset, M. S.: The dynamics of cavitation bubbles, J. Appl. Mech. **16**, 277–282 (1949).

[24] Plesset, M. S., Prosperetti, A.: Bubble dynamics and cavitation, Annu. Rev. Fluid Mech. **9**, 145–185 (1977).

[25] Prosperetti, A., Crum, L. A., Commander, K. W.: Nonlinear bubble dynamics, J. Acoust. Soc. Am. **83**, 502–514 (1988).

[26] Prosperetti, A., Lezzi, A.: Bubble dynamics in a compressible liquid Part 1: First order theory, J. Fluid Mech. **168**, 457–478 (1986).

[27] Lord Rayleigh, Philos. Mag. 6 **34**, 94–98 (1917).

[28] Serrin, J.: Mathematical principles of classical fluid mechanics. In: Flügge, S. (ed.), Handbuch der Physik VIII/1 – Strömungsmechanik 1, 125–263. Springer-Verlag, Berlin - Göttingen - Heidelberg (1959).

[29] Tomita, Y., Shima, A.: On the behavior of a spherical bubble and the impulse pressure in a viscous compressible liquid, Bull. JSME **20**, 1453–1460 (1977).

[30] Trilling, L.,The collapse and rebound of a gas bubble, J. Appl. Phys. bf 23, 14–17 (1952).

[31] Wu, C. C., Roberts, P. H., Shock-wave propagation in a sonoluminescing gas bubble, Phys. Rev. Lett. **70**, 3424–3427 (1993).

[32] Yasui, K.: Effects of thermal conduction on bubble dynamics near the sonoluminescence threshold, J. Acoust. Soc. Amer. **98**, 2772–2782 (1995).

[33] Zein, A.: Numerical methods for multiphase mixture conservation laws with phase transition, PHD thesis, Otto-von-Guericke university Magdeburg (2010).

Chapter 12

Mixture theories for dispersed particles

Bibliographic note: The content of this chapter is published in [H14]: Wolfgang Dreyer, Maren Hantke, and Gerald Warnecke. On balance laws for mixture theories of disperse vapor bubbles in liquid with phase change, *Continuum mechanics and thermodynamics* (2013). DOI 10.1007/s00161-013-0316-7

Abstract: We study averaging methods for the derivation of mixture equations for disperse vapor bubbles in liquids. The carrier liquid is modeled as a continuum, whereas simplified assumptions are made for the disperse bubble phase. An approach due to Petrov and Voinov is extended to derive mixture equations for the case that there is a phase transition between the carrier liquid and the vapor bubbles in water. We end up with a system of balance laws for a multi-phase mixture, which is completely in divergence form. Additional non-differential source terms describe the exchange of mass, momentum and energy between the phases. The sources depend explicitly on evolution laws for the total mass, the radius and the temperature of single bubbles. These evolution laws are derived in a prior article [4] and are used to close the system. Finally numerical examples are presented.

12.1 Introduction

The aim of the paper is to derive mixture balance laws for fluid flows with phase transition. We derive balance laws for mass and momentum as a first step. Analogously, we derive balances for the energy of the phases.

We are considering a mixture of a disperse phase of small ball shaped bubbles of water vapor, immersed in a carrier fluid of the corresponding other liquid phase. The advantage of considering a dispersed phase is that one may use a simpler specific averaging technique to describe it. In a more general approach for two phase mixtures one would use for both phases the averaging that we use only for the carrier fluid.

There are many techniques available to go from some microscopic modeling to macroscopic models. All of them involve a form of averaging in some sense. There is the theory of homogenization which mostly considers periodic structures, see Bensoussan et al. [3], and does the averaging by considering weak limits of periodically fluctuating physical states. There are the methods of moments, which may be seen as weighted global averages, such as those described in Müller and Ruggieri [14] or local averaging techniques such as those we want to consider. There are a number of such local averaging techniques, namely ensemble averaging, time averaging and spatial averaging, see Drew and Passman [5]. Also we want to mention Ishii [10], Stewart and Wendroff [19], Nigmatulin [16] among many other publications. All forms of averaging lead to the same type of macroscopic equations. We pursue spatial averaging.

It is not too difficult to arrive at averaged equations, but most approaches lead to additional variables which need closure relations in the form of state equations. This is not so surprising, since most theories at the level of continuum mechanics need such closure relations to completely determine the mathematical model equations. In the case we consider here, already the microscopic equations for the continuous phase used for the averaging come with equations of state.

There are also some numerical techniques along this line, see for instance Engquist and Hou [6].

Our approach is based on volume averaging techniques due to Voinov and Petrov [23] for the same problems which were studied in detail in a diploma thesis of Rydzewski [17]. In our approach we aim at taking the compressible Euler equations to describe the microscopic flow in the carrier phase whereas Voinov and Petrov [22–24] assumed a potential flow field and made explicit use of the known solution of potential flow around a sphere. Our results are therefore more general than those. But we do take up the idea to use a potential flow in order to determine the interfacial terms on the spherical surfaces between the phases. The remarkable difference to other two phase models is, that our model is completely in divergence form.

We average by using a type of sliding average over a ball of radius $a > 0$ in space. The diameter of the ball $d = 2a$ is the scale at which we want to derive macroscopic equations for the mixture of a liquid phase L occupying most of the space and a dispersed phase consisting of bubbles B consisting of small balls with radii considerably smaller than a.

This averaging is a specific case of volume averaging as described in Drew and Passman [5], though our notation is different and taken from Voinov and Petrov [23]. Drew and Passman argue at the end of Chapter 10 that ensemble averaging, i.e. an approach of statistical physics, is the preferred form of averaging to be used for multi-component fluids. We believe that we are considering a mere change of scale and therefore a fixed scale d introduced by the size of the balls is more adequate to describe the micro-macro transition in modeling. We are assuming that we have a deterministic microscopic model with a given unique dynamics, though existence and uniqueness currently cannot be proven mathematically rigorously for the model equations we are using.

For the microscopic phases we assume that they are not in equilibrium with each other and we want to focus on modeling their interacting dynamics including phase changes between them.

The paper is organized as follows. In Section 12.2 we introduce the averaging procedures and obtain meaningful averaged quantities. We prove a bubble and a general transport theorem. In the next section we derive balance laws for the carrier and the dispersed phase. In Section 11.4 we obtain closure relations for the sources to describe the exchange of mass, momentum and energy between the phases. In Section 12.5 we give some mathematical properties of a radial symmetric submodel. We recall the evolution laws obtained in [4] in Section 12.6 and give some numerical examples in Section 12.7. Finally, some detailed calculations for the proofs can be found in the appendix.

12.2 Local spatial averaging techniques

We assume that the space $\mathbb{R}^3$ contains a mixture of two separated fluids. In this study we consider an ensemble of $\mathcal{N}$ bubbles immersed in a liquid, thus forming the dispersed phase resp. the carrier phase. Further we require that the number of bubbles is constant. In order to take care of nucleation and dissolution of bubbles, we allow for bubbles with zero radius. The merging or breakage of bubbles are excluded in our approach since this would require an additional evolution law for the number of bubbles. The number $\mathcal{N}$ thus gives the maximal number of real bubbles in the system.

Both phases are represented here by different types of averaging operators. Mean values of properties of the dispersed phase consisting of bubbles, indicated by B, are given by sums over the bubbles, whereas in the liquid, indicated by L, we will have integrals over the liquid domain.

For the averaging we take a ball $B_a(0)$ of radius $a > 0$ at the origin, i.e. for a general ball we set $B_a(\mathbf{x}) = \{\mathbf{x}' \in \mathbb{R}^3 \mid |\mathbf{x}' - \mathbf{x}| < a\}$, and denote its volume by $V_a = \frac{4\pi}{3}a^3$. Thereby we define the volume averaging characteristic function or *window function*

$$\chi_a(\mathbf{x}) = \begin{cases} \frac{1}{V_a} & \mathbf{x} \in B_a(0) \\ 0 & \text{otherwise.} \end{cases}$$

Note that by standard smoothing techniques with Friedrichs mollifiers one could also take a smoothed approximation of the characteristic function over $B_a(0)$. If we consider derivatives of non-smooth functions to be taken in the sense of distributions we may avoid this. Either way, it should be noted that there is a mathematical theory making all the arguments below completely rigorous, but care has to be taken in each step. Since we want to concentrate on basic properties of the resulting system of differential equations, we leave out these technical details. They would only obscure the theory without giving additional insight.

Further, we assume that any bounded subset of $\mathbb{R}^3$ contains at most finitely many balls $B_\alpha(t)$ of radius $R_\alpha(t) > 0$ with $R_\alpha(t) \ll a$, with midpoints at $\mathbf{q}_\alpha(t) \in \mathbb{R}^3$, and volume $V_\alpha(t)$, i.e. $B_\alpha(t) = \{\mathbf{x} \in \mathbb{R}^3 \mid |\mathbf{x} - \mathbf{q}_\alpha(t)| < R_\alpha(t)\}$ and $V_\alpha(t) = \frac{4\pi}{3} R_\alpha(t)^3$. Let $\boldsymbol{\eta}_\alpha$ be the vector field of outer unit normals to the surface of $B_\alpha(t)$. To describe the surface points of the balls, we introduce the radial vectors $\mathbf{R}_\alpha(t, \boldsymbol{\eta}_\alpha) = R_\alpha(t)\boldsymbol{\eta}_\alpha$ such that the points $\mathbf{q}_\alpha(t) + \mathbf{R}_\alpha(t, \boldsymbol{\eta}_\alpha)$ lie on the surface of the respective ball. For the surface area we set $O_\alpha(t) = 4\pi R_\alpha(t)^2$. We denote by $m_\alpha(t)$ the mass of the ball $B_\alpha(t)$, by $\mathbf{v}_\alpha(t) = \dot{\mathbf{q}}_\alpha(t)$ the velocity of its midpoint, by $\mathbf{w}_\alpha(t, \boldsymbol{\eta}_\alpha) = \dot{\mathbf{q}}_\alpha(t) + \dot{\mathbf{R}}_\alpha(t, \boldsymbol{\eta}_\alpha)$ the velocity of its boundary, and by $\rho_\alpha(t) = m_\alpha(t)/V_\alpha(t)$ its mass density. For notational convenience we will not always explicitly write out the dependence of the radial vectors and velocities on the unit normals.

The balls just described contain solely the dispersed bubbles B whereas their complement $\Omega_L(t)$

$$\Omega_L(t) = \mathbb{R}^3 \backslash \bigcup_\alpha B_\alpha(t)$$

is filled completely with only the carrier fluid L. Then we define the *volume fraction* of the disperse phase as

$$c(t, \mathbf{x}) = \sum_\alpha \chi_a(\mathbf{x} - \mathbf{q}_\alpha(t)) V_\alpha(t). \tag{12.2.1}$$

The sum is finite for each $\mathbf{x} \in \mathbb{R}^3$ and is taken over all small balls containing the dispersed phase that have their midpoint within a distance a of $\mathbf{x}$. The volume fraction of the carrier fluid is then set to be $1 - c(t, \mathbf{x})$ in order to preserve volume. These volume fractions are step functions, i.e. not smooth.

Note that we are purposely making a small error by taking the full volume of any ball with its center in $B_a(\mathbf{x})$, even if it is not contained completely in $B_a(\mathbf{x})$. At the same time we neglect the volume of some balls that have their center outside and cut it. Otherwise we could have replaced in (12.2.1) $V_\alpha(t)$ by the volume measure $|B_\alpha(t) \cap B_a(\mathbf{x})|$. This would add a notational complication to the averaging formula of the dispersed phase without leading to any substantial changes in the outcome of the averaging. Note that our definition implies that the function c is not continuous where the midpoint of a dispersed phase ball $B_\alpha(t)$ leaves or enters the averaging ball $B_a(\mathbf{x})$.

The dispersed phase is assumed to consist of well separated very small balls. We are aware that in reality a dynamic dispersed phase will not come in spherical shapes, but do not wish to complicate the averaging procedure unnecessarily at this point. So we further assume for simplicity that certain physical properties Ψ, namely density, pressure and temperature are spatially constant and only time dependent within each ball, but may be different in neighboring balls. Note that the velocity must then be radially dependent in order to guarantee local mass conservation. We generically denote these quantities by $\Psi_\alpha(t)$. In the carrier fluid any field quantity Ψ depends on t and the spatial point $\mathbf{x}' \in \Omega_L(t)$.

Next we define the spatial *liquid average* for extensive physical variables by

$$(1 - c)\overline{\Psi}(t, \mathbf{x}) = \int_{\Omega_{L(t)}} \Psi(t, \mathbf{x}')\, \chi_a(\mathbf{x} - \mathbf{x}')\, d\mathbf{x}'\,. \tag{12.2.2}$$

Extensive variables describe those quantities that double in case the system size is doubled. In case that no bubble is cut by the averaging ball B_a, this is equivalent to the definition

$$\overline{\Psi}(t, \mathbf{x}) = \frac{\int_{\Omega_{L(t)}} \Psi(t, \mathbf{x}')\, \chi_a(\mathbf{x} - \mathbf{x}')\, d\mathbf{x}'}{\int_{\Omega_{L(t)}} \chi_a(\mathbf{x} - \mathbf{x}')\, d\mathbf{x}'} \tag{12.2.3}$$

In this study we need both averages, where (12.2.2) is used for establishing the evolution equation, while (12.2.3) is more convenient for numerical calculations.

Correspondingly we define the spatial *average of the dispersed phase* for extensive physical variables as

$$c\,\overline{\Psi_\alpha}(t, \mathbf{x}) = \sum_\alpha \Psi_\alpha(t)\, \chi_a(\mathbf{x} - \mathbf{q}_\alpha(t)) V_\alpha(t). \tag{12.2.4}$$

Note that the form of spatial averaging in (12.2.4) is somewhat different from taking (12.2.2) and assuming that Ψ has piecewise constant values Ψ_α on subsets of volume V_α containing representative points $\mathbf{x}' = \mathbf{q}_\alpha$. The spatial average (12.2.4) leads to step functions whereas the integration in (12.2.3) leads to continuous functions in this case. Also there is a slight deviation due to the fact that (12.2.4) is

taken only over the balls with at least their center point in $B_a(\mathbf{x})$ and we take their full volume, not just their intersection with $B_a(\mathbf{x})$ as a precise application of (12.2.2) would require. On the other hand balls with an intersection having their center outside the averaging domain are completely neglected. This small error is carried through all the arguments. It does not have any influence on the form of the averaged equations to be derived. There is only an imprecision for quantitative predictions. Also note, that our averaging procedure is similar to, but slightly different from the procedure in the book of Nigmatulin [16, p. 28], who also uses spatial averaging techniques.

Further, we point out that in the spatial averaging (12.2.2) we do not have the property $\overline{\overline{\Psi}} = \overline{\Psi}$. The double average involves integration over a ball or radius $2a$. Such a property is only true for ensemble averages or periodic functions averaged over their periods. For our discrete average (12.2.4) a double average is not meaningful because it gives a density that is independent of α. We only use the notation $\overline{\Psi_\alpha}$ to point out that the averaged variable is related to the dispersed balls. Microscopic quantities for the carrier fluid have no index.

Quantities related to the interfaces

$$I_\alpha(t) = \partial B_\alpha(t) = \{\mathbf{x} \in \mathbb{R}^3 \mid \ |\mathbf{x} - q_\alpha(t)| = R_\alpha(t)\}$$

will have an index I_α.

Next we consider special choices for the properties Ψ_α resp. Ψ for the bubbles and the liquid. The only meaningful choices are densities of additive quantities. See Section 11.4 for more details. Note that Nigmatulin [16] did not discuss this point

The simplest choice is $\Psi_\alpha \equiv 1$. This results in representation (12.2.1) of the concentration of the bubbles which is the local mean value of their volumes. The mean values of m_α/V_α, $1/V_\alpha$, $m_\alpha \dot{q}_\alpha/V_\alpha$ and $m_\alpha e_\alpha/V_\alpha$ give the mass density ρ_B, the number density n, the momentum density $\rho_B v_B$ and the total energy density $\rho_B e_B$ of the bubbles. The latter is assumed to be the sum of the internal and the kinetic energy

$$c\rho_B(t,\mathbf{x}) = \sum_\alpha m_\alpha(t)\ \chi_a(\mathbf{x} - \mathbf{q}_\alpha(t)), \tag{12.2.5}$$

$$cn(t,\mathbf{x}) = \sum_\alpha \chi_a(\mathbf{x} - \mathbf{q}_\alpha(t)), \tag{12.2.6}$$

$$c\rho_B\mathbf{v}_B(t,\mathbf{x}) = \sum_\alpha m_\alpha(t)\dot{\mathbf{q}}_\alpha(t)\ \chi_a(\mathbf{x} - \mathbf{q}_\alpha(t)), \tag{12.2.7}$$

$$c\rho_B e_B(t,\mathbf{x}) = \sum_\alpha m_\alpha(t)e_\alpha(t)\ \chi_a(\mathbf{x} - \mathbf{q}_\alpha(t))\,. \tag{12.2.8}$$

In the liquid we only have to define the mass density, the momentum density and the total energy density by the corresponding formulas

$$(1-c)\rho_L(t,\mathbf{x}) \quad = \int_{\Omega_{L(t)}} \rho(t,\mathbf{x}')\ \chi_a(\mathbf{x} - \mathbf{x}')\ d\mathbf{x}', \tag{12.2.9}$$

$$(1-c)\rho_L\mathbf{v}_L(t,\mathbf{x}) = \int_{\Omega_{L(t)}} \rho(t,\mathbf{x}')\mathbf{v}(t,\mathbf{x}')\ \chi_a(\mathbf{x} - \mathbf{x}')\ d\mathbf{x}'\,, \tag{12.2.10}$$

$$(1-c)\rho_L e_L(t,\mathbf{x}) = \int_{\Omega_{L(t)}} \rho(t,\mathbf{x}')e(t,\mathbf{x}')\ \chi_a(\mathbf{x} - \mathbf{x}')\ d\mathbf{x}'\,. \tag{12.2.11}$$

Note that now we have at each point in space a partial density $c\rho_B$ of the bubbles and a partial density $(1-c)\rho_L$ of the liquid. The same is true for the momentum and the energy. All further quantities have to be obtained from the above variables using an equation of state or other closure relations.

Now we study the most important properties of the averaging.

Lemma 12.2.1 (Preservation property)**.** *Let $\Psi(t,\cdot) \in L^1(\Omega_L(t))$ and Ψ_α for finitely many bubbles be any extensive variable, then we have*

$$\int_{\Omega_L(t)} \Psi(t,\mathbf{x})\ d\mathbf{x} + \sum_\alpha \Psi_\alpha(t)V_\alpha(t) = \int_{\mathbb{R}^3} (1-c)\overline{\Psi}(t,\mathbf{x}) + c\overline{\Psi_\alpha}(t,\mathbf{x})\ d\mathbf{x}\,.$$

Proof. Using the definitions (12.2.4), (12.2.2), the Fubini Theorem as well as the fact that $\int_{\mathbb{R}^3} \chi_a\ d\mathbf{x} = 1$

we find

$$\begin{aligned}
&\int_{\mathbb{R}^3} (1-c)\overline{\Psi}(t,\mathbf{x}) + c\overline{\Psi_\alpha}(t,\mathbf{x})\, d\mathbf{x} \\
&\quad = \int_{\mathbb{R}^3} \left[\int_{\Omega_L(t)} \Psi(t,\mathbf{x}')\, \chi_a(\mathbf{x}-\mathbf{x}')\, d\mathbf{x}' + \sum_\alpha \Psi_\alpha(t)\, \chi_a(\mathbf{x}-\mathbf{q}_\alpha(t))V_\alpha(t) \right] d\mathbf{x} \\
&\quad = \int_{\Omega_L(t)} \Psi(t,\mathbf{x}') \int_{\mathbb{R}^3} \chi_a(\mathbf{x}-\mathbf{x}')\, d\mathbf{x}\, d\mathbf{x}' + \sum_\alpha \Psi_\alpha(t) \int_{\mathbb{R}^3} \chi_a(\mathbf{x}-\mathbf{q}_\alpha(t))\, d\mathbf{x}\, V_\alpha(t) \\
&\quad = \int_{\Omega_L(t)} \Psi(t,\mathbf{x}')\, d\mathbf{x}' + \sum_\alpha \Psi_\alpha(t)V_\alpha(t).
\end{aligned}$$

□

Next we derive the transport theorems that describe the dynamics of the averaged quantities.

Lemma 12.2.2 (Bubble transport equation)**.** *We consider any extensive quantity $\Psi_\alpha(t)$ describing the bubble. We use the notation $\nabla_{\mathbf{x}} = \left(\frac{\partial}{\partial x_1}, \frac{\partial}{\partial x_2}, \frac{\partial}{\partial x_3}\right)$ for the spatial gradient. Then the averaged quantity $\overline{\Psi_\alpha}$ satisfies the transport equation*

$$\frac{\partial c\overline{\Psi_\alpha}}{\partial t}(t,\mathbf{x}) + \nabla_{\mathbf{x}} \cdot (c\,\overline{\Psi_\alpha \dot{\mathbf{q}}_\alpha}(t,\mathbf{x})) = c\,\overline{\left(\frac{(\Psi_\alpha V_\alpha)^{\cdot}}{V_\alpha}\right)}(t,\mathbf{x}). \tag{12.2.12}$$

Proof. Using the definition (12.2.4) we find by differentiation in the sense of distributions, see also Appendix B, and again use of (12.2.4)

$$\begin{aligned}
\frac{\partial}{\partial t} c\overline{\Psi_\alpha}(t,\mathbf{x}) &= \sum_\alpha \frac{\partial}{\partial t} \left(\Psi_\alpha(t)\, \chi_a(\mathbf{x}-\mathbf{q}_\alpha(t))V_\alpha(t) \right) \\
&= \sum_\alpha \Big[\Psi_\alpha(t) \nabla_{\mathbf{q}_\alpha}\, \chi_a(\mathbf{x}-\mathbf{q}_\alpha(t)) \cdot \dot{\mathbf{q}}_\alpha(t) V_\alpha(t) + \dot{\Psi}_\alpha(t)\, \chi_a(\mathbf{x}-\mathbf{q}_\alpha(t))V_\alpha(t) \\
&\quad + \Psi_\alpha(t)\, \chi_a(\mathbf{x}-\mathbf{q}_\alpha(t))\dot{V}_\alpha(t) \Big] \\
&= -\nabla_{\mathbf{x}} \cdot \sum_\alpha \Psi_\alpha(t)\, \chi_a(\mathbf{x}-\mathbf{q}_\alpha(t))V_\alpha(t)\dot{\mathbf{q}}_\alpha + \sum_\alpha \dot{\Psi}_\alpha(t)\, \chi_a(\mathbf{x}-\mathbf{q}_\alpha(t))V_\alpha(t) \\
&\quad + \sum_\alpha \Psi_\alpha(t) \frac{\dot{V}_\alpha(t)}{V_\alpha(t)}\, \chi_a(\mathbf{x}-\mathbf{q}_\alpha(t))V_\alpha(t) \\
&= -\nabla_{\mathbf{x}} \cdot \left(c\,\overline{\Psi_\alpha \dot{\mathbf{q}}_\alpha}(t,\mathbf{x}) \right) + c\,\overline{\left(\frac{\dot{\Psi}_\alpha V_\alpha}{V_\alpha}\right)}(t,\mathbf{x}) + c\,\overline{\left(\frac{\Psi_\alpha \dot{V}_\alpha}{V_\alpha}\right)}(t,\mathbf{x}).
\end{aligned}$$

□

Note that from the proof we have

$$c\,\overline{\dot{\Psi}_\alpha}(t,\mathbf{x}) = \frac{\partial}{\partial t}(c\overline{\Psi_\alpha}(t,\mathbf{x})) + \nabla_{\mathbf{x}} \cdot \left(c\,\overline{\Psi_\alpha \dot{\mathbf{q}}_\alpha}(t,\mathbf{x}) \right) - c\,\overline{\left(\frac{\Psi_\alpha \dot{V}_\alpha}{V_\alpha}\right)}(t,\mathbf{x}).$$

Taking $\Psi_\alpha = 1$ in (12.2.12) we obtain

$$\frac{\partial c}{\partial t}(t,\mathbf{x}) + \nabla_{\mathbf{x}} \cdot (c\,\overline{\dot{\mathbf{q}}_\alpha}(t,\mathbf{x})) = c\,\overline{\left(\frac{\dot{V}_\alpha}{V_\alpha}\right)}(t,\mathbf{x}). \tag{12.2.13}$$

This result states that the volume fraction of the bubbles gets transported by the local average velocity of the balls $\overline{\dot{q}_\alpha}$. According to (12.2.13) the volume fraction can also be produced by the source term of the right hand side. This fact indicates that we allow liquid-vapor phase transitions. Note that in Drew and Passman [5] this equation is replaced by the so-called topological equation for the averaged

characteristic function of the set microscopically occupied by one phase. But they have not accounted for the phase transition term.

Since we are assuming a spherical shape of V_α note that

$$\frac{\dot{V}_\alpha}{V_\alpha} = 3\frac{\dot{R}_\alpha}{R_\alpha}\,. \tag{12.2.14}$$

The next equation of our hierarchy describes the evolution of the number density of bubbles. Taking (12.2.6) and $\Psi_\alpha = 1/V_\alpha$ gives

$$\frac{\partial cn}{\partial t}(t,\mathbf{x}) + \nabla_{\mathbf{x}} \cdot (c\,\overline{\dot{\mathbf{q}}_\alpha/V_\alpha}(t,\mathbf{x})) = 0\,. \tag{12.2.15}$$

Note that the total number of bubbles in the system does not change. Taking $\Psi_\alpha = \rho_\alpha$ resp. $\Psi_\alpha = \rho_\alpha \dot{q}_\alpha$ we obtain the transport equations for mean bubble mass

$$\frac{\partial c\rho_B}{\partial t}(t,\mathbf{x}) + \nabla_{\mathbf{x}} \cdot (c\rho_B \mathbf{v}_B(t,\mathbf{x})) = c\,\overline{\left(\frac{\dot{m}_\alpha}{V_\alpha}\right)}(t,\mathbf{x}) \tag{12.2.16}$$

and mean bubble momentum

$$\frac{\partial c\rho_B v_B}{\partial t}(t,\mathbf{x}) + \nabla_{\mathbf{x}} \cdot (c\,\overline{\rho_\alpha \dot{\mathbf{q}}_\alpha \otimes \dot{\mathbf{q}}_\alpha}(t,\mathbf{x})) = c\,\overline{\left(\frac{(\rho_\alpha \dot{\mathbf{q}}_\alpha V_\alpha)^{\cdot}}{V_\alpha}\right)}(t,\mathbf{x}) = c\,\overline{\left(\frac{(m_\alpha \dot{\mathbf{q}}_\alpha)^{\cdot}}{V_\alpha}\right)}(t,\mathbf{x})\,. \tag{12.2.17}$$

Further we obtain with $\Psi_\alpha = \rho_\alpha e_\alpha$ the transport equation for the mean bubble energy

$$\frac{\partial c\rho_B e_B}{\partial t}(t,\mathbf{x}) + \nabla_{\mathbf{x}} \cdot (c\overline{\rho_\alpha e_\alpha \dot{\mathbf{q}}_\alpha}(t,\mathbf{x})) = c\,\overline{\left(\frac{(m_\alpha e_\alpha)^{\cdot}}{V_\alpha}\right)}(t,\mathbf{x})\,. \tag{12.2.18}$$

In order to obtain the corresponding transport equations for the liquid phase we will need differentiation in time of integrals with time dependent integrand and domain of integration of the form

$$\frac{d}{dt}\int_{\Omega(t)} \Psi(t,y)\; dy.$$

This is achieved by the well known Reynolds Transport Theorem assuming that we know a continuously differentiable family of continuously differentiable transformations $\mathbf{X}^t : \Omega(0) \to \Omega(t)$ whereby for each point y_0 we have a trajectory $y(t) = \mathbf{X}^t(y_0)$ leading to a velocity field $\mathbf{u}(t,y) = \dot{y}(t)$.

Theorem 12.2.1 (Reynolds Transport Theorem)**.** *Let $\Psi : \mathbb{R} \times \mathbb{R}^{\mathsf{N}} \to \mathbb{R}$ be a continuously differentiable scalar field and the transformations $\mathbf{X}^t : \mathbb{R}^{\mathsf{N}} \to \mathbb{R}^{\mathsf{N}}$ also continuously differentiable with the velocity field $\mathbf{u}$ as defined above. Then for any bounded control volume $\Omega(t)$ the transport equation*

$$\frac{d}{dt}\int_{\Omega(t)} \Psi(t,y)\; dy = \int_{\Omega(t)} \left[\frac{\partial \Psi}{\partial t}(t,y) + \nabla_y \cdot \Big(\Psi(t,y)\mathbf{u}(t,y)\Big)\right] dy \tag{12.2.19}$$

holds, where $\boldsymbol{\eta}(t)$ is the velocity of the boundary.

Proof. A proof can be found in Serrin [18] or Warnecke [21]. □

Also see Drew and Passman [5, p. 102] for the topological equation. For our purposes we will modify the equation (12.2.19) using the Gauss theorem with the outer unit normal field $\boldsymbol{\eta}(t)$ on the boundary $\partial\Omega(t)$ giving

$$\frac{d}{dt}\int_{\Omega(t)} \Psi(t,y)\; dy = \int_{\Omega(t)} \frac{\partial \Psi}{\partial t}(t,y)\; dy + \oint_{\partial\Omega(t)} \Big(\Psi(t,y)\mathbf{u}(t,y)\Big) \cdot \boldsymbol{\eta}(t,y)\; dS\,. \tag{12.2.20}$$

Lemma 12.2.3 (General transport equation)**.** *Let us assume that a physical quantity Ψ for the carrier fluid satisfies a microscopic balance law*

$$\frac{\partial}{\partial t}\Psi(t,\mathbf{x}') + \nabla_{\mathbf{x}'} \cdot \mathbf{F}(t,\mathbf{x}') = G(t,\mathbf{x}') \tag{12.2.21}$$

for some given flux function $\mathbf{F}$ *and right hand side* G*, e.g. an external force or a source. We set* $I_\alpha(t) = \partial B_\alpha(t)$ *and take* $\boldsymbol{\eta}_\alpha$ *to be the outer unit normal vector of these balls on their surface. We further denote by* $\mathbf{R}_\alpha(t) = R_\alpha(t)\boldsymbol{\eta}_\alpha$ *the vector of length* $R_\alpha(t)$ *so that* $\mathbf{q}_\alpha(t) + \mathbf{R}_\alpha(t)$ *gives an arbitrary point on* $\partial B_\alpha(t)$*. We set* $\mathbf{w}_\alpha = \dot{\mathbf{q}}_\alpha + \dot{\mathbf{R}}_\alpha$*. Further, we assume that the boundary* ∂ *of the ball* $B_a(\mathbf{x})$ *does not intersect any of the small balls* $B_\alpha(t)$*. Then we have by averaging*

$$\begin{aligned}\frac{\partial}{\partial t}(1-c)\overline{\Psi}(t,\mathbf{x}) + \nabla_{\mathbf{x}} \cdot (1-c)\overline{\mathbf{F}}(t,\mathbf{x}) \qquad (12.2.22)\\ = \sum_{\substack{\alpha \\ \mathbf{q}_\alpha \in B_a(\mathbf{x})}} \oint_{I_\alpha(t)} [\mathbf{F}(t,\mathbf{x}') - \Psi(t,\mathbf{x}')\mathbf{w}_\alpha] \cdot \boldsymbol{\eta}_\alpha \, \chi_a(\mathbf{x}-\mathbf{x}') \, dS + (1-c)\overline{G}(t,\mathbf{x}).\end{aligned}$$

The summation is finite and by assumption the quantities $\dot{\mathbf{q}}_\alpha$*,* $\dot{\mathbf{R}}_\alpha$ *are constant with respect to integration on each sphere.*

Proof. We have to take into account that our general averaging integral in (12.2.2) has a time dependent domain of integration and use (12.2.20). The unit normals $\boldsymbol{\eta}_\alpha$ are inner unit normals to $\Omega_{L(t)}$, so we obtain

$$\begin{aligned}\frac{\partial}{\partial t}(1-c)\overline{\Psi}(t,\mathbf{x}) = \frac{\partial}{\partial t}\int_{\Omega_{L(t)}} \Psi(t,\mathbf{x}') \, \chi_a(\mathbf{x}-\mathbf{x}') \, d\mathbf{x}' \qquad (12.2.23)\\ = \int_{\Omega_{L(t)}} \frac{\partial \Psi}{\partial t}(t,\mathbf{x}') \, \chi_a(\mathbf{x}-\mathbf{x}') \, d\mathbf{x}' - \sum_\alpha \oint_{I_\alpha(t)} \Psi(t,\mathbf{x}')\mathbf{w}_\alpha \cdot \boldsymbol{\eta}_\alpha(t) \, \chi_a(\mathbf{x}-\mathbf{x}') \, dS.\end{aligned}$$

The summation is taken over all balls with their center in the support of $\chi_a(\mathbf{x}-\mathbf{x}')$. Now we use the conservation law (12.2.21) and (12.2.2) as well as the shift of differentiation formula for the distribution $\nabla_{\mathbf{x}'} \, \chi_a(\mathbf{x}-\mathbf{x}')$ given in Appendix 12.B to obtain

$$\begin{aligned}\frac{\partial}{\partial t}(1-c)\overline{\Psi}(t,\mathbf{x}) &= -\int_{\Omega_{L(t)}} \nabla_{\mathbf{x}'} \cdot \mathbf{F}(t,\mathbf{x}') \, \chi_a(\mathbf{x}-\mathbf{x}') \, d\mathbf{x}' + \int_{\Omega_{L(t)}} G(t,\mathbf{x}') \, \chi_a(\mathbf{x}-\mathbf{x}') \, d\mathbf{x}' \\ &\quad - \sum_\alpha \oint_{I_\alpha(t)} \Psi(t,\mathbf{x}')\mathbf{w}_\alpha \cdot \boldsymbol{\eta}_\alpha(t) \, \chi_a(\mathbf{x}-\mathbf{x}') \, dS \\ &= -\int_{\Omega_{L(t)}} \nabla_{\mathbf{x}'} \cdot \left[\mathbf{F}(t,\mathbf{x}') \, \chi_a(\mathbf{x}-\mathbf{x}')\right] d\mathbf{x}' + \int_{\Omega_{L(t)}} \mathbf{F}(t,\mathbf{x}') \nabla_{\mathbf{x}'} \, \chi_a(\mathbf{x}-\mathbf{x}') \, d\mathbf{x}' \\ &\quad - \sum_\alpha \oint_{I_\alpha(t)} \Psi(t,\mathbf{x}')\mathbf{w}_\alpha \cdot \boldsymbol{\eta}_\alpha(t) \, \chi_a(\mathbf{x}-\mathbf{x}') \, dS + (1-c)\overline{G}(t,\mathbf{x}).\end{aligned}$$

Using the shift of differentiation formula from Appendix 12.B this gives

$$\begin{aligned}\frac{\partial}{\partial t}(1-c)\overline{\Psi}(t,\mathbf{x}) &= -\int_{\Omega_{L(t)}} \nabla_{\mathbf{x}'} \cdot \left[\mathbf{F}(t,\mathbf{x}') \, \chi_a(\mathbf{x}-\mathbf{x}')\right] d\mathbf{x}' - \nabla_{\mathbf{x}} \cdot \int_{\Omega_{L(t)}} \mathbf{F}(t,\mathbf{x}') \, \chi_a(\mathbf{x}-\mathbf{x}') \, d\mathbf{x}' \\ &\quad - \sum_\alpha \oint_{I_\alpha(t)} \Psi(t,\mathbf{x}')\mathbf{w}_\alpha \cdot \boldsymbol{\eta}_\alpha(t) \, \chi_a(\mathbf{x}-\mathbf{x}') \, dS + (1-c)\overline{G}(t,\mathbf{x}) \\ &= \sum_\alpha \oint_{I_\alpha(t)} \mathbf{F}(t,\mathbf{x}') \cdot \boldsymbol{\eta}_\alpha(t,\mathbf{x}') \, \chi_a(\mathbf{x}-\mathbf{x}') \, dS - \nabla_{\mathbf{x}} \cdot (1-c)\overline{\mathbf{F}}(t,\mathbf{x}) \\ &\quad - \sum_\alpha \oint_{I_\alpha(t)} \Psi(t,\mathbf{x}')\mathbf{w}_\alpha \cdot \boldsymbol{\eta}_\alpha(t) \, \chi_a(\mathbf{x}-\mathbf{x}') \, dS + (1-c)\overline{G}(t,\mathbf{x}).\end{aligned}$$

All terms involving derivatives of χ_a have to be interpreted in the sense of distributions, see Appendix 12.B. □

For the case that small balls $B_\alpha(t)$ intersect $\partial B_a(\mathbf{x})$ we take the same formula (12.2.22) and again make a small error, as in the definition of c.

For a first illustration we consider the special case $\Psi = 1$ to obtain an equation for the concentration c in the liquid setting. We have

$$\begin{aligned}
\frac{\partial}{\partial t}(1-c)(t,\mathbf{x}) = -\frac{\partial c}{\partial t}(t,\mathbf{x}) &= -\frac{\partial}{\partial t}\int_{\Omega_{L(t)}} \chi_a(\mathbf{x}-\mathbf{x}')\, d\mathbf{x}' \\
&= -\sum_\alpha \oint_{I_\alpha(t)} \mathbf{w}_\alpha \cdot \boldsymbol{\eta}_\alpha(t)\, \chi_a(\mathbf{x}-\mathbf{x}')\, dS \\
&= -\sum_\alpha \oint_{I_\alpha(t)} \left(\dot{\mathbf{q}}_\alpha + \dot{\mathbf{R}}_\alpha\right) \cdot \boldsymbol{\eta}_\alpha(t)\, \chi_a(\mathbf{x}-\mathbf{x}')\, dS \\
&= -\sum_\alpha \int_{B_\alpha(t)} \nabla_{\mathbf{x}'} \cdot \left[\dot{\mathbf{q}}_\alpha\, \chi_a(\mathbf{x}-\mathbf{x}')\right]\, d\mathbf{x}' - \sum_\alpha \oint_{I_\alpha(t)} \dot{R}_\alpha\, \chi_a(\mathbf{x}-\mathbf{x}')\, dS. \\
&= \nabla_x \cdot \sum_\alpha \int_{B_\alpha(t)} \left[\dot{\mathbf{q}}_\alpha\, \chi_a(\mathbf{x}-\mathbf{x}')\right]\, d\mathbf{x}' - \sum_\alpha \oint_{I_\alpha(t)} \dot{R}_\alpha\, \chi_a(\mathbf{x}-\mathbf{x}')\, dS.
\end{aligned}$$

Now we may set $\chi_a(\mathbf{x}-\mathbf{q}_\alpha(t)) = \chi_a(\mathbf{x}-\mathbf{x}')$, because we note that in case $a > 2R_\alpha(t)$ for all α, which we assume throughout, we have $B_\alpha(t) \subset B_a(\mathbf{q}_\alpha(t) + \mathbf{R}_\alpha(t))$. So for $\mathbf{x} \in B_a(\mathbf{q}_\alpha(t)) \cap B_a(\mathbf{q}_\alpha(t) + \mathbf{R}_\alpha(t))$ we have using $\mathbf{x}' = \mathbf{q}_\alpha(t) + \mathbf{R}_\alpha(t) \in I_\alpha(t)$

$$\chi_a(\mathbf{x}-\mathbf{q}_\alpha(t)) = \chi_a(\mathbf{x}-(\mathbf{q}_\alpha(t)+\mathbf{R}_\alpha(t))) = \chi_a(\mathbf{x}-\mathbf{x}') = \frac{1}{V_a}\,. \tag{12.2.24}$$

This gives

$$\frac{\partial c}{\partial t}(t,\mathbf{x}) + \nabla_{\mathbf{x}} \cdot \left(c(t,\mathbf{x})\overline{\dot{\mathbf{q}}_\alpha}(t,\mathbf{x})\right) = 3c\overline{\left(\frac{\dot{R}}{R}\right)}\,.$$

Here we refer the reader to the corresponding equations (12.2.13) and (12.2.14) for the concentration in the bubble setting, which gives the same result.

12.3 Mixture balance laws

12.3.1 The microscopic conservation laws within each phase

The liquid is assumed to be described by the inviscid, compressible balances for mass, momentum and energy for the microscopic variables mass density $\rho : \mathbb{R}\times\mathbb{R}^3 \to \mathbb{R}$, velocity $\mathbf{v} : \mathbb{R}\times\mathbb{R}^3 \to \mathbb{R}^3$ and energy $e : \mathbb{R}\times\mathbb{R}^3 \to \mathbb{R}$.

$$\frac{\partial \rho}{\partial t} + \nabla_{\mathbf{x}} \cdot (\rho\,\mathbf{v}) = 0\,, \tag{12.3.1}$$

$$\frac{\partial(\rho\mathbf{v})}{\partial t} + \nabla_{\mathbf{x}}((\rho\mathbf{v}\otimes\mathbf{v}) + p(\rho)\mathbf{1}) = \rho\mathbf{g}\,, \tag{12.3.2}$$

$$\frac{\partial \rho e}{\partial t} + \nabla_{\mathbf{x}} \cdot ((\rho e + p)\mathbf{v} + \mathbf{Q}) = \rho\mathbf{g}\cdot\mathbf{v}\,. \tag{12.3.3}$$

The pressure $p : \mathbb{R}\times\mathbb{R}^3 \to \mathbb{R}$ is given by the equation of state due to Hooke's law applied to an isotropic liquid

$$p = p_{ref} + K(\frac{\rho}{\rho_{ref}} - 1)\,, \tag{12.3.4}$$

where K is the liquid bulk modulus. This means, that the liquid density does not depend on temperature, we neglect thermal expansion. Corresponding to equation (12.3.4) the speed of sound a_L of the liquid is given by

$$a_L = \sqrt{\frac{K}{\rho_{ref}}} \tag{12.3.5}$$

and is obviously constant. The gravitational acceleration is given by $\mathbf{g} = -g(0,0,1)$. For the energy we have

$$e = u + \frac{1}{2}\,\mathbf{v}^2\,,$$

where we use the following constitutive law for the internal energy u

$$u(T,\rho) = c_*(T - T_{ref}) + (p_{ref} - K)\left(\frac{1}{\rho_{ref}} - \frac{1}{\rho}\right) + \frac{K}{\rho_{ref}} \ln \frac{\rho}{\rho_{ref}} + u(T_{ref}, \rho_{ref}) \tag{12.3.6}$$

with the specific heat capacity c_*. Further we have Fourier's law the constitutive law for the heat flux

$$\mathbf{Q} = -\kappa \nabla T$$

with the heat conductivity κ.

We assume that the content of the bubbles behaves as an ideal gas. It is described by the ideal thermal and the caloric equation of state for the pressure and the internal energy

$$p_\alpha = \frac{\rho_\alpha k T_\alpha}{m_0} \qquad \text{and} \qquad u_\alpha(T_\alpha) = z\frac{k}{m_0}(T_\alpha - T_{ref}) + u(T_{ref}) \tag{12.3.7}$$

where m_0 is the molecular mass, k is the Boltzmann constant and $z = 3$ for a polyatomic gas.

The thermodynamic states inside the bubbles are assumed to be homogeneous in space. For this reason we do not need local balance laws here. Instead we take Newton's law of motion for the evolution of the bubble centers $\mathbf{q}_\alpha$, which concerns a moving bubble with changing bubble radius that may gain or lose mass

$$(m_\alpha(t)\dot{q}^j_\alpha(t))^{\cdot} = -\oint_{I_\alpha} p\eta^j_\alpha dS + m_\alpha g^j + \frac{\dot{m}_\alpha(t)}{4\pi R_\alpha(t)^2}\oint_{I_\alpha} v^j(t,\mathbf{x}')dS\,, \tag{12.3.8}$$

for $j = 1, 2, 3$. The first term on the right hand side is the pressure exerted by the fluid onto the particle, the second is the gravitational force and the third term is a momentum change due to mass being lost to the carrier fluid. The special form of these equations is explained in Appendix 12.A.

Further, we have the respective mass, momentum, and energy balance at the interface

$$[\![\rho(v^\eta - w^\eta)]\!] = 0\,, \tag{12.3.9}$$

$$\rho(v^\eta - w^\eta)[\![\mathbf{v}]\!] + [\![p\eta]\!] = 2\sigma k_m \eta\,, \tag{12.3.10}$$

$$\rho(v^\eta - w^\eta)[\![u + \frac{p}{\rho} + \frac{1}{2}(\mathbf{v} - \mathbf{w})^2]\!] + [\![Q]\!] = 0\,, \tag{12.3.11}$$

where the jump brackets denote $[\![\Psi]\!] = \Psi^I_L - \Psi^I_\alpha$ for any physical quantity Ψ, σ denotes the surface tension and k_m denotes the mean curvature.

For a simplified study one can ignore the energy equation. In that case one has to introduce a rule that controls the variation of temperature. For instance we can consider either the isothermal or the adiabatic case. In this paper for simplicity we only investigate the isothermal system mathematically, see Section 12.5. Moreover we illustrate how to deal with source terms resp. evolution laws for the isothermal system, see Section 12.6 and Section 12.7.

12.3.2 Macroscopic mass balances

We first use for the liquid phase (12.2.22) with $\Psi = \rho$, $\mathbf{F} = \rho\mathbf{v}$ and the definition (12.2.10) to obtain from (12.3.1)

$$\begin{aligned}\frac{\partial}{\partial t}[(1-c)\rho_L](t,\mathbf{x}) + \nabla_{\mathbf{x}} \cdot [(1-c)\rho_L \mathbf{v}_L](t,\mathbf{x}) \\ = \sum_\alpha \oint_{I_\alpha(t)} \rho(t,\mathbf{x}')\,[\mathbf{v}(t,\mathbf{x}') - \mathbf{w}_\alpha(t)] \cdot \boldsymbol{\eta}_\alpha\, \chi_a(\mathbf{x} - \mathbf{x}')\, dS\,.\end{aligned} \tag{12.3.12}$$

For the bubbles we take (12.2.12) with $\Psi_\alpha(t) = m_\alpha(t)/V_\alpha(t)$, the definitions (12.2.7) and obtain

$$\frac{\partial(c\rho_B)}{\partial t}(t,\mathbf{x}) + \nabla_{\mathbf{x}} \cdot (c\,\rho_B \mathbf{v}_B)(t,\mathbf{x}) = c\,\overline{\left(\frac{\dot{m}_\alpha}{V_\alpha}\right)}(t,\mathbf{x}). \tag{12.3.13}$$

Overall the total mass of both phases must be conserved. Therefore, we must have a mass balance across the interfaces. The terms on the right hand side must cancel when both equations are added

together. In fact this happens because we conclude: For $\mathbf{x}' = \mathbf{q}_\alpha(t) + \mathbf{R}_\alpha(t) \in I_\alpha(t)$ we have using (12.2.24) for the right hand side of (10.3.48)

$$c\overline{\left(\frac{\dot m_\alpha}{V_\alpha}\right)}(t,\mathbf{x}) = \sum_\alpha \dot m_\alpha\, \chi_a(\mathbf{x} - (\mathbf{q}_\alpha(t) + \mathbf{R}_\alpha(t)) = \sum_\alpha \dot m_\alpha\, \chi_a(\mathbf{x} - \mathbf{x}')\,.$$

Now for $\mathbf{x}' \in \partial B_\alpha(t)$ and $\mathbf{x} \in B_a(\mathbf{q}_\alpha(t)) \cap B_a(\mathbf{q}_\alpha(t) + \mathbf{R}_\alpha(t))$ we obtain the relation

$$\oint_{I_\alpha(t)} \rho(t,\mathbf{x}')\,[\mathbf{v}(t,\mathbf{x}') - \mathbf{w}_\alpha(t)]\cdot\boldsymbol{\eta}_\alpha\, \chi_a(\mathbf{x}-\mathbf{x}')\, dS = -\dot m_\alpha\, \chi_a(\mathbf{x}-\mathbf{x}')$$

for the liquid phase. This equation relates the rate of mass change $\dot m_\alpha$ to the flow and boundary velocities. We use the rate of mass change

$$\dot m_\alpha = -\oint_{I_\alpha(t)} \rho(t,\mathbf{x}')\,[\mathbf{v}(t,\mathbf{x}') - \mathbf{w}_\alpha(t)]\cdot\boldsymbol{\eta}_\alpha\, dS\,. \tag{12.3.14}$$

The total rate of change of mass in $B_\alpha(t)$ equals the mass flux at the moving fluid boundary. A change of bubble mass corresponds to a positive (gain) resp. negative (loss) boundary velocity $w_\alpha = \mathbf{w}_\alpha\cdot\boldsymbol{\eta}_\alpha = (\dot{\mathbf{q}}_\alpha + \dot{\mathbf{R}}_\alpha)\cdot\boldsymbol{\eta}_\alpha$.

Therefore, summation over α gives identical right hand sides of equations (12.3.12) and (10.3.48), i.e. total mass conservation.

12.3.3 Macroscopic momentum balances

For the liquid phase we use (12.2.22) with $\Psi = \rho\mathbf{v}$, $\mathbf{F} = \rho\mathbf{v}\otimes\mathbf{v} + p\mathbf{1}$, set $G = \rho\mathbf{g}$ and take p given by the equation of state (12.3.4) to obtain

$$\begin{aligned}
&\frac{\partial}{\partial t}[(1-c)\rho_L\mathbf{v}_L](t,\mathbf{x}) + \nabla_{\mathbf{x}}\cdot([(1-c)\overline{\rho\mathbf{v}\otimes\mathbf{v}}](t,\mathbf{x}) + (1-c)p_L\mathbf{1}) - (1-c)\rho_L\mathbf{g} \qquad (12.3.15)\\
&\quad= \sum_\alpha \oint_{I_\alpha(t)} [\rho\mathbf{v}(t,\mathbf{x}')\otimes[\mathbf{v}(t,\mathbf{x}') - \mathbf{w}_\alpha] + p(t,\mathbf{x}')\mathbf{1}]\cdot\boldsymbol{\eta}_\alpha\, \chi_a(\mathbf{x}-\mathbf{x}')\, dS\\
&\quad= \sum_\alpha \left(\oint_{I_\alpha(t)} \rho\mathbf{v}(t,\mathbf{x}')\otimes[\mathbf{v}(t,\mathbf{x}') - \mathbf{w}_\alpha]\cdot\boldsymbol{\eta}_\alpha\, \chi_a(\mathbf{x}-\mathbf{x}')\, dS \right.\\
&\qquad \left. + \oint_{I_\alpha(t)} p(t,\mathbf{x}')\boldsymbol{\eta}_\alpha\, \chi_a(\mathbf{x}-\mathbf{x}')\, dS \right).
\end{aligned}$$

For the disperse phase we now take (12.2.12) with $\Psi_\alpha(t) = \rho_\alpha(t)\dot{\mathbf{q}}_\alpha(t)$. This gives

$$\frac{\partial(c\rho_B\mathbf{v}_B)}{\partial t}(t,\mathbf{x}) + \nabla_{\mathbf{x}}\cdot(c\overline{\rho_\alpha\dot{\mathbf{q}}_\alpha\otimes\dot{\mathbf{q}}_\alpha})(t,\mathbf{x}) = c\overline{\left(\frac{(\rho_\alpha\dot{\mathbf{q}}_\alpha V_\alpha)^{\cdot}}{V_\alpha}\right)}(t,\mathbf{x}) = c\overline{\left(\frac{(m_\alpha\dot{\mathbf{q}}_\alpha)^{\cdot}}{V_\alpha}\right)}(t,\mathbf{x}).$$

Now we may consider (12.3.8) on the right hand side. We obtain using (12.2.4)

$$\begin{aligned}
c\overline{\left(\frac{(m_\alpha\dot{\mathbf{q}}_\alpha)^{\cdot}}{V_\alpha}\right)}(t,\mathbf{x}) &= -c\overline{\left(\oint_{I_\alpha} p\boldsymbol{\eta}_\alpha dS/V_\alpha\right)} + c\overline{\left(\frac{m_\alpha}{V_\alpha}\right)}\mathbf{g} + c\overline{\left(\frac{\dot m_\alpha(t)}{4\pi R_\alpha(t)^2}\oint_{I_\alpha}\mathbf{v}dS/V_\alpha\right)}\\
&= \sum_\alpha\left(-\oint_{I_\alpha} p\boldsymbol{\eta}_\alpha dS + \frac{\dot m_\alpha(t)}{4\pi R_\alpha(t)^2}\oint_{I_\alpha}\mathbf{v}dS\right)\chi_a(\mathbf{x}-\mathbf{q}_\alpha(t)) + c\rho_B\mathbf{g}. \qquad (12.3.16)
\end{aligned}$$

Again the momenta must balance across the interfaces. In analogy to the above arguments for the mass balance, we obtain the momentum balance on the interfaces

$$\begin{aligned}
&\oint_{I_\alpha} p\eta_\alpha^j dS - \frac{\dot m_\alpha(t)}{4\pi R_\alpha(t)^2}\oint_{I_\alpha} v^j dS\\
&\qquad\qquad = \oint_{I_\alpha}\rho v^j[\mathbf{v}-\mathbf{w}_\alpha]\cdot\boldsymbol{\eta}_\alpha\, dS + \oint_{I_\alpha} p\eta_\alpha^j\, dS\,.
\end{aligned}$$

This equation obviously holds, because of the mass balance at the interface

$$-\frac{\dot m_\alpha(t)}{4\pi R_\alpha(t)^2}\oint_{I_\alpha} v^j dS = \oint_{I_\alpha}\rho v^j[\mathbf{v}-\mathbf{w}_\alpha]\cdot\boldsymbol{\eta}_\alpha\, dS\,. \tag{12.3.17}$$

12.3.4 Macroscopic energy balances

To obtain an energy balance equation for the liquid phase, we again use (12.2.22) with $\Psi = \rho e$, $\mathbf{F} = (\rho e + p)\mathbf{v} + \mathbf{Q}$ and $G = \rho \mathbf{g} \cdot \mathbf{v}$. We get

$$\begin{aligned}\frac{\partial}{\partial t}(1-c)\rho_L e_L + \nabla_x \cdot (1-c)\overline{(\rho e + p)\mathbf{v} + \mathbf{Q}} - (1-c)\rho_L \mathbf{g}\cdot\mathbf{v}_L \\ = \sum_\alpha \oint_{I_\alpha} ((\rho e + p)\mathbf{v} - \rho e \mathbf{w} + \mathbf{Q}) \cdot \eta \chi_a(\mathbf{x} - \mathbf{q}_\alpha)\, dS \\ = \sum_\alpha \oint_{I_\alpha} (\rho(\mathbf{v}-\mathbf{w})e + p\mathbf{v} + \mathbf{Q}) \cdot \eta \chi_a(\mathbf{x} - \mathbf{q}_\alpha)\, dS \end{aligned} \tag{12.3.18}$$

Again we take for the disperse phase (12.2.12) with $\Psi_\alpha(t) = \rho_\alpha(t) e_\alpha(t)$ to obtain

$$\frac{\partial c\rho_B e_B}{\partial t} + \nabla_{\mathbf{x}} \cdot (c\overline{\rho_\alpha e_\alpha \dot{\mathbf{q}}_\alpha})(t,\mathbf{x}) = c\overline{\left(\frac{(m_\alpha e_\alpha)^{\cdot}}{V_\alpha}\right)}(t,\mathbf{x})\,. \tag{12.3.19}$$

For the right hand side of (12.3.19) we have

$$c\overline{\left(\frac{(m_\alpha e_\alpha)^{\cdot}}{V_\alpha}\right)}(t,\mathbf{x}) + c\rho_B \mathbf{g}\cdot\mathbf{v}_B = -\sum_\alpha \oint_{I_\alpha} (\rho(\mathbf{v}-\mathbf{w})e + p\mathbf{v} + \mathbf{Q}) \cdot \eta \chi_a(\mathbf{x} - \mathbf{q}_\alpha)\, dS\,.$$

This implies energy conservation at the interface.

12.4 Closure relations

The PDE system, we are interested in, relies on the balance equations that were derived in the last section. In these equations several quantities appear that must be related to the variables of the model, namely

$$\overline{\left(\frac{\dot{\mathbf{q}}_\alpha}{V_\alpha}\right)},\quad \overline{\left(\frac{\dot{R}_\alpha}{R_\alpha}\right)},\quad \overline{\left(\frac{\dot{m}_\alpha}{V_\alpha}\right)},\quad \overline{\rho_\alpha(t)\dot{\mathbf{q}}_\alpha \otimes \dot{\mathbf{q}}_\alpha},\quad \overline{\frac{1}{V_\alpha}\oint_{I_\alpha} p\eta_\alpha^j dS},\quad \overline{(\rho e + p)\mathbf{v} + \mathbf{Q}},$$

$$\overline{\left(\frac{\dot{m}_\alpha(t)}{4\pi R_\alpha(t)^2}\oint_{I_\alpha} v^j dS/V_\alpha\right)},\quad \overline{\rho\mathbf{v}\otimes\mathbf{v}},\quad \overline{\rho_\alpha e_\alpha \dot{\mathbf{q}}_\alpha},\quad \overline{\frac{1}{V_\alpha}\oint (\rho(\mathbf{v}-\mathbf{w})e + p\mathbf{v} + \mathbf{Q})\cdot\eta\, ds}.$$

Now we will modify these expressions in order to obtain a closed system of equations. At first we introduce the *cold closure assumption* to simplify the first and fourth term. To this end we decompose the bubble velocity $\dot{\mathbf{q}}_\alpha$ as $\dot{\mathbf{q}}_\alpha = \mathbf{v}_B + \mathbf{C}_\alpha$. The cold closure assumption ignores the excess velocity $\mathbf{C}_\alpha$, this means we ignore any stochastic motion of the bubbles. Using (12.2.6) and (12.2.5) this assumption leads to

$$\overline{\left(\frac{\dot{\mathbf{q}}_\alpha}{V_\alpha}\right)} = n\mathbf{v}_B \qquad \text{and} \qquad \overline{\rho_\alpha(t)\dot{\mathbf{q}}_\alpha \otimes \dot{\mathbf{q}}_\alpha} = \rho_B \mathbf{v}_B \otimes \mathbf{v}_B\,. \tag{12.4.1}$$

Alternatively one could introduce a Reynolds stress tensor. This requires additional modeling in order to close the system. It is no easy task, see e.g. Drew and Passman [5].

Similarly we set

$$\overline{\rho\mathbf{v}\otimes\mathbf{v}} = \rho_L \mathbf{v}_L \otimes \mathbf{v}_L \quad , \quad \overline{\rho_\alpha e_\alpha \dot{\mathbf{q}}_\alpha} = \rho_B \mathbf{v}_B e_B \quad \text{and} \quad \overline{(\rho e + p)\mathbf{v}} = (\rho_L e_L + p_L)\mathbf{v}_L$$

and define the averaged bubble resp. liquid internal energy

$$u_B := e_B - \frac{1}{2}\mathbf{v}_B^2 \qquad \text{and} \qquad u_L := e_L - \frac{1}{2}\mathbf{v}_L^2\,.$$

Further we define the averaged temperatures of the phases

$$T_B := (u_B - u_{ref}(T_{ref}))\frac{m_0}{zk} + T_{ref} \qquad \text{and}$$

$$T_L := \frac{1}{c_*}\left(u_L - u_{ref}(T_{ref},\rho_{ref}) - (p_{ref}-K)\left(\frac{1}{\rho_{ref}}-\frac{1}{\rho_L}\right) - \frac{K}{\rho_{ref}}\ln\frac{\rho}{\rho_{ref}}\right) + T_{ref}$$

with the same reference data as in (12.3.6) and (12.3.7). With this definition we set

$$\overline{\mathbf{Q}} = -\kappa\nabla T_L\,.$$

Next we calculate the second and third expression of our list. At first we have by definition

$$\overline{c\left(\frac{\dot R_\alpha}{R_\alpha}\right)}(t,\mathbf{x}) = \sum_\alpha \frac{\dot R_\alpha(t)}{R_\alpha(t)}\chi_\alpha(\mathbf{x}-\mathbf{q}_\alpha(t))V_\alpha(t)\,,\ \overline{c\left(\frac{\dot m_\alpha}{V_\alpha}\right)}(t,\mathbf{x}) = \sum_\alpha \dot m_\alpha(t)\chi_\alpha(\mathbf{x}-\mathbf{q}_\alpha(t))\,.$$

The evolution of $R_\alpha(t)$ and $m_\alpha(t)$ was studied in [4] for a single bubble. There we considered various model equations without and with phase transition. These equations are used here to determine $\dot R = \overline{\dot R_\alpha}$ and $\dot m = \overline{\dot m_\alpha}$ by the simplifying assumption that we set

$$\overline{\left(\frac{\dot R_\alpha}{R_\alpha}\right)} = \frac{\dot R}{R} \qquad \text{and} \qquad \overline{\left(\frac{\dot m_\alpha}{V_\alpha}\right)} = \frac{\dot m}{V}\,, \tag{12.4.2}$$

where R and V denote the mean bubble radius resp. the mean bubble volume. These quantities are related to the volume fraction c and the number density cn. We have

$$\frac{c}{cn} = \frac{1}{n} = V = \frac{4\pi R^3}{3}\,. \tag{12.4.3}$$

The right hand sides of (12.4.2) are calculated by means of the models from [4], see Section 6 for more details.

Further, we now replace the fifth term and the seventh term of the list. We use equation (12.3.17) and the interfacial momentum balance equation (12.3.10). For the spherical bubble with index α the mean curvature is given by $-1/R_\alpha$. Therefore we have

$$\begin{aligned}\oint_{I_\alpha}\left(\rho v^j[\mathbf{v}-\mathbf{w}_\alpha]\cdot\boldsymbol{\eta}_\alpha + p\eta_\alpha^j\right)\,dS &= \oint_{I_\alpha}\left(\rho_\alpha v_\alpha^j[\mathbf{v}_\alpha-\mathbf{w}_\alpha]\cdot\boldsymbol{\eta}_\alpha + (p_\alpha - \frac{2\sigma}{R_\alpha})\eta_\alpha^j\right)dS\\ &= -\frac{\dot m_\alpha}{4\pi R_\alpha^2}\oint v_\alpha^j\,dS = -\frac{\dot m_\alpha}{4\pi R_\alpha^2}\oint \dot q_\alpha^j\,dS\\ &= -\dot m_\alpha \dot q_\alpha^j\,.\end{aligned} \tag{12.4.4}$$

This expression is zero in the radially symmetric case of a single spherical bubble.

In order to modify the last expression of the list, we use the interface balances for energy (12.3.11) and momentum (12.3.10) as well as the mass balance at the interface (12.3.9) to obtain

$$\begin{aligned}\frac{1}{V_\alpha}\oint(\rho(\mathbf{v}-\mathbf{w})e + p\mathbf{v} + \mathbf{Q})\cdot\eta\,ds &= \frac{1}{V_\alpha}\oint(\rho_\alpha(\mathbf{v}_\alpha-\mathbf{w})e_\alpha + p_\alpha\mathbf{v}_\alpha + \mathbf{Q}_\alpha + 2\sigma k_m\mathbf{w})\cdot\eta\,ds\\ &= -\frac{\dot m_\alpha e_\alpha}{V_\alpha} - \frac{p_\alpha\dot m_\alpha}{\rho_\alpha V_\alpha} + \frac{3p_\alpha\dot R_\alpha}{R_\alpha} - \frac{6\sigma\dot R_\alpha}{R_\alpha^2} + \frac{1}{V_\alpha}\oint\mathbf{Q}_\alpha\cdot\eta\,ds\end{aligned}$$

with

$$\frac{1}{V_\alpha}\oint\mathbf{Q}_\alpha\cdot\eta\,ds = \frac{3Q_\alpha^I}{R_\alpha}\,.$$

Integrating the energy balance equation for a radial symmetric homogeneous bubble

$$r^2 p_\alpha\frac{\partial}{\partial t}\ln\frac{T_\alpha^z}{\rho_\alpha} + \frac{\partial r^2 Q_\alpha}{\partial r} = 0$$

over the whole bubble domain we obtain

$$\frac{3Q_\alpha^I}{R_\alpha} = -\rho_\alpha\dot T_\alpha\frac{kz}{m_0} + \frac{p_\alpha\dot m_\alpha}{\rho_\alpha V_\alpha} - \frac{3p_\alpha\dot R_\alpha}{R_\alpha}\,.$$

As above, we set $\overline{\Pi}_m = \Pi_m$ with

$$\Pi_m^j = -c\frac{\dot{m}v_B^j}{\frac{4}{3}\pi R^3}\,. \tag{12.4.5}$$

Similarly, we define

$$\Pi_c = 3c\frac{\dot{R}}{R} \quad , \quad \Pi_\rho = c\frac{\dot{m}}{\frac{4}{3}\pi R^3} \quad \text{and} \quad \Pi_e = c\frac{\dot{m}e_B}{\frac{4}{3}\pi R^3} + c\rho_B\dot{T}\frac{kz}{m_0} + 6c\frac{\sigma\dot{R}}{R^2}\,. \tag{12.4.6}$$

Thus we end up with 8 partial differential equations for the determination of the variables number density n, volume fraction of the disperse phase c, densities of the phases ρ_L, ρ_B, velocities of the phases $\mathbf{v}_L$, $\mathbf{v}_B$ and energy of the phases e_L, e_B. In summary the system of partial differential equations can be written as

$$\begin{aligned}
\frac{\partial cn}{\partial t} + \nabla_{\mathbf{x}}\cdot(c\,n\mathbf{v}_B) &= 0\,,\\
\frac{\partial c}{\partial t} + \nabla_{\mathbf{x}}\cdot(c\,\mathbf{v}_B) &= \Pi_c\,,\\
\frac{\partial}{\partial t}[(1-c)\rho_L] + \nabla_{\mathbf{x}}\cdot[(1-c)\rho_L\mathbf{v}_L] &= -\,\Pi_\rho\,,\\
\frac{\partial c\rho_B}{\partial t} + \nabla_{\mathbf{x}}\cdot(c\,\rho_B\mathbf{v}_B) &= \Pi_\rho\,,\\
\frac{\partial}{\partial t}[(1-c)\rho_L v_L^j] + \nabla_{\mathbf{x}}\cdot[(1-c)\rho_L v_L^j\mathbf{v}_L] + \frac{\partial(1-c)p_L}{\partial x_j} - (1-c)\rho_L g^j &= -\,\Pi_m^j\,,\\
\frac{\partial(c\rho_B v_B^j)}{\partial t}(t,\mathbf{x}) + \nabla_{\mathbf{x}}\cdot(c\,\rho_B v_B^j\mathbf{v}_B) - c\rho_B g^j &= \Pi_m^j\,,\\
\frac{\partial}{\partial t}(1-c)\rho_L e_L + \nabla_x\cdot(1-c)\left((\rho_L e_L + p_L)\mathbf{v}_L + \mathbf{Q}_L\right) - (1-c)\rho_L\,\mathbf{g}\cdot\mathbf{v}_L &= -\,\Pi_e\,,\\
\frac{\partial c\rho_B e_B}{\partial t} + \nabla_{\mathbf{x}}\cdot(c\rho_B e_B\mathbf{v}_B) - c\rho_B\,\mathbf{g}\cdot\mathbf{v}_B &= \Pi_e\,.
\end{aligned} \tag{12.4.7}$$

Using (12.4.3), the balance equation for the number density can easily be rewritten in terms of the more descriptive quantity R. We obtain

$$\frac{\partial cR}{\partial t} + \nabla_{\mathbf{x}}\cdot(c\,R\mathbf{v}_B) = \frac{4}{3}R\Pi_c\,.$$

With the definition $\Pi_R := 4c\dot{R}$, we give the alternative system (12.4.8) of 8 partial differential equations for the determination of the variables mean bubble radius R, volume fraction of the disperse phase c, densities of the phases ρ_L, ρ_B, velocities of the phases $\mathbf{v}_L$, $\mathbf{v}_B$ and energy of the phases e_L, e_B

$$\begin{aligned}
\frac{\partial cR}{\partial t} + \nabla_{\mathbf{x}}\cdot(c\,R\mathbf{v}_B) &= \Pi_R\,,\\
\frac{\partial c}{\partial t} + \nabla_{\mathbf{x}}\cdot(c\,\mathbf{v}_B) &= \Pi_c\,,\\
\frac{\partial}{\partial t}[(1-c)\rho_L] + \nabla_{\mathbf{x}}\cdot[(1-c)\rho_L\mathbf{v}_L] &= -\,\Pi_\rho\,,\\
\frac{\partial c\rho_B}{\partial t} + \nabla_{\mathbf{x}}\cdot(c\,\rho_B\mathbf{v}_B) &= \Pi_\rho\,,\\
\frac{\partial}{\partial t}[(1-c)\rho_L v_L^j] + \nabla_{\mathbf{x}}\cdot[(1-c)\rho_L v_L^j\mathbf{v}_L] + \frac{\partial(1-c)p_L}{\partial x_j} - (1-c)\rho_L g^j &= -\,\Pi_m^j\,,\\
\frac{\partial(c\rho_B v_B^j)}{\partial t}(t,\mathbf{x}) + \nabla_{\mathbf{x}}\cdot(c\,\rho_B v_B^j\mathbf{v}_B) - c\rho_B g^j &= \Pi_m^j\,,\\
\frac{\partial}{\partial t}(1-c)\rho_L e_L + \nabla_x\cdot(1-c)\left((\rho_L e_L + p_L)\mathbf{v}_L + \mathbf{Q}_L\right) - (1-c)\rho_L\,\mathbf{g}\cdot\mathbf{v}_L &= -\,\Pi_e\,,\\
\frac{\partial c\rho_B e_B}{\partial t} + \nabla_{\mathbf{x}}\cdot(c\rho_B e_B\mathbf{v}_B) - c\rho_B\,\mathbf{g}\cdot\mathbf{v}_B &= \Pi_e\,.
\end{aligned} \tag{12.4.8}$$

Finally it remains to give the equation of state for the liquid pressure. The averaging process is simple here. It relies on the corresponding microscopic equation of state (12.3.4)

$$(1-c)p_L = (1-c)\overline{[p_{ref} + K(\rho/\rho_{ref} - 1)]} = (1-c)\,[p_{ref} + K(\rho_L/\rho_{ref} - 1)]$$

since p_{ref}, K and ρ_{ref} are constants giving a linear relation between ρ and p.

The volume fraction of the carrier phase is always taken to be $1-c$ and does not need to be determined. To solve the system presented one needs a complete set of initial data. In addition to the initial data for the unknowns in (12.4.7), we need initial data for $\dot{R}$. Analogously to previous calculations these data can be found using

$$\dot{R}(t) = \frac{\sum_\alpha R_\alpha^2(t)\dot{R}_\alpha(t)\,\chi_a(\mathbf{x} - \mathbf{q}_\alpha(t))}{c/R(t,\mathbf{x})} \tag{12.4.9}$$

at $t = 0$, which results from the averaging of the change of volume density, see also the following sections.

Next we will explicitly study four problems, in which simplified flows are involved. To illustrate clearly, how to deal with the source terms resp. evolution laws, we restrict ourselves to the isothermal subproblem for a single spherical bubble. First we investigate the mathematical properties of the resulting model in Section 12.5. Several evolution laws are available for the computation of $\dot{R}$, $\dot{m}$ and $\dot{T}$, see [4]. In Section 12.6 we summarize the results of [4] and we explain their application to the system (12.4.7). Numerical results are then presented in Section 12.7.

12.5 Mathematical properties of the radial symmetric system

Considering spherical symmetry and assuming an isothermal process we get the simplest case. This means that we have a bubble with its center in the origin which gives us some test cases for comparisons with the results of our paper [4].

As already mentioned, the gravity terms drop out, further $\Pi_m = 0$ and the energy balances become redundant. The system corresponding to (12.4.7) consists of 6 equations of the following form

$$\frac{\partial c}{\partial t} + \frac{\partial c v_B}{\partial r} = -\frac{2}{r} c v_B + \Pi_c \tag{12.5.1}$$

$$\frac{\partial cn}{\partial t} + \frac{\partial cn v_B}{\partial r} = -\frac{2}{r} cR v_B \tag{12.5.2}$$

$$\frac{\partial c\rho_B}{\partial t} + \frac{\partial c\rho_B v_B}{\partial r} = -\frac{2}{r} c\rho_B v_B + \Pi_\rho \tag{12.5.3}$$

$$\frac{\partial c\rho_B v_B}{\partial t} + \frac{\partial c\rho_B v_B^2}{\partial r} = -\frac{2}{r} c\rho_B v_B^2 \tag{12.5.4}$$

$$\frac{\partial (1-c)\rho_L}{\partial t} + \frac{\partial (1-c)\rho_L v_L}{\partial r} = -\frac{2}{r}(1-c)\rho_L v_L - \Pi_\rho \tag{12.5.5}$$

$$\frac{\partial (1-c)\rho_L v_L}{\partial t} + \frac{\partial (1-c)\rho_L v_L^2}{\partial r} + \frac{\partial (1-c)p_L}{\partial r} = -\frac{2}{r}(1-c)\rho_L v_L^2\,. \tag{12.5.6}$$

Due to the radial symmetry, one obtains additional geometric source terms on the right hand side of the equations. All sources are non-differential, this means, that the system is in divergence form in contrast to other two-phase models, see for instance Baer and Nunziato [2] or Stewart and Wendroff [19].

For a single bubble in the origin it must hold that $v_B(t,r) = 0$ for all t. Indeed, this is the unique solution of the above system with the initial data $v_B(0,r) = 0$. With $v_B(t,r) = 0$ for all t equation (12.5.2) reduces to $\frac{\partial cn}{\partial t} = 0$ and becomes redundant for given initial data $n(0,r)$. Further, the equation (12.5.4) drops out. The system (12.5.1-12.5.6) reduces to a system of only 4 equations of the much more simple form

$$\frac{\partial c}{\partial t} = \Pi_c \tag{12.5.7}$$

$$\frac{\partial c\rho_B}{\partial t} = \Pi_\rho \tag{12.5.8}$$

$$\frac{\partial (1-c)\rho_L}{\partial t} + \frac{\partial (1-c)\rho_L v_L}{\partial r} = -\frac{2}{r}(1-c)\rho_L v_L - \Pi_\rho \tag{12.5.9}$$

$$\frac{\partial (1-c)\rho_L v_L}{\partial t} + \frac{\partial (1-c)\rho_L v_L^2}{\partial r} + \frac{\partial (1-c)p_L}{\partial r} = -\frac{2}{r}(1-c)\rho_L v_L^2\,. \tag{12.5.10}$$

The non-differential sources on the right hand side do not influence the mathematical type of the system. Therefore it is sufficient to investigate the homogeneous system. Using $\frac{\partial p_L}{\partial \rho_L} = \frac{a_L^2}{\rho_L}$ with the sound speed a_L of the liquid for convenience we write the homogeneous system in primitive variables

$$\frac{\partial \mathbf{u}}{\partial t} + \mathbf{A}(\mathbf{u})\frac{\partial \mathbf{u}}{\partial r} = \mathbf{0}\,,$$

where $\mathbf{u} = (c, \rho_B, \rho_L, v_L)^T$ denotes the independent unknowns. The matrix $\mathbf{A}$ is given by

$$\mathbf{A} = \begin{pmatrix} 0 & 0 & 0 & 0 \\ 0 & 0 & 0 & 0 \\ -\frac{\rho_L v_L}{1-c} & 0 & v_L & \rho_L \\ -\frac{p_L}{(1-c)\rho_L} & 0 & \frac{a_L^2}{\rho_L} & v_L \end{pmatrix} \tag{12.5.11}$$

with $p_L = p_{ref} + K(\rho_{ref}/\rho_L - 1)$. After some simple calculations one gets the eigenvalues of $\mathbf{A}$ as

$$\lambda_1 = v_L - a_L \quad \lambda_2 = \lambda_3 = 0\,(= v_B) \quad \lambda_4 = v_L + a_L\,. \tag{12.5.12}$$

and 4 corresponding linearly independent eigenvectors

$$\mathbf{e}_1 = \begin{pmatrix} 0 \\ 0 \\ -\frac{\rho_L}{a_L} \\ 1 \end{pmatrix} \quad \mathbf{e}_2 = \begin{pmatrix} 0 \\ 1 \\ 0 \\ 0 \end{pmatrix} \quad \mathbf{e}_3 = \begin{pmatrix} \frac{a_L^2 - v_L^2}{p_L - \rho_L v_L^2}(1-c) \\ 0 \\ 1 \\ \frac{v_L}{\rho_L}\frac{\rho_L a_L^2 - p_L}{p_L - \rho_L v_L^2} \end{pmatrix} \quad \mathbf{e}_4 = \begin{pmatrix} 0 \\ 0 \\ \frac{\rho_L}{a_L} \\ 1 \end{pmatrix}. \tag{12.5.13}$$

Obviously, the system is non-strictly hyperbolic.

Considering a Riemann problem one obtains the Riemann invariants c, ρ_B of a 1-wave and the 4-wave. This means, that these quantities do not change across the 1- and 4-wave. For the double eigenvalue $\lambda = 0$ one has a contact discontinuity. Here all quantities change. The Riemann invariants are given by

$$(1-c)\rho_L v_L = \text{const} \qquad \text{and} \quad (1-c)(\rho_L v_L^2 + p_L) = \text{const}\,. \tag{12.5.14}$$

Remark 12.5.1. *If one further excludes phase transition, then we have $\Pi_\rho = 0$ and the bubble mass balance becomes redundant as well for given initial data $\rho_B(0, r)$. The system reduces to the equations (12.5.7), (12.5.9), and (12.5.10). In the Jacobian matrix $\mathbf{A}$ the second row and column drop out and one obtains the eigenvalues*

$$\lambda_1 = v_L - a_L \quad \lambda_2 = 0\,(= v_B) \quad \lambda_3 = v_L + a_L$$

and the corresponding eigenvectors

$$\mathbf{e}_1 = \begin{pmatrix} 0 \\ -\frac{\rho_L}{a_L} \\ 1 \end{pmatrix} \quad \mathbf{e}_2 = \begin{pmatrix} \frac{a_L^2 - v_L^2}{p_L - \rho_L v_L^2}(1-c) \\ 1 \\ \frac{v_L}{\rho_L}\frac{\rho_L a_L^2 - p_L}{p_L - \rho_L v_L^2} \end{pmatrix} \quad \mathbf{e}_3 = \begin{pmatrix} 0 \\ \frac{\rho_L}{a_L} \\ 1 \end{pmatrix}.$$

The system is strictly hyperbolic with the Riemann invariant c of the 1- and 3- wave. For the eigenvalue $\lambda = 0$ one has a contact discontinuity with the same Riemann invariants as above, see (12.5.14).

12.6 Production terms

In order to calculate the production terms $(12.4.6)_1$, $(12.4.6)_2$, and (12.4.5), we need evolution laws for the radius $\dot{R}$ as well as the total mass $\dot{m}$ of a single bubble. In [4] several models for a single bubble system were derived. These models take into account resp. neglect the effects of mass transfer, heat conduction, and compressibility of the surrounding liquid according to various choices one can make.

To model the production terms in the paper at hand we use isothermal models for a pure water vapor bubble, see [4]. To derive such a model one assumes a single pure water vapor bubble in a sufficiently large domain, surrounded by pure liquid water. For simplicity we assume spherical symmetry and homogeneity

in the vapor phase. This means that the density ρ_B, and consequently the pressure, depends only on time and is constant in space.

The mass transfer is described by a kinetic relation, based on the classical Hertz-Knudsen theory. For details we refer to Section 2 in [4]. With the further assumption of incompressible liquid water, the evolution of the bubble can be described by the following system of ordinary differential equations

$$\dot{m} = \frac{4\pi R^2 \rho_B m_0}{\sqrt{2\pi m_0 kT}} \left[\frac{1}{\rho_L} \left(\frac{\rho_B kT}{m_0} - \frac{2\sigma}{R} - \bar{p} \right) - \frac{kT}{m_0} \ln \frac{\rho_B kT}{\bar{p} m_0} - \frac{1}{2} \left(\frac{1}{\rho_L} - \frac{1}{\rho_B} \right)^2 \left(\frac{\dot{m}}{4\pi R^2} \right)^2 \right] , \tag{12.6.1}$$

$$\dot{F} = \frac{F^2}{2R^3} - \frac{R}{\rho_L} \left(p_0 - \frac{\rho_B kT}{m_0} + \frac{2\sigma}{R} + \left(\frac{1}{\rho_L} - \frac{1}{\rho_B} \right) \left(\frac{\dot{m}}{4\pi R^2} \right)^2 \right) , \tag{12.6.2}$$

$$\dot{R} = \frac{F}{R^2} + \frac{\dot{m}}{4\pi R^2 \rho_L} . \tag{12.6.3}$$

This is a special case of Case 2 in [4]. There a mixture of water vapor and an inert gas is assumed. The dot $\dot{}$ denotes the time derivative.

Using (12.6.1) one can calculate $\dot{m}$. The equation (12.6.1) is quadratic. The positive root gives the solution. To solve this system of ordinary differential equations one needs values for R, ρ_B and ρ_L. The values ρ_B and ρ_L are given by the values of the system (12.5.7-12.5.10) of partial differential equations. As mentioned before the averaged volume V is given by $V = 1/n$. Therefore, the averaged radius R can be calculated using $R = \sqrt[3]{\frac{3}{4\pi n}}$. In our case we have $\frac{\partial cn}{\partial t} = 0$. This means that

$$R = R_0 \sqrt[3]{\frac{c}{c_0}} \qquad \text{with} \qquad R_0 = \sqrt[3]{\frac{3}{4\pi n_0}} .$$

Further one needs the mass of a single water molecule m_0, the Boltzmann constant k, the outer pressure p_0, the temperature T, and the reference values for the surficial tension σ of water as well as for the saturation pressure $\bar{p}$ corresponding to T.

For a complete set of initial data one needs initial values for $\dot{R}$, see (12.4.9). Alternatively one can assume the system initially to be at rest and set $F(0) = 0$. This implies initial data for $\dot{R}$.

For F we have $F = v_L^I \cdot R^2$, see [4]. Using (12.6.2) and for instance a Runge-Kutta method one gets values for F in a new time step. Using (12.6.1) together with equation (12.6.3) gives values for $\dot{R}$.

In [4] it was shown, that for *large* pressure differences the compressibility of the liquid plays an important role. Taking into account compressibility of the liquid in a weak sense, one starts with the linearized Euler equations and obtains a wave equation. Its solution we denote by Φ. Assuming that the domain is large enough that the bubble is not affected by reflections at the outer boundary, one derives instead of (12.6.2) and (12.6.3) the following equations

$$\Phi'(R - a_L t) = \frac{R}{\rho_L a_L} \left(\frac{\rho_B kT}{m_0} - \frac{2\sigma}{R} - \left(\frac{1}{\rho_L} - \frac{1}{\rho_B} \right) \left(\frac{\dot{m}}{4\pi R^2} \right)^2 - p_0 \right) \tag{12.6.4}$$

$$\dot{R} = -\frac{\Phi(R - a_L t)}{R^2} + \frac{\Phi'(R - a_L t)}{R} + \frac{\dot{m}}{4\pi R^2 \rho_L} , \tag{12.6.5}$$

where a_L denotes the speed of sound in the liquid. As before $\dot{}$ denotes the time derivative, whereas $'$ denotes the derivative for the argument.

Instead of (12.6.1) one gets

$$\dot{m} = \frac{4\pi R^2 \rho_B m_0}{\sqrt{2\pi m_0 kT}} \left[\frac{K}{\rho_L} \ln \left(1 + \frac{\frac{\rho_B kT}{m_0} - \frac{2\sigma}{R} - \left(\frac{1}{\rho_L} - \frac{1}{\rho_B} \right) \left(\frac{\dot{m}}{4\pi R^2} \right)^2}{K} \right) - \frac{kT}{m_0} \ln \frac{\rho_B kT}{m_0 \bar{p}} + \left(\frac{1}{\rho_L^2} - \frac{1}{\rho_B^2} \right) \left(\frac{\dot{m}}{4\pi R^2} \right)^2 \right] \tag{12.6.6}$$

with the liquid bulk modulus K. Because of the logarithm term this equation is transcendent. The calculation of $\dot{m}$ by an iterative method is expensive. Further one has to discuss the non-uniqueness,

what is unnecessarily complicated here. By linearization of the logarithm term one obtains equation (12.6.1), which is a sufficiently good approximation.

Therefore for a compressible model we use the equations (12.6.1), (12.6.4) and (12.6.5). In that case we need initial data for Φ.

Now we have two models taking into account phase transition to calculate the production terms in (12.5.7-12.5.10). If we exclude mass transfer we have $\dot{m} = 0$. The equations (12.6.2) and (12.6.3) resp. (12.6.4) and (12.6.5) then simplify.

12.7 Numerical results

For the current section we choose specific initial data. For these data we give numerical results for the two systems (12.6.1), (12.6.2), (12.6.3) resp. (12.6.1), (12.6.4), (12.6.5) of ordinary differential equations, in each case with and without phase transition. This gives us four test cases.

With the same initial data we solve the system (12.5.7-12.5.10) of partial differential equations for the radial symmetric case numerically and compare these results with the previous for all the four test cases.

12.7.1 Initial data

Let us assume a pure water vapor bubble in the origin surrounded by pure liquid water. This means, for the midpoint of the bubble we have $r = 0$ where r denotes the space coordinate. The outer boundary is chosen to be at $r = R_A = 0.3m$. This guaranties that the bubble is not affected by reflections at the outer boundary during the computation time. The temperature T is assumed to be $T = 293.15K$ and the outer pressure p_0 is the atmospheric pressure, $p_0 = 101300Pa$. Corresponding to T we give the reference values for the surficial tension $\sigma = 0.0725N/m$ and the saturation pressure $\bar{p} = 2330Pa$, see [8] or [25]. The mass of one water molecule is given by $m_0 = 2.9915 \cdot 10^{-26}kg$ and the Boltzmann constant by $k = 1.380658 \cdot 10^{-23}J/K$. Beside this we need the liquid bulk modulus K, which we chose to be $K = 2.08 \cdot 10^9 Pa$.

We choose the initial radius $R(0) = R_0 = 6 \cdot 10^{-4}m$ and assume that the bubble contains 10^{16} water molecules. Therefore the initial bubble mass is given by $m(0) = 2.9915 \cdot 10^{-10}kg$. Whereas, the initial bubble density is given by $\rho_B(0) = 0.3306kg/m^3$.

Further, in the beginning the system is assumed to be at rest. This means that the liquid velocity $v_L(0)$ equals to zero everywhere.

Especially at the interface, we have $v_L^I(0) = 0$. For the incompressible case $v_L^I = F/R^2$ holds, see [4]. We have $F(0) = 0$. According to the compressible case we have $\Phi(R(0)) = 0$.

12.7.1.1 Initial data for the averaged system (12.5.7-12.5.10)

The derivation of the corresponding initial data for the system (12.5.7-12.5.10) of partial differential equations for constant or piecewise constant data is quite simple. For that we need the formulas (12.2.3) and (12.2.4) as well as the radius R_a of the averaging ball. We choose $R_a = 5 \cdot R_0 = 3 \cdot 10^{-3}m$. For the concentration we get $c = 0.0008$ for $0 \leq r \leq 3 \cdot 10^{-3}m$ and $c = 0$ otherwise. For numerical aspects we choose $c = 10^{-8}$ instead of $c = 0$.

The computation of the initial data for the densities ρ_B, ρ_L, and the velocity v_L is trivial. We summarize the initial data in the neighborhood of the bubble in Figure 12.1. Besides the plots for the four unknowns c, ρ_B, ρ_L, v_L, we give plots for the averaged radius R and the liquid pressure p_L.

12.7.2 Numerical results for the ODE-systems

For the initial data given in the previous subsection we now want to calculate numerical results for the four test cases. We use a Runge-Kutta method method and obtain for the two cases without phase transition the results presented in Figure 12.2. In the case of an incompressible liquid one obtains an undamped oscillation for the evolution of the bubble radius, for a compressible liquid the oscillation is damped.

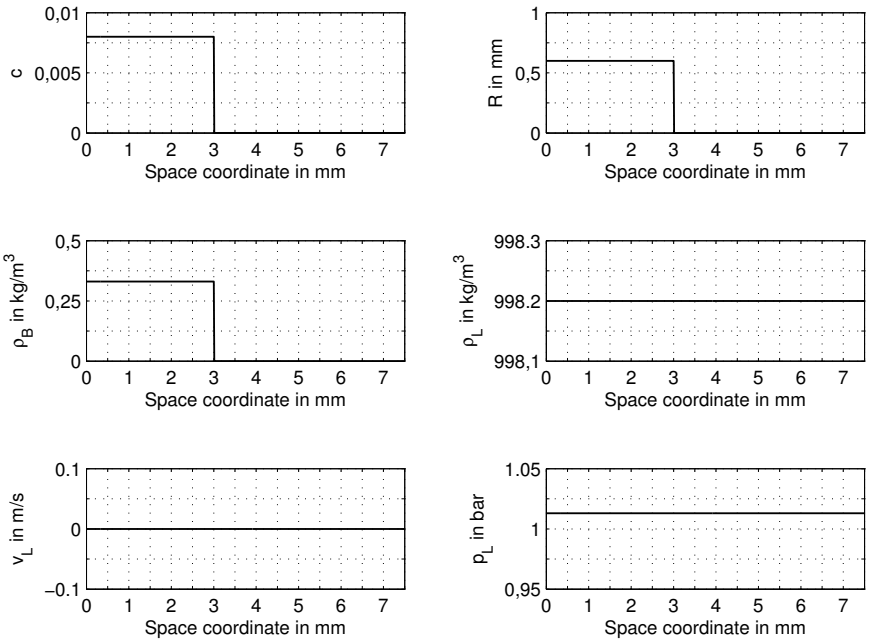

Figure 12.1: Initial data for (12.5.7-12.5.10) in the neighborhood of the bubble

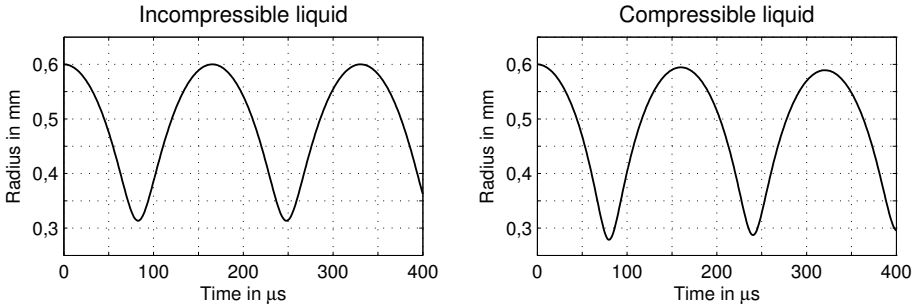

Figure 12.2: Bubble radius vs. time without phase transition, ODE-system

Taking into account mass transfer, it is clear from the physics of this situation that the bubble vanishes, see [4]. The numerical results for the test cases with phase transition are given in the following Figure 12.3.

12.7.3 Numerical results for the averaged system (12.5.7-12.5.10)

To solve the system (12.5.7-12.5.10) numerically we use Godunov operator splitting, see Toro [20], and further a Roe type Riemann solver for the homogeneous part of the system. For the latter finite volume method we follow the procedure in [1] resp. [7].

We denote the conserved variables $c, c\rho_B, (1-c)\rho_L, (1-c)\rho_L v_L$ by $\mathbf{v}$. Then the system (12.5.7-12.5.10) can be written in the form

$$\mathbf{v}_t + \mathbf{F}(\mathbf{v})_r = \mathbf{S}(\mathbf{v}) \qquad \text{with} \qquad \mathbf{v}(t^n, r) = \mathbf{v}^n \,.$$

The vector $\mathbf{S}(\mathbf{v})$ denotes the sources. By the splitting procedure one first solves the homogeneous part

$$\mathbf{v}_t + \mathbf{F}(\mathbf{v})_r = 0 \qquad \text{with} \qquad \mathbf{v}(t^n, r) = \mathbf{v}^n \,, \tag{12.7.1}$$

to obtain $\overline{\mathbf{v}}^{n+1}$. In a second step one determines

$$\frac{d}{dt}\mathbf{v} = \mathbf{S}(\mathbf{v})$$

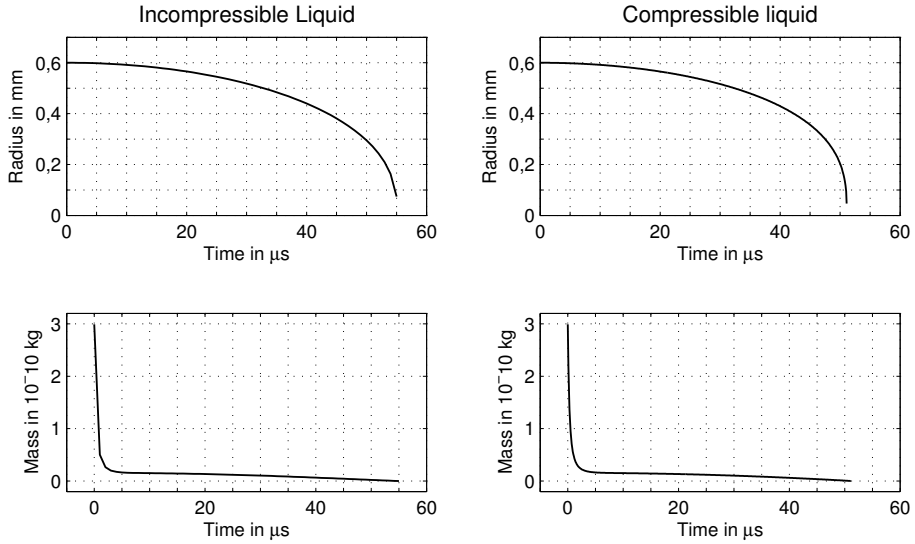

Figure 12.3: Bubble radius and bubble mass vs. time with phase transition, ODE-system

with initial data $\overline{\mathbf{v}}^{n+1}$ to obtain the data for the new time step $\mathbf{v}^{n+1}$.

To solve the homogeneous system (12.7.1) numerically, we again as in Section 12.5 rewrite the system in primitive variables $\mathbf{u}$

$$\frac{\partial \mathbf{u}}{\partial t} + \mathbf{A}(\mathbf{u})\frac{\partial u}{\partial r} = \mathbf{0}\,, \tag{12.7.2}$$

where $\mathbf{A}(\mathbf{u})$ is given in (12.5.11) and $\mathbf{u} = (c, \rho_B, \rho_L, v_L)^T$. At each cell boundary $r_{j+1/2}$ we consider the Riemann problem for (12.7.2) with initial data

$$\mathbf{u}(0,r) = \begin{cases} \mathbf{u}_j & r \le r_{j+1/2} \\ \mathbf{u}_{j+1} & r > r_{j+1/2}\,. \end{cases}$$

We calculate the Jacobian $\mathbf{A}(\overline{\mathbf{u}})$ in the average state $\overline{\mathbf{u}}_{j+1/2} = (\mathbf{u}_j + \mathbf{u}_{j+1})/2$. By eigenvector decomposition of $\mathbf{u}_{j+1} - \mathbf{u}_j$

$$\Delta\mathbf{u} = \mathbf{u}_{j+1} - \mathbf{u}_j = \sum_{n=1}^{4} x_n \mathbf{e}_n$$

we determine the coefficients x_n to find the intermediate state

$$\mathbf{u}^*_{j+1/2} = \mathbf{u}_j + \sum_{\lambda_n < 0} x_n \mathbf{e}_n$$

in the solution of the above Riemann problem, where the eigenvalues λ_n resp. eigenvectors $\mathbf{e}_n$ of $\mathbf{A}$ are given in (12.5.12) resp. (12.5.13). We get

$$\begin{aligned}
x_1 &= \frac{-\Delta\rho_L + \frac{\rho_L}{a_L}\Delta v_L + \frac{\Delta c}{1-c}\frac{1}{a_L}\frac{p_L - \rho_L a_L v_L}{a_L - v_L}}{2\rho_L/a_L} \\
x_2 &= \Delta\rho_B \\
x_3 &= \frac{\Delta c}{1-c}\,\frac{p_L - \rho_L v_L^2}{a_L^2 - v_L^2} \\
x_4 &= \frac{\Delta\rho_L + \frac{\rho_L}{a_L}\Delta v_L - \frac{\Delta c}{1-c}\frac{1}{a_L}\frac{p_L - \rho_L a_L v_L}{a_L - v_L}}{2\rho_L/a_L}\,.
\end{aligned}$$

Using the values $\mathbf{u}^*$ in a Finite Volume method we calculate approximations $\overline{\mathbf{V}}^{n+1}$ for $\overline{\mathbf{v}}^{n+1}$

$$\overline{\mathbf{V}}^{n+1} = \overline{\mathbf{v}}^n - \frac{\Delta t}{\Delta r}\left[\mathbf{v}(\mathbf{u}^+)^n_{j+1/2} - \mathbf{v}(\mathbf{u}^*)^n_{j-1/2}\right]\,.$$

Remark 12.7.1. *If we exclude phase transition the above calculations simplify according to Section 12.5.*

Finally, for the source term integration we again use the explicit Euler method. For our calculations we chose a CFL number of 0.9 and a spatial step size of $\Delta r = 1.2 \cdot 10^{-}5m$ and compute the following results. Note, that we do not plot the whole computational domain but only the bubble and its neighborhood.

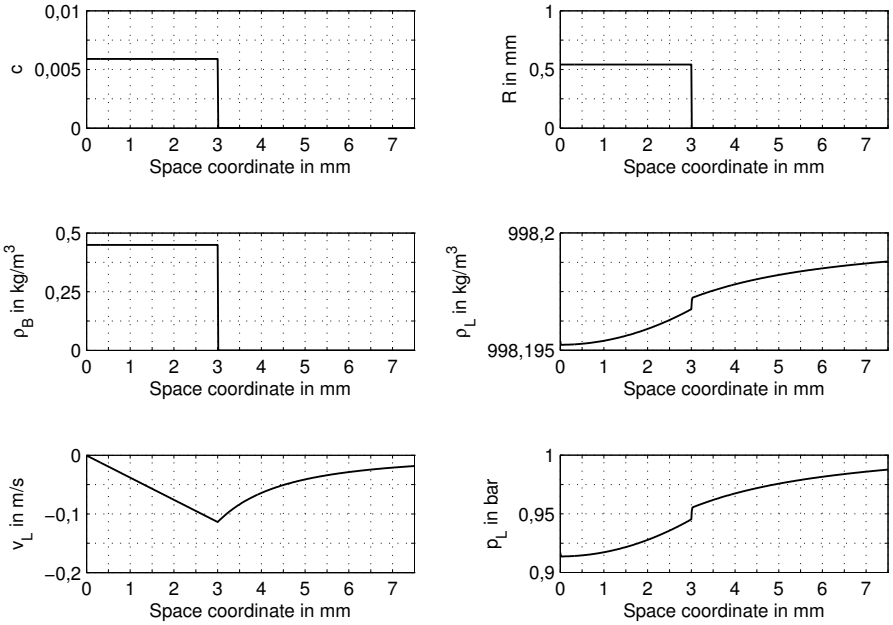

Figure 12.4: Numerical solution for $t = 40\mu s$, incompressible liquid without phase transition

Obviously the solutions for the radius evolution of the ODE systems are in very good agreement with the solutions of the averaged system with the corresponding sources.

12.A Appendix: Newton's second law with non-constant mass

Most textbook examples in classical mechanics deal only with the dynamics of bodies with constant mass. The following argument is taken mostly from Müller [15, Subsection 1.4.6]. Consider a closed system of a rocket R emitting burnt gases B. The masses m_R of the rocket and m_B of the burnt gas are changing in time. The burning rate is $-\dot{m}_R$. Let v be the constant speed relative to the rocket of the gas emitted in the direction of an axis chosen parallel to the movement of the rocket. Let v_R be the speed of the rocket along this axis. The speed of the burnt gas in the resting frame satisfies $v_B = v_R - v$. We have mass conservation $\dot{m}_R(t) + \dot{m}_B(t) = 0$. The total momentum of the burnt gas is given as

$$m_B v_B = -\int_{t_0}^{t} \dot{m}_R(\tau)(v_R(\tau) - v)\, d\tau.$$

Momentum conservation states that

$$0 = \frac{d}{dt}(m_R v_R + m_B v_B) = \dot{m}_R v_R + m_R \dot{v}_R - \frac{d}{dt}\int_{t_0}^{t} \dot{m}_R(\tau)(v_R(\tau) - v)\, d\tau$$

The fundamental theorem of calculus gives

$$0 = \dot{m}_R v_R + m_R \dot{v}_R - \dot{m}_R(t)(v_R(t) - v) = m_R \dot{v}_R + \dot{m}_R v.$$

This implies

$$m_R(t)\dot{v}_R(t) = -\dot{m}_R(t)v$$

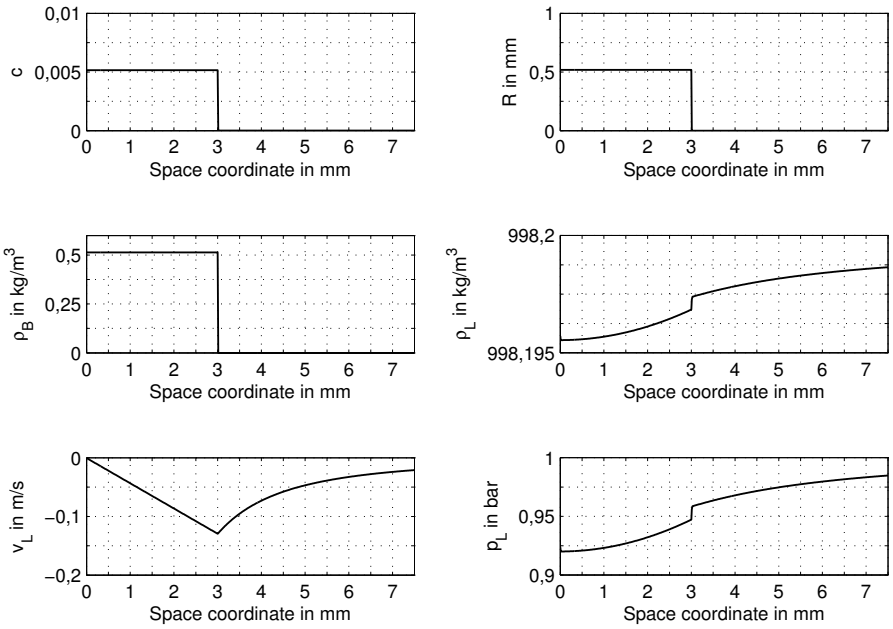

Figure 12.5: Numerical solution for $t = 40\mu s$, compressible liquid without phase transition

i.e. the thrust of the rocket is $\Theta = -\dot{m}_R v$. The above equation leads to

$$\frac{d}{dt}(m_R v_R) = \dot{m}_R v_R + m_R \dot{v}_R = \dot{m}_R(v_R - v) = \dot{m}_R v_B.$$

Identifying the particles with the rocket and the carrier phase with the burnt gas the term on the right hand side motivates the last term in (12.3.8).

12.B Appendix: Distributional derivatives

For the definition of distributional derivatives see e.g. Hörmander [9, Chapter 2], Warnecke [21, Appendix C]. Here we first consider the case of superposition of functions $f \in L^1_{loc}(\mathbb{R}^3)$ with $f(\mathbf{x} - \mathbf{q}(t))$ for a smooth vector field $\mathbf{q} \in \mathbb{R}^3$ needed in proofs of Section 2. We consider this as a distribution in $\mathbb{R}^4$. Take $\phi \in C_0^\infty(\mathbb{R}^4)$ then

$$\begin{aligned}
\langle \frac{d}{dt} f(\cdot - \mathbf{q}(t)) \,,\, \phi \rangle &= -\langle f(\cdot - \mathbf{q}(t)) \,,\, \frac{\partial}{\partial t}\phi \rangle \\
&= -\int_{\mathbb{R}^4} f(\mathbf{x} - \mathbf{q}(t)) \frac{\partial}{\partial t}\phi(t, \mathbf{x}) \; dt\, d\mathbf{x} \\
&= -\int_{\mathbb{R}^4} f(y) \frac{\partial}{\partial t}\phi(t, y + \mathbf{q}(t)) \; dt\, dy \\
&= -\int_{\mathbb{R}^4} f(y) \left[\frac{d}{dt}\phi(t, y + \mathbf{q}(t)) - \nabla_y \phi(t, y + \mathbf{q}(t)) \cdot \dot{\mathbf{q}} \right] \; dt\, dy \\
&= \int_{\mathbb{R}^4} f(y) \nabla_y \phi(t, y + \mathbf{q}(t)) \cdot \dot{\mathbf{q}} \; dt\, dy \\
&= \int_{\mathbb{R}^4} f(\mathbf{x} - \mathbf{q}(t)) \dot{\mathbf{q}} \cdot \nabla_{\mathbf{x}} \phi(t, \mathbf{x}) \; dt\, d\mathbf{x} \\
&= \langle f(\cdot - \mathbf{q}(t)) \dot{\mathbf{q}} \,,\, \nabla \phi \rangle \\
&= -\langle \nabla_{\mathbf{x}} f(\cdot - \mathbf{q}(t)) \cdot \dot{\mathbf{q}} \,,\, \phi \rangle.
\end{aligned}$$

The derivative $\nabla_{\mathbf{x}} \chi_a(\mathbf{x} - \mathbf{x}')$ has to be taken in the sense of distributions on $\mathbb{R}^3$ and is a singular signed vector measure $\boldsymbol{\mu}_{\partial B_a(\mathbf{x})}$ on the boundary $\partial B_a(\mathbf{x})$ with mass $-\boldsymbol{\eta}$ given by the outer normal. Take

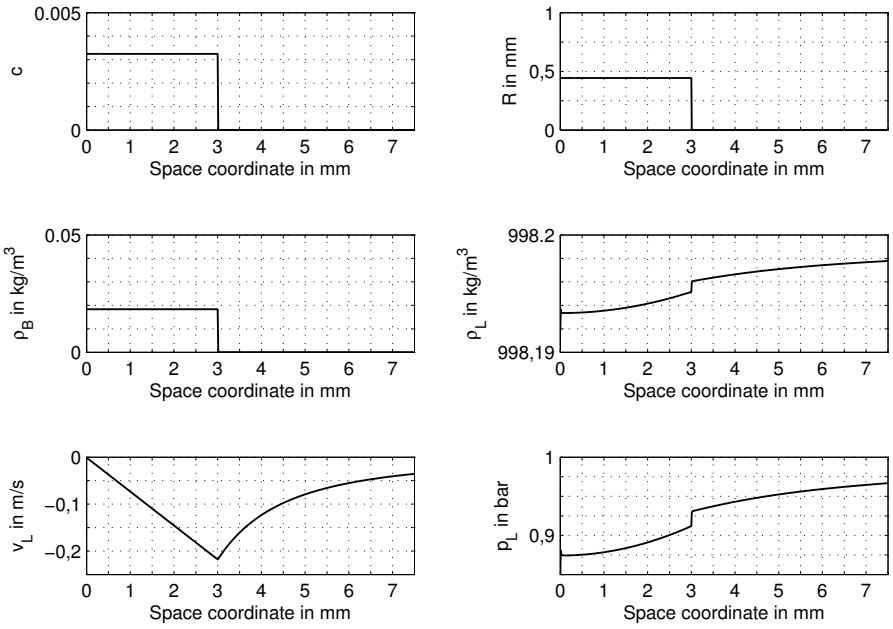

Figure 12.6: Numerical solution for $t = 40\mu s$, incompressible liquid with phase transition

$\phi \in C_0^\infty(\mathbb{R}^3)$ then

$$\begin{aligned}
\langle \frac{\partial}{\partial x^j} \chi_a(\cdot - \mathbf{x}') \,,\, \phi \rangle &= - \langle \chi_a(\cdot - \mathbf{x}') \,,\, \frac{\partial}{\partial x^j}\phi \rangle = - \int_{\mathbb{R}^3} \chi_a(\mathbf{x} - \mathbf{x}') \frac{\partial}{\partial x^j}\phi(\mathbf{x}) \, d\mathbf{x} \\
&= - \int_{B_a(\mathbf{x}')} \frac{\partial}{\partial x^j}\phi(\mathbf{x}) \, d\mathbf{x} = - \int_{\partial B_a(\mathbf{x}')} \eta^j \phi(\mathbf{x}) \, d\mathbf{x} \\
&= \int_{\mathbb{R}^3} \phi(\mathbf{x}) \, d\mu^j_{\partial B_a(\mathbf{x}')} = \langle \mu^j_{\partial B_a(\mathbf{x}')} \,,\, \phi \rangle.
\end{aligned}$$

Now we derive the *shift of differentiation formula* that we needed in the proof of the general transport equation in Lemma 12.2.3. We consider arbitrary test functions $\phi^{\mathbf{x}}, \psi^{\mathbf{x}'} \in C_0^\infty(\mathbb{R}^3)$, use a change of variables and integration by parts to get

$$\begin{aligned}
\langle \frac{\partial}{\partial (\mathbf{x}')^j} \chi_a \,,\, \phi^{\mathbf{x}} \psi^{\mathbf{x}'} \rangle &= - \int_{\mathbb{R}^3} \int_{\mathbb{R}^3} \chi_a(\mathbf{x} - \mathbf{x}') \frac{\partial}{\partial (\mathbf{x}')^j} \psi^{\mathbf{x}'}(\mathbf{x}') \, d\mathbf{x}' \, \phi^{\mathbf{x}}(\mathbf{x}) \, d\mathbf{x} \\
&= \int_{\mathbb{R}^3} \int_{\mathbb{R}^3} \chi_a(y) \frac{\partial}{\partial x^j} \psi^{\mathbf{x}'}(\mathbf{x} - \mathbf{y}) \, d\mathbf{y} \, \phi^{\mathbf{x}}(\mathbf{x}) \, d\mathbf{x} \\
&= \int_{\mathbb{R}^3} \int_{\mathbb{R}^3} \frac{\partial}{\partial x^j} \psi^{\mathbf{x}'}(\mathbf{x} - \mathbf{y}) \phi^{\mathbf{x}}(\mathbf{x}) \, d\mathbf{x} \;\; \chi_a(\mathbf{y}) \, d\mathbf{y} \\
&= - \int_{\mathbb{R}^3} \int_{\mathbb{R}^3} \psi^{\mathbf{x}'}(\mathbf{x} - \mathbf{y}) \frac{\partial}{\partial x^j} \phi^{\mathbf{x}}(\mathbf{x}) \, d\mathbf{x} \;\; \chi_a(\mathbf{y}) \, d\mathbf{y} \\
&= - \int_{\mathbb{R}^3} \int_{\mathbb{R}^3} \chi_a(\mathbf{y}) \psi^{\mathbf{x}'}(\mathbf{x} - \mathbf{y}) \, d\mathbf{y} \;\; \frac{\partial}{\partial x^j} \phi^{\mathbf{x}}(\mathbf{x}) \, d\mathbf{x} \\
&= \int_{\mathbb{R}^3} \int_{\mathbb{R}^3} \chi_a(\mathbf{x} - \mathbf{x}') \psi^{\mathbf{x}'}(\mathbf{x}') \, d\mathbf{x}' \;\; \frac{\partial}{\partial x^j} \phi^{\mathbf{x}}(\mathbf{x}) \, d\mathbf{x} \\
&= - \langle \frac{\partial}{\partial x^j} \chi_a \,,\, \phi^{\mathbf{x}} \psi^{\mathbf{x}'} \rangle.
\end{aligned}$$

12.C Appendix: Exterior potential flow

We take a flow domain around one ball $B_R(\mathbf{q})$ of radius R centered at the the moving point $\mathbf{q}$ with velocity $\dot{\mathbf{q}}$ at time t. Note that in this appendix R is not identical to the macroscopic field for the radius

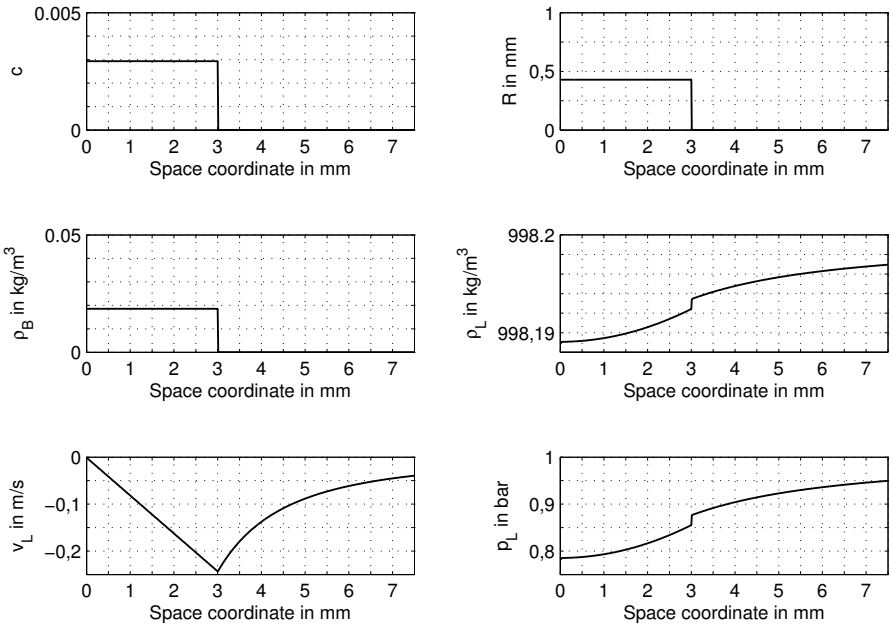

Figure 12.7: Numerical solution for $t = 40\mu s$, compressible liquid with phase transition

equation and here we have $\dot{R} = \frac{dR}{dt}$. We want to use this notation to conform with presentations of the exterior potential problem such as in Landau and Lifshitz [12] or Michlin [13]. We introduce the coordinates $\mathbf{x}$ to be at rest and $\mathbf{r} = \mathbf{x} - \mathbf{q}$ the moving coordinate for which we will formulate a potential. We consider a flow potential Φ satisfying the linear potential equation $\Delta\Phi = 0$ and $\mathbf{v}_\infty \cdot \mathbf{r}$ at infinity. Since $\Phi(\mathbf{r}) = |\mathbf{r}|^{-1} = r^{-1}$ is a solution to this equation outside any ball around the origin, so is any derivative. Due to Maxwell is the ansatz using derivatives of r^{-1}, see Lamb [11, Section 82], using the summation convention where indices appearing twice in a term are summed over 1,2,3,

$$\Phi(t, \mathbf{r}) = v^i_\infty r^i + A\frac{1}{r} + B^i \frac{\partial}{\partial x^i}\frac{1}{r} + C^{ij}\frac{\partial}{\partial x^i \partial x^j}\frac{1}{r} + \dots \ .$$

We will truncate the series after the B^i

$$\Phi = v^i_\infty r^i + A\frac{1}{r} + B^i \frac{\partial}{\partial x^i}\frac{1}{r}.$$

We will see that then we have enough terms to pose appropriate boundary conditions on the ball. We use

$$\frac{\partial r}{\partial x^i} = \frac{x^i - q^i}{r} = \frac{r^i}{r} \quad \text{and} \quad \text{thereby} \quad \frac{\partial r^{-1}}{\partial x^i} = -\frac{x^i - q^i}{r^3} = -\frac{r^i}{r^3}$$

to obtain

$$\Phi = v^i_\infty r^i + A\frac{1}{r} - B^i \frac{r^i}{r^3}.$$

We denote by $\mathbf{R}$ with $R = |\mathbf{R}|$ the coordinates on the surface of the ball. Then the velocity components for $j = 1, 2, 3$ there are given as

$$v^j\Big|_{\mathbf{R}} = \frac{\partial \Phi}{\partial x^j}\Big|_{\mathbf{R}} = v^j_\infty - A\frac{R^j}{R^3} + B^i\left(\frac{3R^iR^j}{R^5} - \frac{\delta_{ij}}{R^3}\right). \tag{12.C.1}$$

Using the assumption that all quantities are constant on the surface (12.3.14) gives

$$\dot{m} = -\rho_L \oint_{\partial B_R(0)} [\mathbf{v}(t, \mathbf{x}') - \mathbf{w}(t)] \cdot \boldsymbol{\eta} \, dS = -4\pi R^2 \rho_L \, [\mathbf{v} - \mathbf{w}(t)] \cdot \boldsymbol{\eta}.$$

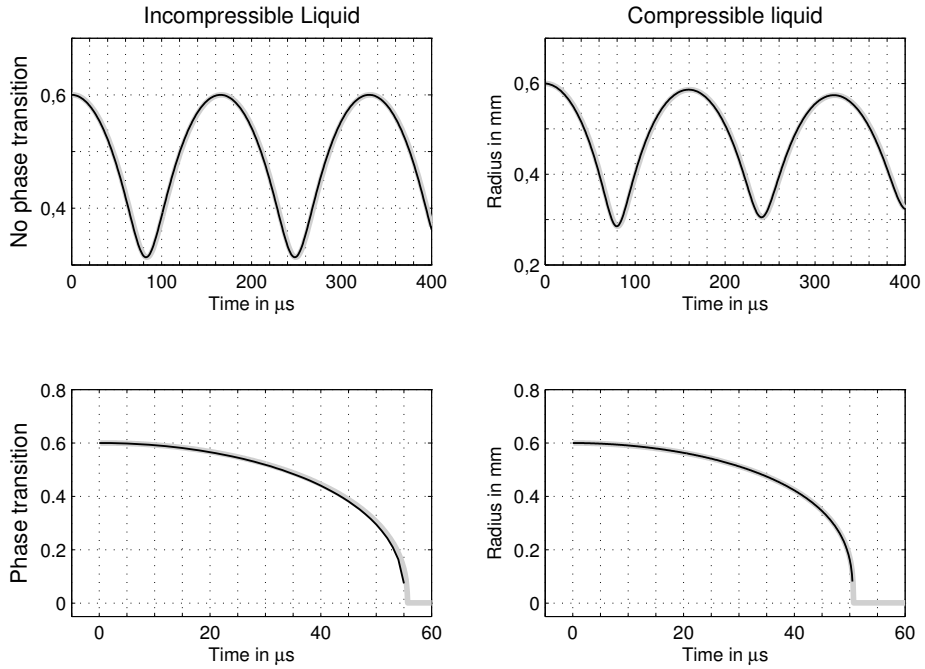

Figure 12.8: Radius vs. time, compressible and incompressible liquid, with and without phase transition, grey: solution of the PDE-system, black: solution of the ODE-system

Note that $\mathbf{w} = \dot{\mathbf{R}} + \dot{\mathbf{q}}$, $\boldsymbol{\eta} = \mathbf{R}/R$, and then $\dot{R} = \boldsymbol{\eta} \cdot \dot{\mathbf{R}}$ giving

$$\mathbf{v} \cdot \boldsymbol{\eta} = -\frac{\dot{m}}{4\pi\rho_L R^2} + \dot{R} + \frac{\dot{\mathbf{q}} \cdot \mathbf{R}}{R}. \tag{12.C.2}$$

Multipying $\eta^j = R^j/R$ to (12.C.1) and comparing the result with (12.C.2) we have

$$\begin{aligned} v^j \eta^j \Big|_{\mathbf{R}} = \frac{\partial \Phi}{\partial x^j} \eta^j \Big|_{\mathbf{R}} &= \frac{v_\infty^j R^j}{R} - \frac{A}{R^2} + B^j R^j \frac{2}{R^4} \\ &= \dot{R} - \frac{\dot{m}}{4\pi\rho_L R^2} + \dot{q}^j \frac{R^j}{R}. \end{aligned}$$

There is a unique solution to the exterior Neumann problem for the potential equation that decays to $\mathbf{v}_\infty \cdot \mathbf{r}$ like r^{-1}, see e.g. Michlin [13, Satz 13.2.2]. It can be expanded uniquely by spherical harmonics, see e.g. Michlin [13, Section 15.4]. This implies that the coefficients in our case are

$$A = \frac{\dot{m}}{4\pi\rho_L} - \dot{R}R^2, \qquad B^j = \frac{1}{2} R^3 (\dot{q}^j - v_\infty^j)$$

leading to

$$\Phi(t, \mathbf{x}) = v_\infty^j r^j + \frac{\dot{m}}{4\pi\rho_L r} - \frac{\dot{R}R^2}{r} - \frac{R^3 r^j (\dot{q}^j - v_\infty^j)}{2r^3}. \tag{12.C.3}$$

We take the Bernoulli equation, see Lamb [11]

$$f(t) = \frac{\partial \Phi}{\partial t} + \frac{1}{2} \frac{\partial \Phi}{\partial x^j} \frac{\partial \Phi}{\partial x^j} + \frac{p}{\rho_L} + g x^3.$$

The aim is to determine the pressure. Using (12.D.1) we obtain

$$\begin{aligned} \frac{1}{\rho_L} \oint_{\partial B_R(0)} p \eta^i \, dS &= - \oint_{\partial B_R(0)} \left(-f(t) + \frac{1}{2} \frac{\partial \Phi}{\partial x^j} \frac{\partial \Phi}{\partial x^j} + \frac{\partial \Phi}{\partial t} + g x^3 \right) \eta^i \, dS \\ &= - \oint_{\partial B_R(0)} \left(\frac{1}{2} \frac{\partial \Phi}{\partial x^j} \frac{\partial \Phi}{\partial x^j} + \frac{\partial \Phi}{\partial t} + g x^3 \right) \eta^i \, dS. \end{aligned} \tag{12.C.4}$$

Now we compute the derivative terms of the potential needed in the Bernoulli equation

$$\left.\frac{\partial\Phi}{\partial x^j}\frac{\partial\Phi}{\partial x^j}\right|_R = v^j_\infty v^j_\infty + 2v^j_\infty B^i\left(\frac{3R^iR^j}{R^5}-\frac{\delta_{ij}}{R^3}\right) - 2v^j_\infty A\frac{R^j}{R^3}$$
$$+A^2\frac{1}{R^4} + B^iB^k\left(\frac{3R^iR^j}{R^5}-\frac{\delta_{ij}}{R^3}\right)\left(\frac{3R^kR^j}{R^5}-\frac{\delta_{kj}}{R^3}\right) - 4AB^i\frac{R^i}{R^6}.$$

We turn to the time derivative and note that

$$\frac{\partial r^j}{\partial t} = \frac{\partial}{\partial t}(x^j - q^j) = -\dot q^j.$$

This gives

$$\frac{\partial r}{\partial t} = -\frac{r^j}{r}\dot q^j$$

and we obtain

$$\begin{aligned}\left.\frac{\partial\Phi}{\partial t}\right|_R &= \frac{\partial}{\partial t}\left(v^j_\infty r^j + A\frac{1}{r} - B^j\frac{r^j}{r^3}\right)\Bigg|_R\\ &= -v^j_\infty\dot q^j + \dot A\frac{1}{R} - A\frac{1}{R^2}\left.\frac{\partial r}{\partial t}\right|_R - \dot B^j\frac{R^j}{R^3} - B^j\frac{1}{R^3}\left.\frac{\partial r^j}{\partial t}\right|_R + 3B^jR^j\frac{1}{R^4}\left.\frac{\partial r}{\partial t}\right|_R\\ &= -v^j_\infty\dot q^j + \dot A\frac{1}{R} + A\frac{R^j}{R^3}\dot q^j - \dot B^j\frac{R^j}{R^3} + B^j\frac{1}{R^3}\dot q^j - 3B^jR^jR^i\dot q^i\frac{1}{R^5}.\end{aligned}$$

The derivatives obtained are now inserted into the formula (12.C.4) for the pressure. We make use of the fact that formulae (12.D.1-12.D.3) imply that we only have to retain terms where the integrand contains a constant times the product of two normal components η^i or depends on a space variable, as in the gravitational term,

$$\begin{aligned}\frac{1}{\rho_L}\oint_{\partial B_R(0)} p\eta^i\,dS &= \oint_{\partial B_R(0)}\left(v^j_\infty A\frac{R^j}{R^3} + 2AB^j\frac{R^j}{R^6} - A\frac{R^j}{R^3}\dot q^j + \dot B^j\frac{R^j}{R^3} - g\delta_{i3}\right)\eta^i\,da\\ &= \frac{4}{3}\pi v^i_\infty A + \frac{8}{3}\pi AB^i\frac{1}{R^3} - \frac{4}{3}\pi A\dot q^i + \frac{4}{3}\pi\dot B^i - g\delta_{i3}\frac{4}{3}\pi R^3\\ &= \frac{4}{3}\pi v^i_\infty A + \frac{4}{3}\pi A(\dot q^i - v^i_\infty) - \frac{4}{3}\pi A\dot q^i + \frac{4}{3}\pi\dot B^i - g\delta_{i3}\frac{4}{3}\pi R^3\\ &= \frac{4}{3}\pi\dot B^i - g\delta_{i3}\frac{4}{3}\pi R^3\end{aligned}$$

giving

$$\begin{aligned}\oint_{\partial B_R(0)} p\eta^i\,dS &= \rho_L\left(\frac{4}{3}\pi\dot B^i - g\delta_{i3}\frac{4}{3}\pi R^3\right)\\ &= \rho_L\left(\frac{2}{3}\pi\left(R^3\dot q^i\right)^{\cdot} - 2\pi R^2\dot R v^i_\infty - g\delta_{i3}\frac{4}{3}\pi R^3\right).\end{aligned}$$

With $v^i_\infty = 0$ we obtain

$$\oint_{\partial B_R(0)} p\eta^i\,dS = \rho_L\left(\frac{2}{3}\pi\left(R^3\dot q^i\right)^{\cdot} - g\delta_{i3}\frac{4}{3}\pi R^3\right). \tag{12.C.5}$$

We compute the $\mathbf{v}$ term in (12.3.8). Note that A and the B^j are constant and contain no normal

components $\eta^i = R^i/R$. Therefore we can use (12.D.1) and (12.D.2) to obtain

$$\begin{aligned}
\oint_{\partial B_R(0)} v^j \, dS &= \oint_{\partial B_R(0)} \frac{\partial \Phi}{\partial x^j} \, dS \\
&= \oint_{\partial B_R(0)} \left(v^j_\infty - A\frac{R^j}{R^3} + B^i \left(\frac{3R^iR^j}{R^5} - \frac{\delta_{ij}}{R^3} \right) \right) dS \\
&= 4\pi R^2 v^j_\infty + \oint_{\partial B_R(0)} B^i \left(\frac{3R^iR^j}{R^5} - \frac{\delta_{ij}}{R^3} \right) dS \\
&= 4\pi R^2 v^j_\infty + \frac{B^i}{R^3} \oint_{\partial B_R(0)} \left(3\frac{R^iR^j}{R^2} - \delta_{ij} \right) dS \\
&= 4\pi R^2 v^j_\infty + \frac{B^i}{R^3} \left(3\frac{4}{3}\pi R^2 - 4\pi R^2 \right) \delta_{ij} = 4\pi R^2 v^j_\infty = 0 \,. \qquad (12.C.6)
\end{aligned}$$

12.D Appendix: Surface integrals

In Appendix C we had to evaluate a number surface integrals for integrands consisting of one, two or three components of the exterior normal vector on $\partial B_R(\mathbf{q})$. For an arbitrary domain Ω allowing the use of the Gauss theorem we have

$$\oint_{\partial\Omega} \eta^i \, dS = \int_\Omega \partial_{x^i} 1 \, d\mathbf{x} = 0. \qquad (12.D.1)$$

We extend the vector field $\boldsymbol{\eta} = \mathbf{R}/R$ by $(\mathbf{x}-\mathbf{q})/R$ to the interior of $B_R(\mathbf{q})$

$$\oint_{\partial B_R(\mathbf{q})} \eta^i \eta^j \, dS = \int_{B_R(\mathbf{q})} \partial_{x^i} \eta^j \, d\mathbf{x} = \frac{\delta_{ij}}{R} \int_{B_R(\mathbf{q})} d\mathbf{x} = \frac{4}{3}\pi R^2 \delta_{ij}. \qquad (12.D.2)$$

Noting that the functions η^j are odd with respect to a plane through the center of the ball we obtain

$$\begin{aligned}
\oint_{\partial B_R(\mathbf{q})} \eta^i \eta^j \eta^k \, dS &= \int_{B_R(\mathbf{q})} \partial_{x^i} \left(\eta^j \eta^k \right) \, d\mathbf{x} \\
&= \int_{B_R(\mathbf{q})} \eta^j \partial_{x^i} \eta^k + \partial_{x^i}(\eta^j) \eta^k \, d\mathbf{x} \\
&= \frac{1}{R} \int_{B_R(\mathbf{q})} \eta^j \delta_{ik} + \eta^k \delta_{ij} \, d\mathbf{x} \\
&= \frac{\delta_{ik}}{R} \int_{B_R(\mathbf{q})} \eta^j \, d\mathbf{x} + \frac{\delta_{ij}}{R} \int_{B_R(\mathbf{q})} \eta^k \, d\mathbf{x} \\
&= 0. \qquad (12.D.3)
\end{aligned}$$

References

[1] Andrianov, N.: Analytical and numerical investigation of two-phase flows. PhD thesis. Otto-von-Guericke University, Magdeburg (2003)

[2] Baer, M., Nunziato, J.: a two-phase mixtute theory for the deflagration-to-detonation transition (DDT) in reactive granular materials. Int. j. Multiphase Flows **12**, 861–889 (1986)

[3] Bensoussan, A., Lions, J.-L., Papanicolaou, G.: Asymptotic analysis for periodic structures. North-Holland Publ. Company, Amsterdam (1978)

[4] Dreyer, W., Duderstadt, F., Hantke, M., Warnecke, G.: Bubbles in liquids with phase transition. Part 1. On phase change of a vapor bubble in liquid water. Cont. Mech. Thermodyn. DOI 10.1007/s00161-0225-6, (2011)

[5] Drew, D. A., Passman, S. L.: Theory of multicomponent fluids. Springer-Verlag, New York (1999)

[6] Engquist, B., Hou, T.: Particle method approximation of oscillatory solutions to hyperbolic differential equations. SIAM J. Numer. Anal. **26**, 289–319 (1989)

[7] Gallouët, T., Masella, J.-M.: Un schema de Godunov approché. C. R. Acad. Sci. Paris Ser. **I 323**, 77–84 (1996)

[8] Grigull, U., Straub, S., Schiebener, P.: Steam Tables in SI-Units, Wasserdampftafeln. Springer-Verlag, Berlin (1990)

[9] Hörmander, L.: The Analysis of Linear Partial Differential Operators I. Springer-Verlag, Berlin (1990.)

[10] Ishii, M.: Thermo-fluid dynamic theory of two-phase flow. Eyrolles, Paris (1975)

[11] Lamb, H.: Hydrodynamics. Dover, New York (1945)

[12] Landau, L. D., Lifshitz, E. M.: Fluid Mechanics, Volume 6 of Course on Theoretical Physics. Pergamon Press, London (1959)

[13] Michlin, S. G.: Partielle Differentialgleichungen in der mathematischen Physik. Akademie-Verlag, Berlin (1978)

[14] Müller, I., Ruggeri, T.: Rational Extended Thermodynamics, Volume 37 of Springer Tracts in Natural Philosophy. Springer-Verlag, New York (1998)

[15] Müller, I.: Grundzüge der Thermodynamik. Springer-Verlag, Berlin (2001)

[16] Nigmatulin, R. I.: Dynamics of Multiphase Media, Vol 1. Hemisphere Publ., New York – Washington – Philadelphia – London (1991)

[17] Rydzewski, R.: Die Feldgleichungen von Suspensionen. Diploma thesis. Technical University Berlin (1985)

[18] Serrin, J.: Mathematical principles of classical fluid mechanics. In: Flügge, S. (ed.) Handbuch der Physik VIII/1 – Strömungsmechanik 1, 125–263. Springer-Verlag, Berlin – Göttingen – Heidelberg, (1959)

[19] Stewart, H. B., Wendroff, B.: Two-phase flow: models and methods. J. Comput. Phys. **56**, 363–409 (1984)

[20] Toro, E.: Riemann Solvers and Numerical Methods for Fluid Dynamics. Springer, Berlin (1999)

[21] Warnecke, G.: Analytische Methoden in der Theorie der Erhaltungsgleichungen, TEUBNER-TEXTE zur Mathematik Band 138. Teubner, Stuttgart-Leipzig (1999)

[22] Voinov, O. V.: Force acting on a sphere in an inhomogeneous flow of an ideal incompressible fluid. J. Appl. Mech. Tech. Phys. **14**, 592–594 (1973)

[23] Voinov, O. V., Petrov, A. G.: On the equation of motion of a liquid with bubbles. J. Appl. Math. Mech. **39**, 811–822 (1975)

[24] Voinov, O. V., Petrov, A. G.: On the stress tensor in a fluid containing disperse particles. J. Appl. Math. Mech. **41**, 362–364 (1977)

[25] Wagner, W., Kretzschmar, H.-J.: International Steam Tables, Springer-Verlag, Berlin – Heidelberg (2008)

Eigene Veröffentlichungen

[H1] B. Dittmar, M. Hantke. Robin function and eigenvalue problems, *Reports on Analysis*, Martin-Luther-Universitt Halle - Wittenberg, 2006.

[H2] B. Dittmar, M. Hantke. The Robin function and its eigenvalues, *Georgian mathematical Journal*, 14 (2006), pp. 403-417.

[H3] A. Zein, M. Hantke, G. Warnecke. Modeling phase transition for compressible two-phase flows applied to metastable liquids, *J. Comput. Phys.*, 229 (2010), pp. 2964-2998.

[H4] B. Dittmar, M. Hantke. About a Polya-Schiffer inequality, *Annales Universitatis Mariae Curie-Sklodowska*, 65 (2011), pp. 29-44.

[H5] W. Dreyer, F. Duderstadt, M. Hantke, G. Warnecke. Bubbles in liquids with phase transition. Part 1: On phase change of a single vapor bubble in liquid water, *Continuum mechanics and thermodynamics* 24 (2012), pp. 461-483.

[H6] M. Hantke, F. Thein. Numerical solutions to the Riemann problem for compressible isothermal Euler equations for two phase flows with and without phase transitions, in: *Proceedings of HYP2012*.

[H7] Ee Han, M. Hantke, G. Warnecke. Exact Riemann solutions to compressible Euler equations in ducts with discontinuous cross-section, *Journal of hyperbolic differential equations* 9 (2012), pp. 403-449.

[H8] M. Hantke, W. Dreyer, G. Warnecke. Exact solutions to the Riemann problem for compressible isothermal Euler equations for two phase flows with and without phase transition, *Quarterly of Applied Mathematics*, vol. LXXI 3 (2013), pp. 509-540.

[H9] Ee Han, M. Hantke, G. Warnecke. Criteria for non uniqueness of Riemann solutions to compressible duct flows, *ZAMM*, Vol. 93/6-7 (2013), pp. 465-475.

[H10] A. Zein, M. Hantke, G. Warnecke. On the modeling and simulation of a laser-induced cavitation bubble, *Int. J. Num. Meth. Fluids*, Vol.73/2 (2013), pp. 172-203. DOI: 10.1002/fld.3796

[H11] W. Dreyer, M. Hantke, G. Warnecke. Bubbles in liquids with phase transition. Part 2: on balance laws for mixture theories of disperse vapor bubbles in liquid with phase change, *Continuum mechanics and thermodynamics* (2013). DOI 10.1007/s00161-013-0316-7

[H12] M. Hantke, F. Thein. Why condensation by compression in pure water vapor cannot occur in an approach based on Euler equations, *Quarterly of Applied Mathematics* 73 (2015), 575-591.

[H13] S. Müller, M. Hantke, P. Richter. Closure conditions for non-equilibrium multi-component models, *Continuum Mech. Thermodyn.* (2016). 28:1157. doi:10.1007/s00161-015-0468-8

[H14] F. Thein, M. Hantke. Singular and selfsimilar solutions for Euler equations with phase transitions, *Bulletin of the Brazilian Mathematical Society*, New Series 47 (2), (2016), 779-786.

[H15] Ee Han, M. Hantke, S. Müller. Efficient and robust relaxation procedures for multi-component mixtures including phase transition, *Journal of Computational Physics*, Vol. 338 (2017), pp. 217-239.

[H16] M. Hantke, C. Matern, G. Warnecke. Numerical solutions for a weakly hyperbolic dispersed two-phase flow model. To appear in: *Proceedings of HYP2016.*

[H17] F. Thein, M. Hantke. A general existence result for isothermal two-phase flows with phase transition. (Submitted)

[H18] M. Hantke, S. Müller. Analysis and simulation of a new multi-component two-phase flow model with phase transitions and chemical reactions. To appear in: *Quarterly of Applied Mathematics*